

# Mechatronic Systems

Rolf Isermann

---

# Mechatronic Systems

## Fundamentals

With 357 Figures



Springer

Professor Dr.-Ing. Dr.h.c. Rolf Isermann  
Institute of Automatic Control, Darmstadt University of Technology,  
Landgraf-Georg-Strasse 4, D-64283, Darmstadt, Germany

British Library Cataloguing in Publication Data  
Isermann, R. (Rolf)

Mechatronic systems : fundamentals  
1.Mechatronics 2.Microelectromechanical systems  
I.Title  
621.3  
ISBN 1852339306

Library of Congress Cataloging-in-Publication Data  
A catalog record for this book is available from the Library of Congress.

Apart from any fair dealing for the purposes of research or private study, or criticism or review, as permitted under the Copyright, Designs and Patents Act 1988, this publication may only be reproduced, stored or transmitted, in any form or by any means, with the prior permission in writing of the publishers, or in the case of reprographic reproduction in accordance with the terms of licences issued by the Copyright Licensing Agency. Enquiries concerning reproduction outside those terms should be sent to the publishers.

ISBN 1-85233-930-6  
Springer Science+Business Media  
[springeronline.com](http://springeronline.com)

© Springer-Verlag London Limited 2005  
2nd printing 2005

The use of registered names, trademarks etc. in this publication does not imply, even in the absence of a specific statement, that such names are exempt from the relevant laws and regulations and therefore free for general use.

The publisher makes no representation, express or implied, with regard to the accuracy of the information contained in this book and cannot accept any legal responsibility or liability for any errors or omissions that may be made.

Typesetting: Electronic text files prepared by author  
Printed in the United States of America  
69/3830-54321 Printed on acid-free paper SPIN 11348962

## Preface

---

Many technical processes and products in the area of mechanical and electrical engineering are showing an increasing integration of mechanics with digital electronics and information processing. This integration is between the components (hardware) and by the information-driven functions (software), resulting in integrated systems called *mechatronic systems*. Their development involves finding an optimal balance between the basic mechanical structure, sensor and actuator implementation, automatic information processing and overall control. Frequently, formerly mechanical functions are replaced by electronically controlled functions, resulting in simpler mechanical structures and increased functionality. The development of mechatronic systems opens a way to many innovative solutions and synergetic effects that are not possible with mechanics or electronics alone. This technical progress has a very large influence on a multitude of products in the area of mechanical, electrical and electronic engineering and changes the design, for example, of conventional electromechanical components, machines, vehicles and precision mechanical devices with increasing intensity.

This book is intended to give an introduction to the development of mechatronic systems, especially by considering the modeling of the dynamics of the components, their interactions and overall behavior and by describing the components of information processing from sensors through microcomputers to actuators. After considering the basic structure of integrated mechanical-electronic systems, typical tasks for the design of mechatronic systems are discussed. The design of the process and the implementation of the information-processing algorithms generally requires a precise knowledge of the static and dynamic relations between input, state and output variables

and the possibilities of influencing them by control functions. Therefore, theoretical (physical) modeling, computer-aided design methods and experimental testing (identification) methods are required.

The first part of the book describes the basics of theoretical modeling, the static and dynamic behavior of lumped parameter processes in a general form and by a unified methodology for different physical domains, like mechanics, electricity and heat. After a classification of the various process elements with regard to energy, matter or information flow, the fundamental equations for processes with energy and matter flow are stated, like balance equations, constitutive equations and phenomenological equations. Here, the analogies between the processes of different physical domains are used by applying power variables for processes with energy flows, like potentials and flows or across and through variables. Special energy balance equations are stated for mechanical and electrical processes and processes with compressible fluids, like gases and steam. For the formulation of the interconnection of the process elements with energy and mass flows, the connection laws are stated, resulting in generalized node and mesh equations. The next chapter then considers the fundamental equations for mechanical systems with moving masses, including Newton's laws of kinetics and the principles of mechanics in the form of d'Alembert's principle and Lagrange equations.

Then, models of mechanical systems with and without motion for a selection of mechanical machine elements are described, from mass-spring-damper systems and bearings, through rotational multi-mass systems, to friction laws. This is followed by models of electrical drives in the form of electromagnets and electrical machines, like DC and AC motors. The basic mathematical models for DC and AC motors with power electronics are developed. Based on these part models, mathematical models of power-generating and power-consuming machines are derived and their static and dynamic properties, like inherent damping, resonance effects and stability, are analyzed. Then, a chapter on the experimental identification and parameter estimation of linear and non-linear dynamic systems follows, including recursive estimators for time-varying systems, artificial neural networks and look-up table representations. Further on, models of harmonic oscillations and their identification are discussed.

The second part is dedicated to the description of the information processing components of mechatronic systems as sensors, actuators and microcomputers. Typical sensors and actuators for mechatronic systems are systematically considered and their properties and performance data are surveyed to ease their selection. In the case of actuators, detailed models of electrical, hydraulic and pneumatic actuators are described. A brief treatment of the basic structure of microcomputers, including microprocessors, microcontrollers and digital signal processors and field bus systems is given in order to obtain an overview. Various tables with technical data should give some hints for the performance of these information-processing components.

In the last chapter, some examples of the development of mechatronic systems are given, including their modeling, control and fault detection, as an industrial robot, a semi-active vehicle suspension, an electrical throttle valve and an electromechanical disc brake. These examples show some applications for the topics treated throughout the book.

Based on the mathematical models of the processes and the surveys of the components of mechatronic systems, the information processing by digital control, supervision with fault diagnosis and optimization can be implemented, which is described in other books. This then enables steps in the direction of mechatronic systems, even with some intelligent properties. Examples in the area of precision mechanical systems are automatic cameras, high-density disk storage, smart actuators, learning robots and mobile robots with automatic navigation. In the area of machines, active damping systems, magnetic bearings with unbalance compensation and fault detection, machine tools with adaptive control, fault diagnosis and maintenance on demand are typical examples. For combustion engines, increasingly more actuator systems, like variable geometry turbochargers, common rail multiple injection, variable valve camshafts, electromechanical-actuated valves and adaptive look-up tables, are developed. Automobiles with electro-hydraulic brakes, electromechanical brakes, steer-by-wire and collision avoidance control with rollover prevention are further typical mechatronic developments.

The book is a revised translation of the German version, "Mechatronische Systeme", with many extensions. It is based on several research projects and lectures at the Darmstadt University of Technology, held since 1992. The general design methodology and some parts also go back to the special research project, "Integrated mechatronic systems (IMES)", at the Darmstadt University of Technology, funded by the Deutsche Forschungsgemeinschaft, in which 11 Institutes of Electrical and Mechanical Engineering cooperated in performing 20 different innovative research projects from 1988 to 2001. The book is dedicated to graduate students of electrical and electronic engineering, mechanical engineering and computer science and practising engineers in research and development, design and manufacturing.

The author is especially grateful to his research associates, who have been helpful in compiling the material. The earlier team was mentioned in the first, German, version. The translation of the German book into English, including many additions, was performed in a combined effort by Markus Börner, Stefan Drogies, Alexander Fink, Frank Kimmich, Michael Kochem, Marco Münchhof, Jürgen Schmitt, Jochen Schaffnit, Anselm Schwarte, Harald Straky, Karsten Spreitzer, Susanne Töpfer, Crina Vlad, Marian Walter, Armin Wolfram and Christof Zosel. Sections 5.4 on AC motors, 5.6 on power electronics and 6.6 on centrifugal pumps were written by Armin Wolfram, 6.7 on automobile drivetrains by Jochen Schaffnit and 8.2.7 on speed signal analysis by Frank Kimmich. Considerable extensions to Chapter 9 on sensors was contributed by Karsten Spreitzer and to Chapter 10 on actuators by Marco

Münchhof. The examples for mechatronic systems in Chapter 12 were contributed by Michael Kochem, Markus Börner and Sascha Semmler. This assistance is highly appreciated, making it possible to publish the English version in time. The final laborious and precise text setting, including the figures and tables in camera-ready form was performed by Brigitte Hoppe. Many thanks for the patient and continuous work go to her.

Darmstadt, August 2002

Rolf Isermann

# Contents

---

<b>List of Symbols</b>	.....	ix
<b>1 Integrated Mechanical Electronic Systems</b>	.....	1
1.1 From Mechanical to Mechatronic Systems	.....	1
1.2 Mechanical Systems	.....	6
1.2.1 Mechanical Systems in Mechanical Engineering	....	8
1.2.2 Mechanical Systems in Precision Mechanic Devices	.....	9
1.2.3 Micromechanics	.....	9
1.2.4 Mechanical Systems in Apparatus (Process Engineering)	.....	10
1.2.5 Confinement of Mechatronic Systems	.....	10
1.3 Functions of Mechatronic Systems	.....	11
1.3.1 Design	.....	11
1.3.2 Distribution of Mechanical and Electronic Functions	.....	12
1.3.3 Operating Properties	.....	13
1.3.4 New Functions	.....	13
1.3.5 Other Developments	.....	14
1.4 Integration Forms of Processes and Electronics	.....	14
1.5 Ways of Information Processing	.....	18
1.5.1 Multi-level Control Systems	.....	18
1.5.2 Special Signal Preprocessing	.....	19
1.5.3 Information Gaining	.....	19

1.5.4	Model-based Methods of Control .....	20
1.5.5	Supervision and Fault Diagnosis .....	21
1.5.6	Intelligent Systems .....	22
1.6	Design Procedures for Mechatronic Systems .....	24
1.7	Contents of this Book .....	29
<b>2</b>	<b>Fundamentals of Theoretical Modeling of Technical Processes</b> .....	<b>33</b>
2.1	Theoretical and Experimental Modeling .....	34
2.2	Classification of Process Elements .....	37
2.2.1	Forms of Matter .....	37
2.2.2	Main Flows and Side Flows .....	38
2.2.3	Process Elements with Lumped Parameters .....	40
2.2.4	Process Elements with Distributed Parameters .....	46
2.3	Fundamental Equations of Process Elements with Energy and Matter Flows .....	46
2.3.1	Balance Equations .....	47
2.3.2	Constitutive Equations .....	51
2.3.3	Phenomenological Equations .....	68
2.4	Energy Balance Equations for Lumped Parameter Processes .....	71
2.4.1	Energy Balance for Mechanical Systems .....	71
2.4.2	Energy Balance for Thermal Systems (Rigid Bodies, Fluids) .....	77
2.4.3	Energy Balance for Gases and Steam .....	79
2.4.4	Energy Balance for Electrical Systems .....	83
2.4.5	Common Properties of Balance Equations .....	85
2.5	Connection of Process Elements .....	88
2.5.1	Node Equation and Mesh Equation .....	88
2.5.2	Causality of Process Elements .....	91
2.6	Analogies between Mechanical and Electrical Systems .....	94
2.7	Summary .....	97
2.8	Problems .....	99
<b>3</b>	<b>Fundamental Equations of the Dynamics of Mechanical Systems with Mobile Masses</b> .....	<b>101</b>
3.1	Newton's Laws of Kinetics .....	102
3.1.1	Translational Motion .....	102
3.1.2	Rotational Motion .....	103
3.2	Principles of Mechanics .....	106
3.2.1	d'Alembert's Principle .....	106
3.2.2	Lagrange's Equations .....	109

3.3	Problems . . . . .	114
<b>4</b>	<b>Mechanical Elements . . . . .</b>	<b>115</b>
4.1	Bars . . . . .	116
4.2	Springs . . . . .	118
4.3	Dampers . . . . .	121
4.3.1	Dampers with Dry and Viscous Friction . . . . .	121
4.3.2	Spring-damper Systems . . . . .	122
4.4	Bearings . . . . .	124
4.4.1	Sliding Bearings . . . . .	124
4.4.2	Roller Bearings . . . . .	125
4.5	One-mass Oscillator (Spring-mass-damper Systems) . . . . .	128
4.5.1	Longitudinal Oscillators . . . . .	128
4.5.2	Torsional Oscillators . . . . .	133
4.6	Multi-mass Oscillators . . . . .	134
4.6.1	Two-mass Torsional Oscillator with One Spring . . . . .	134
4.6.2	Two-mass Torsional Oscillator with Two Springs . . . . .	140
4.6.3	Two-mass Torsional Oscillator with Gear and One Spring . . . . .	142
4.6.4	Power Transmissions . . . . .	146
4.6.5	Belt Drives . . . . .	151
4.6.6	Absorbers and Dampers . . . . .	158
4.7	Mechanical Systems with Friction . . . . .	159
4.8	Mechanical Systems with Backlash . . . . .	162
4.9	Problems . . . . .	164
<b>5</b>	<b>Electrical Drives . . . . .</b>	<b>167</b>
5.1	Types of Electrical Drives . . . . .	167
5.2	Electromagnets . . . . .	170
5.2.1	Types of Electromagnets . . . . .	170
5.2.2	The Magnetic Field . . . . .	171
5.2.3	Static Behavior of Simple Magnetic Circuits . . . . .	173
5.2.4	Dynamic Behavior of Simple Magnetic Circuits . . . . .	175
5.2.5	Static Behavior of Electromagnets . . . . .	177
5.2.6	Dynamic Behavior of Electromagnets and Position Control . . . . .	181
5.3	Direct Current Motors . . . . .	184
5.3.1	Induced Voltage . . . . .	186
5.3.2	Torque Generation . . . . .	187
5.3.3	Dynamic Behavior . . . . .	188

5.3.4	Static Behavior . . . . .	192
5.3.5	Speed and Position Control . . . . .	194
5.3.6	Brushless DC Motors (Electronic Commutation) . . . . .	196
5.3.7	Special Types of DC Motors . . . . .	200
5.4	Alternating Current Motors (AC) . . . . .	205
5.4.1	Induction Motors . . . . .	205
5.4.2	Synchronous Motors . . . . .	215
5.5	Single-phase Motors . . . . .	221
5.5.1	Commutator Motors (Universal Motors) . . . . .	221
5.5.2	Squirrel-cage Motors . . . . .	222
5.6	Power Electronics . . . . .	225
5.6.1	Power Component Parts . . . . .	225
5.6.2	Power Circuits . . . . .	226
5.7	Internally or Externally Commutated Electromotors . .	234
5.8	Problems . . . . .	235
<b>6</b>	<b>Machines and Drivetrains . . . . .</b>	<b>241</b>
6.1	Coupling of Machine Components to Complete Machines . . . . .	243
6.2	Characteristics and Stability of Machines . . . . .	248
6.3	Static Behavior of Power-generating and Power-consuming Machines . . . . .	257
6.4	Dynamic Model of a Combustion Engine Test Stand . . . . .	262
6.5	Dynamic Behavior of a Machine Tool Feed Drive . . .	268
6.5.1	A Feed Drive and its Components . . . . .	268
6.5.2	Identification of the Feed Drive Control System . . . . .	270
6.6	Dynamic Model of an AC Motor and Centrifugal Pump System . . . . .	273
6.6.1	Theoretical Model of Centrifugal Pumps . . . . .	273
6.6.2	Overall Model of the Pumping Plant and Identification . . . . .	274
6.7	Dynamic Model of an Automobile Drivetrain . . . . .	278
6.7.1	Components of an Automotive Drivetrain . . . . .	279
6.7.2	Drivetrain Model with Driveshaft Elasticity . . . . .	280
6.8	Dependency of System Behavior on the Operating Point . . . . .	283
6.8.1	Storage with and without Feedback . . . . .	283
6.8.2	Tuning of Controller Parameters . . . . .	286
6.9	Advanced Control of Mechanical Systems . . . . .	286
6.9.1	Lower Level Feedback Control . . . . .	287

6.9.2	Higher Level Feedback Control .....	289
6.9.3	Adaptive Control .....	290
6.9.4	Fuzzy Control .....	290
6.10	Problems .....	291
<b>7</b>	<b>Identification of Dynamic Systems .....</b>	<b>293</b>
7.1	Identification Methods .....	293
7.1.1	General Procedure .....	293
7.1.2	Classification of Identification Methods .....	294
7.1.3	Identification Methods .....	295
7.1.4	Test Signals .....	298
7.1.5	Closed-loop Identification .....	299
7.1.6	Type of Application .....	299
7.2	Parameter Estimation for Discrete Time Signals .....	299
7.2.1	Method of Least Squares (LS) .....	300
7.2.2	Recursive Method of Least Squares (RLS) .....	303
7.2.3	Modifications of the Least Squares Method .....	303
7.3	Parameter Estimation for Continuous Time Signals .....	303
7.3.1	Method of Least Squares .....	304
7.4	Time-varying Systems .....	306
7.5	Non-linear Processes .....	308
7.5.1	Parameter Estimation with Classical Non-linear Models .....	308
7.5.2	Artificial Neural Networks .....	309
7.5.3	Fuzzy-logic Models .....	323
7.5.4	Grid-based Look-up Tables for Static Systems .....	325
7.5.5	Parameter Estimation for Non-continuously Differentiable Non-linear Processes (Friction and Backlash) .....	327
7.6	Problems .....	331
<b>8</b>	<b>Models of Oscillations and their Identification .....</b>	<b>333</b>
8.1	Harmonic Oscillations .....	333
8.1.1	Single Oscillations .....	334
8.1.2	Superposition .....	334
8.1.3	Amplitude Modulation .....	334
8.1.4	Frequency and Phase Modulation .....	335
8.1.5	Beating (Libration) .....	337
8.1.6	Superposition and Non-linear Characteristics .....	338
8.2	Identification of Harmonic Oscillations .....	339
8.2.1	Bandpass Filtering .....	339

8.2.2	Fourier Analysis . . . . .	340
8.2.3	Correlation Functions . . . . .	340
8.2.4	Fourier Transformation . . . . .	341
8.2.5	Fast Fourier Transformation (FFT) . . . . .	343
8.2.6	Maximum-entropy Spectral Estimation . . . . .	347
8.2.7	Speed Signal Analysis of Combustion Engines . . . . .	353
8.3	Problems . . . . .	357
<b>9</b>	<b>Sensors . . . . .</b>	<b>359</b>
9.1	Measuring System . . . . .	360
9.2	Classification of Sensors . . . . .	360
9.3	Sensor Properties . . . . .	362
9.4	Signal Types, Transducers, Measuring Amplifiers . . . . .	363
9.5	Displacement Measurement . . . . .	364
9.6	Velocity Measurement . . . . .	368
9.7	Acceleration Measurement . . . . .	370
9.8	Vibration and Oscillation Measurement . . . . .	372
9.9	Force and Pressure Measurement . . . . .	372
9.10	Torque Measurement . . . . .	373
9.11	Temperature Measurement . . . . .	373
9.12	Analog-to-Digital Conversion . . . . .	376
9.13	Electromagnetic Compatibility (EMC) . . . . .	377
9.14	Integrated and Intelligent Sensors . . . . .	378
9.15	Problems . . . . .	381
<b>10</b>	<b>Actuators . . . . .</b>	<b>383</b>
10.1	Basic Structures of Actuators . . . . .	384
10.2	General Survey of Actuators . . . . .	387
10.2.1	Types of Auxiliary Energy . . . . .	387
10.2.2	Actuator Behavior and Control . . . . .	389
10.2.3	Requirements for Actuators and Servo-drives . . . . .	392
10.3	Electromechanical Actuator Drives . . . . .	392
10.3.1	Electrical Motors . . . . .	393
10.3.2	Electromagnets . . . . .	404
10.4	Hydraulic Actuators . . . . .	406
10.4.1	Hydraulic Actuation Systems . . . . .	407
10.4.2	Hydraulic Components and their Models . . . . .	408
10.4.3	Models of an Hydraulic Servo-axis: An Example . . . . .	429
10.5	Pneumatic Actuators . . . . .	439
10.5.1	Pneumatic Actuating Systems . . . . .	439

10.5.2	Pneumatic Components and their Models . . . . .	442
10.5.3	Model-based Control of a Pneumatic Servo-axis . . . . .	452
10.5.4	Models of a Pneumatic Valve . . . . .	456
10.6	Unconventional Actuators . . . . .	457
10.6.1	Thermo-bimetals . . . . .	458
10.6.2	Shaped Memory Alloys . . . . .	459
10.6.3	Thermal Expansion Elements . . . . .	462
10.6.4	Electrochemical Actuators . . . . .	463
10.6.5	Electro-rheological and Magneto-rheological Fluids . . . . .	463
10.6.6	Piezoelectric Actuators . . . . .	465
10.6.7	Electrostrictive and Magnetostrictive Actuators . . . . .	469
10.6.8	Micro-actuators . . . . .	470
10.7	Comparison of Application Areas . . . . .	471
10.8	Actuators as System Components . . . . .	474
10.8.1	Ports . . . . .	475
10.8.2	Integration of Actuator and Process . . . . .	475
10.8.3	Implemented Functionality . . . . .	475
10.9	Fault-tolerant Components . . . . .	476
10.9.1	Fault-tolerance for Components . . . . .	476
10.9.2	Fault-tolerance for Control Systems . . . . .	480
10.9.3	Fault Detection for Sensors, Actuators and Mechatronic Servo-systems . . . . .	480
10.9.4	Fault-tolerant Components for Mechatronic Systems . . . . .	481
10.9.5	Fault-tolerant Sensors . . . . .	481
10.9.6	Fault-tolerant Actuators . . . . .	484
10.10	Problems . . . . .	485
11	<b>Microcomputers</b> . . . . .	487
11.1	Microcomputer Structure . . . . .	489
11.2	Standard Processors . . . . .	490
11.2.1	Standard Processor Architecture . . . . .	492
11.2.2	Software for Standard Processors . . . . .	495
11.3	Memory . . . . .	497
11.4	Interfaces to the Process (Peripherals) . . . . .	501
11.4.1	Analog Inputs . . . . .	502
11.4.2	Digital and Binary Inputs . . . . .	504
11.4.3	Analog Outputs . . . . .	504
11.4.4	Digital and Binary Outputs . . . . .	505
11.5	Microcontrollers . . . . .	506

11.6	Signal Processors . . . . .	510
11.7	Application-specific Processors (ASICS) . . . . .	512
11.8	Field Bus Systems . . . . .	514
	11.8.1 Net Topologies . . . . .	515
	11.8.2 Basic Bus Functions . . . . .	517
	11.8.3 OSI (Open System Interconnection) Reference Model . . . . .	517
	11.8.4 Profibus . . . . .	519
	11.8.5 CAN Bus . . . . .	523
<b>12</b>	<b>Examples for the Design of Mechatronic Systems: Modeling, Control and Diagnosis . . . . .</b>	<b>527</b>
12.1	Electromagnetic Actuator: Non-linear Control and Fault Detection . . . . .	527
	12.1.1 Model-based Compensation of Non-linearities .	527
	12.1.2 Electromagnetic Actuator . . . . .	529
12.2	Electrical Throttle Valve for SI Engines: Modeling and Fault Diagnosis . . . . .	535
12.3	Semi-active Vehicle Suspensions . . . . .	538
	12.3.1 Passive Vehicle Suspensions . . . . .	538
	12.3.2 Semi-active Suspensions . . . . .	543
	12.3.3 Dynamic Models of a Quarter-car . . . . .	549
	12.3.4 Identification of a Quarter-car Model . . . . .	551
	12.3.5 Suspension Control . . . . .	554
	12.3.6 Simulations of a Semi-active Two-chamber Air Spring . . . . .	559
12.4	Electromechanical Disc Brake (EMB) . . . . .	560
	12.4.1 Introduction . . . . .	560
	12.4.2 Wheel Module . . . . .	562
	12.4.3 Brake Model . . . . .	564
	12.4.4 Simplified Brake Model . . . . .	567
	12.4.5 Simulation and Measurement . . . . .	568
12.5	Control Prototyping and Hardware-in-the-loop Simulation . . . . .	569
	12.5.1 Simulation Methods . . . . .	569
	12.5.2 Rapid Control Prototyping for Engine Control . . . . .	571
	12.5.3 Hardware-in-the-loop Simulation for Diesel Engines . . . . .	572
12.6	Industrial Robot . . . . .	577
	12.6.1 Modeling . . . . .	578

12.6.2 Control .....	583
12.6.3 System Structure .....	585
Outlook .....	587
References .....	589
Index .....	617

# List of Symbols

---

Only frequently used symbols and abbreviations are given.

## *Letter symbols*

- $a$  parameters of differential or difference equations
- $b$  parameters of differential or difference equations
- $c$  spring constant, constant, concentration, stiffness
- $d$  damping coefficient, diameter
- $e$  equation error, potential difference, control deviation  $e = r - y$ , number  $e = 2,71828\dots$
- $f$  frequency ( $f = 1/T_p$ ,  $T_p$  period), function  $f(\dots)$ , flow
- $g$  gravitational acceleration, function  $g(\dots)$ , impulse response
- $h$  height, compliance, specific enthalpy
- $i$  integer, gear ratio, index,  $\sqrt{-1}$  (imaginary unit)
- $j$  integer, index
- $k$  discrete number, discrete time  $k = t/T_0 = 0,1,2,\dots$  ( $T_0$ : sampling time)
- $l$  index, length
- $m$  mass, order number
- $n$  rotational speed, order number, disturbance signal
- $p$  pressure, index
- $q$  generalized coordinate, heat (relative)
- $r$  index, radius, reference variable
- $s$  thickness, Laplace variable  $s = \delta + i\omega$ , slip, specific entropy, circumference
- $t$  continuous time
- $u$  input signal change  $\Delta U$ , specific internal energy
- $v$  speed, specific volume
- $w$  reference value (exceptionally)
- $x$  space coordinate, state variable
- $y$  output signal change  $\Delta Y$ , space coordinate, control variable change  $\Delta Y$ , signal

- $z$  space coordinate, disturbance variable change  $\Delta Z$ ,  $z$  transform variable
- $A$  area
- $B$  magnetic flux density
- $C$  capacitance
- $D$  damping ratio, diameter
- $E$  module of elasticity, energy, potential
- $F$  filter transfer function, force
- $G$  weight, shear modulus, transfer function
- $H$  enthalpy, magnetic field strength, height
- $I$  electrical current, mechanical pulse, torsion, second moment of area
- $J$  moment of inertia
- $K$  constant, gain
- $L$  inductance, Lagrange function, mechanical work
- $N$  discrete number, windings number
- $P$  power
- $Q$  generalized force, heat
- $R$  electrical resistance, correlation function
- $S$  spectral density
- $T$  absolute temperature, torque, time constant
- $U$  input variable, manipulated variable (control input)
- $V$  volume, voltage
- $W$  mechanical work
- $X$  space coordinate
- $Y$  output variable, space coordinate, control variable
- $Z$  space coordinate, disturbance variable
- $\alpha$  coefficient, heat transfer coefficient, angle
- $\beta$  coefficient, angle
- $\gamma$  specific weight
- $\delta$  decay factor, impulse function
- $\epsilon$  modulus of elasticity (linear strain)
- $\zeta$  resistance coefficient (tube)
- $\eta$  efficiency
- $\vartheta$  temperature
- $\lambda$  thermal conductivity
- $\mu$  friction coefficient, permeability
- $\nu$  kinematic viscosity
- $\pi$  number  $\pi = 3.14159\dots$
- $\rho$  density
- $\sigma$  standard deviation, tensile stress
- $\tau$  time
- $\varphi$  angle
- $\omega$  angular frequency
- $\Delta$  change, deviation
- $\Theta$  magnetomotance, parameter
- $\Pi$  product

- $\Sigma$  sum
- $\Phi$  magnetic flux
- $\Psi$  magnetic flux linkage

*mathematical abbreviations*

- $\exp(x) = e^x$
- $E\{ \}$  expectation of a statistical variable
- dim dimension
- det determinant
- Re real part
- Im imaginary part
- $\dot{Q}$   $dQ(t)/dt$  (first derivative)

# 1

# Integrated Mechanical Electronic Systems

---

Integrated mechanical electronic systems emerge from a suitable combination of mechanics, electronics and control/information processing. Thereby, these fields influence each other mutually. First, a shift of functions from mechanics to electronics is observed and then the addition of extended and new functions. Finally, systems are being developed with certain intelligent or autonomous functions. For these integrated mechanical electronic systems, the term “mechatronics” has been used for several years.

In the following, first the development from mechanical to mechatronic systems is described and the systems concerned in mechanical engineering and in precision mechanics are considered. Several tasks arise and different forms of integration for mechanics and electronics can be distinguished. The integration may be performed, *e.g.*, by the components (hardware) or by the information-driven functions (software). Generally, a development to adaptive or intelligent overall systems shows up. The first chapter ends with a consideration of substantial design steps for mechatronic systems.

## 1.1 FROM MECHANICAL TO MECHATRONIC SYSTEMS

Mechanical systems generate certain motions or transfer forces or torques. For an oriented command of, *e.g.*, displacements, velocities or forces, feedforward and feedback control systems have been applied for many years. The control

systems operate either without auxiliary energy (*e.g.*, fly ball governor), or with electrical, hydraulic or pneumatic auxiliary energy, to manipulate the commanded variables directly or with a power amplifier. A realization with added fixed wired (analog) devices turns out to enable only relatively simple and limited control functions. If these analog devices are replaced with digital computers in the form of, *e.g.*, on-line coupled microcomputers, the information processing can be designed to be considerably more flexible and more comprehensive. Figure 1.1 summarizes this development, beginning with the purely mechanical systems of the nineteenth century to mechatronic systems in the 1980s. The first digitally controlled machines were, *e.g.*, machine tools, where already in around 1973 fixed wired sequential control devices based on transistors were being replaced by digital storage programmable control systems. This was paralleled by the introduction of digital control systems for, *e.g.*, electrical drives, industrial robots and steam turbines and for automotive parts. About 10 years later, the first mechanical systems with integrated sensors, actuators and microcontrollers appeared, *e.g.*, as anti-lock braking systems (ABS) for vehicles or magnetic bearings and in the form of precision electro-mechanical devices as cameras, video recorders, printers and disk storage, thus forming the first mechatronic systems.

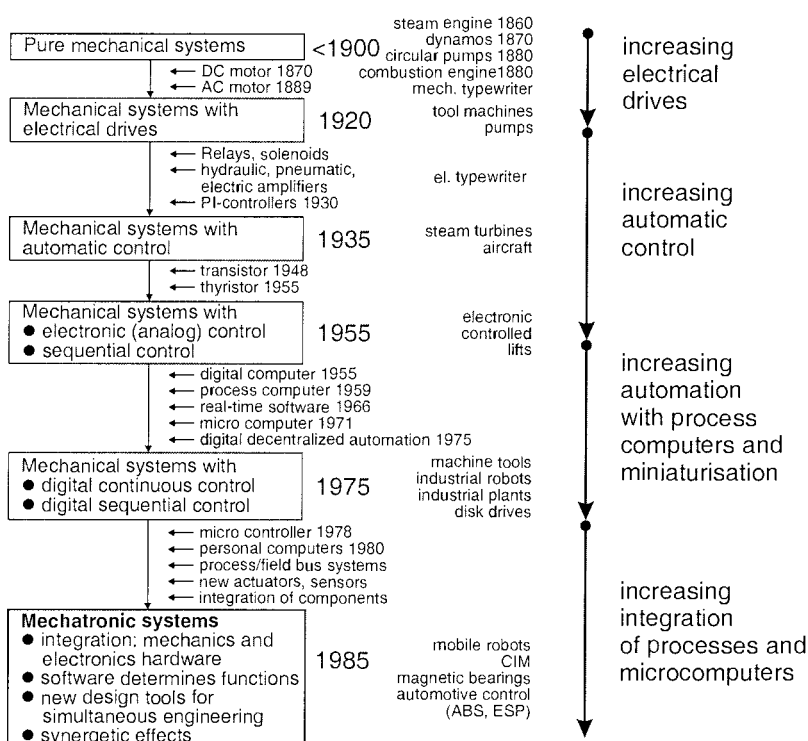


**Figure 1.1.** Historical development of mechanical, electronic and mechatronic systems

Figure 1.2 shows the example of a machine set, consisting of a power-generating machine (DC motor) and a power-consuming machine (circulation pump): (a) a scheme of the components, (b) the resulting signal flow diagram in two-port representation, and (c) the open-loop process with one or several manipulated variables as input variables and several measured variables as output variables.

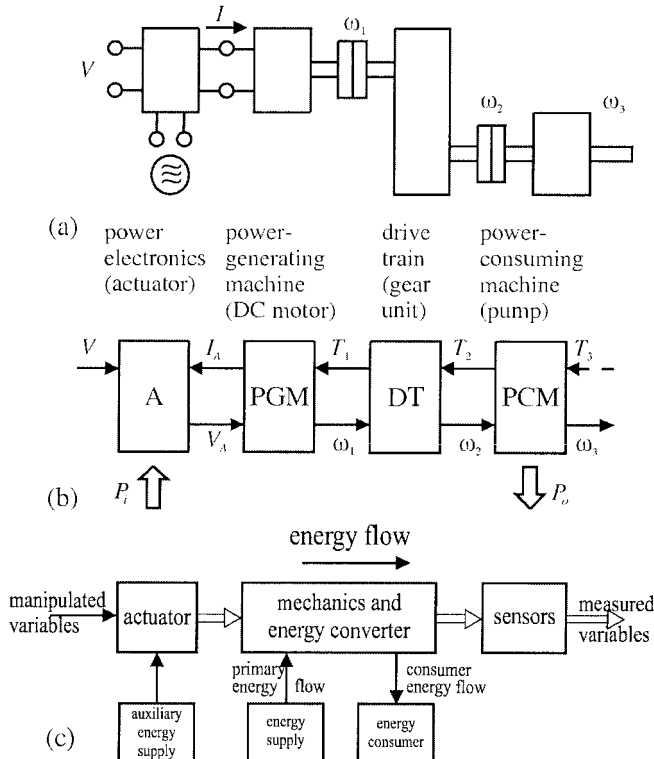


**Figure 1.2.** Schematic representation of a machine set: (a) scheme of the components; (b) signal flow diagram (two-port representation); (c) open-loop process

$V$  voltage;  $V_A$  armature voltage;  $I_A$  armature current;  $T$  torque;  $\omega$  angular frequency;  $P_i$  drive power;  $P_o$  consumer power

This process is characterized by different controllable energy flows (electrical, mechanical, hydraulic). The first and last flow can be manipulated by a manipulated variable of low power (auxiliary power), e.g., through a power electronics device and a flow valve actuator. Several sensors yield measurable variables. For a mechanical-electronic system, a digital electronic system is added to the process. This electronic system acts on the process based on the measurements or external command variables in a feedforward or feedback manner, Figure 1.3. If then the electronic and the mechanical system are merged to an autonomous overall system, an integrated mechanical-electronic system results. The electronics processes

information, and such a system is characterized at least by a mechanical energy flow and an information flow.

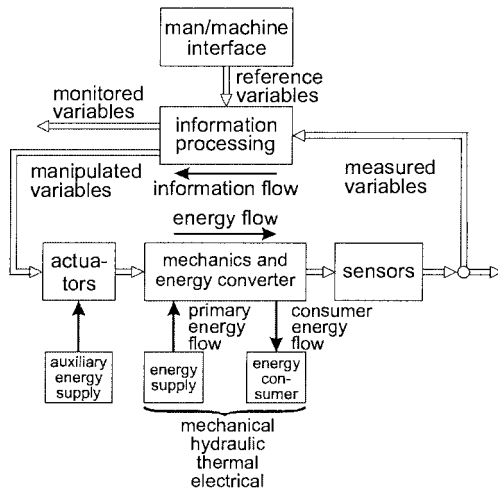


**Figure 1.3.** Mechanical process and information processing develop towards a mechatronic system

These integrated mechanical-electronic systems are increasingly called mechatronic systems.

Thus, MECHANICS and ElecTRONICS are conjoined. The word “mechatronics” was probably first created by a Japanese engineer in 1969, Kyura, Oho (1996). Several definitions can be found in the literature. The journal *Mechatronics* (1991) uses the following scope: “Mechatronics in its fundamental form can be regarded as the fusion of mechanical and electrical disciplines in modern engineering processes. It is a relatively new concept to the design of systems, devices and products aimed at achieving an optimal balance between basic mechanical structures and its overall control.” In the *IEEE/ASME Transactions on Mechatronics* (1996), a preliminary definition is given: “Mechatronics is the synergistic integration of mechanical engineering with electronics and intelligent computer control in the design and manufacturing of industrial products and processes.” (Harashima, Tomizuka (1996)).

The IFAC Technical Committee on Mechatronic Systems, founded in 2000, IFAC-TC 4.2, uses the following description: “Many technical processes and products in the area of mechanical and electrical engineering show an increasing integration of mechanics with electronics and information processing. This integration is between the components (hardware) and the information-driven function (software), resulting in integrated systems called mechatronic systems. Their development involves finding an optimal balance between the basic mechanical structure, sensor and actuator implementation,

automatic digital information processing and overall control, and this synergy results in innovative solutions.”

All definitions agree that mechatronics is an interdisciplinary field, in which the following disciplines act together, Figure 1.4:

1. *mechanical systems* (mechanical elements, machines, precision mechanics);
2. *electronic systems* (microelectronics, power electronics, sensor and actuator technology);
3. *information technology* (systems theory, control and automation, software engineering, artificial intelligence).

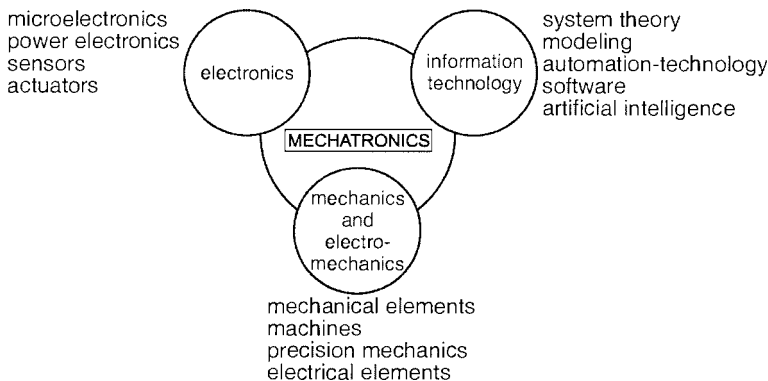


**Figure 1.4.** Mechatronics: synergetic integration of different disciplines

The solution of tasks for designing mechatronic systems is performed as well on the mechanical as on the digital-electronic side. Herewith, interrelations during the design play an important role; because the mechanical system influences the electronic system and *vice versa*, the electronic system has influence on the design of the mechanical system, Figure 1.5. This means that simultaneous engineering has to take place, with the goal of designing an overall integrated system (“organic system”) and also creating synergetic effects.

A further feature of mechatronic systems is the integrated digital information processing. Except for basic control functions, more sophisticated control functions may be realized, *e.g.*, the calculation of non-measurable variables, the adaptation of controller parameters, the detection and diagnosis of faults and, in the case of failures, a reconfiguration to redundant components. Hence, mechatronic systems are developing with adaptive or even learning behavior which can also be called *intelligent mechatronic systems*, see also Section 1.5.

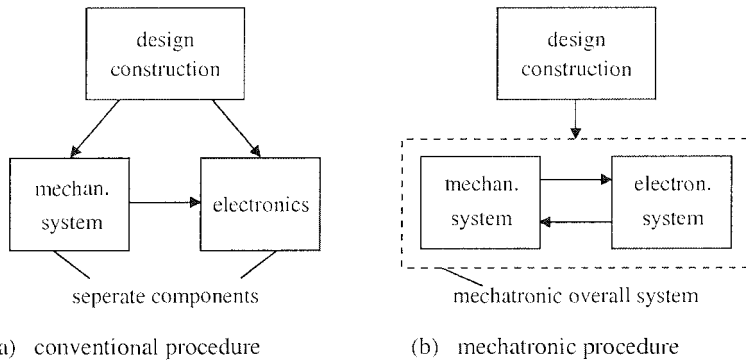


**Figure 1.5.** Interrelations during the design and construction of mechatronic systems

Descriptions of developments up until now can be seen in Schweitzer (1992), Gausemeiser *et al.* (1995), Harashima, Tomizuka (1996), Isermann (1996), Tomizuka (2000), VDI 2006 (2003). An insight into general aspects are given editorially in the journals *Mechatronics* (1991), *Mechatronics System Engineering* (1993), *IEEE/ASME Transactions on Mechatronics* (1996), the conference proceedings of, *e.g.*, UK Mechatronics Forum (1990, 1992, 1994, 1996, 1998, 2000, 2002), IMES (1993), DUIS (1993), ICRAM (1995), AIM (1999, 2001, 2003), IFAC (2000, 2002, 2004), the journal articles by Hiller (1995), Lückel (1995), and the books of Kitaura (1987), Bradley *et al.* (1991), McConaill *et al.* (1991), Heimann *et al.* (1998), Isermann (1999), Bishop (2002).

## 1.2 MECHANICAL SYSTEMS

Mechanical systems can be dedicated to a large area of mechanical engineering. According to their construction, they can be subdivided into mechanical components, machines, vehicles, precision mechanical devices and micro-mechanical components, Figure 1.6. Another classification follows the discipline of *kinematics* according to the theory of engineering mechanics. One distinguishes between free (non-constrained) systems, where the elements can move without any constraints, and constrained systems, where elements have rigid joints. The joined systems can have holonomic constraints which restrict their position, or non-holonomic constraints, which restrict their position and velocity. Most mechanical systems in the frame of mechatronic systems belong to constrained systems.

In the following, examples of such systems are considered, for which an integration with electronics already took place or is to be expected. This is followed by a discussion of which systems may be considered to be mechatronic systems.

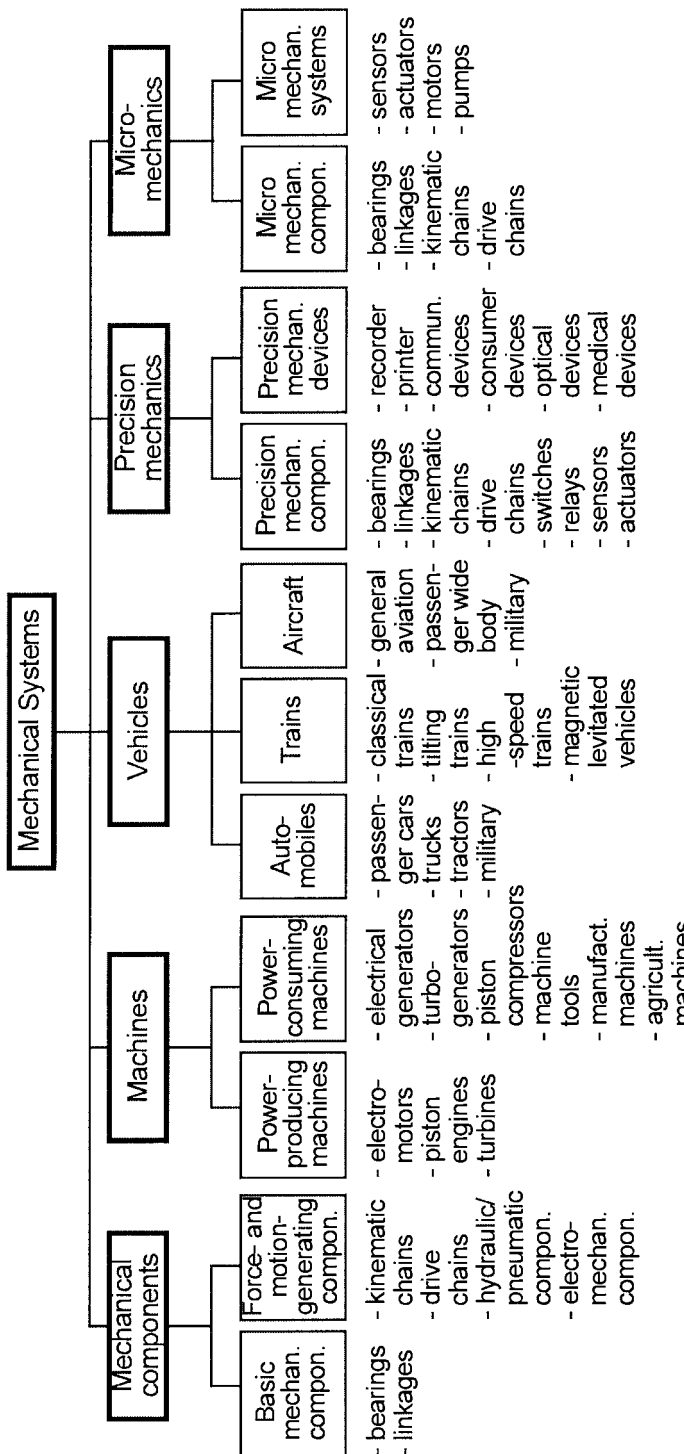


Figure 1.6. Mechanical systems and their classification, with examples

### 1.2.1 Mechanical Systems in Mechanical Engineering

The design of mechanical products is influenced by the interplay of energy, matter and information. With regard to the basic problem and its solution, frequently either the energy, matter or information flow is dominating. Therefore, one *main flow* and at least one *side flow* can be distinguished, Pahl, Beitz (2001).

The classification of machine elements as components in the engineering of machines, apparatus and devices was proposed by, e.g., Beitz (1989), Roth (1982). The classification of machines according to systematic categories as, e.g., economical branches, functions, operating principles, is given by Hupka (1973), see also Beitz, Küttner (1994). However, because of the manifold of possible classifications and the traditionally well-accepted terms, it is obviously not possible to classify all mechanical systems with a unique scheme, see also Green (1992), Smith (1994), Kreith (1998), Kutz (1998).

#### a) Machine elements

Machine elements are usually purely mechanical. Figure 1.6 shows some examples. Properties that can be improved by electronics are, for example, self-adaptive stiffness and damping, self-adaptive free motion or pretension, automatic operating functions like coupling or gear shifting, and supervisory functions. Some examples of mechatronic approaches are hydrobearings for combustion engines with electronic control of damping, magnetic bearings with position control, automatic electronic-hydraulic gears, and adaptive shock absorbers for wheel suspensions.

#### b) Machines

Machines show a particularly rich variability. Power-generating machines are characterized by the conversion of hydraulic, thermodynamic or electrical energy into mechanical energy and delivery of power. Power-consuming machines convert mechanical energy into another form, thereby absorbing energy. For example, vehicles convert mechanical energy into motion and absorb energy. Examples of mechatronic solutions for machines are: Diesel engines with common-rail injection system and electronically controlled variable geometry turbocharger, spark-ignition engines with multidimensional look-up tables, knock control, exhaust oxygen control and misfire detection, spark ignition engines with combustion pressure feedback control and ignition timing, electromagnetic actuated camshafts, turbojet engines with a multitude of control and supervisory functions, hydraulic piston motors and pumps with integrated control box, machine tools with integrated adaptive cutting force control and fault detection, and industrial robots with sensor-based grippers or tools in lightweight construction or command by sensor gloves. Several mechatronic components have been introduced for automobiles (passenger cars and trucks), like anti-lock braking control (ABS) with first realization in

1967 and in series production since 1978, anti-slip control (ASR) 1983, electronic acceleration pedal with electrical throttle in 1979, active chassis control, electronic stability control (ESP) in 1995, feedback-controlled suspensions with adjustable shock absorbers and pneumatic springs, see, *e.g.*, van Zanten (2000), electro-hydraulic brake in 2001 and active front steering in 2003. Mechatronic developments for railway systems are active suspensions, tilting trains and actively steered wheelsets, Goodall, Kortüm (2000).

### 1.2.2 Mechanical Systems in Precision Mechanic Devices

Precision mechanic devices are characterized by the co-operation of, *e.g.*, precision mechanics, electromechanics, electronics and optics. Here of major interest are devices that are more dedicated to information processing than to energy transfer, Davidson (1968), Koller (1985), Walsh (1999). Figure 1.6 lists some examples. Also, actuators of automation technology belong to this class. Examples of mechatronic precision mechanic systems are brushless, electronically commutated DC motors, electromagnets (solenoids) with non-linear adaptive position control and fault detection, pneumatic cylinders with non-linear adaptive friction compensation, disk drives with precision position control and electronic controlled printers, automatic cameras, camcorders and video projectors. The integration of precision mechanics and microelectronics offers many possibilities for the basic design with integrating, mechatronic solutions. Except for the addition of sensors, actuators and decentralized drives, the digital sequence and feedback control has a considerable influence on the design of the devices. Also, the manual operation with keys and displays has a large impact on the design of the human-machine interface.

### 1.2.3 Micromechanics

Based on the continuous efforts of miniaturization, the field of microsystem technology could develop, consisting of, *e.g.*, microelectronic, microelectromechanical (MEMS) and micromechanic systems. The miniaturization began with microelectronics. Here, the first transistor in 1947, the first integrated circuit in 1958 and the first microprocessor in 1971 were important milestones. Steps in the direction of microelectromechanical systems were magnetic hard disk drives in around 1970, followed by, *e.g.*, sensors like accelerometers.

Microsystem technology is characterized by its production methods, including bulk micromachining, surface micromachining, fine-molding technologies and precision machining, Sato (2000). Bulk micromachining generates three-dimensional microstructures by etching materials, surface micromachining by layering thin films over the surface of a silicon substrate, fine-molding by a lithographic method for non-silicon structures like metals or polymers and precision machining by conventional cutting tools for metals,

specially tailored for small dimensions in the 10 µm area.

Microsystem technology also includes microoptics, microfluidics, microheat-exchangers and microreactors. Based on microsystem components, like microactuators, microprocessors and microsensors, *micromechatronic systems* can be built up, including, for example, electrical micromotors, microgears and micropumps. Ehrfeld *et al.* (2000). This is an area where development is just at the beginning. First products, like yaw-rate and flow sensors, microelectronic gyros, ink-jet printer heads, piezoceramic actuators, micromotors with 2 mm diameter, planetary gears with 55 µm diameter, microscanners, micromirrors and micropumps, show the potential, Janocha (2000). Further literature for this fast-progressing field includes Gad-el-Hak (2000), Madon (2001), Lyshevski (2001).

### **1.2.4 Mechanical Systems in Apparatus (Process Engineering)**

Apparatus can be described as technical systems with a primary goal of processing materials and/or enabling material or heat flow, Koller (1985). Examples are mechanical apparatus like pipelines, valves, grinding machines, pneumatic sifters and filters, thermal apparatus like heat-exchangers, boilers and components for heating, ventilation and air conditioning, and burners, chemical reactors and stirring vessels. For these apparatus, an increasing integration with electronic control can also be observed. One example of simultaneous engineering is a design for fast-changing energy and material flows to follow fast load demands, thus saving large storage and investment costs (*e.g.*, for steam boilers, heating boilers, water supply systems). Digital adaptive control can compensate the partially very non-linear behavior, enabling a wide-range operation with high product performance. Also, the precisely adapted automation in the higher levels allows much progress, *e.g.*, in the frame of supervision, optimization and at the human–machine interface. Hence, several integrating design approaches and properties of mechatronic systems for machine elements and machines hold also for some apparatus. However, these partially mechanical systems are usually not considered as part of mechatronic systems.

### **1.2.5 Confinement of Mechatronic Systems**

The previous discussion shows that the integration of electronics and information processing in the sense of mechatronic systems comprises many technical areas. Besides the mechanical process part, in many cases an electrical, thermal, thermodynamical, chemical or information-transferring part exists. One reason is that machines, devices and apparatus are often energy converters that contain energy forms other than just mechanical energy. Then, the non-mechanical process parts cannot be separated from the

mechanical part with regard to the functions and the signal flow. Therefore, mechatronic systems can also include electrical, thermal, thermodynamical, chemical and information-carrying process parts. This leads now to an *extended definition* used in this book.

### **Definition of mechatronic systems:**

*“Mechatronic systems result from the simultaneous design and integration of following disciplines:*

- mechanical and coupled systems;
- electronic systems;
- control and information technology.

*The integration is between the components (hardware) and the information-driven functions (software), oriented towards finding an optimal balance between the basic mechanical structure, sensor and actuator implementation, automatic digital information processing and overall control. In addition, synergetic effects are created, resulting in enhanced functionality and innovative solutions.”*

This definition leans on IFAC-TC (2000). The field of mechatronics therefore can be seen to comprise, except for the purely mechanical machine elements, modern machines and precision mechanical devices, and also a small part of apparatus, like transporting systems, mills, oil and gas burners. However, the border between mechatronic systems and other with electronics integrated systems, for which until now no special term exists, is not crisp, but gradual.

## **1.3 FUNCTIONS OF MECHATRONIC SYSTEMS**

Mechatronic systems enable, after the integration of the components, many improved and also new functions. This will be discussed by using examples.

### **1.3.1 Design**

The basic *mechanical construction* first has to satisfy the task of transferring the mechanical energy flow (force, torque) to generate motions or special movements, *etc.* Known traditional methods are applied, like material selection, calculation of strengths, manufacturing, production costs, *etc.* By attaching sensors, actuators and mechanical controllers, in earlier times, simple control functions were realized, *e.g.*, the flyball governor. Then gradually pneumatic, hydraulic and electrical *analog controllers* were used. After the advent of *digital control systems*, especially with microprocessors

in around 1975, the information processing part could be designed to be much more sophisticated. These digitally controlled systems had been first added to the basic mechanical construction and their limitations were given by the properties of the sensors, actuators and electronics, *i.e.*, they were frequently not satisfying reliability and lifetime requirements under the rough environmental conditions (temperature, vibrations, contamination) and had a relatively large space requirement, cable connections and low computational speed. However, many of the initial drawbacks have been removed during time, and since about 1980 the *electronic hardware* is much more *miniaturized, robust* and *powerful* and connected by field bus systems. Hence, the emphasis on the electronic side could be increased and the mechanical construction could be designed as a mechanical-electronic system from the very beginning. The aim was to result in more autonomy, for example, by decentralized control, field bus connections, plug-and-play approaches, distributed energy supply, *etc*, such that self-contained units emerge.

### 1.3.2 Distribution of Mechanical and Electronic Functions

Mechatronic systems permit many improved and new functions. This will be discussed by considering some examples.

In the design of mechatronic systems, the *interplay for the realization of functions* in the mechanical and electronic part is crucial. Compared to pure mechanical realizations, the use of amplifiers and actuators with electrical auxiliary energy has already led to considerable simplifications, as can be seen from watches, electronic typewriters and cameras. A further considerable simplification in the mechanics resulted from introducing microcomputers in connection with decentralized electrical drives, *e.g.*, for electronic typewriters, sewing machines, multi-axis handling systems and automatic gears.

The design of *lightweight constructions* leads to elastic systems that are weakly damped through the material itself. An *electronic damping* through position, speed or vibration sensors and electronic feedback can be realized with the additional advantage of an adjustable damping through the algorithms. Examples are elastic drivetrains of vehicles with damping algorithms in the engine electronics, elastic robots, hydraulic systems, far-reaching cranes and space constructions (*e.g.*, with flywheels).

The addition of closed-loop control, *e.g.*, for position, speed or force, does not only result in a precise tracking of reference variables, but also an approximate *linear overall behavior*, though the mechanical systems show non-linear behavior. By omitting the constraint of linearization on the mechanical side, the effort for construction and manufacturing may be reduced. Examples are simple mechanical pneumatic and electromechanical actuators and flow valves with electronic control.

With the aid of freely programmable reference variable generation, the adaptation of non-linear mechanical systems to the *operator* can be improved.

This is already used for the driving pedal characteristics within the engine electronics for automobiles, telemanipulation of vehicles and aircraft and in the development of hydraulic actuated excavators and electric power steering.

However, with increasing number of sensors, actuators, switches and control units, the cables and electrical connections also increase such that *reliability, cost, weight* and the required *space* are major concerns. Therefore, the development of suitable bus systems, plug systems and fault-tolerant and reconfigurable electronic systems are challenges for the design.

### 1.3.3 Operating Properties

By applying *active feedback control*, the precision of, *e.g.*, a position is reached by comparison of a programmed reference variable with measured control variable and not only through the high mechanical precision of a passively feedforward-controlled mechanical element. Therefore, the mechanical precision in design and manufacturing may be reduced somewhat and more simple constructions for bearings or slideways can be used. An important aspect is hereby the compensation of a larger and time-variant friction by *adaptive friction compensation*, Isermann *et al.* (1992). Then also a larger friction on the cost of backlash may be intended (*e.g.*, gears with pretension), because it is usually easier to compensate for friction than for backlash. *Model-based* and *adaptive control* further allow an operation in more operating points (wide-range operation), compared to fixed control with unsatisfactory performance (danger of instability or sluggish behavior). A combination of robust and adaptive control allows a wide-range operation to become possible, *e.g.*, for flow-, force-, speed-control and for processes involving engines, vehicles and aircraft. A better control performance allows the reference variables to be moved closer to constraints with improved efficiencies and yields (*e.g.*, higher temperatures, pressures for combustion engines and turbines, compressors at stalling limits, higher tensions and higher speed for paper machines and steel mills).

### 1.3.4 New Functions

Mechatronic systems also allow functions that could not be performed without digital electronics. Firstly, *non-measurable quantities* can be calculated on the basis of measured signals and influenced by feedforward or feedback control. Examples are time-dependent variables like the slip for tires, internal tensions, temperatures, the slip angle and ground speed for steering control of vehicles or parameters like damping and stiffness coefficients and resistances. The automatic adaptation of parameters, like damping and stiffness for oscillating systems based on measurements of displacements or accelerations, is another example. Integrated *supervision* and *fault diagnosis* becomes more and more important with increasing automatic functions, increasing complexity and

higher demands on reliability and safety. Then, *fault-tolerance* by triggering of redundant components and system reconfiguration, maintenance on request and any kind of *teleservice* makes the system more “intelligent”.

### 1.3.5 Other Developments

Mechatronic systems frequently allow a *flexible adaptation* to boundary conditions. A part of the functions and also precision becomes programmable and fast changeable. Advance simulations enable the reduction of experimental investigations with many parameter variations. Also, a faster time-to-market is possible if the basic elements are developed in parallel and the functional integration results from the software.

A far-reaching *integration of the process and the electronics* is much easier if the customer obtains the functioning system from one manufacturer. Usually, this is the manufacturer of the machine, the device or the apparatus. Although this manufacturer has to cope intensively with the electronics and the information processing, they get the chance to add to the value of the product. For small devices and machines with large production numbers, this is obvious. In the case of larger machines and apparatus, the process and its automation frequently comes from different manufacturers. Then, special effort is needed to result in integrated solutions.

Table 1.1 summarizes some properties of mechatronic systems compared to conventional electromechanical systems and Table 1.2 shows practical examples for the corresponding rows of Table 1.1.

## 1.4 INTEGRATION FORMS OF PROCESSES AND ELECTRONICS

Figure 1.7a shows a general scheme of a *classical mechanical-electronic system*. Such systems resulted from adding available sensors and actuators and analog or digital controllers to the mechanical components. The limits of this approach were the lack of suitable sensors and actuators, the unsatisfactory lifetime under the rough operating conditions (acceleration, temperature, contamination), the large space requirements, the required cables and relatively slow data processing. With increasing improvements of the miniaturization, robustness and computing power of microelectronic components, one can now try to put more weight on the electronic side and to design the mechanical part from the beginning with a view to a *mechatronic overall system*. Then, more autonomous systems can be envisaged, *e.g.*, in the form of capsules units with touchless signal transfer or bus connections and robust microelectronics.

**Table 1.1.** Properties of conventional and mechatronic designed systems

conventional design	mechatronic design
added components	integration of components (hardware)
simple control	integration by information processing (software)
1 bulky 2 complex 3 cable problems 4 connected components	compact simple mechanisms bus or wireless communication autonomous units
5 stiff construction  6 feedforward control, linear (analog) control  7 precision through narrow tolerances  8 non-measurable quantities change arbitrarily  9 simple monitoring 10 fixed abilities	elastic construction with damping by electronic feedback programmable feedback (non-linear) digital control precision through measurement and feedback control control of non-measurable estimated quantities supervision with fault diagnosis adaptive and learning abilities

**Table 1.2.** Realization examples for the properties given in Table 1.1

conventional design	mechatronic design
added components	integration of components (hardware)
simple control	integration by information processing (software)
1 electromechanical typewriter 2 mechanically controlled injection pump with rotating piston 3 many wiring 4 belt-driven auxiliaries	electronic printer high pressure pump and magnetic injection valves (common rail) bus cable decentralized driven auxiliaries
5 stiff drivetrain  6 mechanical gas pedal 7 feedforward-controlled actuator  8 manual steering of cars during spinning  9 monitoring of exhaust gases through maintenance or inspection 10 rail vehicles	elastic drivetrain with algorithmic damping through engine control electronic non-linear throttle control feedback-controlled actuator with friction compensation feedback control of slip angle by state observer and individual wheel braking on-board misfire detection by speed measurement of engine crankshaft mobile vehicle with automatic navigation

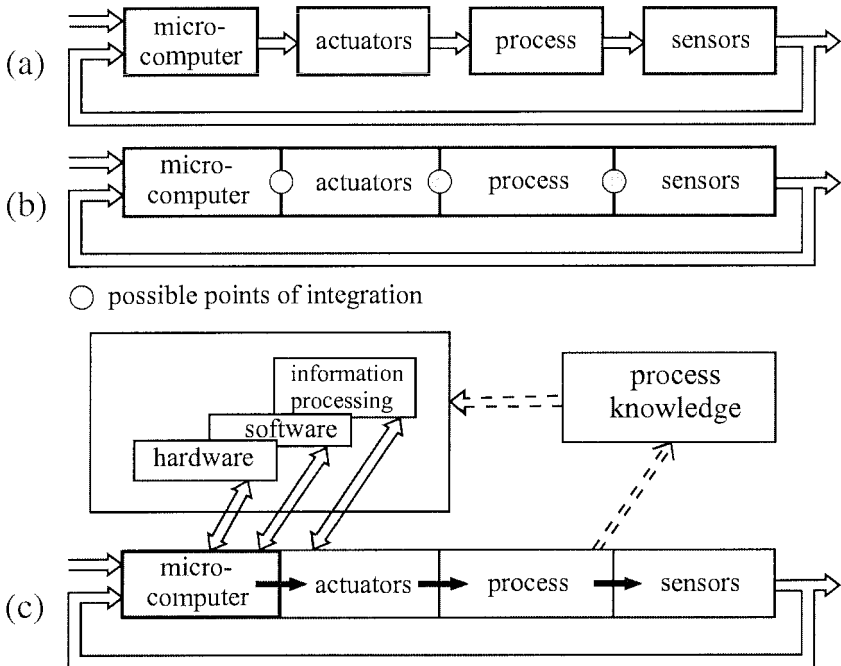


**Figure 1.7.** Integration of mechatronic systems: (a) general scheme of a (classical) mechanical-electronic system; (b) integration through components (hardware integration); (c) integration through functions (software integration)

The integration within a mechatronic system can be performed mainly in two ways, through the integration of components and through integration by information processing.

The *integration of components (hardware integration)* results from designing the mechatronic system as an overall system and embedding the sensors, actuators and microcomputers into the mechanical process, see Figure 1.7b. This spatial integration may be limited to the process and sensor or the process and actuator. The microcomputers can be integrated with the actuator, the process or sensor, or be arranged at several places.

Integrated sensors and microcomputers lead to *smart sensors* and integrated actuators and microcomputers develop into *smart actuators*. For larger systems, bus connections will replace the many cables. Hence, there are several possibilities for building an integrated overall system by proper integration of the hardware.

*Integration by information processing (software integration)* is mostly based on advanced control functions. Besides a basic feedforward and feedback control, an additional influence may take place through the process knowledge and corresponding on-line information processing, see Figure 1.7c. This means a processing of available signals in higher levels, as to be discussed in the next section. This includes the solution of tasks like supervision

with fault diagnosis, optimization and general process management. The respective problem solutions result in an *on-line information processing*, especially by real-time algorithms, which must be adapted to the mechanical process properties, *e.g.*, expressed by mathematical models in the form of static characteristics, differential equations, *etc*, see Figure 1.8. Therefore, a *knowledge base* is required, comprising methods for design and information gain, process models and performance criteria. In this way, the mechanical parts are governed in various ways through higher level information processing with intelligent properties, possibly including learning, thus forming an integration by process adapted software.

Both types of integration are summarized in Figure 1.8. In the following, mainly the integration through information processing will be considered further.

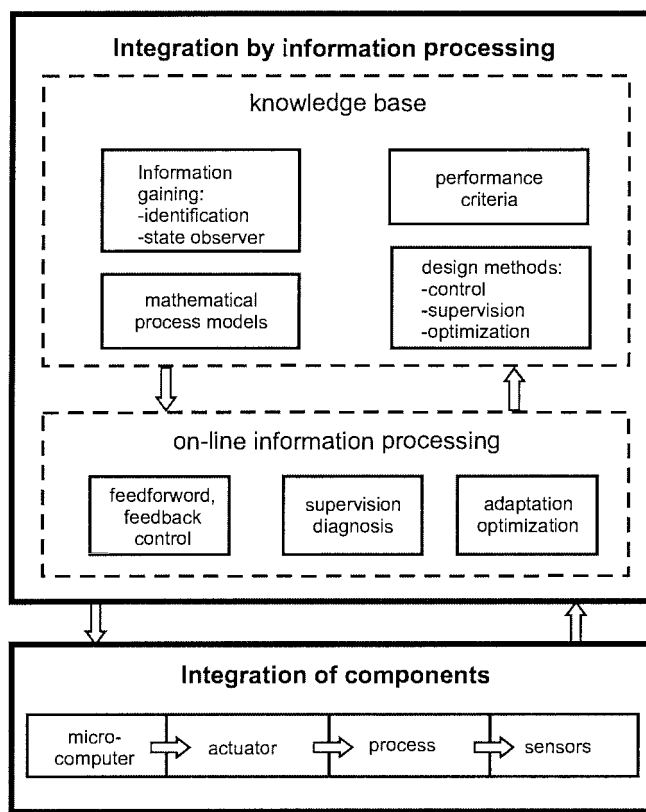


**Figure 1.8.** Integration of mechatronic systems: integration of components (hardware integration); integration by information processing (software integration)

## 1.5 WAYS OF INFORMATION PROCESSING

The governing of mechanical systems is usually performed through actuators for changing of positions, speeds, flows, forces or torques, and voltages. The directly measurable output quantities are frequently positions, speeds, accelerations or forces and currents. The different ways of information processing methods can be subdivided into multi-level process automation, special signal processing, model-based and adaptive control and intelligent systems.

### 1.5.1 Multi-level Control Systems

The information processing of direct measurable input and output signals can be organized in several levels, compare Figure 1.9:

- level 1a: low-level control (feedforward, feedback for damping, stabilization, linearization);
- level 1b: high-level control (advanced feedback control strategies);
- level 2: supervision including fault diagnosis;
- level 3: optimization, coordination (of processes);
- level 4: general process management.

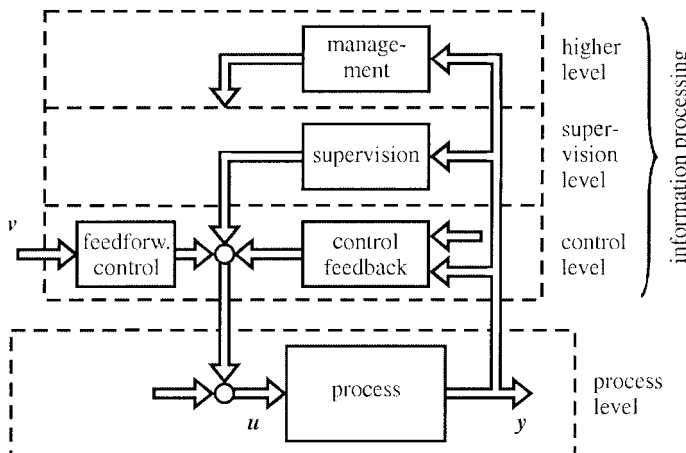


**Figure 1.9.** Different levels of information processing for process automation  
 $u$ : manipulated variables;  $y$ : measured variables;  $v$ : input variables;  $r$ : reference variables

Generally, it can be observed:

- lower levels: react fast, act locally,
- higher levels: react slowly, act globally.

Recent approaches for mechatronic systems mostly use signal processing in the lower levels, *e.g.*, damping or control of motions or simple supervision. Digital information processing, however, allows the solutions of many more tasks, such as adaptive control, learning control, supervision with fault diagnosis, decisions for maintenance or even fault-tolerance actions, economic optimization and coordination. The tasks of the higher levels are sometimes summarized as “process management”.

### 1.5.2 Special Signal Preprocessing

The methods described above are partially also applicable to non-measurable quantities that are reconstructed by using mathematical process models. In this way, it is possible to control, *e.g.*, damping ratios, material and heat stress and slip or to supervise quantities like resistances, capacitances, temperatures within components, or parameters of wear and contamination. This signal processing may require special filters to determine amplitudes or frequencies of vibrations, to determine derived or integrated quantities, or state variable observers, compare Figure 1.10.

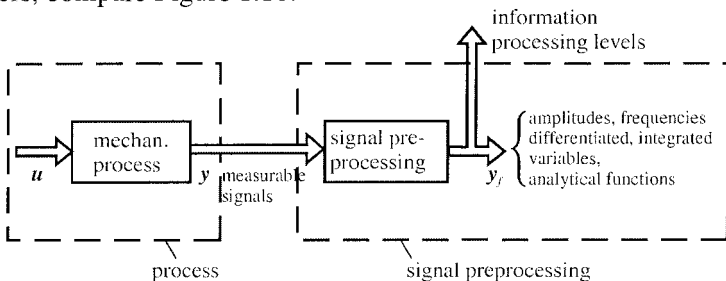


**Figure 1.10.** Special signal processing to obtain non-measurable quantities (signal pre-processing)

### 1.5.3 Information Gaining

A precondition for precisely adapted algorithms for feedforward and feedback control, for damping by electronic feedback, for fault detection, *etc.*, is the knowledge of mathematical process models for static and dynamic behavior. In the case of mechanical processes, the model structure and some model parameters can frequently be obtained through theoretical modeling. Based on this model structure in the form of linear and non-linear differential equations, the measured input and output variables can be brought into their causal relationships and information on the internal process behavior can be obtained.

#### *Parameter estimation*

The output error  $e(t)$  between the measured output signal  $y(t)$  and the output

signal  $y_M(t)$  of a virtual parallel model (or the equation error) is formed, Figure 1.11a. The parameters  $\Theta$  of the model are then estimated by searching for the minimum of the sum of the squared errors (method of least squares). Well-proven algorithms and software modules in non-recursive or recursive form exist, also for continuous time, discrete time and slowly time-variant parameters and some non-linear models, see Chapter 7.

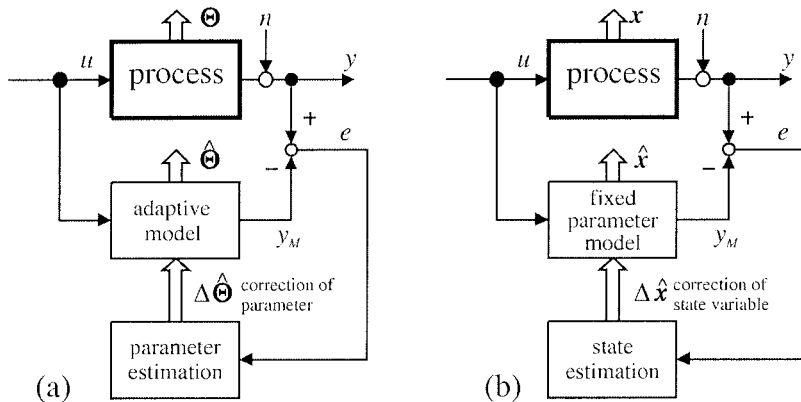


**Figure 1.11.** Model-based methods to obtain information of dynamical processes  
output error:  $e(t) = y(t) - y_M(t)$

(a) parameter estimation

$\Theta$  : real process parameters

$\hat{\Theta}$  : estimated process parameters

(b) state estimation

$x$  : real process state variables

$\hat{x}$  : estimated process state variables

### State estimation

If the parameters  $\Theta$  or  $\mathbf{A}, \mathbf{b}, \mathbf{c}$  of a state variable model are known, the output error  $e(t)$  can be fed back and the time-variant state variables  $\mathbf{x}(t)$  can be corrected by  $\Delta\mathbf{x}(t)$ , Figure 1.11b. With a design for deterministic signals, a state observer is obtained and for stochastic signals a state estimation (Kalman filter) results. Then, non-measurable, internal process variables can be estimated, Föllinger (1992), Ogata (1997), Franklin *et al.* (1998), Dorf, Bishop (2000), see Chapter 7.

The results of the parameter estimation can, for example, be used for adaptive control or damping or for model-based fault detection. State variable estimates are the basis for state feedback to control and stabilize systems with difficult behavior, or for the control of non-measurable variables and fault detection with state observers.

#### 1.5.4 Model-based Methods of Control

The information processing is, at least in the lower levels, performed by simple algorithms or software modules under real-time conditions. These algorithms contain free adjustable parameters, which have to be adapted to the

static and dynamic behavior of the process. In contrast to manual tuning by trial and error, the use of mathematical models allows precise and fast automatic adaptation.

The mathematical models can be obtained by identification and parameter estimation, which use the measured and sampled input and output signals. These methods are not restricted to linear models, but also allow the identification of several classes of non-linear systems. If the parameter estimation methods are combined with appropriate control algorithm design methods, adaptive control systems result, which can be used for precise controller tuning permanently or only for commissioning, Åström, Wittenmark (1994), Isermann *et al.* (1992), Figure 1.12.

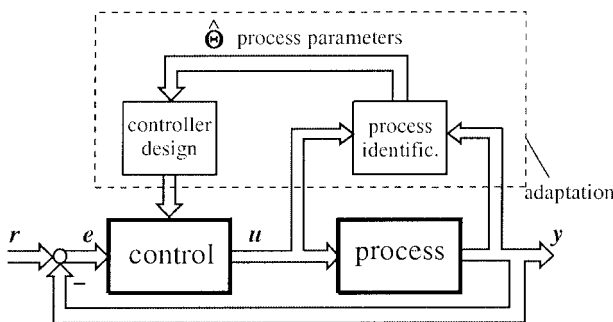


**Figure 1.12.** Adaptive control through permanent process identification and controller design

### 1.5.5 Supervision and Fault Diagnosis

With the increasing number of automatic functions (autonomy) including electronic components, sensors and actuators, increasing complexity and increasing demands on reliability and safety, integrated supervision with fault diagnosis becomes more and more important. This is, therefore, a significant natural feature of an intelligent mechatronic system. Figure 1.13 shows a process influenced by faults. These faults indicate unpermitted deviations from normal states and can be generated either externally or internally. External faults are, *e.g.*, caused by the power supply, contamination or collision, internal faults by wear, missing lubrication, actuator or sensor faults. The classical method for fault detection is the limit value checking or plausibility checks of a few measurable variables. However, incipient and intermittent faults cannot usually be detected and an in-depth fault diagnosis is not possible with this simple approach. Therefore, model-based fault detection and diagnosis methods have been developed in recent years, allowing early detection of small faults with normally measured signals, also in closed loops, Isermann (1997, 2005), Gertler (1999), Chen, Patton (1999). Based on measured input signals  $U(t)$ , output signals  $Y(t)$  and process models,

features are generated by, *e.g.*, parameter estimation, state and output observers and parity equations, Figure 1.13.

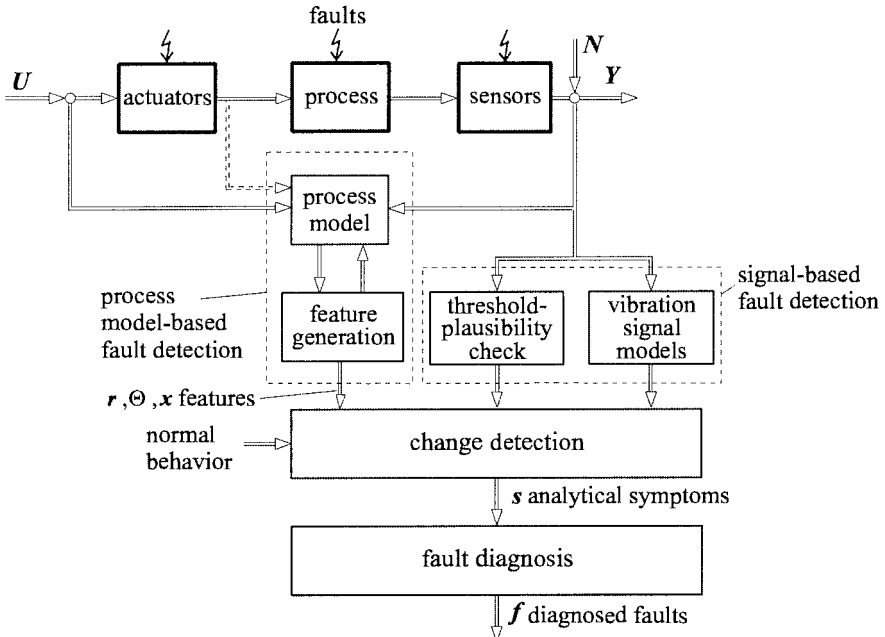


Figure 1.13. Scheme for a model-based fault detection

These features are then compared with the features for normal behavior, and with change detection methods, analytical symptoms are obtained. Then, a fault diagnosis is performed via methods of classification or reasoning.

A considerable advantage is that the same process model can be used for both the (adaptive) controller design and the fault detection. In general, continuous time models are preferred if fault detection is based on parameter estimation or parity equations. For fault detection with parameter estimation, state estimation and also parity equations discrete time models can also be used.

Advanced supervision and fault diagnosis is a basis for improving reliability and safety, state-dependent maintenance, triggering of redundancies and reconfiguration for fault-tolerant systems, Isermann (2000).

### 1.5.6 Intelligent Systems

The information processing within mechatronic systems may range between simple control functions and “intelligent” control. Various definitions of intelligent control systems do exist, *e.g.*, Saridis, (1977), Saridis, Valavanis (1988), Åström (1991), White, Sofge (1992), Antsaklis (1994), Gupta, Sinha (1996), Harris (1994). An intelligent control system may be organized as an on-line expert system according to Figure 1.14 and comprises:

1. multi-control functions (executive functions);
2. knowledge base;
3. inference mechanisms;
4. communication interfaces.

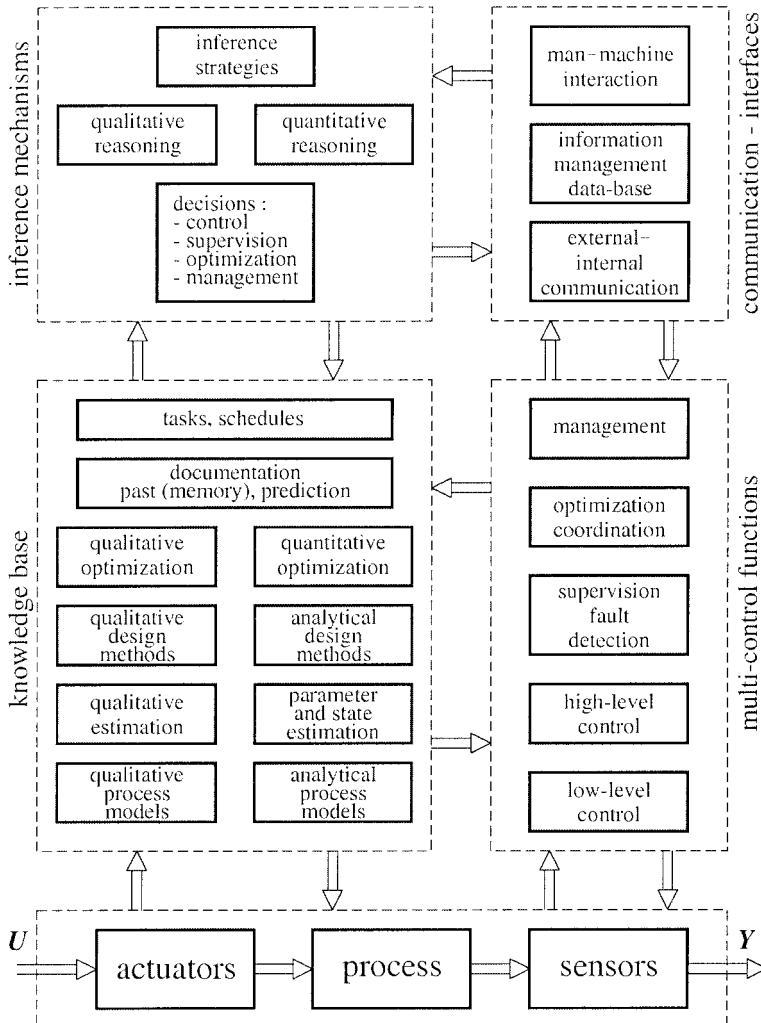


**Figure 1.14.** Advanced intelligent automatic system with multi-control levels, knowledge base, inference mechanism and interfaces

The *on-line control functions* are usually organized in multi-levels, as already described. The *knowledge base* contains quantitative and qualitative knowledge. The quantitative part operates with analytical (mathematical)

process models, parameter and state estimation methods, analytical design methods (*e.g.*, for control and fault detection) and quantitative optimization methods. Similar modules hold for qualitative knowledge, *e.g.*, in the form of rules (fuzzy logic and soft computing). Further knowledge is the past history of events and the possibility of predicting the behavior. Finally, tasks or schedules may be included.

The *inference mechanism* draws conclusions either by quantitative reasoning (*e.g.*, Boolean methods) or by qualitative reasoning (*e.g.*, possibilistic methods) and takes decisions for the executive functions.

Finally, *communication between* the different modules, an information management database and the man–machine interaction has to be organized.

Based on these functions of an on-line expert system, an intelligent system can be built up with the ability “to model, reason and learn the process and its automatic functions within a given frame and to govern it towards a certain goal”. Hence, *intelligent mechatronic systems* can be developed, ranging from the “low-degree intelligent” such as intelligent actuators, to “fairly intelligent systems” such as self-navigating automatic guided vehicles.

An intelligent mechatronic system can adapt the controller to mostly non-linear behavior (adaptation) and store its controller parameters dependent on the position and load (learning), supervise all relevant elements and perform a fault diagnosis (supervision) to request for maintenance or if a failure occurs (decisions on actions). In the case of multiple redundant components, supervision may help to switch off the faulty component and to perform a reconfiguration of the controlled process, thus making the mechatronic system fault-tolerant.

## 1.6 DESIGN PROCEDURES FOR MECHATRONIC SYSTEMS

The design of mechatronic systems requires a systematic development and use of modern software design tools. As with any design, mechatronic design is also an iterative procedure. However, it is much more involved than for pure mechanical or electrical systems. Figure 1.15 shows that in addition to the traditional domain specific engineering an integrated, simultaneous (concurrent) engineering is required. It is the integration of engineering across traditional boundaries that is typical of the development of mechatronic systems.

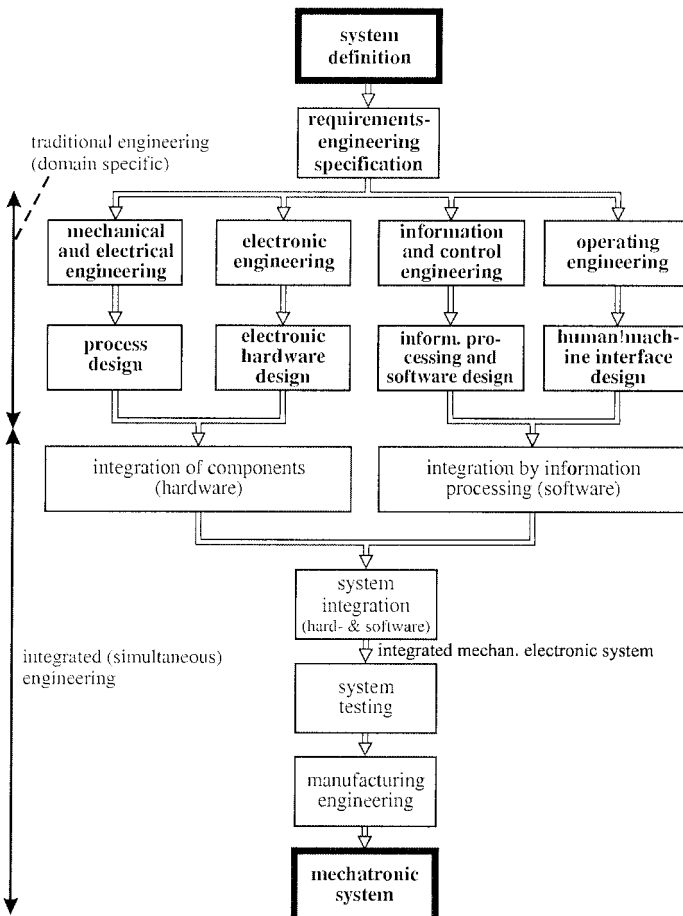


**Figure 1.15.** From domain specific traditional engineering to integrated, simultaneous engineering (iteration steps are not indicated)

A similar representation of important design steps, which distinguishes especially between the mechatronic *system design* and *system integration* is depicted in Figure 1.16. This scheme is represented in form of a “V”-model, which originates probably from software development, STARTS guide (1989), Broehl (1995), see also VDI 2206 (2003). The design and development of mechatronic systems comprises, for example, the following steps.

### 1. Requirements engineering

- definition of general functions and data (rated values) of the final product or process or system;
- traditional solution versus new approaches;
- reliability and safety requirements;
- requirements for development and manufacturing costs;
- requirements on timely development and mile stones;

- continuous updating during design process;
  - deliverable: requirements document.
2. *Specification*
    - definition of the developed product or process or system that fulfils the requirements;
    - first partitioning into manageable modules;
    - specification of the modules;
    - measures to meet the required functions, technical data and performances;
    - measures to meet the reliability and safety requirements;
    - consideration of the sources and limitations for the development and production of the final product;
    - deliverable: specification documents.
  3. *System design*
    - detailed partitioning into developed or off-the-shelf modules:
      - mechanical, hydraulic, pneumatic, electrical, thermal, ... components;
      - electronic components (integrated circuits, microcomputers, interfaces, amplifiers, filters, ...);
      - sensors, actuators;
      - automatic control and information processing software;
      - operator's console and human-machine-interface (HMI);
    - task distribution between mechanical, electrical and electronic modules;
    - redesign of traditional solutions:
      - simplification of mechanical and electrical design;
      - generation of special kinematic functions through servo-drives and control algorithms;
      - replacement of linearization by mechanical or electrical design through non-linear control algorithms;
      - lightweight construction with damping through electronic feedback;
    - realization of power-related functions by mechanical, pneumatic, hydraulic or electrical components;
    - realization of information and control-related functions by mechanical, pneumatic, hydraulic or electronic (analog or digital) components;
    - addition of sensors, actuators and information carrying buses (compared to traditional solutions);
    - electronic hardware architecture (microprocessors, bus systems, cabling and harness, plug systems);
    - software architecture (structure, language, compilers, real-time solutions);
    - control engineering design (feedforward and feedback control, classical or model-based controllers, state-observers, parameter estimation, controller tuning and adaptation);
    - realization of synergies (effects which are possible by the integrated approach);
    - FMEA study: behavior in the case of faults and consequences for a fault-tolerant design;
    - deliverable: system design document.
  4. *Modeling and simulation*
    - model-based development is required to simulate the components' overall behavior of the mechatronic product;

- mathematical models of the components (theoretically designed or experimentally gained models, granularity or degree of simplifications dependent on application);
- use of modeling tools, like MODELICA, VHDL-AMS, ...;
- simulation of components and systems behavior with regard to strength of material, compatibility of components, required power, reachable control performance, *etc.*;
- use of simulation tools, like MATLAB/SIMULINK;
- software-in-the-loop simulation (SiL): components and control algorithms are simulated on an arbitrary computer without real-time requirements;
- fault sensitivity: behavior in case of faults and failures;
- deliverables: design data, mathematical models, dynamic requirements, placement and type of actuators and sensors, performance measures for microcomputer, periphals and buses.

#### 5. Component design

- domain specific design with integration aspects;
- use of available CASE-tools (only examples listed)
  - mechanics: CAD/CAE: 2D-, 3D-design (*e.g.*, AutoCAD);
  - fluidics: CFD-tools;
  - electronics: circuit board layout (PADS), microelectronic circuits (VHDL);
  - control: CADCS-tools (MATLAB);
- human-machine-interface:
  - electronic buttons, pedals, sticks or wheels;
  - haptic force feedback;
  - graphic displays, instruments, screens;
  - operator supervision and emergency assistance;
  - tele-operation with visual or tactile feedback;
- reliability and safety design:
  - fail operational, fail-safe, fail-silent property;
  - fault detection and reconfiguration;
  - fault tolerance through hardware or analytical redundancy;
- deliverables: single prototype components ready for integration.

#### 6. Prototypes

- building of laboratory prototypes;
- modification of former products;
- use of of-the-shelf components;
- use of by-pass computers with high-level software in addition to series-electronic-control units for rapid prototyping of control functions;
- deliverables: single prototype components, ready for integration.

#### 7. Mechatronic components

- components ready for integration: mechanics, electronics, control, HMI;
- electronic control unit (ECU) with implemented software.

#### 8. Component testing

- stress and strength testing of hardware components;
- hardware-in-the-loop simulation (HiL): individual real components are tested with their real-time simulated environment. (Saves development time and test rigs and may include dangerous operation states);

- deliverables: hints for design and redesign.
9. *System integration (hardware)*
- spatial integration of mechanical components and electronics (embedding into mechanics);
  - integration of sensors, actuators, cables, plugs;
  - mutual fine adaptation;
  - creation of synergetic effects:
    - use of same components for different tasks;
    - improvement of precision by feedback control;
    - use of submodul masses for vibration damping;
    - use of actuators as sensors for driven mechanics;
    - use of mathematical models for control and fault detection;
  - deliverable: hardware integrated mechatronic product or system.
10. *System integration (software)*
- calculated features from signal analysis methods;
  - model-based computation of non-measurable variables;
  - compensation of nonlinearities by control-algorithms;
  - damping of oscillations by proper feedback algorithms;
  - wide operating conditions through adaptive control algorithms and state observation;
  - special control algorithms for start-up, warm-up, normal operation, shutdown;
  - automatic fault detection and diagnosis;
  - fault-tolerance through analytical redundancy;
  - learning behavior;
  - fault detection and maintenance on demand;
  - deliverable: hardware and software integrated mechatronic product or system.
11. *System testing*
- testing of all functions on test rigs or final environment (extreme loads and environmental conditions).
  - electromagnetic compatibility (EMC);
  - reliability and safety tests;
  - verification: testing that the product meets its specifications;
  - deliverable: redesign of components, if required.
12. *Field testing*
- testing of final product for all functions under customers conditions;
  - statistics on performance measures, faults, failures;
  - human-machine interplay;
  - certification by authorities;
  - validation: testing if final product is appropriate for its purpose with regard to the requirements
  - deliverable: redesign, if required.
13. *Production*
- similar V-modules exist for the production of mechatronic products (VDI 2206);
  - planning of manufacturing should be parallel and simultaneous to design and development;

- includes: available technologies for manufacturing, assembling, until quality control.

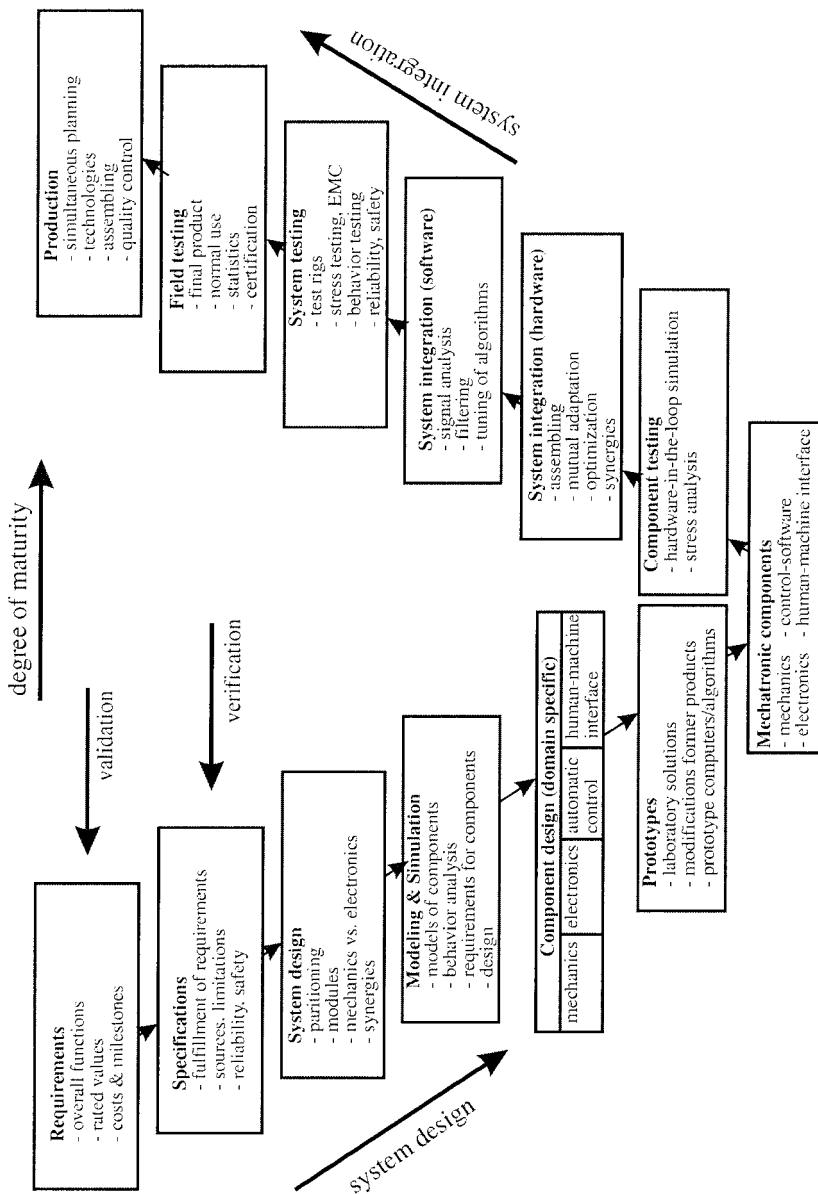


Figure 1.16. A "V" development scheme for mechatronic systems

Stepping through the V-model results in an increasing degree of maturity of the mechatronic product or system. It includes many iterations, which are not indicated in the scheme of Figure 1.16.

Depending on the type of mechanical system, the intensity of the single

development steps is different. For *precision mechanical devices*, fairly integrated mechatronic systems already exist. The influence of the electronics on *mechanical elements* may be considerable, as shown by adaptive dampers, anti-lock system brakes and automatic gears. However, *complete machines* and *vehicles* show first a mechatronic design of some components and then slowly a redesign of parts of the overall structure as can be observed in the development of machine tools, robots and vehicle bodies.

The computer-aided development of mechatronic systems comprises:

1. constructive specification in the engineering development stage using CAD and CAE tools;
2. model building for obtaining static and dynamic process models;
3. transformation into computer codes for system simulation;
4. programming and implementation of the final mechatronic software.

Some software tools are described, for example, in Otter, Gruebel (1993). A broad range of CAD/CAE tools is available for 2D and 3D mechanical design, such as AutoCAD with a direct link to CAM (computer-aided manufacturing); PADS for multi-layer printed circuit board layout, *etc.* However, computer-aided modeling has not advanced as much, see Section 2.1. Object-oriented languages such as DYMOLA, MOBILE and MODELICA for modeling of large combined systems are described in Otter, Gruebel (1993), Elmquist (1993), Hiller (1995). These packages are based on specified ordinary differential equations, algebraic equations and discontinuities. Modeling and simulation tools for special domains are, *e.g.*, AMESim for hydraulics, SABER and SPICE for electrical circuits, ADAMS for mechanics. A description of the state of computer-aided control system design can be found in James *et al.* (1995). For system simulation (and controller design), a variety of program systems exist, like ACSL, SIMPACK, MATLAB/SIMULINK. These simulation techniques are valuable tools for the design, as they allow the study of the interaction of components and the variations of design parameters before integration. However, they are in general not suitable for real-time simulation.

## 1.7 CONTENTS OF THIS BOOK

The previous general considerations on mechatronic systems show that for the design, the start-up and the operation of mechatronic systems, the following aspects are important:

- *systematic description of the processes*, consisting of the mechanical, electrical, thermal and thermodynamic process parts;
- *systematic description of the information-transferring components*, as

sensors, actuators and microelectronics;

- *modeling and simulation* of the static and dynamic behavior of the components and the overall mechatronic system;
- *architecture* of the digital computers and buses;
- *methods of information processing* for control, supervision, optimization, etc.;
- *software design tools* for modeling, simulation, mechanical design, computer-aided design, implementation, experimental test procedures, etc.;
- *operating engineering* (human–machine interface design);
- *entirely and unified treatment* in all development phases.

For many of the sub-areas there exists much literature, books and handbooks. First representations in its entirety appeared mainly in the frame of control engineering as, e.g., Oppelt (1953, 1972), Töpfer, Kriesel (1977, 1983). A first, more comprehensive, book on mechatronics was published by Bradley *et al.* (1991). It mainly considers the information-transferring components and system aspects.

In this book, the basics of modeling for the static and dynamic behavior of technical processes are treated in the first part. After classification of process elements, the fundamental equations for processes with energy and matter flows are stated in unified form for processes with lumped parameters in Chapter 2. Herewith, the equations are subdivided into balance equations, constitutive equations, phenomenological equations and connection laws. The resulting causalities are described and a general procedure for theoretical modeling is given. This is followed by the principles of mechanics for systems with many mobile masses in Chapter 3. One goal for the unified systematic treatment of modeling is the possibility of a unified representation of mechanical, electrical and thermal processes in the form of differential equations, state space equations and for the development of transparent block diagrams or for object-oriented software tools.

Then, frequently appearing models of mechanical elements, such as linkages and different machine elements (bearings, gears), and one-mass and multi-mass oscillators are considered in Chapter 4. This is followed in Chapter 5 by a survey of the most important electrical drives as electromagnets and electromotors in the form of direct current and alternating current motors for use in mechatronic systems. Basic models for the dynamic behavior of electromagnets, DC motors and inductance motors are described, and for several types the main characteristics of the static and dynamic behavior are given.

Modeling of machines is based on the previously established elementary models and leads to equation systems, preferably stated in state space representation, in Chapter 6. Then, the general behavior of machines is considered through the interaction of the characteristics of power-generating

and power-consuming machines. Of special interest are the stability, the resulting dynamics and the dependency on the operation point.

In addition to theoretical modeling, a survey of the most important methods of experimental modeling or *identification* is given for continuous and discrete time, in Chapter 7. Of main interest are on-line methods for parameter estimation and artificial neural networks. Also, models for harmonic oscillations and their identification are considered, especially Fourier analysis and spectral estimation in Chapter 8.

The components for information transfer in mechatronic systems are considered in the second part of the book. This begins with a survey of the most important sensors and measurement devices for mechanical and thermal systems in Chapter 9. After a discussion of signal types and sensor properties, different measurement principles for displacements, velocities, accelerations, forces, *etc.*, are briefly described. Different types of actuators are considered for electrical, pneumatic and hydraulic auxiliary energy in Chapter 10. Basic structures of controlled actuators, consisting of a motor and an actuating element, are treated. This is followed by a systematic survey of electromagnetic, fluidic and unconventional motors. The advantages and disadvantages and their application areas and properties as system components are discussed. Finally, Chapter 11 gives a brief survey of microcomputers from an application viewpoint as embedded computers in mechatronic systems. Standard processors, microcontrollers, signal processors and bus systems are considered and some technical data, relevant for the application, are shown.

One goal of the book is to describe the single components with unified principles and to represent them in mathematical models for the design of integrated mechatronic overall systems. A suitable compromise between the multiplicity and details of the components, their models and the length of the book had to be made. Therefore, the main focus is the systematic description and representation of selected components with regard to their behavior within a mechatronic system. The modeling of the components could therefore be performed only exemplarily and had to be restricted to selected cases. However, to facilitate ease of reading, many tables and graphic representations are given throughout the book.

In designing mechatronic systems, traditional borders of the various disciplines have to be passed. This means for the classical mechanical engineer that frequently knowledge on the electronic components, information processing and systems theory has to be deepened, and for the electrical/electronic engineer that knowledge on thermodynamics, fluid mechanics and engineering mechanics has to be enlarged. For both, more knowledge on modern control principles, software engineering and information technology may be necessary. The book is addressed to students of electrical engineering, mechanical engineering and computer science and to practicing engineers, and tries to add to the respective knowledge.

## 2 Fundamentals of Theoretical Modeling of Technical Processes

---

The temporal behavior of technical systems can be described with the help of system theory according to uniform methods. For this, however, mathematical models must exist for the static and dynamic behavior of the system components or the processes.

A *system* is understood as a bounded arrangement of formations influencing one another. Here, these formations are processes. A *process* is characterized by the conversion and/or the transport of matter, energy and/or information. With respect to the following, it will be differentiated between overall processes, subprocesses and process elements.

The derivation of mathematical models can take place in a theoretical or experimental way. Therefore, it is called theoretical or experimental analysis resp. modeling.

For mechatronic systems, mathematical models for different technical areas have to be set up and combined, *e.g.*, for mechanics, electricity, electronics and thermodynamics. The procedure during theoretical modeling is in principle known for the individual areas, and there also exists analogies for models between different areas. In the following, the basic methodology for theoretical modeling is treated. Thereby, it is aimed at a unified representation for the different technical areas.

## 2.1 THEORETICAL AND EXPERIMENTAL MODELING

During theoretical modeling, also called *theoretical analysis*, the model is set up on the basis of mathematically formulated laws of nature. For this, first the process elements are considered. By combining their models, one obtains models of subprocesses and overall processes. The theoretical modeling always begins with simplifying assumptions about the process, which simplifies the calculations or enables them at all with a tolerable expenditure. One can distinguish the following types of basic equations:

1. balance equations for stored masses, energies and impulses;
2. constitutive equations (physical-chemical state equations) of special elements;
3. phenomenological equations, if irreversible processes (equalizing processes) take place (e.g., equations for thermal conduction, diffusion or chemical reaction);
4. entropy balance equations, if several irreversible processes take place (if not already considered by 3.);
5. connection equations (describe the interconnection of the process elements).

For *distributed parameter systems*, the dependency on the space and time has to be considered. This usually leads to partial differential equations. If the space dependency is negligible, the systems can be considered with *lumped parameters*. These are described by ordinary differential equations as a function of time.

By summarizing the basic equations of all process elements, one receives a system of ordinary and/or partial differential equations of the process. This leads to a *theoretical process model* with a certain structure and certain parameters, if it can be solved explicitly. Frequently, this model is extensive and complicated, so it must be simplified for further applications.

The simplifications are made by linearization, reduction of the model order or approximation of systems with distributed parameters by lumped parameters when limiting on fixed locations, see Figure 2.1. The first steps of these simplifications can be already made by simplifying assumptions while stating the basic equations.

But also if the set of equations cannot be solved explicitly, the individual equations supply important hints for the model structure. So, e.g., balance equations are always linear and some phenomenological equations are linear in wide areas. The constitutive equations often introduce non-linear relations.

During experimental modeling, which is called *identification*, one obtains the mathematical model of a process from measurements. Here,

one always proceeds from *a priori* knowledge, which was gained, e.g., from the theoretical analysis or from preceding measurements. Then, input and output signals are measured and evaluated by means of identification methods in such a way that the relation between the input and output signal is expressed in a mathematical model. The input signals can be naturally operating signals (occurring in the system) or artificially introduced test signals. Depending upon the application purpose, one can use identification methods for parametric or non-parametric models. The result of the identification then is an experimental model. A detailed description of the different techniques can be found, e.g., in Eykhoff (1974), Isermann (1992) and Ljung (1987).

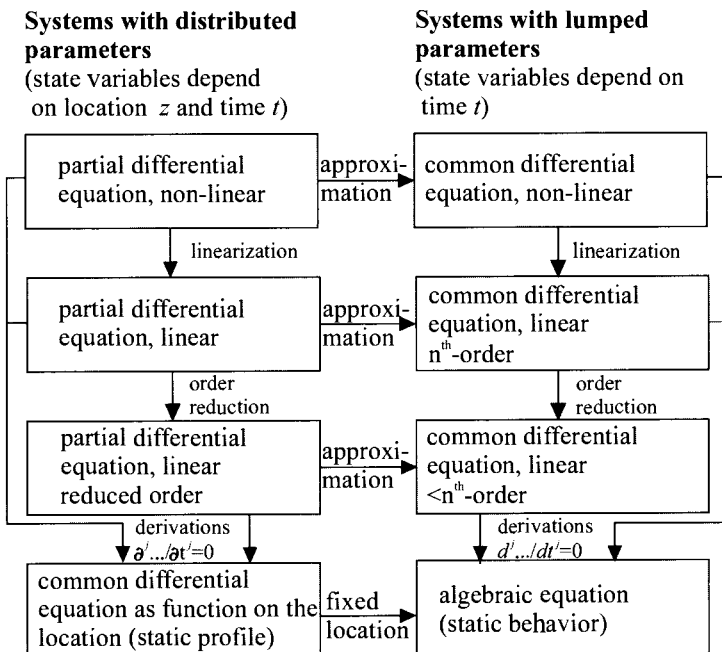


**Figure 2.1.** Relationships of models with distributed and lumped parameters

The theoretical and the experimental model can be compared, provided both types of modeling can be realized. If both models do not agree, then one can conclude from the type and size of the differences which particular steps of the theoretical or experimental modeling have to be corrected.

Theoretical and experimental modeling thus mutually complete themselves. The theoretical model contains the functional description between the physical data of the process and its parameters. Therefore, one will use this model, e.g., if the process is to be favorably designed with regard to dynamical behavior or if the process behavior has to be simulated before construction. The experimental model on the other hand, contains parameters as numeric values whose functional relation with the physical basic data of the process remains unknown. In many

cases, the real dynamic behavior can be described more exactly or it can be determined at smaller expenditure by experimentally obtained models, which, e.g., is better suited to the adjustment of a feedback controller, the prediction of signals or for fault detection. The experimental modeling is described in Chapter 7.

In the following, the procedure of the theoretical modeling of technical processes is treated. In doing so, it is desirable, despite the large variety of existing process elements, to reach a certain systematic model. This is supported by many similarities and analogies between not only the mechanical and electrical, but also thermal, thermodynamic and chemical processes. The statement of models for different process elements is described, e.g., in Campbell (1958), Profos (1962), Shearer *et al.* (1967), Isermann (1971). Analogies between mechanical and electrical systems are covered by several books, e.g., Firestone (1957), Olsen (1958), Crandall *et al.* (1968). A systematic method for modeling a larger variety of technical processes is described by MacFarlane (1964, 1967, 1970). For example, terms were introduced like “effort” and “flow” or “across-variable” and “through-variable”. A continuation of these concepts and, in particular, the consideration of mechanical, electrical and thermal processes and the energy as a central variable is described by Karnopp, Rosenberg (1970) and Wellstead (1979), see also Gawthrop, Smith (1996). These approaches to the modeling of processes with energy flows are also the basis of the “bond graph models”, which were introduced by Paynter (1961) and were further developed by Karnopp, Rosenberg (1970), Wellstead (1979), Karnopp *et al.* (1990), Thoma (1990), Cellier (1991) and Gawthrop, Smith (1996).

The following systematic representation of the modeling of technical processes introduces a methodology that can be applied to most of the technical systems. It is aimed primarily at mechanical, electrical, hydraulic, thermal and partially also thermodynamic processes.

A first approach consists of regarding the elements of these processes and stating the appropriate equations. One will then recognize many analogies later on and the approach will result in common model structures. However, it is more appropriate to consider the typical physical basic equations after a classification of the elementary components and to consider the similarities and analogies in this earlier stage of the modeling, resp. during the set-up of the equations. This has several advantages. First, a superimposed scheme results from setting up the basic equations. Then, the structure of the models results from the common form of the basic equations and is thus straightforward, e.g., the structure of signal flow diagrams in a particularly descriptive way can be obtained. It is then possible to recognize early the common model structures and to reach a unified representation of the dynamic behavior of technical processes. This is also the foundation for programming software tools for computer-aided modeling.

Therefore, the next steps will be as follows:

- classification of the process elements (Section 2.2);

- statement of the basic equations according to physical principles (Sections 2.3, 2.4);
- interconnection of the process elements to processes (Section 2.5).

Here, primarily processes with lumped parameters are considered.

## 2.2 CLASSIFICATION OF PROCESS ELEMENTS

### 2.2.1 Forms of Matter

In order to reach a certain systematic method for the modeling of technical processes, one can first proceed from the different appearances of matter, Figure 2.2.

First, resting and moved matter are distinguished from one another. Then, as sub-groups, further distinction between fluids (liquids, gases) and solids are made. The types of energy stored and/or transported in these different forms of matter are:

- mechanical energy;
- thermal energy;
- electrical energy;
- chemical energy;
- nuclear energy.

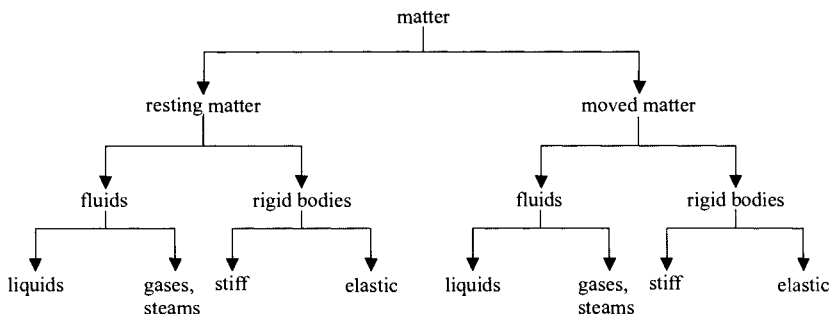


**Figure 2.2.** Different forms of matter

In mechatronic systems, one will predominantly find mechanical, thermal and electrical, occasionally also chemical, energy as with combustion engines.

A further partitioning of the technical processes arises as a result of the spatial distribution of the process elements. Processes with distributed parameters have state variables, which are dependent on both space and time. They are described by partial differential equations (example:

heat conductor). For the mathematical treatment of processes with lumped parameters it is assumed that state variables are considered to be concentrated in one zero-dimensional point. They are therefore described by ordinary differential equations (example: gas pressure in tank).

For theoretical modeling, the processes are divided into individual elements, so that they can be described by physical laws in the form of equations.

## 2.2.2 Main Flows and Side Flows

Many technical processes are an interaction of energy flow, matter flow and information flow, Pahl, Beitz (2001). Frequently, one of the energy, matter or information flows is dominating, depending on the problem or the solution. Thus, a main flow and either none, or one or more side flows can usually be distinguished, see Figure 2.3. Processes that have energy as the main flow exist without matter and information flow, as, e.g., many mechanical, thermal or electrical processes, or with matter flow, like, e.g., thermodynamic, power and hydraulic processes.

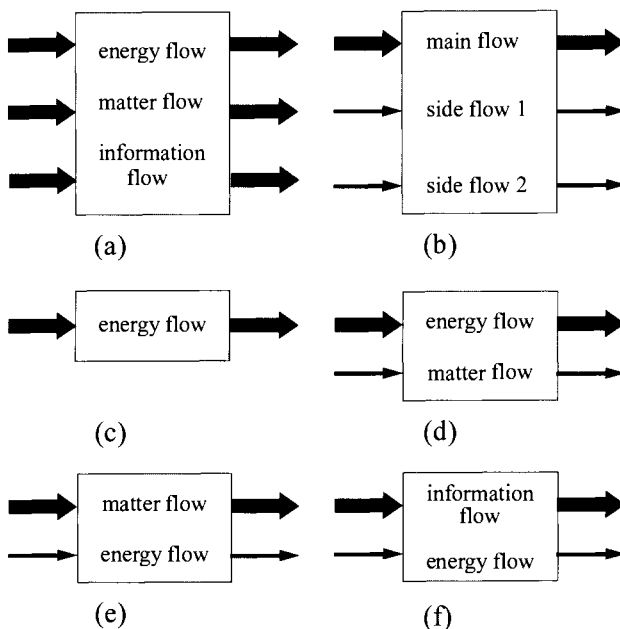


**Figure 2.3.** Interaction of energy, matter and information: (a) different flows; (b) main and side flows; (c) processes with energy flow without matter flow (mechanics, electrical engineering, heat systems); (d) processes with energy flow and matter flow (power engineering, hydraulics, thermodynamics); (e) processes with matter flow and energy flow (conveying systems, chemical engineering); (f) processes with information flow and energy flow (precision instrument technology, telecommunication)

Processes with matter flow (e.g., conveyer systems and chemical processes) and also with information flow (e.g., precision instrument technology and telecommunication), however, always have an energy

flow as a side flow. Therefore, an energy flow is usually always involved. Examples of these flows are:

- *mechanical energy flow*
- piston rod motion

$$\dot{E} = Fv [N \cdot \frac{m}{s}] \hat{=} [W]$$

( $F$  force,  $v$  velocity);

- rotating shaft

$$\dot{E} = T\omega [Nm \cdot \frac{1}{s}] \hat{=} [W]$$

( $T$  torque,  $\omega$  angular speed);

- *electrical energy flow*

- direct current (DC)

$$\dot{E} = VI [V \cdot A] \hat{=} [W]$$

( $V$  voltage,  $I$  current)

- alternating current (AC, real power)

$$\dot{E}_{real} = \frac{1}{T} \int_0^T \dot{E}(t) dt = \frac{1}{T} \int_0^T V_0 \sin \omega t \cdot I_0 \sin(\omega t + \varphi) dt = V_0 I_0 \cos \varphi [W]$$

( $V_0$  voltage amplitude,  $I_0$  current amplitude,  $\varphi$  phase angle);

- *thermal energy flow*

- thermal conduction

$$\dot{E} = \lambda A \frac{\partial T}{\partial z} \left[ \frac{J}{mKs} \cdot m^2 \cdot \frac{K}{m} \right] \hat{=} \left[ \frac{J}{s} \right] \hat{=} [W]$$

( $\lambda$  thermal conductivity,  $A$  cross-section area,  $T$  temperature,  $z$  local coordinate)

- convection

$$\dot{E} = \dot{m}h \left[ \frac{kg}{s} \cdot \frac{J}{kg} \right] \hat{=} \left[ \frac{J}{s} \right] \hat{=} [W]$$

( $\dot{m}$  mass flow,  $h$  specific enthalpy);

- *matter flow*

- fluid matter flow

$$\dot{m} = \frac{dm}{dt} = A \rho v \left[ m^2 \frac{kg}{m^3} \frac{m}{s} \right] \hat{=} \left[ \frac{kg}{s} \right]$$

( $dm$  mass element,  $dt$  time interval,  $A$  cross-sectional area,  $\rho$  density,  $v$  velocity);

- information flow

- character rate

$$\dot{I} = \frac{\Delta I}{\Delta t} \left[ \text{characters} \cdot \frac{1}{s} \right]$$

- bus transfer rate

$$\dot{I} = \frac{\Delta I}{\Delta t} \left[ \text{bit} \cdot \frac{1}{s} \right] \hat{=} [\text{baud}] .$$

### 2.2.3 Process Elements with Lumped Parameters

In the following, the terms energy, matter and information are called *quantity*. If one considers processes with lumped parameters, then the elements of technical processes can be classified according to the following idealized types, see Karnopp *et al.* (1990), MacFarlane (1967, 1970):

*sources, storages, transformers, converters, sinks.*

These elements are represented in Figures 2.4 and 2.5. The connecting lines represent the flows between the elements in the form of [quantity/time]. The arrows indicate the direction of the flows.

*Sources* deliver an output quantity from a large supply. They can be distinguished as:

- *ideal sources*: the output quantity is produced without losses;
- *real sources*: the output quantity is produced with (usually small) losses. (Ideal sources with integrated sink.)

*Storages* take up a quantity and deliver it again in the same form. The difference between input and output quantity is accumulated internally, thus stored. One can partition as:

- *ideal storages*: the quantity is stored without losses;
- *real storages*: the storage takes place with losses. (Ideal storage with sink.)

*Transformers* take up a quantity and deliver it again in the same form, without storing it. One can also call transformers *couplers*. They can be distinguished as:

- *ideal transformers*: the input quantity is delivered as output quantity without losses;

- *real transformers*: the input quantity is delivered as output quantity with (usually small) losses. (Ideal transformers with sink.)

*Converters* take up a quantity in a certain form and deliver it after conversion into another form, without storing it. Converters thus transfer input quantity into another output quantity. Thereby, the following types can be distinguished generally:

- *ideal converters*: the input quantity is converted completely into an output quantity. If there are no losses, they are conservative processes;
- *real converters*: the input quantity is not completely converted into the output quantity, losses occur. (Ideal converters with sink.)

*Sinks* take up an input quantity and consume it in the same or another form completely or in a substantial portion. Since mainly losses occur, they are dissipative processes. One can distinguish between:

- *ideal sinks*: the input quantity is completely consumed;
- *real sinks*: the input quantity is not completely consumed.

A further distinction of the process elements can be made with regard to their controllability with an additional auxiliary energy:

- *passive elements*: the transferred quantity is not controllable by an additional auxiliary energy. Examples are passive storages, e.g., capacitances, passive transformers as, e.g., fixed gear transmissions, or passive converters, e.g., fans with constant speed;
- *active elements*: a quantity is controlled by an actuator. Thereby, an electrical or mechanical auxiliary energy usually has to supply the actuator. Examples are controllable sources as, e.g., voltage sources, controllable transformers as, e.g., electrical amplifiers and controllable converters, e.g., electromagnets.

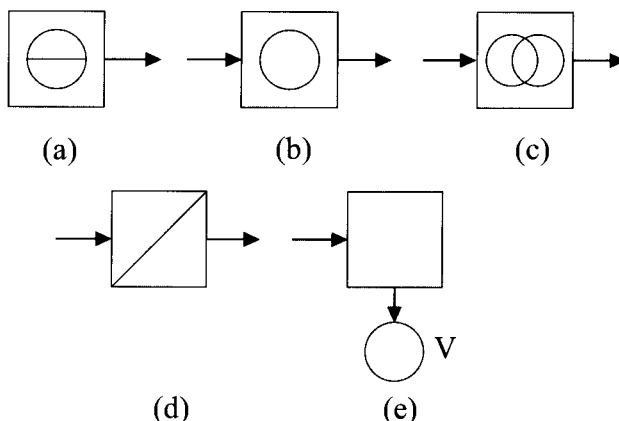
With these definitions, basic process elements result, as shown in Figures 2.4 and 2.5.

The storages basically show a dynamic, usually an integral, behavior. Sources, transformers, converters and sinks can have both a mainly static transfer behavior as well as a distinct dynamic transfer behavior.

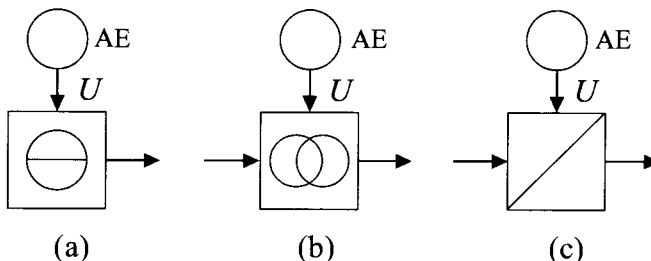
The basic structure of technical processes (process scheme) results from interconnecting the process elements such as sources, storages, transformers, converters and sinks. Figure 2.6 shows some simple examples of interconnections.

Figure 2.7a, for example, represents a pumping plant, which transports liquid into a tank. The following process elements can be distinguished, Figure 2.7b:

1. converter: electricity is withdrawn from the electrical network (controllable source);
2. direct current or asynchronous motor (electromechanical converter);
3. transmission (transformer, with small losses);
4. centrifugal pump (converter of mechanical shaft energy into mechanical flow energy, with losses);
5. pipeline (transformer of liquid to other places, with losses of energy);
6. elevated tank (storage of potential energy).



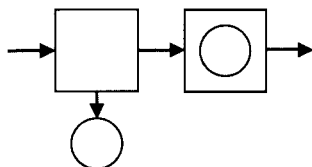
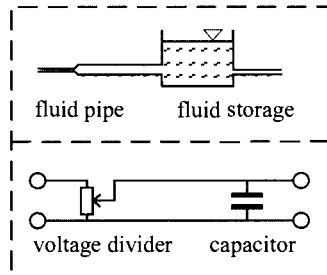
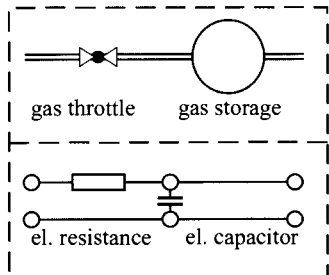
**Figure 2.4.** Symbols of passive process elements: (a) source; (b) storage; (c) transformer; (d) converter; (e) sink ( $V$ : losses) - energy, matter or information flow



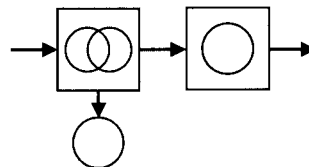
**Figure 2.5.** Symbols of active process elements (the process element is controlled by an actuator, which is supplied by an auxiliary energy. AE: auxiliary energy;  $U$ : manipulated variable): (a) source with auxiliary energy; (b) transformer with auxiliary energy; (c) converter with auxiliary energy

The process elements can be represented as one-port and two-port elements, Figure 2.7c, and the corresponding signal flow diagram in Figure 2.7d, Takahashi *et al.* (1972). This will be treated in Section 2.3.

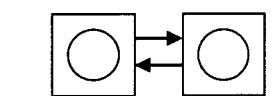
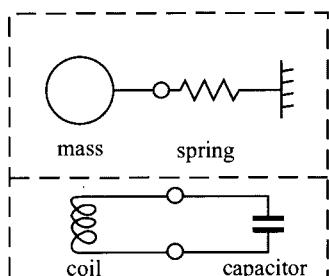
According to the defined terms of the different processes and process elements, Table 2.1 shows examples of storages, transformers, converters, sources and sinks for different forms of energy. The energy flow (with regard to the problem) is essentially considered as main flow and a possible matter or information flow is considered as side flow.



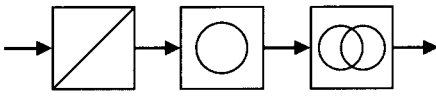
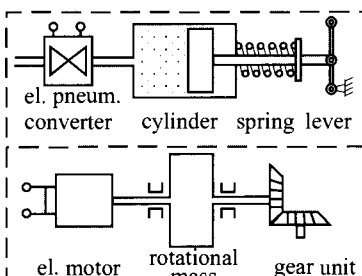
(a) sink storage



(b) transformer storage



(c) two different storages



(d) converter-storage-transformer

**Figure 2.6.** Examples of the connection of process elements: upper picture: schematic representation of the process (process scheme); lower picture: unified process elements with flows

Table 2.2 shows a corresponding representation of different matter forms as main flow. Here, one can also differentiate according to storages, transformers, converters, etc.

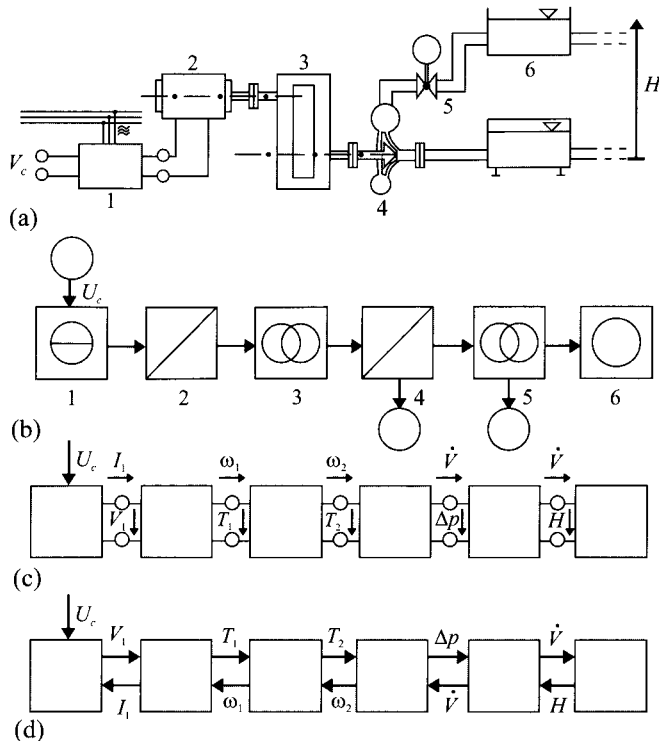


**Figure 2.7.** Schematic representation of a pumping plant with an elevated tank: (a) process scheme: scheme of the constructional arrangement; (b) energy flow scheme: process elements with energy flows; (c) multi-port scheme: one-port and two-port elements (with flows and potentials); (d) multi-port signal flow diagram: signal flow diagram with one- and two-port elements (for speed control or flow rate control)

1 converter (controllable source); 2 electrical motor (controllable converter); 3 transmission (transformer); 4 centrifugal pump (converter with losses); 5 pipeline (transformer with losses); 6 elevated tank (storage)

Table 2.1 Processes with different energy forms, where the energy flow is the main flow (examples)

energy form	mechanical	thermal	thermo-dynamic	electrical	chemical
potential	kinetic			electrostatic	electromagnetic
matter form	solid fluid gaseous	solid fluid	gaseous vaporous	solid	solid fluid gaseous
energy storage	mass in field of gravity, elasticity	moved mass	thermal capacity	condensor	inductivity
energy converter	lever joint	gear fluid flow	thermal inductance thermal radiation fluid flow	vaporization condensation	el. conductor transformer
energy transformer	flow piston in cylinder aerofoil	Peltier element	compression expansion	electrostat. motor piezoactuat.	electromagnet electromotor generator
energy source	water reservoir wind		solar radiation heat of earth combustion chem. exoth. reaction	accumulator electr. nets	exothermal reaction combustion
energy sink	friction	cold environment	throttling	resistance eddy current receiver	endothalmic reactions

**Table 2.2.** Processes with different matter forms, where the matter flow is the main flow (examples)

<b>matter form</b>	<b>rigid bodies</b>	<b>fluids</b>	<b>gases</b>	<b>steams</b>
matter storages	container	tank	storage	tank
matter transformers	conveyor lift	duct pipeline	pipeline bottles	pipeline
matter converters	transformation separation crushing smelting chemical reaction combustion	vaporization rectification crystallization chemical reaction combustion	condensation diffusion chemical reaction combustion	condensa- tion diffusion chemical reaction combustion
matter sources	earth (mining)	earth sea	earth atmosphere	earth sea
matter sinks	container earth disposal	tank environment disposal	storage atmosphere disposal	container atmosphere disposal

### 2.2.4 Process Elements with Distributed Parameters

For processes with distributed parameters, process elements such as storages, transformers, converters and sinks are distributed over space. By partitioning into infinitesimally small elements, one can determine process elements with lumped parameters, whose state variables are location-dependent from element to element, see, e.g., Gilles (1973).

The partitioning of the processes according to different matter forms, different flows and corresponding process elements enables the statement of basic equations of the process elements according to certain principles. This leads to transparent superordinated principles, similarities and analogies.

## 2.3 FUNDAMENTAL EQUATIONS OF PROCESS ELEMENTS WITH ENERGY AND MATTER FLOWS

After the definition of suitable cuts, the process is divided into elements such as sources, storages, transformers, converters and sinks for energies and matters in order to set up the basic equations. Then, types of basic equations can be distinguished for lumped parameter processes as follows:

- *balance equations* (general storages, junction points);
- *constitutive equations*, physical state equations (sources, transformers, converters, special storages);

- *phenomenological equations* (sinks, dissipative elements).

This partitioning then applies both to processes with energy flows and matter flows.

### 2.3.1 Balance Equations

Since the laws for conservation of mass, energy and momentum are fundamental, they are regarded as the first type of equations. The balance equations, which are derived from these conservation laws, basically apply independently of the construction of the processes. They describe the global behavior. The mass balance applies to processes with moved matter, the energy balance to processes with all types of energy and the momentum balance to processes with moved masses.

#### a) Mass balance

The principle of the conservation of mass applies to a bounded area, where no mass enters or leaves.

$$\sum_{v=1}^n m_v = \text{const.} \quad (2.3.1)$$

whereby  $n$  different matters with mass  $m_v$  exist, Figure 2.8a. If a mass  $\Delta m_e(t)$  enters through the boundaries of an arbitrary control area and a mass  $\Delta m_o(t)$  escapes through the boundaries in a time interval  $\Delta t$ , then it follows from the mass conservation theorem that

$$\Delta m_i(t) - \Delta m_o(t) = \Delta m_s(t) \quad (2.3.2)$$

Compare Figure 2.8b. Herewith,  $\Delta m_s(t)$  is the mass remaining in the control area, the stored mass per  $\Delta t$ .

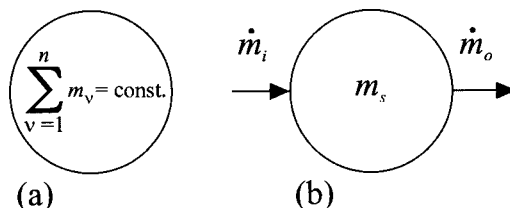


**Figure 2.8.** Mass balance: (a) bounded area; (b) mass storage

The control surface thus encloses a mass storage. From (2.3.2), it follows that

$$\frac{\Delta m_i(t)}{\Delta t} - \frac{\Delta m_o(t)}{\Delta t} = \frac{\Delta m_s(t)}{\Delta t} \quad (2.3.3)$$

In the limit it follows that with  $\Delta t \rightarrow 0$

$$\lim_{\Delta t \rightarrow 0} \frac{\Delta m}{\Delta t} = \frac{dm}{dt} = \dot{m}$$

and thus

$$\frac{dm_i(t)}{dt} - \frac{dm_o(t)}{dt} = \frac{dm_s(t)}{dt} \quad (2.3.4)$$

and it applies for the mass flow balance of a mass storage, Figure. 2.8b

$$\dot{m}_i(t) - \dot{m}_o(t) = \frac{d}{dt} m_s(t) \quad (2.3.5)$$

energy inflow	energy outflow	stored energy flow
---------------	----------------	--------------------

Now small deviations are introduced around the equilibrium point  $\bar{m}$

$$\dot{m}(t) = \bar{\dot{m}} + \Delta\dot{m}(t)$$

Then, it yields

$$\frac{d\dot{m}}{dt} = \frac{d\Delta\dot{m}}{dt}; \frac{d\bar{\dot{m}}}{dt} = 0 \quad (2.3.6)$$

and it follows that

$$\bar{\dot{m}}_i + \Delta\dot{m}_i(t) - \bar{\dot{m}}_o - \Delta\dot{m}_o(t) = \frac{dm_s(t)}{dt}$$

For the equilibrium state (ES) it is  $d(\dots)/dt = 0$ , and it follows that

$$\bar{\dot{m}}_i = \bar{\dot{m}}_o$$

Thus, the mass flow balance equation for small deviations reads

$$\Delta\dot{m}_i(t) - \Delta\dot{m}_o(t) = \frac{d}{dt} m_s(t) \quad (2.3.7)$$

Figure 2.9 shows the resulting signal flow or block diagram, whereby the individual variables represent signals.

The mass flow balance is represented by the summation point. An integrator (storage) determines the stored mass remaining in the process.

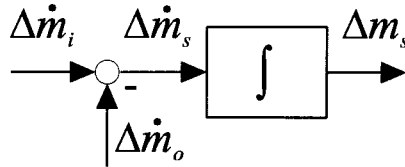


Figure 2.9. Block diagram of the mass flow balance

### b) Energy balance in general form

For a bounded area, where no energy enters or leaves, the theorem of energy conservation applies

$$\sum_{v=1}^n E_v = \text{const.} \quad (2.3.8)$$

whereby  $n$  different types of energy  $E_v$  may exist, see Section 2.2 and Figure 2.10. Here, mechanical, thermal and electrical energy are of particular interest.

If an energy  $\Delta E_e(t)$  enters an arbitrary control area through its control boundaries per time interval  $\Delta t$  and an energy  $\Delta E_o(t)$  is withdrawn, then it follows from the principle of conservation of energy that

$$\Delta E_i(t) - \Delta E_o(t) = \Delta E_s(t) \quad (2.3.9)$$

Herewith,  $\Delta E_s(t)$  is the energy remaining in the control area, the *stored energy per  $\Delta t$  in an energy storage*. Then applies

$$\frac{\Delta E_i(t)}{\Delta t} - \frac{\Delta E_o(t)}{\Delta t} = \frac{\Delta E_s(t)}{\Delta t} \quad (2.3.10)$$

and it follows that in the limit with  $\Delta t \rightarrow 0$

$$\frac{dE_i(t)}{dt} - \frac{dE_o(t)}{dt} = \frac{d}{dt} E_s(t) \quad (2.3.11)$$

and thus the energy flow balance, see Figure 2.10b

$$\begin{array}{ccc} \dot{E}_i(t) & - & \dot{E}_o(t) \\ \text{energy} & & \text{energy} \\ \text{inflow} & & \text{outflow} \end{array} = \frac{d}{dt} E_s(t) \quad (2.3.12)$$

stored  
energy flow

Derived from this some special cases follow

a) Only an energy inflow or outflow.

$$\dot{E}(t) = \frac{d}{dt} E_s(t)$$

b) The energy storage capacity is zero.

$$\dot{E}_i(t) = \dot{E}_o(t)$$

After introduction of small deviations

$$\dot{E}(t) = \bar{\dot{E}} + \Delta \dot{E}(t)$$

$$\bar{\dot{E}}_i = \bar{\dot{E}}_o$$

the energy flow balance equation for small deviations follows from (2.3.12)

$$\Delta \dot{E}_i(t) - \Delta \dot{E}_o(t) = \frac{d}{dt} E_s(t) \quad (2.3.13)$$

The corresponding block diagram is shown in Figure 2.11.

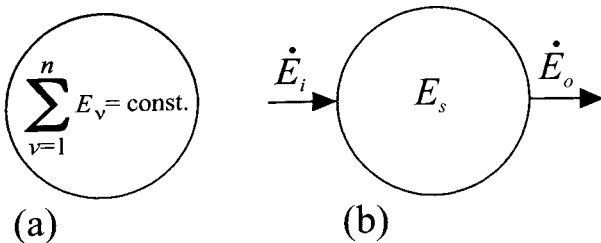


Figure 2.10. Energy balance: (a) bounded area; (b) energy storage

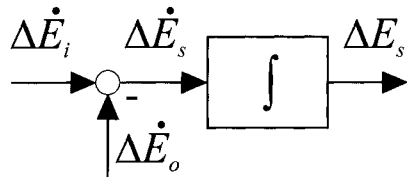


Figure 2.11. Block diagram of the energy flow balance

The energy flow balance equation in this form applies to all types of energy. Frequently, the energy inflows and outflows and the stored energy are composed of different, special types of energy. Then, special forms of energy flow balance equations emerge from these types, see Section 2.4.

Since the mass flow and energy flow balance have, in principle, the same form, a *generalized balance equation*

$$\begin{array}{ccccc} \dot{Q}_i(t) & - & \dot{Q}_o(t) & = & \frac{d}{dt} Q_s(t) \\ \text{inflow} & & \text{outflow} & & \text{stored flow} \end{array} \quad (2.3.14)$$

can be stated, Figure 2.12. A corresponding vectorial type exists for moved masses in the form of *momentum balance*, see (2.4.11), (2.4.12).

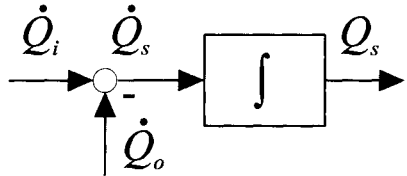


Figure 2.12. Block diagram of an energy or mass storage (balance equation)

Balance equations for energy stores thus lead to an integrating transfer element and cause a dynamically delayed behavior. A balance equation has to be set up for each storage. For processes with distributed parameters, one puts the boundary surface around an infinitesimally small volume. The balance equations will be treated in more detail in

Section 2.4, since special forms have to be considered for some process types.

The balance equations also describe the flows at the interconnection points of process elements, if the storage capacity is set to zero. Balance equations are also called *continuity equations*, see Section 2.5.

### 2.3.2 Constitutive Equations

The coherence between input and output variables of the process elements in the form of sources, transformers, converters, sinks and also storage elements can be expressed by special physical laws in analytical form or by characteristic curves from experiments. The mentioned equations are called *constitutive equations* or *physical state equations*.

There exist many different physical laws that apply to the individual process elements. However, regarding the input/output behavior, several similarities exist.

#### a) Processes with energy flows

For technical processes which primarily transfer energy at their interconnections, it follows from the energy balance equation (2.3.12) without storage  $\dot{E}_s(t) = 0$  that the transferred energy per time interval resp. the power

$$P(t) = \frac{dE(t)}{dt} \quad (2.3.15)$$

is always equal at the interconnections between the process elements. Therefore, it is appropriate to determine the state variables in such a way that at the interfaces between process elements or subprocesses they describe a power, e.g., as in Figure 2.7c. If one determines the interfaces in analogy to electrical transfer elements as a terminal pair, then the different process elements can be described as one-port systems (two-pole systems), two-port systems (four-pole systems) or generally multi-port systems (multi-pole systems), see Figure 2.13. One can always distinguish two variables for a terminal pair at the transfer elements, Karnopp, Rosenberg (1970), Karnopp *et al.* (1990), Takahashi *et al.* (1972):

1. potential difference  $e(t)$ : variables like electrical voltage, force, pressure difference appear as a difference between two terminals. They are called “effort”.
2. flow  $f(t)$ : variables like electrical current, velocity, volume flow enter in one of the terminals. They are called “flow”.

The product of both terms is the transferred power

$$P(t) = f(t) \cdot e(t) \quad (2.3.16)$$

power = flow · potential difference

Here,  $f(t)$  and  $e(t)$  are assigned covariables, which are also called *generalized power variables*. In Table 2.3a, these variables are shown for important technical systems with energy flows according to this potential-flow classification.

The definition of the arrow direction for one-port systems requires a special discussion. The directions of the arrows are arbitrary. They should be determined in such a way that the transferred power  $P$  at the terminals indicates the real direction. If the one-port system receives power according to Figure 2.13a and thus the power input is positive, then the flow flows into the system. Thus, the potential at the upper terminal must be larger than at the lower terminal. Now, the arrow of the potential difference  $e$  is determined in such a way that it points from the higher potential to the lower potential, as this is usual for electrical engineering (so-called consumer arrow system), see Figure 2.13a. For consumers, the potential arrow and flow arrow point in the same direction, for sources they are opposite. For two-port systems, the arrow directions are determined accordingly. The flow  $f_2$  flows out of the process element towards the terminals, Figure 2.13b.

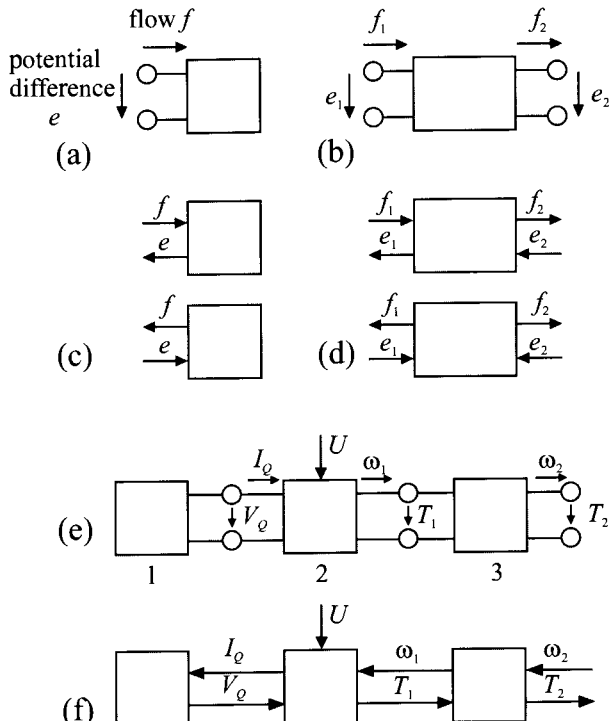


**Figure 2.13.** Representation of one-port and two-port systems for process elements with power variables: (a) one-port system in terminal representation; (b) two-port system in terminal representation; (c) one-port system with input and output signals; (d) two-port system with input and output signals (2 of 4 possibilities); (e) example of an active converter with transformer. 1 source; 2 actuator (converter: direct current motor with voltage actuator) 3 transformer (transmission); (f) input and output signals for Example (e)

One-port systems with a terminal pair represent the simplest form of process elements, Figure 2.13a. For a one-port system, only one of the variables can be influenced independently from the outside, thus only  $e$  or only  $f$ . The other power variable then is a dependent variable.

The variables are now represented as signals, supplying information. (For this, one can imagine that the variables at the interconnection points are measured with appropriate measuring instruments. The displays of the measuring instruments are then the signals.) For a one-port system, the two resulting possibilities are shown in Figure 2.13c, whereby the independent variable is the input signal and the dependent variable is the corresponding output signal. Corresponding signal flow diagrams apply to two-port systems, Figure 2.13d. An example of the interconnection of different process elements can be seen in Figures 2.13e and f.

For some representations, it is appropriate to calculate not only with the power but also with the energies. This is appropriate, e.g., for the state space representation, see Karnopp *et al.* (1990). To do so, the following generalized energy variables are defined

$$\text{displacement: } q(t) = \int_0^t f(\tau) d\tau \quad (2.3.17)$$

$$\text{momentum: } p(t) = \int_0^t e(\tau) d\tau \quad (2.3.18)$$

These notations follow mechanical systems with (translational) moved masses

$$q = \int v(\tau) d\tau = \int dz = z \quad (\text{displacement})$$

$$I = \int F(\tau) d\tau = m \int \frac{dv(\tau)}{d\tau} d\tau = mv \quad (\text{momentum})$$

From (2.3.17), (2.3.18), it follows that

$$\frac{dq(t)}{dt} = f(t) \quad ; \quad dq(t) = f(t) dt \quad (2.3.19)$$

$$\frac{dp(t)}{dt} = e(t) \quad ; \quad dp(t) = e(t) dt \quad (2.3.20)$$

For the energy transferred in time  $t$ , with (2.3.16)

$$E(t) = \int_0^t P(\tau) d\tau = \int_0^t f(\tau) e(\tau) d\tau \quad (2.3.21)$$

and with (2.3.19), (2.3.20), it follows that

$$E(t) = \int_0^t e(\tau) dq(\tau) \quad (2.3.22)$$

$$E(t) = \int_0^t f(\tau) dq(\tau) \quad (2.3.23)$$

For some systems,  $e$  depends directly on  $q$  and  $f$  on  $p$  (e.g., for storages, see Example 2.1). This yields

$$E(q_1) = \int_0^{q_1} e(q) dq \quad (2.3.24)$$

$$E(p_1) = \int_0^{p_1} f(p) dp \quad (2.3.25)$$

The transferred energy then is a function of the generalized energy variables. In Table 2.4, energy variables are put together for different systems. Figure 2.14 shows the corresponding one- and two-port systems, and in Figure 2.15 the relation between the power and energy covariab-les is presented.

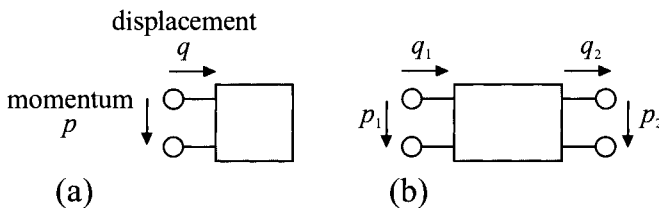


**Figure 2.14.** One- and two-port system representation for process elements with energy variables

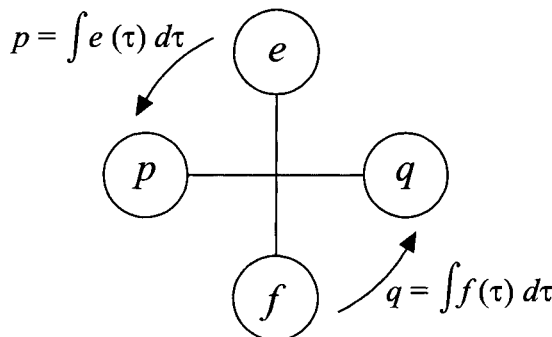


**Figure 2.15.** Relation between the power covariables ( $e, f$ ) and the energy covariables ( $p, q$ )

Another possible definition of power covariables follows from the distinction of across-variables and through-variables after the spatial expansion and the measurement principle:

1. *across-variables*: variables like electrical voltage, velocity and pressure difference can be measured between two terminals.

- Therefore, they are also called two-point-variables and trans-variables;
2. *through-variables*: variables like electric current, force and volume flow can be measured at one terminal. Therefore, they are also called one-point-variables and per-variables.

The assignment for this across-through classification partially agrees with the assignment for the potential-flow classification, e.g., for the electrical and fluid variables. However, in the case of the mechanical variables, an opposite (dual) assignment results, see Table 2.3b.

**Table 2.3.** Power variables for systems with energy flows. Here,  $P = fe$  is a power

(a) potential-flow classification

system	flow $f$				potential difference $e$		
electrical	el. current	$I$	$A$		el. voltage	$V$	$V$
mechanical (translation)	speed	$v$	$\frac{m}{s}$	power	$F$	$N$	
mechanical (rotation)	angular speed	$\omega$	$\frac{1}{s}$	torque	$T$	$Nm$	
hydraulic	volume flow	$\dot{V}$	$\frac{m^3}{s}$	pressure diff.	$p$	$Pa = \frac{N}{m^2}$	
thermodynamic	entropy flow	$\dot{s}$	$\frac{W}{K}$	temperature	$T, \vartheta$	$K$	

(b) across-through classification

system	through variable $f$				across variable $e$		
electrical	el. current	$I$	$A$		el. voltage	$V$	$V$
mechanical (translation)	power	$F$	$N$	speed	$v$	$\frac{m}{s}$	
mechanical (rotation)	torque	$T$	$Nm$	angular speed	$\omega$	$\frac{1}{s}$	
hydraulic	volume flow	$\dot{V}$	$\frac{m^3}{s}$	pressure diff.	$p$	$Pa = \frac{N}{m^2}$	
thermodynamic	entropy flow	$\dot{s}$	$\frac{W}{K}$	temperature	$T, \vartheta$	$K$	

**Table 2.4.** Generalized energy variables for systems with energy transfer

system	displacement $q(t)$			momentum $p(t)$		
electrical	charge	$q$	$As$	flux density	$\Phi$	$Vs$
mechanical (translation)	displacement	$z$	$m$	momentum	$I$	$\frac{kgm}{s}$
mechanical (rotation)	angle	$\varphi$	rad	angular momentum	$L$	$\frac{kgm^2}{s}$
hydraulic	volume	$V$	$m^3$	pressure momentum	$\Gamma$	$\frac{kg}{ms}$

The definition of these different variables is treated in Firestone (1957), Crandall *et al.* (1968), MacFarlane (1964, 1967, 1970), also with notes that the definitions are not always consistent for all systems.

For processes with energy flows in one-port, two-port and multi-port system representation, the bond graph method was developed, see, e.g., Paynter (1961), Karnopp *et al.* (1990, 2000). It is a graphic of multi-port systems with energy transfer. Herewith, the interconnections between one- and two-port systems are replaced by an energy bond, which is a half arrow in the direction of the energy flow, Figure 2.16. The potential difference  $e$  is written above the bond, the flow  $f$  below the bond. In this way, systems with different types of energy can be represented uniformly in abstract form. Together with signals (active bonds), junction points and some rules, one then succeeds in systematically modeling different processes, e.g., electrical, mechanical and hydraulic processes. Problems result, however, in the case of thermal and thermodynamic processes and if energy flows are coupled with mass flows, Karnopp *et al.* (1990).

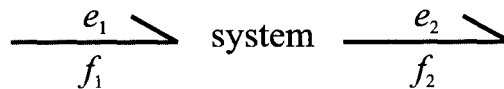


Figure 2.16. Representation of a two-port system as an energy bond graph

According to the usual analogies and general practice for electrical and thermal systems with thermal conduction, one would take the temperature difference  $T$  for the potential difference  $e$  and the heat flow  $\dot{Q}$  for the flow  $f$ . Since the heat flow represents power, however, the product  $\dot{Q}T$  is not power. From thermodynamics, it follows that power is the product of entropy flow and temperature difference  $T$ , Table 2.3. Thus, one would also have to operate with thermodynamic laws for thermal systems, which is more complicated than using laws of heat transfer. Therefore, a practical way to handle it is by the implementation of pseudo bond graphs, where  $e$  and  $f$  are not power variables. However, one cannot couple these directly to normal bond graphs.

### b) Processes with different flows

The previous reflections were limited to processes that exclusively transfer energy flows, thus processes according to Figure 2.3c. For matter flows (solids, liquids, steams, gases), it is practical to use the mass flow  $\dot{m}(t)$  as flow  $f(t)$ , since the mass balance equation is a substantial basic equation. If one uses the usual variables for the potential difference  $e(t)$ , denoted in Table 2.5, the product  $e(t) f(t)$  is not always power  $P(t)$  according to (2.3.16).

At the interconnection points between process elements, power  $P(t)$  (energy flows), (2.3.15), as well as the mass flows

$$\dot{m}(t) = \frac{dm(t)}{dt} \quad (2.3.26)$$

have to be equal between the process elements at any time. Therefore, one uses the mass flow as a further state variable at the interfaces. Only for incompressible matter can one also take the volume flow rate

$$\dot{V}(t) = \frac{1}{\rho} \dot{m}(t)$$

since the density  $\rho$  is constant.

For heat flows that are transferred by convection and therefore are coupled to a mass with heat capacity, the product according to Table 2.5 is power (in the case of convection by fluids it has to be multiplied by the specific heat). This does not apply to thermal conduction in matter, however, if one selects the heat flow as flow  $f$ , since the heat flow itself represents power, Table 2.5, last row.

For powers, it has to be determined if it is the power needed for the transportation of a mass flow, e.g., hydraulic power or the power that is transported by the mass flow, e.g., thermal energy flow.

In the following, examples of physical state equations are considered for different process elements, subdivided by energy storages, sources, transformers, converters and sinks. The examples consider both process elements with energy flows and with mass flows.

**Table 2.5.** Variables for flow and potential difference for matter flows and heat flows

system	flow $f$		potential difference $e$		$ef$	power
hydraulic	mass flow	$\dot{m}$	$\frac{kg}{s}$	pressure difference	$p$	$\dot{m}p$
thermal – convection through liquids – convection through gas, steam	mass flow	$\dot{m}$	$\frac{kg}{s}$	temperature difference	$T$	$K$
	mass flow	$\dot{m}$	$\frac{kg}{s}$	enthalpy difference	$h$	$\frac{J}{kg}$
chemical	mass flow	$\dot{m}_i$	$\frac{kg}{s}$	concentration	$c_i$	$\frac{mol}{kg}$
thermal – heat conduction	heat flow	$\dot{q}$	$W$	temperature difference	$T$	$K$
					$\dot{q}T$	$\dot{q}$

### c) Sources

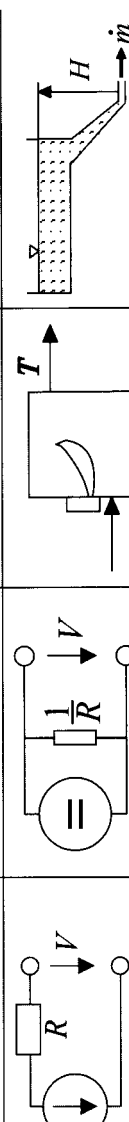
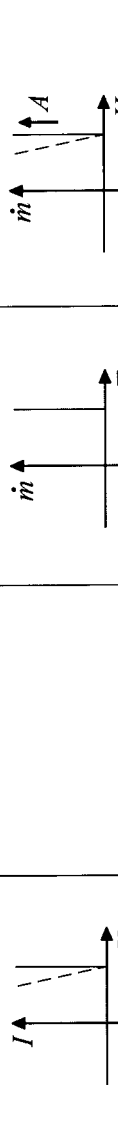
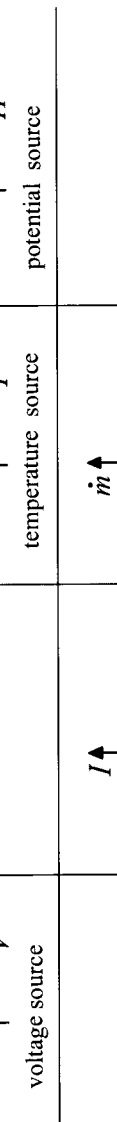
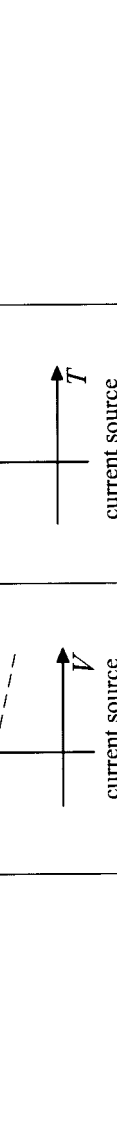
The constitutive equations of some sources are shown in Table 2.6. Herewith, it can be distinguished:

1. *potential source*. The potential supplied by an ideal potential source is independent of the electrical current

$$e = e_0 \quad (2.3.27)$$

(Example: electrical accumulator);

Table 2.6. Sources: examples and constitutive equations

	electrical-electrical	chemical-electrical	chemical-thermal	mechanical
converter element	voltage source	current source	firing	water power station
				
kind of source	accumulator	DC current battery charger	oil, gas burning	water storage with pipeline
constitutive equation	$V = V_0 - RI$	$I = I_0 - \frac{1}{R} V$	$\dot{Q} = mc_p T$ $T = T_0$	$p_s = \rho g H$ $\dot{m} = A \rho \sqrt{2gH} = \sqrt{2\rho p_s}$
characteristics				

2. *current source.* The current supplied by an ideal current source is independent of the potential

$$f = f_0 \quad (2.3.28)$$

(Example: DC voltage battery charger).

The characteristic curve of these ideal sources are vertical lines in the  $f$ - $e$  diagram, since they are independent in each case of the other variable. The delivered power is

$$P(t) = e_0 f(t) \text{ or } P(t) = f_0 e(t) \quad (2.3.29)$$

The potential or the flow usually can be manipulated by an actuator with a control variable, see Figure 2.5a. Because of internal losses or losses of the actuator, the characteristic curves of real sources decline in comparison to the ideal characteristic curve, as some examples show in Table 2.6.

#### d) Storages

Table 2.7 first shows some examples of constitutive equations of storage elements. Special equations result for the storage elements dependent on the components of the energy storages and due to the different physical laws. The elementary state equations can be partially shaped to the generalized balance equation (2.3.14). This is treated in Section 2.4 for mechanical, thermal and electrical storages.

For energy storages, the stored energy in time  $dt$  is then

$$dQ_s(t) = dE_s(t) = P(t)dt = f(t)e(t)dt \quad (2.3.30)$$

Due to the physical laws of the electrical and mechanical storage elements, the variables of flow  $f(t)$  and potential difference  $e(t)$  depend on each other, see Table 2.7. It can be distinguished:

1. *potential storage.* The stored size is proportional to the accumulated flow

$$e(t) = \frac{1}{C} \int f(t)dt \text{ or } C \frac{de(t)}{dt} = f(t) \quad (2.3.31)$$

Then, it follows that with (2.3.30)

$$dQ_s = C \frac{de(t)}{dt} e(t) dt = C e de \quad (2.3.32)$$

and the stored energy becomes

$$Q_s = C \int_0^{e_0} e de = \frac{1}{2} C e_0^2 \quad (2.3.33)$$

The stored energy depends thus only on the potential. Therefore, this storage is called potential storage. The stored energy is potential energy;

Table 2.7. Storage elements: examples and constitutive equations of energy and mass storages

kind of process	mechanical	electrical	thermal	hydraulic
storage elements	spring	capacitance	heat storage	fluid storage
stored variable				
constitutive equation	$F = c z$ $F = c \int v \, dt$	$I = IC \frac{dV}{dt}$ $V = \frac{1}{C} \int I \, dt$	$\dot{Q} = mc_p \frac{dT}{dt}$ $T = \frac{1}{mc_p} \int \dot{Q} \, dt$	$\dot{m} = A\rho \frac{dH}{dt}$ $H = \frac{1}{A\rho} \int \dot{m} \, dt$
stored energy	$\frac{1}{2} c z_0^2$	$\frac{1}{2} CV_0^2$	$mc_p T_0$	$A\rho H$
storage elements	moved mass	inductance		
stored variable			magnetic energy	
constitutive equation	$F = m \frac{dv}{dt}$ $v = \frac{1}{m} \int F \, dt$	$V = L \frac{dI}{dt}$ $I = \frac{1}{L} \int V \, dt$		
stored energy	$\frac{1}{2} mv_0^2$	$\frac{1}{2} LI_0^2$		

2. flow storage. The flow is proportional to the accumulated potential

$$f(t) = \frac{1}{L} \int e(t) \, dt \text{ or } L \frac{df(t)}{dt} = e(t) \quad (2.3.34)$$

Then applies

$$dQ_s(t) = L \frac{df(t)}{dt} f(t) \, dt = L f df \quad (2.3.35)$$

and the stored energy becomes

$$Q_s(t) = L \int_0^{f_0} f \, df = \frac{1}{2} L f_0^2 \quad (2.3.36)$$

The stored energy depends only on the flow. The storage is therefore called flow storage. The stored energy is kinetic energy. Some examples are given below for illustration:

### **Example 2.1.** Electrical and mechanical storages

#### a) *Electrical components*

Stored energy per time interval  $dt$  yields with the current  $f = I$  and the voltage  $e = V$

$$dQ_s(t) = V(t)I(t)dt \quad (2.3.37)$$

A *capacitor* behaves according to the charge law

$$I(t) = C \frac{dV(t)}{dt} \quad \text{resp.} \quad V(t) = \frac{1}{C} \int I(t)dt \quad (2.3.38)$$

For the stored energy, it holds that

$$dQ_s = C V dV \quad (2.3.39)$$

The stored energy thus only depends on the voltage and the capacity, and it is

$$Q_s = C \int_0^{V_0} V \, dV = \frac{1}{2} C V_0^2 \quad (2.3.40)$$

The capacitor is thus a potential storage. For *inductance*, the induced voltage is

$$V(t) = L \frac{dI(t)}{dt} \quad \text{resp.} \quad I(t) = \frac{1}{L} \int V(t) dt \quad (2.3.41)$$

For the stored energy, it holds that

$$dQ_s = L I \, dI \quad (2.3.42)$$

$$Q_s = L \int_0^{I_0} I \, dI = \frac{1}{2} L I_0^2 \quad (2.3.43)$$

The inductance is thus a flow storage.

#### b) *Mechanical components*

Stored energy per  $dt$  in mechanical systems is with the force  $e = F$  and the velocity  $f = v$

$$dQ_s(t) = F(t)v(t)dt \quad (2.3.44)$$

For a linear spring, it holds that

$$F(t) = c \cdot z(t) = c \int v(t) dt \quad (2.3.45)$$

For the stored energy, it follows that

$$dQ_s = c \cdot z \cdot dz \quad (2.3.46)$$

$$Q_s = c \int_0^{z_0} z dz = \frac{1}{2} c \cdot z_0^2 \quad (2.3.47)$$

The spring is thus a potential storage and stores potential energy. For the moved mass, applies accordingly

$$F(t) = m \frac{dv(t)}{dt} \quad \text{resp.} \quad v(t) = \frac{1}{m} \int F(t) dt \quad (2.3.48)$$

The stored energy becomes

$$dQ_s = m \cdot v \cdot dv \quad (2.3.49)$$

$$Q_s = m \int_0^{v_0} v \cdot dv = \frac{1}{2} m \cdot v_0^2 \quad (2.3.50)$$

The moved mass is a flow storage and stores kinetic energy. □

### e) Transformers

A selection of constitutive relations for transformers is shown in Table 2.8. If one represents the transformer as two-port network, see Figure 2.13b, the power balance of a loss-free transformer may be written as

$$P_1 - P_2 = 0 \quad (2.3.51)$$

and with (2.3.16), it follows that

$$f_1 e_1 - f_2 e_2 = 0 \quad (2.3.52)$$

This means that the power  $f_1 e_1$ , which flows at the input port into the transformer, leaves it again as power  $f_2 e_2$  at the output port.

Table 2.8 shows for the special case of static behavior that the potential differences of the transformers are proportional to each other

$$e_2 = i \cdot e_1 \quad (2.3.53)$$

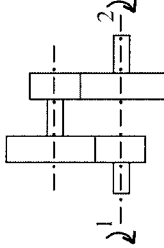
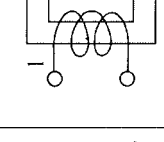
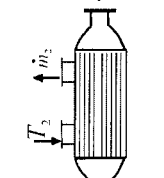
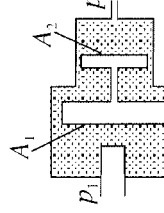
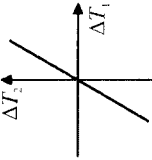
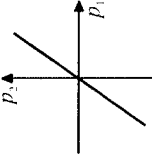
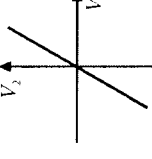
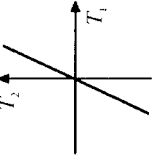
where  $i$  is the transfer factor. By using (2.3.52), it follows that for the flows

$$f_2 = \frac{1}{i} f_1 \quad (2.3.54)$$

The output flow  $f_2$  is thus inversely proportional to the transfer factor  $i$ . (However, if one considers the dynamic behavior, the differences of potential and flows are also coupled, see the examples of the transmissions in Section 4.6.) Hence, with idealized assumptions, one obtains a linear relationship. When losses occur, increasing deviations arise from the idealized characteristics dependent on the transferred power.

Figures 2.17a and b shows the resulting signal flow diagram for the static behavior of some idealized transformers. Here, the respective inputs (independent variables) are  $e_1, f_2$  or  $e_2, f_1$ .

Table 2.8. Transformers: examples and constitutive equations

kind of process	mechanical	electrical	thermal	hydraulic
transformer element	transmission transformer		heat exchanger	pressure transmission
				
kind of transformation		magnetism	heat transfer	pressure transmission
state equation	$T_2 = iT_1$ $\omega_2 = \frac{1}{i}\omega_1$	$V_2 = iV_1$ $I_2 = \frac{1}{i}I_1$	$\Delta T_1 = \frac{c_p \dot{m}_2}{c_p \dot{m}_1} \Delta T_2 = i \Delta T_2$	$p_2 = i p_1; i = \frac{A_1}{A_2}$ $v_2 = v_1$
characteristics				
				
				

### f) Converters

Table 2.9 shows some examples of converters, in which the constitutive equations exhibit a large variation. In the case of the idealized view of static behavior, a simple structure results for some special converters: each potential difference is coupled with a flow

$$e_2 = g_1(f_1) ; e_1 = h_1(f_2) \quad (2.3.55)$$

For the generator applies, e.g.,

$$e_2 = g_1 f_1 ; e_1 = g_1 f_2 \quad (2.3.56)$$

see Figures 2.17c and d.

These relations show, compared with the appropriate relations (2.3.53), (2.3.54) of the transformer, that potential  $e_1$  and flow  $f_1$  are interchanged. The appropriate converters are called *gyrators*, since a one-side supported gyroscope approximately follows these equations, see, e.g., Karnopp *et al.* (1990). A direct current motor leads to the structures shown in Figures 2.17e and f. A direct coupling of the variables  $f_2$ ,  $e_2$  or  $e_1$ ,  $f_1$  is added by the armature resistance. If one neglects the armature resistance, a gyrator structure will result.

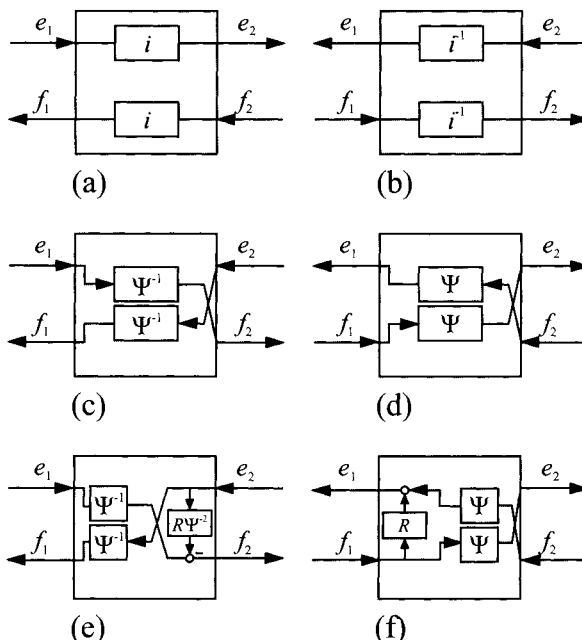


**Figure 2.17.** Signal flow diagrams for the static behavior of some two-port network processes with different inputs: (a), (b) transformer: transmission, transformer ( $i$  transfer factor); (c), (d) converter: generator (gyrator structure); (e), (f) converter: direct current motor ( $\Psi$  magnetic flux linkage,  $R$  armature resistance).

For (c) and (e) the inputs are the armature voltage  $e_1$  and the torque  $e_2$  and the outputs are the armature current  $f_1$  and the angular speed  $f_2$ ; for (d) and (f) the inputs are the armature current  $f_1$  and the angular speed  $f_2$  and the outputs are the armature voltage  $e_1$  and the torque  $e_2$ .

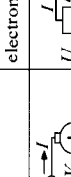
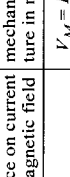
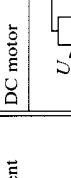
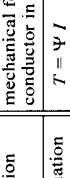
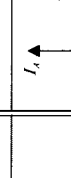
Generally, however, for converters, currents and potential differences are dependent on each other in a different way. Therefore, it is usually advisable to regard the special case. For the representation of the characteristics of the individual process elements, there are usually several possibilities for two-port networks. It is recommended, however, to represent the characteristic curves for the currents and potential differences at the input in the form  $e_1(f_1)$  and at the output in the form  $e_2(f_2)$ , since in this representation the intersection of the characteristic curves of the stationary operating points can be directly obtained for interconnected process elements, see Example 2.4.

*Active converters* allow the control of the conversion process of the input quantity into the output quantity by an actuator, which is controlled by an auxiliary quantity, see Figure 2.13e. In Table 2.10, some examples are presented. Through an actuator, for example, an electrical voltage (or fluid pressure, or strength) or an electrical current (or fluid flow, or heat flow) is controlled. The actuator energy needed for the control is usually small compared to the energy flow of the conversion. The resulting characteristic curve of the active converter then depends on the cooperation of actuator and converter.

**Table 2.9.** Converters: examples and constitutive equations

kind of process	electrical-mechanical	mechanical-electrical	mechanical-hydraulic	mechanical-pneumatic
converter element	moved conductor in magnetic field	generator	circular pump	fan
kind of conversion				
constitutive equation	$F = BlI$ $V_I = Blv$ $Rl = V - V_I$	$\frac{V_I}{I} = \Psi \omega$ $T = \Psi I$	$p = c_1 \omega^2 - c_2 \dot{m}$ $- c_3 \dot{m}^2$	$T(\omega, m)$ $P(\dot{m}, \omega)$
characteristics	  			
symbols	$l$ length $B$ magnetic flux density $R$ resistance $I$ current $V$ voltage $v$ speed	$V$ induced voltage $\Psi$ flux linkage $\omega$ frequency $T$ torque	$p$ head (pressure difference) $\omega$ frequency $\dot{m}$ mass flow $T$ torque	$P$ head (pressure difference) $\omega$ frequency $\dot{m}$ mass flow $T$ torque

Table 2.10. Active converters (converters with actuator): examples and constitutive equations

kind of process	electrical-mechanical	electrical-mechanical	hydraulic-mechanical	hydraulic-mechanical	thermodynamic-mechanical
converter element	DC motor	electromagnet	hydraulic piston-cylinder	combustion engine	
					
kind of conversion	mechanical force on current conductor in magnetic field	mechanical force on armature in magnetic field	mechanical force on piston through fluidic pressure	fuel combustion in cylinder	
constitutive equation	$T = \Psi I$ $T = c_1 V_A - c_1 \omega$	$V_M = RI$ $F = F(U, \omega)$	$F = A p_i$ $\dot{z} = m/A \cdot p$	$\dot{Q}_B = m_B (U) H_u$ $T = T(U, \omega)$	
characteristics					
symbols	$T$ $\omega$ $V_A$ $I_A$	$V_M$ $I$ $F$ $Y$ $U$	$V_M$ $I$ $F$ $Y$ $U$	$F$ $z$ $\dot{m}$ $p_V$ $p_i$ $A$ $U$	$\dot{m}_B$ $H_u$ $T$ $\omega$ $U$ $\dot{Q}_B$

### 2.3.3 Phenomenological Equations

In the case of sinks and losses in some transformers and converters, the internal process runs only in one direction and is not reversible (without additional energy supply). Examples are thermal conduction, diffusion or chemical reaction. The appropriate processes are characterized by irreversible equalization processes with increasing entropy. The reasons for the entropy increase are the dissipation of mechanical and electrical power, the exchange of mass and heat and chemical reactions, Ahrendts (1989). Thus, dissipative systems can be represented as sinks, Table 2.11. The irreversible transients are described by phenomenological equations. Some examples are outlined below:

a) *Fourier's law of heat conduction*

$$\dot{q}_z = -\lambda \frac{\partial T}{\partial z} = -\lambda \text{ grad}_z T \quad (2.3.57)$$

( $\dot{q}_z$  (heat flow density,  $\lambda(k)$  thermal conductivity,  $T$  temperature,  $z$  space coordinate)).

b) *Fick's law of diffusion*

$$\dot{m}_z = -D \frac{\partial c}{\partial z} = -D \text{ grad}_z c \quad (2.3.58)$$

( $\dot{m}_z$  (mass flow density,  $D$  diffusion coefficient,  $c$  concentration)).

c) *Chemical reaction law*

A first order reaction  $A_i \rightarrow B_i$  with  $c_{Ai}$  and  $c_{Bi}$  for the concentrations yields

$$r_z = -k c_{Ai} \left[ \frac{\text{kmol}}{\text{m}^3 \text{s}} \right] \quad (2.3.59)$$

$$k = k_\infty e^{-\frac{E}{RT}} \quad (\text{Arrhenius law}) \quad (2.3.60)$$

( $r_z$  reaction rate,  $k$  reaction rate coefficient,  $c_{Ai}$  concentration of component  $A_i$ ,  $E$  activation energy,  $k_\infty$  frequency factor).

d) *Ohm's law of electrical current*

$$i_z = -\kappa \frac{\partial u}{\partial z} = -\kappa \text{ grad}_z u \quad (2.3.61)$$

( $i$  current density,  $\kappa$  conductivity =  $1/\rho$ ,  $\rho$  specific resistance,  $[\Omega/m]$ ,  $\text{grad}_z u [V/m]$  ).

e) *Resistance laws for fluid flows*

Assuming laminar flow conditions (Reynold's number

$Re = v D/\nu < 2320$ ), the pressure loss is

$$\Delta p = -c_{Rl}v \quad \text{resp.} \quad v = \frac{1}{c_{Rl}} \Delta p$$

$$c_{Rl} = 32 \rho v \frac{l}{D^2} \quad (2.3.62)$$

and in the case of turbulent flow ( $Re > 2320$ )

$$\Delta p = -c_{Rt}v^2 \quad \text{resp.} \quad v = \frac{1}{\sqrt{c_{Rt}}} \sqrt{\Delta p}$$

$$c_{Rt} = 0.1582 \rho \frac{l}{D} Re^{-0.25} \quad (2.3.63)$$

( $\Delta p$  pressure loss,  $v$  velocity,  $\rho$  density,  $\nu$  kinematic viscosity,  $l$  length,  $D$  diameter,  $c_R$  resistance coefficient).

Some phenomenological equations ((a), (b), (d), (e) (laminar)) are composed as follows

$$\text{flow density} = -\frac{1}{\text{specific resistance}} \text{ potential gradient.} \quad (2.3.64)$$

They are linear in a relatively wide range.

#### f) General sinks, dissipative converters

Phenomenological equations show partially linear behavior, e.g., in the case of viscous dampers or Ohm's resistances, and partially strong non-linear behavior as in the case of throttles or friction, see Table 2.11. In the linear case, when using the one-port representation, e.g., the resistance equation applies

$$f_1 = \frac{1}{R} e_1 \quad (2.3.65)$$

where  $R$  is the resistance coefficient. (The negative sign in (2.3.64) is necessary because the gradient is used with regard to the location. With the assumed definition of the signs of the potential differences at the terminal pairs of a one-port, Figure 2.13, the positive sign has to be used in (2.3.65), since  $f_1$  is a flow into the one-port element, if  $e_1$  is positive.)

Dry friction has a direction-dependent discontinuous characteristic curve

$$F = F_{G0} \quad \dot{z} > 0$$

$$F = -F_{G0} \quad \dot{z} < 0 \quad (2.3.66)$$

This leads to force-displacement characteristics in the form of rectangular hysteresis characteristics, whose range depends on the amplitude  $z_0$ , Figure 2.18.

Table 2.11. Dissipative converters (sinks): examples and constitutive equations

kind of process	mechanical	mechanical	electrical	hydraulic	thermal
converter element	damper	friction	resistance	throttle	heat conductor
designation	viscous damping	Coulomb friction	Ohm's law	hydraulic resistance	Fourier's law
	$F = d \dot{z}$ $\dot{z} = \frac{1}{d} F$	$F = \mu F_n \operatorname{sign} z$	$V = RI$ $I = \frac{1}{R} V$	$p = c_r m^2$ $\dot{m} = \frac{1}{c_r} \sqrt{p}$	$\dot{Q} = \frac{1}{R} V$
phenomenological equation					
symbols	$F$ $d$ $\dot{z}$	$F$ $\mu$ $F_n$	$V$ $I$ $R$	$p$ $\dot{m}$ $c_r$	$\dot{Q}$ $T$ $R$
part of conversion into heat	completely	completely	completely	large	—

The energy used during a cycle is

$$\begin{aligned} E &= \oint F \, dz = \int_A^B F_{G0} dz + \int_C^D (-F_{G0}) dz \\ &= 2 F_{G0} z_0 \end{aligned} \quad (2.3.67)$$

This dissipative energy is converted completely into heat.

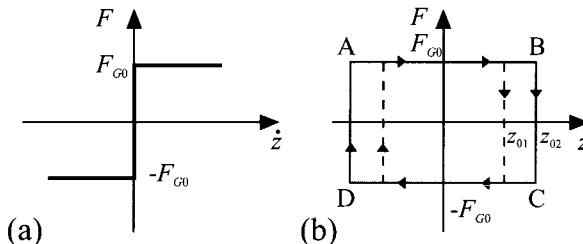


**Figure 2.18.** Discontinuous friction force characteristics: (a) characteristic curve of the dry friction  $F(\dot{z})$  (b) hysteresis curve of  $F(z)$

Table 2.12 gives an overview of the typical characteristics for all five types of process elements. Thereby, simple process elements are considered where only energy flow occurs. With the help of this representation in the form of symbols, multi-ports, basic equations and corresponding characteristics, it is possible to partition a process and to model a process systematically by using the treated generalized laws.

## 2.4 ENERGY BALANCE EQUATIONS FOR LUMPED PARAMETER PROCESSES

The balance equations presented in Section 2.3.1 result from the conservation laws of physics and have, in principle, the general form as presented in (2.3.14). In the following, the energy balance equations for mechanical, thermodynamic and electrical processes are discussed in detail and are presented in a way that is appropriate for a systematic modeling approach. For those cases, some special features are to be considered.

### 2.4.1 Energy Balance for Mechanical Systems

Modeling of complex mechanical systems is treated in more detail in Chapter 3 according to the principles of mechanics. In this section, in connection with the balance equations, the two energy forms of mechanical systems, potential and kinetic energy, are discussed, in order to integrate them into the general modeling approach. Additionally, the

interaction with two frequently appearing coupled energy storages is considered.

**Table 2.12.** Process elements with energy flows in one-port and two-port representation (constitutive and phenomenological equations for simple cases)  $e$  potential difference;  $f$  flow

process element	source	storage	transformer	converter	sink
symbolic presentation (energy flows)					
multi-port presentation					
basic equations	<p>potential source:  <math>e = e_o</math></p> <p>flow source:  <math>f = f_o</math></p>	<p>potential storage:  <math>e_1(t) = c_p(f_1(t) - f_2(t))dt</math>  <math>e_1(t) = e_2(t)</math></p> <p>flow storage:  <math>f_1(t) = c_p(e_1(t) - e_2(t))dt</math>  <math>f_1(t) = f_2(t)</math></p>	<p>potential transformation:  <math>e_2 = ie_1</math>  <math>e_2 = g f_1</math></p> <p>flow transformation:  <math>f_2 = \frac{1}{R}f_1</math></p>	<p><math>e_2 = \frac{1}{R}e</math></p>	
characteristics					

### a) Potential energy of translation

It is assumed that an external impressed force  $\mathbf{F}^{(e)}$  with a potential  $E_p$  acts on a body, Figure 2.19a. For this force in the coordinate system  $x, y, z$  holds (3.1.6). It acts on the position vector  $\mathbf{r}$ , (3.1.7). The performed work between point  $A$  and point  $B$  is then

$$\begin{aligned} W &= \int_A^B \mathbf{F}^{(e)T} d\mathbf{r} \\ &= \int_A^B F_x dx + F_y dy + F_z dz \end{aligned} \quad (2.4.1)$$

If the potential  $E_p(x,y,z)$  equals

$$-dE_p = F_x dx + F_y dy + F_z dz \quad (2.4.2)$$

then the resulting work

$$W = \int_A^B -dE_p = - (E_{pB} - E_{pA}) \quad (2.4.3)$$

is independent of the trajectory between the points  $A$  and  $B$ . The external force  $\mathbf{F}^{(e)}$  is called conservative and  $E_p(x,y,z)$  is the force potential, also called the potential energy.

The total differential of the potential

$$dE_p = \frac{\partial E_p}{\partial x} dx + \frac{\partial E_p}{\partial y} dy + \frac{\partial E_p}{\partial z} dz \quad (2.4.4)$$

results from (2.4.2)

$$F_x = - \frac{\partial E_p}{\partial y} \quad F_y = - \frac{\partial E_p}{\partial x} \quad F_z = - \frac{\partial E_p}{\partial z} \quad (2.4.5)$$

Introducing the gradient

$$\text{grad } E_p = \frac{\partial E_p}{\partial x} \mathbf{e}_x + \frac{\partial E_p}{\partial y} \mathbf{e}_y + \frac{\partial E_p}{\partial z} \mathbf{e}_z \quad (2.4.6)$$

with the unit vectors according to (3.1.6) leading in vector notation from (2.4.5) to

$$\mathbf{F}^{(e)} = - \text{grad } E_p \quad (2.4.7)$$

Therefore, the applied external force in a conservative system equals the negative gradient of the potential.

Considering a closed trajectory in a potential, the performed work according to (2.4.1) is

$$\begin{aligned} W &= \oint \mathbf{F}^{(e)T} d\mathbf{r} = \int_A^B \mathbf{F}^{(e)T} d\mathbf{r} + \int_B^A \mathbf{F}^{(e)T} d\mathbf{r} \\ &= 0 \end{aligned} \quad (2.4.8)$$

Then it is not necessary to add or remove energy: the potential energy remains unchanged.

A first example for the potential is the gravitation potential of the earth

$$E_p = G z = mg z \rightarrow \text{grad } E_p = mg$$

A second example is the spring force

$$E_p = \int_0^z c z \, dz = \frac{c}{2} z^2 \rightarrow \text{grad } E_p = c z$$

### b) Kinetic energy of translation

If an external force  $\mathbf{F}$  acts on a body with mass  $m$  and momentum

$$\mathbf{I} = m\mathbf{v} \quad (2.4.9)$$

then according to Newton's second law of momentum, see Section 3.1 and Figure 2.19b, it holds that for a *translation* that

$$\frac{d\mathbf{I}(t)}{dt} = \frac{d}{dt}[m(t)\mathbf{v}(t)] = \mathbf{F}(t) \quad (2.4.10)$$

and for  $m = \text{const.}$

$$\frac{d\mathbf{I}(t)}{dt} = m \frac{d\mathbf{v}(t)}{dt} = \mathbf{F}(t) \quad (2.4.11)$$

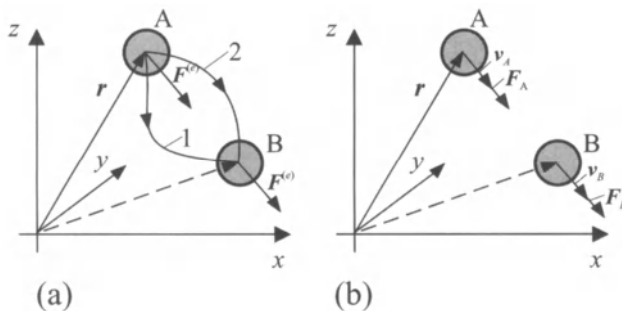


**Figure 2.19.** Illustration for the energy conservation law of mechanical systems: (a) external force acting on a body with potential  $E_p$ ; (b) force acting on a mass  $m$  with kinetic energy  $E_k$

If, e.g., a driving force  $F_1(t)$  and a resistance force  $F_2(t)$  are acting in a moving direction (scalar, one-dimensional case), then

$$F_1(t) - F_2(t) = \frac{d\mathbf{I}(t)}{dt} = m \frac{d\mathbf{v}(t)}{dt} \quad (2.4.12)$$

(2.4.10) is also called a *momentum balance equation* and is the vector notation of the generalized balance equation (2.3.14).

The force  $\mathbf{F}$  in (2.4.10), which modifies the momentum, leads to the work increment

$$dW = \mathbf{F}^T(t)dr = m \frac{dw^T(t)}{dt} dr \quad (2.4.13)$$

Inserting  $dr(t) = w(t)dt$  yields

$$\begin{aligned} dW &= m dv^T v(t) = m v^T(t) dv(t) \\ &= m (v_x(t)dv_x + v_y(t)dv_y + v_z(t)dv_z) \end{aligned} \quad (2.4.14)$$

thus leading to the work between two trajectory points A and B

$$\begin{aligned} W &= \int_A^B m v^T(t) dv = m \left[ \frac{v_x^2}{2} + \frac{v_y^2}{2} + \frac{v_z^2}{2} \right] \Big|_A^B \\ &= \frac{m}{2} [(v_{xB}^2 - v_{xA}^2)^2 + (v_{yB}^2 - v_{yA}^2) + (v_{zB}^2 - v_{zA}^2)] \end{aligned} \quad (2.4.15)$$

where

$$E_k = \frac{m}{2} v^2 = \frac{m}{2} [v_x^2 + v_y^2 + v_z^2] \quad (2.4.16)$$

is the kinetic energy of the moving mass. This leads to

$$W = E_{kB} - E_{kA} \quad (2.4.17)$$

thus resulting in the *principle of work*: the work that has to be carried out between the two points of the trajectory of a moving mass is equal to the change of the kinetic energy.

If the acting force is an externally applied conservative force  $\mathbf{F}^{(e)}$ , then it results from (2.4.3) and (2.4.14)

$$- (E_{pB} - E_{pA}) = E_{kB} - E_{kA}$$

or

$$E_{pA} + E_{kA} = E_{pB} + E_{kB} = \text{const.} \quad (2.4.18)$$

From this follows the *law of conservation of energy for conservative mechanical systems*:

If the externally applied forces have a potential, then the sum of kinetic and potential energy of a moved mass is constant.

$$E_p + E_k = \sum_{i=p}^k E_i(t) = E_0 = \text{const.} \quad (2.4.19)$$

potential energy      kinetic energy

Differentiating yields the *energy flow balance equation* for conservative mechanical systems

$$\begin{array}{ccc} \frac{dE_p(t)}{dt} & + & \frac{dE_k(t)}{dt} = 0 \\ \text{potential} & & \text{kinetic} \\ \text{energy flow} & & \text{energy flow} \end{array} \quad (2.4.20)$$

Friction forces are not conservative but are *dissipative forces* that transfer work into heat. In this case, the law of energy conservation as stated in (2.4.19) does not apply.

### Example 2.2. Spring-mass system

A spring-mass system is considered, according to Figure 2.20, to be a system with two energy storages. The energy flow between mass and spring is, according to (2.3.30)

$$\frac{dQ_s(t)}{dt} = F(t)v(t)$$

where  $e = F$  is a force and  $f = v$  is the velocity.

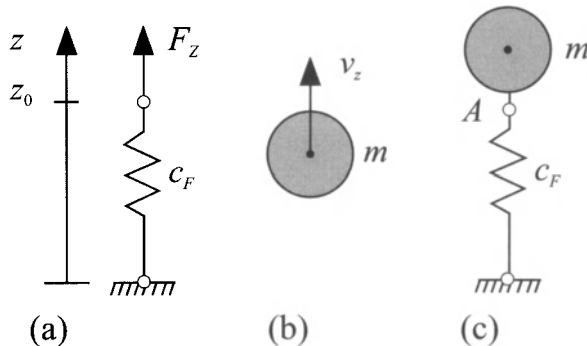


**Figure 2.20.** Mechanical energy storages (examples): (a) spring as storage for potential energy; (b) mass as storage for kinetic energy; (c) spring-mass-damper system: storage for potential and kinetic energy

In Section 2.3, it has been shown that the variables force (potential difference) and velocity (flow) are not independent for these energy storages.

Considering energy flows for the spring holds, according to (2.3.46)

$$\frac{dQ_{sF}(t)}{dt} = c z(t) \frac{dz(t)}{dt}$$

and for the mass, according to (2.3.49)

$$\frac{dQ_{sm}(t)}{dt} = m v(t) \frac{dv(t)}{dt}$$

Hence, with the energy flow balance equation (2.4.20) results

$$c z(t) \frac{dz(t)}{dt} + m \frac{dv(t)}{dt} \frac{dz(t)}{dt} = 0$$

and in the case  $dz(t)/dt \neq 0$

$$c z(t) = - m \frac{dv(t)}{dt}$$

or

$$m \ddot{z}(t) + c z(t) = 0$$

However, this equation may be directly derived from the physical state equations for storages and the force balance equation (node equation) as an interconnection condition for point *A*, Figure 2.20c. Thus, this approach, in the case of one or some few masses, is simpler than using the principle of energy flow balance.

□

### c) Kinetic energy of rotation

In the case of rotation, the *angular momentum balance equation* holds

$$\frac{d\mathbf{L}_{s(t)}}{dt} = \frac{d}{dt} [\mathbf{J}(t)\boldsymbol{\omega}(t)] = \mathbf{T}(t) \quad (2.4.21)$$

where the angular momentum is

$$\mathbf{L}_s = \mathbf{J} \boldsymbol{\omega} \quad (2.4.22)$$

with  $J$  the inertia tensor and  $T$  the torque vector. In the scalar case

$$T_1(t) - T_2(t) = J \frac{d\omega(t)}{dt} \quad (2.4.23)$$

for  $J = \text{const.}$

The axial moment of inertia of a disc with thickness  $b$  and radius  $R$  is calculated from

$$J = \int_m r^2 dm = b \int_0^R 2\pi \rho r^3 dr = \frac{\pi}{2} \rho b R^4 = m \frac{R^2}{2} \quad (2.4.24)$$

## 2.4.2 Energy Balance for Thermal Systems (Rigid Bodies, Fluids)

A *solid body* is now considered as thermal energy storage that stores for a constant mass  $m$  and a constant specific heat value  $c_p$  and a temperature change  $dT$  the heat quantity

$$dQ_s(t) = dE_s(t) = m c_p dT = C_T dT \quad (2.4.25)$$

where  $C_T = m c_p$  is the thermal capacity. The heat flow into the storage is

$$\dot{Q}_s(t) = \frac{dQ_s(t)}{dt} = C_T \frac{dT}{dt} \quad (2.4.26)$$

From this, results

$$dQ_s(t) = C_T \frac{dT}{dt} dt \quad (2.4.27)$$

and by comparison with (2.3.16) it can be seen that it is not possible to define the variables  $f(t)$   $e(t) = P(t)$ . This relies on the fact that the heat

flow  $\dot{Q}$  is an energy flow and that there exists only a potential energy storage and no flow energy storage. The difference to the mechanical and electrical storages becomes evident by considering the stored energy that is proportional to the temperature  $T$

$$\dot{Q}_s = C_T \int_{T_1}^{T_2} dT = C_T (T_2 - T_1) \quad (2.4.28)$$

and not proportional to  $z_0^2, v_0^2, V_0^2, I_0^2$ , see Table 2.7.

(A representation  $f(t)e(t)$  for the energy flow, however, is obtained by using the entropy flow  $\dot{s}(t)$  and the absolute temperature  $T(t)$ , Ahrendts (1989), Karnopp *et al.* (2000).)

The temperature distribution inside a body follows the law of heat conduction. Assuming that the conduction of heat is infinitely fast, or that there is no thermal resistance, then each mass has at each position the same temperature  $T$ . This may be assumed if the solid body is a thin layer. In this case, it holds that for the heat flow balance, see Figure 2.21a

$$\dot{Q}_i(t) - \dot{Q}_o(t) = \frac{d}{dt} Q_s(t) \quad (2.4.29)$$

heat inflow	heat outflow	stored heat flow
-------------	--------------	------------------

with

$$\dot{Q}_s(t) = m \cdot c_p \frac{dT(t)}{dt}$$

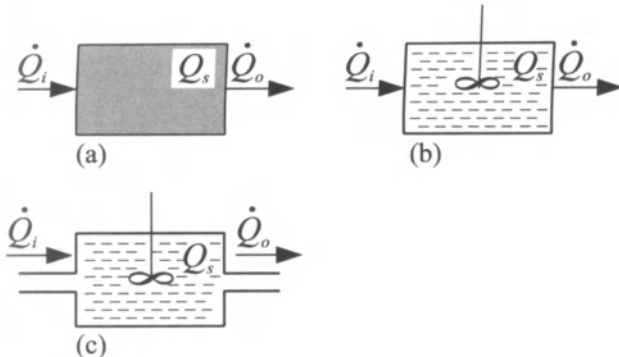


**Figure 2.21.** Energy balance of thermal systems: (a) solid body; (b) stationary incompressible fluid; (c) flowing fluid

The same relation holds if the heat storage element is a *stationary incompressible fluid*, which is ideally mixed, Figure 2.21b. If the heat storage is passed by a fluid flow, then the heat inflow and heat outflow are

$$\dot{Q}_i(t) = \dot{m}_i(t)c_p T_i(t)$$

$$\dot{Q}_o(t) = \dot{m}_o(t)c_p T_o(t)$$

Compare Figure 2.21c; (2.4.29) holds for an ideal mixture inside the storage and therefore it follows that

$$T_i(t) - T_o(t) = \frac{\dot{m}}{\dot{m}} \frac{dT(t)}{dt} \quad (2.4.30)$$

for  $\dot{m}_i = \dot{m}_o = \dot{m}$ .

### 2.4.3 Energy Balance for Gases and Steam

Gas and steam are compressible and therefore mechanical work occurs in combination with the compressibility. This leads to the introduction of enthalpy as a special energy measure.

- *Stationary gas quantity in a closed control volume*

$U$  denotes the internal energy of a resting body. It is the sum of all energies of a gas mixture in a closed control volume

$$U(t) = E_s(t) \quad (2.4.31)$$

The energy balance per time increment  $\Delta t$  then takes the general form

$$\Delta E_i(t) - \Delta E_o(t) = \Delta E_s(t) \quad (2.4.32)$$

For a gas quantity in a closed control volume, according to Figure 2.22, it results that from the first law of thermodynamics with  $\Delta t \rightarrow dt$

$$dQ(t) - dL(t) = dU(t) \quad (2.4.33)$$

Herewith,  $dQ$  is the supplied heat and  $dL$  is the performed mechanical work.

The mechanical work delivered during the expansion of the gas mixture becomes  $p = \bar{p} = \text{const.}$ , compare Figure 2.22

force	displacement	
$dL = \bar{p}A \cdot dz$		
$= \bar{p} \cdot dV$		(2.4.34)

From this, yields

$$L = \int_{V_1}^{V_2} pdV = \bar{p} \int_{V_1}^{V_2} dV = \bar{p}[V_2 - V_1] \quad (2.4.35)$$

respectively

$$L = \bar{p} \Delta V$$

$$dL = p dV$$

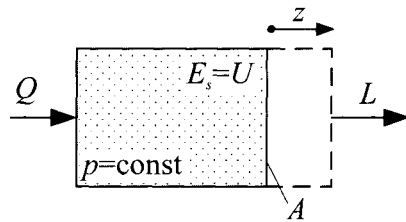


**Figure 2.22.** Energy balance of an expanding closed gas quantity

Consequently, the energy balance for an expanding gas mixture in a closed control volume with constant pressure becomes

$$dQ(t) - pdV(t) = dU(t) \quad (2.4.36)$$

where  $dL(t)$  is the displacement work.

● *Flowing gas quantity (technical thermodynamic process)*

For technical processes, generally flowing gas quantities are of interest and not closed gas quantities. Figure 2.23 shows the scheme of a thermodynamic process. On the left, gas is flowing into the system with internal energy  $U_i$  and, on the right, gas is flowing out of the system with internal energy  $U_o$ .

– Equilibrium state

For the equilibrium state it holds that

$$\frac{d}{dt}(\dots) = 0$$

(no energy storage) and therefore, according to the general energy balance equation (2.3.9)

$$\Delta E_i(t) - \Delta E_o(t) = 0$$

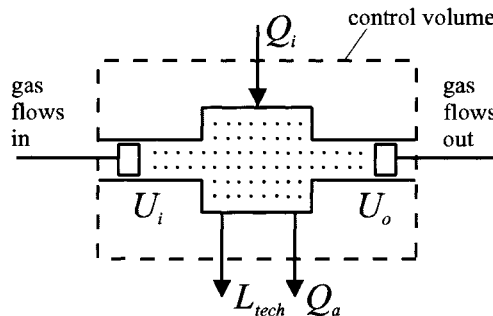


**Figure 2.23.** Energy balance of a flowing gas quantity of a thermodynamic process (e.g., power engine)

From the first law of thermodynamics (2.4.33), results accordingly

$$dQ - dL - dU = 0$$

Assuming lumped parameters, the energy balance equation is obtained for an increment  $\Delta t$

$$(Q_i - Q_o) + (L_i - L_o) + (U_i - U_o) = 0 \quad (2.4.37)$$

heat supplied change of  
supply external inner  
work energy

Without heat supply, it holds that

$$(Q_i - Q_o) = 0$$

and

$$(L_i - L_o) + (U_i - U_o) = 0 \quad (2.4.38)$$

For the external work, it follows that with (2.4.35)

$$(L_i - L_o) = -L_{tech} + p_i V_i - p_o V_o \quad (2.4.39)$$

delivered supplied delivered  
usable displacement work  
work

This results in the balance equation, according to (2.4.37)

$$p_i V_i - p_o V_o - L_{tech} + U_i - U_o = 0$$

or

$$(U_i + p_i V_i) - (U_o + p_o V_o) - L_{tech} = 0 \quad (2.4.40)$$

Introducing the enthalpy as a new state variable yields

$$H = U + pV \quad (2.4.41)$$

and the enthalpy balance equation (without heat supply) in the stationary case is

$$H_i - H_o - L_{tech} = 0 \quad (2.4.42)$$

The enthalpy  $H$  considers the inner energy  $U$  and the displacement work  $pV$ , which is necessary for maintaining the continuous operation.

Now, the *usable work* (also called *technical work*) is considered more closely.

From (2.4.41), results

$$dH = dU + pdV + Vdp$$

According to the first law of thermodynamics (2.4.36), it holds that

$$dU = dQ - pdV$$

and therefore

$$dH = dQ - pdV + pdV + Vdp$$

or

$$dH = dQ + Vdp \quad (2.4.43)$$

heat technical usable  
supply work

From this, results with  $dQ = 0$

$$dH = Vdp$$

From (2.4.42), yields the enthalpy balance equation

$$dH - dL_{tech} = 0$$

Therefore, without heat flow, it holds that

$$dL_{tech} = Vdp \text{ or } L_{tech} = \int_{p_o}^{p_i} Vdp \quad (2.4.44)$$

In the case of  $V=\text{const.}$ , one obtains for the usable work

$$L_{tech} = V \int_{p_o}^{p_i} dp = V(p_i - p_o) \quad (2.4.45)$$

The enthalpy balance equation with heat flow in the stationary case results from (2.4.37) and (2.4.39)

$$(H_i - H_o) - L_{tech} + (Q_i - Q_o) = 0 \quad (2.4.46)$$

### - Dynamic relationship

In the case of a dynamic state, the variables of (2.4.46) become time-dependent and therefore the storing of energy has to be considered according to (2.4.29).

The energy balance relation per  $\Delta t$  is therefore

$$\begin{aligned} \frac{\Delta H_i(t)}{\Delta t} - \frac{\Delta H_o(t)}{\Delta t} - \frac{\Delta L_{tech}(t)}{\Delta t} + \frac{\Delta Q_i(t)}{\Delta t} - \frac{\Delta Q_o(t)}{\Delta t} \\ = \frac{\Delta U(t)}{\Delta t} = \frac{\Delta E_s(t)}{\Delta t} \end{aligned} \quad (2.4.47)$$

With the limit consideration

$$\lim_{\Delta t \rightarrow dt} (\dots)$$

it holds that

$$\frac{dH_i(t)}{dt} = \dot{H}_i(t) \quad (\text{enthalpy flow})$$

and therefore

$$\dot{H}_i(t) - \dot{H}_o(t) - \dot{L}_{tech}(t) + \dot{Q}_i(t) - \dot{Q}_o(t) = \frac{d}{dt} U(t) \quad (2.4.48)$$

Introducing specific variables yields

$$\dot{H}(t) = \frac{dH(t)}{dt} = \frac{dH(t)}{dm} \frac{dm}{dt} = h(t) \dot{m}(t) \quad (2.4.49)$$

$$dU = \frac{dU}{dm} dm = u dm \quad (2.4.50)$$

with

$h(t)$ : specific enthalpy [J/kg]

$u(t)$ : specific inner energy [J/kg].

From this follows, by using (2.4.48), the *enthalpy balance equation for flowing gases and steam*

$$\dot{m}_i(t)h_i(t) - \dot{m}_o(t)h_o(t) - \dot{L}_{tech}(t) + \dot{Q}_i(t) - \dot{Q}_o(t) = \frac{d}{dt}[u(t)m_s(t)] \quad (2.4.51)$$

- $\dot{m}_i h_i$ : thermal energy flow into the system due to the fluid flow
- $\dot{m}_o h_o$ : thermal energy flow out of the system due to the fluid flow
- $\dot{L}_{tech}$ : technical power output
- $\dot{Q}_i$ : heat flow into the system
- $\dot{Q}_o$ : heat flow out of the system
- $\frac{d}{dt}(um_s)$ : stored energy flow.

#### Annotation:

- The term for the technical work (2.4.44) includes the potential and kinetic energy. They provoke a pressure difference  $dp$ :
  - (i) hydrostatic pressure difference  $-dp$ ;
  - (ii) pressure difference due to acceleration  $-dp$ .
- For the technical work caused by friction or throttling, it holds that

$$L_{tech} = \int_{p_i}^{p_o} V dp = + Q_e \quad (2.4.52)$$

supplied   delivered

$L_{tech}$  is the technical work that is delivered from the system and is supplied to it again in the form of (additional) heat  $Q_e$ . This has to be considered in the balance relation.

## 2.4.4 Energy Balance for Electrical Systems

The two energy forms of electrical systems, electrical and magnetic energy, occur in connection with the storage elements, capacitor and inductance.

For the energy flow stored in these components, it holds that

$$\frac{dQ_s(t)}{dt} = V(t)I(t) \quad (2.4.53)$$

It has been shown in Section 2.3 that the variables' voltage (potential difference) and current are not independent of each other for these storage elements but are coupled by physical state equations.

### Example 2.3. Electrical oscillating circuit

Now, as an example, an ideal oscillating circuit, Figure 2.24, is discussed. For the energy flow into the capacity, it then holds that

$$\frac{dQ_{sC}(t)}{dt} = V(t)I(t) = C V(t) \frac{dV(t)}{dt}$$

and for the inductance

$$\frac{dQ_{sL}(t)}{dt} = V(t)I(t) = L I(t) \frac{dI(t)}{dt}$$

The energy balance yields

$$Q_{sC}(t) + Q_{sL}(t) = Q_0 = \text{const.}$$

and for the energy flow balance equation, results

$$\frac{dQ_{sC}(t)}{dt} + \frac{dQ_{sL}(t)}{dt} = 0$$

From this, it follows that

$$C V(t) \frac{dV(t)}{dt} + L I(t) \frac{dI(t)}{dt} = 0$$

Because the voltage at the capacity equals the voltage at the inductance,  $V(t)$  may be replaced by

$$V(t) = L \frac{dI(t)}{dt}$$

and therefore it results that

$$L^2 C \frac{dI(t)}{dt} \frac{d^2 I(t)}{dt^2} + L I(t) \frac{dI(t)}{dt} = 0$$

and with  $dI(t)/dt \neq 0$  yields

$$L C \ddot{I}(t) + I(t) = 0$$

This equation may be directly derived from the physical state equation of both energy storages and the voltage balance (Kirchhoff's voltage law) as a coupling relation. As this way is simpler to apply than the utilization of the energy flow balance equations it should be preferred (in the case of a few components). Note the analogy to the spring-mass system in Section 2.4.1 (Example 2.2).

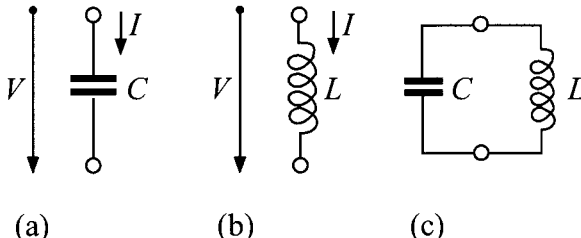


**Figure 2.24.** Energy balance of electrical systems: (a) capacitor; electric (electrostatic) energy; (b) inductance; electric (electromagnetic) energy; (c) electrical oscillating circuit

□

### 2.4.5 Common Properties of Balance Equations

The generalized flow balance equation

$$\dot{Q}_i(t) - \dot{Q}_o(t) = \frac{dQ_s(t)}{dt} \quad (2.4.54)$$

which was introduced in Section 2.3, is valid for storages of mass, energy (different types) and also for momentum in vector notation, see (2.4.12). Here,  $\dot{Q}(t)$  stands for a generalized flow with the following corresponding notations:  $\dot{Q} \triangleq M, \dot{Q} \triangleq \dot{E}; \dot{Q} \triangleq K$ . (In the field of fluid mechanics,  $\dot{Q}$  is also called “momentum flow”.)

The balance equations are basically linear and are represented as a sum element in the block diagram. If one is interested in the stored variable  $Q_s(t)$ , as an output an integral element succeeds the sum element, Figure 2.12. Without feedback, *integral behavior* is obtained.

Introducing relative variables and referring the variables to the equilibrium state (ES) denoted by  $\bar{Q}_s$  and  $\bar{Q}$ , leads to

$$\dot{q}(t) = \frac{\Delta \dot{Q}(t)}{\bar{Q}} ; q_s(t) = \frac{\Delta Q_s(t)}{\bar{Q}_s} \quad (2.4.55)$$

resulting in

$$\frac{\Delta \dot{Q}_i(t)}{\bar{Q}} - \frac{\Delta \dot{Q}_o(t)}{\bar{Q}} = \frac{\bar{Q}_s}{\bar{Q}} \frac{d}{dt} \left[ \frac{\Delta Q_s(t)}{\bar{Q}_s} \right]$$

respectively

$$\dot{q}_i(t) - \dot{q}_o(t) = T_q \frac{dq_s(t)}{dt} \quad (2.4.56)$$

with the integral action time

$$T_q = \frac{\bar{Q}_s}{\bar{Q}} = \frac{\text{stored quantities in ES}}{\text{flow in ES}} \quad (2.4.57)$$

Compare Figure 2.25 ( $T_q$  is not to be mistaken for the time constant of a first order time lag). Instead of referring to the equilibrium state, other variables might be chosen.

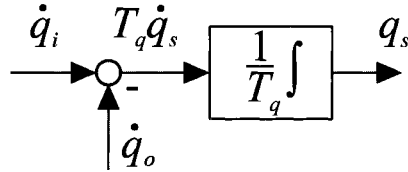


**Figure 2.25.** Signal flow representation of the balance equation of a process with lumped parameters and relative variables

Frequently, the stored variable  $Q_s$  influences the output flow  $\dot{Q}_o$  or the input flow  $\dot{Q}_i$ , either directly or by other process elements. Examples are (linearized):

- tank:  $\Delta \dot{M}_p(t) = c \Delta M_s(t)$
- throttle in a fluid flow:  $\Delta \dot{M}_o(t) = c \Delta p(t)$
- viscous friction:  $\Delta F_2(t) = c \Delta v(t)$
- electrical resistance:  $\Delta V(t) = c \Delta I(t)$

The feedback by the constant  $c$  is then for small deviations in general form, cf. Figure 2.26

$$\Delta \dot{Q}_o(t) = c \Delta Q_s(t) \quad (2.4.58)$$

and with the balance equation for small deviations

$$\Delta \dot{Q}_i(t) - \Delta \dot{Q}_o(t) = \frac{dQ_s(t)}{dt} \quad (2.4.59)$$

results

$$T \Delta \dot{Q}_s(t) + \Delta Q_s(t) = K \Delta \dot{Q}_i(t) \quad (2.4.60)$$

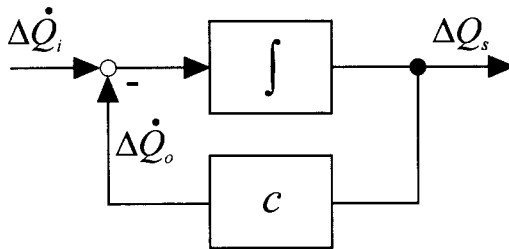
Hence, a proportional acting first order time delay with time constant

$$\begin{aligned} T &= \frac{1}{c} = \frac{\Delta Q_s(t)}{\Delta \dot{Q}_o(t)} \\ &= \frac{\text{change of stored variable}}{\text{change of outflow}} \end{aligned} \quad (2.4.61)$$

and gain

$$K = \frac{1}{c} \quad (2.4.62)$$

is obtained.

**Figure 2.26.** Storage with proportional acting feedback

After the termination of a transient state (e.g., step response) which started at a steady state for  $t = 0$  with  $\Delta \dot{Q}_i(0^-) = 0$ ;  $\Delta \dot{Q}_o(0^-) = 0$ ;  $\Delta Q_s(0^-) = 0$ , it results that as  $t \rightarrow \infty$

$$T = \frac{1}{c} = \frac{\Delta Q_s(\infty)}{\Delta \dot{Q}_o(\infty)} = \frac{\Delta Q_s(\infty)}{\Delta \dot{Q}_i(\infty)} \quad (2.4.63)$$

Both the time constant and the gain depend only on the feedback.

The interpretation of (2.4.61) only holds for one input flow or one output flow. For processes with multiple feedback, the interpretation of the time constant has to be modified. In Chapter 6, this is treated in more detail.

Introducing the relative variables

$$q_s(t) = \frac{\Delta Q_s(t)}{\bar{Q}_s}; \dot{q}(t) = \frac{\Delta \dot{Q}(t)}{\bar{Q}}$$

leads to

$$\frac{1}{c} \frac{dq_s(t)}{dt} + q_s(t) = \frac{1}{c} \frac{\bar{Q}}{\bar{Q}_s} \Delta \dot{Q}_i(t) \quad (2.4.64)$$

$$T = \frac{1}{c} \quad K = \frac{1}{c} \frac{\bar{Q}}{\bar{Q}_s}$$

The gain changes by introducing the relative variables. However, the time constant does not.

As the balance relations are basically linear, non-linear transfer elements result from non-linear relations in the forward path between the storage variable and the interested output variable  $Y(t)$

$$Y(t) = f_{NL}(Q_s(t))$$

see Figure 2.27a, or from non-linear relations in the feedback path between the output variable  $Y(t)$  and output flow

$$\dot{Q}_o(t) = f_{NL}(Y(t))$$

see Figure 2.27b.

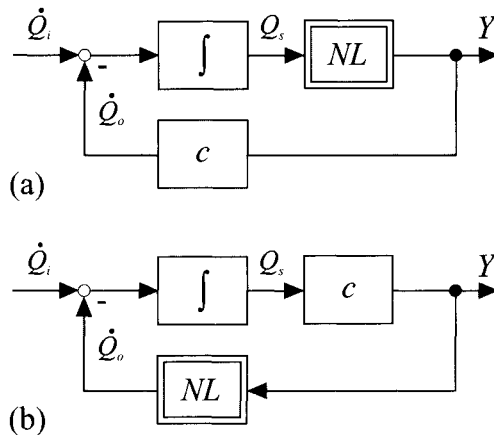


**Figure 2.27.** Storage elements with feedback: (a) non-linearity in the forward path; (b) non-linearity in the feedback path

## 2.5 CONNECTION OF PROCESS ELEMENTS

### 2.5.1 Node Equation and Mesh Equation

Up to now, the process elements have been treated separately. By interconnecting or coupling respectively, new conditions arise which depend on the type of interconnection. The two main connection types are the parallel connection and the serial connection.

Now, process elements are considered whose connections are characterized by an energy flow  $P = ef$ . A connection of two or more ports or terminals is called a *node*. A connection between two nodes is a *branch*.

For the parallel connection of two elements, according to Figure 2.28a, it holds that

$$\begin{aligned} e &= e_1 = e_2 \quad (\text{between node A and B}) \\ f_3 - f_1 - f_2 &= 0 \quad (\text{at node A}) \\ -f_3 + f_1 + f_2 &= 0 \quad (\text{at node B}) \end{aligned} \tag{2.5.1}$$

The total flow  $f_3$  before or after the node is composed of the sum of all flows into and out of the system, *i.e.*, the sum of all flows at each node respectively equals zero.

$$\sum_{i=1}^n f_i(t) = 0 \tag{2.5.2}$$

This equation is thus a *continuity equation*, which is also called a *node equation*. It is a flow balance equation for each node without storage of flow. This balance relation differs from the flow balance equations of Section 2.3.1 by the fact that previously, process elements (with lumped parameters) that store a flow were considered.

For a serial connection, according to Figure 2.28b,

$$\begin{aligned} f &= f_1 && \text{(at node A)} \\ f &= f_2 && \text{(at node B)} \\ e_3 &= e_1 + e_2 && \text{(between node A and B)} \end{aligned} \quad (2.5.3)$$

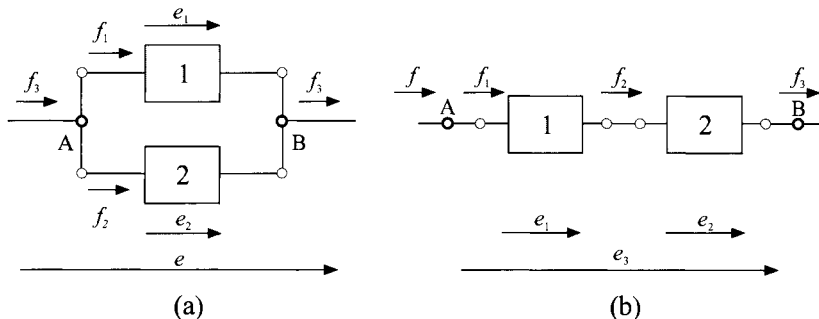


**Figure 2.28.** Interconnections of two process elements with energy flow  $P = ef$  as flown through blocks (equivalent diagram): (a) parallel connection; (b) serial connection

Thus, the flow through both elements is of the same size and the total potential difference equals the sum of all potential differences connected in series. Considering the potential differences of a closed loop (a mesh), the sum of all potential differences is zero.

$$\sum_{i=1}^n e_i(t) = 0 \quad (2.5.4)$$

This equation is a *compatibility equation* and is also called a *mesh equation*. In the case of electrical process elements, (2.5.2) and (2.5.4) are called *first* and *second Kirchhoff's law*.

Figure 2.29 shows the same interconnection as Figure 2.28 in a one-port (or two-pole) representation. In Figure 2.30, several elements are shown as flowing through blocks. They clarify again the node equation (2.5.2) of node B and the mesh equation (2.5.4).

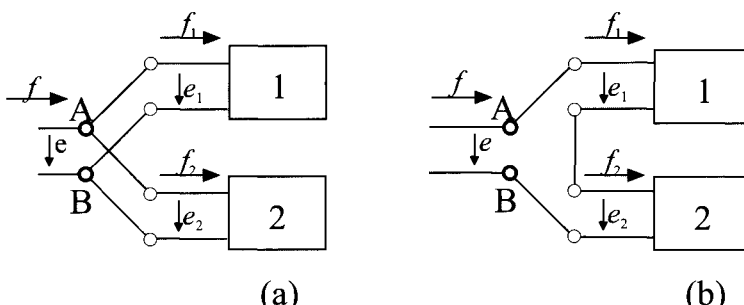


**Figure 2.29.** Interconnections of two process elements as a one-port representation (equivalent diagram): (a) parallel connection; (b) serial connection

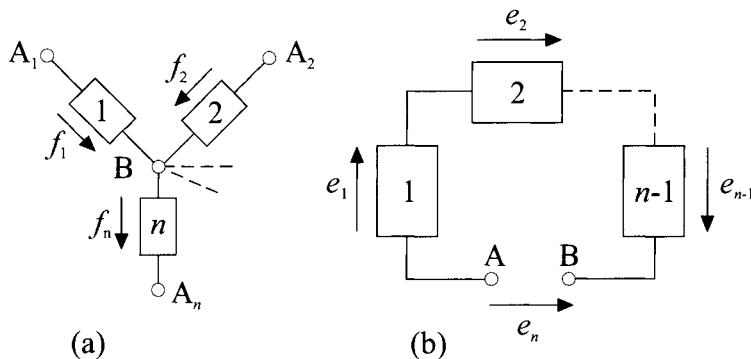


**Figure 2.30.** Arrangements of process elements for the continuity and the compatibility equation: (a) node B:  $\sum$  flows = 0; (b) mesh (loop) A-B-A:  $\sum$  potential differences = 0

Table 2.13 summarizes the corresponding equations for the different physical systems with energy and mass flows. A unified representation is obtained, which is characterized by the superposition of flows and potential differences. Hence, the interconnection equations are linear.

**Table 2.13.** Node and mesh equations for different systems with mass or energy flows

	system	node equation	mesh equation
a	electrical	$\sum I = 0$ 1. Kirchhoff's law	$\sum V = 0$ 2. Kirchhoff's law
b	magnetic	$\sum \Phi = 0$ magnetic flux balance eq.	$\sum \Theta = 0$ magnetomotance compatibility
c	mechanical (translation)	$\sum F = 0$ force balance eq.	$\sum v = 0$ kinematic equation
d	mechanical (rotation)	$\sum T = 0$ torque balance eq.	$\sum \omega = 0$ kinematic equation
e	hydraulic – incompressible – compressible	$\sum \dot{V} = 0$ volume flow balance eq. $\sum \dot{m} = 0$ mass flow balance eq.	$\sum p = 0$ $\sum p = 0$ pressure compatibility
f	thermal – convection fluid – thermal conduction	$\sum \dot{Q} = 0$ heat flow balance eq.	$\sum T = 0$ temperature compatibility
g	chemical	$\sum \dot{m}_i = 0$ mass flow balance eq.	

The corresponding node relations result from the general balance relations of process elements with lumped parameters if the storage capacity is set to zero, *i.e.*, without storage. For this reason, the node equation for mechanical systems may be derived from the principle of linear momentum if the mass is set to zero. This also results from d'Alembert's principle (3.2.3).

In the case of hydraulic systems, the mechanical energy flow, according to Table 2.3, is the product of volume flow  $\dot{V}$  and pressure difference  $p$ . The node equation therefore uses the volume flow for incompressible fluids.

In the case of a compressible fluid, the node equations result from the mass balance. The node equation of a thermal system may be derived from the heat flow balance relation (2.4.29) without energy storage. For chemical processes with mixed phase flow, the mass balance relation applies.

The mesh equations result mostly from the fact that the potentials according to (2.5.4) are zero along a closed loop due to the compatibility condition. For mechanical systems, this compatibility is achieved by using the geometric or kinematic variable velocity or its integral, the displacement, respectively. If one compares the different node and mesh equations for energy flows that result from the physical continuity and compatibility equations at the connection point with the power variables  $f$  and  $e$  as with the potential-flow classification, see Table 2.3a, the following becomes evident. The node and mesh equations according to (2.5.2) and (2.5.4) with flows and potential differences as defined in Table 2.3a are valid for electrical, magnetic and hydraulic systems (incompressible). For mechanical (translational and rotational) systems it is, however, advisable to use the corresponding (dual) power variables according to the across-through classification, see Table 2.3b.

The node and mesh equations resulting from the interconnection conditions of the process elements combine the variables to describe the overall technical system. After defining the independent input variables and the dependent output variables, the compatibility equations of the coupled process elements result. This leads to the applied variables of the sequentially coupled process elements in sequential order.

## 2.5.2 Causality of Process Elements

An explicit causality of a physical element exists if a cause has as an outcome a certain effect, *i.e.*, if the following rule is valid:

if <cause> then <effect>

Considering potentials and flows as cause, they can be interpreted as applied variables and can be described as signals. A certain output variable of a causal element is the function of a certain input variable

$$x_o = f(x_i)$$

and the inversion is therefore not valid

$$x_i \neq f^{-1}(x_o)$$

However, if the inversion is valid, an explicit causality does not exist. Cause and effect may then not be unique.

For different process elements, the following behavior is observed: In the case of ideal sources, a distinction can be made between sources with applied flow  $f = f_0$  (flow sources) and sources with applied potential  $e = e_0$  (potential sources). In the first case, the flow  $f$  is the cause which is independent of the potential  $e$ , whereas in the second case the potential  $e$  is the cause which is independent of the flow  $f$ . The resulting causality during operation depends on the connected elements. Because the applied variables are always the cause and the character of the effect is known, sources are one-ports with unique causality. This also applies to non-ideal and controllable sources.

In the case of ideal energy storages, a distinction can be made between effort storages that relate the potential to the integral of the flow and flow storages that relate the flow to the integral of the potential. In the same manner, the flow storage may be seen as a function of the potential's time derivative and *vice versa*. For mass storages, the stored mass results from the integral of the mass flow. Again, the inversion is also valid. Therefore, storages are usually one- or two-ports without explicit causality.

In the case of ideal energy transformers, the input flow  $f_1$  or the input potential  $e_1$  are related to the output flow  $f_2$  or the output potential  $e_2$  by a certain ratio (transformer gain). These relations also apply *vice versa* and therefore energy transformers are usually process elements without explicit causality.

For energy converters, potentials and flows are mutually related to each other in different ways. If the relations also hold in the inverse case, energy converters are two-ports without explicit causality. Active converters change the characteristic curve of the input and output relation on by an actuator. This does not change the assigned causality.

Sinks are characterized by a flow  $f$  that depends on the potential difference  $e$ . However, as the inversion is also valid, sinks are usually one-ports without explicit causality.

These considerations lead to the conclusion that the causality of the overall system is determined by connecting all process elements with the source. From this, the signal flow of the overall system results. This is shown by a simple example.

#### **Example 2.4.** Connecting a source with a sink

A voltage or current source is connected serially with a resistor, see Figure 2.31. For the resistance, it holds that according to Ohm's law either

$$V_R = R I_R$$

or

$$I_R = \frac{1}{R} V_R$$

and therefore no explicit causality exists.

For the ideal voltage source, it holds that

$$V_Q = V_{Q0} \text{ for all } I_Q$$

The interconnection equations are

$$V_Q - V_R = 0 \rightarrow V_R = V_Q \quad (\text{mesh equation})$$

$$I_Q - I_R = 0 \rightarrow I_Q = I_R \quad (\text{node equation})$$

The current through the resistance becomes, from the mesh relation

$$I_{R1} = \frac{1}{R} V_{Q0}$$

For an ideal voltage source, it holds that

$$I_Q = I_{Q0} \text{ for all } V_Q$$

and the voltage drop at the resistance becomes, from the node equation

$$V_{R2} = R I_{Q0}$$

These relations are be illustrated by the characteristic curves in Figure 2.32.

This simple example shows that:

- a) The isolated (unconnected) sink itself has no explicit causality. Either  $V_R = f(I_R)$  or  $I_R = f^{-1}(V_R)$  is valid.
- b) The sources impose the causality of a system by their characteristics of being a source with either an applied current or an applied source. The effect is then either a current or a voltage between the terminals if a sink is connected. Therefore, an explicit causality of the source exists. However, one terminal variable remains unknown without knowing the sink.
- c) By connecting the source to the sink, the causality of the sink is determined as well as the unknown terminal variable of the source.
- d) The connection of the source and sink results, therefore, within the overall system in a unique cause-effort relationship. If, e.g., the voltage  $\Delta V_{Q0}$  of a controllable voltage source is changed, this cause results in a change of the current in the electric circuit by  $\Delta I_{R1} = \frac{1}{R} \Delta V_{Q0}$  and thus an explicit signal flow direction follows.

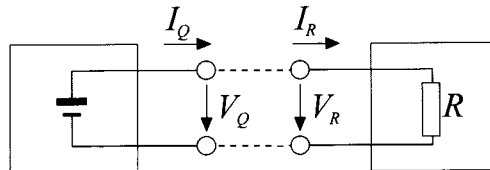


Figure 2.31. Circuit diagram with source and sink

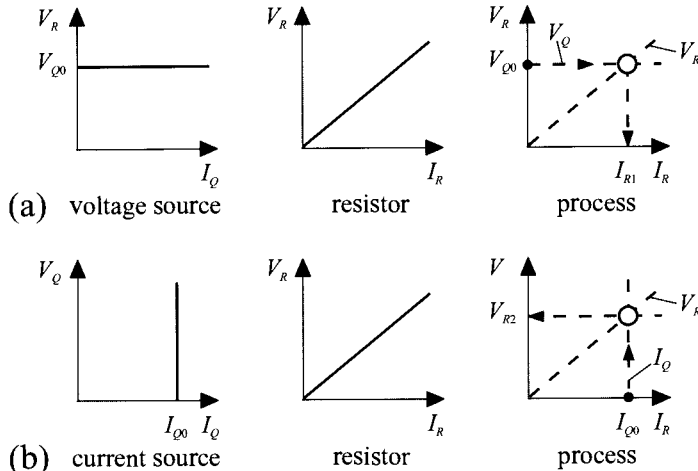


Figure 2.32. Characteristic curves of the circuit diagram of Figure 2.31: (a) voltage source; (b) current source

□

## 2.6 ANALOGIES BETWEEN MECHANICAL AND ELECTRICAL SYSTEMS

The discussion of the constitutive equations for systems with energy flows in Section 2.3.2 has shown that there exist many similarities for sources, storage elements, transformers and sinks (not so much for converters). This holds especially for mechanical and electrical storages and sinks, leading to direct analogies between the signals and the *parameters* of the components, see also Olson (1958).

Table 2.14 summarizes these analogies. Beginning with the electrical elements, two cases of analogies can be stated, depending on the selected power variables of the one-port elements, compare Tables 2.3a and b. The potential-flow classification leads to the analogy (correspondence) of the signals

$$V \triangleq F \quad I \triangleq v$$

and the analogy of the parameters

$$R \triangleq d \quad L \triangleq m \quad C \triangleq 1/c$$

If, however, the across-through classification is used, with

$$V \triangleq v \quad I \triangleq F$$

the analogy of the parameters becomes

$$R \triangleq 1/d \quad L \triangleq 1/c \quad C \triangleq m$$

This shows that the analogies between mechanical and electrical elements are not unique.

**Table 2.14.** Analogies between electrical and mechanical elements

electrical elements	resistance	inductance	capacitance
a) potential-flow classification $V \triangleq F; I \triangleq v$			
analogy of the signals	$V_R \triangleq F_d$ $I_R \triangleq v_d$	$V_L \triangleq F_m$ $I_L \triangleq v_m$	$V_C \triangleq F_c$ $I_C \triangleq v_c$
analogy of the parameters	$R \triangleq d$	$m \triangleq L$	$C \triangleq \frac{1}{c}$
b) across-through classification $V \triangleq v; I \triangleq F$			
analogy of the signals	$V_R \triangleq v_d$ $I_R \triangleq F_d$	$V_L \triangleq v_c$ $I_L \triangleq F_c$	$V_c \triangleq v_m$ $I_c \triangleq F_m$
analogy of the parameters	$R \triangleq \frac{1}{d}$	$L \triangleq \frac{1}{c}$	$C \triangleq m$

The interconnection of the elements leads to the agreements following, compare Table 2.13:

- parallel connection (node equation)

$$\sum_{i=0}^n f_i(t) = 0 \rightarrow \sum_{i=1}^n I_i = 0 \triangleq \sum_{i=1}^n F_i = \mathbf{0}$$

- serial connection (mesh equation)

$$\sum_{i=0}^n e_i(t) = 0 \rightarrow \sum_{i=1}^n V_i = 0 \triangleq \sum_{i=1}^n v_i = \mathbf{0}$$

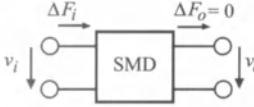
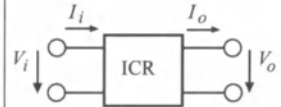
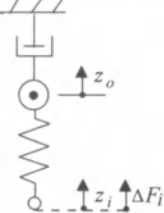
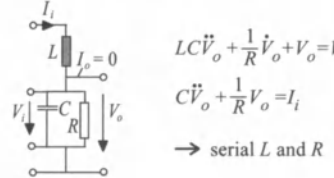
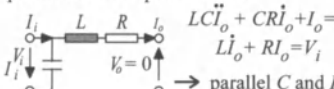
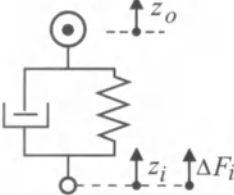
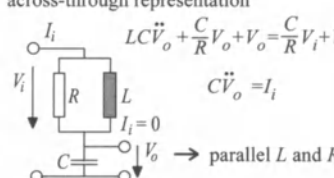
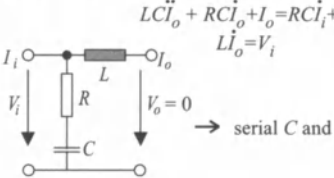
This means that the across-through classification should be used if the parallel and serial connections for both the electrical and mechanical elements have the same topology.

Table 2.15 illustrates for a mechanical spring-mass-damper system, with a serial and a parallel connection of the spring (c) and damper (d)

and bottom excitation, each two electrical connections (circuits) for across-through and potential-flow representation.

This also shows that for the connection types of basic electrical and mechanical elements, different analogies exist, *e.g.*, mechanical series connections compared to electrical parallel connections in the case of the potential-flow classification and *vice versa*. However, for the across-through representation, a corresponding serial connection of the analog elements  $L$  and  $R$  results, *i.e.*, the same connection type.

**Table 2.15.** Analogies of mechanical and electrical connections for a spring-mass-damper system and inductance-capacitance-resistor system

mechanical connection	electrical connection	analogy of signals	analogy of parameters
			
 $\frac{m}{c} \ddot{v}_o + \frac{d}{c} \dot{v}_o + v_o = v_i$ $m v_o + d \dot{v}_o = \Delta F_i$ $\rightarrow$ serial connection of $c$ and $d$	<p>across-through representation</p>  <p>potential-flow representation</p> 	$v \triangle V$ $F \triangle I$	$R \triangle \frac{1}{d}$ $C \triangle m$ $L \triangle \frac{1}{c}$
 $\frac{m}{c} \ddot{v}_o + \frac{d}{c} \dot{v}_o + v_o = \frac{d}{c} \dot{v}_i + v_i$ $m \dot{v}_o = \Delta F_i$ $\rightarrow$ parallel connection of $c$ and $d$	<p>across-through representation</p>  <p>potential-flow representation</p> 	$v \triangle V$ $F \triangle I$	$R \triangle \frac{1}{d}$ $C \triangle m$ $L \triangle \frac{1}{c}$

Because of the non-uniqueness of the analogies between electrical and mechanical (and also other) systems, special care has to be taken with regard to their applications. As mechatronic systems have to deal with connections of elements from different physical domains, it is im-

portant to represent the interfaces (terminals, cuts) in a consistent way. Therefore, the multi-port representation introduced in Section 2.3.2 and summarized in Table 2.12 seems to be a practical procedure as an intermediate step in modeling connected elements with energy flow. Because of the agreement of different connection laws, the across-through representation earns some preference.

## 2.7 SUMMARY

By following the systematic approach described in this chapter, a consistent procedure for the modeling of processes with energy and mass flows results. The individual steps are arranged in Table 2.16. First, all process elements and their interfaces have to be determined. Sources and sinks are usually one-ports, storages, transformers and converters are multi-ports. Then, the basic equations of the process elements are stated. The following types of basic equations can be distinguished:

- balance equations;
- constitutive equations;
- phenomenological equations.

The balance equation for mass and energy can be stated in unified form. Special representations exist for potential and kinetic energy, if the respective storages are interconnected and for the energy balance of gases and steam. The balance equations are linear in principle, result in a summing point and an integrator in the block diagram representation, see Figure 2.12, and are one reason for the dynamic behavior of processes. In the case of mechanical systems with kinetic energy, it is usually easier for simple set-ups with few mass points not to take the energy balances but the momentum balance equation that follows from differentiating the energy balance equation. For multi-mass systems with constrained forces that are generated, *e.g.*, by guideways, it is advisable to apply the principles of mechanics, *e.g.*, the Lagrange equations, see Chapter 3 (which are based on energies with generalized coordinates). Also, for simple electrical circuits, it is simpler to use the special state equation of the storages instead of the energy balance equations. Therefore, balance equations are generally used for the following processes:

- mass storages;
- heat storages (rigid bodies, fluids);
- thermodynamic storages (gases, steam).

The constitutive equations of sources, storages, transformers, passive and active converters vary from each other. They may behave statically or dynamically and may exhibit both linear and non-linear behavior. For

particular component classes, a couple of general rules may be formulated, mainly for the multi-port representation.

**Table 2.16.** General procedure for modeling of processes with lumped parameters

	steps of modeling	
1	definition of main and side flows	<ul style="list-style-type: none"> <li>- energy flow</li> <li>- matter flow</li> </ul>
2	definition of process elements	<ul style="list-style-type: none"> <li>- sources</li> <li>- storages</li> <li>- transformers</li> <li>- converters</li> <li>- sinks</li> </ul>
3	basic equation of process elements	
3.1a	balance equations storages (general)	<ul style="list-style-type: none"> <li>- mass flow balance</li> <li>- energy flow balance</li> <li>- momentum balance</li> </ul>
	balance equations energy storages (special forms)	<ul style="list-style-type: none"> <li>- potential, kinet. mech. energy</li> <li>- principals of mechanics</li> <li>- electrical, magnetic energy</li> <li>- energy balance for gases and steam</li> </ul>
3.2a	constitutive equations for energy flows	<ul style="list-style-type: none"> <li>- flows</li> <li>- potential differences for:</li> <li>- sources</li> </ul>
	constitutive equations for energy and matter flow: special constitutive equation	<ul style="list-style-type: none"> <li>- storages</li> <li>- transformers</li> <li>- converters (passive, active)</li> </ul>
3.3	phenomenological equations for irreversible processes	<ul style="list-style-type: none"> <li>- sinks (general)</li> <li>- mechanical dissipation</li> <li>- electrical dissipation</li> <li>- thermal conduction</li> <li>- diffusion</li> <li>- chemical reaction</li> </ul>
4	interconnection equations	<ul style="list-style-type: none"> <li>- node equation (continuity equation)</li> <li>- mesh equation (compatibility equation)</li> </ul>
5	definition of input and output variable	<ul style="list-style-type: none"> <li>- independent variables (e.g., manipulated variables)</li> <li>- dependent variables</li> </ul>
6	overall model	<ul style="list-style-type: none"> <li>- signal flow diagram</li> <li>- in/output model</li> <li>- state variables model</li> <li>- linearization</li> </ul>

The phenomenological equations for irreversible processes, *i.e.*, dissipative processes, describe the behavior of sinks. They may be linear or non-linear.

In addition to the different types of basic equations of each process element, the interconnection equations have to be included. Based on the continuity and compatibility conditions, node equations for parallel connections and mesh equations for serial connections result in a unique

form for various physical systems. They represent superpositions and are linear. Imposed by the causality of the source, the causality of the overall system results from the interconnection of the process elements.

Using these particular equations, an equation system for the process follows. From this, a signal flow diagram may be systematically composed and the state space equations as well as the differential equations for the input and output variables may be derived. If desired, a linearization around the operating point may be carried out. Examples for this are to be found in the following chapters.

The treated systematic approach and unified procedure allows not only the identification of many similarities but is also a prerequisite for computer-aided modeling with modern software tools.

The following Chapters 4 to 6, 10 and 12 comprise many examples for the procedure of theoretical modeling.

## 2.8 PROBLEMS

- 2.8.1 Design a schematic representation of an automobile including energy flows and multi-port signal flow diagram, as in Figure 2.7.
- 2.8.2 Which main flows and side flows exist in a combustion engine?
- 2.8.3 State the balance equations and constitutive equations for a cylindrical water tank in horizontal orientation with cross-section  $A = 1 \text{ m}^2$  and liquid level  $h = 2 \text{ m}$ , one inflow valve over the liquid surface and outflow at the bottom. Derive the transfer function for the liquid level as output and the inlet valve position as input (maximum inlet flow  $0.2 \text{ m}^3/\text{s}$ ) for a flow of  $0.1 \text{ m}^3/\text{s}$ .
- 2.8.4 Model the dynamic behavior of an electrically driven vehicle. The components are a battery, DC motor, gear, axles, wheels. Follow the steps from multi-port diagrams through basic equations and characteristics according to Tables 2.6 to 2.12.
- 2.8.5 What are the differences between constitutive and phenomenological equations? To which type of equations belong: Ohm's law, induction law, heat conduction, Newton's laws?
- 2.8.6 Model the dynamic behavior of the temperature in a stirred warm water tank with cold water inflow ( $\vartheta_{CW} = 20^\circ\text{C}$ ) of  $\dot{m}_{CW} = 0.1 \text{ m}^3/\text{s}$ , warm water inflow ( $\vartheta_{WW} = 60^\circ\text{C}$ ) of  $\dot{m}_{WW} = 0.2 \text{ m}^3/\text{s}$ , volume  $V = 1 \text{ m}^3$  for a change of  $\Delta\dot{m}_{WW} = 0.01 \text{ m}^3/\text{s}$ . Show the dependence of the gain and time constant on the total flow rate.

Consider all steps from multi-port diagrams to the differential equation according to Tables 2.14 to 2.16.

- 2.8.7 State the basic equations of a rotating mass with  $m = 5 \text{ kg}$  and  $R = 0.1 \text{ m}$ . The driving torque is  $M_1 = 1 \text{ Nm}$  and independent of the angular speed. The resistance torque is  $M_2 = (k_1 + k_2 \omega^2)$  with  $k_1 = 0.5 \text{ Nm}$  and  $k_2 = 0.5 \cdot 10^{-4} \text{ Nms}^2$ . Derive the linearized differential equation for  $\Delta M_1$  as input and  $\Delta\omega$  as output for the operating point and calculate the gain and time constant.
- 2.8.8 An undamped spring-mass system oscillates at 1 kHz. The mass is 0.1 g. Calculate the spring constant  $c$ . Design an electrical inductance-capacitance system with the same frequency by using coils from loud speakers with  $L = 3 \text{ mHenry}$ .
- 2.8.9 State the analogies between an electrical RLC element and a mechanical mdc element (mass-damper-spring) for the signals and the parameters and the across-through classification.
- 2.8.10 A hydraulic system consists of a valve with input position  $U_1$ , pressure at input  $p_1$ , an elastic connection tube with stiffness  $c_2$  and pressure  $p_2$ , a connected cylinder with a piston of area  $A_3$  and pressure  $p_3 = p_2$  acting against a spring with stiffness  $c_4$  and fixed at the other end.  
 Develop a scheme of the arrangement, an energy flow scheme, multi-port scheme, also with signal flows according to Figure 2.7, and derive the equations and the block diagram for the dynamic behavior of the system with  $U_1$  as input and position of the piston rod  $Z_3$  as output.

# 3 Fundamental Equations of the Dynamics of Mechanical Systems with Mobile Masses

---

Mechanics deals with the mathematical modeling of mechanical systems. The application of abstract mathematical models to specific technical applications is taught in engineering mechanics and machine dynamics. A possible subdivision of the subject mechanics into its sub-subjects is shown in Figure 3.1.

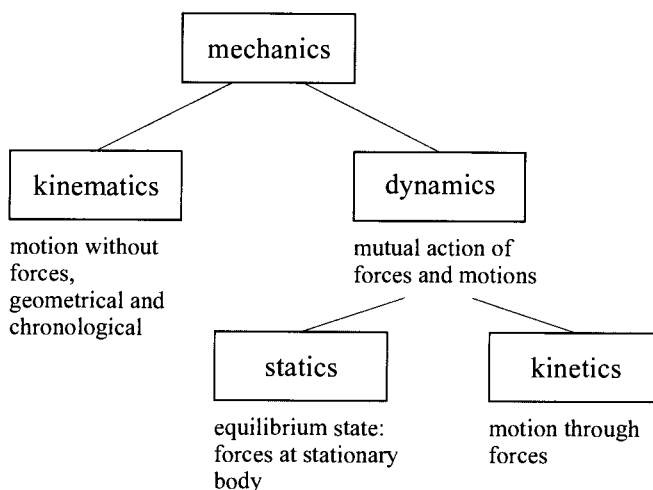


**Figure 3.1.** Subdivision of engineering mechanics

Due to the fact that the modeling of the dynamical behavior of mobile masses, *i.e.*, the *kinetics*, plays a significant role in mechatronic

systems, a summary of the most basic equations is presented in the following.

A more fundamental treatment on kinetics may be looked up elsewhere, *e.g.*, Schiehlen (1986), Hauger *et al.* (1989), Pfeiffer (1989), Hagedorn (1990), Sneck (1991), Meriam, Kraige (1997), Kessel, Fröhling (1998).

The following section introduces Newton's laws of kinetics for the three-dimensional case. They are axioms that cannot be proved but which are postulated from experimental observations. Other formulations of mechanics may be derived from the principles of mechanics – of which the d'Alembert principle and the Lagrange equations are presented here – these are, however, equivalent to Newton's laws.

## 3.1 NEWTON'S LAWS OF KINETICS

### 3.1.1 Translational Motion

The translational motions of a point mass are considered in the following. When the geometric extension of a body has no influence on the motion of a body, its total mass can be assumed to be concentrated in a single geometric coordinate, *i.e.*, a *point mass*. Newton's three laws (1687), which are based on experience, are formulated as follows:

**Newton's first law:** The momentum  $\mathbf{I}$  of the point mass  $m$  which moves with the velocity  $\mathbf{v}$  is a vector pointing in the direction of  $\mathbf{v}$  and is given by

$$\mathbf{I} = m \mathbf{v} \quad (3.1.1)$$

Newton's first law states that, "The momentum  $\mathbf{I}$  of a point mass remains constant if and only if the sum of all forces which act upon it is zero."

$$\mathbf{I} = m \mathbf{v} = \text{const.} \quad (3.1.2)$$

A point mass performs a uniform rectilinear motion with  $\mathbf{v} = \text{const.}$  as long as no force is being applied to it. This is equivalent with the law of inertia given by Galilei (1638).

**Newton's second law:** When a resulting force  $\mathbf{F}$  acts upon a point mass  $m$ , then

$$\frac{d\mathbf{I}}{dt} = \frac{d(m\mathbf{v})}{dt} = \mathbf{F} \quad (3.1.3)$$

"The derivative of the momentum with respect to time is equal to the force acting upon the point mass." This is also called the *principle of linear momentum*.

In the case of constant mass, (3.1.3) becomes

$$m \frac{d\mathbf{v}}{dt} = m \mathbf{a} = \mathbf{F} \quad (3.1.4)$$

where the acceleration vector  $\mathbf{a}$  is parallel to the force vector  $\mathbf{F}$ . From  $\mathbf{F} = 0$  and (3.1.4) follows (3.1.2), i.e., the first fundamental law can be considered to be a special case of Newton's second fundamental law.

Newton's laws apply to inertial systems, which are reference systems with either zero or constant velocity. For many technical applications, the coordinate system of the earth is sufficiently approximated by an inertial system with zero velocity. Thus, (3.1.4) is also referred to as the "conservation of linear momentum".

**Newton's third law:** The law of bodies with interaction due to central forces states that if one body exerts a force on another body, then the latter also exerts a force on the former that is of equal magnitude but opposite direction: "action = reaction". Therefore, Newton's third law enables the transition from a mechanical system that consists of just a single point mass to one with many point masses, e.g., extended bodies.

If the mobility of a point mass is unconstrained with respect to its spatial coordinates – as it is, for example, in the case of unconstrained movements of thrown bodies – then the point mass has *three degrees of freedom* due to the three spatial coordinates. However, when a body is being forced to move on a given surface or along a trajectory, then it has two or one degrees of freedom respectively. In that case, not only central/applied forces  $\mathbf{F}^{(e)}$ , which are independent of any constraints, exist, but also so-called *forces of constraint*  $\mathbf{F}^{(z)}$  are then being exerted, which, as reacting forces, always apply perpendicularly to the particle's trajectory. Newton's second fundamental law incorporates by definition the total force and has to be re-formulated accordingly

$$m \mathbf{a} = \mathbf{F}^{(e)} + \mathbf{F}^{(z)}. \quad (3.1.5)$$

applied forces	+	forces of constraint
-------------------	---	-------------------------

### 3.1.2 Rotational Motion

In the case of rotational motions, the following fundamental equations hold. Assume that in a spatial coordinate system  $x, y, z$  with the vectors of unity  $\mathbf{e}_x, \mathbf{e}_y, \mathbf{e}_z$ , a force

$$\mathbf{F} = F_x \mathbf{e}_x + F_y \mathbf{e}_y + F_z \mathbf{e}_z \quad (3.1.6)$$

may be applied at a coordinate vector

$$\mathbf{r} = r_x \mathbf{e}_x + r_y \mathbf{e}_y + r_z \mathbf{e}_z \quad (3.1.7)$$

Then, the torque is defined with respect to the origin of the coordinate systems as

$$\mathbf{T} = \mathbf{r} \times \mathbf{F} \quad (3.1.8)$$

which includes the notation of an *outer product*, or *vector product*. The vector  $\mathbf{T}$  is orthogonal to the plane which is defined by  $\mathbf{r}$  and  $\mathbf{F}$ , Figure 3.2. The magnitude of the torque is equal to the area of the parallelogram which is spanned by  $\mathbf{r}$  and  $\mathbf{F}$

$$|\mathbf{T}| = |\mathbf{F}| |\mathbf{r}| \sin\varphi \text{ or } \mathbf{T} = \mathbf{F} \mathbf{r} \sin\varphi \quad (3.1.9)$$

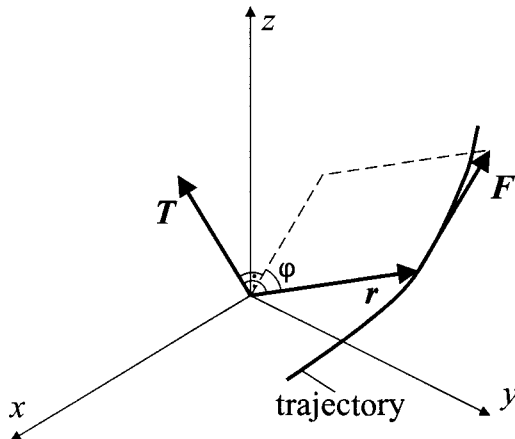


Figure 3.2. Definition of the torque vector

The vector product vanishes in the case of two parallel vectors ( $\varphi = 0$ ). In the case when two vectors are orthogonal to each other,  $\sin \varphi = 1$ . The vectors of unity are therefore related to each other by

$$\begin{aligned} \mathbf{e}_x \times \mathbf{e}_x &= 0 & \mathbf{e}_x \times \mathbf{e}_y &= \mathbf{e}_z & \mathbf{e}_x \times \mathbf{e}_z &= -\mathbf{e}_y \\ \mathbf{e}_y \times \mathbf{e}_x &= -\mathbf{e}_z & \mathbf{e}_y \times \mathbf{e}_y &= 0 & \mathbf{e}_y \times \mathbf{e}_z &= \mathbf{e}_x \\ \mathbf{e}_z \times \mathbf{e}_x &= \mathbf{e}_y & \mathbf{e}_z \times \mathbf{e}_y &= -\mathbf{e}_x & \mathbf{e}_z \times \mathbf{e}_z &= 0 \end{aligned} \quad (3.1.10)$$

Hence

$$\begin{aligned} \mathbf{T} = \mathbf{r} \times \mathbf{F} &= (r_y F_z - r_z F_y) \mathbf{e}_x + (r_z F_x - r_x F_z) \mathbf{e}_y \\ &\quad + (r_x F_y - r_y F_x) \mathbf{e}_z \\ &= T_x \mathbf{e}_x + T_y \mathbf{e}_y + T_z \mathbf{e}_z \end{aligned} \quad (3.1.11)$$

The outer product may also be written in the form of a determinant

$$\mathbf{T} = \mathbf{r} \times \mathbf{F} = \begin{vmatrix} \mathbf{e}_x & \mathbf{e}_y & \mathbf{e}_z \\ r_x & r_y & r_z \\ F_x & F_y & F_z \end{vmatrix} \quad (3.1.12)$$

If a point mass moves along a trajectory with velocity  $\mathbf{v}$  and if the vector  $\mathbf{r}$  represents the coordinate of the point mass with respect to the origin, see also Figure 3.3, then it follows that with the definitions in (3.1.1) and (3.1.8), the following outer product, which may be defined as the *angular momentum*

$$\mathbf{L} = \mathbf{r} \times \mathbf{I} = \mathbf{r} \times m \mathbf{v} \quad (3.1.13)$$

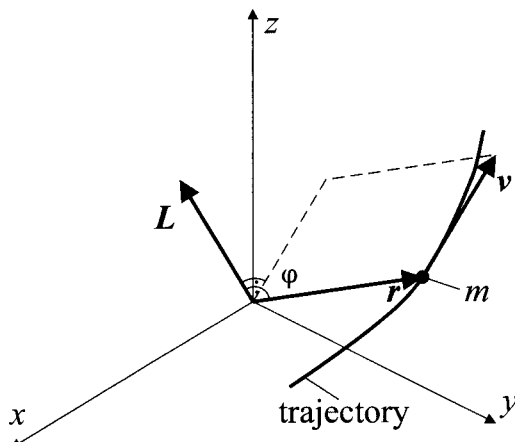


Figure 3.3. Computation of the angular momentum

From Newton's second law (3.1.3) and the definition of the torque (3.1.12), it follows that

$$\mathbf{r} \times m \frac{d\mathbf{v}}{dt} = \mathbf{r} \times \mathbf{F} = \mathbf{T} \quad (3.1.14)$$

The derivative of (3.1.13) with respect to time and presumed constant mass is

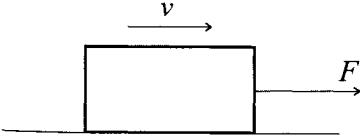
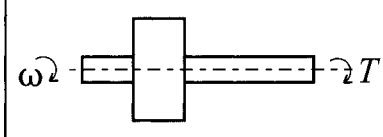
$$\frac{d\mathbf{L}}{dt} = \frac{d}{dt}(\mathbf{r} \times m \mathbf{v}) = \frac{d\mathbf{r}}{dt} \times m \mathbf{v} + \mathbf{r} \times m \frac{d\mathbf{v}}{dt}$$

The first summand is zero since  $\mathbf{v} = d\mathbf{r}/dt$ , which proves the *angular momentum conservation law*:

"The temporal derivative of the angular momentum with respect to a spatially fixed coordinate system is equal to the torque exerted at the point mass." This is also called the *principle of angular momentum*. The physical equations of a rigid body (infinite number of rigidly con-

nected point masses) for translational and rotational motions, which follow from the fundamental relations mentioned above, are shown in Table 3.1.

**Table 3.1** Basic equations for translation and rotation

translation in one direction	rotation for one axis
	
<i>s</i>	displacement
$v = \dot{s}$	speed
$a = \ddot{v} = \ddot{s}$	acceleration
<i>m</i>	mass
<i>F</i>	force
$I = mv$	momentum
$F = ma$	Newton's second law
$E_k = \frac{1}{2}mv^2$	kin. energy
$v = \int F ds$	work
$P = Fv$	power
	angle
	$\omega = \dot{\phi}$
	$\dot{\omega} = \ddot{\phi}$
	$\theta$
	$T$
	$L = \theta\omega$
	$T = \theta\dot{\omega}$
	$E_K = \frac{1}{2}\theta\omega^2$
	$W = \int T d\phi$
	$P = T\omega$
	angular velocity
	angular acceleration
	momentum of inertia
	torque on axis
	angular momentum
	Newton's second law
	kin. energy
	work
	power

## 3.2 PRINCIPLES OF MECHANICS

The dynamics of mechanical systems, which consist of multiple rigid bodies, is evaluated, due to Newton's laws, by isolating all rigid bodies and stating the corresponding applied forces and constrained forces on each of the rigid sub-bodies. Then, the forces of constraint have to be eliminated in the corresponding equations. This rather cumbersome procedure, *e.g.*, the sub-division of the system into its components and the explicit computation of the forces of constraint, can easily be avoided by employing the principles of mechanics. The procedure given below is particularly useful for complicated cases.

### 3.2.1 d'Alembert's Principle

Newton's second law for the case of constant mass is, according to (3.1.4)

$$\mathbf{F} - m\mathbf{a} = \mathbf{0} \quad (3.2.1)$$

Now, define a force of inertia  $\mathbf{F}_T$  (d'Alembert's auxiliary force), which is a *fictitious force* (non-Newtonian force) of acceleration due to the fact that no reaction forces exist

$$\mathbf{F}_T = -m\mathbf{a} \quad (3.2.2)$$

Thus

$$\mathbf{F} + \mathbf{F}_T = \mathbf{0} \quad (3.2.3)$$

"The sum of applied forces  $\mathbf{F}$  and d'Alembert's force of inertia  $\mathbf{F}_T$  is zero (dynamical equilibrium)". Therefore, forces of inertia  $\mathbf{F}_T$  have to be included in an equation describing the dynamics of an isolated sub-system.

The computation of the equations of motion, which are either motivated by Newton's laws or by d'Alembert's principle, requires that all exerted forces onto a system are taken into account. This includes the forces of constraint that confine the body to its restricted motion. The explicit formulation of (holonomic) constraints for just a few bodies may already become complicated. d'Alembert developed a mathematical method that does not explicitly include reaction forces.

Consider the restricted motion of a point mass along a pre-defined trajectory: it follows from Newton's law that

$$m\mathbf{a} = \mathbf{F}^{(e)} + \mathbf{F}^{(z)} \quad (3.2.4)$$

$\mathbf{F}^{(e)}$ : applied forces

$\mathbf{F}^{(z)}$ : forces of constraint

Forces of constraint are, by definition, perpendicular to the trajectory, which leads, for a virtual displacement  $\delta\mathbf{r}$  along the trajectory, to a vanishing virtual work  $\delta W$

$$\delta W = (\mathbf{F}^{(z)})^T \delta\mathbf{r} = 0 \quad (3.2.5)$$

Whereby  $\delta\mathbf{r}$  is an infinitesimally small displacement, which is consistent with the constraint of a point mass. It is presumed that no dry friction forces occur. Herewith follows d'Alembert's principle.

See also Figure 3.4.

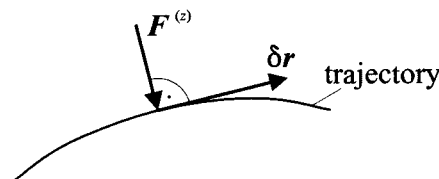


Figure 3.4. Forces of constraint and virtual displacement along a pre-defined trajectory

"A point mass moves along a trajectory such that the forces of constraint do no virtual work". For example, in the two-dimensional case, it holds that

$$\begin{aligned}\mathbf{F}^T \delta \mathbf{r} &= \begin{bmatrix} F_x & F_y \end{bmatrix} \begin{bmatrix} \delta_x \\ \delta_y \end{bmatrix} = F_x \delta_x + F_y \delta_y \\ &= |\mathbf{F}| |\delta \mathbf{r}| \cos \varphi\end{aligned}\quad (3.2.6)$$

where  $\varphi$  is the angle between the vector  $\mathbf{F}$  and  $\delta \mathbf{r}$ . (3.2.6) defines a *scalar product* or *inner product* of the two vectors  $\mathbf{F}$ ,  $\delta \mathbf{r}$ .

The sum the virtual work of a point mass can be calculated by inserting (3.2.4) into (3.2.5) and multiplying  $-1$

$$(\mathbf{F}^{(e)})^T - m \mathbf{a}^T \delta \mathbf{r} = 0 \quad (3.2.7)$$

Here, the virtual work may be introduced by applied forces and forces of inertia

$$\left. \begin{aligned}\delta W &= (\mathbf{F}^{(e)})^T \delta \mathbf{r} \\ \delta W_T &= (\mathbf{F}_T)^T \delta \mathbf{r} = -m \mathbf{a}^T \delta \mathbf{r}\end{aligned}\right\} \quad (3.2.8)$$

Thus

$$\delta W + \delta W_T = 0 \quad (3.2.9)$$

Therefore, the principle of virtual work states that, “A point mass moves along a trajectory such that for all time and any virtual displacement the sum of virtual work of applied forces and d’Alembert’s forces of inertia vanish.”

Note that (3.2.9) no longer contains any forces of constraint. A system of several point masses with rigid constraints is given by (see also Figure 3.5)

$$m_i \ddot{\mathbf{r}}_i = \mathbf{F}_i^{(e)} + \mathbf{F}_i^{(z)} \quad i = 1, \dots, n \quad (3.2.10)$$

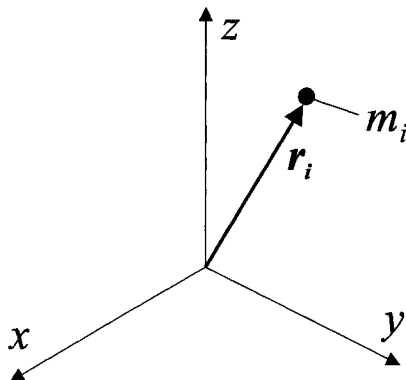


Figure 3.5. Masses  $m_i$  with position vector  $\mathbf{r}_i$

A virtual displacement does not lead to any virtual work; as before in (3.2.5)

$$\sum_i \left( \mathbf{F}_i^{(z)} \right)^T \delta \mathbf{r}_i = 0 \quad (3.2.11)$$

After (3.2.10) has been multiplied by  $\delta \mathbf{r}_i$ , (3.2.11) becomes

$$\begin{aligned} \sum_i [(\mathbf{F}_i^{(z)})^T - m_i \ddot{\mathbf{r}}_i^T] \delta \mathbf{r}_i &= 0 \\ \underbrace{\sum_i (\mathbf{F}_i^{(z)})^T \delta \mathbf{r}_i}_{\delta W} + \underbrace{\sum_i -m_i \ddot{\mathbf{r}}_i^T \delta \mathbf{r}_i}_{\delta W_T} &= 0 \end{aligned} \quad (3.2.12)$$

Hence, the principle of virtual work, as given in (3.2.9), is also valid for a system of point masses with rigid constraints, *i.e.*, rigid bodies. The number of virtual displacements is thereby equal to the number of equations of motion.

### 3.2.2 Lagrange's Equations

The number of Newton's equations for a system of point masses is equal to the number of point masses. Establishing the equations of motion can be simplified by choosing:

- special generalized coordinates; and
- rearranging the terms stemming from the principle of virtual work.

This holds as long as (holonomic) constraints reduce the degrees of freedom. In the following, it is assumed that the interconnection between point masses is rigid. The position of each of the  $n$  point masses inside the system of point masses is given by  $i = 1, \dots, n$  spatial coordinate vectors  $\mathbf{r}_i$ . If there exist  $r$  holonomic constraints, then the configuration of the system of  $n$  point masses is completely defined by  $f = n - r$  generalized coordinates  $q_j$ ,  $j = 1, \dots, f$ , which then allows the introduction of the fundamental relation

$$\mathbf{r}_i = \mathbf{r}_i(q_1, \dots, q_j, \dots, q_f) \quad (3.2.13)$$

between generalized coordinates  $q_j$  and spatial coordinates  $\mathbf{r}_i$ . As with d'Alembert's principle, the coordinate vector  $\delta \mathbf{r}_i$  and the scalar  $\delta q_j$  denote virtual displacements. The total differential of the virtual displacement vector

$$\delta \mathbf{r}_i = \frac{\partial \mathbf{r}_i}{\partial q_1} \delta q_1 + \dots + \frac{\partial \mathbf{r}_i}{\partial q_f} \delta q_f = \sum_j \frac{\partial \mathbf{r}_i}{\partial q_j} \delta q_j \quad (3.2.14)$$

may then be employed to reformulate d'Alembert's principle which, as in (3.2.12), results in no virtual work for  $n$  point masses with rigid inter-

connections

$$\sum_i \left[ \left( \mathbf{F}_i^{T(e)} - m_i \ddot{\mathbf{r}}_i^T \right) \left( \sum_j \frac{\partial \mathbf{r}_i}{\partial q_j} \delta q_j \right) \right] = 0 \quad (3.2.15)$$

The total sum of the virtual work of  $n$  point masses with respect to the virtual displacements of  $f$  generalized coordinates can now be expanded by multiplication into

$$\sum_i \mathbf{F}_i^{T(e)} \left( \sum_j \frac{\partial \mathbf{r}_i}{\partial q_j} \delta q_j \right) - \sum_i m_i \dot{\mathbf{r}}_i^T \left( \sum_j \frac{\partial \mathbf{r}_i}{\partial q_j} \delta q_j \right) = 0 \quad (3.2.16)$$

The sum of quantities of virtual work is by definition associative, which allows exchange of the order of summation

$$\sum_j \sum_i \mathbf{F}_i^{T(e)} \frac{\partial \mathbf{r}_i}{\partial q_j} \delta q_j - \sum_j \sum_i m_i \dot{\mathbf{r}}_i^T \frac{\partial \mathbf{r}_i}{\partial q_j} \delta q_j = 0 \quad (3.2.17)$$

The product rule of differentiation implies that

$$\frac{d}{dt} \left[ m_i \dot{\mathbf{r}}_i^T \frac{\partial \mathbf{r}_i}{\partial q_j} \delta q_j \right] = m_i \dot{\mathbf{r}}_i^T \frac{\partial \mathbf{r}_i}{\partial q_j} \delta q_j + m_i \dot{\mathbf{r}}_i^T \frac{\partial \dot{\mathbf{r}}_i}{\partial q_j} \delta q_j$$

The rearrangement of the three terms in that equation with respect to the second one leads to

$$m_i \dot{\mathbf{r}}_i^T \frac{\partial \mathbf{r}_i}{\partial q_j} \delta q_j = \frac{d}{dt} \left[ m_i \dot{\mathbf{r}}_i^T \frac{\partial \mathbf{r}_i}{\partial q_j} \delta q_j \right] - m_i \dot{\mathbf{r}}_i^T \frac{\partial \dot{\mathbf{r}}_i}{\partial q_j} \delta q_j \quad (3.2.18)$$

By applying the chain rule of differentiation to (3.2.13), it becomes

$$\frac{\partial \mathbf{r}_i}{\partial t} = \sum_j \frac{\partial \mathbf{r}_i}{\partial q_j} \frac{\partial q_j}{\partial t} \quad (3.2.19)$$

which, in turn, may be differentiated with respect to  $\dot{q}_j$ , leaving only a single term in the sum unequal to zero

$$\frac{\partial \dot{\mathbf{r}}_i}{\partial \dot{q}_j} = \frac{\partial \mathbf{r}_i}{\partial q_j} \quad (3.2.20)$$

Thus, (3.2.18) becomes for one mass

$$\begin{aligned} m_i \dot{\mathbf{r}}_i^T \frac{\partial \mathbf{r}_i}{\partial q_j} &= \frac{d}{dt} \left[ m_i \dot{\mathbf{r}}_i^T \frac{\partial \mathbf{r}_i}{\partial \dot{q}_j} \right] - m_i \dot{\mathbf{r}}_i^T \frac{\partial \dot{\mathbf{r}}_i}{\partial q_j} \\ &= \frac{d}{dt} \left[ \frac{\partial}{\partial \dot{q}_j} \left( \frac{1}{2} m_i \dot{\mathbf{r}}_i^T \dot{\mathbf{r}}_i \right) \right] - \frac{\partial}{\partial q_j} \left( \frac{1}{2} m_i \dot{\mathbf{r}}_i^T \dot{\mathbf{r}}_i \right) \end{aligned} \quad (3.2.21)$$

Because with, e.g.,

$$\mathbf{r}_i^T = [r_{i1}, r_{i2} \dots]$$

the first term is equal to

$$\begin{aligned}\frac{\partial}{\partial \dot{q}_j} \left( \frac{1}{2} m_i \dot{\mathbf{r}}_i^T \dot{\mathbf{r}}_i \right) &= \frac{\partial}{\partial \dot{q}_j} \left( \frac{1}{2} m_i (\dot{r}_{i1}^2 + \dot{r}_{i2}^2 + \dots) \right) \\ &= m_i \left( \dot{r}_{i1} \frac{\partial \dot{r}_{i1}}{\partial \dot{q}_j} + \dot{r}_{i2} \frac{\partial \dot{r}_{i2}}{\partial \dot{q}_j} + \dots \right) \\ &= m_i \dot{\mathbf{r}}_i^T \frac{\partial \dot{\mathbf{r}}_i}{\partial \dot{q}_j}\end{aligned}$$

and accordingly for the second term.

The kinetic energy for  $n$  point masses  $m_i$  is given by

$$E_k = \sum_i \left( \frac{1}{2} m_i \dot{\mathbf{r}}_i^T \dot{\mathbf{r}}_i \right) \quad (3.2.22)$$

Therefore, (3.2.21) becomes

$$\sum_i m_i \dot{\mathbf{r}}_i^T \frac{\partial \dot{\mathbf{r}}_i}{\partial q_j} = \frac{d}{dt} \frac{\partial E_k}{\partial \dot{q}_j} - \frac{\partial E_k}{\partial q_j} \quad (3.2.23)$$

The definition of the generalized applied forces in the direction of  $q_j$  is

$$Q_j = \sum_i \mathbf{F}_i^{T(e)} \frac{\partial \mathbf{r}_i}{\partial q_j} \quad (3.2.24)$$

and the identities in (3.2.17) and (3.2.23) imply, for the virtual work of  $n$  point masses for any displacement  $\delta q_j$ , that

$$\sum_j \left[ Q_j - \frac{d}{dt} \left( \frac{\partial E_k}{\partial \dot{q}_j} \right) + \frac{\partial E_k}{\partial q_j} \right] \delta q_j = 0 \quad (3.2.25)$$

The generalized coordinates are, by definition, independent of each other, and so the virtual displacements  $\delta q_j$  are also independent, i.e., each summand in (3.2.25) must be equal to zero

$$\frac{d}{dt} \left( \frac{\partial E_k}{\partial \dot{q}_j} \right) - \frac{\partial E_k}{\partial q_j} = Q_j \quad j = 1, \dots, f \quad (3.2.26)$$

These are *Lagrange's equations*. They are derived from the kinetic energy of point masses. In the case of  $f$  generalized coordinates, there exist  $f$  corresponding equations. Newton's laws require for  $n$  point masses  $3n$  equations of motion and  $r$  equations formulating the holonomic constraints, which means that  $3n + r$  equations have to be solved simultaneously. The number of Lagrange's equations is therefore always smaller than the number of Newton's equations as long as  $r > 0$ , becau-

se

$$f = 3n - r < 3n + r \quad r \neq 0$$

Now, consider the *virtual work of the applied forces*  $\mathbf{F}_i^{(e)}$ , see, for example, (3.2.8) and (3.2.12)

$$\delta W = \sum_i \mathbf{F}_i^{T(e)} \delta \mathbf{r}_i. \quad (3.2.27)$$

The total differential of the virtual displacement  $\delta \mathbf{r}_i$ , see also (3.2.14), may be written as

$$\begin{aligned} \delta W &= \sum_i \mathbf{F}_i^{T(e)} \left( \sum_j \frac{\partial \mathbf{r}_i}{\partial q_j} \delta q_j \right) \\ &= \sum_j \underbrace{\sum_i \mathbf{F}_i^{T(e)} \frac{\partial \mathbf{r}_i}{\partial q_j}}_{Q_j} \delta q_j \\ &= \sum_j Q_j \delta q_j \end{aligned} \quad (3.2.28)$$

This shows that the virtual work  $\delta W$  of the applied forces  $\mathbf{F}_i^{(e)}$  can be represented by the generalized forces  $Q_j$  and the corresponding virtual displacements  $\delta p_j$ . The Lagrange equations may be simplified in the case where there exists a potential  $E_p$  corresponding to the applied forces  $\mathbf{F}_i^{(e)}$ , i.e.,

$$\delta W = -\delta E_p \quad (3.2.29)$$

since in this case there is virtual work  $\delta W$  done by the decrease of the potential energy  $\delta E$ . The virtual change of the potential energy is given by the total differential

$$\delta E_p(q_j) = \frac{\partial E_p}{\partial q_1} \delta q_1 + \dots + \frac{\partial E_p}{\partial q_f} \delta q_f = \sum_j \frac{\partial E_p}{\partial q_j} \delta q_j \quad (3.2.30)$$

(3.2.29) is taking (3.2.28) and (3.2.30) into account, which is equivalent to

$$Q_j = -\frac{\partial E_p}{\partial q_j}$$

The substitution of this relation into (3.2.26) results in

$$\frac{d}{dt} \left( \frac{\partial E_k}{\partial \dot{q}_j} \right) - \frac{\partial E_k}{\partial q_j} + \frac{\partial E_p}{\partial q_j} = 0 \quad (3.2.31)$$

Now, the *Lagrange function* (or *Lagrangian*) is defined as the difference

between kinetic and potential energy

$$L = E_k - E_p \quad (3.2.32)$$

whereby the potential energy is independent of  $\dot{q}_j$ :

$$\frac{\partial E_p}{\partial \dot{q}_j} = 0 \quad (3.2.33)$$

The Lagrange equation for conservative systems with potential  $E_p$  then follows immediately from (3.2.31)

$$\frac{d}{dt} \left( \frac{\partial L}{\partial \dot{q}_j} \right) - \frac{\partial L}{\partial q_j} = 0 \quad j = 1, \dots, f \quad (3.2.34)$$

Establishing the equations of motion only requires the explicit composition of kinetic and potential energy of each generalized coordinate and their derivatives. The previously derived equations for systems of point masses are obviously also valid for rigid bodies. Lagrange's equations can be formulated for electrical and electromechanical systems as well, where certain analogies are drawn, see, for example, Wells (1967), MacFarlane (1970).

Further principles of mechanics, for example, *Jourdain's principle*, which utilizes the approach of virtual power, or *Hamilton's principle*, which employs the sum of kinetic and potential energy, can be found elsewhere, for example in Pfeiffer (1992), Schiehlen (1986).

### 3.3 PROBLEMS

- 3.3.1 Derive the equations of motion of the torsional system, consisting of two rotational masses, shown in Figure 4.25, by applying Lagrange equations.
- 3.3.2 Two masses  $m_1$  and  $m_2$  are coupled together by a linear spring ( $c_1$ ) and a linear damper ( $d_1$ ) (dashpot). Mass  $m_2$  is connected by a linear second spring ( $c_2$ ) and damper ( $d_2$ ) with a wall. Derive the equations for the positions  $z_1(t)$  and  $z_2(t)$  for the masses if a force  $F_1(t)$  acts on mass  $m_1$  by applying Lagrange equations.
- 3.3.3 A robot arm of length  $l = 1$  m carries a load of  $m = 100$  kg with an angle of  $\varphi_1 = 30^\circ$  to the horizontal axis. Derive the equations of motion with torque  $T_1(t)$  as input and  $\varphi_1(t)$  as output signal. Linearize the equations around the operation point (mass and damping of robot arm is negligible).

- 3.3.4 An inverted pendulum with mass  $m_2$  is mounted on a cart of mass  $m_1$ . An applied force  $F_1(t)$  acts on the cart. Derive the equations for the car displacement  $z(t)$  and the angle  $\varphi(t)$  of the pendulum with Lagrange equations. Frictions can be neglected.
- 3.3.5 A cart with mass  $m_1$  is connected with a linear spring  $F = cx$  to a wall. Damping and friction can be neglected. The cart carries a pendulum with mass  $m_2$ , length  $l$  and angle  $\varphi$ . Derive the equations of motion for  $x$  and  $\varphi$  applying Lagrange equations. Verify the equations for the special case  $l = 0$  and  $x = 0$ .
- 3.3.6 A mass  $m$  follows a parabolic trajectory  $y = cx^2$  under the influence of gravity. Derive the equation of motion for  $x(t)$  by using the Lagrange equation.
- 3.3.7 A pendulum consists of a linear spring and a mass  $m$  at the end resulting in a motion of length  $l(t)$  and angle  $\varphi(t)$ . The length of the spring without tension is  $l_0$ . Derive the equations of motion for  $\varphi(t)$  and  $l(t)$ . Verify the equations for  $\varphi \approx 0$  and the case that the spring becomes a rod of length  $l_0$ .

# 4 Mechanical Elements

---

Mechanical systems, machines and devices usually consist of:

- masses (point masses, rigid bodies);
- connecting elements (bars, beams, springs, belts, dampers);
- machine elements (bearings, gears, guidances, cylinders with pistons).

In this chapter, the mathematical models of frequently used mechanical elements are considered. It will be shown in principle how the models, important for the design of mechatronic systems, will be set up with regard to the overall mechanical system dynamics. A more profound consideration can be found in special books on engineering mechanics and machine dynamics such as Krämer (1984), Bremer (1988), Paul (1989), Pfeiffer (1989), Jensen (1991), Sneed (1991), Holzweißig, Dreßig (1992), Bremer, Pfeiffer (1993), Smith (1994), Meriam, Kraige (1997), Kessel, Fröhling (1998), Kutz (1998), Walsh (1999).

The modeling of mechanical elements (this chapter) and machines (Chapter 6) follows according to Chapters 2 and 3. It is advisable to firstly set up equivalent block diagrams and multi-port diagrams for the representation of the principal arrangement and couplings of the different elements. Then, basic equations of the elements and their connections are stated, resulting in a system of differential equations. After defining input and output variables, vector differential equations for state space representation and transfer functions can be formulated.

## 4.1 BARS

Examples of bars are the tension bar and the torsional bar. These bars are used as supports, tubes or shafts. A common characteristic is that their diameter is smaller than their length as well as the connection of all center of gravity cross-sections to form a straight line. Depending on the type of imposed stresses, one can distinguish between tension, compression or torsion bars or bending beams.

Assume that a tension bar is fixed on one side as shown in Figure 4.1a. Then, a tensile force  $F$  results in an alteration of length  $\Delta l$ . An element of length  $dz$  and area  $A(z)$  is extended by  $dl$ . According to Hooke's law, the force  $F$  is proportional to the extension  $\epsilon$

$$\epsilon = \frac{dl}{dz} = \frac{F}{EA} \quad (4.1.1)$$

With

$A$  cross-sectional area

$E$  modulus of elasticity [ $\text{N/m}^2$ ].

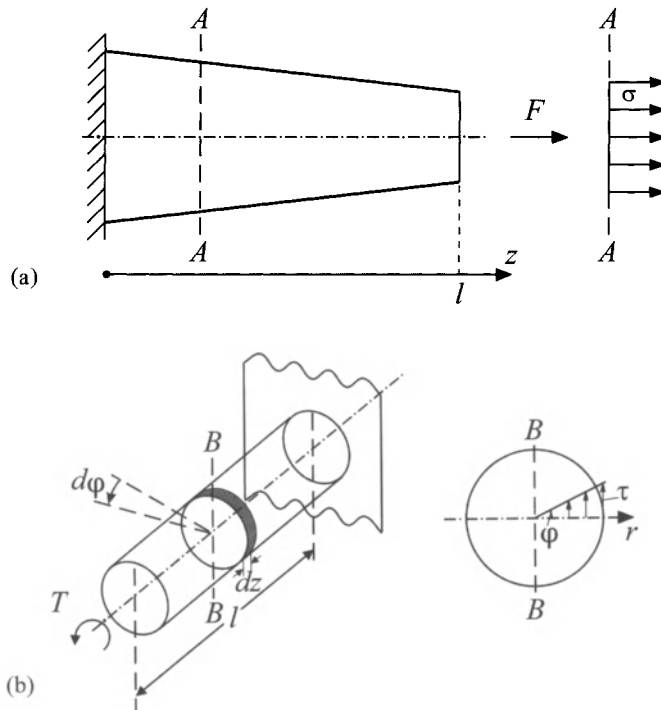


**Figure 4.1** Bars: (a) tension bar with tensile stress  $\sigma$ ; (b) torsion bar with the torsional shearing stress  $\tau$

With the tensile stress

$$\sigma = \frac{F}{A} \quad (4.1.2)$$

the longitudinal expansion is

$$\epsilon = \frac{1}{E} \sigma \quad (4.1.3)$$

The length deviation of the bar becomes

$$\Delta l = \int_0^l dl = \int_0^l \epsilon dz = F \int_0^l \frac{1}{EA(z)} dz \quad (4.1.4)$$

With  $A(z) = \text{const.}$  it follows that

$$\Delta l = \frac{F}{EA} l \quad (4.1.5)$$

The following equation describes the compliance

$$h = \frac{\Delta l}{F} = \int_0^l \frac{1}{EA(z)} dz \quad [m/N] \quad (4.1.6)$$

and the stiffness

$$c = \frac{1}{h} = \frac{F}{\Delta l} \quad [N/m] \quad (4.1.7)$$

If  $E = \text{const.}$  and  $A = \text{const.}$ , the following applies

$$h = \frac{l}{EA} \text{ and } c = \frac{EA}{l} \quad (4.1.8)$$

Now, a torsion bar fixed on one side, Figure 4.1b, is considered. Applying a torque  $T$  at the free end results in an angle deviation  $\Delta\varphi$ . This causes shearing stresses  $\tau$ , proportional to the radius, to appear in all cross-sections, Figure 4.1b. For the twist or torsion of an element of length  $dz$ , applies

$$\frac{d\varphi}{dz} = \frac{T}{GI} \quad (4.1.9)$$

with

$G$  shear modulus

$$I \text{ torsional or polar moment of inertia } I = \int r^2 dA.$$

The angle deviation, assuming  $T = \text{const.}$  is

$$\Delta\varphi = \int_0^l d\varphi = T \int_0^l \frac{1}{GI(z)} dz \quad (4.1.10)$$

and with  $I(z) = \text{const.}$

$$\Delta\varphi = \frac{T}{GI} l \quad (4.1.11)$$

The following equation describes the torsional compliance

$$h_T = \frac{\Delta\varphi}{T} = \int_0^l \frac{1}{GI(z)} dz \quad (4.1.12)$$

and

$$c_T = \frac{T}{\Delta\varphi} = \frac{1}{h_T} \quad (4.1.13)$$

the torsional stiffness.

Assuming  $G = \text{const.}$  and  $I = \text{const.}$ , the compliance becomes

$$h_T = \frac{l}{GI} \text{ and } c_T = \frac{GI}{l}\sigma \quad (4.1.14)$$

## 4.2 SPRINGS

Springs pick up, save and release mechanical energy. They decrease the imposed forces from shocks or oscillating loads and can also be used to create forces or torques. One can distinguish between:

- metal springs for compression, extension, bending or torsion;
- gas or pneumatic springs;
- rubber springs.

For small excitations, the majority of springs behave linearly. Then, it follows from the basic equations of the tensile bar for infinitesimally small changes of the force  $dF$  and the length  $dz$  that

$$\text{spring stiffness: } c = \frac{dF}{dz} \quad (4.2.1)$$

$$\text{compliance: } h = \frac{1}{c} \quad (4.2.2)$$

$$\text{deformation work: } W = \int F \, dz \quad (4.2.3)$$

$$\begin{aligned} \text{parallel connection: } F_{tot} &= \sum_i F_i \\ c_{tot} &= \sum_i c_i \end{aligned} \quad (4.2.4)$$

$$\text{series connection: } z_{tot} = \sum_i z_i \\ h_{tot} = \frac{1}{c_{tot}} = \sum_i \frac{1}{c_i} = \sum_i h_i \quad (4.2.5)$$

A helical spring, according to Figure 4.2a, picks up mechanical energy via a torsional deformation. Therefore, its characteristic values can be calculated based upon the basic equations of the torsional bar. For  $n$  windings, the following applies

$$\text{longitudinal stiffness: } c_T = \frac{dT}{d\varphi} = \frac{GI}{l} = \frac{Gd^4}{64Dn} \quad (4.2.6)$$

$$c = \frac{dF}{dl} = \frac{Gd^4}{8D^3n} \quad (4.2.7)$$

For loads  $\Delta x$  orthogonal to the length deviation  $\Delta l$ , the

$$\text{lateral stiffness: } c = \frac{\Delta F_q}{\Delta x} \quad (4.2.8)$$

is effective, compare also Krämer (1984), Walsh (1999). The smaller  $l/D$  the larger is the lateral stiffness.

A gas spring picks up mechanical energy via compression of gaseous fluids according to the polytropic state equation

$$p \cdot V^n = k' \quad n = 1 \dots 1,4 \quad (4.2.9)$$

(Figure 4.2b), where  $k'$  is a constant. With  $F = pA$  and  $V = A(l-z)$ , it follows that

$$F = A^{1-n}(l-z)^{-n}k' \quad (4.2.10)$$

with  $n = 1$  for isothermal and  $n = 1.4$  for adiabatic state changes (bi-atomic gases).

For the spring's stiffness, it follows that

$$c = \frac{dF}{dz} = nA^{1-n}(l-z)^{-(n+1)}k'$$

and after substituting (4.2.9)

$$c = \frac{A}{(l-z)} np \quad (4.2.11)$$

The spring's stiffness increases inversely proportionally to the length ( $l-z$ ), it is therefore progressive.

From (4.2.10), it follows that (compare also Figure 4.2b)

$$\frac{F_1}{F_2} = \left( \frac{l-z_2}{l-z_1} \right)^n \quad (4.2.12)$$

For the modulus of elasticity, applies, according to (4.1.8) and (4.2.11)

$$E = \frac{c(l-z)}{A} = p \cdot n \quad (4.2.13)$$

It is proportional to the pressure  $p$  and the polytropic exponent  $n$ .

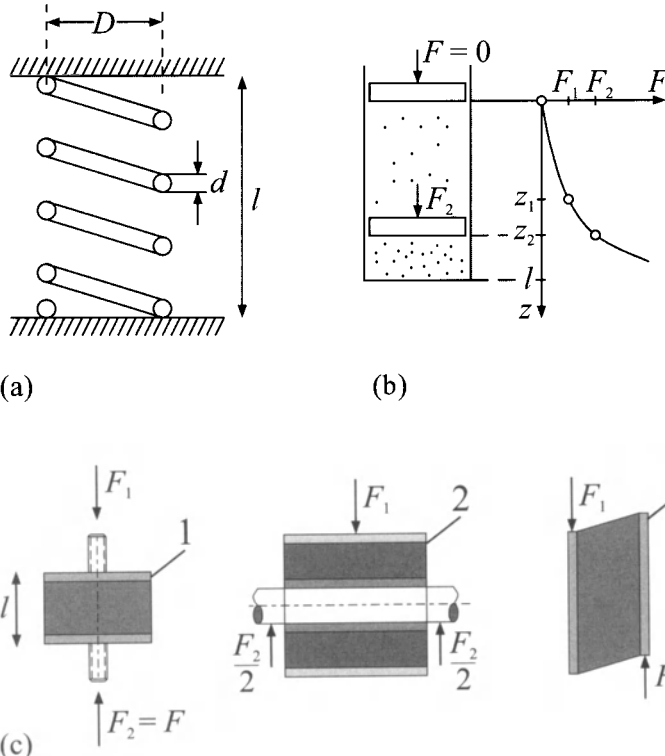


**Figure 4.2.** Springs: (a) helical spring; (b) gas/pneumatic spring; (c) rubber springs 1,2 compression spring, 3 parallel thrust spring

Rubber springs pick up mechanical energy by compression and/or extension deformation, compare Figure 4.2c. The springs can be made of natural or artificial rubber (elastomers). For the spring's stiffness, applies, in the case of compression deformation according to the tensile bar (Figure 4.2c left hand side)

$$c = \frac{EA}{l} \quad (4.2.14)$$

The elasticity module strongly depends, besides the type of rubber, on the temperature, the frequency, amplitude and the steady stress component. The module increases with increasing hardness and frequency while it decreases for rising temperature, see also Göbel (1969), Krämer (1984), Walsh (1999).

Rubber springs are mainly used for vibration isolation and for elastic couplings. They have quite a good self-damping property.

## 4.3 DAMPERS

Damping in oscillating systems causes a decrease in free oscillations and a reduction of the amplitude resulting from forced oscillations, particularly within the resonance range. Mechanical energy is converted into other forms of energy, mostly into heat. It is possible to divide damping into the following categories:

- material damping (internal damping);
- contact damping (sliding points. Joints: screws, rivets);
- fluid damping (surrounding medium: air, oil).

### 4.3.1 Dampers with Dry and Viscous Friction

Figure 4.3 illustrates elementary damping systems with different kinds of sliding frictions. The dry friction force (Coulomb friction) is described by (Figure 4.3a)

$$F_c = -\mu F_N \operatorname{sign} \dot{z} \quad |\dot{z}| > 0 \quad (4.3.1)$$

$F_N$  : normal force

$\mu$  : friction coefficient.

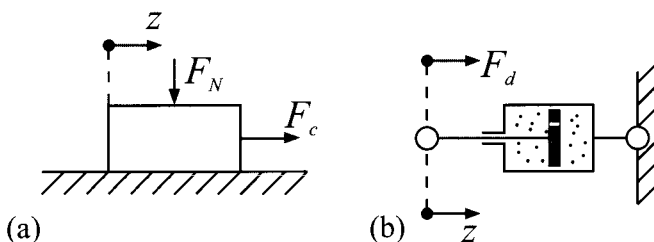


Figure 4.3. Elementary dampers: (a) dry friction; (b) viscous friction

The friction coefficient  $\mu$  depends on the material combination and the surface of the contact surfaces. It ranges normally within  $0.1 \leq \mu \leq 0.6$ . The viscous friction or liquid friction occurs if a lubricated liquid is in between the sliding bodies. It also appears in fluid dampers, in which a moving piston squeezes the fluid through a throttle point. This leads with small speeds and laminar flow to

$$F_d = -d \dot{z} \quad (4.3.2)$$

and with large speeds and turbulent flow to

$$F_d = -d \dot{z}^2 \quad (4.3.3)$$

### 4.3.2 Spring-damper Systems

Damping often occurs together with elasticities and this results in different damper models. Figure 4.4 shows some basic configurations of spring-damper systems: (a), (b) and (c) are described by two parameters, (d) and (e) by three parameters.

As an example, the Kelvin-Voigt model for a frequently occurring viscoelastic damper according to Figure 4.4a is considered. For the external force, applies

$$F(t) = -F_f(t) - F_d(t) = c_f z(t) + d \dot{z}(t) \quad (4.3.4)$$

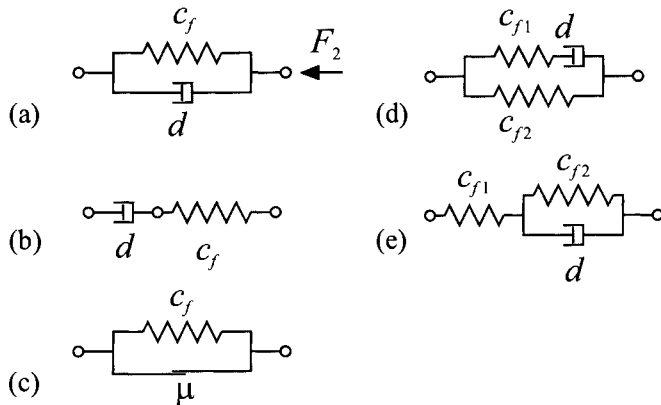


**Figure 4.4.** Basic configurations of damper models: (a) Kelvin-Voigt model; (b) Maxwell model; (c) Coulomb model; (d) combination 1; (e) combination 2

The Laplace transformation leads to

$$F(s) = [c_f + ds]z(s) \quad (4.3.5)$$

and the transfer function becomes

$$G(s) = \frac{F(s)}{z(s)} = c_f + ds = c_f \left(1 + \frac{ds}{c_f}\right) = c_f (1 + T_D s) \quad (4.3.6)$$

Hence, a proportional differentiating element results with the locus of the frequency response  $G(i\omega)$  for  $s = i\omega$  shown in Figure 4.5.

In the case of sinusoidal excitation,

$$z(t) = z_0 \sin \omega t \quad (4.3.7)$$

The resulting force can be described by

$$F(t) = F_0 \sin(\omega t + \alpha) \quad (4.3.8)$$

with the amplitude

$$F_0 = c_f \sqrt{1 + \left(\frac{d}{c_f}\right)^2 \omega^2} \quad (4.3.9)$$

and the phase lead angle

$$\alpha = \arctg \frac{Im(\omega)}{Re(\omega)} = \arctg T_D \omega \quad (4.3.10)$$

The force  $F(t)$  leads the deflection  $z(t)$  by the lead angle  $\alpha$ . This leading increases with higher frequencies to a maximum of  $90^\circ$ . The individual amplitudes of the force components can be written as

$$\begin{aligned} \text{spring force } F_{f0} &= c_f z_0 \\ \text{damping force } F_{d0} &= d\omega z_0 \end{aligned}$$

The damping force increases proportionally to the angular frequency  $\omega$  of the excitation.

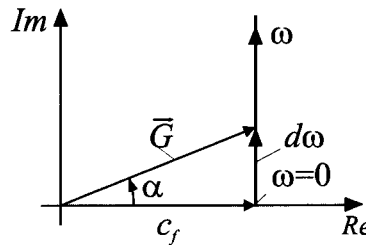


**Figure 4.5** Locus of the frequency response  $G(i\omega) = c_f(1+T_D\omega i)$  of the Kelvin Voigt model

According to DIN 1311, the special designations apply

$$\text{dissipation factor: } \eta_v = \frac{F_{do}}{F_{f0}} = \frac{d\omega}{c_f} \quad (4.3.11)$$

$$\text{loss angle: } \alpha = \arctg \eta_v \quad (4.3.12)$$

The loss angle is identical to the lead angle. The dissipation factor relates the damping force to the spring force. (The expression *loss angle* probably derives from the fact that the movement  $z(t)$  lags behind the resulting force  $F(t)$ .)

The work applied by the damper during one period can be calculated by using the power

$$\frac{dE}{dt} = F(t)\dot{z}(t) \quad (4.3.13)$$

This leads to the work

$$E = \int_0^T F(t)\dot{z}(t)dt \quad (4.3.14)$$

From (4.3.7), it follows that

$$\dot{z}(t) = z_0 \omega \cos \omega t \quad (4.3.15)$$

and from (4.3.2)

$$F_d(t) = d\dot{z}(t) = z_0 d\omega \cos \omega t \quad (4.3.16)$$

This inserted in (4.3.13) results in

$$E = z_0^2 d\omega^2 \int_0^T \cos^2 \omega t dt = \pi d\omega z_0^2 \quad (4.3.17)$$

Hence, the dissipated mechanical work during one oscillation period is proportional to the angular frequency  $\omega$ , to the damping factor  $d$  and to the square of the amplitude  $z_0$ .

## 4.4 BEARINGS

The main purpose of a bearing is the transmission of forces between moving mechanical elements relative to each other and the restriction of their movements to certain directions. One distinguishes between sliding bearings, roller bearings and magnetic bearings. In the following, the underlying friction laws for sliding and roller bearings will be described, as required for modeling. Friction in mechanical systems in general is covered in Section 4.7 of this book.

### 4.4.1 Sliding Bearings

Starting from a certain rotational speed, a lubrication film accumulates between adjacent surfaces, allowing viscous friction. This results in an eccentric position  $e$  of the shaft (or journal), Figure 4.6, Sneed (1991). The rotating shaft transports the lubricant through the bearing gap, resulting in the generation of oil pressures. Implementing certain lubrication channels can influence the flow of the lubricant. The friction coefficient  $\mu$  depends on the Sommerfeld number, Czichos (1989)

$$So = \frac{\bar{p}\psi^2}{\eta \cdot \omega} \quad (4.4.1)$$

Where

$\bar{p} = F/B D$  mean surface pressure

$D, B$  diameter and width of the bearing

$\psi = s/D$  relative clearance

$s = D-d$  working clearance

$\eta$  dynamic viscosity

$\omega$  rotational speed.

For the friction factor, the following applies

$$\mu = k \frac{\psi}{So} \quad So < 1 : \text{low load} \quad (4.4.2)$$

$$\mu = k \frac{\psi}{\sqrt{So}} \quad So > 1 : \text{high load} \quad (4.4.3)$$

where  $k = 2 \dots 3.8$ , depending on the bearing design. For low loads, the friction factor is proportional to  $\omega$ , whereas it is proportional to  $\sqrt{\omega}$  for high loads.

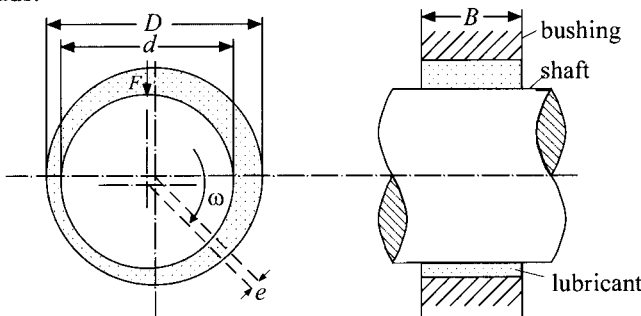


**Figure 4.6.** Scheme of a sliding bearing (fluid film bearing)

#### 4.4.2 Roller Bearings

According to the variety of bearing strains (axial, radial), mounting properties, clearance adjustment, *etc.*, there exists a wide variety of different bearing designs. Figure 4.7 shows three examples.

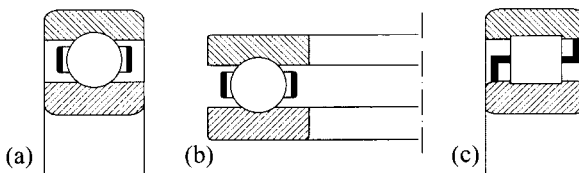


**Figure 4.7.** Different forms of roller bearings: (a) ball bearing (deep groove ball bearing); (b) axial type ball bearing for axial forces; (c) cylindrical roller bearing (as movable bearing) for radial forces

An exact mathematical description of the roller friction phenomenon is quite complicated. Therefore, in the following, a simple description of the characteristic friction in roller bearings will be given. Palmgren (1964) found these empirical equations by performing a number of experiments.

The different motions of the bearing components cause different kinds of friction within the bearing. At the contact areas between rollers and bearing races, one observes rolling with partial gliding. Also, sliding friction losses occur at the contact points between rollers and the cage, the other bearing parts and the lubricant.

The following characteristics have a more or less strong influence on the friction-dependent behavior of the bearing:

- the bearing type, such as the dimensions and internal design;
- the amount and special properties of the lubricant;
- operation properties, such as temperature, speed, imposed stresses and wear.

For high rotational speeds and small loads (high-speed bearings), the hydrodynamic dissipative moments are predominant, because the rolling motion presses the lubricant (grease or oil) between the adjacent touching bearing parts. This causes the rolling resistance to be mainly dependent on the amount of lubricant, its viscosity (which strongly depends on the temperature) and the rotating speed of the rollers.

In the case that the thickness of the covering lubricant drops below the surface roughness of the adjacent, relatively moving parts, the hydrodynamic assumption does not hold. Then, the following very small, mainly velocity-independent, friction torque applies

$$T_{F0} = 10^{-7} d_m^3 f_0^3 \sqrt{(\nu)^2} \quad \text{for } \nu \geq 2000 \quad (4.4.4a)$$

$$T_{F0} = 10^{-7} d_m^3 f_0 160 \quad \text{for } \nu < 2000 \quad (4.4.4b)$$

with

$T_{F0}$  load-independent friction torque of the roller bearing [Nmm]

$d_m$  mean bearing diameter [mm]

$f_0$  constant, depending on bearing type and lubrication (e.g., 1.5...4)

$n$  rotational speed [rpm]

$\nu = f(\theta)$  kinematic viscosity of the lubricant [ $\text{mm}^2/\text{s}$ ] (typically 5...200).

However, roller bearings are hardly driven within that range.

For low rotational speeds and high loads (low-speed bearings), the friction losses mainly depend on local (partial) gliding of adjacent areas of the bearing components (rollers and tracks). The losses depend to a great extent on the molecular properties of the boundary layer. In this case, the load mainly determines the friction torque

$$T_{F1} = d_m f_1 P_1 \quad (4.4.5)$$

with

$T_{F1}$  load-dependent friction torque of the roller bearing [Nmm]

$d_m$  mean bearing diameter [mm]

$f_1$  constant, depending on bearing type and lubrication

$P_1$  friction torque-decisive bearing load in [N].

For general operating conditions, these friction parts have to be superimposed

$$T_F = T_{F1} + T_{F0} \quad (4.4.6)$$

This yields, under the assumption of a symmetrical friction characteristic, for both rotating directions

$$T_F = T_{F0} \text{sign}(\omega) + T_{F1} \sqrt[3]{\omega^2} \text{sign}(\omega) \quad (4.4.7)$$

with

$T_F$	total bearing friction [Nm]
$T_{F0}$	dry (Coulomb) friction coefficient [Nm]
$T_{F1}$	viscous (fluidic) friction coefficient (rolling and sliding friction)
$\omega$	angular bearing speed [rad/s].

where  $T_{F0}$  and  $T_{F1}$  represent state- and environment-dependent coefficients.

This equation basically describes mathematically the friction losses of a roller bearing within the whole operating range (large signal behavior).

Since  $T_{F1}$  is not transparent with regard to its physical unit

$$\left( \text{kgm}^2/\sqrt[3]{\text{s}^4 \text{rad}^2} \right)$$

the viscous friction part is approximated by a polynomial of the lowest possible order. To obtain an expression that incorporates a linear damping part as well as approximating the non-linear roller bearing characteristic, a third order polynomial is used

$$\begin{aligned} T_{F1}(\omega) &= \sum_{\mu=1}^3 T_{F1\mu} \omega^\mu (\text{sign}(\omega))^{\mu+1} \\ &= T_{F11}\omega + T_{F12}\omega^2 \text{sign}(\omega) + T_{F13}\omega^3 \end{aligned} \quad (4.4.8)$$

The second order part in (4.4.8) describes mainly the influence of air friction, which is of minor importance for the approximation of the roller bearing characteristics. Neglecting this part ( $T_{F12} = 0$ ) and considering the remaining viscous frictions parts from (4.4.7), a polynomial describing the friction characteristics of a roller bearing results

$$T_F(\omega) = T_{F0} \text{sign}(\omega) + T_{F1}\omega + T_{F3}\omega^3 \quad (4.4.9)$$

Now, the physical unit [Nms/rad] of the damping coefficient  $T_{F1}$  is meaningful. Since it is a degressive characteristic, the coefficient  $T_{F3}$  [ $\text{kgm}^2/\text{s}^3 \text{rad}^3$ ] is negative.

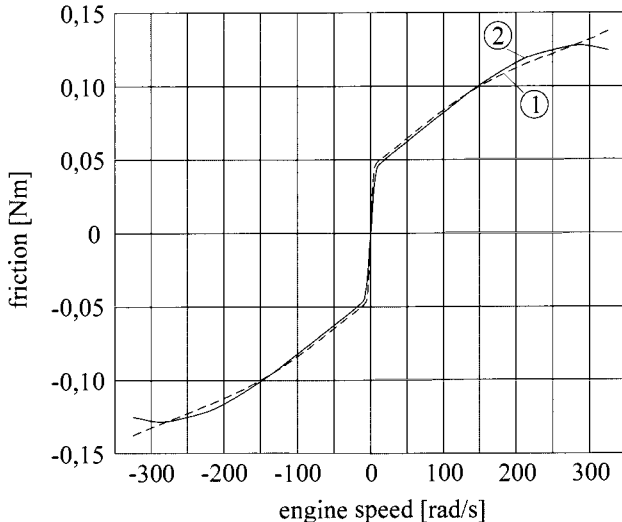
This approach has been successfully verified using a special correlation method with a robot's drive containing several gears and bearings for high rotational speeds (up to approximately 4000 rpm), Freyermuth (1990).

Figure 4.8 shows the comparison between the roller bearing (4.4.7) and the approximation (4.4.9). It shows only small deviations over the considered operating range, which justifies the approximation for practical purposes.

If the degressive characteristic is of minor importance for a certain application because only a small section of the characteristic is used (small signal behavior), the third order part can be set equal to zero. If the roller bearing friction is significantly asymmetrical with respect to the rotating direction, one has to distinguish between positive  $+ (\omega > 0)$  and negative  $- (\omega < 0)$  rotation direction. Then, the structure of the friction model is the same for both directions, but the parameters may

have different values. The indices (+) and (-) indicate the valid friction coefficients with regard to the rotation direction.

$$T_F(\omega) = \begin{cases} T_{F0+} \text{sign}(\omega) + T_{F1+} \omega + T_{F3+} \omega^3 & \text{for } \omega > 0 \\ T_{F0-} \text{sign}(\omega) + T_{F1-} \omega + T_{F3-} \omega^3 & \text{for } \omega < 0 \end{cases} \quad (4.4.10)$$



**Figure 4.8.** Roller bearing friction characteristic of a robot's axis, Freyermuth (1990). 1: roller bearing characteristic according to (4.4.7); 2: polynomial approximation according to (4.4.9)

Further descriptions, calculations and tables regarding forces and motion in roller bearings, applicable load, lifetime, lubrication, service and possible material wear, *etc.*, can be found in Palmgren (1990), Sneed (1991).

## 4.5 ONE-MASS OSCILLATOR (SPRING-MASS-DAMPER SYSTEMS)

In the next section, some simplified, linear models for oscillators with one degree of freedom are presented. There are three different types of oscillators: longitudinal, flexural (bending) and torsional.

### 4.5.1 Longitudinal Oscillators

#### a) Force excitation

An external force  $F_i$  excites the longitudinal oscillator with a serial configuration of spring and damper as in Figure 4.9a. The force  $F_i$  can be written using the principle of linear momentum as

$$m \ddot{Z}_o(t) = F_i(t) + F_c(t) + F_d(t) - G \quad (4.5.1)$$

Here,  $G = mg$  is the weight of the mass.

Applying the constitutive equation of the spring leads to

$$F_c(t) = -c Z_o(t)$$

and applying the phenomenological equation to the damper yields

$$F_d(t) = -d \dot{Z}_o(t)$$

Insertion into (4.5.1) results in

$$m \ddot{Z}_o(t) = F_i(t) - c Z_o(t) - d \dot{Z}_o(t) - G \quad (4.5.2)$$

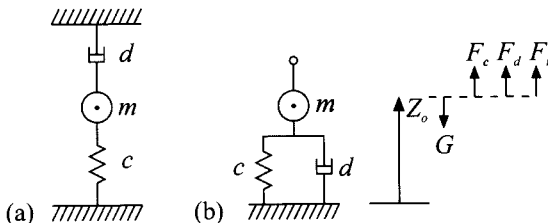


**Figure 4.9.** Longitudinal oscillators with excitation by force  $F_i$ : (a) serial configuration of spring and damper; (b) parallel configuration of spring and damper

For the equilibrium, one obtains by setting the derivations to zero

$$\bar{Z}_o = - \frac{G - \bar{F}_i}{c}$$

which is the static compression.

Now, changes  $z = \Delta Z = Z - \bar{Z}_o$  and  $\Delta F_i = F_i(t) - \bar{F}_i$  around this equilibrium state are considered. This leads to

$$m \ddot{z}_o(t) + d \dot{z}_o(t) + c z_o(t) = \Delta F_i(t) \quad (4.5.3)$$

The transfer function becomes

$$\begin{aligned} G_{zF}(s) &= \frac{z_o(s)}{\Delta F_i(s)} = \frac{1}{ms^2 + ds + c} = \frac{\frac{1}{c}}{\frac{m}{c}s^2 + \frac{d}{c}s + 1} \\ &= \frac{K}{\frac{1}{\omega_0^2}s^2 + \frac{2D}{\omega_0}s + 1} = \frac{K}{T_2^2 s^2 + T_1 s + 1} \end{aligned} \quad (4.5.4)$$

with the characteristic values

$$\omega_n = \frac{1}{T_2} = \sqrt{\frac{c}{m}} \quad \text{undamped natural freq. } (D=0)$$

$$\zeta = \frac{T_1}{2T_2} = \frac{d}{2} \frac{1}{\sqrt{cm}} \quad \text{damping ratio}$$

$$\delta = D\omega_0 = \frac{d}{2m} \quad \text{decaying (damping) constant}$$

$$\omega_e = \omega_0\sqrt{1-D^2} = \sqrt{\frac{c}{m} - \frac{d^2}{4m^2}} \quad \text{damped natural frequency } (D<1)$$

$$\omega_{res} = \omega_0\sqrt{1-2D^2} = \sqrt{\frac{c}{m} - \frac{d^2}{2m^2}} \quad \text{resonance angular frequency}$$

$$(0 < D < 1/\sqrt{2}) \quad (4.5.5)$$

If (4.5.3) is written in the form

$$m\ddot{z}_o(t) = -cz_o(t) - d\dot{z}_o(t) + \Delta F_i(t)$$

then the block diagram according to Figure 4.10a results for the input  $\Delta F_i(t)$ . This is the elementary block diagram of the spring-mass-damper system in serial configuration. It directly follows from the differential equation for the principle of linear momentum, the constitutive equation for the spring and the phenomenological equation for the damper.

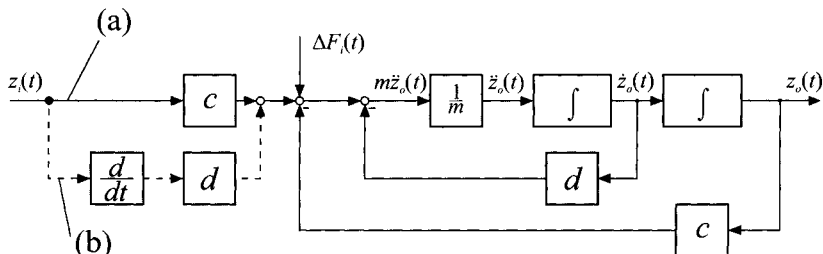


**Figure 4.10.** Elementary block diagram of the spring-mass-damper system for force excitation  $\Delta F_i(t)$  and base excitation  $z_i(t)$ : (a) serial configuration of spring and damper according to Figure 4.9a for force excitation  $\Delta F_i(t)$  and base excitation  $z_i(t)$ : straight lines; (b) parallel configuration of spring and damper according to Figure 4.9b: additionally dashed lines for base excitation  $z_i(t)$

For many applications, e.g., for simulation or state control, the state representation of the system is required. The outputs of the storages (integrators) may be selected as state variables, according to Figure 4.10, as

$$x_1(t) = z_o(t); x_2(t) = \dot{z}_o(t) \quad (4.5.6)$$

Then, using the transformed differential equation (4.5.3)

$$\begin{aligned}\ddot{z}_o(t) + \frac{d}{m} \dot{z}_o(t) + \frac{c}{m} z_o(t) &= \frac{1}{m} \Delta F_i(t) \\ \ddot{z}_o(t) + a_1 \dot{z}_o(t) + a_0 z_o(t) &= b_0 \Delta F_i(t)\end{aligned}\quad (4.5.7)$$

with the parameters

$$a_1 = \frac{d}{m}; \quad a_0 = \frac{c}{m}; \quad b_0 = \frac{1}{m} \quad (4.5.8)$$

and with the input  $u(t) = F_i(t)$ , one gets

$$\begin{aligned}\dot{x}_1(t) &= x_2(t) \\ \dot{x}_2(t) &= -a_0 x_1(t) - a_1 x_2(t) + b_0 u(t) \\ y(t) &= x_1(t) = z_o(t)\end{aligned}$$

The state space representation is then given by

$$\begin{aligned}\begin{bmatrix} \dot{x}_1(t) \\ \dot{x}_2(t) \end{bmatrix} &= \begin{bmatrix} 0 & 1 \\ -a_0 & -a_1 \end{bmatrix} \begin{bmatrix} x_1(t) \\ x_2(t) \end{bmatrix} + \begin{bmatrix} 0 \\ b_0 \end{bmatrix} u(t) \\ y(t) &= [1 \quad 0] \begin{bmatrix} x_1(t) \\ x_2(t) \end{bmatrix}\end{aligned}\quad (4.5.9)$$

The choice of the state variables is not unique. In system theory and control theory, certain canonical state space representations are used that are transferred to each other by linear transformations, see, e.g., Föllinger (1992), Isermann (1989), Ogata (1997), Ellis (2000). For the design of control systems, the *controllable canonical form* is suitable, which can be obtained by choosing the appropriate state variables

$$x_1(t) = \frac{1}{b_0} z_o(t); \quad x_2(t) = \frac{1}{b_0} \dot{z}_o(t) \quad (4.5.10)$$

From

$$\frac{1}{b_0} \ddot{z}_o(t) + a_1 \frac{1}{b_0} \dot{z}_o(t) + a_0 \frac{1}{b_0} z_o(t) = \Delta F_i(t) \quad (4.5.11)$$

and  $u(t) = F_i(t)$  follows the state space representation

$$\begin{aligned}\begin{bmatrix} \dot{x}_1(t) \\ \dot{x}_2(t) \end{bmatrix} &= \begin{bmatrix} 0 & 1 \\ -a_0 & -a_1 \end{bmatrix} \begin{bmatrix} x_1(t) \\ x_2(t) \end{bmatrix} + \begin{bmatrix} 0 \\ 1 \end{bmatrix} u(t) \\ y(t) &= [b_0 \quad 0] \begin{bmatrix} x_1(t) \\ x_2(t) \end{bmatrix}\end{aligned}\quad (4.5.12)$$

The corresponding block diagram is shown in Figure 4.11. The observed canonical form is given, e.g., in Isermann (1989).

For a parallel configuration of spring and damper, according to Figure 4.9b, one obtains for the case of force excitation  $F_i(t)$  the same differential equation as that given in (4.5.3).

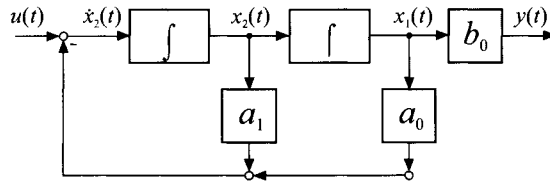


**Figure 4.11.** Block diagram of the serial spring-mass-damper system with state space representation in controllable canonical form.  $u(t) = \Delta F_i(t)$ ,  $y(t) = z_o(t)$ , according to Figure 4.10a

### b) Basic excitation

A deflection at the base generates in the case of serial configuration, according to Figure 4.12, movements around the steady state condition

$$\begin{aligned} m\ddot{z}_o(t) &= c(z_i(t) - z_o(t)) - d\dot{z}_o(t) \\ m\ddot{z}_o(t) + d\dot{z}_o(t) + cz_o(t) &= cz_i(t) \end{aligned} \quad (4.5.13)$$

with the transfer function

$$G_{zz}(s) = \frac{z_o(s)}{z_i(s)} = \frac{c}{ms^2 + ds + c} \quad (4.5.14)$$

Except for the gain, it is the same type as (4.5.4). The block diagram Figure 4.10a follows with the input  $z_i(t)$ .

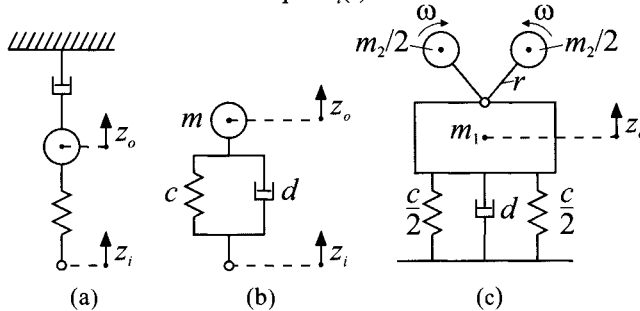


**Figure 4.12** Longitudinal oscillators with excitation by: (a), (b) base deflection; (c) unbalance

Now, the parallel configuration according to Figure 4.12b is considered. The movement around the steady state condition for base excitation  $z_i(t)$  is

$$\begin{aligned} m\ddot{z}_o(t) &= c(z_i(t) - z_o(t)) + d(\dot{z}_i(t) - \dot{z}_o(t)) \\ m\ddot{z}_o(t) + d\dot{z}_o(t) + cz_o(t) &= cz_i(t) + d\dot{z}_i(t) \end{aligned} \quad (4.5.15)$$

The transfer function then results in

$$G_{zz}(s) = \frac{z_o(s)}{z_i(s)} = \frac{ds + c}{ms^2 + ds + c} \quad (4.5.16)$$

In comparison to (4.5.3) and (4.5.14), a lead effect results, see Figure 4.10b. The parameters (4.5.5) remain the same, since the denominator polynomial does not change.

### c) Excitation by unbalance

To receive an excitation in the vertical direction, according to Figure 4.12c, two counteracting masses  $m_2/2$  are mounted onto mass  $m_1$ . The excitation force is

$$F_u(t) = m_2 r \omega^2 \sin \omega t \quad (4.5.17)$$

and this leads to

$$(m_1 + m_2) \ddot{z}_o(t) = -d\dot{z}_o(t) - cz_o(t) + m_2 r \omega^2 \sin \omega t$$

$$m \ddot{z}_o(t) + d\dot{z}_o(t) + cz_o(t) = m_2 r \omega^2 \sin \omega t \quad (4.5.18)$$

This corresponds, in (4.5.3), to an excitation force at the mass of

$$F_i(t) = F_0 \sin \omega t \quad (4.5.19)$$

with the amplitude of unbalance

$$F_0 = m_2 r \omega^2$$

Hence, the amplitude of the deflection of the mass is proportional to the unbalance mass  $m_2$ , to the radius  $r$  and to the square of the angular frequency  $\omega$ .

## 4.5.2 Torsional Oscillators

For a torsional oscillator with one fixed end, according to Figure 4.13, with moment of inertia  $J$  and torsional stiffness  $c$ , it follows that from the principle of angular momentum (4.1.15) according to (4.1.13)

$$\begin{aligned} J\ddot{\phi}(t) &= T(t) - c\phi(t) - d\dot{\phi}(t) \\ J\ddot{\phi}(t) + d\dot{\phi}(t) + c\phi(t) &= T(t) \end{aligned} \quad (4.5.20)$$

Small changes around the equilibrium leads to

$$T(t) = \bar{T} + \Delta T(t); \quad \phi(t) = \bar{\phi} + \Delta\phi(t)$$

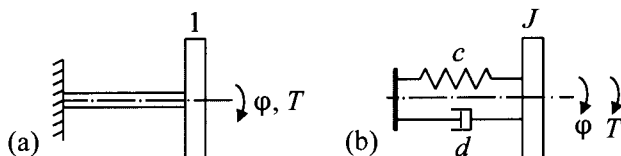


**Figure 4.13.** Torsional oscillators with one fixed end: (a) configuration; (b) equivalent scheme

For the equilibrium state, it follows, from (4.5.20), that

$$\bar{\phi} = \frac{\bar{T}}{c}$$

and for small changes

$$J\Delta\ddot{\phi}(t) + d\Delta\dot{\phi}(t) + c\Delta\phi(t) = \Delta T(t)$$

(This equation has the same form as (4.5.20). Using  $\bar{T}=0$  and  $\bar{\phi}=0$ , both equations are identical. Hence, (4.5.20) describes small changes around the operating point  $T=0$ ,  $\phi=0$ .)

The transfer function is described by

$$G_{\phi T}(s) = \frac{\Delta\phi(s)}{\Delta T(s)} = \frac{1}{Js^2 + ds + c} \quad (4.5.21)$$

Therefore, the torsional oscillator has the same transfer function as the longitudinal oscillator (4.5.4), if  $J$  is replaced by  $J \triangleq m$ .

The natural angular frequency is

$$\omega_0 = \sqrt{\frac{c}{J}}$$

and the damped natural frequency is

$$\omega_i = \sqrt{\frac{c}{J} - \frac{d^2}{4J^2}} \quad (D < 1)$$

## 4.6 MULTI-MASS OSCILLATORS

As examples for multi-mass oscillators, which frequently occur in machines, different two-mass torsional oscillators without and with gearboxes will be considered.

### 4.6.1 Two-mass Torsional Oscillator with One Spring

In the configuration according to Figure 4.14a, it is assumed that the rotational masses are concentrated on the left and right side and that the moment of inertia of the shaft is negligible. The torsional stiffness and torsional damping is assumed to be concentrated in the shaft. This configuration frequently occurs for drives, e.g., if  $J_1$  essentially contains the moment of inertia of an electric motor or a combustion engine and if the drivetrain essentially contains a torque shaft with a rotational mass  $J_2$  at the end.

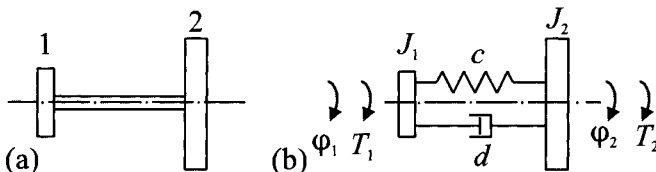


**Figure 4.14.** Two-mass torsional oscillators with a spring: (a) configuration; (b) equivalent scheme of the unbounded torsional oscillator

For the description of the dynamic behavior, the following two cases can be differentiated:

a) *Free torsional oscillator*

Both rotational masses move freely. The turning actions can be overlaid to give a rotation with constant rotating speed.

b) *Fixed torsional oscillator*

One of the rotational masses or the associated end of the torsion spring is fixed (according to Figure 4.13). This is applied with a fixed mass or a very large rotational mass, or if the associated movement (rotating speed) is given or applied.

In both cases, a different dynamic behavior arises, e.g., expressed by the result of the angular frequencies  $\omega_0$  of the undamped oscillator. This natural frequency depends in case a) on both moments of inertia  $J_1$  and  $J_2$  and in case b) either on  $J_1$  or on  $J_2$ .

For the free torsional oscillator, an equivalent scheme results according to Figure 4.14b. After isolating the rotational masses, the *differential equations* for the free bodies can be obtained from the principle of angular momentum

$$\begin{aligned} J_1 \ddot{\varphi}_1(t) &= -c(\varphi_1(t) - \varphi_2(t)) - d(\dot{\varphi}_1(t) - \dot{\varphi}_2(t)) + T_1(t) \\ J_2 \ddot{\varphi}_2(t) &= -c(\varphi_2(t) - \varphi_1(t)) - d(\dot{\varphi}_2(t) - \dot{\varphi}_1(t)) + T_2(t) \end{aligned} \quad (4.6.1)$$

respectively

$$\begin{aligned} J_1 \ddot{\varphi}_1(t) + d\dot{\varphi}_1(t) + c\varphi_1(t) &= T_1(t) + c\varphi_2(t) + d\dot{\varphi}_2(t) \\ J_2 \ddot{\varphi}_2(t) + d\dot{\varphi}_2(t) + c\varphi_2(t) &= T_2(t) + c\varphi_1(t) + d\dot{\varphi}_1(t) \end{aligned}$$

Figures 4.15a and b show two associated block diagrams for the case that the torque inputs are given by  $T_1$  and  $T_2$ . Figure 4.15a directly results from (4.6.1). For each of the rotational masses and the common torsional spring, one block diagram results. If the torsional torque resulting after isolation is described by

$$\begin{aligned} T_T(t) &= T_{T1}(t) - T_{T2}(t) \\ &= (c\varphi_1(t) + d\dot{\varphi}_1(t)) - (c\varphi_2(t) + d\dot{\varphi}_2(t)) \\ &= c(\varphi_1(t) - \varphi_2(t)) + d(\dot{\varphi}_1(t) - \dot{\varphi}_2(t)) \\ &= c\Delta\varphi^*(t) + d\Delta\dot{\varphi}^*(t) \end{aligned}$$

then the block diagram Figure 4.15b follows. By the introduction of the turning angle  $\Delta\varphi^*$ , the block diagram becomes simpler. Herewith, both the rotational masses and the torsional spring get individual parts of the block diagram. Multiple feedback paths can be seen in both block diagrams. A vectorial representation follows from (4.6.1)

$$\begin{bmatrix} J_1 & 0 \\ 0 & J_2 \end{bmatrix} \begin{bmatrix} \ddot{\varphi}_1(t) \\ \ddot{\varphi}_2(t) \end{bmatrix} + \begin{bmatrix} d & -d \\ -d & d \end{bmatrix} \begin{bmatrix} \dot{\varphi}_1(t) \\ \dot{\varphi}_2(t) \end{bmatrix} + \begin{bmatrix} c & -c \\ -c & c \end{bmatrix} \begin{bmatrix} \varphi_1(t) \\ \varphi_2(t) \end{bmatrix} = \begin{bmatrix} 1 & 0 \\ 0 & 1 \end{bmatrix} \begin{bmatrix} T_1(t) \\ T_2(t) \end{bmatrix} \quad (4.6.2)$$

$$J \ddot{\varphi}(t) + D \dot{\varphi}(t) + C \varphi(t) = F T(t) \quad (4.6.3)$$

which is a *second order vector differential equation*. Also, chains of torsional oscillators with more than two torsional oscillators can be re-

presented in the form of (4.6.3). According to the number  $n$  of the torsional oscillators, the order of the vectors and matrices increases to  $n$ .

A state representation corresponding to that of a one-mass oscillator (4.5.9) can be received by choice of the state variables

$$\dot{x}^T(t) = [\varphi_1(t)\dot{\varphi}_1(t)\varphi_2(t)\dot{\varphi}_2(t)] = [x_1(t)x_2(t)x_3(t)x_4(t)] \quad (4.6.4)$$

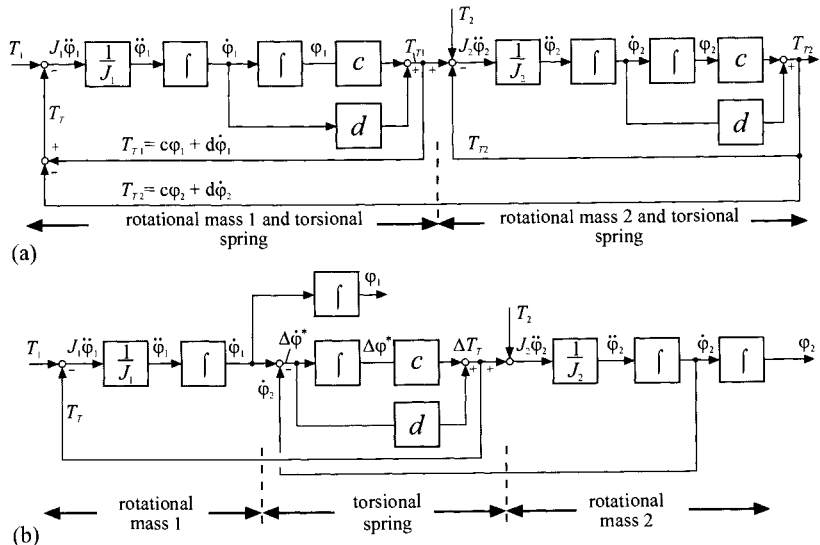


Figure 4.15. Block diagrams of the two-mass oscillator according to Figure 4.14: (a) two subsystems; (b) three subsystems

(4.6.1) is written in the form of

$$\begin{aligned}\ddot{\varphi}_1(t) &= -\frac{c}{J_1}\varphi_1(t) + \frac{c}{J_1}\varphi_2(t) - \frac{d}{J_1}\dot{\varphi}_1(t) + \frac{d}{J_1}\dot{\varphi}_2(t) + \frac{1}{J_1}T_1(t) \\ &= -a_{10}\varphi_1(t) + a_{10}\varphi_2(t) + a_{11}\dot{\varphi}_1(t) + a_{11}\dot{\varphi}_2(t) + b_{10}T_1(t)\end{aligned} \quad (4.6.5)$$

$$\begin{aligned}\ddot{\varphi}_2(t) &= -\frac{c}{J_2}\varphi_2(t) + \frac{c}{J_2}\varphi_1(t) - \frac{d}{J_2}\dot{\varphi}_2(t) + \frac{d}{J_2}\dot{\varphi}_1(t) + \frac{1}{J_2}T_2(t) \\ &= -a_{20}\varphi_2(t) + a_{20}\varphi_1(t) - a_{21}\dot{\varphi}_2(t) + a_{21}\dot{\varphi}_1(t) + b_{20}T_2(t)\end{aligned} \quad (4.6.6)$$

This yields

$$\begin{bmatrix} \dot{\varphi}_1(t) \\ \ddot{\varphi}_1(t) \\ \dot{\varphi}_2(t) \\ \ddot{\varphi}_2(t) \end{bmatrix} = \begin{bmatrix} 0 & 1 & 0 & 0 \\ -a_{10} & -a_{11} & -a_{10} & -a_{11} \\ 0 & 0 & 0 & 1 \\ a_{20} & a_{21} & -a_{20} & -a_{21} \end{bmatrix} \begin{bmatrix} \varphi_1(t) \\ \dot{\varphi}_1(t) \\ \varphi_2(t) \\ \dot{\varphi}_2(t) \end{bmatrix} + \begin{bmatrix} 0 & 0 \\ b_{10} & 0 \\ 0 & 0 \\ 0 & b_{20} \end{bmatrix} \begin{bmatrix} T_1(t) \\ T_2(t) \end{bmatrix}$$

$$\dot{x}(t) = A x(t) + B u(t) \quad (4.6.7)$$

$$y(t) = \varphi_2(t) = [0 \ 0 \ 1 \ 0] \ x(t) = c^T x(t) \quad (4.6.8)$$

A further representation possibility for chains of torsional oscillators is the *two-port network representation* according to Figure 4.16. With such a two-port network, the coupling of several components can be represented in block form. The cut between two components is defined by a power, see Chapter 2. Therefore, torques and rotating speeds are the input and output signals for torsional oscillators.

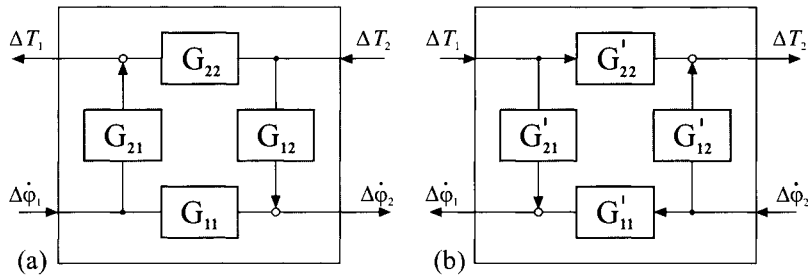


**Figure 4.16** Two-port network representation of a two-mass torsional oscillator: (a) inputs:  $\Delta\dot{\phi}_1$  and  $\Delta T_2$ ; (b) inputs:  $\Delta T_1$  and  $\Delta\dot{\phi}_2$

For converters, the following variables can be independent inputs in the stationary case, compare Figure 2.17a, b:

- a) Applied angular speed  $\dot{\phi}_1$  or applied torque  $T_2$ .
- b) Applied torque  $T_1$  or applied angular speed  $\dot{\phi}_2$ .

For these two cases, the transfer functions are derived for small changes. For each input, only one output is considered and the other two variables are set to zero. Then, it follows that each one angular speed is either zero, or it is an applied input. In the block diagram, Figure 4.15a, which is shown for the inputs  $T_1$  and  $T_2$  and the output values  $\dot{\phi}_1$  and  $\dot{\phi}_2$ , it is, e.g., in case a).  $\Delta\dot{\phi}_2 = f(\Delta T_2)$  for  $\Delta\dot{\phi}_1 = 0$  and in case b)  $\Delta\dot{\phi}_1 = f(\Delta T_1)$  for  $\Delta\dot{\phi}_2 = 0$ . Therefore, only one part of the block diagram becomes effective, either the right part for rotational mass 2 and the torsional spring or the left part for the rotational mass 1 and the torsional spring.

For small changes around the equilibrium, it is

$$\begin{aligned} T_1(t) &= \bar{T}_1 + \Delta T_1(t) ; \Delta T_2(t) = \bar{T}_2 + \Delta T_2(t) \\ \varphi_1(t) &= \bar{\varphi}_1 + \Delta\varphi_1(t) ; \varphi_2(t) = \bar{\varphi}_2 + \Delta\varphi_2(t) \end{aligned}$$

After inserting in (4.6.1), one obtains for the equilibrium

$$\bar{T}_1 = \bar{T}_2 = c(\bar{\varphi}_1 - \bar{\varphi}_2)$$

The transfer functions of the differential equations (4.6.1) then follow by Laplace transformation

a) Inputs:  $\Delta \dot{\phi}_1$  and  $\Delta T_2$

$$\begin{aligned}
 G_{11}(s) &= \left. \frac{\Delta \dot{\phi}_2(s)}{\Delta \dot{\phi}_1(s)} \right|_{\Delta T_2=0} = \frac{ds + c}{J_2 s^2 + ds + c} \\
 G_{21}(s) &= \left. \frac{\Delta T_1(s)}{\Delta \dot{\phi}_1(s)} \right|_{\Delta T_2=0} = \frac{J_1 J_2 s^3 + d(J_1 + J_2)s^2 + c(J_1 + J_2)s}{J_2 s^2 + ds + c} \\
 G_{12}(s) &= \left. \frac{\Delta \dot{\phi}_2(s)}{\Delta T_2(s)} \right|_{\Delta \dot{\phi}_1 = 0} = \frac{s}{J_2 s^2 + ds + c} \\
 G_{22}(s) &= \left. \frac{\Delta T_1(s)}{\Delta T_2(s)} \right|_{\Delta \dot{\phi}_1 = 0} = \frac{ds + c}{J_2 s^2 + ds + c} = G_{11}(s)
 \end{aligned} \tag{4.6.9}$$

b) Inputs:  $\Delta T_1$  and  $\Delta \dot{\phi}_2$

$$\begin{aligned}
 G_{11}'(s) &= \left. \frac{\Delta \dot{\phi}_1(s)}{\Delta \dot{\phi}_2(s)} \right|_{\Delta T_1=0} = \frac{ds + c}{J_1 s^2 + ds + c} \\
 G_{12}'(s) &= \left. \frac{\Delta T_2(s)}{\Delta \dot{\phi}_2(s)} \right|_{\Delta T_1=0} = \frac{J_1 J_2 s^3 + (J_1 + J_2)ds^2 + (J_1 + J_2)cs}{J_1 s^2 + ds + c} \\
 G_{21}'(s) &= \left. \frac{\Delta \dot{\phi}_1(s)}{\Delta T_1(s)} \right|_{\Delta \dot{\phi}_2 = 0} = \frac{s}{J_1 s^2 + ds + c} \\
 G_{22}'(s) &= \left. \frac{\Delta T_2(s)}{\Delta T_1(s)} \right|_{\Delta \dot{\phi}_2 = 0} = \frac{ds + c}{J_1 s^2 + ds + c} = G_{11}'(s)
 \end{aligned} \tag{4.6.10}$$

Figure 4.16 shows the associated block diagrams. In the stationary state, only the main transfer elements  $G_{11}$ ,  $G_{22}$  or  $G_{11}'$ ,  $G_{22}'$  are effective, as indicated in Figure 2.17a, b, for the case of the transformers. In the dynamic state, the coupling elements  $G_{12}$ ,  $G_{21}$  or  $G_{12}'$ ,  $G_{21}'$  are additionally effective. In case a, e.g., for applied  $\Delta \dot{\phi}_1$  of rotational mass 1, the undamped natural frequency of the oscillator according to (4.5.5) is

$$\omega_n = \sqrt{c/J_2}$$

and depends on the freely oscillating rotational mass 2. In case b), with, e.g., applied torque  $\Delta T_1$ , the undamped natural frequency is

$$\omega_n' = \sqrt{c/J_1}$$

and therefore depends on the freely oscillating rotational mass 1.

One example of a two-mass torsional oscillator is an electric motor with moment of inertia  $J_1$ , which drives a centrifugal pump with  $J_2$  over

an elastic clutch. Another example is a combustion engine with  $J_1$ , which turns a ship's propeller with  $J_2$ .

The model of a two-mass torsional oscillator can also be used as an equivalent model for elastic shafts with moment of inertia  $J$ . Then, for one section of a shaft with the same geometrical properties,  $J_1 = J_2 = J/2$  can be assumed.

Using transfer functions in each case, the inputs set to zero have to be observed. The two-mass torsional oscillators are usually not driven in such a way, because a working process with a coupling of  $\Delta T_2(t)$  and  $\Delta\varphi_2$  follows on the output side. Examples for this are a centrifugal pump or a vehicle. With a change of inputs, all transfer functions of the two-port network representation are then excited. Therefore, usually the complete coupled configurations (two-port network chains) have to be considered.

If oscillations of the free two-mass torsional oscillator for the relative movement of the two rotational masses are of interest, one introduces

$$\Delta\varphi^*(t) = \varphi_1(t) - \varphi_2(t) \quad (4.6.11)$$

Then, it follows that by subtraction of the two equations in (4.6.1)

$$\frac{J_1 J_2}{J_1 + J_2} \Delta\ddot{\varphi}^*(t) + d\Delta\dot{\varphi}^*(t) + c\Delta\varphi^*(t) = \frac{J_2}{J_1 + J_2} T_1(t) - \frac{J_1}{J_1 + J_2} T_2(t) \quad (4.6.12)$$

with the effective rotational mass

$$J_{\text{eff}} = \frac{J_1 J_2}{J_1 + J_2} = \frac{1}{\frac{1}{J_2} + \frac{1}{J_1}}$$

and the undamped natural frequency

$$\omega_0^2 = \frac{c}{J_{\text{eff}}} = \frac{c(J_1 + J_2)}{J_1 J_2}$$

The undamped natural frequency is therefore determined by the stiffness  $c$  and both moments of inertia  $J_1$  and  $J_2$ .

If one of the moments of inertia is dominating, it holds that

$$J_{\text{eff}} \Big|_{J_1 \gg J_2} \approx J_2 ; J_{\text{eff}} \Big|_{J_1 \ll J_2} \approx J_1$$

Hence, for the undamped natural angular frequency  $\omega_0$  of the oscillations, the smaller moment of inertia is the determining factor.

The equations for a rigid two-mass system can be received by isolating the rotational masses in Figure 4.14a and setting  $\varphi_1 = \varphi_2$

$$J_1 \ddot{\varphi}_1(t) = T_1(t) + T_1'(t)$$

$$J_2 \ddot{\varphi}_1(t) = T_2(t) + T_2'(t)$$

with  $T_1' = -T_2'$  as a coupling torque. This leads to

$$(J_1 + J_2) \ddot{\phi}_1(t) = T_1(t) + T_2(t) \quad (4.6.13)$$

In the motion equation, the sum of the single moments of inertia then appears.

### 4.6.2 Two-mass Torsional Oscillator with Two Springs

Many machines have several torsional oscillators. This leads to serially connected torsional oscillators as shown in Figure 4.17. If one considers two torsional oscillators, then the following equations can be obtained after isolating the rotational masses using the principle of angular momentum

$$\begin{aligned} J_1 \ddot{\phi}_1(t) &= T_{T1}(t) + T_1(t) \\ T_{T1}(t) &= c_1(\phi_0(t) - \phi_1(t)) + d_1(\dot{\phi}_0(t) - \dot{\phi}_1(t)) \\ &= c_1 \Delta\phi_1^*(t) + d_1 \Delta\dot{\phi}_1^*(t) \\ T_{T1}(t) &= T_0(t) \end{aligned} \quad (4.6.14)$$

$$\begin{aligned} J_2 \ddot{\phi}_2(t) &= T_{T2}(t) + T_2(t) \\ T_{T2}(t) &= c_2(\phi_1(t) - \phi_2(t)) + d_2(\dot{\phi}_1(t) - \dot{\phi}_2(t)) \\ &= c_2 \Delta\phi_2^*(t) + d_2 \Delta\dot{\phi}_2^*(t) \\ T_1(t) &= -T_{T2} \quad (\text{coupling}) \end{aligned} \quad (4.6.15)$$

where it holds for the turning angles of the shafts that

$$\Delta\phi_1^* = \phi_0 - \phi_1 ; \Delta\phi_2^* = \phi_1 - \phi_2 \quad (4.6.16)$$

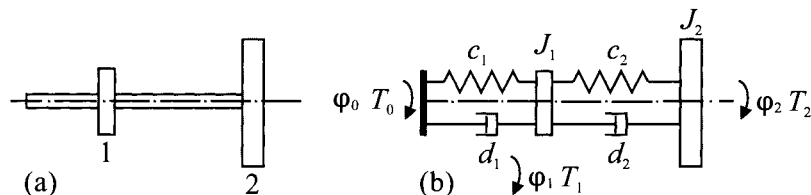


**Figure 4.17.** Two-mass torsional oscillators with two springs: (a) configuration; (b) equivalent diagram

Using this equation, the block diagram for the turning angles is shown in Figure 4.18.  $T_{T1}$  and  $T_{T2}$  are the dynamic torques transferred in the shafts. Several feedbacks appear. In contrast to Figure 4.15b, the rotational masses possess different torsional stiffness and damping.

A two-port network representation of two coupled torsional oscillators is represented in Figure 4.19 for the changes of angles and torques. The individual transfer functions of a torsional oscillator can be obtained through Laplace transformation of the differential equations (4.6.14) and (4.6.15).

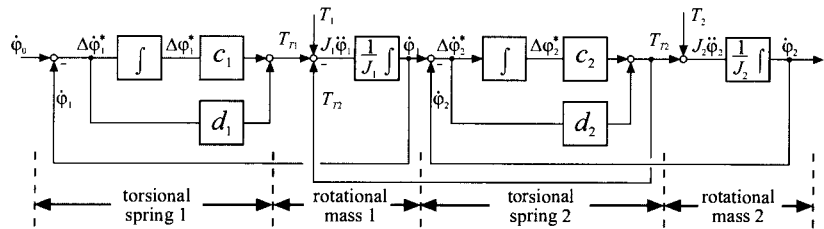


**Figure 4.18.** Block diagram of the two-mass oscillator according to Figure 4.17 for torsional angles

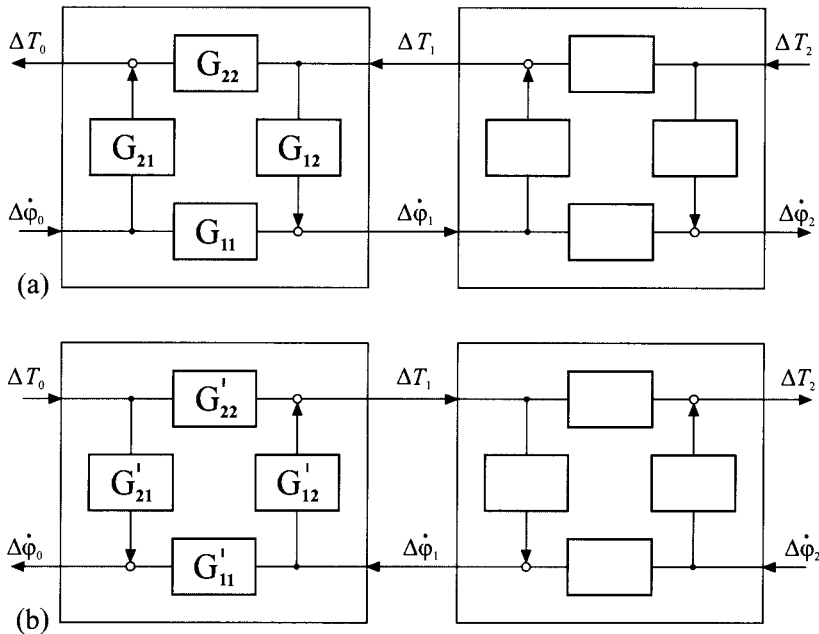


**Figure 4.19.** Two-port network representation of two coupled torsional oscillators with two springs according to Figure 4.17: (a) inputs:  $\Delta \dot{\phi}_0$  and  $\Delta T_2$ ; (b) inputs:  $\Delta T_0$  and  $\Delta \dot{\phi}_2$

For the first torsional oscillator with moment of inertia  $J_1$ , the following transfer functions result by using (4.6.14):

a) Inputs:  $\Delta \dot{\phi}_0$  and  $\Delta T_1$

$$\begin{aligned}
 G_{11}(s) &= \left. \frac{\Delta \dot{\phi}_1(s)}{\Delta \dot{\phi}_0(s)} \right|_{\Delta T_1=0} = \frac{c_1 + d_1 s}{J_1 s^2 + d_1 s + c_1} \\
 G_{21}(s) &= \left. \frac{\Delta T_0(s)}{\Delta \dot{\phi}_0(s)} \right|_{\Delta T_1=0} = \frac{J_1 s (c_1 + d_1 s)}{J_1 s^2 + d_1 s + c_1} \\
 G_{12}(s) &= \left. \frac{\Delta \dot{\phi}_1(s)}{\Delta T_1(s)} \right|_{\Delta \dot{\phi}_0 = 0} = \frac{s}{J_1 s^2 + d_1 s + c_1} \\
 G_{22}(s) &= \left. \frac{\Delta T_0(s)}{\Delta T_1(s)} \right|_{\Delta \dot{\phi}_0 = 0} = \frac{c_1 + d_1 s}{J_1 s^2 + d_1 s + c_1}
 \end{aligned} \tag{4.6.17}$$

b) Inputs:  $\Delta T_0$  and  $\Delta \dot{\phi}_1$

$$\begin{aligned}
 G_{11}^+(s) &= \left. \frac{\Delta \dot{\phi}_0(s)}{\Delta \dot{\phi}_1(s)} \right|_{\Delta T_0=0} = 1 \\
 G_{12}^+(s) &= \left. \frac{\Delta T_1(s)}{\Delta \dot{\phi}_1(s)} \right|_{\Delta T_0=0} = J_1 s \\
 G_{21}^+(s) &= \left. \frac{\Delta \dot{\phi}_0(s)}{\Delta T_0(s)} \right|_{\Delta \dot{\phi}_1 = 0} = \frac{s}{c_1 + d_1 s} \\
 G_{22}^+(s) &= \left. \frac{\Delta T_1(s)}{\Delta T_0(s)} \right|_{\Delta \dot{\phi}_1 = 0} = 1
 \end{aligned} \tag{4.6.18}$$

In the steady state, only the main transfer elements are effective,  $G_{11}^+ = 1$ ,  $G_{22}^+ = 1$ ,  $G_{11}^- = 1$ ,  $G_{22}^- = 1$ . In the dynamic state, the coupling elements have to be added. For the second torsional oscillator, the relations given in Section 4.6.1 are valid.

### 4.6.3 Two-mass Torsional Oscillators with Gear and One Spring

Now, a two-mass torsional oscillator with gearbox according to Figure 4.20 is considered. It is assumed that the gear wheels have a negligible small moment of inertia and have no backlash. Torsional stiffness  $c_i$  and torsional damping  $d_i$  are concentrated in the driveshaft. This means that for the driven shaft,  $\varphi_2 = \dot{\varphi}_2$  applies. The gear ratio follows from  $\varphi_1 r_1 = -\dot{\varphi}_2 r_2$  (equilibrium state:  $\varphi_1 r_1 = -\dot{\varphi}_2 r_2$ )

$$i = -\frac{\dot{\varphi}_1}{\dot{\varphi}_2} = \frac{r_2}{r_1} = -\frac{\dot{\varphi}_1}{\dot{\varphi}_2} = -\frac{\dot{\varphi}_1}{\dot{\varphi}_2} = -\frac{\text{input angular speed}}{\text{output angular speed}} \tag{4.6.19}$$

- $i > 1$  speed reducing ratio  
 $i < 1$  speed increasing ratio

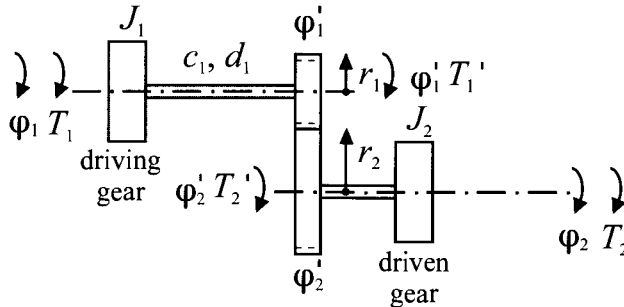


Figure 4.20. Two-mass torsional oscillators with gear

The turning angle is described by using the gears with  $r_1$  and  $r_2$

$$\dot{\varphi}_1 = -\frac{r_2}{r_1} \dot{\varphi}_2 = -i\dot{\varphi}_2 ; \quad \dot{\varphi}_2 = -\frac{r_1}{r_2} \dot{\varphi}_1 = -\frac{1}{i} \dot{\varphi}_1 \quad (4.6.20)$$

and for the torque at the gears, it follows that

$$T_1' = -(-iT_1) = iT_1 \quad (4.6.21)$$

For the driveshaft, it follows from the principle of angular momentum after isolating the rotational masses that

$$\begin{aligned} J_1 \ddot{\varphi}_1(t) &= -c_1(\varphi_1(t) - \dot{\varphi}_1(t)) - d_1(\dot{\varphi}_1(t) - \ddot{\varphi}_1(t)) + T_1(t) \\ J_2 \ddot{\varphi}_2(t) &= i c_1(\dot{\varphi}_1(t) - \varphi_1(t)) + i d_1(\dot{\varphi}_1(t) - \dot{\varphi}_2(t)) + T_2(t) \end{aligned} \quad (4.6.22)$$

With (4.6.20), this leads to

$$\begin{aligned} J_1 \ddot{\varphi}_1(t) &= -c_1(\varphi_1(t) + i\varphi_2(t)) - d_1(\dot{\varphi}_1(t) + i\dot{\varphi}_2(t)) + T_1(t) \\ \frac{J_2}{i} \ddot{\varphi}_2(t) &= c_1(-i\varphi_2(t) - \varphi_1(t)) + d_1(-i\dot{\varphi}_2(t) - \dot{\varphi}_1(t)) + \frac{1}{i} T_2(t) \end{aligned} \quad (4.6.23)$$

or

$$\begin{aligned} J_1 \ddot{\varphi}_1(t) + d_1 \dot{\varphi}_1(t) + c_1 \varphi_1(t) &= T_1(t) - c_1 i \varphi_2(t) - d_1 i \dot{\varphi}_2(t) \\ \frac{J_2}{i^2} \ddot{\varphi}_2(t) + d_1 \dot{\varphi}_2(t) + c_1 \varphi_2(t) &= \frac{1}{i^2} T_2(t) - \frac{c_1}{i} \varphi_1(t) - \frac{d_1}{i} \dot{\varphi}_1(t) \end{aligned} \quad (4.6.24)$$

Using spare variables

$$\varphi_2^{ii} = -i\varphi_2; \quad \varphi_1^{ii} = -\frac{1}{i}\varphi_1; \quad J_2^{ii} = \frac{J_2}{i^2}; \quad T_2^{ii}(t) = -\frac{1}{i^2} T_2(t) \quad (4.4.25)$$

then one obtains

$$\begin{aligned} J_1 \ddot{\varphi}_1(t) + d_1 \dot{\varphi}_1(t) + c_1 \varphi_1(t) &= T_1(t) + c_1 \varphi_2^{ii}(t) + d_1 \dot{\varphi}_2^{ii}(t) \\ J_2^{ii} \ddot{\varphi}_2(t) + d_1 \dot{\varphi}_2(t) + c_1 \varphi_2(t) &= -T_2^{ii}(t) + c_1 \varphi_1^{ii}(t) + d_1 \dot{\varphi}_1^{ii}(t) \end{aligned} \quad (4.6.26)$$

a) Inputs:  $\Delta \dot{\phi}_0$  and  $\Delta T_1$

$$\begin{aligned}
 G_{11}(s) &= \left. \frac{\Delta \dot{\phi}_1(s)}{\Delta \dot{\phi}_0(s)} \right|_{\Delta T_1=0} = \frac{c_1 + d_1 s}{J_1 s^2 + d_1 s + c_1} \\
 G_{21}(s) &= \left. \frac{\Delta T_0(s)}{\Delta \dot{\phi}_0(s)} \right|_{\Delta T_1=0} = \frac{J_1 s (c_1 + d_1 s)}{J_1 s^2 + d_1 s + c_1} \\
 G_{12}(s) &= \left. \frac{\Delta \dot{\phi}_1(s)}{\Delta T_1(s)} \right|_{\Delta \dot{\phi}_0 = 0} = \frac{s}{J_1 s^2 + d_1 s + c_1} \\
 G_{22}(s) &= \left. \frac{\Delta T_0(s)}{\Delta T_1(s)} \right|_{\Delta \dot{\phi}_0 = 0} = \frac{c_1 + d_1 s}{J_1 s^2 + d_1 s + c_1}
 \end{aligned} \tag{4.6.17}$$

b) Inputs:  $\Delta T_0$  and  $\Delta \dot{\phi}_1$

$$\begin{aligned}
 G_{11}^+(s) &= \left. \frac{\Delta \dot{\phi}_0(s)}{\Delta \dot{\phi}_1(s)} \right|_{\Delta T_0=0} = 1 \\
 G_{12}^+(s) &= \left. \frac{\Delta T_1(s)}{\Delta \dot{\phi}_1(s)} \right|_{\Delta T_0=0} = J_1 s \\
 G_{21}^+(s) &= \left. \frac{\Delta \dot{\phi}_0(s)}{\Delta T_0(s)} \right|_{\Delta \dot{\phi}_1 = 0} = \frac{s}{c_1 + d_1 s} \\
 G_{22}^+(s) &= \left. \frac{\Delta T_1(s)}{\Delta T_0(s)} \right|_{\Delta \dot{\phi}_1 = 0} = 1
 \end{aligned} \tag{4.6.18}$$

In the steady state, only the main transfer elements are effective,  $G_{11}^+ = 1$ ,  $G_{22}^+ = 1$ ,  $G_{11}^- = 1$ ,  $G_{22}^- = 1$ . In the dynamic state, the coupling elements have to be added. For the second torsional oscillator, the relations given in Section 4.6.1 are valid.

### 4.6.3 Two-mass Torsional Oscillators with Gear and One Spring

Now, a two-mass torsional oscillator with gearbox according to Figure 4.20 is considered. It is assumed that the gear wheels have a negligible small moment of inertia and have no backlash. Torsional stiffness  $c_1$  and torsional damping  $d_1$  are concentrated in the driveshaft. This means that for the driven shaft,  $\varphi_2 = \dot{\varphi}_2$  applies. The gear ratio follows from  $\varphi_1 r_1 = -\varphi_2 r_2$  (equilibrium state:  $\dot{\varphi}_1 r_1 = -\dot{\varphi}_2 r_2$ )

$$i = -\frac{\dot{\varphi}_1^+}{\dot{\varphi}_2^+} = \frac{r_2}{r_1} = -\frac{\dot{\varphi}_1^+}{\dot{\varphi}_2^+} = -\frac{\dot{\varphi}_1}{\dot{\varphi}_2} = -\frac{\text{input angular speed}}{\text{output angular speed}} \tag{4.6.19}$$

With increasing gear reduction,  $i$  higher frequencies are excited by speed changes  $\Delta\varphi_1$  or by torque changes  $\Delta T_2$  on the driving side. The effective moment of inertia of the driven side then influences the eigen-behavior with  $J_2/i^2$  and can often be neglected for  $i \gg 10$ .

The ratio  $i$  does not have effect on the eigen-behavior in case b), because the rotational mass  $J_1$  freely oscillates for applied driving torque  $\Delta T_1$  and applied speed  $\Delta\varphi_2$ . The ratio  $i$  affects, however, the gain of the transfer elements  $G_{21}^+(s)$ .

For the investigation of oscillations, the relative movement of the rotational masses is of interest

$$\Delta\varphi^*(t) = \varphi_1(t) - \varphi_1^i(t) \quad (4.6.29)$$

After inserting in (4.6.22), one obtains by subtraction of both equations in (4.6.20)

$$\begin{aligned} \frac{J_1 J_2}{J_2 + i^2 J_1} \Delta \ddot{\varphi}_1^*(t) + d_1 \Delta \dot{\varphi}_1^*(t) + c_1^* \Delta \varphi_1(t) \\ = \frac{J_2}{J_2 + i^2 J_1} T_1(t) + \frac{J_1 i}{J_2 + i^2 J_1} T_2(t) \end{aligned} \quad (4.6.30)$$

with the effective rotational mass

$$J_{eff} = \frac{J_1 J_2}{J_2 + i^2 J_1} = \frac{J_1 \left( \frac{J_2}{i^2} \right)}{\left( \frac{J_2}{i^2} \right) + J_1} = \frac{J_1 J_2^{ii}}{J_2^{ii} + J_1}$$

and the undamped natural frequency

$$\omega_n^2 = \frac{c_1}{J_{eff}} \quad \frac{c_1 \left( J_2 + i^2 J_1 \right)}{J_1 J_2} = \frac{c_1 \left( \frac{J_2}{i^2} + J_1 \right)}{J_1 \left( \frac{J_2}{i^2} \right)}$$

If the moment of inertia is reduced to one shaft  $J_2^{ii} = J_2/i^2$ , the same relation as in the case of the two-mass torsional oscillator without gear is obtained. The natural frequency of the oscillation depends on the stiffness  $c_1$  and on both moments of inertia.

The rotational mass that is relevant for the oscillations and the resulting angular natural frequency depends as follows on the ratio  $i = r_2/r_1$

$$\begin{aligned} J_{eff} \Big|_{i \ll 1} &\approx J_1 & ; \quad \omega_n^2 \Big|_{i \ll 1} &\approx \frac{c_1}{J_1} \\ J_{eff} \Big|_{i \gg 1} &\approx \frac{J_2}{i^2} = J_2^{ii} & ; \quad \omega_n^2 \Big|_{i \gg 1} &\approx \frac{c_1}{J_2/i^2} \end{aligned}$$

In the case of a small ratio  $i$  ( $r_2 \ll r_1$ , i.e., speed increasing ratio:  $\dot{\varphi}_2 > \dot{\varphi}_1$ ), the effective moment of inertia is determined by the more slowly running rotational mass 1 with  $J_1$ . In the case of a large ratio  $i$  ( $r_2 > r_1$ , i.e., speed reducing ratio:  $\dot{\varphi}_2 < \dot{\varphi}_1$ ), the effective moment of inertia is determined also by the more slowly running rotational mass 2 by  $J_2/i^2$ . According to the case for the torsional oscillator without gearboxes, the smaller of the moments of inertia  $J_1$  or  $J_2/i^2$  is decisive for the resultant oscillations.

If the rotational masses with gear can be regarded as a *rigid two-mass system*, one obtains with  $\varphi_1(t) = \varphi_1^1(t)$  and  $\varphi_2(t) = -\varphi_2^1(t)$  and Figure 4.20

$$J_1 \ddot{\varphi}_1(t) = T_1(t) + T_1^1(t)$$

$$J_2 \ddot{\varphi}_2(t) = T_2(t) + T_2^1(t)$$

and by insertion of (4.6.20) and (4.6.21)

$$\left( J_1 + \frac{J_2}{i^2} \right) \ddot{\varphi}_1(t) = T_1(t) - \frac{1}{i} T_2(t) \quad (4.6.31)$$

The moment of inertia on the output side effects the motion equation in the case of torque changes on the driving side  $\Delta T_1(t)$  with  $J_2/i^2$ . In the case of large transmission ratios  $i \gg 1$ , it can be seen that the effects of the moment of inertia  $J_2$  can be neglected if  $J_2/i^2 \gg J_1$  (e.g., for robots with  $i = 100 \dots 300$  for the main axes). Correspondingly, one obtains for the dynamics of the driven side

$$(J_2 + i^2 J_1) \ddot{\varphi}_2(t) = T_2(t) - i T_1(t) \quad (4.6.32)$$

The effective moment of inertia of the driving side therefore depends for torque changes on the driven side of  $i^2 J_1$ .

#### 4.6.4 Power Transmissions

Motion transformers in the form of mechanisms are gear trains or power transmissions to transfer and transform rotational or translational motion. They are used when a change of the kind of motion or a change of speed or torque is needed. There exists a large variety of transmission mechanisms. Therefore, only an extract of some possibilities can be mentioned here. For more details, see respective handbooks, e.g., Bradley *et al.* (1991), Bolton (1996), FVA (1992), Walsh (1999).

##### a) Fixed ratio motion transformers

In many applications, the driving motor runs with a higher speed than the driven machine. Table 4.1 shows some examples of the transformation of rotary motion into rotary or linear motion. Gears are used for the transmission of rotary motion between *parallel shafts* (and for shafts that are inclined to one another: bevel gears). The larger gear wheel is often called the spur or crown wheel and the smaller the pinion. Gears with parallel shafts may have axial teeth, called *spur gears*. Otherwise,

they may have helical teeth called *helical gears*. Because of their gradual engagement of the individual teeth this results in a smoother drive and larger lifetime. The gear ratio is given by the ratio, of the number of teeth of both wheels. For large gear ratios several stages of wheel pairs are required, leading to *gear trains*. A simple gear train results if each shaft carries one gear wheel, with idler wheels between. If two intermediate wheels are mounted on a common shaft, this is called a compound gear train. Then, the input and output shaft can be in one line.

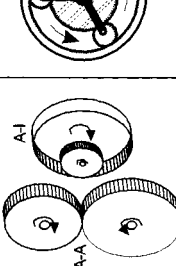
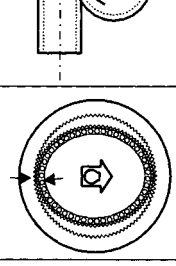
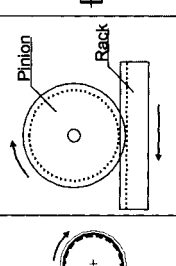
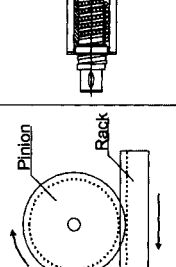
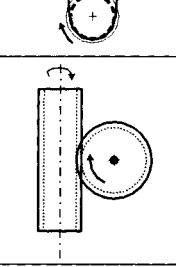
*Planetary* or *epicyclic* gears have parallel shafts and coaxial input and output shafts. One or more wheels are mounted on an arm that can rotate about the main axis, see Table 4.1. Such wheels are called *planets* and the wheel around which the planets revolve is called the *sun*. The planet wheels mesh with the internal teeth of an outer ring (annulus). For fixed ratio, the input is normally taken at the planet carrier and the output from the sun wheel, while the outer ring remains fixed in the casing. By fixing different parts of the planetary gear, different gear ratios can be obtained. For example, the ring may rotate and the arm of the sun may be kept fixed. The planetary gears lead to compact transmissions and are the basis of most car automatic gear boxes.

One disadvantage of the parallel shaft and planetary gears is the backlash, which cannot be avoided totally. With each stage, the overall backlash increases. This is usually no problem if the external load is unidirectional. However, for a load reversal, this is not acceptable if high-precision motions have to be generated, like for robot arms. Here, *harmonic drives* are widely used. A central input gear is eccentrically driven within an outer ring via rolls and a flexible tooth ring. The ring gear advances only by one tooth per revolution of the input wheel and therefore large reduction gear ratios are possible with one single stage.

For relatively large speed reduction and change in the direction of the input and output axis of  $90^\circ$ , *worm gears* are a common solution. In addition, for ratios of 15:1 and more they reliably hold under load when the motor is deactivated. The disadvantage is their relatively low efficiency.

*Belt drives* consist of a pair of wheels (pulleys) and a belt for the transmission of the motion. The simplest configuration is a series of cylindrical pulleys connected by a flat belt. Here, the friction that develops between the pulley and the arc of contact is used to transmit a torque. The transmitted torque is the difference between the tension that occurs in the tight side and the slack side of the belt. However, slip may occur. Belt drives have the advantage that the belt length can easily be adjusted to a wide range of shaft-to-shaft distances and the system is automatically protected against overload because slipping then occurs. However, the gear ratio is limited to about three to maintain an adequate arc of contact.

Table 4.1. Fixed ratio transmissions

gear type	gear drives					straight gears
	parallel shaft gear	planetary gear	harmonic-drive gear	worm gear	recirculating ball spindle	
construction principle (example)						
number of stages	1-15	1-5	1	1-10	$\geq 2$	1
gear ratio/stage $i$	3-6	3-10	50-320	10-80	3	—
nominal speed $n$ min <sup>-1</sup>	< 90000	< 80000	$\leq 5000$	< 3800	< 6000	—
movement speed m/s	—	—	—	—	—	< 2.5
displacement m/s	—	—	—	—	—	< 30
overall efficiency $\eta$	0.75-0.99	0.5-0.9	0.85-0.98	0.25- 0.8	0.8-0.97	0.8-0.85
nominal torque at driven shaft kNm	< 700	< 3500	$\leq 9$	< 350	—	0.5-0.6
feed force kN	—	—	—	—	—	—
backlash °	< 0.15	< 0.35	< 0.05	< 0.13	—	< 2000
self-locking	no	no	conditional yes	no	no	conditional yes
characteristics	— spur gear: high noise level — helical gear: higher load, lower noise	— compact design	— no backlash — high stiffness — compact design	— low noise level — increased heat-up	— cost efficient — little maintenance required — flexible installation	— high damping — small backlash

V or wedge belts and poly V-type belts can be used for high power up to 1000 kW. The effect of the V configuration is to produce a wedging action between the sides of the pulley groove and the belt. The greater the torque, the greater becomes the lateral pressure and therefore the tractive force. These belt types don't have a constant ration of speed, because creep occurs due to the belt elasticity, at around 1 to 2%.

*Toothed belts* avoid this disadvantage. They consist of a composite belt that is reinforced with polymer filament or steel wire and provides stiff and backlash-free drive with a constant gear ratio. However, they are limited to lower powers, *i.e.*, less than 20 kW, and temperatures less than 120°C. They can be used as timing belt drives, have low inertia and need no lubrication or maintenance. They are, *e.g.*, used for the driving of engine overhead camshafts or for the traverse mechanisms of printers and plotters.

*Chain drives* are used mostly for higher power where no slip can be tolerated (camshafts, motorcycles). They have rollers and need some pretension to avoid backlash and oscillation, and need lubrication.

*Rack and pinion* is a simple form of transforming rotational to linear motion or vice versa (*e.g.*, steering of car front wheels). If backlash has to be avoided, the pinion can be split on the centerline with tooth halves displaced to each other.

*Screw nut combinations* transform rotary motion into linear motions via balls. They can be used for high-precision motion of a load with low friction, like the feed drive of a machine tool. The balls are usually recirculated.

### b) Variable ratio motion transformers

For many applications, a continuously adjustable ratio of the transmission is required. This has led to a large variety of mechanical solutions, of which only some are discussed here, compare Table 4.2. They are partly known as continuously variable transmissions (CVT) and feature, *e.g.*, in recent automatic gear boxes for automobiles. CVTs have to be seen as competition to speed-controlled electrical drives, due to the progress in power electronics.

*Conical pulley and disc transmissions* consist of cone-faced wheels on adjacent shafts and a wedge-type belt. The variable gear ratio is obtained by moving both conical wheels in opposite directions by a linkage system and therefore changing the effective radius. The linkage mechanism may be manipulated by pneumatic or hydraulic actuators. Polymer-based belts can be used for lower power, whereas for higher power, steel belts or solid rings are required. A realization with a belt form of stacks with thin steel slats is the positive infinitely variable (PIV) drive. Other realizations use balls or wheels between conical or toroidally shaped discs, FVA (1992).

*Hydrodynamic transmissions* are the most widely used type of variable transmission for automobiles. They consist of a circulation pump, a fluid turbine and a leading (reaction) wheel to carry a difference tor-

que between pump and turbine, which is either fixed or may idle. They are suitable for higher powers and allow a smooth transition of speed and torque. Without the reaction wheel, the hydrodynamic transmission acts as fluid coupling without control, e.g., for starting high loads or with a controlled amount of oil in the circuit.

**Table 4.2.** Variable ratio transmissions

gear type	hydraulic transmissions			control range $R = n_{out,max}/n_{at\ min}$	$n$ nominal speed $\text{min}^{-1}$	efficiency $\eta$	nominal torque at driven shaft kNm	characteristics
	continuous variable transmission (CVT)	conical pulley belt drive	hydrostatic transmission					
visco clutch				$R < 15$	$R < 3$	$R < 0.95^*$		
silicon oil primary disc			hydrodynamic transmission	$R < 6$	$< 20000$	$0.7-0.97$	$< 22000$	$R < 0.95^*$
secondary disc								$< 0.95^*$ )
								$< 0.5$
								- passive torque change - temperature dependent torque change *) estimate
								- high power density - smooth transition - low efficiency for high slip

A disadvantage of the hydrodynamic transmissions is the low efficiency for high slip and therefore heat production. Therefore, modern gearboxes for cars possess a torque converter clutch for direct coupling of pump and turbine for operations where no slip is required (e.g., around steady state).

*Hydrostatic transmissions* consist of a piston pump and a piston motor connected by an oil circuit. The piston unit works as well as a pump as a motor and may be of axial or radial type with or without a variable displacement mechanism. Because of geometric relations between the pumped oil and the received flow and pressure at the motor, torque-speed characteristics can be adjusted to a driven working machine by adjusting the piston displacements. These hydrostatic transmissions have an excellent power/weight ratio, are used for high-power applications and also allow very low motor speed.

The *visco clutch* is an encapsulated multiple disc (lamina) clutch with silicon fluid, where the torque increases strongly with the difference speed or slip. It can be used for passively changing the transmitted torque between two shafts (like in the drivetrain of four-wheel-driven cars) or for changing the transmitted torque in temperature-dependent situation (like for cooling fans in cars), Braess, Seiffert (2000).

#### 4.6.5 Belt Drives

Figure 4.21 shows the scheme of a belt drive. The belt loops the pulleys onto the driver and driven shaft, where a peripheral force  $F_v$  at the discs is created as the difference between the load force of the tight side  $F_1(t)$  and the slack side  $F_2(t)$ . These forces generate the torques and rotating speeds of the pulleys. The belt can be considered as a transformer element with spring-damper behavior.

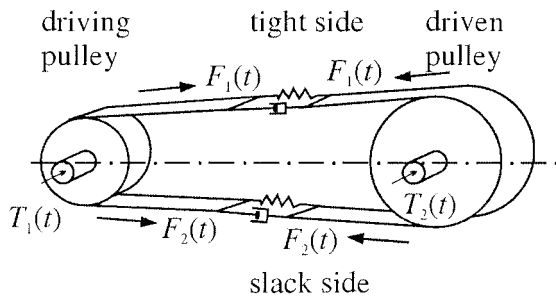


Figure 4.21. Belt drive

With regard to modeling a belt drive, different belt types have to be distinguished, compare Section 4.6.4:

- *Friction belt drives*

Flat belt or V-belt transmission, etc. The power transmission follows the principle of the rope friction. The speed transforma-

tion is reached for correct design with a low, load-dependent slip and an almost constant transmission ratio;

- *Toothed belt drives*

Synchronous or positive belt drives. The tangential forces are generated without slip and therefore a constant transmission ratio is obtained.

To obtain a frictional engagement for the friction belts and to achieve optimal drive behavior for the toothed belts, a type-dependent minimum pretensioning is required.

Figure 4.22 shows an equivalent model for the belt drives of Figure 4.21 for modeling of the dynamic behavior, He (1993). The following simplifying assumptions are met:

- the belt is massless;
- the shaft distance is constant;
- the effect of centrifugal forces is neglected;
- the deformation of the wheels and the shafts is neglected compared to the belt deformations;
- for a certain load status, the modulus of elasticity is constant over the total belt length, such that Hooke's law applies;
- for friction belts, extension slip only occurs.

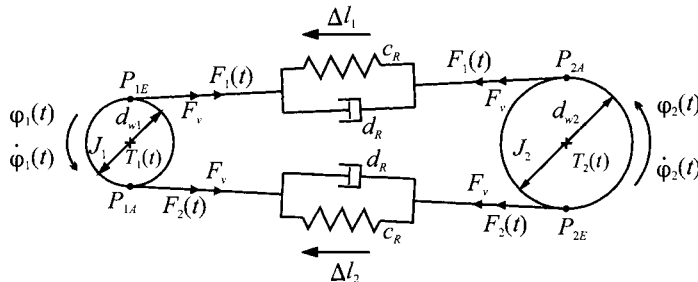


**Figure 4.22.** Equivalent model of a belt drive

The following symbols are used:

$A$  belt cross-sectional area

$T$  torque

$F$  force of belt

$F_v$  pretensioning force

$\varphi$  turning angle change

$\dot{\varphi}$  angular speed

$J$  moment of inertia

$d_w$  effective diameter

$c_R$  belt spring stiffness

$d_R$  belt-damping coefficient

$\Delta l$  length variation of the belt relative to pretensioned status.

The indices used are:

- 1 tight side belt, driving pulley;
- 2 slack side belt, driven pulley.

The belt spring stiffness  $c_R$  can be estimated by the following formula

$$c_R = \frac{EA}{l_R} \quad (4.6.33)$$

with

$EA$  belt stiffness factor

$l_R$  belt length on tight or slack side.

The calculation of  $EA$  values in dependence on the belt type and belt load is exemplarily described in Erxleben (1984), see also Walsh (1999).

The belt-damping coefficient  $d_R$  can be calculated according to Klingenberg (1978)

$$d_R = \frac{\Psi c_R}{2\pi \dot{\varphi}_{10}} \quad (4.6.34)$$

$\dot{\varphi}_{10}$  is the angular speed of the driving pulley at the operating point and  $\Psi$  the relative damping of the belt, which can be experimentally determined according Erxleben (1984).

With these assumptions, the following angular momentum balances at the two wheels can be stated by referring to Figure 4.22.

At the driving pulley, it holds that

$$J_1 \ddot{\varphi}_1(t) = T_1(t) - \frac{d_{w1}}{2}(F_1(t) - F_2(t)) \quad (4.6.35)$$

and at the driven pulley

$$J_2 \ddot{\varphi}_2(t) = -T_2(t) + \frac{d_{w2}}{2}(F_1(t) - F_2(t)) \quad (4.6.36)$$

with

$$F_1(t) = F_v + c_R \Delta l_1(t) + d_R \Delta \dot{l}_1(t) \quad (4.6.37)$$

$$F_2(t) = F_v - c_R \Delta l_2(t) - d_R \Delta \dot{l}_2(t) \quad (4.6.38)$$

with  $\Delta l_1$  as the increase of the length of the tight side and  $\Delta l_2$  as the decrease of the length of the slack side.

By inserting (4.6.37) and (4.6.38) into (4.6.35) and (4.6.36) respectively, one obtains the following equations for the belt drive

$$J_1 \ddot{\varphi}_1(t) + \frac{d_{w1}}{2} [c_R(\Delta l_1(t) + \Delta l_2(t)) + d_R(\Delta \dot{l}_1(t) + \Delta \dot{l}_2(t))] = T_1(t) \quad (4.6.39)$$

$$J_2 \ddot{\varphi}_2(t) - \frac{d_{w2}}{2} [c_R(\Delta l_1(t) + \Delta l_2(t)) + d_R(\Delta \dot{l}_1(t) + \Delta \dot{l}_2(t))] = -T_2(t) \quad (4.6.40)$$

The pretensioning  $F_v$  disappears.

In the following, the non-measurable quantities  $\Delta l_1$ ,  $\Delta l_2$  are calculated.

### a) Flat belt drive (friction belt)

Frictionally engaged belt drives always operate with a slightly load-dependent extension slip, i.e., the speed of the driven pulley is smaller than the speed of the driving pulley.

The slip can be described as

$$s = \frac{v_1 - v_2}{v_1} \quad (4.6.41)$$

where the pulley's peripheral speed is

$$v_1 = \frac{d_{w1}}{2} \dot{\varphi}_1; \quad v_2 = \frac{d_{w2}}{2} \dot{\varphi}_2 \quad (4.6.42)$$

The ratio of the belt drive is

$$i = \frac{n_1}{n_2} = \frac{\dot{\varphi}_1}{\dot{\varphi}_2} = \frac{\text{driving speed}}{\text{driven speed}} \quad (4.6.43)$$

and by inserting (4.6.42) in (4.6.41), one obtains

$$s = \frac{d_{w1} \dot{\varphi}_1 - d_{w2} \dot{\varphi}_2}{d_{w1} \dot{\varphi}_1} = 1 - \frac{d_{w2} \dot{\varphi}_2}{d_{w1} \dot{\varphi}_1} \Rightarrow \frac{\dot{\varphi}_1}{\dot{\varphi}_2} = \frac{1}{1-s} \frac{d_{w2}}{d_{w1}}$$

This leads to the actual ratio of a flat belt

$$i = \frac{\dot{\varphi}_1}{\dot{\varphi}_2} = \frac{1}{1-s} \frac{d_{w2}}{d_{w1}} = \frac{1}{1-s} i_0 \quad (4.6.44)$$

from which the idle ratio follows for  $s = 0$

$$i_0 = \frac{d_{w2}}{d_{w1}} \quad (4.6.45)$$

The lagging of the driven shaft is only a consequence of the engagement and disengagement of the forces over the pulleys. By moving over the pulleys, the belt undergoes different elongations, which cause changes in the belt speed.

The belt speed  $v_{1E}$  at the break-in point  $P_{1E}$  of the driving pulley (for no sliding slip) is equal to the peripheral speed  $v_1$  of the pulley:  $v_{1E} = v_1$ . The belt speed  $v_{2E}$  at the break-in point  $P_{2E}$  of the driven pulley is equal to the peripheral speed  $v_2$  of the pulley:  $v_{2E} = v_2$ . Because of belt stretching by  $\Delta l_1$  on the tight side, it holds that  $v_{2A} < v_1$  and it follows that

$$\Delta l_1(t) = v_{1E}(t)\Delta t - v_{2A}(t)\Delta t = v_1(t)\Delta t - v_{2A}(t)\Delta t \quad (4.6.46)$$

The decreasing of the elongation  $\Delta l_2$  in the slack side leads with  $v_{1A} > v_2$  to

$$\Delta l_2(t) = v_{1A}(t)\Delta t - v_{2E}(t)\Delta t = v_{1A}(t)\Delta t - v_2(t)\Delta t \quad (4.6.47)$$

with:

- $v_{1E}$  belt speed at the break in point of the driving pulley  $P_{1E}$
- $v_{1A}$  belt speed at the break out point of the driven pulley  $P_{1A}$
- $v_{2E}$  belt speed at the break in point of the driven pulley  $P_{2E}$
- $v_{2A}$  belt speed at the break out point of the driven pulley  $P_{2A}$

For these speeds, it holds that by the assumption of an extension slip

$$s = 1 - \frac{v_2}{v_1} \quad \text{or} \quad (1-s) = \frac{v_2}{v_1}$$

In order to eliminate unknown speeds  $v_{1A}$  and  $v_{2A}$  in (4.6.46) and (4.6.47), one assumes

$$v_{1A} \approx v_2, \quad v_{2A} \approx v_1$$

From the slip definition, (4.6.41), it then follows that

$$\begin{aligned} s &= 1 - \frac{v_2}{v_1} \approx 1 - \frac{v_{1A}}{v_1} \\ v_{1A} &\approx (1-s)v_1 \end{aligned} \quad (4.6.48)$$

$$\begin{aligned} s &= 1 - \frac{v_2}{v_1} \approx 1 - \frac{v_2}{v_{2A}} \\ v_{2A} &\approx \frac{1}{1-s} v_2 \end{aligned} \quad (4.6.49)$$

Hence, from (4.6.46)–(4.6.49) and  $\Delta\varphi(t) = \dot{\varphi}(t) = \ddot{\varphi}(t)\Delta t$

$$\Delta l_1(t) = \frac{d_{w1}}{2}\dot{\varphi}_1(t) - \frac{1}{1-s} \frac{d_{w2}}{2}\dot{\varphi}_2(t) \quad (4.6.50)$$

$$\Delta \dot{l}_1(t) = \frac{d_{w1}}{2}\ddot{\varphi}_1(t) - \frac{1}{1-s} \frac{d_{w2}}{2}\ddot{\varphi}_2(t) \quad (4.6.51)$$

$$\Delta l_2(t) = (1-s) \frac{d_{w1}}{2}\dot{\varphi}_1(t) - \frac{d_{w2}}{2}\dot{\varphi}_2(t) \quad (4.6.52)$$

$$\Delta \dot{l}_2(t) = (1-s) \frac{d_{w1}}{2}\ddot{\varphi}_1(t) - \frac{d_{w2}}{2}\ddot{\varphi}_2(t) \quad (4.6.53)$$

With the help of (4.6.45) and (4.6.50)–(4.6.52) and the model equations (4.6.39), (4.6.40), one finally obtains the following differential equation system for flat belt transmissions

$$J_1 \ddot{\phi}_1(t) + d_{DT}(\dot{\phi}_1(t) - i\dot{\phi}_2(t)) + c_{DT}(\phi_1(t) - i\phi_2(t)) = T_1(t) \quad (4.6.54)$$

$$J_2 \ddot{\phi}_2(t) - i_0[d_{DT}(\dot{\phi}_1(t) - i\dot{\phi}_2(t)) + c_{DT}(\phi_1(t) - i\phi_2(t))] = -T_2(t) \quad (4.6.55)$$

with

$$c_{DT} = (2-s)\left(\frac{d_{w1}}{2}\right)^2 c_R \text{ - dynamical torsional stiffness [Nm/rad]} \quad (4.6.56)$$

$$d_{DT} = (2-s)\left(\frac{d_{w1}}{2}\right)^2 d_R \text{ - damping coefficient [Nm/rads]} \quad (4.6.57)$$

(4.6.54), (4.6.55) describe the dynamic behavior of a two-mass oscillator, compare (4.6.1). Figure 4.23 represents the corresponding, simplified equivalent model for flat belt transmissions.

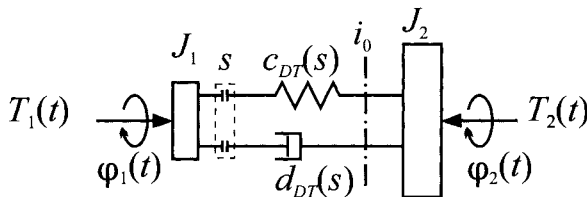


Figure 4.23. Simplified equivalent model of the flat belt drive

The transfer functions in the two-port representation becomes, for small changes, according to (4.6.9)

$$\begin{aligned} G_{11}(s) &= \frac{\Delta \dot{\phi}_2(s)}{\Delta \dot{\phi}_1(s)} = \frac{i_0(d_{DT}s + c_{DT})}{J_2 s^2 + i_0 i d_{DT} s + i_0 i c_{DT}} \\ G_{21}(s) &= \frac{\Delta T_1(s)}{\Delta \dot{\phi}_1(s)} = \frac{J_1 J_2 s^3 + d_{DT}(i_0 i J_1 + J_2)s^2 + c_{DT}(i_0 i J_1 + J_2)s}{J_2 s^2 + i_0 i d_{DT} s + i_0 i c_{DT}} \\ G_{12}(s) &= \frac{\Delta \dot{\phi}_2(s)}{\Delta T_2(s)} = \frac{s}{J_2 s^2 + i_0 i d_{DT} s + i_0 i c_{DT}} \\ G_{22}(s) &= \frac{\Delta T_1(s)}{\Delta T_2(s)} = \frac{i(d_{DT}s + c_{DT})}{J_2 s^2 + i_0 i d_{DT} s + i_0 i c_{DT}} = G_{11}(s) \end{aligned} \quad (4.6.58)$$

### b) Synchronous belt drive (toothed belt)

Because of the positive engagement, a slip-free transmission with constant ratio results.

$$s = 0 \text{ and } i = i_0 = \frac{d_{w2}}{d_{w1}} \quad (4.6.59)$$

Therefore, the following mathematical model for synchronous belt drives is obtained from (4.6.54)–(4.6.55), see also Figure 4.24

$$J_1 \ddot{\varphi}_1(t) + d_{DT}(\dot{\varphi}_1(t) - i\dot{\varphi}_2(t)) + c_{DT}(\varphi_1(t) - i\varphi_2(t)) = T_1(t) \quad (4.6.60)$$

$$J_2 \ddot{\varphi}_2(t) - i[d_{DT}(\dot{\varphi}_1(t) - i\dot{\varphi}_2(t)) + c_{DT}(\varphi_1(t) - i\varphi_2(t))] = -T_2(t) \quad (4.6.61)$$

with the dynamic torsional stiffness and the damping factor

$$c_{DT} = \frac{d_{w1}^2}{2} c_R \text{ and } d_{DT} = \frac{d_{w1}^2}{2} d_R$$

The corresponding transfer functions of the two-port representation (small signal changes) for the synchronous belt drive with speed  $\Delta\dot{\varphi}_1$  and torque  $\Delta T_2$  as inputs are

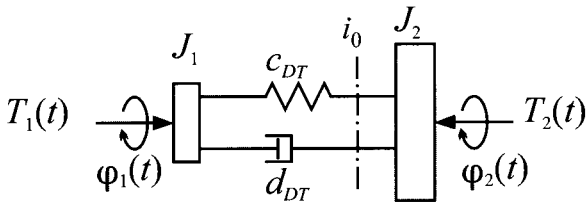


**Figure 4.24.** Simplified equivalent model of the synchronous belt drive

$$\begin{aligned} G_{11}(s) &= \frac{\Delta \dot{\varphi}_2(s)}{\Delta \dot{\varphi}_1(s)} = \frac{i(d_{DT}s + c_{DT})}{J_2 s^2 + i^2 d_{DT}s + i^2 c_{DT}} \\ G_{21}(s) &= \frac{\Delta T_1(s)}{\Delta \dot{\varphi}_1(s)} = \frac{J_1 J_2 s^3 + d_{DT} (i^2 J_1 + J_2) s^2 + c_{DT} (i^2 J_1 + J_2) s}{J_2 s^2 + i^2 d_{DT}s + i^2 c_{DT}} \\ G_{12}(s) &= \frac{\Delta \dot{\varphi}_2(s)}{\Delta T_2(s)} = \frac{s}{J_2 s^2 + i^2 d_{DT}s + i^2 c_{DT}} \\ G_{22}(s) &= \frac{\Delta T_1(s)}{\Delta T_2(s)} = \frac{i(d_{DT}s + c_{DT})}{J_2 s^2 + i^2 d_{DT}s + i^2 c_{DT}} \end{aligned} \quad (4.6.62)$$

These transfer functions are identical to the two-mass torsional oscillator with gear, (4.6.28), except for the signs.

### 4.6.6 Absorbers and Dampers

To reduce oscillations, absorbers or dampers are mounted at the shaft ends, see Figure 4.25. An absorber is a spring-mass component without substantial damping. It shifts the resonance frequency of the overall system. A vibration damper additionally contains a damping element and converts part of the oscillation energy into heat.

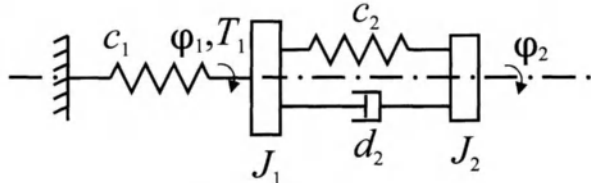


**Figure 4.25.** Equivalent model of a torsional oscillator 1 with vibration damper respectively vibration absorber 2

By simplifying the oscillating system through an equivalent model with moment of inertia  $J_1$  and spring stiffness  $c_1$ , the following differential equations hold, according to Figure 4.25

$$J_1 \ddot{\varphi}_1(t) = -c_1 \varphi_1(t) - c_2(\varphi_1(t) - \varphi_2(t)) - d_2(\dot{\varphi}_1(t) - \dot{\varphi}_2(t)) + T_1(t) \quad (4.6.63)$$

$$J_2 \ddot{\varphi}_2(t) = -c_2(\varphi_2(t) - \varphi_1(t)) - d_2(\dot{\varphi}_2(t) - \dot{\varphi}_1(t)) \quad (4.6.64)$$

$T_1(t)$  is an excitation torque, e.g., harmonically with frequency  $\omega_1$

$$T_1(t) = T_{10} \sin \omega_1 t \quad (4.6.65)$$

The transfer function for the oscillation amplitudes  $\varphi_1$  and  $\varphi_2$  then becomes

$$G_{11}(s) = \frac{\varphi_1(s)}{T_1(s)} = \frac{J_2 s^2 + d_2 s + c_2}{(J_1 s^2 + d_2 s + (c_1 + c_2))(J_2 s^2 + d_2 s + c_2) - (c_2 + d_2 s)^2} \quad (4.6.66)$$

$$G_{21}(s) = \frac{\varphi_2(s)}{T_1(s)} = \frac{c_2 + d_2 s}{(J_1 s^2 + d_2 s + (c_1 + c_2))(J_2 s^2 + d_2 s + c_2) - (c_2 + d_2 s)^2} \quad (4.6.67)$$

Based on (4.6.66), it follows from (4.6.65) for an absorber with  $d_2 = 0$  and the condition that the amplitudes become  $\varphi_1 = 0$  by excitation with  $T_1$  that

$$J_2(i\omega_1)^2 + c_2 = 0$$

therefore

$$\omega_1^2 = c_2/J_2 \quad (4.6.68)$$

By a suitable choice of  $c_2/J_2$ , it is therefore possible that the oscillations  $\varphi_1$  of the rotational mass  $J_1$  disappear. However, two new resonance frequencies below and above this frequency appear, which disturb the starting and stopping. In addition, the torque  $T_1$  has to be taken up by the absorber spring. This is why vibration dampers with a spring and damper are better used, e.g., rubber components or springless dampers, if the spring load has to be avoided, Holzweißig, Dresig (1992).

## 4.7 MECHANICAL SYSTEMS WITH FRICTION

Friction plays an essential role in many mechanical processes. It appears between relatively moving adjacent bodies, see also Section 4.4, and can be classified as dry (Coulomb) friction, fluidic (viscous) friction or a mixture of both.

In the case of dry friction, both of the bodies touch each other directly without lubricant. Then, one may distinguish between static friction  $F_{Fs}$  and kinetic friction  $F_{Fk}$ . Static friction appears between the bodies before they are moving. To achieve this, the adhesive force, described by the static friction number  $\mu_s$ , at the contact surfaces has to be overcome (*stiction*, starting friction). For relatively moving objects, the sliding friction with the sliding friction number  $\mu_c$  applies. The following friction law can be applied for both kinds of friction

$$F_{Fs} = \mu_s F_N \quad ; \quad F_c = \mu_c F_N \quad (4.7.1)$$

where  $F_N$  is the normal force at the touching surfaces, Figure 4.3a. The values for the static and sliding friction numbers are

$$\mu_s \approx 0.15 \dots 0.8$$

$$\mu_c \approx 0.1 \dots 0.6.$$

Generally, the static friction is higher than the sliding friction.

If there is a lubricating fluid layer between the sliding bodies, the friction occurs within the fluidic layer. This kind of friction depends on the relative speed  $v$  and is usually smaller than the dry friction. Then, for fluidic or viscous friction, the following approximately applies for low velocities  $v$  and laminar flow

$$F \sim v \quad (4.7.2)$$

and for high velocities and turbulent flow

$$F \sim v^2 \quad (4.7.3)$$

Between pure dry friction and pure viscous friction there exists a state where both of the aforementioned kinds of friction apply at the same time. It is also known as *mixed friction*  $F_{Fm}$  and appears if the lubri-

cant's thickness  $h$  and the mean roughness value  $\sigma$  have a ratio  $\lambda = h/\sigma$  ranging from 1...3.

Drawing the friction numbers with respect to the velocity gives a characteristic as depicted in Figure 4.26. It is called the Stribeck characteristic curve, according to Stribeck (1902).

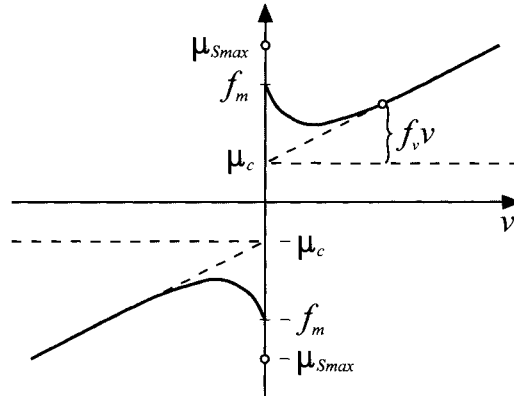


**Figure 4.26.** Friction characteristic according to Stribeck (1902) for the sliding friction  $\mu_c$  dry / Coulomb friction;  $f_v v$  viscous friction;  $f_m$  friction threshold for  $v > 0$ ;  $\mu_{smax}$  maximum stick friction

The overall friction characteristics can be described by the following equation, Tustin (1947), see also Armstrong-Hélouvy (1991)

$$f_F = -\mu_c \operatorname{sign} v + f_v v + f_m e^{-c|v|} \operatorname{sign} v \quad (v > 0) \quad (4.7.4)$$

Then, the friction force becomes

$$F_F = f_F F_N \quad (4.7.5)$$

and the following also applies

$$F_F = F_c \operatorname{sign} v + F_v v + F_m e^{-c|v|} \operatorname{sign} v \quad (v > 0). \quad (4.7.6)$$

It should be noted that in the case of  $v = 0$ , i.e., stand still, the static friction  $F_{F_s} < F_{F_{smax}}$  applies. Here,  $F_{smax}$  is the maximum static friction for which the system is still not moving. The static friction is, according to "action = reaction", always as large as the driving force  $F$ . As soon as  $F > F_{F_{smax}}$  the system starts moving abruptly. Then, the friction force agrees with the friction characteristics in Figure 4.26.

Now, a spring-mass-damper system with friction is considered according to Figure 4.27a. The differential equation

$$m \ddot{z}_2(t) + d\dot{z}_2(t) + cz_2(t) + F_F(t) = c z_1(t) \quad (4.7.7)$$

applies for the distance  $z_1(t)$  being the input. In the moving state  $v_2 = \dot{z}_2(t) \neq 0$ , the friction force arises by means of sliding friction for which a dry and viscous part is assumed

$$F_F(t) = F_T \operatorname{sign} \dot{z}_2(t) + F_v \dot{z}_2(t) \quad (4.7.8)$$

For the movement in the direction  $\dot{z}_2(t) > 0$ , applies

$$m\ddot{z}_2(t) + (d + F_v)\dot{z}_2(t) + cz_2(t) + F_c = c z_1(t) \quad (4.7.9)$$

and in the direction  $\dot{z}_2(t) < 0$ :

$$m\ddot{z}_2(t) + (d + F_v)\dot{z}_2(t) + cz_2(t) - F_c = c z_1(t) \quad (4.7.10)$$

Thus, the coefficient  $F_v$  is added to the coefficient  $d$  of the damper. The dry friction appears as a constant value, whose sign depends on the direction of the velocity  $\dot{z}_2(t)$ . The affiliated block diagram is depicted in Figure 4.27b.

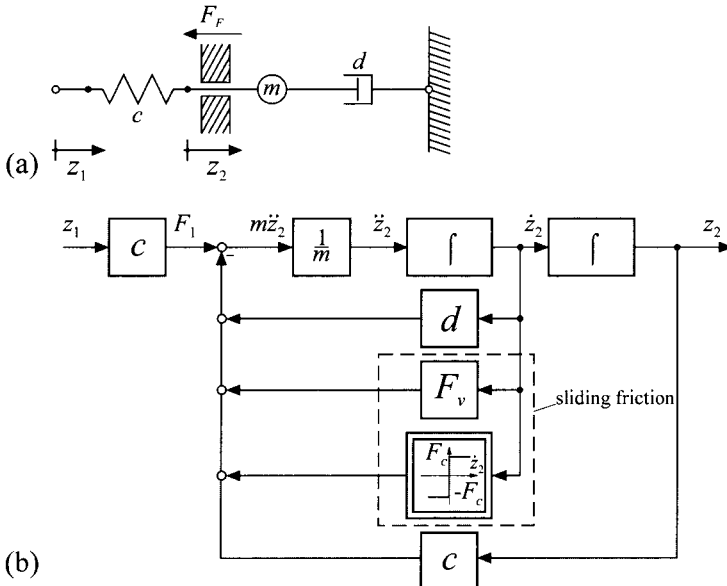


**Figure 4.27.** Mechanical oscillator with friction: (a) schematic arrangement; (b) signal flow diagram for dry and viscous friction

For the linear part, the following transfer function applies

$$G(s) = \frac{z_2(s)}{F_2(s)} = \frac{1}{ms^2 + (d + F_v)s + c} \quad (4.7.11)$$

with a partial sum of forces

$$F_2(t) = cz_1(t) - F_c \operatorname{sign} \dot{z}_2(t) \quad (4.7.12)$$

Figure 4.28 shows the resulting equivalent circuit diagram. The effects of the constant part of the sliding friction can be interpreted as an offset with changing sign.

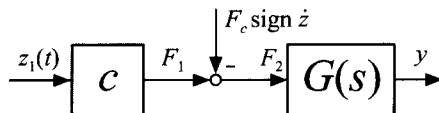


**Figure 4.28.** Equivalent circuit diagram of a linear system with sliding friction

$$s = 0 \text{ and } i = i_0 = \frac{d_{w2}}{d_{w1}} \quad (4.6.59)$$

Therefore, the following mathematical model for synchronous belt drives is obtained from (4.6.54)–(4.6.55), see also Figure 4.24

$$J_1 \ddot{\varphi}_1(t) + d_{DT}(\dot{\varphi}_1(t) - i\dot{\varphi}_2(t)) + c_{DT}(\varphi_1(t) - i\varphi_2(t)) = T_1(t) \quad (4.6.60)$$

$$J_2 \ddot{\varphi}_2(t) - i[d_{DT}(\dot{\varphi}_1(t) - i\dot{\varphi}_2(t)) + c_{DT}(\varphi_1(t) - i\varphi_2(t))] = -T_2(t) \quad (4.6.61)$$

with the dynamic torsional stiffness and the damping factor

$$c_{DT} = \frac{d_{w1}^2}{2} c_R \text{ and } d_{DT} = \frac{d_{w1}^2}{2} d_R$$

The corresponding transfer functions of the two-port representation (small signal changes) for the synchronous belt drive with speed  $\Delta\dot{\varphi}_1$  and torque  $\Delta T_2$  as inputs are

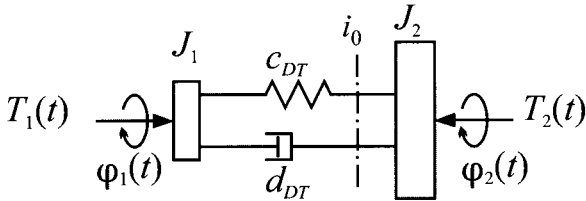


**Figure 4.24.** Simplified equivalent model of the synchronous belt drive

$$\begin{aligned} G_{11}(s) &= \frac{\Delta \dot{\varphi}_2(s)}{\Delta \dot{\varphi}_1(s)} = \frac{i(d_{DT}s + c_{DT})}{J_2 s^2 + i^2 d_{DT}s + i^2 c_{DT}} \\ G_{21}(s) &= \frac{\Delta T_1(s)}{\Delta \dot{\varphi}_1(s)} = \frac{J_1 J_2 s^3 + d_{DT} (i^2 J_1 + J_2) s^2 + c_{DT} (i^2 J_1 + J_2) s}{J_2 s^2 + i^2 d_{DT}s + i^2 c_{DT}} \\ G_{12}(s) &= \frac{\Delta \dot{\varphi}_2(s)}{\Delta T_2(s)} = \frac{s}{J_2 s^2 + i^2 d_{DT}s + i^2 c_{DT}} \\ G_{22}(s) &= \frac{\Delta T_1(s)}{\Delta T_2(s)} = \frac{i(d_{DT}s + c_{DT})}{J_2 s^2 + i^2 d_{DT}s + i^2 c_{DT}} \end{aligned} \quad (4.6.62)$$

These transfer functions are identical to the two-mass torsional oscillator with gear, (4.6.28), except for the signs.

If the backlash is combined with a spring, Figure 4.31a, the backlash element is pressed against one of the two limits depending on the direction of the spring's force. Then, the following applies

$$\begin{aligned} z_2(t) &= z_1(t) - z_t \text{ for } z_1(t) \geq z_t \\ z_2(t) &= z_1(t) + z_t \text{ for } z_1(t) \leq -z_t \\ z_2(t) &= 0 \quad \text{for } -z_t < z_1(t) < z_t \end{aligned} \quad (4.8.2)$$

The resulting characteristic is called a *dead zone*, Figure 4.31b. Depending on the type of connected mechanical elements, a backlash yields two different characteristics.

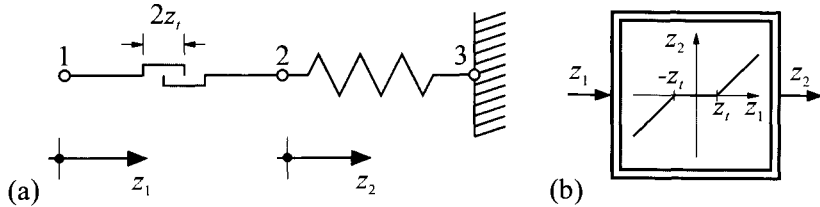


**Figure 4.31.** Mechanical element with spring and backlash: (a) schematic arrangement; (b) signal flow diagram with characteristic

Now, a mechanical oscillator with a backlash of width  $2 z_t$  is considered, Figure 4.32. For the oscillator without backlash, applies

$$m\ddot{z}_2(t) + d\dot{z}_2(t) + cz_2(t) = cz_3(t) \quad (4.8.3)$$

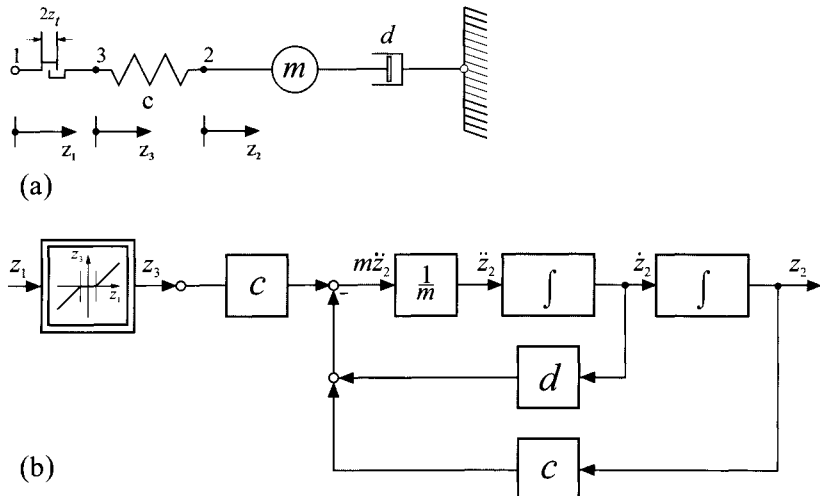


**Figure 4.32.** Mechanical oscillator with backlash (dead zone): (a) schematic arrangement; (b) signal flow diagram for  $z_1(t) > z_1$  and  $z_1(t) < -z_1$

(4.8.2) describes the effect of the backlash for a slow motion. In the case that the backlash is located at one of its limits, such that  $z_1(t) > z_t$ , the following applies

$$m\ddot{z}_2(t) + d\dot{z}_2(t) + cz_2(t) + cz_t = cz_1(t) \quad (4.8.4)$$

and at the other limit

$$m\ddot{z}_2(t) + d\dot{z}_2(t) + cz_2(t) - cz_t = cz_1(t) \quad (4.8.5)$$

Therefore, the backlash appears as a constant, whose sign depends on  $z_1(t)$ . For the range within the backlash, it holds that  $z_3(t) = 0$  and only the characteristic system dynamics of the oscillator applies

$$m\ddot{z}_2(t) + d\dot{z}_2(t) + cz_2(t) = 0 \quad (4.8.6)$$

But this is only if point 3 of the schematic diagram is fixed (*e.g.*, due to friction). The spring force disappears if point 3 moves freely within the range of the backlash. Then,  $c$  in (4.8.6) is set equal to zero.

A simplified diagram of the overall system for the range outside the backlash results, as depicted in Figure 4.33. (Possible shock forces at both limits of the backlash have been neglected in this case.)

In this chapter, only the modeling of some mechanical elements could be covered in an exemplary way. Besides the discussed spring-mass-damper systems for translation and rotation, there exist many other mechanical systems, such as special guidances, crank mechanisms, multi-chained linkages to generate special movements or forces, compare also Hain (1973), VDI (1978), Jensen (1991), Sneck (1991).

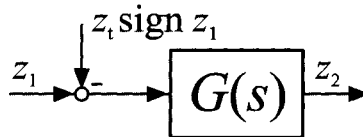


Figure 4.33. Equivalent circuit diagram of a linear system with backlash for  $|z_1(t)| > |z_t|$

## 4.9 PROBLEMS

- 4.9.1 Calculate the torsional spring stiffness  $c$  of a steel rod with length  $l = 1$  m and diameter  $d = 0.01$  m.
- 4.9.2 Determine the force-displacement characteristics of an air spring according to Figure 4.2b for  $d=0.1$  m and  $l=0.3$  m.
- 4.9.3 A linearized suspension system of a vehicle with neglected wheel mass and wheel stiffness shows the following data for a quarter car:  $m = 250$  kg;  $c = 20000$  N/m;  $d = 1100$  Ns/m.  
Determine the frequency response for the road excitation  $z_r(t)$  as input and the displacement  $z_o(t)$  of the body as output and draw the Bode diagram. Then, calculate the eigen-frequency, resonance frequency and damping ratio, poles and zeros.

- 4.9.4 The axle of a vehicle's rear drive between the differential and the wheel has the data  $c = 6000 \text{ Nm/rad}$ ;  $d = 20 \text{ Nms/rad}$ . The wheel has a ratio inertia  $J = 0.35 \text{ kgm}^2$ . Calculate the natural and eigen-frequency.
- 4.9.5 A passenger car wheel with radius  $r = 0.30 \text{ m}$  has an unbalanced mass of  $m = 50 \text{ g}$ . Determine the amplitude of the resulting force in the vertical direction for the car speed  $v = 60, 120, 180 \text{ km/h}$ . How large is the amplitude of the spring deflection of the freely rotating wheel (not touching the road), if the wheel mass is  $32 \text{ kg}$  and the body is assumed not to oscillate. The spring stiffness is  $c = 22.5 \text{ kN/m}$  and the damping coefficient of the shock absorber  $d = 1100 \text{ Ns/m}$ .
- 4.9.6 A robot arm of length  $l = 1.2 \text{ m}$  with a mass of  $m = 10 \text{ kg}$  at its end effector is driven by a DC motor with gear ratio  $i = 140$ . The moment of inertia of the DC motor is  $J_1 = 25 \text{ kgcm}^2$  and that of the rotor arm without mass is  $J_2 = m \cdot l/2 = 14.4 \text{ kgm}^2$ . The torque of the DC motor is  $T_1 = k_1 I$  with the current in [A] and  $k_1 = 30 \text{ Nsm/A}$ .  
Derive the differential equation for the current  $I$  as input and the robot arm angle  $\varphi_2$  as output. How is the overall ratio of inertia changed by increasing the load mass to  $m = 20 \text{ kg}$ ?
- 4.9.7 An electrical AC generator is directly connected to the crank-shaft pinion of a four-cylinder four-stroke combustion engine through a V-belt. Determine the first harmonic oscillation frequency of the angular speed of the belt drive for the crankshaft speed of 500 to 6000 rpm.  
The ratio of inertia of the generator with its pinion is  $J = 2 \cdot 10^{-3} \text{ kgm}^2$ , the belt stiffness is  $c_2 = 700 \text{ Nm/rad}^2$  and the belt damping factor is  $d_2 = 0.1 \text{ Nms/rad}$ . It can be assumed that the slip is zero. The effective radius of the crankshaft pinion is  $r_1 = 30 \text{ mm}$  and the generator pinion is  $r_1 = 15 \text{ mm}$ .  
Determine the dynamic behavior of the generator's angular speed  $\omega_2$  depending on changes of the crankshaft speed  $\omega_1$ . State the differential equation and the frequency response. Determine the rotational acceleration of the generator depending on the angular speed, the resonance frequency and eigen-frequency, assuming that the amplitude of the crankshaft oscillation is 20 rpm.
- 4.9.8 A rotating wheel with ratio of inertia  $J = 5 \cdot 10^{-3} \text{ kgm}^3$ , bearing viscous damping factor  $d = 2 \cdot 10^{-3} \text{ Nms}$  and Coulomb friction  $T_c = 0.2 \text{ Nm}$  has been accelerated to a constant speed of 1000 rpm. Determine the time behavior of the speed for idling, i.e., with driving torque zero, with and without Coulomb friction.

- 4.9.4 The axle of a vehicle's rear drive between the differential and the wheel has the data  $c = 6000 \text{ Nm/rad}$ ;  $d = 20 \text{ Nms/rad}$ . The wheel has a ratio inertia  $J = 0.35 \text{ kgm}^2$ . Calculate the natural and eigen-frequency.
- 4.9.5 A passenger car wheel with radius  $r = 0.30 \text{ m}$  has an unbalanced mass of  $m = 50 \text{ g}$ . Determine the amplitude of the resulting force in the vertical direction for the car speed  $v = 60, 120, 180 \text{ km/h}$ . How large is the amplitude of the spring deflection of the freely rotating wheel (not touching the road), if the wheel mass is  $32 \text{ kg}$  and the body is assumed not to oscillate. The spring stiffness is  $c = 22.5 \text{ kN/m}$  and the damping coefficient of the shock absorber  $d = 1100 \text{ Ns/m}$ .
- 4.9.6 A robot arm of length  $l = 1.2 \text{ m}$  with a mass of  $m = 10 \text{ kg}$  at its end effector is driven by a DC motor with gear ratio  $i = 140$ . The moment of inertia of the DC motor is  $J_1 = 25 \text{ kgcm}^2$  and that of the rotor arm without mass is  $J_2 = m \cdot l/2 = 14.4 \text{ kgm}^2$ . The torque of the DC motor is  $T_1 = k_1 I$  with the current in [A] and  $k_1 = 30 \text{ Nsm/A}$ .  
Derive the differential equation for the current  $I$  as input and the robot arm angle  $\varphi_2$  as output. How is the overall ratio of inertia changed by increasing the load mass to  $m = 20 \text{ kg}$ ?
- 4.9.7 An electrical AC generator is directly connected to the crank-shaft pinion of a four-cylinder four-stroke combustion engine through a V-belt. Determine the first harmonic oscillation frequency of the angular speed of the belt drive for the crankshaft speed of 500 to 6000 rpm.  
The ratio of inertia of the generator with its pinion is  $J = 2 \cdot 10^{-3} \text{ kgm}^2$ , the belt stiffness is  $c_2 = 700 \text{ Nm/rad}^2$  and the belt damping factor is  $d_2 = 0.1 \text{ Nms/rad}$ . It can be assumed that the slip is zero. The effective radius of the crankshaft pinion is  $r_1 = 30 \text{ mm}$  and the generator pinion is  $r_1 = 15 \text{ mm}$ .  
Determine the dynamic behavior of the generator's angular speed  $\omega_2$  depending on changes of the crankshaft speed  $\omega_1$ . State the differential equation and the frequency response. Determine the rotational acceleration of the generator depending on the angular speed, the resonance frequency and eigen-frequency, assuming that the amplitude of the crankshaft oscillation is 20 rpm.
- 4.9.8 A rotating wheel with ratio of inertia  $J = 5 \cdot 10^{-3} \text{ kgm}^3$ , bearing viscous damping factor  $d = 2 \cdot 10^{-3} \text{ Nms}$  and Coulomb friction  $T_c = 0.2 \text{ Nm}$  has been accelerated to a constant speed of 1000 rpm. Determine the time behavior of the speed for idling, i.e., with driving torque zero, with and without Coulomb friction.

# 5 Electrical Drives

---

Mechatronic systems comprise a large variety of electrical drives. Their main purpose is to generate translational or rotational forces or to change the position of mechanical components. Electrical power-generating machines, which are used to drive power-consuming machines, and electrical actuators (control motors, servo drives), which are employed to drive control valves, are typical examples. In both cases, a distinction can be made between rotational and translational forces and motions. In the following sections, the construction and modeling of electromagnets, DC and AC motors will be outlined. The most important equations of these electromagnetic components will be stated in such a form that they can be used to describe the static and dynamic behavior of mechatronic overall systems.

## 5.1 TYPES OF ELECTRICAL DRIVES

Electrical drives used for direct translational motion are first and foremost electromagnets and linear drives. Electromagnets are usually employed as actuators, provided the desired displacement is small. In general, electromagnets can be divided into the following:

- DC magnets;
- AC magnets;
- polarized electromagnets.

Depending on the design of the magnetic body, the armature and the exciting field coil, one can distinguish between different basic designs, see Section 5.2. Electromagnetic linear drives are mainly incorporated for direct conversion of electrical energy into translational mo-

tion, as – for instance – in conveying systems and magnetic levitation railways.

Electrical drives for the direct generation of rotational motions are electrical motors, for which a vast variety of different designs exists. One can differentiate between small-power motors up to 75 W, fractional horse power motors (FHP motors) up to 750 W and large-power motors up to approximately 100 MW. Small-power motors and FHP motors are the dominating drives for actuators with small power settings, see Chapter 10. However, they are also used as power generators and therefore as small-power drives. Examples are household appliances, feed drives in machine tools and robots and devices for communications technology. Consequently, the power range of electrical drives extends from about  $10^{-6}$  W to  $10^8$  W, spanning approximately 14 powers of ten, Gray (1989), Meyer (1985), Wildi (1981).

For mechatronic systems, the interest lies in small-power electrical drives with an output of up to about 30 kW. Table 5.1 gives an overview of some basic types, illustrating torque characteristics and corresponding control inputs, see Töpfer, Kriesel (1983), Fraser, Milne (1994).

The electrical machines considered here have in common the fact that electric conductors move in a magnetic field. According to Faraday's law, a voltage is induced in these conductors. If this induced voltage sends a current through an external electric circuit, then this current will cause a force in the magnetic field and will generate a torque opposite to the direction of rotation. In this case, electric power is produced and the machine acts as a power-consuming machine (generator). If an external voltage, opposite in sign to the induced voltage and larger in magnitude, drives the electrical current, then this will generate a torque in the same direction as the rotational velocity. Hence, the system operates as a power-generating machine (motor, drive). Electrical power will be consumed and, at the same time, mechanical power will be delivered.

Many electrical machines can be used both as drives and generators. In the following, only motors will be considered.

The most important types of electric motors can be divided into the following:

## 1. DC motors

- series-wound motors;
- shunt-wound motors;
- permanent-field motors.

## 2. Three-phase AC motors

- induction motors (asynchronous motors);
- synchronous motors.

**Table 5.1.** General survey of electric motors with small power

motor	DC shunt-wound motor	DC series-wound motor	three-phase synchronous motor (DC excitation of rotor)	single-phase asynchronous motor (universal motor)	single-phase asynchronous motor with condensator	single-phase asynchronous motor (Ferraris motor)
circuit diagram						
torque-speed characteristics						
torque characteristics for manipulation	different manipul. variables: — — — normal:					
manipulated variables	$\Delta V_a$ $\Delta I_f$ $\Delta R_a$	$\Delta V_a$ $\Delta I_f$ $\Delta R_a$	$\Delta V_a$ $\Delta \omega$ $\Delta R$	$\Delta V_a$ $\Delta \omega$ $\Delta R$	$\Delta V_a$ $\Delta \omega$ $\Delta R$	$\Delta V_a$ $\Delta \omega$ $\Delta R$
			voltage frequency rotor resistance	frequency armature resistance	voltage armature resistance	manipulated voltage

### 3. Single-phase AC motors

- commutator motors (universal motors);
- squirrel cage motors.

## 5.2 ELECTROMAGNETS

Electromagnets are widely used as actuators (servo-drives, switches, relays) generating force or motion. Magnets are divided into DC magnets, AC magnets and polarized electromagnets, which can be used for small translational or for rotational motions. In the following, some important types as well as simplified models capturing the static as well as dynamic behavior of DC magnets are presented. For an in-depth review, see Kallenbach *et. al* (1994), Philippow (1976), Fraser, Milne (1994), Stadler (1995).

### 5.2.1 Types of Electromagnets

There exists a wide variety of different designs for electromagnets. All of these designs belong to one of the three basic designs shown in Figure 5.1. The field coil creates a magnetic field. A magnetic circuit is formed by the fixed magnet body (iron yoke), the movable armature and the variable air gap. The armature can either move in a translational manner, as illustrated in Figure 5.1, or in a rotational manner. A return mechanism, *e.g.*, a spring, can be added. With respect to their functions, one can differentiate between *positioning magnets* (lifting magnets, pulling magnets, switching magnets), *holding magnets* (without armature, clamping magnets) and *force-generating magnets* (clutch, brake).

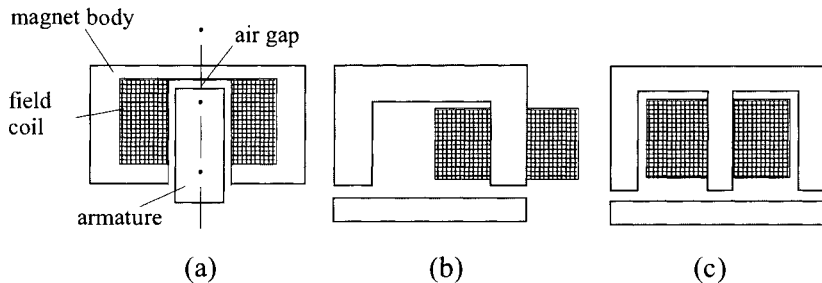


**Figure 5.1** Basic types of electromagnets for translational armature movement: (a) solenoid; (b) U-magnet; (c) E-magnet

For positioning magnets, on which the main focus will be, the magnetic force-displacement characteristic plays a prominent role. Magnets can be dimensioned differently by designing the magnet body and armature accordingly. For proportional magnets, one is interested in using designs that result in a linear relation between magnetic force and

current, or displacement and current respectively. For switching magnets, only the stop positions are of interest (e.g., magnetic valves).

### 5.2.2 The Magnetic Field

A conductor carrying a current  $I_1$  generates a magnetic field with field lines shaped as concentric circles, as shown in Figure 5.2. The *magnetic field strength* at a distance  $r$  from the conductor is given by

$$H(I, r) = \frac{I_1}{2\pi r} \quad \left[ \frac{A}{m} \right] \quad (5.2.1)$$

and does not depend on the properties of the surrounding medium. The electrical current is given as

$$I_1 = Hs \quad (5.2.2)$$

where  $s$  denotes the length of a field line. If one proceeds piece-wise on different field lines (different values of  $r$ ), then one gets

$$I_1 = \sum_j H_j \Delta s_j \quad (5.2.3)$$

and in the limiting case,  $\Delta s_j \rightarrow ds$ , one gets

$$I_1 = \oint_L H ds \quad (5.2.4)$$

where the integral must be evaluated over one circulation  $L$ . This law is called the *law of magnetomotance*. (Quite often, textbooks refer to a different form of this law, termed *Ampere's law*.)

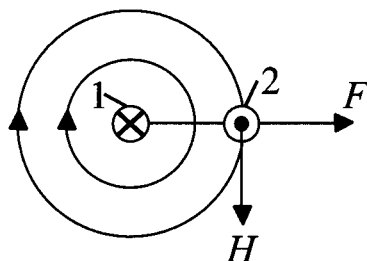


**Figure 5.2.** Magnetic field  $H$  of a wire 1 of infinite length. (The direction of the field lines and the direction of the current flow form a screw with a right handed thread.) Force  $F$  acting on conductor 2.  $\otimes$  current flows into plane,  $\bullet$  current flows out of plane

For multiple currents, the law can be written as

$$\oint_L H ds = \sum I = \Theta \quad (5.2.5)$$

where  $\Theta$  denotes the *magnetomotance*.

Experiments have revealed a law of the form

$$F = \frac{\mu I_1}{2\pi r} I_2 l = B_1 I_2 l \quad (5.2.6)$$

for the force acting on a conductor 2, carrying a current  $I_2$  in the presence of a conductor 1, which is placed at a distance  $l$  away from conductor 2.  $B_1$  is termed the *magnetic flux density*. The magnetic flux density

$$B = \mu \frac{I}{2\pi r} \left[ \frac{Vs}{m^2} = \text{Tesla} \right] \quad (5.2.7)$$

is proportional to the magnetic field strength, which was defined in (5.2.1), yielding;

$$B = \mu H \quad (5.2.8)$$

In this equation,  $\mu$  is the permeability that describes the influence of the medium on the flux density. In a vacuum,  $\mu$  is given as

$$\mu_0 = 4\pi 10^{-7} \left[ \frac{Vs}{Am} \right]$$

In general

$$\mu = \mu_r \mu_0 \quad (5.2.9)$$

where the relative permeability can be:

- $\mu_r < 1$  for diamagnetic materials
- $\mu_r > 1$  for paramagnetic materials
- $\mu_r \gg 1$  for ferromagnetic materials.

For the latter – ferromagnetic – materials such as iron, cobalt, and nickel, the relation between the magnetic field strength  $H$  and the magnetic flux density  $B$  is highly non-linear and depends on the time history. Figure 5.3 shows a typical magnetization curve. If the material has not been magnetized before, then the relation between  $B$  and  $H$  is given by the initial magnetization curve 1 until saturation is reached. Then, a hysteresis loop will build up and  $\mu$  is given by

$$\mu(H) = \frac{B}{H}$$

In order to determine the integral effect of the flux density within an area  $A$ , the *magnetic flux* can be calculated by

$$\Phi = \int_A B dA \quad [Vs = Wb] \quad (5.2.10)$$

if  $A$  and  $B$  are perpendicular to each other. The magnetic flux density is therefore given by

$$B = \frac{d\Phi}{dA} \quad (5.2.11)$$

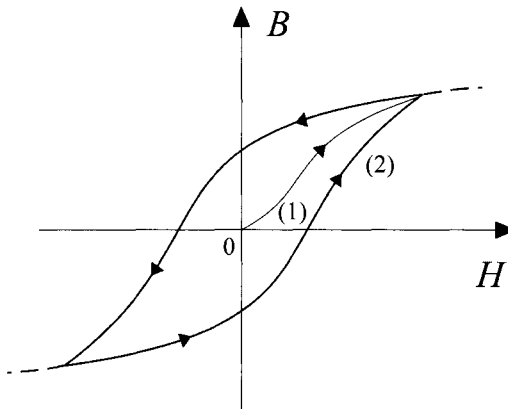


**Figure 5.3.** Magnetization characteristic for a ferromagnetic material: (1) initial magnetization curve, (2) hysteresis curve

### 5.2.3 Static Behavior of Simple Magnetic Circuits

Magnetic circuits will form under the condition that ferromagnetic materials are positioned such that the magnetic field lines, which may be created by a coil with  $N$  turns, will mainly flow through the ferromagnetic parts. The high permeability of ferromagnetic materials leads to this formation of the electromagnet field. A simple magnet circuit is shown in Figure 5.4. For further development, the following assumptions will be made: (a) the magnetic field within the iron ring is homogeneous (cross-sectional area  $A$  small); (b) the length of the air gap  $l_L$  is small with respect to the width. Under these assumptions,

$$B = B_E = B_L$$

will hold and application of the law of magnetomotance yields

$$H_E J_E + H_L l_L = NI = \Theta \quad (5.2.12)$$

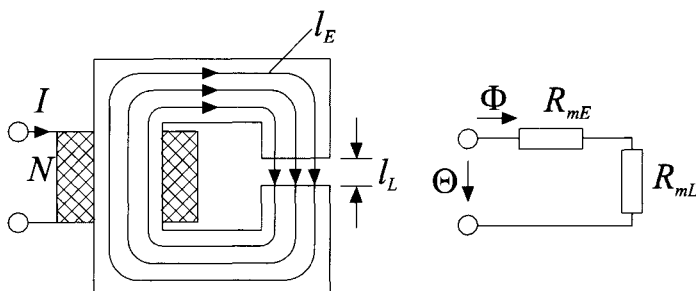


**Figure 5.4.** Simple magnetic circuit and magnetic equivalent circuit diagram

By substituting  $B = \mu H$  and the magnetic flux  $\Phi$ , one gets

$$\Phi \left( \frac{l_E}{\mu_E A} + \frac{l_L}{\mu_L A} \right) = \Theta \quad (5.2.13)$$

Comparing this equation with the equation describing the resistance of a conductor of length  $l$ , which is given by  $R = l/\gamma A$  ( $\gamma$ , conductivity), leads to the notion of magnetic resistance given by

$$R_m = \frac{l}{\mu A} \quad (5.2.14)$$

Therefore, the behavior of the magnetic circuit can be described by

$$(R_{mE} + R_{mL}) \Phi = \Theta \quad (5.2.15)$$

As an analogy to Ohm's law for electrical circuits, which can be written as

$$R I = V \quad (5.2.16)$$

one can define *Ohm's law for magnetic circuits*, given by

$$R_M \Phi = \Theta \quad (5.2.17)$$

In this equation, the magnetic flux  $\Phi$  corresponds to the electric current and the magnetomotance  $\Theta$  corresponds to the voltage. Employing these analogies, an equivalent circuit diagram can be derived, as shown in Figure 5.4. However, the non-linear magnetization curve,  $B = f(H)$ , respectively  $\mu = g(H)$ , has to be taken into account.

For a coil, where the cross-sectional area  $A$  is identical to the area enclosed by a wire loop, one denotes the magnetic flux linked with that particular loop with  $\Psi$ . For a coil with  $N$  turns, the *magnetic flux linkage* is calculated by

$$\Psi = \sum_N \Phi = \sum_N \int_A B dA \quad (5.2.18)$$

and – provided each loop creates the same amount of flux per turn –  $\Psi$  is given by

$$\Psi = N\Phi = N \int_A B dA \quad (5.2.19)$$

For linear magnetic circuits, the magnetic flux linkage is proportional to the current as given by

$$\Psi = LI \quad [Vs = mN/A] \quad (5.2.20)$$

where  $L$  denotes the inductance. For non-linear magnetic circuits, the relation  $L = f(I)$  has to be taken into account. The term

$$L_d = \frac{d\Psi}{dI} \quad (5.2.21)$$

is denoted as the differential inductance.

The inductance of a coil can be calculated by

$$L = \frac{\Psi}{I} = N^2 \frac{\Phi}{\Theta} = N^2 \frac{1}{R_m} \quad (5.2.22)$$

exploiting (5.2.20), (5.2.19), and (5.2.12).

### 5.2.4 Dynamic Behavior of Simple Magnetic Circuits

In the preceding section, all calculations were carried out for the conductor being at rest in the magnetic field. Whenever a conductor of length  $l$  is moved with constant speed  $v$  perpendicular to a magnetic field with magnetic flux density  $B$ , a voltage will be induced. The equation

$$V_i = -Blv = -Bl \frac{dz}{dt} = -B \frac{dA}{dt} = -\frac{d\Phi}{dt} \quad (5.2.23)$$

is called Faraday's law: the induced voltage is proportional to the time-rate of change of the magnetic flux, which is encompassed by the conductor loop of cross-sectional area  $A$ .

Faraday's law can also be applied if the conductor is at rest and the magnetic flux varies over time. Substituting (5.2.10), one can rewrite (5.2.23) as

$$V_i = -\frac{d\Phi}{dt} = - \int_A \frac{\partial B}{\partial t} dA \quad (5.2.24)$$

For coils, the magnetic flux linked with the turns  $\Psi$  must be used instead of  $\Phi$ . This leads to

$$V_i = -\frac{d\Psi}{dt} \quad (5.2.25)$$

For electromagnets, changes in the magnetic flux are caused by changes in the magnetic field of other, coupled, magnets (mutual induction) or changes in the own magnetic field (self-induction). For the latter case, two important practical examples will now be considered.

#### a) Dynamic behavior in the presence of changes in the voltage

A simple magnet as shown in Figure 5.5 can be represented by the equivalent circuit diagram shown in Figure 5.6, which consists of a resistor  $R$  and a (mostly non-linear) inductance  $L$  connected in series.

The system response due to a step change in the voltage  $V(t)$  can be calculated using Kirchhoff's second law (voltage law)

$$V(t) - RI(t) - \frac{d\Psi(t)}{dt} = 0 \quad (5.2.26)$$

For a linear magnetic circuit, this can be rewritten using (5.2.20) as

$$L \frac{dI(t)}{dt} + RI(t) = V(t)$$

or

$$\frac{L}{R} \frac{dI(t)}{dt} + I(t) = \frac{1}{R} V(t) \quad (5.2.27)$$

which represents a first order differential equation whose time constant is  $T = L/R$ . Hence, the time-rate of change of the flux  $d\Psi(t)/dt$  causes an induced voltage, which is opposite in sign to the impressed voltage  $V(t)$  and which delays the current rise.

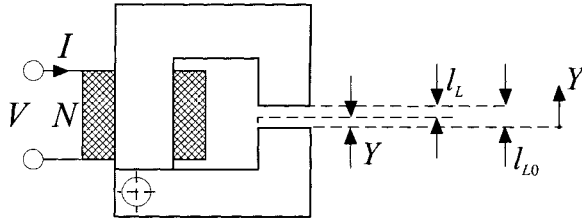


Figure 5.5. Electromagnet with hinged armature

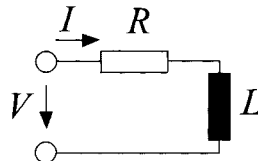


Figure 5.6. Equivalent circuit diagram for the electromagnet shown in Figure 5.5

### b) Dynamic behavior in the presence of air gap changes

According to (5.2.14), a change in the air gap  $l_L$  will lead to a change in the magnetic resistance. From (5.2.20) and (5.2.22), it follows that

$$\begin{aligned} \frac{d\Psi}{dt} &= \frac{d}{dt} (N^2 R_m^{-1}(t) I(t)) \\ &= N^2 \left[ -R_m^{-2} \frac{dR_m}{dt} I(t) + R_m^{-1} \frac{dI(t)}{dt} \right] \\ &= N^2 R_m^{-1} \left[ -R_m^{-1} \frac{1}{\mu_L A} \frac{dl_L(t)}{dt} I(t) + \frac{dI(t)}{dt} \right] \end{aligned} \quad (5.2.28)$$

Combining this result with (5.2.26) will lead to the non-linear differential equation

$$L \frac{dI(t)}{dt} + \left[ R - \frac{L}{R_m \mu_L A} \frac{dl_L(t)}{dt} \right] I(t) = V(t) \quad (5.2.29)$$

A reduction in the air gap results in  $dl_L(t)/dt < 0$ , and the effective magnetic resistance increases. Therefore, a reduction or even short-time reversal in the current rise  $dI(t)/dt$  follows.

### 5.2.5 Static Behavior of Electromagnets

A simple electromagnet as shown in Figure 5.5 will be considered in the following, with the characteristics

$\Theta = NI$	magnetomotance
$l_E, l_L$	effective length of the magnetic flux in the iron core respectively the air gap
$A$	cross-section (constant)
$B = B_E = B_L$	magnetic flux density
$F_m$	magnetic force acting along displacement $Y$ .

The mechanical energy is given by

$$dE_{mech} = F_m dY \quad (5.2.30)$$

The magnetic energy in the iron core can be calculated by using (5.2.25), multiplying by  $I(t)dt$  and using (5.2.11), (5.2.12). The magnetic energy is given by

$$\begin{aligned} dE_m &= Id\Psi = INd\Phi = INA dB \\ &= l_E H A dB = V_E H_E dB \end{aligned} \quad (5.2.31)$$

where  $V = l_E A$  denotes the volume of the iron core, Clausert, Wiesemann (1986). Under the condition of a homogenous magnetic field and the relation given in (5.2.8), the equation

$$dE_m = \frac{V_E}{\mu} B dB \quad (5.2.32)$$

can be derived. For a constant permeability this can be integrated, yielding

$$E_m = \frac{V_E}{\mu} \int_0^{B_E} B dB = \frac{1}{2} \frac{B_E^2}{\mu} V_E \quad (5.2.33)$$

Subsequently, the magnetic energy can be stated as

$$E_m = \frac{1}{2} \mu H^2 V = \frac{1}{2} BHV = \frac{1}{2} \frac{B^2}{\mu} V \quad (5.2.34)$$

This equation can be used to calculate the amount of energy stored in the iron core and the air gap by using (5.2.11), (5.2.13) and  $\mu_L = \mu_0$ .

$$\begin{aligned} E_m &= A l_E \frac{1}{2} \frac{B^2}{\mu_E} + A l_L \frac{1}{2} \frac{B^2}{\mu_L} = \frac{\Phi^2}{2} \left( \frac{l_E}{\mu_E A} + \frac{l_L}{\mu_0 A} \right) \\ &= \frac{\Theta^2}{2} \frac{1}{\frac{l_E}{\mu_E A} + \frac{l_L}{\mu_0 A}} \end{aligned} \quad (5.2.35)$$

In the following, the variable length of the air gap will be substituted as  

$$l_L = l_{L0} - Y \quad (5.2.36)$$

The underlying geometry can be seen in Figure 5.5. It is possible to calculate the magnetic force using (5.2.30) with  $dE_{\text{mech}} = dE_m$ , which results in

$$F_m = \frac{dE_m}{dY} = \frac{\Theta^2}{2} \frac{\frac{1}{\mu_0 A}}{\left( \frac{l_E}{\mu_E A} + \frac{l_{L0} - Y}{\mu_0 A} \right)^2} \quad (5.2.37)$$

For the maximum length of the air gap, characterized by  $Y = 0$ , the force can be determined by using (5.2.13) and (5.2.11) as

$$F_m(0) = \frac{\Theta^2}{2} \frac{\frac{1}{\mu_0 A}}{\left( \frac{l_E}{\mu_E A} + \frac{l_{L0}}{\mu_0 A} \right)^2} = \frac{1}{2} \frac{\Phi^2}{\mu_0 A} = \frac{1}{2} \frac{B^2}{\mu_0} A = F_{m\min} \quad (5.2.38)$$

Similarly, for the minimum length of the air gap, i.e.,  $Y = l_{L0}$ , the relationship

$$F_m(l_{L0}) = \frac{\Theta^2}{2} \frac{\frac{1}{\mu_0 A}}{\left( \frac{l_E}{\mu_E A} \right)^2} = F_{m\max} \quad (5.2.39)$$

follows.

The representative shape of the magnetic force over displacement curve is sketched in Figure 5.7.

For the simple electromagnet considered here, consisting of a flat armature and a flat counterpart, the magnetic force is primarily determined by the magnetic resistance of the air gap. The influence of the iron core can be neglected in wide ranges since  $\mu_E \ll \mu_0$ . This results in

$$F_m \approx \frac{\Theta^2}{2} \frac{\frac{1}{\mu_0 A}}{\left( \frac{l_{L0} - Y}{\mu_0 A} \right)^2} = \frac{\Theta^2}{2} \frac{\mu_0 A}{(l_{L0} - Y)^2} = \frac{\Theta^2}{2} \frac{\mu_0 A}{l_L^2} = \frac{N^2 I^2}{2} \frac{\mu_0 A}{l_L^2} \quad (5.2.40)$$

Roughly speaking, the force is inversely proportional to the squared length of the air gap, proportional to the squared current and proportional to the squared number of turns. The effect of the magnetic resistance of the iron core will only become noticeable for a very small air gap.

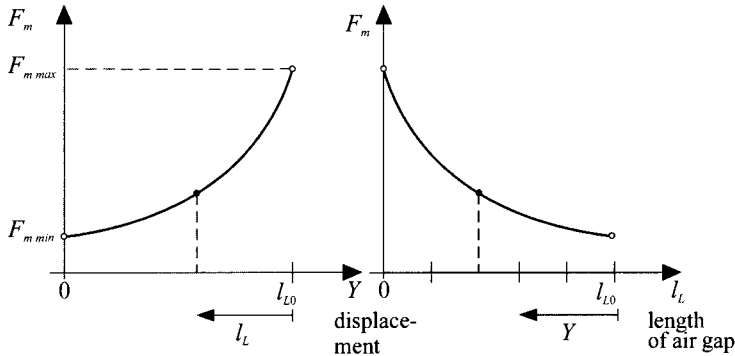


**Figure 5.7.** Magnetic force-displacement characteristics for the electromagnet shown in Figure 5.5 under simplifying assumptions

Recordings of magnetic force curves for positioning magnets, in which all effects come into play, are characterized by a shape as shown in Figure 5.8. The resulting curves are non-linear and show hysteretic behavior. The hysteresis stems from both magnetic hysteresis and dry bearing friction, Kallenbach *et al.* (1994), Raab (1993). For the magnetic force-current curve, one can identify three different regions:

- initial region (I):  $F_m \sim I^2$   
(magnetic resistance of the air gap is predominant, magnetic resistance of the iron core can be neglected due to weak excitation);
- linear region (II):  $F_m \sim I$ ;
- saturation region (III):  $F_m \sim I^{1/2}$   
(The magnetic circuit is close to saturation, a current increase will only cause a small increase in force.)

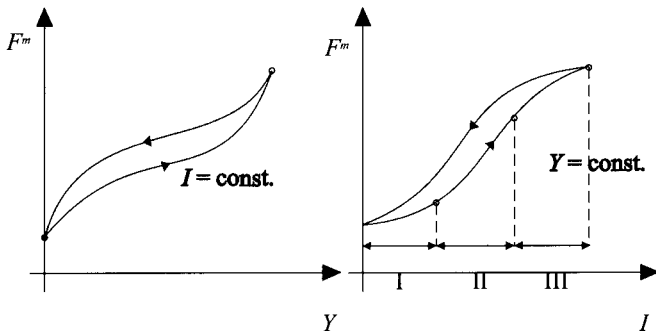


**Figure 5.8.** Measured magnetic force characteristic for positioning magnets: (a) magnetic force-displacement characteristic; (b) magnetic force-current characteristic

The magnetic force-displacement curve can be influenced by the shape of the armature and the counterpart. The shaping determines the displacement dependency of the magnetic energy by means of the air

gap's extension, not only in the longitudinal but also the radial direction, the geometric properties and the non-linear magnetization curve  $B = f(H)$  respectively  $\Psi = f(I)$ , Kallenbach *et al.* (1994).

Figure 5.9 provides some examples, showing that the field of characteristics  $\Psi = f(I)$  is almost linear for the simple design shown in Figure 5.9a and non-linear for the designs shown in Figure 5.9b and 5.9c. The electromagnets shown in Figure 5.9b and 5.9c have armatures and counterparts designed to shape the characteristics.

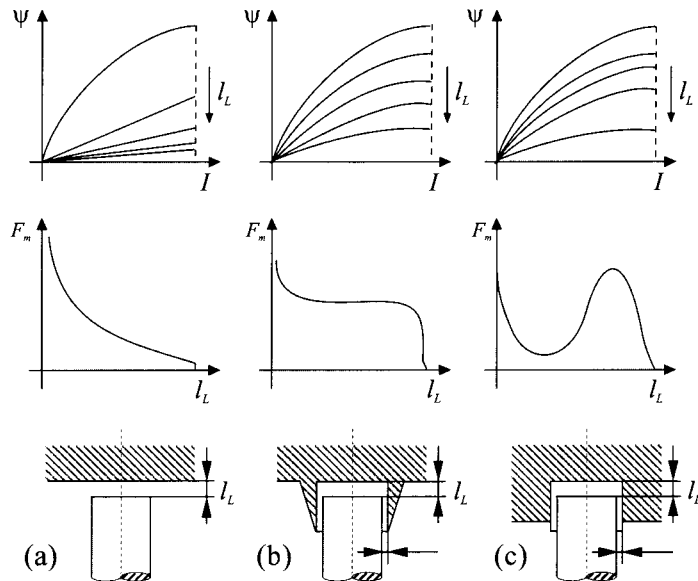


**Figure 5.9.** Characteristics for different armature counterparts, Kallenbach *et. al* (1994)

Now, a positioning magnet with a linearly moving armature and a return spring is considered, as shown in Figure 5.10. The force-displacement curves are illustrated in Figure 5.11. A stable operating point exists whenever the slope of the magnetic force curve is less than the slope of the curve describing the spring characteristic, which can be stated as

$$\frac{\partial F_m}{\partial Y} < \frac{\partial F_c}{\partial Y}$$

This notion is described in Section 6.2. For an electromagnet with shaping of the characteristic curve, as shown in Figure 5.11a, the gains and time constants will vary less and the stable control range with respect to the achievable maximum displacement  $Y_{max}$  is larger compared to a magnet designed without measures to shape the characteristics.

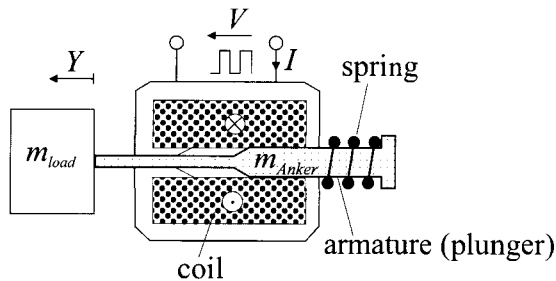


**Figure 5.10.** Solenoid with a linearly movable armature

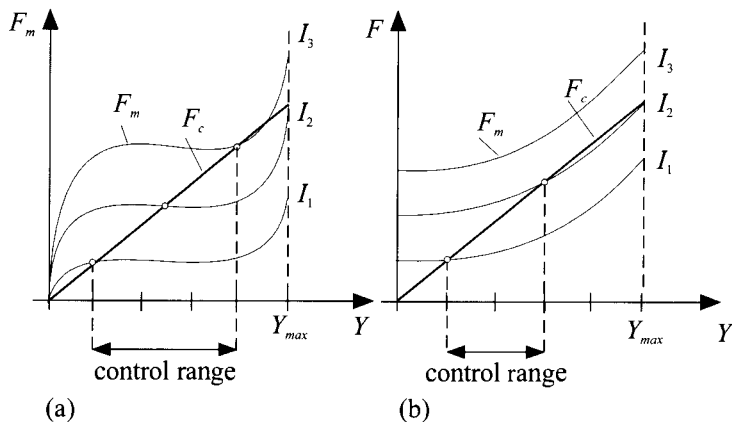


**Figure 5.11.** Force-displacement characteristic for magnet and return spring (without hysteresis): (a) with shaping of the characteristic curve; (b) without shaping of the characteristic curve

### 5.2.6 Dynamic Behavior of Electromagnets and Position Control

Under the following assumptions, the dynamics of an electromagnet as shown in Figure 5.10 can be described by linear equations:

- the magnetic flux linkage can be described by

$$\Psi = \Psi_0 + L_d I + c_Y Y \quad (5.2.41)$$

- $(L_d$  differential inductance as derived in (5.2.21));
- eddy current losses are neglected;
- effects due to hysteretic magnetization effects will be neglected.

Under these assumptions, the magnet circuit, as described in (5.2.26), is governed by

$$U(t) = RI(t) + L_d \frac{dI(t)}{dt} + c_Y \frac{dY}{dt} \quad (5.2.42)$$

$$F_m(t) = c_Y I(t) \quad (5.2.43)$$

which follows from (5.2.41), Kallenbach *et al.* (1994). The behavior of the spring-mass system in the presence of viscous friction is given by

$$F_m(t) = m \ddot{Y}(t) + d \dot{Y}(t) + c_F Y(t) \quad (5.2.44)$$

Upon selecting the voltage  $V(t)$  as the variable to be manipulated, a block diagram can be drawn as shown in Figure 5.12. Application of the Laplace transform results in the transfer function

$$G_{YV}(s) = \frac{Y(s)}{V(s)} = \frac{\frac{c_Y}{c_F R}}{\frac{mL_d}{c_F R} s^3 + \left( \frac{m}{c_F} + \frac{dL_d}{c_F R} \right) s^2 + \left( \frac{d}{c_F} + \frac{L_d}{R} + \frac{c_Y^2}{c_F R} \right) s + 1} \quad (5.2.45)$$

describing a third order system.

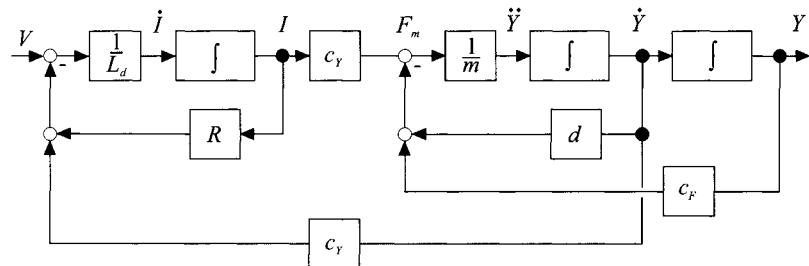


**Figure 5.12.** Block diagram for the linearized electromagnet with return spring fed by direct current

In the following, the non-linear behavior of a non-idealized electromagnet will be considered. For this, the non-linear curves  $\Psi(I, Y)$ , the magnetic hysteresis  $F_m(I, Y)$  and the friction force  $F_f(\dot{Y})$  have to be taken into account, which will lead to the set of equations

$$V(t) = RI(t) + \frac{d}{dt} \Psi(I, Y) \quad (5.2.46)$$

$$\Psi = L(I, Y) I \quad (5.2.47)$$

$$F_m(I, Y) \quad (\text{characteristic curves}) \quad (5.2.48)$$

$$F_m(t) = m \ddot{Y}(t) + c_F Y(t) + F_f(\dot{Y}) \quad (5.2.49)$$

$$F_f(\dot{Y}) = F_{f0} \operatorname{sign} \dot{Y}(t) + d \dot{Y}(t) \quad (5.2.50)$$

$F_{f0}$  denotes the coefficient of dry friction, whereas  $d$  is the viscous friction coefficient. (5.2.46) and (5.2.47) can be combined into

$$\begin{aligned} V(t) &= RI(t) + \dot{I}(t)L(I,Y) + I(t) \frac{\partial L(I,Y)}{\partial Y} \dot{Y}(t) \\ &\quad + I(t) \frac{\partial L(I,Y)}{\partial I} \cdot \dot{I}(t) \end{aligned}$$

and

$$\left[ L(I,Y) + \frac{\partial L(I,Y)}{\partial I} I(t) \right] \frac{dI(t)}{dt} + \left[ R + \frac{\partial L(I,Y)}{\partial Y} \dot{Y}(t) \right] I(t) = V(t) \quad (5.2.51)$$

respectively.

The magnetic hysteresis influences the quantities  $L(I,Y)$ ,  $\partial L(I,Y)/\partial I$  and  $\partial L(I,Y)/\partial Y$ . This influence depends on the direction of the movement. The hysteretic effects caused by dry friction are incorporated into (5.2.49) by means of the signum function. Figure 5.13 shows the corresponding block diagram.

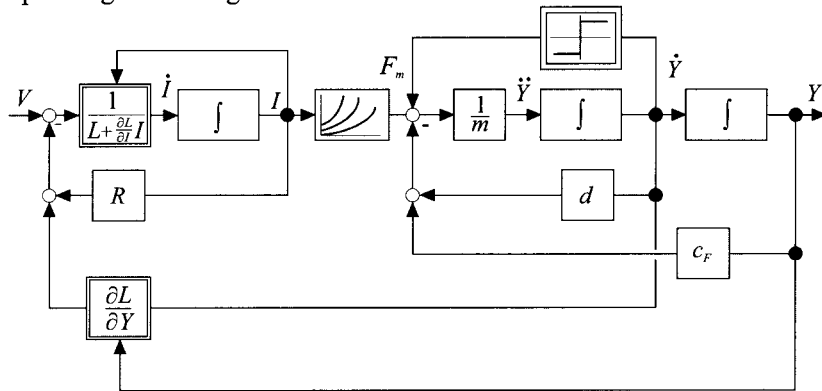


**Figure 5.13.** Block diagram for the non-linear electromagnet with return spring fed by a direct current

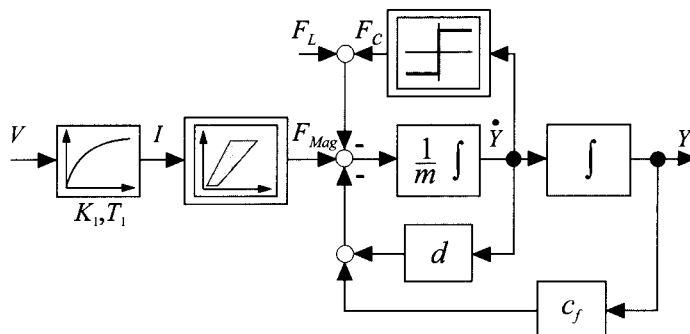


**Figure 5.14.** Simplified block diagram for the non-linear electromagnet that can be used for the design of controls, Raab (1993);  $F_L$ : forces of load

The design of model-based displacement controllers requires simplified mathematical models that still capture the essential input/output behavior. The block diagram shown in Figure 5.14 shows a suitable model. A positioning magnet fitted with an inner current control loop, can be described by a first order model. The output of this block is subject to the magnetic force-displacement curve, which rises and descends linearly although with different slopes and a current-dependent hysteresis width. Next to this block is the model of the mechanical system, which includes the second hysteresis stemming from dry friction. This simplified non-linear model leads to third order difference equations with direction-dependent parameters. For a non-linear adaptive digital control system, the unknown parameters will be estimated based on the recorded signals  $V(k)$  and  $Y(k)$ . Raab (1993) showed how the control performance of the displacement control of a positioning magnet could be increased substantially by compensation of the non-linear magnetic force curve and the dry friction. By employing this software-based adaptive characteristic curve linearization, the need for constructive measures to linearise the characteristic curve has vanished. This means a relocation of this function from the constructive linearisation to the information-processing domain, which is a characteristic of the mechatronic approach.

### 5.3 DIRECT CURRENT MOTORS

In the following section, the construction of different electric motors will be briefly discussed. First of all, modeling and speed control of separately excited (shunt-wound) motors are addressed. Then, some special designs of DC motors will be considered. Subsequently, modeling and speed control of the most important constructions of induction motors (AC motors, single-phase motors) involving the basic operational behavior will be regarded. This is followed by a section on power electronics.

A general survey of the individual circuit diagrams, steady state torque characteristics and manipulated variables is shown in Table 5.1, compare Töpfer, Kriesel (1983). Further surveys are given by Gray (1989), Sen (1989), Wildi (1981), Lindsay, Rashid (1986), Fraser, Milne (1994), Leonhard (1974, 1996), Beitz, Küttner (1981), Stölting, Beisse (1987), Weißmantel (1991), Janocha (1992), Pfaff (1994), Moczala (1993), Schröder (1995).

An extensive, systematical survey of electric small-type motors up to powers of 1 kW is composed by Jung, Schneider (1984) in the form of a construction catalogue, see also DIN 42027.

The stator of DC motors, designed for higher power carries several field coils with 1 up to  $n$  pairs of magnetic north and south poles, in order to produce one or more stationary magnetic fields, compare Figure 5.15. The armature windings are placed in 2 up to  $m$  axial rotor slots

forming several coils. The corresponding connectors of the individual coils are connected to one bar of the commutator. The commutator is a rotary body that consists of pairs of sector-shaped, individually insulated copper lamellas. These lamellas are connected in series so that the overall voltage results from the sum of the voltages induced in the individual partial windings. The rotor coils are fed with armature current by means of brushes (sliding contacts).

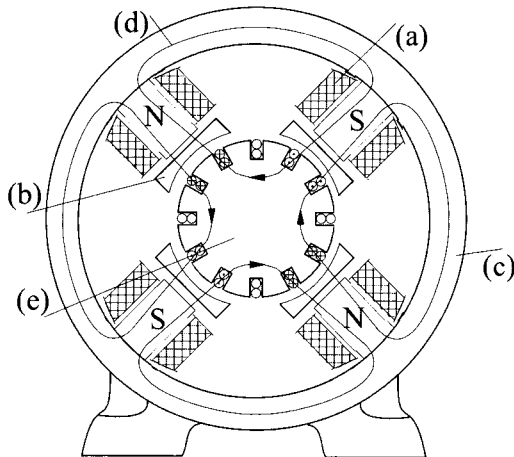


**Figure 5.15.** DC motor with four poles: (a) excitation coils; (b) pole shoe; (c) yoke; (d) magnetic flux; (e) rotor

In the case of turning the rotor through the constant magnetic field produced by the stator windings, alternating voltages are induced in the armature coils according to Faraday's induction law. This is because the armature coils change their inclination (rotation angle) with regard to the magnetic field, alternately passing a north or a south pole. In order to achieve a rectified voltage, the polarity of the contact between connector and partial armature winding has to be reversed whenever the sign of the induced voltage changes. This is accomplished by the commutator, which therefore consists of the same number of brush pairs like the armature winding pairs. In this case, the angular position of the brushes is equivalent to those of the field poles. Thus, adjacent brushes yield alternately positive and negative poles.

The main types of construction of small-power DC motors can be primarily distinguished by considering the mode of excitation. If the electromagnetic excitation is performed by means of a field coil in the stator, it can be either supplied independently (separately excited DC motor) or in the form of a parallel circuit (shunt-wound motor) or a series connection with the armature coil (series-wound motor), compare Table 5.1. Above all, the specified circuit configurations result in different speed-torque curves.

In the case of parallel connection of the armature and field coils and separately excited field coils, the produced torque decreases at constant

armature voltage linearly with the angular velocity. The speed can be controlled over a wide speed range by varying the armature voltage. For separately excited DC motors the decrease of the exciting current (field weakening) yields a further speed rise if the rated armature voltage is already reached. This motor type can be employed as a speed-variable drive in a multitude of applications, such as machine tools, robots and actuating drives (servo-drives).

With series connection of the armature and field coils, the resulting magnetic field depends on the load. The speed-torque curve shows large torque for small speed, whereas with higher speed the torque decreases rapidly. In view of the large starting torque, this machine type is, for instance, used as a starting motor for combustion engines.

Permanently excited DC motors, by employing ferrites or Al-Ni-Co magnets, comply with separately excited DC motors with constant excitation and show equivalent characteristics. This type of construction is often used for low-power motors.

In consideration of the universal applicability, separately excited DC motors will be discussed in detail within the following section, see also Bödefeld, Sequenz (1971), Leonhard (1974, 1996), Nürnberg, Hantsch (1987), Pfaff (1994), Richter (1949), Schröder (1995).

### 5.3.1 Induced Voltage

In Figure 5.15 the schematic set-up and in Figure 5.16 the equivalent circuit diagram of a DC motor are depicted. The excitation windings in the stator are fed by a DC current  $I_E$ . Thus, a magnetic field with field strength  $H$  and corresponding flux density  $B = \mu H$  is produced. The arising exciting field effects a linked magnetic flux  $\Psi$  in the current-carrying armature coils. Hence, in accordance with Faraday's induction law, a voltage is induced in the moved armature windings, (5.2.25)

$$V_i(t) = - \frac{d\Psi(\varphi, t)}{dt} = - \frac{\partial\Psi}{\partial t} - \frac{\partial\Psi}{\partial\varphi} \frac{d\varphi}{dt} \quad (5.3.1)$$

whereby  $\partial\Psi/\partial t$  is the derivative of the flux linkage with regard to time. In the presence of constant excitation (also valid for permanent magnet excitation), this term can be neglected. The term  $\partial\Psi/\partial\varphi$  describes the change of the flux linkage in dependence on the angle of rotation. Considering an armature coil, which is inclined at angle  $\varphi$ , the flux linkage can be specified by

$$\Psi(\varphi) = \Psi^* \sin \varphi \quad (5.3.2)$$

and therefore

$$\frac{d\Psi}{d\varphi} = \Psi^* \cos \varphi$$

In the case of DC motors with several armature windings and commuta-

tor segments, the corresponding angle  $\varphi$  is comparably small, so that  $\cos\varphi \approx 1$  can be assumed. Thus, the induced voltage results in

$$V_i = -\Psi^* \omega \quad (5.3.3)$$

whereupon  $\omega = d\varphi/dt$  specifies the angular velocity. The induced voltage (5.3.3) is also denoted as electromotive force (EMF).

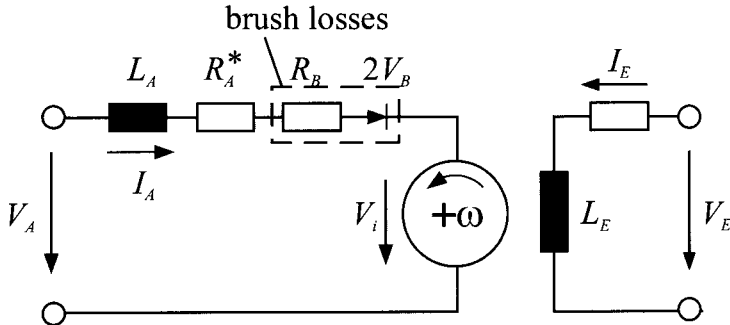


Figure 5.16 Schematic circuit diagram of a separately excited DC motor

### 5.3.2 Torque Generation

When the current  $I_A$  flows through a conductor of length  $l$ , the conductor will experience the following force (Lorentz force) in the presence of an external magnetic field  $B$ , according to (5.1.6)

$$F = I_A \times B \cdot l \quad (5.3.4)$$

Hence, the conductor moves with distance  $r$  (radius relative to the shaft) perpendicular towards the magnetic field, resulting in the torque

$$T_{el} = r I_A B l \quad (5.3.5)$$

The driving power at the shaft is therefore

$$P_{mech} = T_{el} \omega \quad (5.3.6)$$

In this case, the electrical power within the armature coils is

$$P_{el} = V_i I_A = \Psi^* \omega I_A \quad (5.3.7)$$

and with the help of the power balance, the produced torque can be denoted by

$$T_{el} = \Psi^* I_A \quad (5.3.8)$$

where from (5.3.5) and (5.3.8), it follows that

$$\Psi^* = r B l \quad (5.3.9)$$

In the following,  $\Psi^* = \Psi$  is assumed.

### 5.3.3 Dynamic Behavior

According to the circuit diagram in Figure 5.16, the main electrical quantities of the armature circuit can be specified as follows:

$R_A^*$	armature resistance
$L_A$	armature inductance
$R_B$	brush resistance
$2V_B$	brush voltage loss (twice)
$E_A$	induced rotation voltage
$R_A = R_A^* + R_B$	overall armature resistance.

The current transfer at the twofold brushes is connected with losses. These can be regarded by considering an Ohm's component  $R_B$  and a direct voltage loss  $V_v = 2V_B$  similarly to the on-resistance of a diode, Vogt (1988). (It is  $V_B \approx 1V$  for carbon brushes and high currents.) The dynamic behavior of the armature circuit can therefore be specified as follows

$$\begin{aligned} L_A \dot{I}_A(t) + R_A I_A(t) &= V_A(t) - V_i(t) - 2V_B \operatorname{sign} I_A(t) \\ &= V_A(t) - \Psi \omega(t) - 2V_B \operatorname{sign} I_A(t) \end{aligned} \quad (5.3.10)$$

(In the case of generating the armature voltage by means of an inverter based on pulse width modulation, the brush voltage losses can be better approached by the term  $V_v = K_B I |\omega|$ , Höfling (1996).) Thus, a first order differential equation with the armature time constant

$$T_A = \frac{L_A}{R_A}$$

emerges. As for the mechanical subsystem of the DC motor the following values are of interest:

- $J$  moment of inertia
- $T_{el}$  electrical motor torque
- $T_R$  friction torque
- $T_L$  load torque.

Due to (4.7.8) and (4.4.6), the friction torque can be partitioned into solid and viscous friction terms, see Chapter 4.

$$T_F(t) = T_{F0} \operatorname{sign} \omega(t) + T_{F1} \omega(t) \quad (5.3.11)$$

Furthermore, the torque balance yields

$$\begin{aligned} J \ddot{\omega}(t) &= T_{el}(t) - T_F(t) - T_L(t) \\ &= \Psi I_A(t) - T_{F0} \operatorname{sign} \omega(t) - T_{F1} \omega(t) - T_L(t) \end{aligned} \quad (5.3.12)$$

which is a first order differential equation with the mechanical time constant

$$T_M = \frac{J}{T_{F1}}$$

Considering (5.3.10) and (5.3.12), the electrical and mechanical subsystems of a DC motor with constant excitation are summarized in the block diagram of Figure 5.17. The armature voltage  $V_A$  as well as the load torque  $T_L$  can be regarded as input values. Output values are the armature current  $I_A$  and the angular velocity  $\omega$ . Neglecting the non-linear terms for the dry friction and the brush voltage loss, the block diagram is equivalent to that of the linearized electromagnet with the velocity  $\dot{Y}$  as output value, see Figure 5.12. The electrical and mechanical sub-models are coupled via the armature flux linkage  $\Psi$ , on the one hand, for the generation of torque in the feedforward branch and, on the other hand, for the generation of the induced EMF in the feedback branch.

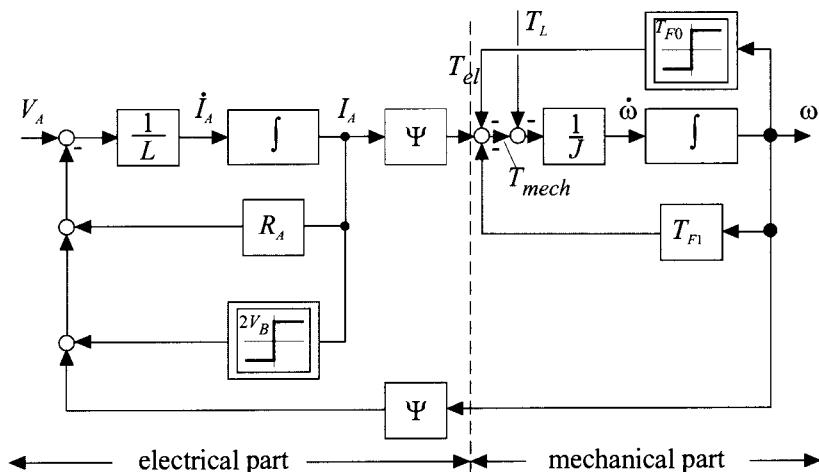


**Figure 5.17.** Block diagram for the dynamical behavior of the separately excited DC motor with constant excitation

Furthermore, the description of the DC motor will be considered in a two-port representation. In accordance with Chapter 2, the following variables of the converter can be regarded as independent input values:

- Applied armature voltage  $V_A$  and applied load torque  $T_L$ .
- Applied armature current  $I_A$  and applied angular velocity  $\omega$ .

Neglecting the mostly small impacts of dry friction as well as brush voltage loss and considering therefore  $T_{F0} = 0$  and  $V_B = 0$ , the following transfer functions for small changes around an operating point can be derived by transforming the differential equations into the Laplace domain:

a) Inputs:  $\Delta V_A$  and  $\Delta T_L$

$$\begin{aligned} G_{11}(s) &= \frac{\Delta \omega(s)}{\Delta V_A(s)} \Bigg|_{\Delta T_L=0} = \frac{\Psi}{\Psi^2 + T_{F1} R_A + s(JR_A + T_{F1} L_A) + s^2 JL_A} \\ G_{21}(s) &= \frac{\Delta I_A(s)}{\Delta V_A(s)} \Bigg|_{\Delta T_L=0} = \frac{T_{F1} + sJ}{\Psi^2 + T_{F1} R_A + s(JR_A + T_{F1} L_A) + s^2 JL_A} \\ G_{12}(s) &= \frac{\Delta \omega(s)}{\Delta T_L(s)} \Bigg|_{\Delta V_A=0} = \frac{-(sL_A + R_A)}{\Psi^2 + T_{F1} R_A + s(JR_A + T_{F1} L_A) + s^2 JL_A} \\ G_{22}(s) &= \frac{\Delta I_A(s)}{\Delta T_L(s)} \Bigg|_{\Delta V_A=0} = \frac{\Psi}{\Psi^2 + T_{F1} R_A + s(JR_A + T_{F1} L_A) + s^2 JL_A} \end{aligned} \quad (5.3.13a)$$

b) Inputs:  $\Delta I_A$  and  $\Delta \omega$

$$\begin{aligned} G_{11}'(s) &= \frac{\Delta T_L(s)}{\Delta I_A(s)} \Bigg|_{\Delta \omega=0} = \Psi \\ G_{21}'(s) &= \frac{\Delta V_A(s)}{\Delta I_A(s)} \Bigg|_{\Delta \omega=0} = R_A + L_A s \\ G_{12}'(s) &= \frac{\Delta T_L(s)}{\Delta \omega(s)} \Bigg|_{\Delta I_A=0} = -(T_{R1} + Js) \\ G_{22}'(s) &= \frac{\Delta V_A(s)}{\Delta \omega(s)} \Bigg|_{\Delta I_A=0} = \Psi \end{aligned} \quad (5.3.13b)$$

The corresponding block diagrams of the arising two-ports are illustrated in Figure 5.18.

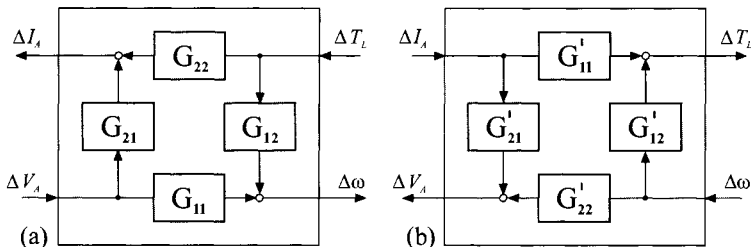


Figure 5.18. Two-port representation of a DC motor

In case a), all transfer functions show the same denominator of second order. Thus, the poles  $s_{1/2} = -\delta_e \pm i\omega_e$  for the discussed transfer functions can be specified as

$$s_{1/2} = \frac{-JR_A - T_{F1} L_A \pm \sqrt{J^2 R_A^2 - 2T_{F1} JL_A R_A + T_{F1}^2 L_A^2 - 4\Psi^2 JL_A}}{2JL_A} \quad (5.3.14)$$

In consideration of the negative radicand, a conjugate complex pole

pair emerges. The damping factor  $D$  and the characteristic angular frequency  $\omega_0$  of the system are

$$D = \frac{JR_A + T_{F1}L_A}{2\sqrt{JL_A(\Psi^2 + T_{F1}R_A)}} \quad (5.3.15)$$

$$\omega_0 = \sqrt{\frac{\Psi^2 + T_{F1}R_A}{JL_A}}$$

If the armature time constant  $T_A = L_A/R_A$  is negligible, the following transfer functions with  $L_A = 0$  can be denoted

$$G_{11}(s) = \frac{\Delta\omega(s)}{\Delta V_A(s)} = \frac{\Psi}{\Psi^2 + T_{F1}R_A + sJR_A} \quad (5.3.16)$$

$$G_{12}(s) = \frac{\Delta\omega(s)}{\Delta T_L(s)} = \frac{-R_A}{\Psi^2 + T_{F1}R_A + sJR_A}$$

$$G_{21}(s) = \frac{\Delta I_A(s)}{\Delta V_A(s)} = \frac{T_{F1} + sJ}{\Psi^2 + T_{F1}R_A + sJR_A}$$

$$G_{22}(s) = \frac{\Delta I_A(s)}{\Delta T_L(s)} = \frac{\Psi}{\Psi^2 + T_{F1}R_A + sJR_A}$$

The considered transfer functions have only one pole at

$$s_1 = -\frac{\Psi^2 + T_{F1}R_A}{JR_A} \quad (5.3.17)$$

and the corresponding time constant  $T_{Mot}$  of the DC motor becomes

$$T_{Mot} = \frac{JR_A}{\Psi^2 + T_{F1}R_A} \quad (5.3.18)$$

The resulting transfer functions in case b) are much simpler.  $G_{11}^+$  and  $G_{22}^+$  are proportionally acting elements,  $G_{21}^+$  contains the armature time constant

$$T_A = \frac{L_A}{R_A}$$

and  $G_{12}^+$  is dependent on the mechanical time constant

$$T_m = \frac{J}{T_{F1}}$$

Assuming  $L_A = 0$ , the transfer function  $G_{21}^+$  shows proportional behavior as well.

A state space representation of the motor equations can be specified by considering the armature current  $I_A$  and the angular velocity  $\omega$  as state variables. Based on the linear differential equations with  $T_{F0} = 0$  and  $V_B = 0$ , (5.3.10), (5.3.12),

$$\begin{aligned} L_A \dot{I}_A(t) + R_A I_A(t) &= V_A(t) - \Psi \omega(t) \\ J \dot{\omega}(t) + T_{F1} \omega(t) &= \Psi I_A(t) - T_L(t) \end{aligned} \quad (5.3.19)$$

the state space representation can be specified as

$$\begin{bmatrix} \dot{I}_A(t) \\ \dot{\omega}(t) \end{bmatrix} = \begin{bmatrix} -\frac{R_A}{L_A} & -\frac{\Psi}{L_A} \\ \frac{\Psi}{J} & -\frac{T_{F1}}{J} \end{bmatrix} \cdot \begin{bmatrix} I_A(t) \\ \omega(t) \end{bmatrix} + \begin{bmatrix} \frac{1}{L_A} & 0 \\ 0 & -\frac{1}{J} \end{bmatrix} \cdot \begin{bmatrix} V_A(t) \\ T_L(t) \end{bmatrix}$$

$$\mathbf{x}(t) = \mathbf{A} \mathbf{x}(t) + \mathbf{B} \mathbf{u}(t) \quad (5.3.20)$$

### Example 5.1

From a data sheet, the following values of a permanently excited DC motor have been extracted ( $P_N = 500 \text{ W}$ ,  $n_N = 2500 \text{ rpm}$ ):

moment of inertia	$J$	$= 0.75 \cdot 10^{-3} \text{ kgm}^2$
torque constant	$K_T$	$= 0.35 \text{ Nm/A} = 0.35 \text{ Vsec}$
back-EMF constant	$K_E$	$= 36.0 \text{ V/1000 rpm} \approx K_T$
armature resistance	$R_A$	$= 0.95 \Omega$
armature inductance	$L_A$	$= 1.9 \cdot 10^{-3} \text{ H}$
viscous friction	$T_{F1}$	$= 70.6 \cdot 10^{-3} \text{ Nm/1000 rpm}$
dry friction	$T_{F0}$	$= 0.18 \text{ Nm.}$

Note that  $\omega = 2\pi n$  is considered in the unit 1/s (respectively rad/s). Hence, some of the constants have to be converted. As can be easily shown, the back-EMF constant and the torque constant must be equal to the flux linkage  $K_T = K_E = \Psi$ . Finally, the dynamic model results in

$$\begin{bmatrix} \dot{I}_A \\ \dot{\omega} \end{bmatrix} = \begin{bmatrix} -\frac{500}{s} & -184.2A \\ \frac{467}{As^2} & -\frac{0.899}{s} \end{bmatrix} \cdot \begin{bmatrix} I_A \\ \omega \end{bmatrix} + \begin{bmatrix} \frac{526.3A}{Vs} & 0 \\ 0 & -\frac{1333}{VAs^3} \end{bmatrix} \cdot \begin{bmatrix} V_A \\ L_L \end{bmatrix} \quad (5.3.21)$$

The poles of the system are obtained by solving the equation  $\det(sI - \mathbf{A}) = 0$ . This yields

$$s_{1/2} = -250 \frac{1}{s} \pm 154 \frac{1}{s} \quad (5.3.22)$$

□

### 5.3.4 Static Behavior

Within the static operating conditions (5.3.10) of the armature circuit, it follows that with  $d(.)/dt = 0$  and  $V_B = 0$

$$I_A = \frac{1}{R_A} (V_A - \Psi \omega) \quad (5.3.23)$$

For the mechanical torque produced by the motor, the following relationship holds

$$T_{\text{mech}} = T_{\text{el}} - T_F = \Psi I_A - T_F \quad (5.3.24)$$

with friction torque  $T_F$ .

If the friction torque consists of a dry and a viscous term as specified in (5.3.11), the mechanical torque can be written as

$$T_{\text{mech}} = \frac{\Psi}{R_A} \left[ V_A - \left( \Psi + \frac{R_A}{\Psi} T_{F1} \right) \omega \right] - T_{F0} \quad (5.3.25)$$

Hence, the torque decreases proportionally with the angular velocity, see Figure 5.19a. The maximum torque at standstill ( $\omega = 0^+$  due to the friction relationship) is given by

$$T_{\text{mech}}(0^+) = T_{\max,0} = \frac{\Psi}{R_A} V_A - T_{F0} \quad (5.3.26)$$

and the maximum speed at idling (no-load operation) ( $T_{\text{mech}} = 0$ ) can be specified as

$$\omega_{\max,0} = \frac{V_A \Psi - R_A T_{F0}}{\Psi^2 + R_A T_{F1}} \quad (5.3.27)$$

(Herewith, the armature feedback  $\Psi(I_A)$  is neglected.)

Thus, the torque characteristic can be shifted in parallel by varying the armature voltage  $V_A$ , Figure 5.19a. For a given load torque, it is therefore possible to control the angular velocity  $\omega$  over a wide speed range by adapting the armature voltage  $V_A$  by means of a power converter. The control range then comprises speeds between standstill and the velocity that corresponds to the rated armature voltage  $V_{A0}$ .

$$\omega_{\max} = \frac{V_{A0} \Psi + T_{F0} - T_{\text{mech}}}{\Psi^2 + R_A T_{F1}} \quad (5.3.28)$$

On the other hand, the angular velocity can also be adjusted by adapting the field strength and therefore the flux linkage  $\Psi(I_E)$ . This can be done by means of the exciting current  $I_E$  corresponding to the saturation characteristic, (5.3.25) and Figure 5.19b. As the rated flux linkage is usually chosen to be near the saturation limit, the flux can only be weakened. This decreases the gradient of the torque curve, Figure 5.19b and the angular velocity becomes smaller for larger loads and higher in the case of smaller loads. The field weakening causes higher armature currents at identical load torques, which can lead to commutation problems and finally ends in brush sparking. Hence, field weakening for the purpose of speed control is just employed at higher speeds and smaller load torques if the motor is already supplied with the rated armature voltage. The armature current is thereby restricted to its maximum value  $I_{A\max}$ . In the case of producing constant power

$$P = T_{\text{mech}} \omega \approx \Psi(\omega) I_{A\max} \quad (5.3.29)$$

the flux linkage

$$\Psi(\omega) \approx \frac{P}{I_{A\max}\omega} \quad (5.3.30)$$

is adjusted inversely proportionally to the angular velocity. This can be achieved by controlling the induced armature voltage, Leonhard (1974), Schröder (1995). Under consideration of a constant armature current, the characteristic curves of a separately excited DC motor are depicted in Figure 5.20. If the DC motor operates below its base speed, the armature voltage  $V_A$  is controlled, and above base speed in the field weakening region the exciting current  $I_E$  is adapted. Therefore, the produced torque decreases at higher speeds, as it is adequate, e.g., for machine tools with rapid motion between machining operation or for rolling mills and coilers.

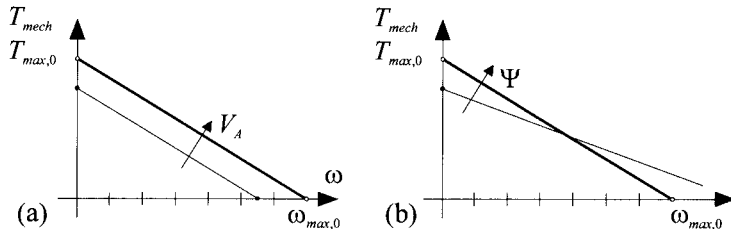


**Figure 5.19.** Torque-speed characteristics of a DC motor: (a) variable armature voltage  $V_A$ ; (b) variable flux linkage  $\Psi$

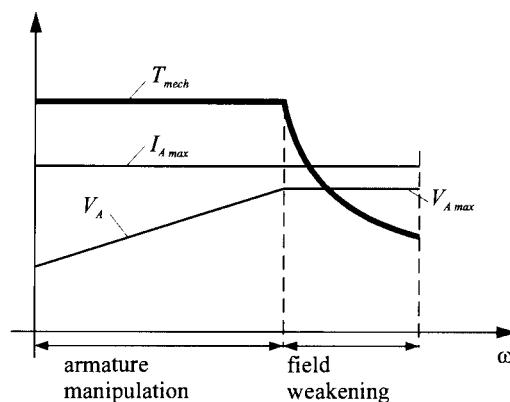


**Figure 5.20.** Feedforward control of a separately excited DC motor at constant armature current: basic operation area: adaptation of the armature voltage; field weakening area: adjustment of the exciting voltage

### 5.3.5 Speed and Position Control

As can be seen from Figure 5.19, the armature voltage is an especially appropriate manipulated variable for speed control. Since the armature current can be easily measured, a cascade control structure with secondary current control loop seems to be appropriate, see Figure 5.21. For the current controller, both a PI-controller

$$G_{RI}(s) = \frac{V_A(s)}{I_A(s)} = K_{RI} \left( 1 + \frac{1}{T_{Nl}s} \right) \quad (5.3.31)$$

or a P-controller can be used. Considering that this control loop works against the current decrease arising from the mutual induction, the electrical torque rises faster. For selection of the speed controller, the dynamic behavior of the coupled load, *e.g.*, a power-consuming machine, has to be taken into account. In most cases, the controlled system shows proportional behavior and thus, PI-controllers

$$G_{Rn}(s) = \frac{I_r(s)}{\omega(s)} = K_{Rn} \left( 1 + \frac{1}{T_{Nn}s} \right) \quad (5.3.32)$$

yield good results. For the adjustment of the speed controller, the secondary current control loop can be simplified as first order lag, according to

$$\frac{I_A(s)}{I_r(s)} = \frac{K_1}{1 + T_1 s} \quad (5.3.33)$$

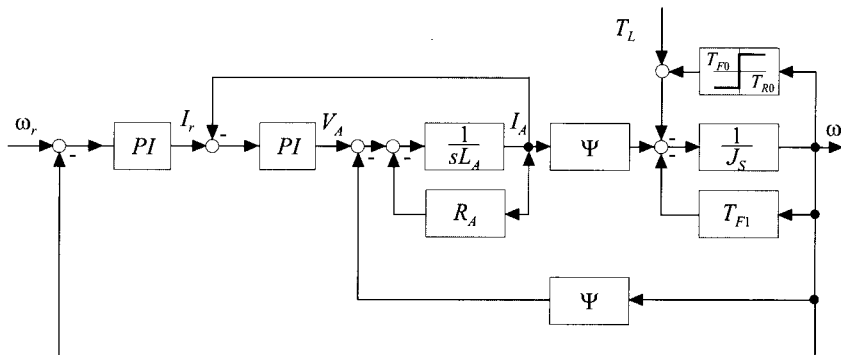


Figure 5.21. Speed cascade control of a separately excited DC motor

The resulting transfer functions that describe the speed control loop are of third order

$$G_{\omega_r}(s) = \frac{\omega(s)}{\omega_r(s)} = \frac{1 + T_{Nn}s}{1 + T_{Nn}s + \frac{T_{Ns}J}{K_{Rn}\Psi}s^2 + \frac{T_{Ns}J T_1}{K_{Rn}\Psi}s^3} \quad (5.3.34)$$

$$G_{\omega_M}(s) = \frac{\omega(s)}{T_L(s)} = \frac{(1 + T_1 s) \frac{T_{Nn}s}{K_{Rn}\Psi}}{1 + T_{Nn}s + \frac{T_{Ns}J}{K_{Rn}\Psi}s^2 + \frac{T_{Ns}J T_1}{K_{Rn}\Psi}s^3} \quad (5.3.35)$$

In the case of controlling the position  $\varphi$  (actuator, robot), a further integrator has to be considered. In addition to the speed controller, a second superimposed P-controller is introduced and consequently a two-fold P-PI-PI-cascade control emerges (gain  $K_{R\varphi}$ ). Neglecting the time constant of the current control loop,  $T_1 = 0$ ,  $K_1 = 1$ , the control behavior is given by

$$G_{\varphi r}(s) = \frac{\varphi(s)}{\varphi_r(s)} = \frac{1 + T_{Nn}s}{1 + \left( T_{Nn} + \frac{1}{K_{R\varphi}} \right) s + \frac{T_{Nn}^2 + T_{Nn}J}{K_{Rn} K_{R\varphi} \Psi} s^2 + \frac{T_{Nn}^2 J}{K_{Rn} \Psi} s^3} \quad (5.3.36)$$

The choice of the controller parameters has a significant influence on the dynamic behavior of the drive.

### 5.3.6 Brushless DC Motors (Electronic Commutation)

The advantages of DC motors are that the angular velocity can be controlled over a wide speed range by adjusting the DC supply voltage and that the motors are supplied with DC current (batteries). On the other hand, disadvantages emerge due to the employment of mechanical commutation since the life expectancy of the brushes/commutator construction is restricted. Furthermore, mechanical commutators lead to losses and contact uncertainties at small voltages and can cause electrical disturbances (sparking) and operating noise.

Therefore, brushless DC motors have been developed. Such motors consist of a permanent magnet rotor and several stator windings that can be electronically switched depending on the rotor position, Figure 5.22. The rotor angle can be measured, e.g., by means of Hall sensors, inductive or optical position sensors. The current flowing in at least three stator coils is supplied by transistors in a manner that the angle between the magnetomotive force in the stator and flux linkage in the rotor amounts to approximately  $90^\circ$ . Hence, a rotating field is generated whose rotation frequency depends on the angular velocity. Therefore, electronically commutated DC motors combine the mechanical robustness of polyphase motors with the good speed control properties of DC motors. Further advantages are: smooth running, high durability, good starting behavior (no brush resistance), higher efficiency rate, no sparking (radio frequency interference suppression, explosion protection). The speed-torque curves correspond to those of DC shunt motors. The motors have a power range from 0.5 to 300 W.

Analog to the DC motor with brush commutation, Section 5.3.2–5.3.4, a dynamic model for a brushless electronically commutated DC motor will be considered, Moseler, Isermann (2000). Figure 5.22 shows a scheme of the rotor, stator, hall sensors and electronic commutation circuits. The Y-connected three-phase square-wave motor with a four-pole permanent-magnet rotor is driven by a pulse width modulation (PWM), see Figure 5.23. The rotor position, which determines

the switching scheme implemented in the inverter logic, is described in Hendershot, Miller (1994), Pillay, Krishnan (1987).

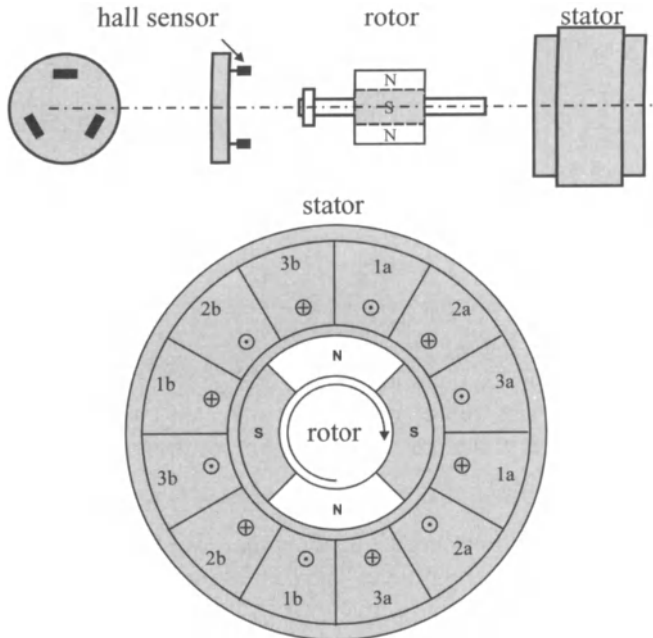


**Figure 5.22.** Dismounted brushless DC motor

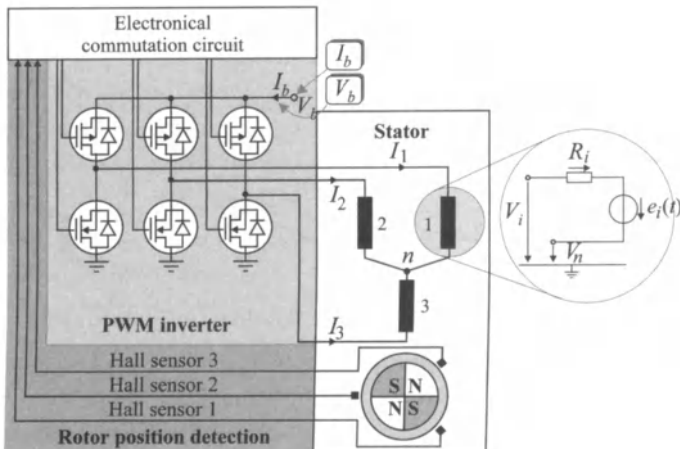


**Figure 5.23.** PWM inverter connected to the three-phase brushless DC motor

The mathematical model of the motor can be divided into two subsystems – an electrical and a mechanical model.

The motor speed is controlled by adjusting the input voltage of the stator coils. For that purpose, the PWM rate is modulated on the active (conducting) transistor of the upper transistor row. If one neglects the inductance of the stator coils, *i.e.*,  $L = 0$ , the mathematical model on one coil (*e.g.*, coil 1) can be derived as follows

$$V_1 - V_n = R_1 V_1 + e_1 \quad (5.3.37)$$

The trapezoidal back-EMF of phase 1 is  $e_1 = k_{E1}\omega(t)$ , where  $\omega(t)$  is the angular velocity of the rotor and  $k_{E1} = \Psi$  is the back-EMF constant for one coil.  $V_1$  denotes the phase voltage with respect to a reference potential and  $V_n$  is the voltage at the star point.

Hence, for all three phases, the following system of equation holds

$$\begin{pmatrix} V_1 - V_n \\ V_2 - V_n \\ V_3 - V_n \end{pmatrix} = \begin{pmatrix} R_1 & 0 & 0 \\ 0 & R_2 & 0 \\ 0 & 0 & R_3 \end{pmatrix} \begin{pmatrix} I_1(t) \\ I_2(t) \\ I_3(t) \end{pmatrix} + \begin{pmatrix} k_{E1} \\ k_{E2} \\ k_{E3} \end{pmatrix} \omega(t) \quad (5.3.38)$$

Usually, the star point is not accessible. Therefore, the respective voltage is unknown. As one of the coils is always open, the equation becomes simpler and one can eliminate  $V_n$  in (5.3.38). Providing that coils 1 and 2 are conducting, the conditions  $V_1 = V_{pwm}$ ,  $V_2 = V_0$ ,  $I_2 = -I_1$ , and  $I_3=0$  are substituted in the previous equation, resulting in

$$V_{pwm}(t) - V_0 \text{sign}(pwm) = (R_1 + R_2)I_1(t) + (k_{E1} + k_{E2})\omega(t) \quad (5.3.39)$$

The term  $V_{pwm}(t) = pwm(t)V_b$  denotes the PWM-modulated supply voltage  $V_b$  of the six-pulse bridge. The continuously variable pulse-pause ratio  $PWM \in [0, 1]$  for the active transistors is generated by an external controller.  $V_0$  is the voltage drop in the power inverter, which is supposed to be approximately constant. Equivalent equations can be derived for the five other cases.

To provide a reasonably cheap solution and to avoid measurement of all phase currents and voltages, only the input and current of the six-phase full-bridge circuit  $I_b$ , the supply voltage  $V_b$ , and the rotor's angular velocity  $\omega$  are measured. The average phase current  $\bar{I}$  can be derived from the bridge current by considering the power balance

$$V_b I_b(t) = V_{pwm}(t) \bar{I}(t) = pwm(t) V_b \bar{I} \quad (5.3.40)$$

Hence

$$\bar{I} = I_b(t)/pwm(t) \quad (5.3.41)$$

Using this relation and forming the mean value of (5.3.39) for all five cases, one gets

$$V_{pwm}(t) - V_0 = \frac{2}{3}(R_1 + R_2 + R_3)\bar{I}(t) + \frac{2}{3}(k_{E1} + k_{E2} + k_{E3})\omega(t) \quad (5.3.42)$$

This equation is valid for controlling the forward rotating direction. For reverse operation, a second switching scheme is applied to the transistors. Shifting from a positive to negative scheme is indicated by a logical bit to the controller. For ease of mathematical description, both cases are combined by extending the range of PWM from  $[0, 1]$  to  $[-1, 1]$ . Thus, the voltage applied to the coils can be described for both operation directions by  $\bar{V}(t) = V_{pwm}(t) - V_0 \text{sign}(pwm(t))$ . Finally, substituting  $2/3(R_1 + R_2 + R_3)$  with  $R$  and  $2/3(k_{E1} + k_{E2} + k_{E3})$  with  $k_E$  leads to the

equation for the electrical subsystem

$$\bar{V}(t) = R\bar{I}(t) + k_E \omega(t) \quad (5.3.43)$$

The magnetic force resulting from the influence of the permanent magnet's field on the currents of the stator coils produces a rotor torque  $T_{el}$ , which is the input of the mechanical subsystem. The torque is proportional to the magnetic flux linkage  $\Psi$  and the average phase current. Hence

$$T_{el} = \Psi \bar{I}(t) = k_T \bar{I}(t) \quad (5.3.44)$$

with  $k_T$  denoting the torque constant. For an ideal square-wave motor, it equals the back-EMF constant  $k_E$ . The equation for the mechanical subsystem can be derived from the torque balance

$$J\dot{\omega}(t) = T_{el} - T_F - T_L \quad (5.3.45)$$

$J$  denotes the inertia of the rotor. The losses  $T_F$  result from friction. It can be split up into Coulomb  $T_{F0}$  sign ( $\omega(t)$ ) and viscose friction  $T_{F1}\omega(t)$ . Thus, (5.3.45) finally yields

$$J\dot{\omega}(t) = k_T \bar{I} - T_{F0} \text{ sign } (\omega(t)) - T_{F1} \omega(t) \quad (5.3.46)$$

Hence, the mathematical model of the brushless DC motor can be summarized by (5.3.43) and (5.3.45). The resulting model is depicted in Figure 5.24.

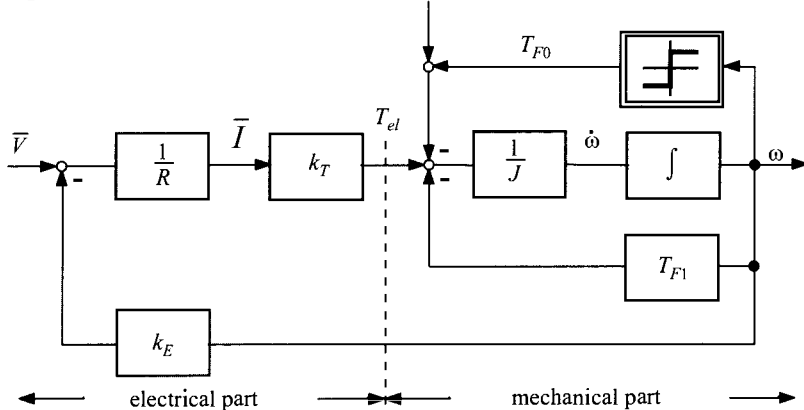


Figure 5.24. Block diagram for the dynamic behavior of a brushless DC motor

### Example 5.2

Some technical data for a permanently excited brushless DC motor (three-phase, Y-connected, four magnetic poles,  $P_{max} = 20 \text{ W}$ ):

nominal torque  
stall torque  
nominal voltage  
nominal current  
nominal speed  
idle speed

$T_n = 37 \text{ Ncm}$   
 $T_{stall} = 130 \text{ Ncm}$   
 $V_n = 28 \text{ V}$   
 $I_n = 1 \text{ A}$   
 $n_n = 5130 \text{ rpm}$   
 $n_{idle} = 7200 \text{ rpm}$

electrical time constant	$T_{el} = 0.2 \text{ ms}$
mechanical time constant	$T_{mech} = 8.6 \text{ ms}$
rotor inertia	$J = 1.5 \cdot 10^{-6} \text{ kgm}^2$
back-EMF constant	$k_E = 0.0372 \text{ Vs/rad}$
coil resistance	$R = 8 \Omega$
viscose friction	$T_{F1} = 2 \cdot 10^{-5} \text{ Nms/rad}$
Coulomb friction	$T_{F0} = 1 \cdot 10^{-4} \text{ Nm.}$

□

### 5.3.7 Special Types of DC Motors

#### a) Permanently excited DC motor

For small-power applications up to 1 kW, in the first place permanently excited DC motors instead of machines equipped with stator excitation coils are employed, Figure 5.25a, b. As for the materials of the permanent magnet's ferrites, Al-Ni-Co, Se-Co, Sm-Co are used. The operational behavior is equivalent to that of DC shunt-wound motors. Permanently excited DC motors can be manufactured with smaller dimensions compared to those with excitation coils. Due to the non-existing excitation loss, the efficiency rate is naturally better. The rotors are, for instance, realized as iron slot rotors with several windings and mechanical commutators with brushes. For the sake of small time constants, the moment of inertia must be small. In the following, a few constructive possibilities to achieve small time constants are discussed:

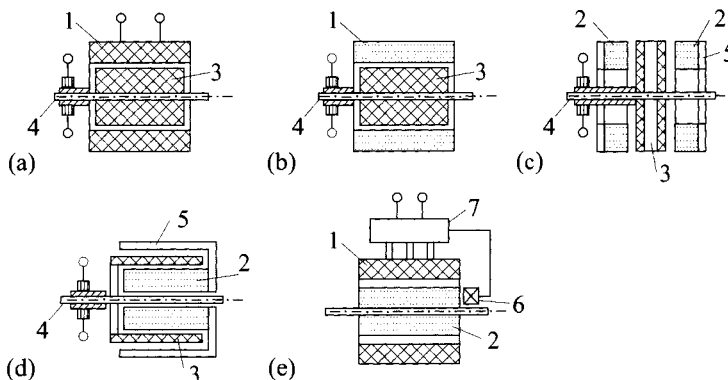


**Figure 5.25.** Basic types of DC motors: (a) separately excited with inner drum rotor; (b) permanently excited with drum rotor; (c) permanently excited with plate rotor; (d) permanently excited with bell rotor; (e) brushless, electronically commutated with permanent rotor

1 excitation coil; 2 permanent magnet; 3 rotor with coil; 4 commutator with brushes; 5 magnetic back flow; 6 position sensor; 7 electronic control

- *DC motors with slim armature*

The rate of the armature length with regard to the diameter of the armature is chosen to be comparatively high ( $l/d = 3$  up to 5).

- *DC motors with plate rotor*

The armature windings are printed on a plate, which is realized without magnetic material in order to obtain a small mass, Figure 5.25c. The collector is also implemented on the plate. These types of DC motors show very small armature time constants  $T_A \approx 0.3$  msec, mechanical time constants  $T_m \approx 5 \dots 20$  msec, and permit high current overloads. The power range can be found in the area of approximately 25 W up to 5 kW.

– *DC motors with ironless rotors*

The rotors are designed as a hollow body that consists of armature windings and, e.g., insulating resin. In general, this rotor is opened at one side (cylindrical and bell rotors) and rotates around a fixed permanent magnet which is placed inside, Figure 5.25d. The rotor also carries the commutator. The corresponding power range is between 1 W and 20 W.

Another special construction of DC motors are the so-called *torque motors*. These motors are used as servo-motors or actuators in order to produce high torque at standstill and low speeds. The motors are designed for applications such as gearless drives, which are capable of rapidly and accurately adjusting certain angular positions as well as generating high holding torque (cooling and fatigue problems). Typical realizations are characterized by permanent excitation, slim rotor and commutators with large diameters generating torques of up to 1000 Nm. Areas of application are, e.g., aerial drives, robot drives and general servomotors, Pfaff (1994).

### b) Stepper motors

Stepper motors consist of a stator with coils that can be supplied individually. The rotors contain permanent magnets and work on the basis of the reluctance principle by employing star-shaped arranged poles or cogs. Defined changes of the angle of rotation can be performed by supplying certain stator coils with DC current control pulses.

If during the start-up process and the phase out respectively no steps get lost, the angle change is defined by the number of trigger pulses according to an open control chain (magnetic grid). Denoting the step angle by  $\alpha$ , the number of pulses or steps by  $v$  and the angle of rotation by  $\varphi$ , the following relationship can be specified

$$\varphi = \alpha v \quad (5.3.47)$$

If a constant pulse sequence with pulse frequency  $f_s$  is applied to the step motor, the mean angular velocity

$$\omega = \frac{d\varphi}{dt} = \alpha f_s \quad (5.3.48)$$

can be observed.

The functionality corresponds to that of synchronous motors, since the rotor follows the stepwise-controlled angle change of the stator

field. The electromechanical construction basically resembles brushless DC motors.

Different designs of stator and rotor exist in several types of construction. The stator is equipped with several windings that are, for instance, interconnected in  $m_s = 1, 2, 3$  or  $4$  phases (one- up to four-phase step motor), see Figure 5.26. In this case,  $p_s = m_s$  stator poles are obtained. In the event of switching between two adjacent windings, the rotor will be placed in the center of the pole axis. This is called the *full step operation* and produces a comparatively high torque. The step angle is bisected if only one winding is interconnected between two full step positions whereas the produced torque decreases and becomes more inhomogeneous. This mode of operation is called the *half step operation*. In the case of a stepwise increase of the current within one winding and a synchronous decrease in the adjacent coils, even smaller step angles can be produced. The corresponding operating method is called the *micro-step operation*. In order to reverse the speed direction, one possibility is to reverse the current that flows in the windings. Another possibility is to switch one of two differently wound coils.

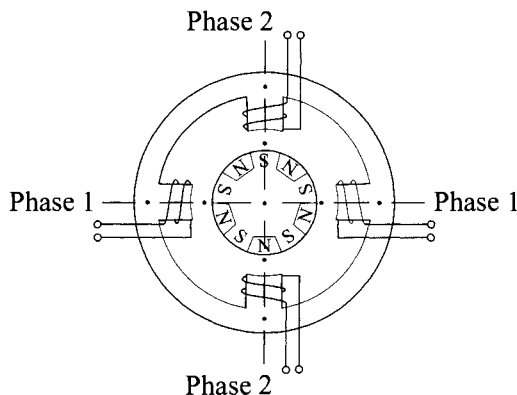


**Figure 5.26.** Simplified example of a stepper motor with permanent magnet rotor: stator: four windings;  $m_s = 2$  phases;  $p_s = 2$  pole pairs; rotor:  $p_R = 5$  pole pairs

The rotor can consist of permanent magnets that are arranged in a star-shaped fashion with alternating polarity, e.g., with up to  $p_R = 12$  pole pairs. Due to the permanent magnets, a locking torque arises at zero current conditions. *Reluctance rotors* are made up of a soft iron-toothed rim with  $z$  teeth that are not premagnetized. The teeth and slot series effects a variable magnetic resistance that leads to the production of torque. This constructional form allows small step angles but, on the other hand, no locking torque can be provided.

Another alternative is the *hybrid rotor*, which can be seen as a combination: the rotor comprises of a permanent magnet that is magnetized in the axial direction. The magnet has toothed pole heads on both sides that are made up of soft iron. The teeth of the toothed rims are displaced half of a partition in each case and form north poles on the one side

and south poles on the other. Thus, small step angles, a comparatively high power and a locking torque can be achieved. If high dynamics are required, a small moment of inertia can be accomplished by means of permanently excited plate rotors.

Figure 5.26 depicts schematically the construction of a stepper motor with permanent rotor. The stator contains four coils and  $m_s = 2$  phases ( $p_s = 2$  pole pairs). By reversing the polarity of a stator pole pair in each case (semi-step operation), four steps can be performed. The rotor consists of  $p_R = 5$  pole pairs or  $2p_R = 10$  poles ( $z$  teeth at the reluctance rotors). In the case of reversing one pole pair of the stator, the rotor turns for half a rotor pole (half a tooth) as it takes a magnetic mid position. This results in 20 steps per rotation or a corresponding step angle of  $18^\circ$ .

The step angle of a stepper motor is defined by the number of coils and the number  $m_s$  of phases within the stator respectively and by the number  $p_R$  of pole pairs in the rotor (respectively  $2p_R$  of the poles or  $z$  of the teeth) and in the case of semi-step operation the following expression can be specified

$$\alpha = \frac{360^\circ}{2m_s p_R} = \frac{360^\circ}{m_s z} \quad (5.3.49)$$

This step angle can be further minimized if each pole head is designed with several teeth, and parallel stators (multiple stator step motors) are arranged so that they are displaced by certain angles, e.g., for half of the step angle.

As for permanent motors, typical step widths are  $30^\circ$  up to  $90^\circ$ , for reluctance motors  $0.2\text{--}15^\circ$  and for hybrid motors  $0.2\text{--}3.6^\circ$ . During the design, it has to be taken into account that for the smallest required resolution, several steps always have to be planned, to cope with starting cycles and phase out.

The control unit is realized by means of highly integrated circuits for standard step motors and microprocessors in the case of higher and special power demands taking acceleration and braking conditions into account. Transistor circuits are employed for power amplification. Step motors are provided for powers of up to approximately 500 W, speeds up to 5000 rpm and  $z = 12\ldots 1000$  steps per rotation.

The application area of stepper motors is mainly the feedforward-controlled exact low-power positioning, as long as the appearance of disturbance torques can be neglected. Otherwise, the exact position has to be measured and adjusted via feedback control. In this case, the employment of DC motors is often preferable. Typical application examples are printers, typewriters, disk drives and feed drives for plotters.

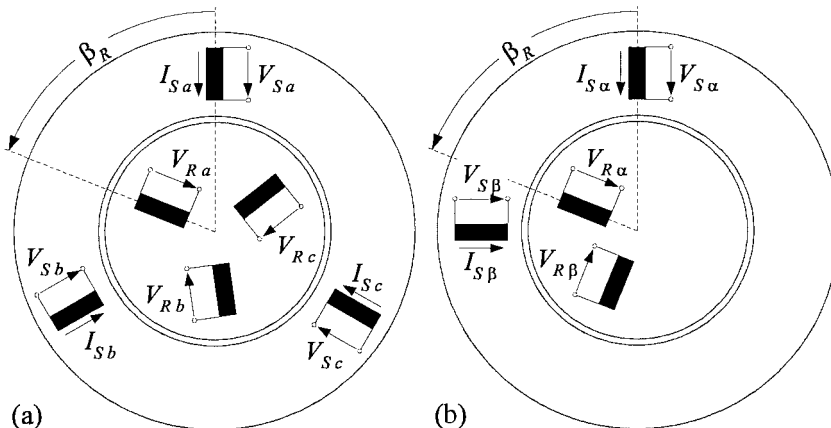
Further details can be found in Kuo (1974), Kenjo (1984), Kreuth (1985), Acarnley (1982), Janocha (1992), Moczala (1993) and Kallenbach *et al.* (1994). Some properties of different DC motors are summarized in Table 5.2.

Table 5.2. Properties of DC motors of small power up to 1 kW (Jung, Schneider (1984))

	DC shunt-wound motor with			DC motor with electronic control	
	excitation coil	permanent excitation	disc rotor	ironless rotor	stepper motor
power range	W	10–1000	0.1–1000	0.05–1000	0.1–250 1.5–1000 0.5–300 < 500
rated voltage	V	12–500	3–220	2.5–64	1.5–48 12–220 12–90 3–48
efficiency		0.3–0.7	0.4–0.8	0.4–0.8 –0.7	0.3–0.7 0.2–0.8
rated speed	rpm	6000	12000	11000	15000 27000 > 20000 9000
controlled speed range		1 : 800	1 : 1000	1 : 3000	1 : 1000 1 : 3000 —

## 5.4 ALTERNATING CURRENT MOTORS (AC)

Alternating current motors consist of three winding circuits placed in stator slots that are interconnected with the individual phases of a three-phase supply system either in delta- or  $Y$ -connection, see Figure 5.27. Hence, a rotating magnetic field is generated, whose angular velocity depends on the power frequency  $f$  and on the number of pole pairs  $p$  within the stator. If the motor consists of one pole pair per phase ( $p = 1$ ), the windings of the individual phases are displaced from each other by  $120^\circ$  and the speed frequency  $f_d$  corresponds to the supply frequency, thus at  $f = 50 \text{ Hz}$ :  $n_d = 3000 \text{ rpm}$ . In the case of two pole pairs ( $p = 2$ ), the windings are displaced from each other by  $60^\circ$  and  $f_d = f/p = f/2$  and therefore  $n_d = 1500 \text{ rpm}$ . In consideration of the different rotor constructions, induction motors and synchronous motors can be distinguished. In the following sections, simplified models and the basic operational behavior of both types will be considered.



**Figure 5.27.** Schematic configuration of the stator and rotor winding systems: (a) three-phase representation of the induction motor without one pole pair per phase; (b) two-phase equivalent circuit of (a)  $\beta_R$ : electrical rotor angle,  $\beta_m$ : mechanical rotor angle, with  $\beta_R = p \cdot \beta_m$  for  $p$  pole pairs.

### 5.4.1 Induction Motors

#### *Modeling of symmetrical three-phase induction motors*

In order to derive a mathematical model describing the dynamic behavior of induction machines a generic motor equipped with three-phase winding systems both in the stator and the rotor is considered. Both winding systems can be supplied by independent three-phase voltage sources.

In order to reduce the complexity of the model, several further assumptions are made:

- the distributed windings can be replaced by lumped windings;

- the runs of all spatially distributed physical variables (e.g., flux density) are sinusoidal along the air gap perimeter. Thus, only fundamental space and time components are considered;
- saturation effects of magnetic circuits are neglected. Hence, the inductance of the windings can be regarded as a constant parameter;
- the magnetic permeability of iron is considered to be infinite so that the flux crosses the air gap in radial lines;
- hysteresis behavior and eddy currents are neglected;
- the resistors and inductances are constant. Hence, dynamic temperature effects are not considered.

For each rotor and stator winding, the voltage equation takes the form

$$V_n = R_n I_n + \frac{d\Psi_n}{dt} \quad \text{with} \quad \Psi_n = L_n I_n + \sum_v M_{nv} I_v \quad (5.4.1)$$

in which  $V_n$  denotes the terminal voltage of the winding  $n$ ,  $I_n$  is the winding current,  $R_n$  and  $L_n$  state the resistance and self-inductance of the winding and  $M_{nv}$  specifies the mutual inductance between the winding  $n$  under consideration and another stator or rotor winding  $v$ , compare Figure 5.27a. With this, the electrical model of the considered three-phase induction machine comprises of six coupled differential equations that are not very transparent. Much progress concerning the modeling of induction motors can be achieved if the three-phase stator and rotor winding systems are transformed into two-phase systems, each consisting of two orthogonally placed windings, see Figure 5.27b, Leonhard (1996), Novotny, Lipo (1996), Lyshevski (2000), also known as Clarke-Park transforms.

The conversion of the corresponding physical values  $V$ ,  $I$  and  $\Psi$  into the two-phase representation can be performed as follows, whereupon instead of physical variables the neutral values  $U_x$  are employed

$$U_\alpha(t) = \frac{2}{3} (U_a(t) + U_b(t)\cos(120^\circ) + U_c(t)\cos(-120^\circ)) \quad (5.4.2)$$

$$U_\beta(t) = \frac{2}{3} (U_b(t)\sin(120^\circ) + U_c(t)\sin(-120^\circ)) \quad (5.4.3)$$

The values  $U_\alpha$  and  $U_\beta$  in two-phase representation can also be combined by employing complex terms

$$U(t) = U_\alpha(t) + jU_\beta(t) = \frac{2}{3} (U_a(t) + U_b(t)e^{j120^\circ} + U_c(t)e^{-j120^\circ}) \quad (5.4.4)$$

and the corresponding complex numbers  $U$  are called space vectors. In this notation, the normalization factor 2/3 effects that in the case of symmetrical sinusoidal values  $U_{a, b, c}$ , which are displaced from each other by  $120^\circ$ , the absolute value of the vector complies with the amplitude of the three-phase variables. In this case, the phase of the vector

of the two-phase system corresponds to that of the three-phase system, so that the space vector moves on a circle with the angular frequency  $\omega$ :  $U_a(t) = \hat{U} \cos(\omega t + \varphi) \rightarrow \mathbf{U}(t) = \hat{U} e^{j(\omega t + \varphi)}$ , with  $\hat{U} = \sqrt{U_a^2 + U_\beta^2}$ .

The inverse transformation can be written in the form

$$\begin{bmatrix} U_a \\ U_b \\ U_c \end{bmatrix} = \frac{1}{2} \begin{bmatrix} 2 & 0 \\ -1 & \sqrt{3} \\ -1 & -\sqrt{3} \end{bmatrix} \begin{bmatrix} U_\alpha \\ U_\beta \end{bmatrix} \quad (5.4.5)$$

Krause (1986), Vas (1990), Leonhard (1996).

Considering the two-phase space vector representation of the induction motor, the following voltage equations for the stator and rotor winding systems can be specified in accordance with (5.4.1), whereupon the parameters  $R_s$  and  $R_r$  denote the stator and the rotor winding resistance respectively

$$\mathbf{V}_S^S(t) = R_s \mathbf{I}_S^S(t) + \frac{d\Psi_S^S(t)}{dt} \quad (5.4.6)$$

$$\mathbf{V}_R^R(t) = R_r \mathbf{I}_R^R(t) + \frac{d\Psi_R^R(t)}{dt} \quad (5.4.7)$$

In this notation, the subscript indices state the winding system that the individual variables belong to. The superscript indices refer to the reference frame in which the space vectors are specified. The reference frames have to be distinguished, as an observer situated in the stator-fixed coordinate system realizes other space vectors than a second observer moving, *e.g.*, with the rotor.

The flux linkages in the individual windings are, on the one hand, determined by the magnetic fields aroused by the windings themselves and, on the other, the remaining windings also contribute a certain proportion to the resulting flux linkages depending on the angle between the individual magnetic axes. The following flux linkages of the stator and rotor winding systems are obtained

$$\Psi_S^S(t) = L_S \mathbf{I}_S^S(t) + M \mathbf{I}_R^R(t) e^{j\beta_R} \quad (5.4.8)$$

$$\Psi_R^R(t) = L_R \mathbf{I}_R^R(t) + M \mathbf{I}_S^S(t) e^{-j\beta_R} \quad \text{with } \beta_R = p \beta_m \quad (5.4.9)$$

with the stator and rotor self-inductances  $L_s$ ,  $L_r$  and the mutual inductance  $M$  between stator and rotor. The total stator and rotor self-inductances can be split up into the corresponding leakage inductances  $L_{s\sigma}$ ,  $L_{r\sigma}$  and the mutual inductance according to

$$L_S = L_{s\sigma} + M \quad \text{and} \quad L_R = L_{r\sigma} + M \quad (5.4.10)$$

Considering (5.4.6) ... (5.4.9), the big advantage of the space vector representation becomes obvious: without immoderate effort the vectors

can be transferred into other reference frames. The transformation of an arbitrary space vector  $\mathbf{U}(t)$  in any, with the angle  $\varphi_k(t)$  rotating reference frame  $K$  is performed by means of

$$\mathbf{U}^K(t) = \mathbf{U}(t) e^{-i\varphi_k(t)} \quad (5.4.11)$$

In this manner, the specified model of the induction machine can be transformed into an arbitrary common coordinate system  $K$  rotating with the angular velocity  $\omega_K(t)$  with respect to the stator. Hence,  $\omega_K$  is the angular velocity of the rotor flux with regard to the stator coordinates. Then the following machine equations are obtained:

$$\mathbf{V}_S^K(t) = R_S \mathbf{I}_S^K(t) + \frac{d\Psi_S^K(t)}{dt} + i\omega_k(t)\Psi_S^K(t) \quad (5.4.12)$$

$$\mathbf{V}_R^K(t) = R_R \mathbf{I}_R^K(t) + \frac{d\Psi_R^K(t)}{dt} + i(\omega_k(t) - \omega_R(t))\Psi_R^K(t) \quad (5.4.13)$$

$$\Psi_S^K(t) = L_S \mathbf{I}_S^K(t) + M \mathbf{I}_R^K(t) \quad (5.4.14)$$

$$\Psi_R^K(t) = L_R \mathbf{I}_R^K(t) + M \mathbf{I}_S^K(t) \quad (5.4.15)$$

The electrical system of induction motors is therefore specified by a fourth order coupled non-linear differential equation system. The motor torque is generated by the force that the air gap field generates upon the current-carrying rotor windings. The torque  $T_{el}(t)$  can be evaluated by

$$T_{el}(t) = \frac{3}{2} p \operatorname{Im}\left\{\mathbf{I}_S^K(t) \Psi_S^{K*}(t)\right\} = -\frac{3}{2} p \operatorname{Im}\left\{\mathbf{I}_R^K(t) \Psi_R^{K*}(t)\right\} \quad (5.4.16)$$

Thus, a torque is only generated if the stator flux vector and the stator current vector are not parallel, Leonhard (1996), Novotny, Lipo (1996).

The mechanical system corresponds to that which was previously introduced for the DC motor

$$T_{el}(t) = J \ddot{\omega}_m(t) + T_{F0} \operatorname{sign}(\omega_m(t)) + T_{F1} \omega_m(t) \quad (5.4.17)$$

### *Types of induction motors*

In connection with induction motors, constructions with slip-ring rotor and squirrel-cage rotor can be distinguished. The *slip-ring* rotor contains a winding system similar to the stator, which is equally distributed along the perimeter with the same number of pole pairs. The rotor windings can be interconnected in delta- or  $Y$ -connection and the remaining connectors can be accessed via slip-rings. Hence, it is feasible to connect the rotor windings with additional resistances that lead to improvements concerning the starting performance when feeding the motor with a stiff three-phase system.

Another type are *squirrel-cage* induction motors operating with a symmetrical rotor construction that consists of circularly arranged bars in the axial direction, see Figure 5.28. These rotor bars, which are short-circuited at the front and back side via end-rings, are commonly

made of copper, aluminium or brass. Although the rotor does not comprise of a conventional three-phase system, the corresponding motor model leads to the previously derived relationships, whereupon the rotor voltage vector is of course always zero ( $\mathbf{V}_R(t) = \mathbf{0}$ ) in (5.4.7) and (5.4.13). Unfortunately, the torque characteristic cannot be adjusted as in the case of slip-ring rotors by adapting the rotor resistance. In this case, the only possibility to influence the rotor resistance is to choose a suitable form of the bars in such a way that at lower speed the effective resistance is higher than at synchronous speed. This is especially favorable by starting a squirrel-cage machine directly from the grid. At low speeds, the frequencies of the rotor currents are in the range of the supply frequency. Because of the skin effect, the resulting rotor resistance may be significantly higher compared to the situation at low rotor current frequencies. There are some special constructions of squirrel-cage rotors developed for this purpose such as *double-cage* or *deep bar* rotors.

In consideration of the robust construction, this motor type is employed for nearly all kinds of drive applications. During the last few years, the importance of induction machines with squirrel cages has been growing drastically, especially in the field of speed- or even of position-controlled drives, Leonhard (1996), Sarma (1996).

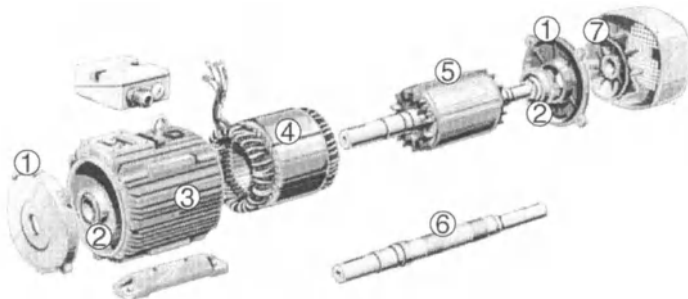


**Figure 5.28.** Cut-away drawing of a squirrel-cage induction motor: 1 cover ; 2 ball bearing; 3 stator casing; 4 stator coil; 5 squirrel-cage rotor ; 6 shaft; 7 fan wheel. (Courtesy of VEM motors, Thurm GmbH, Zwickau, Germany)

#### *Control of induction motors*

On the basis of the proposed dynamic induction motor model with respect to an arbitrary reference frame, an approach for the control of inverter-fed induction motors can be derived. Within the following considerations, the rotor windings and rotor bars are assumed to be short circuited ( $\mathbf{V}_R(t) = \mathbf{0}$ ). Straightforward relationships are obtained if the dynamic equations are oriented on the rotor-flux  $\Psi_R$ . In this reference frame, the real part of the individual space vectors is denoted by  $d$  (direct) component and the imaginary part as  $q$  (quadrature) component ( $\mathbf{U} = U_d + i U_q$ ). As the rotor-flux defines the reference frame, the rotor-flux comprises only a real component ( $\Psi_R(t) = \Psi_{Rd}$ ). After some conversions of (5.4.12)...(5.4.16), the following relationships for the rotor-flux  $\Psi_{Rd}$  and the motor torque  $T_{el}$  are obtained:

$$T_R \frac{d\Psi_{Rd}(t)}{dt} + \Psi_{Rd}(t) = MI_{Sd}(t) \quad \text{with } T_R = \frac{L_R}{R_R} \quad (5.4.18)$$

$$T_{el}(t) = \frac{3}{2} p \frac{M}{L_R} \Psi_{Rd}(t) I_{Sq}(t) \quad (5.4.19)$$

Thus, the torque  $T_{el}$  just depends on the  $q$ -stator-current component  $I_{Sq}$  and on the rotor-flux  $\Psi_{Rd}$ . Equation (5.4.18) shows that the rotor-flux is only dependent on the stator current  $I_{Sd}$ , whereby the dynamical behavior of the flux can be regarded as a first order lag. Similar to separately excited DC motors, two independently manipulated variables for the control of the field and torque values emerge.

The relationship between the stator currents and the stator voltages within the rotor-flux-oriented reference frame can be derived from

$$(5.4.12)\dots(5.4.15) \text{ and results with } \left( \sigma = 1 - \frac{M^2}{L_S L_R} \right)$$

$$V_{Sd} = \left( R_S + R_R \frac{M^2}{L_R^2} \right) I_{Sd} + \sigma L_S \frac{dI_{Sd}}{dt} - \sigma L_S \omega_K I_{Sq} - \frac{R_R M}{L_R^2} \Psi_{Rd} \quad (5.4.20)$$

$$V_{Sq} = \left( R_S + R_R \frac{M^2}{L_R^2} \right) I_{Sq} + \sigma L_S \frac{dI_{Sq}}{dt} + \sigma L_S \omega_K I_{Sd} - \frac{M}{L_R} \omega_R \Psi_{Rd} \quad (5.4.21)$$

Hence, the equations approximately show a first order lag dependency between the stator current components and the parallel stator voltage components. Unfortunately, both equations are not ideally decoupled, as they also contain terms that are dependent on the orthogonal current components. The remaining terms depending on the rotor-flux can be regarded as EMF. Thus, in the case of changing one stator voltage component both current components are affected, which, of course, is undesirable. A decoupling unit that eliminates all terms leading to deviations from the first order lag characteristic between the parallel current and voltage components may help to overcome this problem. The voltages  $V_{Sd}$  and  $V_{Sq}$  supplied to the stator windings are therefore given by

$$V_{Sd} = \tilde{V}_{Sd} - \sigma L_S \omega_K I_{Sq} - \frac{R_R M}{L_R^2} \Psi_{Rd} \quad (5.4.22)$$

$$V_{Sq} = \tilde{V}_{Sq} + \sigma L_S \omega_K I_{Sd} + \frac{M}{L_R} \omega_R \Psi_{Rd} \quad (5.4.23)$$

whereupon  $\tilde{V}_{Sd}$  and  $\tilde{V}_{Sq}$  specify the decoupled stator voltages.

In the 1970s, the rotor-flux vector was measured directly by adequate sensors, whereas nowadays, due to progress in microprocessor technology, indirect approaches are preferred. The absolute value of the rotor-flux linkage can be evaluated by employing the so-called current

model (5.4.18). The major advantage of this model is that the stator voltages need not be measured. The vector angle  $\beta_K$  with respect to the stator is evaluated by means of

$$\beta_K = \int_0^t \omega_K(\tau) d\tau \quad \text{with} \quad \omega_K = \omega_R + \frac{M}{T_R} \frac{I_{Sq}}{\Psi_{Rd}} \quad (5.4.24)$$

which can be derived from the proposed model equations. With this, the so-called *field-oriented* or *vector control* scheme can be specified, which is capable of controlling inverter-fed induction motors, see Figure 5.29. Firstly, the measured currents have to be transformed into the two-phase coordinate system, which can be performed by means of (5.4.2) and (5.4.3). Subsequently, the two field-oriented stator currents are evaluated by transforming the stator currents into the basis defined by the flux angle  $\beta_K$  with the help of (5.4.11). The corresponding control structure is not unlike that of a separately excited DC motor. Finally, the manipulated voltage values  $V_{Sd}$  and  $V_{Sq}$  in the rotor-flux reference frame have to be transformed in the stator-fixed coordinate system. The three stator voltages  $V_{Sa,b,c}$  are obtained from the two-phase representation by employing (5.4.5).

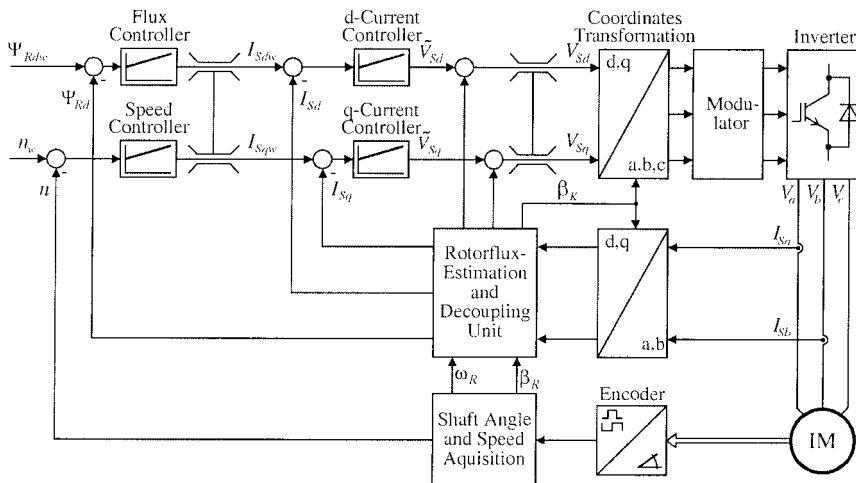


**Figure 5.29.** Block diagram of the field-oriented control of induction motors

In order to obtain high dynamic performance, the same strategy as with the DC machine seems adequate. The reference value of the rotor flux  $\Psi_{Rdw}$  is kept up to the rated speed on a constant level. In consideration of the ceiling voltage of the converter, higher speeds can only be achieved by decreasing the rotor-flux linkage, which simultaneously reduces the maximum torque. This can, for example, be performed by decreasing the rotor-flux indirectly proportionally to the speed. More advanced methods also take the saturation behavior of the mutual inductance into account, Vas (1990), Leonhard (1996), Novotny, Lipo (1996).

The time constant of the first order lags describing the dependency between the stator currents and the stator voltages according to (5.4.20) and (5.4.21) amounts, in the case of small induction motors (rated power: 1.5 kW) to approximately 5 ms, whereas the time constant of the rotor-flux first order lag regarding (5.4.18) is, at approximately 190 ms, many times higher.

### *Steady state operation of induction motors*

In most cases, induction motors are still supplied by stiff power grids, in order to drive loads at nearly constant speed. In this case, the steady state behavior is of paramount interest. A static operating point appears if the mechanical speed is constant ( $\dot{\omega}_m = 0$ ). The dynamic equations of induction motors within the stator reference frame ( $\omega_K = 0$ ) according to

$$\mathbf{V}_S^S(t) = R_S \mathbf{I}_S^S(t) + L_S \frac{d\mathbf{I}_S^S(t)}{dt} + M \frac{d\mathbf{I}_R^S(t)}{dt} \quad (5.4.25)$$

$$\mathbf{0} = R_R \mathbf{I}_R^S(t) + L_R \frac{d\mathbf{I}_R^S(t)}{dt} + M \frac{d\mathbf{I}_S^S(t)}{dt} - i\omega_R(t) (L_R \mathbf{I}_R^S(t) + M \mathbf{I}_S^S(t)) \quad (5.4.26)$$

serve as a starting point for the following considerations, whereby the rotor windings (squirrel-cage rotor) are assumed to be short-circuited ( $\mathbf{V}_R = \mathbf{0}$ ). In this case, the different current and voltage space vectors move on circles

$$\mathbf{V}_S^S(t) = V_S e^{i\omega_N t}(t), \mathbf{I}_S^S(t) = \mathbf{I}_S e^{i\omega_N t}, \mathbf{I}_R^S(t) = \mathbf{I}_R^R e^{i\omega_R t} = \mathbf{I}_S e^{i\omega_N t} \quad (5.4.27)$$

with constant radius and phase angle. The corresponding angular speed complies with the feeding frequency of the power grid ( $\omega_N = 2\pi f_N$ ). Note that the rotor current vector, which originally moves with slip frequency, also rotates within the stator reference frame with net frequency. Substituting (5.4.27) and the stray inductances from (5.4.10) into Equations (5.4.25) and (5.4.26) respectively and omitting the redundant terms, the following relationships are obtained

$$\mathbf{V}_S = R_S \mathbf{I}_S + i\omega_N L_{S\sigma} \mathbf{I}_S + i\omega_N M (\mathbf{I}_S + \mathbf{I}_R) \quad (5.4.28)$$

$$\mathbf{0} = \frac{R_R}{s} \mathbf{I}_R + i\omega_N L_{R\sigma} \mathbf{I}_R + i\omega_N M (\mathbf{I}_S + \mathbf{I}_R) \quad (5.4.29)$$

Equation (5.4.29) is normalized by the slip  $s$ , which is defined by

$$s = \frac{\omega_N - \omega_R}{\omega_N} = \frac{\omega_N - P\omega_m}{\omega_N} \quad (5.4.30)$$

where  $\omega_m$  denotes the rotor speed. These results lead directly to the so-called single-phase equivalent circuit diagram as depicted in Figure 5.30. The equivalent circuit, which complies with those of a transformer apart from the slip  $s$ , is only valid during steady state operation when feeding the induction motor with a symmetrical three-phase voltage system.

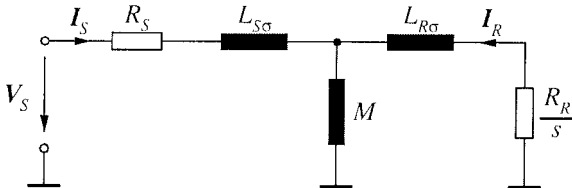


**Figure 5.30.** Single-phase equivalent circuit valid within steady state operation

Starting from the equivalent circuit, special operating conditions can be discussed. If the rotor, *e.g.*, turns with supply frequency divided by the number of pole pairs ( $s = 0$ ), the rotor-flux stays constant and thus no voltage is induced within the rotor. Hence, the rotor current tends to zero within the equivalent circuit, see Figure 5.30. At standstill ( $s = 1$ ), the equivalent circuit corresponds exactly to that of a transformer that is short-circuited on the secondary side. Considering the derived stationary relationships, the stator current can be evaluated depending on the stator voltage and slip by employing the total leakage factor  $\sigma$  where

$$\sigma = 1 - \frac{M^2}{L_S L_R}$$

$$I_S = \frac{R_R + i\omega_N L_R s}{R_R(R_S + i\omega_N L_S) + i\omega_N L_R(R_S + i\omega_N \sigma L_S)s} V_S \quad (5.4.31)$$

The equation can be regarded as conformal mapping and thus the corresponding complex locus of the current vector depending on the slip can be found on a circle. The circle diagram is also called Ossanna's or Heyland's circle and is illustrated in Figure 5.31a.

Within the diagram, three regions can be distinguished: for the sector  $0 \leq s \leq 1$ , the rotor runs below the synchronous speed  $n_s = f_N/p$  and the machine therefore operates as a motor, whereas in the case  $s < 0$  the rotor turns faster than the stator field and the induction machine acts as a generator supplying active power to the line. The induction motor needs to be connected to the power grid even while operating as a generator, since the reactive power causing the magnetization of the rotor has to be provided by the net. Within the region  $s > 1$  the stator field and the rotor are moving in different directions. As can be seen from the diagram, the motor consumes active power at very high stator currents, and acts as a brake. Therefore, this mode of operation is called *countercurrent braking*, Leonhard (1996), Sarma (1996).

The rated slip of induction motors is in the range  $s_r \leq 5\%$ , since otherwise the power loss is too large.

The speed-torque curve can be derived by considering the power balance. Usually, in connection with symmetrical three-phase systems rather than the amplitude, the corresponding root-mean-square (RMS) value is employed, with, *e.g.*,  $V_{rms} = \hat{V}/\sqrt{2}$ . Thus, RMS values are used within the following considerations. As can be seen from the equivalent circuit in Figure 5.30, the active power that is transferred contactless

via the air gap to the rotor is the active power  $P_{el}$  supplied by the grid minus the loss  $P_{SL}$  aroused by the stator resistance. It is called air gap power  $P_\delta$  and is defined as the product between the torque  $T_{el}$  and the angular frequency of the power grid  $\omega_N$

$$P_{el} = P_{SL} + P_\delta \rightarrow 3 \operatorname{Re} \left( V_{S\text{rms}} I_{S\text{rms}}^* \right) = 3 |I_{S\text{rms}}|^2 R_S + \omega_N T_{el} \quad (5.4.32)$$

Inserting (5.4.31) into (5.4.32) results in

$$T_{el} = 3 \frac{V_{S\text{rms}}^2}{\omega_N} \frac{s(1-\sigma)(i\omega_N L_s)(i\omega_N L_R)R_R}{(R_S R_R - s\sigma(i\omega_N L_S)(i\omega_N L_R))^2 + (sR_s(i\omega_N L_R) + R_R(i\omega_N L_S))^2} \quad (5.4.33)$$

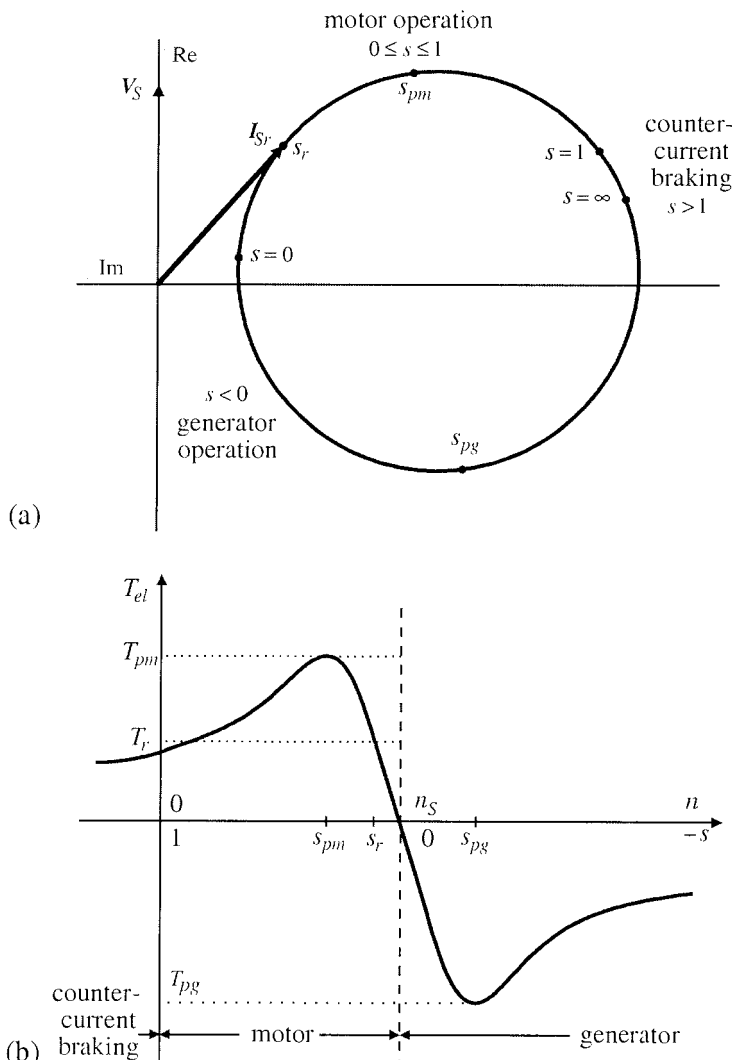


**Figure 5.31.** Characteristic curves of induction motors at steady state operation: (a) circle diagram of the stator current; (b) torque as a function of speed and slip

The torque depends on the square of the stator voltage and a voltage drop of approximately 10% effects therefore a torque decrease of about 20%. The corresponding speed-torque curve depicted in Figure 5.31b shows an extremum within both generating and motoring operations, the so-called pull-out torques  $T_{pm}$  and  $T_{pg}$  respectively. The pull-out slip of medium size motors is  $s_{pm} < 0.25$ . Stable operation is only possible in the range between both pull-out torques, compare Figure 5.31b. The stability of operating points is discussed in detail in Section 6.2.

If the stator resistance can be neglected ( $R_s = 0$ ), which is valid in the case of larger machines operating at line frequency, a simplified relationship, the so-called Kloss equation for the speed-torque curve

$$T_{el} = T_p \frac{2}{\frac{s}{s_p} + \frac{s_p}{s}} \quad \text{with} \quad T_p = \frac{3}{4} p \frac{M^2}{\sigma L_S^2 L_R} \left( \frac{V_{Srms}}{\omega_N} \right)^2 \quad (5.4.34)$$

can be specified. In this case, the absolute value of the motoring pull-out torque complies with the generating one, Leonhard (1996), Sarma (1996).

## 5.4.2 Synchronous Motors

### *Modeling of symmetrical three-phase synchronous motors*

In view of the electrical and magnetical properties, the stator of the synchronous motor is similarly constructed to that of the induction motor, whereas the rotor is designed in a manner such that a constant magnetic field along one axis is produced ( $p = 1$ ). In the case of more than one pole pair ( $p > 1$ ) the magnetic field of the rotor is spread over a corresponding number of axes.

Firstly, synchronous motors equipped with salient-pole rotors are discussed. The salient-pole rotor comprises of distinct poles as shown in Figure 5.32 and has a single excitation coil wound on a core. The rotor field winding is fed with direct current through slip-rings.

The modeling of synchronous motors with a salient-pole rotor can be performed similarly to that of induction motors. For the sake of simplicity, the same restrictions and assumptions as in the case of induction motors are considered.

In view of the excitation field produced by the rotor windings, no slip between the stator field and the electrical speed  $\omega_R = p \cdot \omega_m$  emerges. Hence, the synchronous motor always rotates with the speed that results from the supply frequency divided by the number of pole pairs. The speed can therefore only be adjusted by changing the frequency of the feeding symmetrical voltage system. As no alternating magnetical fields appear in the rotor, no eddy currents are induced and the core need not be designed to be laminated.

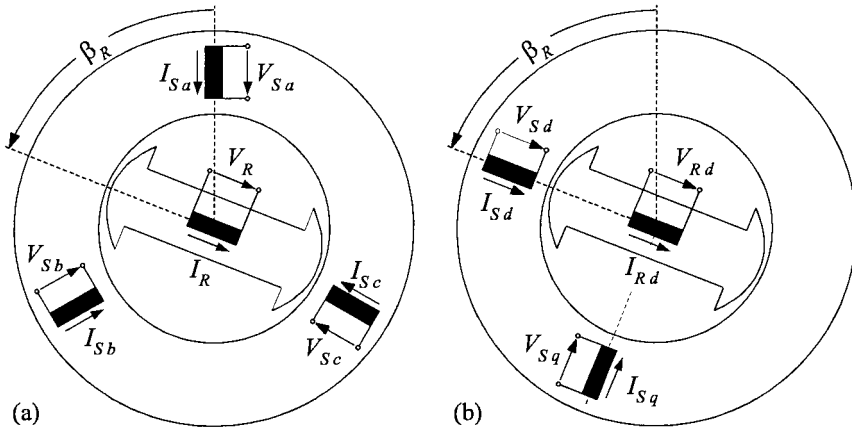


**Figure 5.32.** Schematic configuration of salient-pole synchronous motors: (a) three-phase representation of the synchronous motor; (b) two-phase equivalent circuit in the rotor-oriented reference frame

In view of the special constructive situation, it seems to be appropriate to consider the equations in a reference frame that runs with the rotor. The resulting components in the longitudinal direction are denoted by  $d$  (direct) components and the corresponding orthogonal values are specified as  $q$  (quadrature) components. In consideration of the form of the voltage equations (5.4.1) and the relationship for the transformation into arbitrary reference frames (5.4.11), the following model in the rotor-oriented coordinate system of synchronous motors with a salient-pole rotor is derived

$$\mathbf{V}_S^R = \mathbf{R}_S \mathbf{I}_S^R + \frac{d\boldsymbol{\Psi}_S^R}{dt} + i\omega_R \boldsymbol{\Psi}_S^R \quad (5.4.35)$$

$$\boldsymbol{\Psi}_S^R = \boldsymbol{\Psi}_{Sd}^R + i\boldsymbol{\Psi}_{Sq}^R \text{ with } \boldsymbol{\Psi}_{Sd}^R = L_{Sd} I_{Sd}^R + M I_{Rd}^R \text{ and } \boldsymbol{\Psi}_{Sq}^R = L_{Sq} I_{Sq}^R \quad (5.4.36)$$

$$\mathbf{V}_{Rd}^R = \mathbf{R}_R \mathbf{I}_{Rd}^R + \frac{d\boldsymbol{\Psi}_{Rd}^R}{dt} \quad (5.4.37)$$

$$\boldsymbol{\Psi}_{Rd}^R = L_{Rd} I_{Rd}^R + M I_{Sd}^R \quad (5.4.38)$$

The torque  $T_{el}$  produced by the motor can be computed by inserting (5.4.36) into (5.4.16)

$$T_{el} = \frac{3}{2} P \left( M_{Rd} I_{Rd}^R I_{Sq}^R + (L_{Sd} - L_{Sq}) I_{Sd}^R I_{Sq}^R \right) \quad (5.4.39)$$

Because of the special form of the rotor, the inductances  $L_{Sd}$  and  $L_{Sq}$  in the  $d$ - and  $q$ -axis are different, since they have different magnetic resistances (see also Section 5.2.3). As can be seen from (5.4.39), a torque is even generated if no excitation field is produced by the rotor winding ( $I_R = 0$ ). This torque is called *reluctance torque*.

The derived model is closely related to the rotor-flux-oriented representation of the induction motor, as the torque in the case of negligible reluctance ( $L_{Sd} = L_{Sq}$ ) and constant excitation ( $I_R = \text{const.}$ ) is only dependent on the  $q$ -current component  $I_{Sq}^R$ . Furthermore, the rotor-flux can be adjusted by means of the excitation current  $I_R$ , Vas (1990), Leonhard (1996), Novotny, Lipo (1996), Sarma (1996), Lyshevski (2000).

#### *Types of synchronous motors*

Synchronous motors with a salient-pole rotor are mainly employed in order to achieve high numbers of pole pairs and therefore low speeds, see Figure 5.32. Regarding the large centrifugal force that is proportional to the square of the speed, salient-pole rotors are not applicable for higher speeds.

In order to overcome this problem, *cylindrical rotors* are applied. Because of the rotational symmetry of the rotor, no reluctance emerges ( $L_{Sd} = L_{Sq}$ ). The derived model (5.4.35)...(5.4.39) can be adequately simplified. The rotors are frequently equipped with damper windings in order to damp oscillations of the rotor effected by load changes. The damper windings also serve to perform the start-up or to reduce unavoidable harmonics.

For low-power applications, *permanently excited synchronous motors* are employed. The advantage is that the slip-ring construction can be omitted in order to supply the rotor windings with DC current. Furthermore, the power loss produced in the excitation windings does not appear so that high efficiency rates can be achieved. As for the permanent magnets, often rare earth magnetic materials such as Sm-Co are employed, since they provide high flux densities (1T).

As no excitation rotor winding has to be taken into account, the generic model simplifies for permanently excited synchronous motors according to

$$\mathbf{V}_S^R = R_S I_S^R + \frac{d\Psi_S^R}{dt} + i\omega_R \Psi_S^R \quad (5.4.40)$$

$$\Psi_S^R = L_S \mathbf{I}_S^R + \Psi_{Rd} \quad (5.4.41)$$

$$T_{el} = \frac{3}{2} p \Psi_{Rd} I_{Sq}^R \quad (5.4.42)$$

The arising equations in the rotor-oriented reference frame are closely related to those of permanently excited DC motors, Vas (1990), Leonhard (1996).

#### *Control of permanently excited synchronous motors*

The control of inverter-fed permanently excited synchronous machines can be performed similarly to the rotor-flux-oriented control of induction motors. The equations comprising the behavior between the stator currents and the stator voltages within the rotor-oriented reference fra-

me (neglecting the reluctance effects) is, according to (5.4.40) and (5.4.41)

$$V_{Sd} = R_S I_{Rd} + L_S \frac{dI_{Sd}}{dt} - L_S \omega_R I_{Sq} \quad (5.4.43)$$

$$V_{Sq} = R_S I_{Sq} + L_S \frac{dI_{Sq}}{dt} + L_S \omega_R I_{Sd} + \omega_R \Psi_{Rd} \quad (5.4.44)$$

The relationship between the stator current components and the parallel stator voltage components can be specified apart from coupling terms and the EMF term by first order lags. Since both equations are not ideally decoupled, a decoupling unit has to eliminate all the terms leading to deviations from the first order lag characteristic. Note the similarity to DC motors, Section 5.3.

In the case of feeding the synchronous machine with a variably adjustable three-phase voltage system, the manipulated variables are the stator voltages  $V_{Sd}$  and  $V_{Sq}$ . Controlled variables are the speed  $n$  as well as both stator currents  $I_{Sd}$  and  $I_{Sq}$ . Thus, the control can be performed by means of a cascade structure with secondary current control loops, as depicted in Figure 5.33.

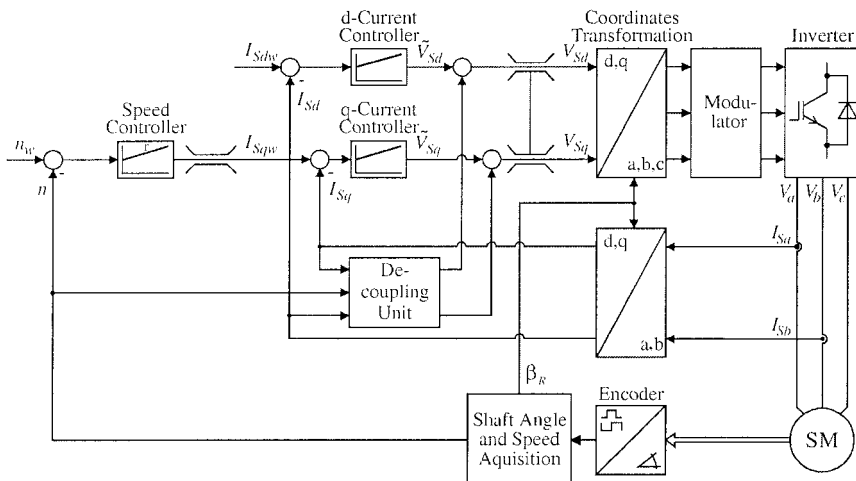


Figure 5.33. Control scheme of permanently excited synchronous motors

As the flux-producing current component  $I_{Sd}$ , according to (5.4.42), does not affect the torque, the reference value  $I_{sdw} = 0$  is chosen. In this case, the motor is driven as efficiently as possible with the smallest possible stator current.

Then, (5.4.44) simplifies to

$$V_{Sq} = R_S I_{Sq} + L_S \frac{dI_{Sq}}{dt} + \omega_R \Psi_{Rd} \quad (5.4.45)$$

After considering small changes around the operation point, the last EMF term vanishes because it can be assumed to be constant. The dynamic current behavior can then be described by the transfer function

$$G_{IV}(s) = \frac{\Delta I_{Sq}(s)}{\Delta V_{Sq}(s)} = \frac{\frac{1}{R_S}}{1 + \frac{L_S}{R_S}s} \quad (5.4.46)$$

If a PI-current-controller is used

$$G_C(s) = \frac{\Delta V_{Sq}(s)}{\Delta I_{Sq}(s)} = \frac{K_c}{T_I s} (1 + T_I s) \quad (5.4.47)$$

and pole-zero cancellation with  $T_I = L_S/R_S$  is applied, the closed-loop behavior is

$$G_{II}(s) = \frac{\Delta I_{Sq}(s)}{\Delta I_{Sqw}(s)} = \frac{1}{1 + T_q s} \quad (5.4.48)$$

with the closed-loop time constant

$$T_q = \frac{L_S}{K_c} \quad (5.4.49)$$

The closed-loop current behavior can therefore be described by a first order lag. The torque then follows from (5.4.42)

$$T_{el} = \Psi' I_{Sq} \text{ with } \Psi' = \frac{3}{2} p \Psi_{Rd} \quad (5.4.50)$$

If a reference value different from zero is chosen ( $I_{Sd} \neq 0$ ), a magnetic field towards  $I_{Sd} > 0$  or in the opposite direction  $I_{Sd} < 0$  of the field generated by the permanent magnet is produced. According to the magnetization curve of the permanent magnet, compare, e.g., Figure 5.3 the rotor-flux can be adapted by specifying a certain value  $I_{Sdw}$ . In this manner, field weakening is even possible. This has to be done carefully in order to avoid the degaussing of the permanent magnet, Vas (1990), Leonhard (1996), Novotny, Lipo (1996).

#### *Steady state operation of synchronous motors*

As synchronous motors are often employed for applications at stiff power grids with feeding frequency  $\omega_N$ , the steady state properties are discussed in the following.

For the sake of simplicity, the reluctance influences are neglected ( $L_{Sd} = L_{Sq}$ ) and the rotor winding is assumed to be constantly excited ( $\Psi_R = \Psi_{Rd} = \text{const.}$ ). In order to describe the steady state behavior of synchronous motors, the dynamic equations (5.4.40) and (5.4.41) valid for constant excitation are considered. Since the individual vectors are constant phasors within the rotor-oriented reference frame, the derivative  $d\Psi^R_s/dt$  tends to zero. The stator voltage equation can therefore be simplified according to

$$\mathbf{V}_S = R_S \cdot \mathbf{I}_S + i\omega_N L_S \cdot \mathbf{I}_S + \mathbf{E} \text{ with } \mathbf{E} = i\omega_N \Psi_{Rd} \quad (5.4.51)$$

with the EMF  $E$ . This result is used to derive the single-phase equivalent circuit as depicted in Figure 5.34, which is not unlike that of separately excited DC motors.

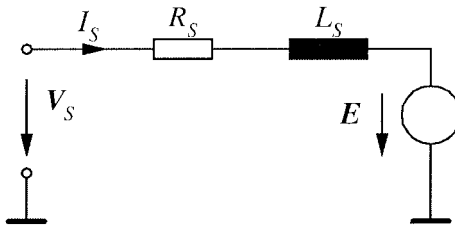


Figure 5.34. Single-phase equivalent circuit

As the synchronous machine is supplied by stiff power grids ( $V_s = \text{const.}$ ,  $\omega_N = \text{const.}$ ), the absolute value of the EMF  $E$  is constant due to the constant mechanical speed ( $\omega_m = \omega_N/p$ ). Depending on the load, a certain rotor displacement angle  $\delta$  between  $V_s$  and  $E$  emerges, which determines the amplitude and the phase of the stator current vector  $I_s$ . In Figure 5.35, the corresponding phasor diagram for a certain steady state operating point is illustrated in the case of negligible stator resistance ( $R_s = 0$ ).

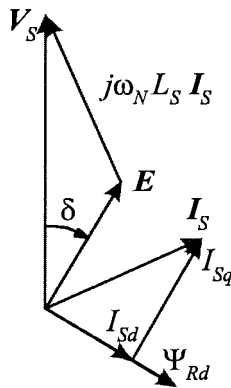


Figure 5.35. Phasor diagram of a synchronous motor with  $R_s = 0$

The torque during steady state operation is evaluated by considering the power balance. If the stator resistance can be neglected ( $R_s = 0$ ), which is valid for larger machines, the power balance under consideration of (5.4.51) is given by

$$\frac{3}{2} \operatorname{Re}(V_s I_s^*) = T_{el} \frac{\omega_N}{p} \quad \text{with } I_S = \frac{V_s - E}{i\omega_N L_S} \quad (5.4.52)$$

Thus, after some conversions, the torque can be specified depending on the rotor displacement angle  $\delta$ , see Figure 5.35,

$$T_{el} = T_p \sin(\delta) \text{ with } T_p = 3p \frac{V_{Srms} E_{rms}}{\omega_N^2 L_S} \quad (5.4.53)$$

In this equation, the RMS values of the corresponding phase variables are employed, with, e.g.,  $V_{rms} = \hat{V}/\sqrt{2}$ . According to (5.4.53), synchronous motors also show pull-out torques  $T_p$  that appear at the rotor displacement angles  $\delta = \pm 90^\circ$ . The corresponding torque curves are depicted in Figure 5.36.

In contrast to induction motors, the pull-out torque of synchronous machines only depends linearly on the stator voltage amplitude. Thus, the torque is not as much affected by oscillations of the power grid as in the case of induction motors, compare (5.4.34), Leonhard (1996), Sarma (1996).

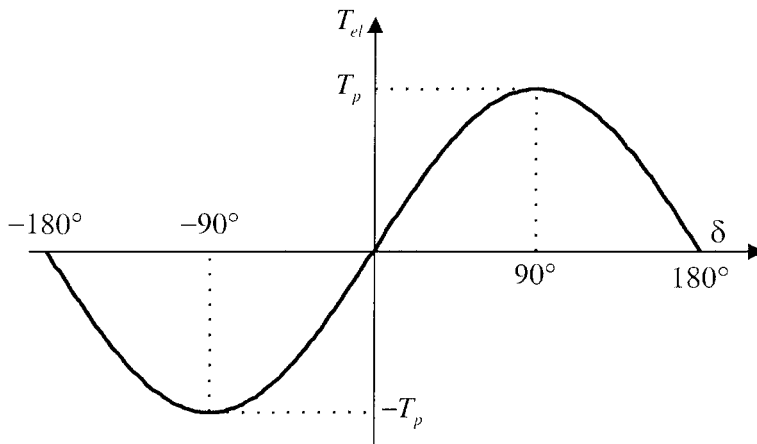


**Figure 5.36.** Torque curve of a synchronous motor depending on the rotor displacement angle  $\delta$

## 5.5 SINGLE-PHASE MOTORS

In the case of low drive powers up to 1 kW, it is common to feed the motors with one-phase AC current in order to keep the set-up as simple as possible. For this purpose, different constructions with commutator or squirrel-cage rotors exist.

### 5.5.1 Commutator Motors (Universal Motors)

Considering DC shunt- and DC series-wound motors, the change of the sign of the armature current leads to the reversal of the magnetic field  $B$  and thus of the armature current. In accordance with (5.3.4) and (5.3.5), the direction of the torque stays constant. Thus, DC motors can be generally supplied by a one-phase AC voltage source. However, in order

to reduce the iron loss caused by the alternating magnetic field, the stator has to be made of laminated iron.

In the case of DC series-wound motors, the stator and rotor current have the same phase, and hence, a maximum pulsating torque arises. The transformatory voltage induced by the alternating main field complicates the commutation and leads to high sparking voltages.

The torque curve of DC series-wound motors fed by AC voltages shows a high starting torque and decreases with rising speed similar to that of DC voltage fed motors, see Table 5.1. The speed can be cost-efficiently adjusted over a wide speed range by employing variable dropping resistors, variable transformers or phase control. The phase control is the easiest AC power converter. The use of permanent magnets instead of stator windings is another interesting constructive option to design low-power DC motors, Stölting (1996). Commutator motors are mainly employed in household appliances or electrical tool devices.

### 5.5.2 Squirrel-cage Motors

Especially straightforward constructions of one-phase AC motors are obtained if a rotating field is generated by two stator windings displaced from each other by  $90^\circ$ . This can be performed by attaching additionally to the main excitation winding an auxiliary winding that is fed by an auxiliary current with a phase delay of  $90^\circ$ . The phase shift can be generated by means of a capacitor (*capacitor motor*), see Figure 5.37 and Table 5.1. However, the arising rotating fields are not circular but ellipsoidal, which leads to lower starting pull-out torques and smaller efficiency rates. In this case, squirrel-cage rotors are mainly employed.

The torque curve is similar to that of a squirrel-cage induction motor, Table 5.1. With rising slip, the torque increases up to the pull-out torque and decreases for higher slips. In order to improve the starting torque, an additional capacitor can be interconnected during the start-up process.

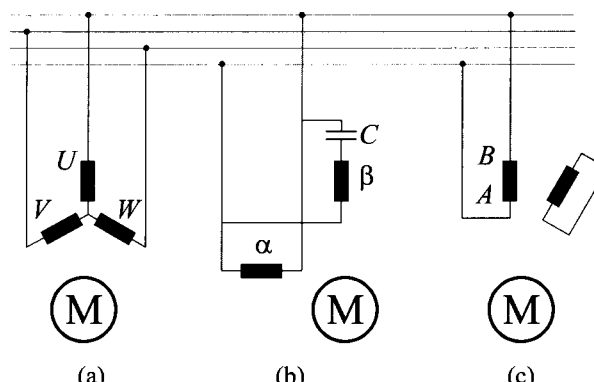


**Figure 5.37.** Asynchronous squirrel-cage motors (from Ramminger (1992)): (a) AC squirrel-cage induction motor; (b) AC capacitor motor; (c) AC shaded-pole motor

A second possibility for the generation of rotating fields is to place the auxiliary winding at a split-pole, Figure 5.37c. With the help of the induction in the short-circuit rings, the magnetic field shows another phase position within this subdomain, which effects an ellipsoidal rotating field. The torque curve of these *shaded-pole motors* is closely related to that of capacitor motors, although the starting torque and the efficiency rate is even smaller. The rotor of both capacitor and shaded-pole motors is laminated. The speed decrease between idle running and rated load is comparatively small (approximately 10%), whereas a distinctive pull-out torque emerges. Thus, in the case of constant supply frequency, these motors are not qualified for speed control.

In the case of feeding one winding with constant AC voltage and the second with a  $90^\circ$  phase-shifted AC voltage with variable amplitude, see Table 5.1, an ellipsoidal rotating field is generated. If the rotor is additionally interconnected to a large resistor, the pull-out torque is shifted to the left and falling-off curves within the whole speed range are obtained. In this case, the speed can be adjusted from zero to the idle speed by means of the control voltage. This principle is applied with the *Ferraris motor*. It comprises a bell rotor (hollow cylinder) made of copper or aluminium so that within the whole rotor eddy currents are produced. The resulting heat is discharged by the large rotor surface. In connection with the small rotor diameters, low moments of inertia are achieved that can be used to construct speed, adjustable AC servo-drives that can be driven even in the range of low speeds for positioning control.

These servo-drives have the advantage that no electrical connection to the rotor is required and they only need an AC amplifier in order to supply the control voltage. The  $90^\circ$  phase shift can be either generated by means of a capacitor (single-phase AC motor) or an AC amplifier with corresponding circuit (two-phase AC motor), e.g., Pfaff (1994). Some properties of low-power AC and single-phase motors are compiled in Table 5.3. Electrical drives that especially serve as actuators will be discussed in Chapter 10.

**Table 5.3.** Properties of low-power (up to 1 kW) AC and single-phase motors, according to Jung, Schneider (1984), Meyer (1985)

	three-phase motors		single-phase motor		
	asynchronous motors	synchronous motors	commutator (universal)	capacitor	shaded pole
power range	<i>W</i> 2-1000	0.01-500	5-1000	0.1-2200	1-100
rated voltage	<i>V</i> 380	220	12-230	220	220
efficiency $\eta_{max}$	0.5-0.8	0.1-0.6	0.3-0.7	0.4-0.7	0.1-0.4
rated speed	rpm 700-30000	40-30000	1000-9000	1200-2850	1200-2700
controlled speed range	1 : 10	1 : 15	1 : 100	—	—
speed control through change of	supply frequency	supply frequency	voltage (phase modulation) shunt	not in use	voltage

## 5.6 POWER ELECTRONICS

In order to build up power electronic circuits, electronic valves are needed that can be transferred alternately in the conducting and the insulating state. On the one hand, the electronic power switching between the two conductance conditions can be performed with the help of so-called *non-controllable valves* depending on the direction of an electrical voltage. Another possibility are electronic components that have an additional connector for an external control signal. Those electronic component parts are *controllable valves*, which can be split up into so-called *self-locking valves* that can either be turned-on and turned-off by means of external control pulses, or *turn-on valves* that can only be turned on. In the following, the most important components are discussed.

### 5.6.1 Power Component Parts

The simplest electronic valve is the semiconductor *diode* belonging to the group of non-controllable valves. In the case of positive voltages, the diode is in the conducting state whereas at negative voltages no current flow occurs.

The *thyristor* is a controllable turn-on valve that is capable of blocking in the case of both positive and negative voltages. In contrast to diodes, an additional connector – the so-called *gate* exists. By introducing a (positive) current pulse  $I_G$ , the thyristor is brought into the conducting state.

The thyristor, however, regains (comparable to diodes) its blocking ability if a negative voltage  $V_T$  emerges and a current flows for a certain time in the opposite direction.

So-called *gate-turn-off* (GTO) *thyristors* additionally provide the property of transferring the component from the conducting into the insulating state by introducing an adequate (negative) gating current  $I_G$ . Therefore, GTO thyristors belong to the category of self-locking electronic valves. In contrast to conventional thyristors, the control current  $I_G$  must be present during the whole period of conduction.

Commonly, thyristors have the property of switching especially high electrical powers ( $\geq 500$  kW). In consideration of the charge carriers that have to be injected in and removed from the different semiconductor layers, thyristors show particularly high turn-on and turn-off delays. On the other hand, the switching frequencies are restricted by the high switching losses. Hence, only considerably low switching frequencies ( $< 1$  kHz) can be applied.

*Bipolar transistors* represent another type of self-locking valve. Transistors are current-controlled component parts that can be transferred into the conducting state by feeding the base with a positive current  $I_B$ . In order to accelerate the removal of the charge carriers during the shut-down cycles, the transistors are not driven saturated. Bipolar

transistors show comparatively low forward losses but high switching losses and are therefore employed at lower switching frequencies ( $\leq 10$  kHz) in order to switch small powers.

*Metal oxide field effect transistors* (MOSFET) are voltage-controlled self-locking valves that can be brought into the conducting state by introducing a positive control voltage  $V_{GS}$ . The advantage is that field effect transistors can be turned on and off rapidly in consideration of the low storage charge within the gate. Thus, by employing MOSFET, high switching frequencies ( $\leq 1000$  kHz) can be achieved. In view of the high forward losses, this component part can only be applied in order to switch low powers.

The advantages of both the bipolar and MOSFET transistors are combined in the so-called *insulated gate bipolar transistors* (IGBT). These transistors are voltage-controlled self-locking valves that have a MOS structure at the input and a bipolar structure at the output. The valves unify the straightforward controllability and high-switching frequencies of MOSFET and the low forward losses of bipolar transistors. Thus, it is feasible to switch even medium powers with high switching frequencies ( $\leq 100$  kHz), Krein (1998).

The symbols of the individual valves along with the most important data and characteristic curves are summarized in Table 5.4.

### 5.6.2 Power Circuits

In order to drive the proposed motor types with variable speed over a wide speed range, actuators are needed for the conversion of electrical energy in order to provide the required voltage and current sources. A variety of power circuits are known that differ from the form of their input and output values. In general, four basic types of circuits can be distinguished, Erickson (1997), Trzynadlowski, Legowski (1998):

- *DC–DC converter*: these devices have the task of transforming a DC voltage or a DC current of a certain magnitude and polarity into a DC voltage or DC current with different magnitude and/or polarity;
- *AC–AC converter*: converts an available AC voltage or AC current system with defined amplitude, frequency and number of phases into a different AC voltage or AC current system;
- *DC–AC converter*: generates out of a certain DC voltage or DC current an AC voltage or AC current system with particular amplitude, frequency and number of phases;
- *AC–DC converter (rectifier)*: a defined AC voltage or AC current system is transformed into a DC voltage or DC current with certain magnitude and polarity.

**Table 5.4.** Survey of some electronic valves

valves	diode	thyristor	GTO	bipolar transistor	MOSFET	IGBT
symbol						
properties	- non-controllable valve	- controllable turn-on valve - turned on with a current pulse	- controllable self-locking valve - turned on and off with a current pulse	- controllable self-locking valve - current-controlled	- controllable self-locking valve - voltage-controlled	- controllable self-locking valve - voltage-controlled
characteristic curve						
voltage range	... 8000 V	600 ... 8000 V	2500 ... 6000 V	500 ... 1200 V	50 ... 200 ... 1000 V	600 ... 1200 ... 3300 V
current range	... 5000 A	300 ... 5000 A	1500 ... 4000 A	15 ... 500 A	5 ... 50 ... 200 A	15 ... 100 ... 1200 A
max. switching frequency		800 ... 1000 Hz	800 ... 1000 Hz	2 ... 10 kHz	10 ... 100 kHz	5 ... 100 kHz
turn-on delay	2 $\mu$ s	2 $\mu$ s	2 $\mu$ s	1 ... 20 $\mu$ s	0.1 ... 1 $\mu$ s	0.1 ... 1 $\mu$ s
turn-off delay	-	10 ... 25 $\mu$ s		0.1 ... 2 $\mu$ s	0.1 ... 2 $\mu$ s	0.1 ... 2 $\mu$ s

In consideration of the high practical importance, a special class of circuits shall be considered that are capable of converting input voltages into certain output voltages. The idea behind these circuits is that, for instance, a particular mean value with respect to a certain interval can be achieved by turning a given DC voltage on and off. The approach is called *pulse width modulation* (PWM), which will be described in the following by the example of so-called *buck converters*.

The basic circuit of buck converters consists of a self-locking controllable valve (e.g., IGBT) and a non-controllable valve (diode) and serves to convert a positive input DC voltage source into a (not necessarily constant) smaller output voltage. The corresponding circuit burdened with a DC motor is depicted in Figure 5.38.

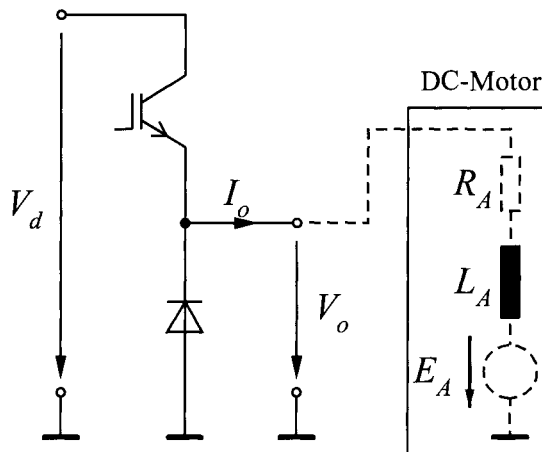


**Figure 5.38.** Scheme of a buck converter supplying a DC motor

The output voltage  $V_o$  is equivalent to the input voltage if the IGBT is turned on and zero when it is turned off. By varying the duration for which the controllable valve is conducting and then insulating, the average output voltage can be varied, but the output voltage is not pure DC. In fact, the output voltage contains an average voltage with a square-voltage superimposed on it. The resulting signal curves are depicted in Figure 5.39.

In order to perform the PWM, the present reference values of the output voltage  $V_{or}$ , valid within the pulse interval  $T_p$ , are compared to a triangular signal that is periodical with the pulse frequency  $f_p$ . As long as the reference  $V_{or}$  is below the triangle, the IGBT is turned on by feeding the gate with an appropriate control voltage. Hence, the characteristic curve of the output voltage  $V_o$ , illustrated in Figure 5.39, arises.

The determination of the switching times by means of triangular signals is based on the following relationships

$$T_{on} = \frac{V_{or}}{V_d} \quad T_{off} = T_p - T_{on} \quad (5.6.1)$$

whereupon  $T_{on}$  and  $T_{off}$  specify the time intervals during which the voltage  $V_d$  is turned on and off respectively, Holtz (1992), Pressman (1997).

The described buck converter circuit can only be applied to the feeding of loads whose impedance shows a low-pass characteristic. Otherwise, high currents would appear. Commonly, this premise is fulfilled by electric motors and hence the emerging output currents  $I_o$  are much more smooth in comparison to the voltages  $V_o$ . This circuit is mainly applied as a power supply for DC motors. The resulting currents in the case of feeding a DC motor with pulse width-modulated voltages are depicted in Figure 5.39. One major drawback of buck converters is that a current flow  $I_o$  can only be performed in the positive direction.

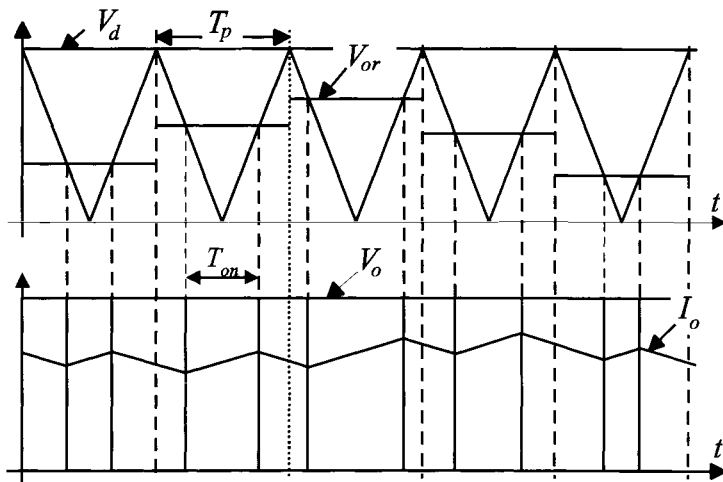


**Figure 5.39.** Pulse width modulation: reference value  $V_{or}$  actual value  $V_o$  and resulting current  $I_o$

A similar circuit, which is called a *boost converter*, emerges if both valves are transposed. Here, the output current can only flow in the negative direction and the output voltage  $V_o$  therefore has to be larger compared to the input voltage  $V_d$ . The PWM can be applied similarly as in the case of buck converters with the exception that the self-locking controllable valve is turned on whenever the output voltage has to be zero. Boost converters can be employed to supply DC motors driven within generating operating points. As both buck and boost converters can only operate within one quadrant (positive output voltage, either positive or negative output current), these circuits are also called *one-quadrant converters*.

By combining the circuits of buck and boost converters, so-called *two-quadrant converters* arise that are capable of conducting the output current in both directions, Figure 5.40. By employing this circuit, it is, for instance, feasible to drive a DC motor within both motoring and generating operating points. Assuming constant input voltages  $V_d$ , only one rotational direction is possible as the output voltage can only be

positive. The circuit is also driven by applying the PWM technique, not unlike the situation in buck and boost converters. Note that both controllable valves (*e.g.*, IGBT) may only be alternately in the conducting state to avoid short circuits that would destroy the valves. The PWM scheme depicted in Figure 5.39 can be directly adopted. The output voltage  $V_o$  is equivalent to the input voltage when the IGBT connected with the positive DC voltage bus is turned on and zero if the other IGBT is turned on.

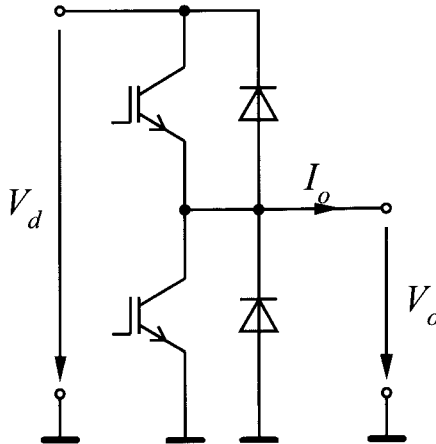


Figure 5.40. Two-quadrant converter

The two-quadrant converter is the basis for more advanced circuits. The *four-quadrant converter* comprises of two paralleled two-quadrant converters as depicted in Figure 5.41. With these circuits, both output voltage and output current can be provided in both directions. The output voltage is the difference between both output voltages of the two-quadrant converters ( $V_o = V_+ - V_-$ ). Thus, the reference values of the two-quadrant converters have to be referred to half of the input voltage and are therefore given by

$$V_{+r} = \frac{1}{2}(V_d + V_{or}) \quad \text{and} \quad V_{-w} = \frac{1}{2}(V_d - V_{or}) \quad (5.6.2)$$

On the one hand, four-quadrant converters are mainly employed to feed DC motors, since motoring and generating operation is available here in both rotational directions. On the other hand, these converters can also be utilized for the generation of single-phase sinusoidal AC voltages. In this case, the PWM approach is also denoted *sine-triangle modulation*.

A *three-phase converter* arises by three parallel two-quadrant converters, as depicted in Figure 5.42. In the following, the feeding of symmetrical earth-free loads, such as AC motors, is considered. In order to specify the reference values for the individual three-quadrant converters, the potential of the neutral point with respect to the ground

is defined as half of the input voltage. The reference values for the individual two-quadrant converters can be denoted by

$$V_{1,2,3r} = V_{Sa,b,c} + \frac{V_d}{2} \quad (5.6.3)$$

whereupon the amplitudes of  $V_{Sa,b,c}$  are restricted to  $\pm \frac{V_d}{2}$ . In connection

with symmetrical voltage systems, the maxima and minima of the individual phase voltages do not appear at the same time. Thus, higher phase voltage amplitudes can be achieved by superposing the constant part of the potential of the neutral point to an appropriate AC component. In this manner, the amplitudes can be increased by approximately 15%. An equivalent approach is the so-called space vector modulation. The proposed circuits are summarized in Table 5.5, including equivalent circuit diagrams and the corresponding operating ranges.

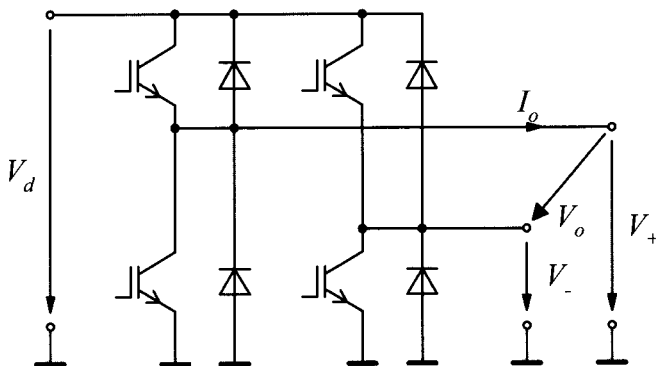


Figure 5.41. Four-quadrant converter

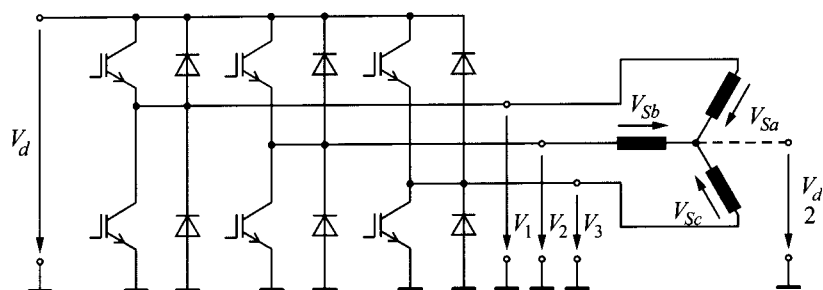


Figure 5.42. Scheme of a three-phase converter

Table 5.5. Survey of controlled power circuits

power circuit	buck converter	boost converter	two-quadrant converter	four-quadrant converter	three-phase converter
type	DC-DC converter	DC-DC converter	DC-DC converter	DC-DC converter and DC-AC (one phase) converter	DC-AC (three phase) converter
equivalent circuit					
restriction	$I_o \leq 0$	$I_o \geq 0$			
range of operation					

Up to now, only circuits that are capable of producing AC voltages from a DC voltage source have been considered. The described principle of four-quadrant and three-phase converters can also be reversed, with the effect that the proposed circuits are capable of working as rectifiers (AC–DC converter). The previous outputs are fed by the AC voltages that have to be rectified, whereas the previous input supplies feed the desired DC voltage. Usually, the DC voltage also contains, apart from the mean value, higher harmonics that can be suppressed by means of smoothing capacitors.

Non-controlled rectifier circuits arise if the controlled valves are omitted and just the free-wheeling diodes remain, compare Figure 5.43. The DC voltage in the case of the four-quadrant converter is below the magnitude of the AC voltage amplitude, whereas in the case of the three-phase converter the DC voltage is in the dimension of  $\sqrt{3} \cdot \hat{V}$  with the phase voltage amplitude  $\hat{V}$ . Note that those circuits are only capable of supplying electric power unidirectionally from the grid to the DC link. The corresponding circuits are depicted in Figure 5.43.

Recent power grid-fed converters for the supply of AC motors consist of a line-side AC–DC converter, which rectifies the symmetrical grid voltage system, and a motor-side three-phase DC–AC converter that generates a three-phase system with variable frequency and amplitude. Commonly, these inverters are called *voltage source DC link converters* as they are based on voltage intermediate circuits. The corresponding block diagram is illustrated in Figure 5.44, Bose (1997), Erickson (1997), Pressman (1997), Trzynadlowski, Legowski (1998).

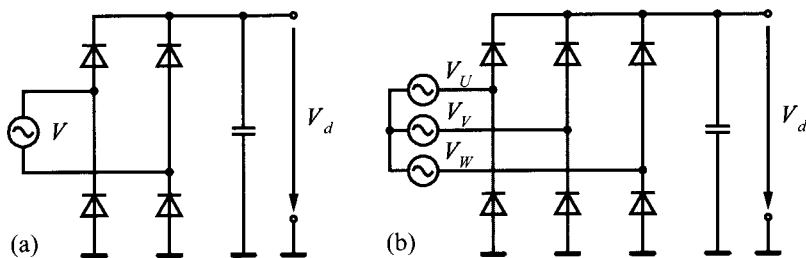


**Figure 5.43.** Non-controlled rectifier with smoothing capacitor: (a) one-phase rectifier circuit; (b) three-phase rectifier circuit

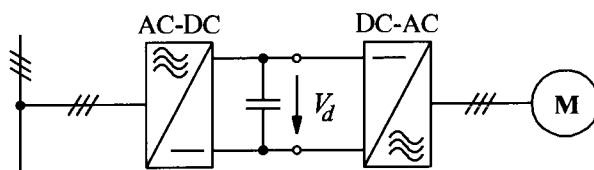


**Figure 5.44.** Voltage source DC link converter scheme for feeding AC motors

On the other hand, converters exist that rely on intermediate current circuits (current source inverter). Instead of the voltages, here the phase currents are pulse width modulated, Bose (1997). Furthermore, so-cal-

led resonant DC link converters are also employed, whose intermediate voltage and current is not constant any more, Erickson (1997). Finally, so-called matrix converters exist, which directly convert three-phase AC systems into other three-phase AC systems with controllable magnitude and frequency. These converters do not have any intermediate circuit, Huber, Borojevic (1995).

## 5.7 INTERNALLY OR EXTERNALLY COMMUTATED ELECTROMOTORS

The previous consideration of the individual electric motors shows a variety of different constructions that are determined by the various properties of the motors and their corresponding areas of application. In view of the significance of feedforward or feedback speed-controlled motors in mechatronic systems employed as servo-drives in actuators or drive motors, the electric motors are finally further classified concerning the generation and control of the rotating magnetic field:

### 1. *Internally commutated motors* (self-commutated)

The armature windings or stator windings are switched over depending on the rotor position:

#### Mechanical commutator

- DC commutator motors;
- AC commutator motors.

#### Electrical commutator

- DC motors (permanent-magnet rotor);
- DC step motors.

### 2. *Externally commutated motors*

The stator windings are excited depending on the frequency of the supply voltage (applied rotating field):

- induction motors;
- synchronous motors;
- squirrel cage motors.

Commonly, the speed control of externally controlled electromotors has to be performed by adapting the frequency of the rotating field. The operation in few (two or three) speed steps can be performed by changing the number of pole pairs. In order to control the speed continuously, variable frequency converters are required, which are quite costly. Externally controlled electromotors are very robust due to their simple construction, low cost, low wear and low noise.

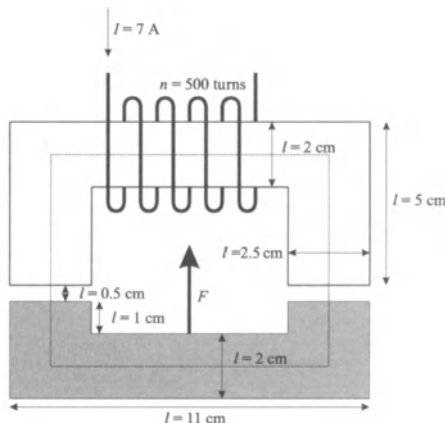
In the case of internally controlled electromotors, the speed control can be performed easier within larger speed ranges, hence only adjustable voltage sources or resistances are needed. These motors are mainly employed as speed-variable drives within the small power range. In contrast to externally controlled machines, internally controlled motors are smaller and of lighter weight but are more expensive with regard to their production. Mechanically commutated motors are characterized by brush/commutator wear and higher noise level but cheaper manufacturing costs. Electronically commutated motors comprise less complex, low-wear and low-noise constructions but are comparatively expensive due to the required rotor position sensors and gating electronics.

The development goes on, in general, from low-power continuously speed-variable electromotors with wide speed range towards simply constructed motors (with rising magnetic fields), electronic commutation and electronic speed control, Stölting (1996). Hence, the application of mechatronic principles can be observed here, too.

A comparison of the various electrical motor principles with regard to the application for actuators is considered in Section 10.3.

## 5.8 PROBLEMS

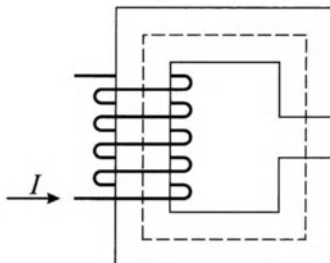
- 5.8.1 An electromagnet is given, which is used to lift a steel beam as shown in the figure below. The magnet core has a relative permeability of  $\mu_r = 5000$ , while the steel beam has a relative permeability of  $\mu_r = 2000$ . The depth of both the iron core and the steel beam is given as 2 cm. Calculate the lifting force  $F$  exerted on the beam.



- 5.8.2 An electromagnet is given as shown in the diagram below. For the iron core, the magnetization curve is given by  $H/B$  pairs as listed in the table. The relationship can be linearly interpolated between the points. Calculate  $H$ ,  $\Theta$ ,  $B$ ,  $\Phi$ . The cross-sectional area is given as  $5 \text{ cm}^2$ . The average magnetic field line in the

iron core is  $l = 50$  cm long. The air gap is 1 mm wide. The coil has  $n = 1000$  turns and carries a current of  $I = 7.5$  A.

$H \left[ \frac{A}{m} \right]$	0	100	200	300	400	600	1000	1500	2500
$B [T]$	0	0.6	1	1.3	1.4	1.5	1.65	1.75	1.76



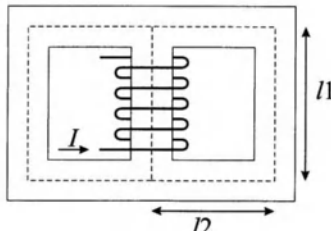
- 5.8.3 A coil is given, which is supported so that it can rotate in a magnetic field. The magnetic field is created by a permanent magnet. Calculate the torque exerted on the coil if a current  $I$  is conducted by the coil. The coil has a radius  $r$  and has a depth  $l$ . Calculate the maximum allowable current  $I_{max}$  if a rotational spring is attached to the coil and if the maximum rotational displacement is limited to  $\alpha_{max}$ . This set-up represents the functional principle of the d'Arsonval galvanometer, which is widely used to measure currents and also voltages employing Ohm's law.

Parameters:  $n = 250$ ,  $I = 0.5$  mA,  $B = 0.3$  T,  $M_{spring} = \frac{\mu \text{ Nm}}{\text{rad}}$ ,

$\alpha_{max} = 1.4 \approx 80^\circ$ ,  $r = 7$  mm, and  $l = 15$  mm.

- 5.8.4 For the magnetic circuit as shown in the diagram, the permeability of the iron core is constant and denoted by  $\mu$ . The cross-sectional area is given as  $A$ . The coil has  $n$  turns. Calculate the self-inductance  $L$ . How does the self-inductance correlate to the magnetic resistance?

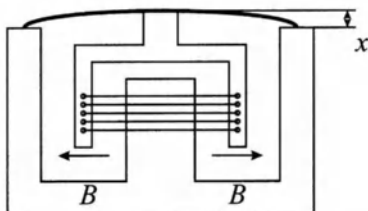
Parameters:  $n = 500$ ,  $A = 16 \text{ cm}^2$ ,  $l_1 = 10 \text{ cm}$ ,  $l_2 = 5 \text{ cm}$ , and  $\mu = 4000 \mu_0$ .



- 5.8.5 A moving coil can be used to construct a microphone. The functional principle can be seen from the figure. A moving coil is immersed into the magnetic field of a permanent magnet. The radial magnetic field is given by  $B$  at the position of the windings of the coil. The coil has  $n$  turns and a radius  $r$ .

If sound waves excite the membrane, then the coil is also displaced. This change of displacement results in an induced voltage. Calculate the output voltage for a membrane displacement of  $x(t) = A \sin(\omega t)$ .

Parameters:  $B = 0.5$  T,  $n = 500$ ,  $A = 0.5$  cm,  $r = 1.5$  cm,  
 $\omega = 2\pi \times 400 \frac{\text{rad}}{\text{sec}}$ .



- 5.8.6 For the DC motor with data as in Example 5.1, calculate the torque-speed characteristic for  $V_A = 50$  V and 100 V.
- 5.8.7 Calculate the parameters for the dynamic model of (5.3.20) for the DC motor in Example 5.1. Determine the armature and the mechanical time constant.
- 5.8.8 A shunt-wound motor supplied with 200 V runs at 1000 rpm with an armature current of 20 A. The armature resistance is 0.6  $\Omega$ . Calculate the required armature voltage, neglecting friction. Calculate the armature voltage for 500 rpm and the current 10 A.
- 5.8.9 Determine the torque-speed characteristic of the brushless DC motor of Example 5.2 for 28 V and 14 V.
- 5.8.10 An induction motor with three phases (50 Hz) runs at 3000 rpm on no load and at 2800 rpm with load. How many poles has the motor and how large is the slip with load?
- 5.8.11 A medium size induction motor with negligible stator resistance ( $R_s = 0$  W) is considered.
- Outline the single-phase equivalent circuit for steady state operation.
  - Derive a relationship for the calculation of the stator current depending on the stator voltage and the slip.

- c) The motor is fed in  $Y$ -connection by a three-phase voltage system ( $\rightarrow$ phase voltage:  $V_S = V_r/\sqrt{3}$ ). The rated values are:  $V_r = 400$  V,  $f_N = 50$  Hz,  $s_r = 0.05$ ,  $R_S = 0$  W,  $R_R = 0.6$  W,  $L_{Ss} = 2.55$  mH,  $L_{Rs} = 3.18$  mH,  $M = 56.0$  mH. Draw the corresponding circle diagram of the stator current.
- d) Mark the operating points at standstill ( $s = 1$ ), at synchronous speed ( $s = 0$ ), at rated speed ( $s = s_r$ ) and at pull-out slip  $s_{pm}$ .

5.8.12 An induction motor with slip-ring rotor is fed in  $Y$ -connection by a three-phase voltage system ( $\rightarrow$ phase voltage:  $U_S = U_r/\sqrt{3}$ ) with constant frequency  $f_N$  and amplitude  $U_r$ .

- a) Specify a relationship for the static torque depending on the phase voltage  $U_S$  in case of a negligible stator resistance ( $R_S = 0 \Omega$ ).
- b) Outline qualitatively the torque as a function of speed. Specify the operating regimes in which the motor acts as motor and generator, respectively.
- c) The induction motor is burdened by a load, whose static torque is constant within the relevant speed range and below the pull-out torque of the motor. Which operating points are stable and unstable respectively?
- d) The input connection scheme of the induction motor is changed from  $Y$ - to  $D$ -connection. Thus, the phase voltages increase, with  $V_S = V_r$ . Outline the arising speed-torque curve regarding the result of a). Specify the corresponding pull-out torque in  $D$ -connection depending on the pull-out torque in  $Y$ -connection.
- e) The induction motor is fed in  $Y$ -connection by a power supply (inverter) with variable frequency and voltage amplitude:
  - i) the voltage amplitude is supposed to be constant  $V_S = V_r/\sqrt{3}$ . Outline the resulting speed-torque curve for the supply frequencies  $f_N/2$ ,  $3/4 \times f_N$  and  $f_N$ ;
  - ii) how has the voltage amplitude depending on the supply frequency to be adjusted in order to keep the pull-out torque on a constant level?
 Note: take equation (5.4.34) into consideration.
- f) The motor is fed by the original power grid in  $Y$ -connection. Furthermore, the slip-ring rotor construction enables the increase of the rotor resistance by interconnecting external resistors  $R_{Ra}$ . Outline the resulting speed-torque curve in the case of an increase of the rotor resistance. For which speeds is this proceeding advantageous?

- 5.8.13 A squirrel-cage induction motor is considered. In the following, the balanced distributed windings can be replaced by means of lumped coils. Furthermore, saturation effects of magnetic circuits are neglected. In this problem, dynamic models of induction motors are derived.
- a) Outline the schematic configuration of the stator and rotor winding systems, both for the original three-phase system and the derived two-phase representation.
  - b) Specify in the case of the two-phase system the equations of the stator and rotor-flux linkages. Use space vectors as described in Section 5.4.1.
  - c) Derive the voltage equations for the stator and rotor coils, employing space vector representation.
  - d) Transform the equations obtained in b) and c) in the common reference-frame defined by the stator.
  - e) The dynamic equation system in an arbitrary common coordinate system according to (5.4.12)...(5.4.16) has to be oriented on the rotor-flux  $\Psi_R$ :
    - i) specify the rotor-flux in the rotor-flux-oriented reference-frame;
    - ii) transform the relationship (5.4.16) into the rotor-flux-oriented coordinate system;
    - iii) the so-called current model can be derived by inserting the rotor current of (5.4.15) into (5.4.13), whereupon in the case of squirrel-cage rotors the rotor voltage is zero. Orient the relationship on the rotor-flux and specify the resulting equations for both components. Which current component therefore controls the rotor-flux? Derive furthermore a relationship for the slip-frequency ( $\omega_2 = \omega_K - \omega_R$ ).

# 6 Machines and Drivetrains

---

According to Chapter 1 and the classification of mechatronic systems, machines in general can be divided into power-generating machines (engines), power-consuming machines (working machines) and vehicles. With regard to energy flows these machines may be characterized as follows. Power engines turn primary energy into mechanical energy. On their output side, power engines deliver mechanical energy. Power-consuming machines turn mechanical energy into the specific energy of the consumer or load. On their input side, they take in mechanical energy and deliver energy in various forms such as heat, deformation energy or mechanical potential energy at the output. Vehicles may also be considered as machines. The energy consumer is the vehicle with the (mechanical) rolling-, ascending- and air-resistance. In addition to the energy flow, there may also be a flow of material (*e.g.*, in combustion engines or pumps). In the case of an electric engine (motor), there is no additional flow of material. A further characteristic property of a machine is the generation of movement according to its transversal or rotational kinematics.

Figure 6.1 shows the scheme of a power-generating machine (engine, motor). The primary energy supply is, for example, an electrical or hydraulic network or fuel. This primary energy is converted by the power engine (*e.g.*, electric, hydraulic or combustion engine) into mechanical energy (rotating shaft with torque). This energy is transmitted into the desired torque-speed range by a transmission such as a mechanical or hydraulic torque converter. This mechanically transformed energy then drives an energy consumer (*e.g.*, working machine or vehicle). Actuators (*e.g.*, power converters, valves, fuel injectors) are applied to manipulate the energy transformation. They are supplied by an auxilia-

ming machine, and according to its  $T(\omega)$  characteristic, a speed  $\omega$  results in the intersection point of the two characteristics. This speed  $\omega_0$  acts back on the motor and determines the voltage  $V_0$  of the current source. Hence, the manipulated variable  $U_c$  primarily determines the torque and the speed is a dependent variable.

This example also shows that the kind of source with applied voltage or applied current determines the causality of the motor, the working machine and their sink. This results in a unique cause-effect relation of the overall systems, as shown by Example 2.4.

The two discussed operating principles are typical for many machines and vehicles. Further examples are:

- *speed manipulation*: machines tools, industrial robots, lifts, actuators;
- *torque manipulation*: combustion engine in vehicles, hydraulic motors, ships, trains, aircraft.

### b) Mathematical models of machines

A machine consisting of a power engine, a drivetrain and a power-consuming machine is shown in Figure 6.4. The drivetrain consists of a belt drive or an elastic clutch, a shaft and a gearbox. Table 6.1 summarizes the mathematical models of some components, which are partly derived in Chapters 4 and 5. Shafts are modeled as two-mass systems. Several components are described by linear differential equations. The friction of plain bearings and guidances can be described by a direction-dependent torque

$$T_{F1}(t) = T_{F10} \operatorname{sign}\dot{\phi}(t) + T_{F11} \dot{\phi}(t) \quad (\dot{\phi}(t) \neq 0) \quad (6.1.1)$$

$T_{F10}$  is the Coulomb friction coefficient (dry friction) and  $T_{F11}$  is the viscous friction coefficient (see Section 4.7). The model of the complete machine may be derived as shown in detail in Chapter 2 by:

- stating the equations of the process elements (balance equations, constitutive equations and phenomenological equations);
- stating the interconnection equations (continuity equations for parallel systems and compatibility equations for serial systems);
- defining the inputs and outputs.

In simple cases, the equations may be solved by eliminating non-interesting variables, resulting in the differential equation for the input/output behavior, see also Chapter 4. Generally, it is more convenient to write the equations in the form of a vector differential equation. If all partial models can be linearized, an  $n^{\text{th}}$  order state vector and a state model follows.

The working process is a consumer (*e.g.*, increasing the pressure by the supply of kinetic energy, metal cutting, transport of piece good material). The working process absorbs mechanical energy and transforms it into a different form of energy. Depending on the process, the mechanical energy is transformed with losses to, *e.g.*, potential energy, cutting energy or size reduction energy, or remains in the energy consumer itself. The losses are generally of a dissipative nature (friction, flow resistance) and appear as a flow of thermal energy in the consumer or its surrounding.

Mechanical systems and machines can now be modeled using the component models shown in Chapters 4 and 5. In the sequel, the coupling of components, resulting characteristic curves, static and dynamic behavior, stability and the dependency on different operating points are discussed.

## 6.1 COUPLING OF MACHINE COMPONENTS TO COMPLETE MACHINES

### a) Speed control and torque control

Machines are either operated automatically or by a human operator. In both cases, the machine is being operated at a low level of information processing in an open- or closed-loop control. Depending on the task and possible manipulated variables, either the position, speed or force is controlled for machines with translational movement (*e.g.*, presses, material testing apparatus or machine tools). Correspondingly for rotating machines, the angle, speed or torque is controlled (*e.g.*, electric engines, industrial robots, combustion engines, test stands for engines or vehicles).

In order to look at some general properties of these two different kinds of control, the coupling of a power-generating machine with a power-consuming machine is analyzed, see Figure 6.3. The rules for connecting process elements (Chapters 2 and 4) are applied and only feedforward control is regarded.

The power supply of the power-generating machine is controllable by the control input  $U_c$ , either as a potential or flow source. In the following example, a DC motor and a centrifugal pump are considered. The pump feeds a liquid into a pipe with a constant throttle dimension at a volume flow rate  $\dot{V}$ . (The required torque can be approximated by  $T = k_m \omega^2$ .) The following steady state characteristics are drawn for idealized cases.

Figure 6.3a shows the scheme with one- and two-port. Accordingly, two operating modes of this machine can be distinguished:

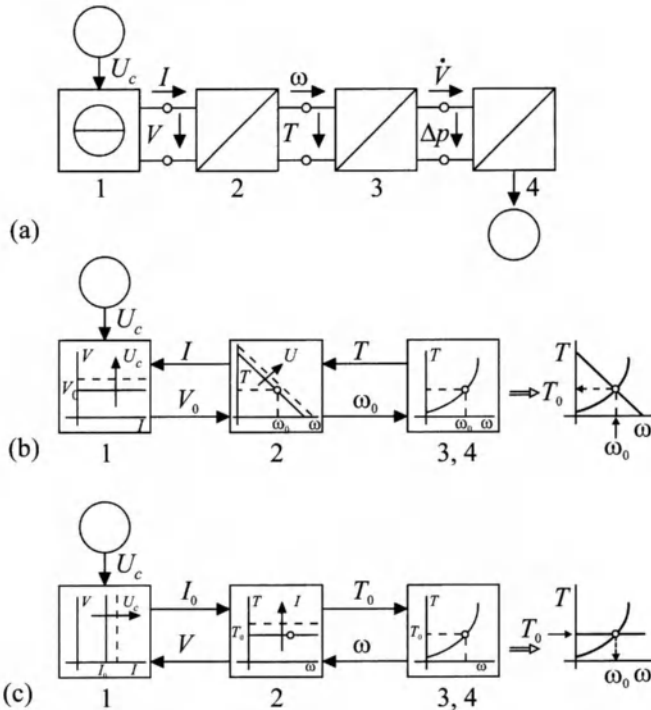


**Figure 6.3.** Connection of a controlled power-generating machine (e.g., DC motor) with a power-consuming machine (e.g., circular pump). Idealized characteristics for 1, 2: (a) block diagram of the one- and two-ports. 1: energy source, 2: power-generating machine (DC engine), 3: power-consuming machine (circular pump), 4: sink (pipe); (b) signal flow and characteristics for *speed manipulation*  $\omega_0 = f(U_c)$  with simplified characteristics. 1: voltage source, 2: speed-manipulated power-generating machine, 3,4: speed-manipulated power-consuming machine with sink; (c) signal flow and characteristics for *torque manipulation*  $T_0 = f(U_c)$  with simplified characteristics. 1: current source, 2: torque-manipulated power-generating machine, 3,4: torque-manipulated power-consuming machine with sink

### a) Speed manipulation

As shown in Figure 6.3b, it is possible to adjust the voltage  $V_0$  of the voltage source with the manipulated variable input  $U_c$ . The voltage  $V_0$  is applied (impressed) on the DC motor. Depending on the  $T(\omega)$  characteristic of the motor, a certain speed  $\omega$  is applied on the power-consuming machine. According to their  $T(\omega)$  characteristic, a torque acts back to the motor. An equilibrium point is reached for the same  $T_0$ ,  $\omega_0$ , i.e., the intersection point of both characteristics. The motor torque  $T_0$  then determines the current  $I_0$  of the voltage source. Hence, the manipulated variable  $U_c$  determines primarily the speed and the torque is a dependent variable.

### b) Torque manipulation

As shown in Figure 6.3c, the current  $I_0$  of the DC motor is adjusted by the manipulated variable  $U_c$ . The current  $I_0$  is applied on the motor, generating a certain torque  $T_0$ . This torque  $T_0$  acts on the power-consum-

ming machine, and according to its  $T(\omega)$  characteristic, a speed  $\omega$  results in the intersection point of the two characteristics. This speed  $\omega_0$  acts back on the motor and determines the voltage  $V_0$  of the current source. Hence, the manipulated variable  $U_c$  primarily determines the torque and the speed is a dependent variable.

This example also shows that the kind of source with applied voltage or applied current determines the causality of the motor, the working machine and their sink. This results in a unique cause-effect relation of the overall systems, as shown by Example 2.4.

The two discussed operating principles are typical for many machines and vehicles. Further examples are:

- *speed manipulation*: machines tools, industrial robots, lifts, actuators;
- *torque manipulation*: combustion engine in vehicles, hydraulic motors, ships, trains, aircraft.

### b) Mathematical models of machines

A machine consisting of a power engine, a drivetrain and a power-consuming machine is shown in Figure 6.4. The drivetrain consists of a belt drive or an elastic clutch, a shaft and a gearbox. Table 6.1 summarizes the mathematical models of some components, which are partly derived in Chapters 4 and 5. Shafts are modeled as two-mass systems. Several components are described by linear differential equations. The friction of plain bearings and guidances can be described by a direction-dependent torque

$$T_{F1}(t) = T_{F10} \operatorname{sign}\dot{\phi}(t) + T_{F11} \dot{\phi}(t) \quad (\dot{\phi}(t) \neq 0) \quad (6.1.1)$$

$T_{F10}$  is the Coulomb friction coefficient (dry friction) and  $T_{F11}$  is the viscous friction coefficient (see Section 4.7). The model of the complete machine may be derived as shown in detail in Chapter 2 by:

- stating the equations of the process elements (balance equations, constitutive equations and phenomenological equations);
- stating the interconnection equations (continuity equations for parallel systems and compatibility equations for serial systems);
- defining the inputs and outputs.

In simple cases, the equations may be solved by eliminating non-interesting variables, resulting in the differential equation for the input/output behavior, see also Chapter 4. Generally, it is more convenient to write the equations in the form of a vector differential equation. If all partial models can be linearized, an  $n^{\text{th}}$  order state vector and a state model follows.

Table 6.1. Mathematical models for the dynamic behavior of several mechanical components

components	equations for dynamic behavior	symbols
DC motor	$J_M \ddot{\omega} = T_M - T_e - T_R - T_L$ $= \Psi I_A$ $= T_{\text{no}} \text{ sign } \omega + T_F \omega$ $L_A \dot{I}_A + R_A I_A = V_A - \Psi \omega$	$J_M$ $L_A$ $R_A$ $\Psi$ $T_F$ $T_L$ $\omega$
shaft	$J_1 \ddot{\Phi}_1 = c_s (\Phi_2 - \Phi_1) + d_s (\dot{\Phi}_2 - \dot{\Phi}_1) + T_1$ $J_2 \ddot{\Phi}_2 = c_s (\Phi_1 - \Phi_2) + d_s (\dot{\Phi}_1 - \dot{\Phi}_2) + T_2$	$J_1, J_2$ $c_s$ $d_s$
belt drive	$J_3 \ddot{\Phi}_3 = c_{DT} (i_1 \Phi_4 - \Phi_3) + d_{DT} (i_1 \dot{\Phi}_4 - \dot{\Phi}_3) + T_3$ $J_4 \ddot{\Phi}_4 = c_{DT} (\Phi_3 - i_1 \Phi_4) + d_{DT} (\dot{\Phi}_3 - i_1 \dot{\Phi}_4) + T_4$	$J_3, J_4$ $c_{DT}$ $d_{DT}$ $i_1 = i_o/(1-s)$ $s$ $d_{w3}, d_{w4}$ $i_0 = d_{w4}/d_{w3}$ $\text{gear ratio}$ $\text{ratios of inertia}$ $\text{torsional stiffness}$ $\text{damping coefficient}$
gear $\Phi_5$	$J_5 \ddot{\Phi}_5 = -c_g (\Phi_6 - i_g \Phi_5) + d_g (\dot{\Phi}_6 - i_g \dot{\Phi}_5) + T_5$ $J_6 \ddot{\Phi}_6 = [c_g (-i_g \Phi_5 - \Phi_6) + d_g (-i_g \dot{\Phi}_5 - \dot{\Phi}_6)] l_g + T_6$	$i_g = r_d/r_s$ $c_g J_s$ $d_g$ $\text{gear ratio}$ $\text{ratios of inertia}$ $\text{stiffness}$ $\text{damping coefficient}$
roller bearing	$T_7 = T_{\text{no}} \text{ sign } \omega_7 + T_F \omega_7 + T_{F3} \dot{\omega}_7$	$T_{F3}$ $T_F$ $\omega_7 = \dot{\omega}_7$ $T_7$ $\text{friction coefficient}$ $\text{angular speed}$

$$\dot{\mathbf{x}}^T(t) = [\dot{\varphi}_1(t)\varphi_1(t)\dot{\varphi}_2(t)\varphi_2(t) \dots \dot{\varphi}_n(t)\varphi_n(t)] \quad (6.1.2)$$

$$\dot{\mathbf{x}}(t) = \mathbf{A} \mathbf{x}(t) + \mathbf{b} u(t) + \mathbf{f} z(t) \quad (6.1.3)$$

$$y(t) = \mathbf{c}^T \mathbf{x}(t) \quad (6.1.4)$$

The transfer function with  $u(t)$  as the input and  $y(t)$  as the output can be deduced from the state model as follows:

$$G_P(s) = \frac{y(s)}{u(s)} = \mathbf{c}^T [s \mathbf{I} - \mathbf{A}]^{-1} \mathbf{b} = \frac{B(s)}{A(s)} \quad (6.1.5)$$

From this transfer function, the differential equation of the complete machine can be derived by reverse Laplace transformation.

$$a_n y^{(n)}(t) + \dots + a_1 y^{(1)}(t) + y(t) = b_0 u(t) + \dots + b_m u^{(m)}(t) \quad (6.1.6)$$

In many cases, the model may be simplified. For closed-loop control design, the high frequency modes can be ignored and for vibrational problems the lower frequency modes may not be of interest. A physically based reduction of the model should be preferred. Generally, only the poles and zeros within the frequency ranges of interest are taken into account.

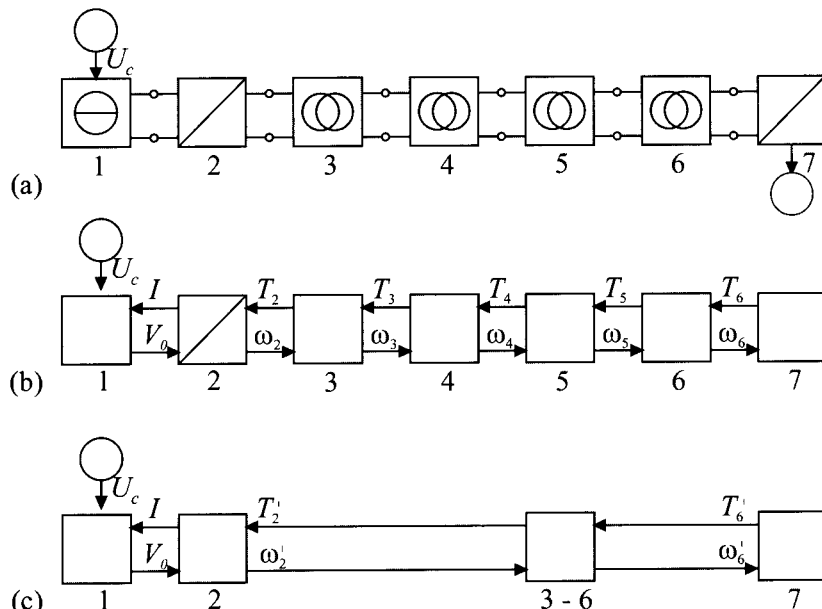


**Figure 6.4.** Schematic diagram of a machine consisting of a power-generating machine, drivetrain and a power-consuming machine; 1. energy source, 2. electrical motor, 3. belt drive, 4. shaft, 5. gearbox, 6. spindle, 7. working process: (a) block diagram of the components as one- and two-ports; (b) block diagram for speed manipulation; (c) block diagram for speed manipulation with simplified models for 3–6

Mathematical models of mechanical systems and machines often show the following characteristics:

- shafts can be linearized;
- bearings and guidances can be linearized if the motion is unidirectional. The Coulomb (dry) friction generates a hysteresis when changing the direction of motion. This requires a non-linear model. It is possible to work with direction-dependent linear models as it is done for positioning tasks, Maron (1991), Raab (1993);
- power-generating machines and power-consuming processes often have non-linear behavior. In such cases, it is possible to combine non-linear characteristics for the steady state behavior and linear models for the dynamic behavior. These combined models are then operating point-dependent linear models;
- some parameters are known with sufficient accuracy (masses, stiffness), other parameters like damping, friction, inertia or load are not well known and often underlie changes during operation;
- for complex systems ( $8 \leq n \leq 20$ ), it is advisable to use computational tools to generate the mathematical models (e.g., computer algebra).

Examples of generating a model and of linking components to a machine are described in Sections 6.3 and 6.4, see also Laschet (1988).

## 6.2 CHARACTERISTICS AND STABILITY OF MACHINES

Now, the characteristic behavior and the stability of machines is analyzed using fundamental equations, block diagrams and characteristics. A circular pump driven by a DC motor as shown in Figure 6.5 is used as an example. The circular pump delivers water in a higher reservoir with geodetic height  $H$  above the pump. The following presentation is based on Profos (1982) and Isermann (1984).

The steady state characteristics of the pump and the steady state characteristic of the pipe and reservoir are shown in Figures 6.6a and b. In the equilibrium and for a specific speed  $n$ , an operating point, with specific pressure  $\Delta P$  and mass flow  $\dot{m}$ , is derived from the intersection of both characteristics, see Figure 6.6c.

Now, the dynamic behavior of the mass flow  $\dot{m}(t)$  is analyzed. Therefore, we assume the dynamic behavior of the pump and of the DC motor to be negligible. Under this assumption

$$m \frac{dv(t)}{dt} = A [\Delta P_p(t) - \Delta P_L(t)] \quad (6.2.1)$$

$$\dot{m}(t) = A \rho v(t) \quad (6.2.2)$$

$$T_I \frac{d\dot{m}(t)}{dt} = \Delta P_p(t) - \Delta P_L(t) \quad (6.2.3)$$

$$T_I = l/A \quad (6.2.4)$$

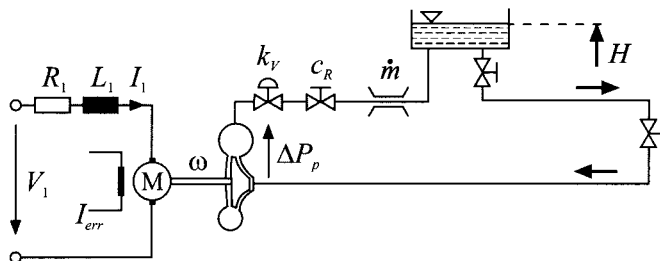


**Figure 6.5.** Scheme of a circular pump with separately excited DC motor

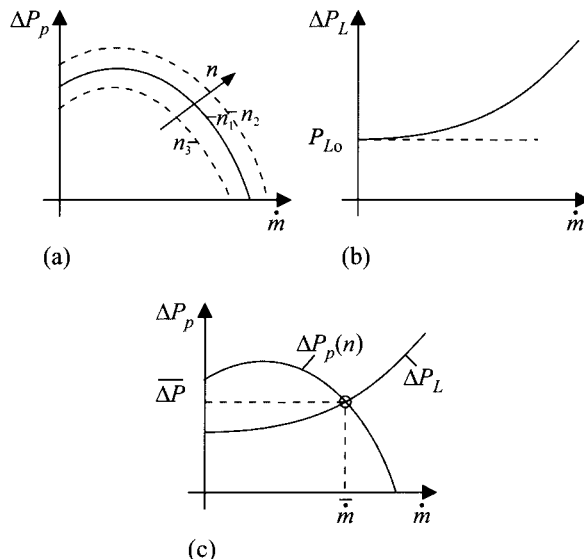


**Figure 6.6.** Characteristics: (a) pump  $\Delta P_p(\dot{m}, n)$ ; (b) pipe  $\Delta P_L(\dot{m})$ , static pressure  $P_{L0} = \rho g H$ ; (c) pump and pipe with operating point  $\bar{\Delta P}, \bar{\dot{m}}$

The pressure difference of the pump is

$$\Delta P_p = \Delta P_p(U, \dot{m}) \quad (6.2.5)$$

$$\Delta P_L = \rho g H + \zeta \frac{\rho}{2} v^2 \quad (6.2.6)$$

with

$U$  manipulated variable for the pump speed

$\zeta$  flow resistance coefficient of the transmission line (pipe).

From (6.2.3), (6.2.5) and (6.2.6), the block diagram shown in Figure 6.7 follows. The summing point represents the balance equation, the resistance characteristic represents a *first feedback* on the momentum storage (resistance), the pump characteristic a *second feedback* (drive: dependence on the mass flow) and the characteristic  $\Delta P_p(U)$  a feedforward input action (drive: dependence on the manipulated variable).

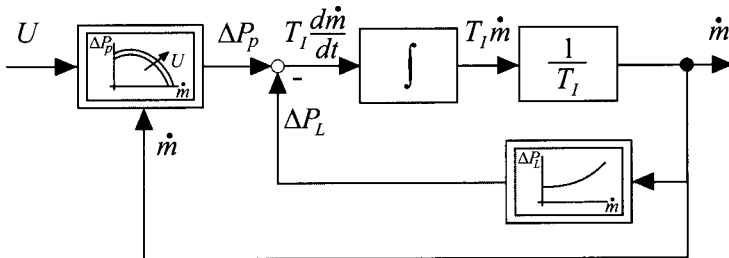


**Figure 6.7.** Block diagram for the dynamic behavior of the pump system with mass flow  $\dot{m}$  as output and the manipulated variable  $U$  (speed) as input

This block diagram is often encountered with machines. Figure 6.8 shows a corresponding block diagram with the following generalized variables

- $Y \triangleq \dot{m}$  output signal
- $\dot{Q}_s \triangleq T_I \dot{m}$  stored variable (momentum)
- $\dot{Q}_i, \dot{Q}_o$  input and output flow of the storage.

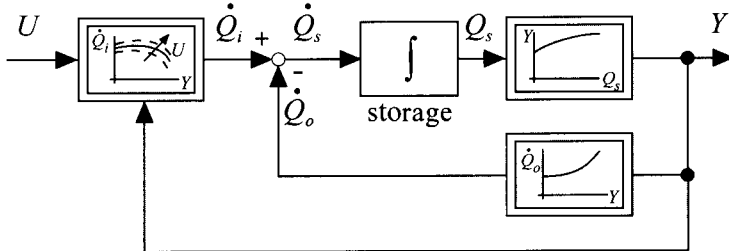


**Figure 6.8.** Block diagram of a proportional acting dynamic process

The process is proportional acting of first order. The constitutive and phenomenological equations complement the balance equation of the momentum by the following effects:

- $Y = f(Q_s)$  feedforward on the output
- $\dot{Q}_o = g(Y)$  feedbackward on the output
- $\dot{Q}_i = h(Y)$  feedbackward on the input (with the input signal  $U$  as a parameter).

If the constitutive and phenomenological equations are slightly non-linear, they may be linearized around the operating point, Figure 6.9.

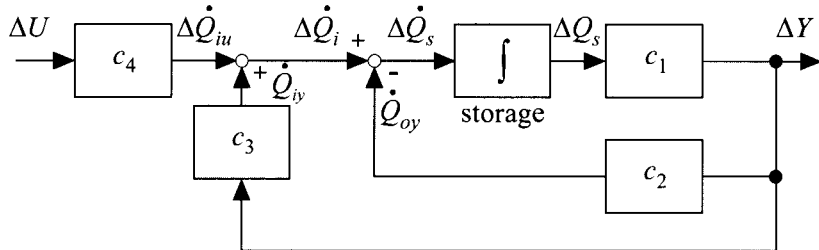


Figure 6.9. Linearized block diagram of Figure 6.8

The feedback by  $c_2$  is negative and influences the process as a stabilizing feedback, while the feedback by  $c_3$  is positive and therefore destabilizes.

Processes with proportional action are characterized by the fact that constant inputs  $U$  result in an equilibrium state (steady state) for all physical variables.

For  $U(t) = U = \text{const.}$  and therefore  $\Delta U(t) = 0$ , Figure 6.10 results from Figure 6.8. In the steady state, the following equations are valid:

$$\begin{aligned} Y(t) &= \text{const.} \rightarrow \frac{dY(t)}{dt} = 0 \\ Q_s(t) &= \text{const.} \rightarrow \frac{dQ_s(t)}{dt} = 0 \\ \Rightarrow \dot{Q}_i(t) &= \dot{Q}_o(t) \quad \text{resp.} \quad \bar{\dot{Q}}_i = \bar{\dot{Q}}_o \end{aligned} \quad (6.2.7)$$

Therefore, with these equations, Figure 6.11a results from Figure 6.10. In the steady state, the operating point results from the intersection of the characteristics  $\dot{Q}_i(Y)$  and  $\dot{Q}_o(Y)$ , Figure 6.10b.

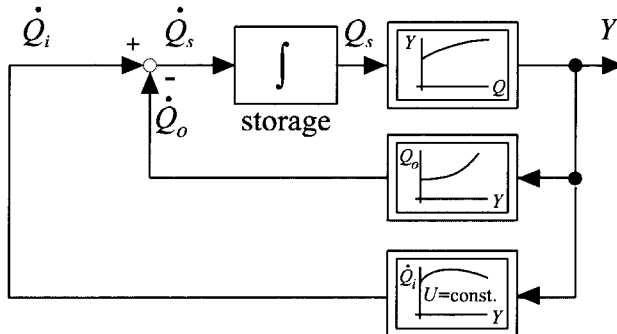


Figure 6.10. Block diagram of constant input variable  $U$

Now, the *stability* of the steady state of this linearized process is examined. It holds that

$$\dot{Q}_s = \dot{Q}_i(Y) - \dot{Q}_o(Y), \quad Y = f(Q_s) \quad (6.2.8)$$

The steady states lead to

$$\bar{Q}_s, \bar{Y}, \bar{\dot{Q}}_i = \bar{\dot{Q}}_o$$

$$Q_s(t) = \bar{Q}_s + \Delta Q_s(t)$$

$$\dot{Q}_s(t) = \frac{dQ_s(t)}{dt} = \frac{d\Delta Q_s(t)}{dt} = \Delta \dot{Q}_s(t)$$

$$\dot{Q}_i(t) = \bar{\dot{Q}}_i + \underbrace{\left( \frac{\partial \dot{Q}_i}{\partial Y} \right)}_{c_3} \Delta Y(t), \quad \dot{Q}_o(t) = \bar{\dot{Q}}_o + \underbrace{\left( \frac{\partial \dot{Q}_o}{\partial Y} \right)}_{c_2} \Delta Y(t)$$

$$Y(t) = \bar{Y} + \underbrace{\left( \frac{\partial Y}{\partial Q_s} \right)}_{c_1} \Delta Q_s(t) \quad (6.2.9)$$

Inserting in (6.2.8) yields

$$\Delta \dot{Q}_s(t) = \bar{\dot{Q}}_i + c_3 \Delta Y(t) - \bar{\dot{Q}}_o - c_2 \Delta Y(t)$$

and with

$$\Delta Y(t) = c_1 \Delta Q_s(t)$$

it follows that

$$\Delta \dot{Q}_s(t) + c_1(c_2 - c_3) \Delta Q_s(t) = 0 \quad (6.2.10)$$

or

$$\frac{1}{c_1} \Delta \dot{Y}(t) + (c_2 - c_3) \Delta Y(t) = 0 \quad (6.2.11)$$

which is a first order differential equation.

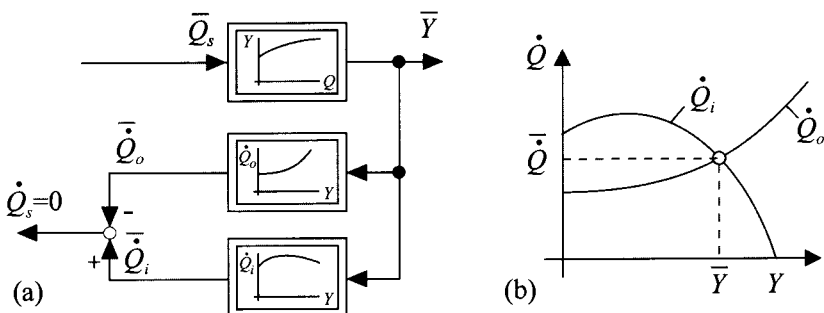


**Figure 6.11.** Process with proportional action in steady state: (a) signal flow diagram; (b) static characteristics of the process

Now, the *stability conditions* for the linear system are investigated. As it is a first order system, it is asymptotically stable according to the Hurwitz criterium if all parameters are present and have the same sign. With the assumption that  $c_1 > 0$ , the system is asymptotically stable if

$$c_2 > c_3 \text{ resp. } \frac{\partial \dot{Q}_o}{\partial Y} > \frac{\partial \dot{Q}_i}{\partial Y} \quad (6.2.12)$$

It is monotonously unstable if

$$c_2 < c_3 \text{ resp. } \frac{\partial \dot{Q}_o}{\partial Y} < \frac{\partial \dot{Q}_i}{\partial Y} \quad (6.2.13)$$

This means that the overall feedback  $\Delta \dot{Q}_s(t) = -c_1(c_2 - c_3)\Delta Q_s(t)$  must be negative, *i.e.*, the negative feedback must be greater than the positive feedback for the system to be stable. Therefore, for two possible intersections of the characteristics as shown in Figure 6.12, intersection *S* is stable and intersection *I* is unstable.

A *disturbance* causes the steady state characteristic  $\dot{Q}_i$  to shift in parallel by  $\Delta \dot{Q}_i$  for constant  $\dot{Q}_o$  as shown in Figure 6.13.

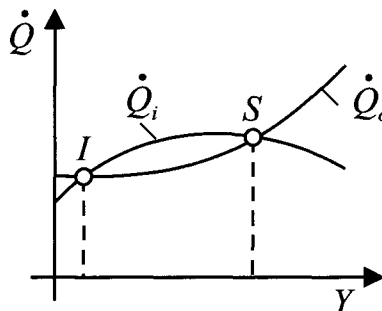


**Figure 6.12.** Static characteristic of a proportional action process and a stable steady state *S*:  $c_2 > c_3$  and an unstable steady state *I*:  $c_2 < c_3$

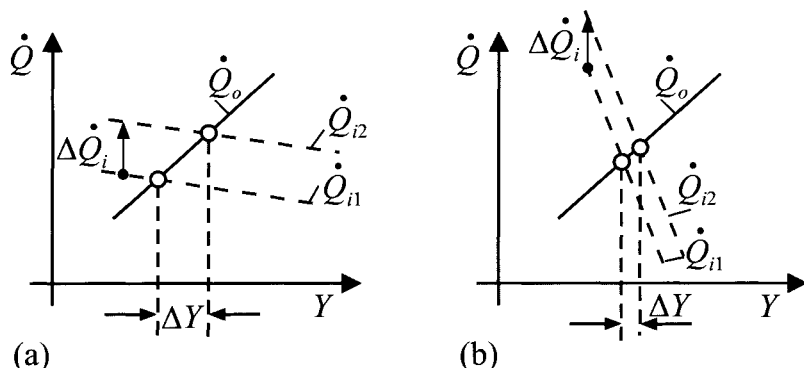


**Figure 6.13.** Influence of a disturbance  $\Delta \dot{Q}_i$  on  $Y$  for: (a) flat characteristic  $\dot{Q}_i$ ; (b) steep characteristic  $\dot{Q}_i$

The figure clearly shows that the influence of disturbances is wea-

ker the steeper the characteristics  $\dot{Q}_i$  and  $\dot{Q}_o$  are.

Now, the relationship between the intersection of the characteristics and the dynamic behavior is considered. In Figure 6.14, several stable, limit stable, and unstable intersections of characteristics are shown. It is assumed that  $c_1 = \text{const.} = 1$  (scale factor) and that the characteristic  $\dot{Q}_o$  has a constant gradient ( $c_2 = \text{const.}$ ). The systems are stable for  $c_2 - c_3 > 0$  and unstable for  $c_2 - c_3 < 0$ . The characteristics also give information about the relative dynamic transient behavior (eigen-behavior) as the poles are given by

$$s_1 = -\frac{1}{T} = -c_1(c_2 - c_3) \quad (6.2.14)$$

This follows from

$$T \Delta \dot{Y}(t) + \Delta Y(t) = 0 \quad (6.2.15)$$

$$T = \frac{1}{c_1(c_2 - c_3)} \quad (6.2.16)$$

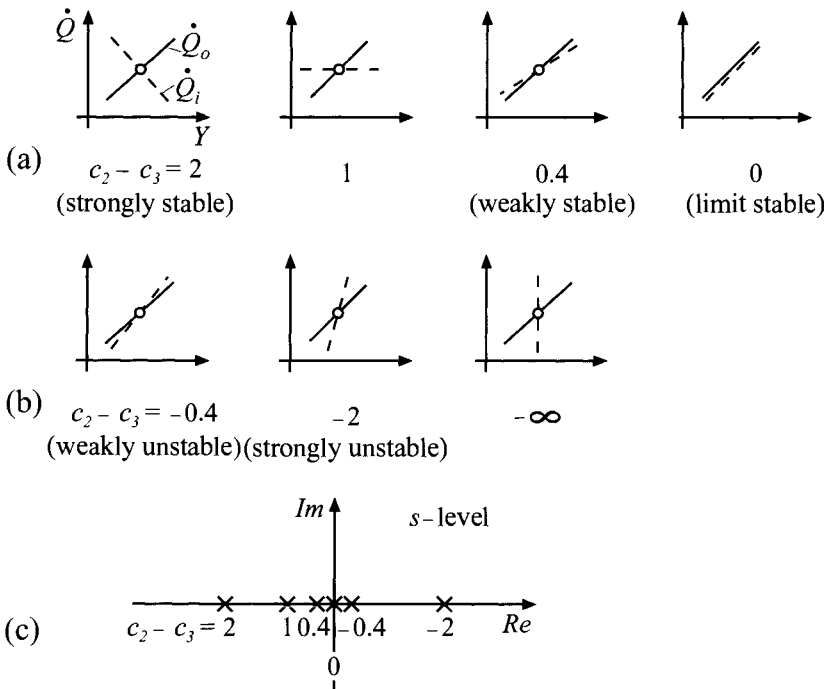


**Figure 6.14.** Various intersections of steady state characteristics for  $c_2 = \text{const.}$ : (a) stable steady state, limit stable state; (b) unstable steady state; (c) corresponding relative pole positions

The position of the poles is relative because  $c_1$  cannot be derived from the steady state characteristics. If the negative and positive feedback is expressed as a function of the output of the storage

$$\dot{Q}_o = f(Q_s), \dot{Q}_o = h(Q_s)$$

and the following is therefore valid

$$\Delta \dot{Q}_o = c_1 c_2 \Delta Q_s = c_2' \Delta Q_s ; \Delta \dot{Q}_i = c_1 c_3 \Delta Q_s = c_3' \Delta Q_s \quad (6.2.17)$$

$c_2'$  negative feedback parameter

$c_3'$  positive feedback parameter

then it follows that

$$T \Delta \dot{Q}_s(t) + \Delta Q_s(t) = 0 \quad (6.2.18)$$

with the time constant

$$T = \frac{1}{c_2' - c_3'} = \frac{1}{\text{negative feedback parameter} - \text{positive feedback parameter}} \quad (6.2.19)$$

Then, the characteristics also reveal also information about the absolute dynamic behavior of the storage variable  $\Delta Q_s(t)$ .

Hence, the stability condition for asymptotic stability is

$$c_2' > c_3' \quad \begin{matrix} \text{negative feedback parameter} & \text{positive feedback parameter} \end{matrix} \quad (6.2.20)$$

In Figure 6.15, the stable intersection of the characteristics are shown again.

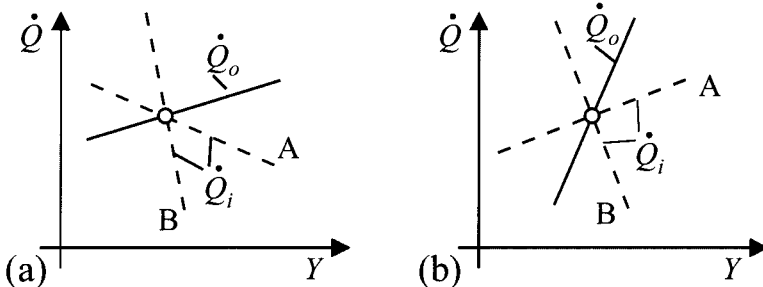


**Figure 6.15.** Stable characteristic intersections: (a) flat characteristics; (b) steep characteristics; A: strong influence by disturbance, slow dynamic transient; B: small influence by disturbance, fast dynamic transient

To achieve a small sensitivity towards disturbance and a fast dynamic transient response, case B should be selected. Therefore,  $(c_2 - c_3)$  should be large by using

- different signs of the gradients  $c_2$  and  $c_3$ ;
- steep characteristics.

Now, the transfer behavior according to Figure 6.9 is considered.

With

$$c_4 = \frac{\partial \dot{Q}_{eu}}{\partial U} \quad (6.2.21)$$

it follows that, according to (6.2.10), (6.2.14),

$$T\Delta \dot{Q}_s(t) + \Delta Q_s(t) = K_1 \Delta U(t)$$

or

$$T\Delta \dot{Y}(t) + \Delta Y(t) = K_2 \Delta U(t) \quad (6.2.22)$$

with

$$T = \frac{1}{c_1(c_2 - c_3)}; \quad K_1 = \frac{c_4}{c_1(c_2 - c_3)}; \quad K_2 = \frac{c_4}{c_2 - c_3} \quad (6.2.23)$$

If the constants from (6.2.9)

$$c_1 = \frac{\Delta Y}{\Delta Q_s}; \quad c_2 = \frac{\Delta \dot{Q}_{oy}}{\Delta Y}; \quad c_3 = \frac{\Delta \dot{Q}_{iy}}{\Delta Y}$$

are inserted in (6.2.23), the time constant may be interpreted as

$$T = \frac{1}{c_1(c_2 - c_3)} = \frac{\Delta Q_s(t)}{\Delta \dot{Q}_{oy}(t) - \Delta \dot{Q}_{iy}(t)}$$

and with the variables in the steady state (SS) after a transient

$$\begin{aligned} T &= \frac{1}{c_1(c_2 - c_3)} = \frac{\Delta Q_s(\infty)}{\Delta \dot{Q}_{oy}(\infty) - \Delta \dot{Q}_{iy}(\infty)} \\ &= \frac{\text{change of the storage variable in SS}}{\text{change (inflow - outflow) through feedback in SS}} \end{aligned} \quad (6.2.24)$$

A special case appears if  $c_3 = 0$ , i.e., no positive feedback exists. Now, the time constant becomes

$$T = \frac{1}{c_1 c_2} = \frac{\Delta Q_s(\infty)}{\Delta \dot{Q}_{oy}(\infty)} = \frac{\text{change of storage variable in SS}}{\text{change of the outflow in SS}} \quad (6.2.25)$$

This equation is identical to (2.4.63).

The initial gradient of the transient function is  $\Delta \dot{Y}(t) = c_1 c_4 \Delta U(0)$ .

The initial gradient is therefore independent of the feedback elements and is only influenced by the feedforward-acting elements, Figure 6.9.

Until now, the dynamic was of first order. For a second order system, the results so far remain unchanged. For a third order system or even higher orders, see Figure 6.16, further stability examinations have to be included, see Profos (1982).

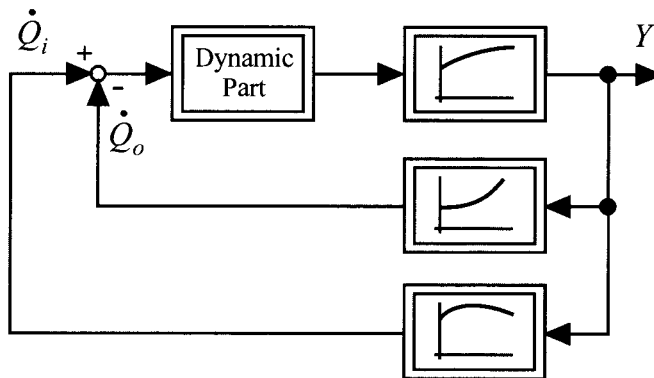


**Figure 6.16.** Simplified block diagram of a higher order non-linear process

### 6.3 STATIC BEHAVIOR OF POWER-GENERATING AND POWER-CONSUMING MACHINES

In the preceding section, the considerable influence of the static characteristics of sources and sinks or power-generating and power-consuming machines on the operational performance of a variety of machines was shown. In the following, some typical shapes of characteristic curves are discussed.

Figures 6.17a–c show the full-load characteristics of power-generating machines, like electric motors (see Chapter 5), combustion engines and hydrostatic motors.

The shown curves represent the typical behavior of the corresponding machine. However, they are subject to modification by a specific machine design. DC motors produce maximum torque at standstill, asynchronous motors just below nominal speed, spark ignition and diesel engines at low or medium speed, whereas hydrostatic motors produce maximum torque at low speed. The considered machines correspond to the fact that torque lowers at high speed.

Power-consuming machines in general increase torque at high engine speed as shown in Figure 6.18. Exceptions to this rule are cutting turning machines, Spur, Stöferle (1979), and rolling mills, Leonhard (1996) and Meyer (1985).

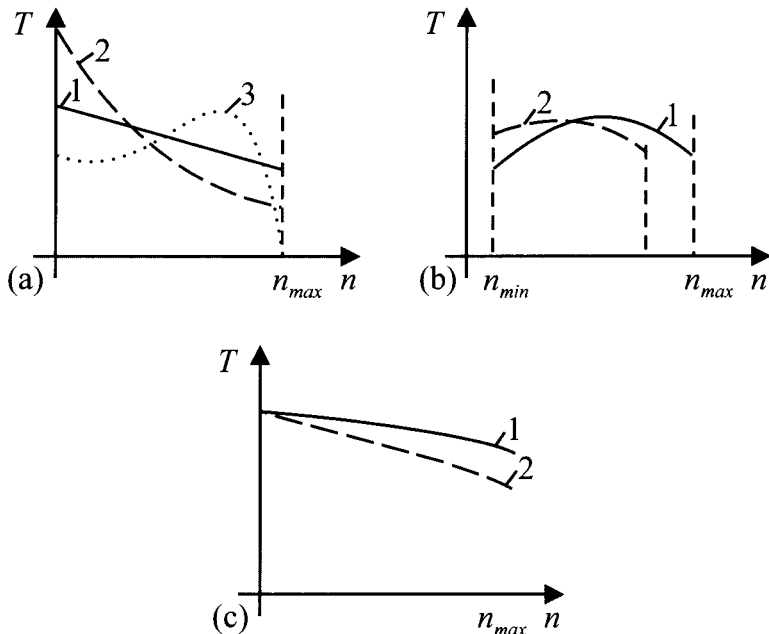


**Figure 6.17.** Full-load torque-speed characteristics of power-generating machines: (a) electric motors (full-load), 1 DC motor (shunt-wound), 2 DC motor (series-wound), 3 three-phase asynchronous motor; (b) combustion engines (full-load), 1 spark-ignition engine, 2 diesel engine; (c) hydrostatic motors, 1 hydraulic motor without throttle valve, 2 hydraulic motor with throttle valve

### Example 6.1. DC motor and circulation pump

The *coupling* of a power-generating machine to a power-consuming machine will be illustrated by considering a DC motor and a circulation pump, see Figure 6.5. The water of the lower tank is pumped through a pipe into a water tank at a higher level.

For the DC shunt motor, the dynamics of the armature circuit can be neglected ( $L = 0$ ). Equations (5.3.10) and (5.3.12) lead to:

$$R_A I_A(t) = V_A(t) - \Psi \omega(t) \quad (6.3.1)$$

$$I_{tot} \dot{\omega}(t) = T_{mech}(t) - T_P(t) \quad (6.3.2)$$

$$T_{mech}(t) = \Psi I_A(t) - T_{F1} \omega(t) \quad (6.3.3)$$

Using (6.3.3) and (6.3.1), the torque of the DC motor can be calculated

$$T_{mech}(t) = \frac{\Psi}{R_A} \left[ V_A(t) - \left( \Psi + \frac{R_A}{\Psi} T_{F1} \right) \omega(t) \right] \quad (6.3.4)$$

see (5.3.22).  $J_{tot} = J_M + J_P$  represents the total moment of inertia of the DC motor and circulation pump. Neglecting the dynamics of the water, the torque of the circulation pump is given by

$$T_P(t) = T_{P0} + T_{P1} \omega^2(t) \quad (6.3.5)$$

The resulting block diagram is shown in Figure 6.19 and corresponds to Figure 6.8. The torque characteristics of the power-consuming machine represents a negative feedback, whereas with the power-generating machines the characteristics lead to positive feedback.

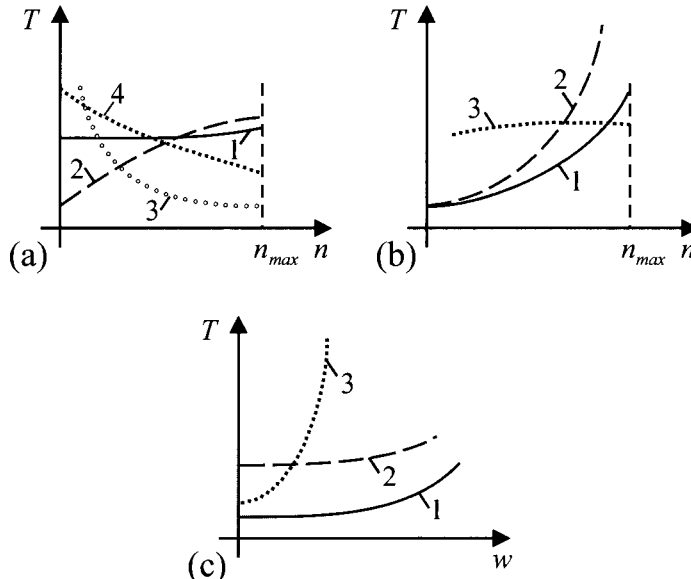


**Figure 6.18.** Full-load characteristics of power-consuming machines: (a) conveyor machines, reforming machines, and machine tools, 1 lifting appliance, cold mill (steel), 2 warm rolling mill, 3 turning machine, 4 cold rolling mill (aluminium); (b) turbo machines, 1 circular pump (constant delivery head), 2 circular pump (constant discharge port), 3 reciprocating piston pump; (c) vehicles, 1 passenger car, 2 truck, 3 ship

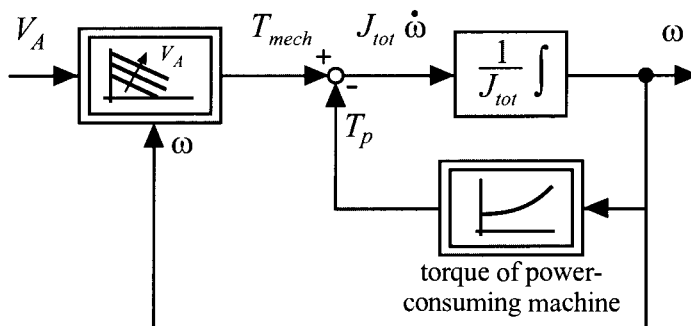


**Figure 6.19.** Simplified block diagram of the dynamics of a DC motor and circulation pump, considering the armature voltage as a manipulated variable

In order to provide an asymptotically stable system behavior the following must be true, see (6.2.12)

$$\left. \frac{\partial T}{\partial n} \right|_{\text{power-consuming machine}} > \left. \frac{\partial T}{\partial n} \right|_{\text{power-generating machine}} \quad (6.3.6)$$

In the considered example, the system behavior of the (uncontrolled) engine is therefore stable on principle. □

### **Example 6.2. Characteristics of a passenger car**

Figure 6.20 shows the torque characteristics of a passenger car with spark-ignition engine and manual transmission (six cylinders; 2.5 l; 125 kW at 6000 rpm; 227 Nm maximum torque; total mass 1250 kg). Figure 6.20a shows the torque characteristics at the clutch for various throttle angles  $\alpha$  depending on the engine speed. The torque curve at full load ( $\alpha = 90^\circ$ ) is quite flat, whereas for smaller throttle angles, engine torque decreases with increasing engine speed. In Figure 6.20b, the engine torque at the transmission output shaft for full load and various road gradients is given. For a road gradient of 0%, the point of intersection of the characteristic curve of the fifth gear gives the maximum speed of 233 km/h. Maximum speed in the fifth gear reduces with increasing road gradients to 200 km/h and 170 km/h for road gradients of 3% and 5% respectively.

In the fifth gear, a further increase of the road gradient from 5% to 7% leads to a speed drop to values between 85 km/h and 50 km/h. Exact values cannot be given due to the parallel curves in this region. A downshift to the fourth gear results in a smaller speed drop from 187 km/h to 153 km/h.

A downshift to the fourth gear results in a higher speed of 187 km/h at a road gradient of 5%, and reduces to 153 km/h at 7% road gradient, *i.e.*, the speed loss is less than in the fifth gear. For the first, second and third gear, no points of intersection exist for the considered road gradients of up to 10% and the considered engine speed, which is limited by the overspeed governor. The respective torque difference is available for accelerating the vehicle.

Figure 6.20c gives the torque characteristics for partial load (throttle angle 30°). Due to the larger decline of the engine torque at partial load, stable operating conditions also exist for the lower gears; for better clarity the characteristic curves of the first, second and fourth gear only are depicted.

The points of intersection indicate the stationary speed values shown in Table 6.2. Due to the steeper curve shapes of the driving torque after the transmission, the lower the gear, the smaller is the influence of a change of the characteristic curve on a change of the operating condition, see Figure 6.15, case B.

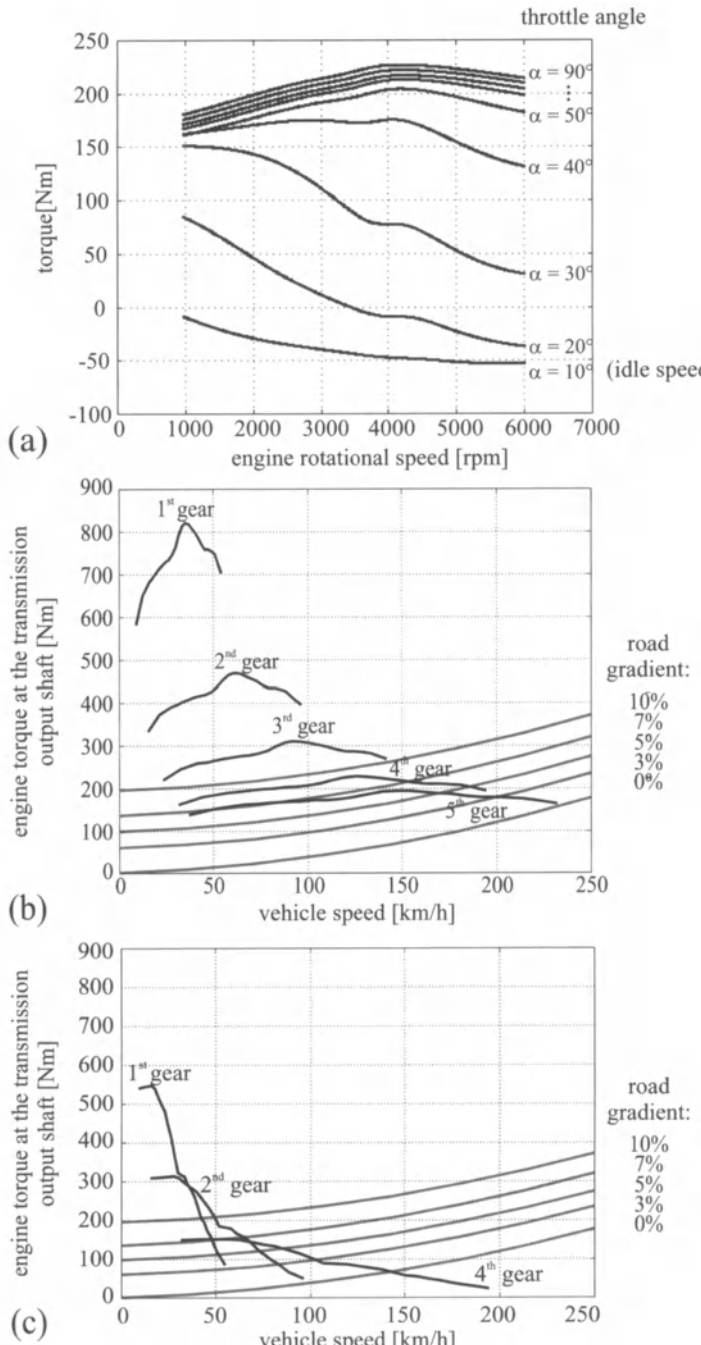


**Figure 6.20.** Torque characteristics of engine and vehicle of a passenger car with spark-ignition engine: (a) torque at the clutch of a six-cylinder spark-ignition engine, as a function of the crankshaft rotational speed for various throttle angles  $\alpha$ ; (b) torque characteristics at the transmission output shaft at full load ( $\alpha = 90^\circ$ ); (c) torque characteristics at the transmission output shaft at partial load ( $\alpha = 30^\circ$ )

**Table 6.2.** Influence of gear on the change of vehicle speed as a result of a change in the road gradient (at throttle angle  $\alpha = 30^\circ$ )

road gradient	5%	7%	change of vehicle speed [km/h]
vehicle speed [km/h]	fourth gear	867351	536547
	second gear		33
	first gear		8
			4

□

The characteristic curves of power-generating and power-consuming machines indicate which combinations are favorable. A favorable system behavior is based on a “small disturbing influence” and a “fast transient response”, which requires the characteristic curves in Figure 6.15 to have opposite sign and steep slopes, according to (6.3.6). Considering power-consuming machines, the torque characteristics of turning machines and rolling mills are unfavorable. For power-generating machines, the torque characteristics of the asynchronous motor are poor for engine speeds smaller than the pull-out speed, for spark ignition engines the torque characteristics are unfavorable at low engine speed. Table 6.3 comments on some combinations of power-generating and power-consuming machines.

**Table 6.3.** System behavior of combinations of power-generating and power-consuming machines as a result of torque characteristics.

power-consuming machine	power-generating machine	comments
circular pump or lifting appliance	DC motor asynchronous motor combustion engine	favorable favorable favorable
reciprocating pump	DC motor asynchronous motor combustion engine	still favorable still favorable unfavorable
cold rolling mill	DC motor asynchronous motor	unfavorable favorable for $n > n_{\text{pull-out}}$
turning machine	DC motor asynchronous motor	stable only for large $n$ favorable for $n > n_{\text{pull-out}}$

## 6.4 DYNAMIC MODEL OF A COMBUSTION ENGINE TEST STAND

As an example of dynamic behavior of a machine, in the following a combustion engine test stand is studied. Figure 6.21 shows the arrangement of a dynamic engine test stand. It consists of a DC motor, a spring

shackle clutch, a belt transmission, a torque transducer and a flange to couple the combustion engine. The dynamometer applies a dynamic load torque on the combustion engine, which corresponds, e.g., to a specific emission test cycle with gear shifts. Due to this, the torque control of a dynamic engine test stand must be very fast and accurate. Hence, for the design of the controller and for the compensation of the dynamics of the drivetrain with the DC motor, a very accurate mathematical model is required. The input signal of the model is the armature current, the output signal is the torque at the torque transducer, Voigt (1991), Pfeiffer (1997).

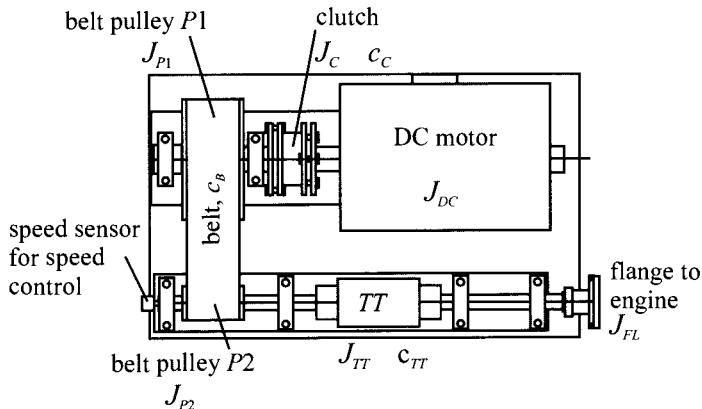


Figure 6.21. Arrangement of the engine test stand

Figure 6.22 shows the equivalent circuit diagram with five ratios of inertia. The Coulomb friction at the roller bearings is modeled as viscous friction. The resulting block diagram is shown in Figure 6.23, where with regard to the angles of torsion, only the relative rotation angles are relevant.

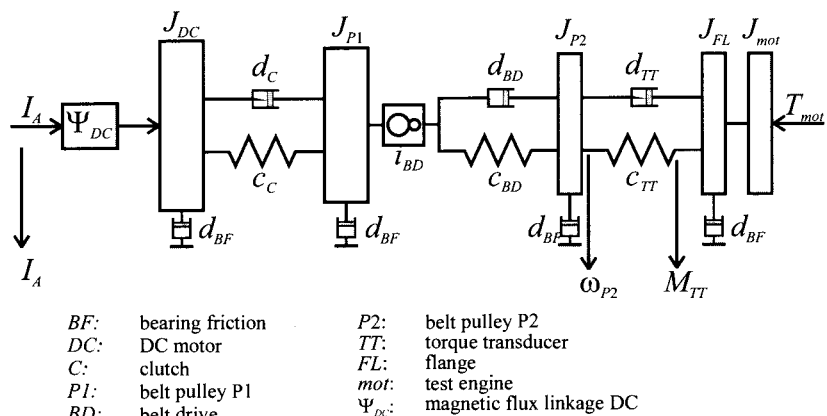


Figure 6.22. Equivalent circuit diagram of the mechanical part of the engine test stand

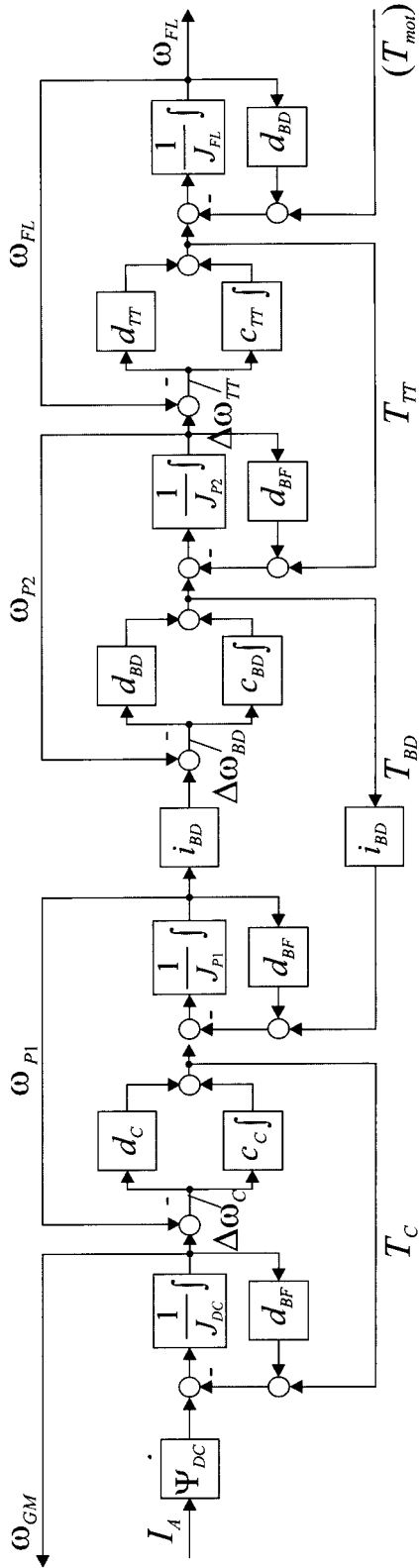


Figure 6.23. Block diagram of the mechanical parts of a combustion engine test stand

The dynamic behavior can be described with a linear state space model

$$\dot{\mathbf{x}}(t) = \mathbf{A} \mathbf{x}(t) + \mathbf{b} u(t) + \mathbf{g} n(t) \quad (6.4.1)$$

$$\mathbf{y}(t) = \mathbf{C} \mathbf{x}(t) \quad (6.4.2)$$

with

$$\begin{aligned} u(t) &= I_A(t) & n(t) &= T_{mot}(t) \\ \mathbf{x}^T(t) &= \left[ \omega_{FL}(t) \Delta\varphi_{TT}(t) \omega_{P2}(t) \Delta\varphi_{BD}(t) \omega_{P1}(t) \Delta\varphi_C(t) \omega_{DC}(t) \right] \\ \mathbf{y}^T(t) &= \left[ T_{TT}(t) \omega_{P2}(t) \right] \end{aligned} \quad (6.4.3)$$

$$\mathbf{A} = \begin{bmatrix} -\frac{d_{TT}+d_{BF}}{J_{FL}+J_{mot}} & \frac{c_{TT}}{J_{FL}+J_{mot}} & \frac{d_{TT}}{J_{FL}+J_{mot}} & 0 & 0 & 0 & 0 \\ -1 & 0 & 1 & 0 & 0 & 0 & 0 \\ \frac{d_{TT}}{J_{P2}} & -\frac{c_{TT}}{J_{P2}} & -\frac{d_{BD}+d_{TT}+d_{BF}}{J_{P2}} & \frac{c_{BD}}{J_{P2}} & \frac{i_{BD}d_{BD}}{J_{P2}} & 0 & 0 \\ 0 & 0 & -1 & 0 & i_{BD} & 0 & 0 \\ 0 & 0 & \frac{i_{BD}d_{BD}}{J_{P1}} & -\frac{i_{BD}c_{BD}}{J_{P1}} & -\frac{i_{BD}^2d_{BD}+d_C+d_{BF}}{J_{P1}} & \frac{c_C}{J_{P1}} & \frac{d_C}{J_{P1}} \\ 0 & 0 & 0 & 0 & -1 & 0 & 1 \\ 0 & 0 & 0 & 0 & \frac{d_C}{J_{DC}} & -\frac{c_C}{J_{DC}} & -\frac{d_C+d_{BF}}{J_{DC}} \end{bmatrix} \quad (6.4.4)$$

$$\begin{aligned} \mathbf{b}^T &= \left[ 0 \ 0 \ 0 \ 0 \ 0 \ 0 \ \frac{\Psi_{DC}}{J_{DC}} \right] \\ \mathbf{g}^T &= \left[ \frac{1}{J_{FL}+J_{mot}} \ 0 \ 0 \ 0 \ 0 \ 0 \ 0 \right] \\ \mathbf{C} &= \left[ \begin{matrix} 0 & c_{TT} & 0 & 0 & 0 & 0 & 0 \\ 0 & 0 & 1 & 0 & 0 & 0 & 0 \end{matrix} \right] \end{aligned} \quad (6.4.5)$$

The transfer function consists of elements of the transfer function matrix

$$\mathbf{G}(s) = \mathbf{C}(s)[sI - \mathbf{A}]^{-1} \mathbf{b} \quad (6.4.6)$$

Considering  $I_A(s)$  and  $T_{TT}(s)$  as input and output signals, the model is seventh order

$$G_{IT}(s) = \frac{T_{TT}(s)}{I_A(s)} = \frac{b_0 + b_1 s}{1 + a_1 s + a_2 s^2 + \dots + a_7 s^7} \quad (6.4.7)$$

The parameters of the transfer function depend on the physical parameters of the system;  $a_1$ , for instance, can be calculated by

$$\begin{aligned}
 a_1 = & \frac{J_{DC} + J_{P1} + i_{BD}^2(J_{FL} + J_{mot} + J_{P2})}{2d_{BF}(i_{BD}^2 + 1)} + \frac{2d_{BF} + d_{BD}(i_{BD}^2 + 1)}{c_{BD}(i_{BD}^2 + 1)} \\
 & + \frac{2d_{TT}(i_{BD}^2 + 1) + d_{BF}(i_{BD}^2 + 2)}{2c_{TT}(i_{BD}^2 + 1)} + \frac{2d_C(i_{BD}^2 + 1) + d_{BF}(2i_{BD}^2 + 1)}{2c_C(i_{BD}^2 + 1)} \quad (6.4.8)
 \end{aligned}$$

Figure 6.24 shows the poles and zeros of the transfer function. Three pairs of conjugate poles are obtained, as well as a real pole and a real zero, the latter are located close to each other. The zero is due to the derivative action of the damping friction  $d_{BF}$  on the right hand side of the torque transducer. Due to this friction, the pole at the origin (integral action) shifts to the left, resulting in the real pole with small negative value.

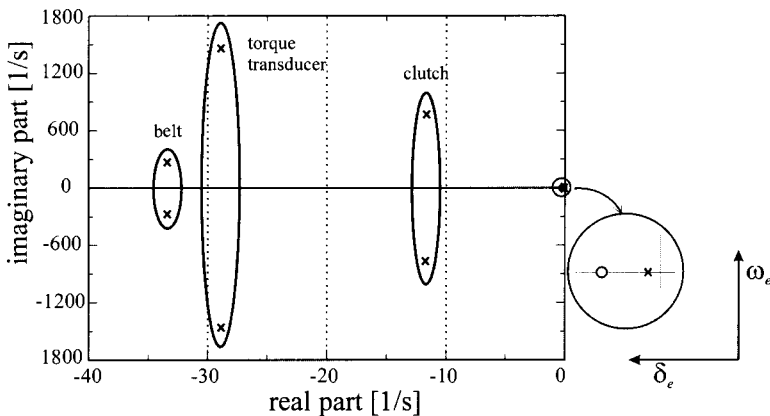


Figure 6.24. Poles and zeros of the transfer function of the engine test stand

The following natural angular eigen-frequencies can be distinguished:  $\omega_{e,C}$ : clutch;  $\omega_{e,TT}$  torque transducer;  $\omega_{e,BD}$ : belt.

The smallest damping coefficient (decay factor  $\delta$ ) is related to the clutch, the largest damping coefficient refers to the belt.

Considering the not-coupled elements as undamped second order oscillators, the characteristic frequencies can be calculated by

$$\begin{aligned}
 f_{0,C} &= \frac{1}{2\pi} \sqrt{\frac{c_C(J_{DC} + J_{P1})}{J_{DC}J_{P1}}} = 154.7 \text{ Hz (clutch)} \\
 f_{0,BD} &= \frac{1}{2\pi} \sqrt{\frac{c_{BD}(J_{P1} + J_{DC}) + i_{BD}^2(J_{P2} + J_{FL})}{(J_{P1} + J_{DC})(J_{P2} + J_{FL})}} = 34.5 \text{ Hz (belt)} \\
 f_{0,TT} &= \frac{1}{2\pi} \sqrt{\frac{c_{TT}(J_{P2} + J_{FL})}{J_{P2}J_{FL}}} = 229.6 \text{ Hz (torque transducer)} \quad (6.4.9)
 \end{aligned}$$

Figure 6.25 shows the measured frequency response of the system

without combustion engine. The three resonance frequencies of the belt (approximately 45 Hz), clutch (120 Hz) and torque transducer (250 Hz) can be clearly recognized. The results show good agreement with the measured frequency response, see Isermann *et al.* (1992), Pfeiffer (1997).

The obtained model allows the design of a digital torque control with the connected combustion engine, compensating the dynamics of the test stand with accurate powertrain models up to frequencies of 12 Hz.

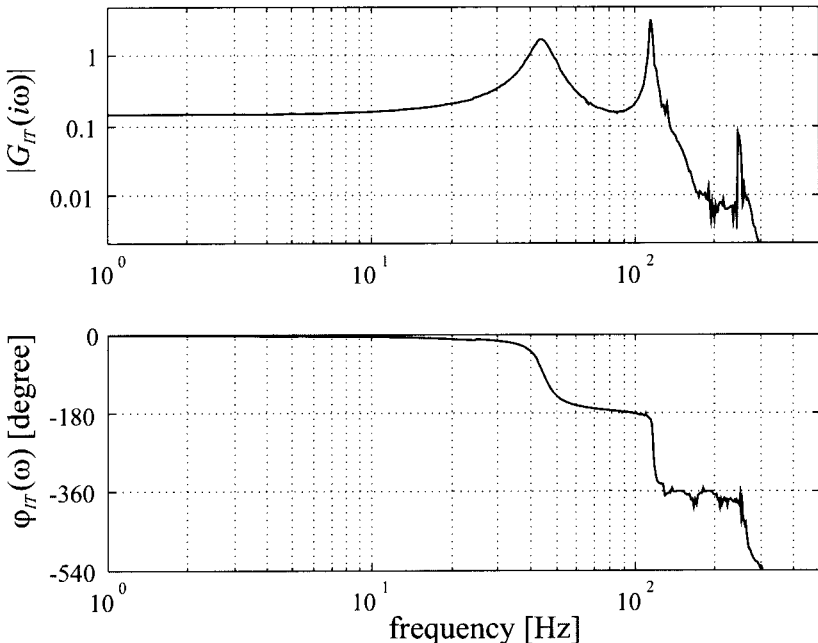


**Figure 6.25.** Measured frequency response of the mechanical part of the engine test stand for current  $I_A$  as input and the torque  $T_T$  as output

Further examples for the theoretical modeling and identification of the dynamic behavior of machines can be found in the following publications:

Grinding machines: Janik (1993), Fuchs (1992); cutting and drilling machines: Reiß (1993), Wanke (1993), Konrad (1997), Nolzen (1997); industrial robots: Specht (1989), Freyermuth (1993), Held (1992), Böhm (1994); vehicles: Germann (1997), Würtenberger (1997).

For the investigation of complex arrangements of rotating machinery, *e.g.*, large turbo generators with multi-stage steam turbines, finite-element methods are applied, see, *e.g.*, Schwibinger, Nordmann (1990), Gasch *et al.* (2002).

## 6.5 DYNAMIC BEHAVIOR OF A MACHINE TOOL FEED DRIVE

### 6.5.1 A Feed Drive and its Components

For cutting and other machine tools, feed drives are used to move the machine table with high precision. The feed drives, usually controlled by a digital control unit, yield the feed motion per turn for the cutting process, Stute (1991), Weck (1982). In the case of, e.g., milling, the machine table carries the workpiece and, in the case of turning, the cutting tool. For the design of precise position and trajectory control and for model-based fault detection, accurate dynamic models of the feed drives are required. As an example, the x-feed drive as shown in Figure 6.26 is considered, which moves the workpiece in a horizontal direction, see Konrad (1997).

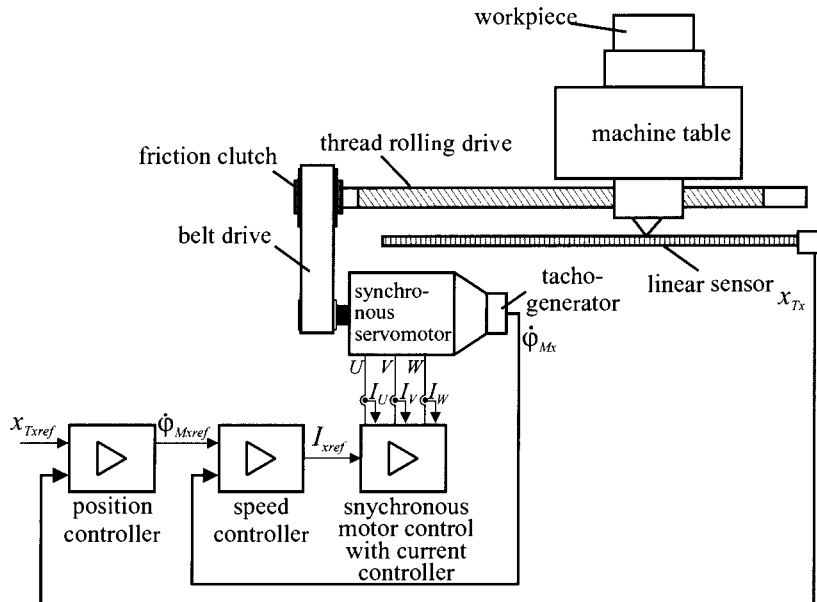


Figure 6.26. Scheme of the x-feed drive control

#### Servomotor

The servomotor used is a synchronous motor with constant excitation as described in Section 5.4.2. With some simplifying assumptions, the dynamic behavior can be described by a first order lag, compare (5.4.48)

$$G_{IT}(s) = \frac{T_{elx}(s)}{I_{xref}(s)} = \frac{\Psi_x}{1 + T_{1Mx}(s)}$$

### Mechanical transmission system

The mechanical part of the feed drive can be described as a system of coupled mass-spring oscillators that can be modeled based on coupling the elementary one-mass oscillation as described in Section 4.5. The feed drive consists of a motor shaft connected to a belt drive. The belt drive moves the feed screw by a friction clutch. The feed screw converts the rotational motion into translational motion and moves the machine table sitting on the feed screw nut. It consists of the belt drive with the rotational mass of the motor with the first pulley, the rotational mass of the second pulley and thread spindle and the translational mass of the thread drive screw and the machine table. Then, a three-mass oscillator results as shown in Figure 6.27a.

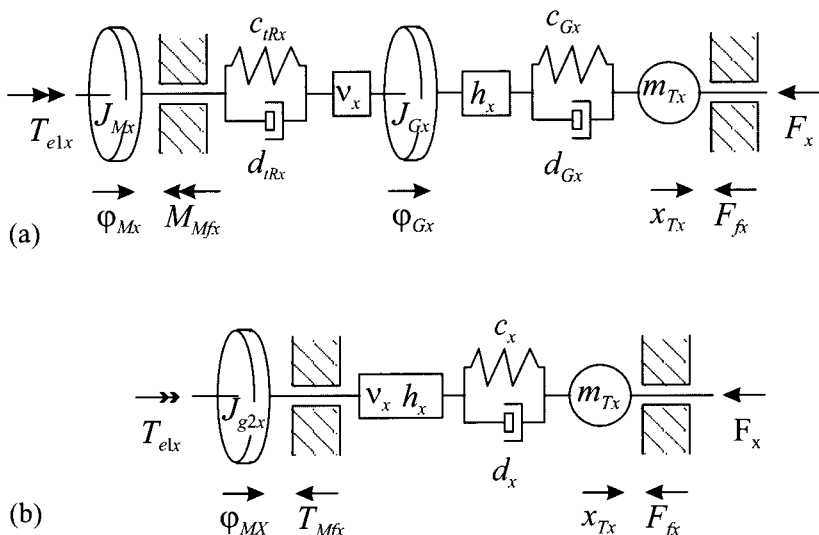


**Figure 6.27.** Model structure of the mechanical part of the feed drive: (a) three-mass system; (b) two-mass system

With the assumption that the elasticity of the belt drive can be neglected, the angle  $\varphi_{Gx}$  of the thread spindle is equal to the angle  $\varphi_{Mx}$  multiplied by the belt gear ratio  $v_x$ . This leads to the two-mass oscillator system shown in Figure 6.27b. Coulomb friction is assumed for the motor/belt system and the table motion.

### The control system

The measured variables are the speed  $\dot{\varphi}_{Mx}$  of the servomotor and the position  $x_{Tx}$  of the machine table by a linear incremental sensor with high resolution (500 slots/min). To achieve high accuracy of the table position and fast dynamics, the feed drive is controlled by a cascade control system with the motor speed controller as slave and the position controller as master, see Figure 6.28.

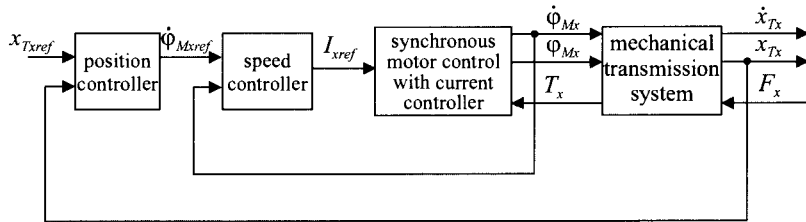


Figure 6.28. Cascade control system for the position control

The reference value of the position  $x_{Txref}$  is calculated in the numerical control (NC) unit. The position controller is programmed as a proportional acting controller:

$$G_{Px}(s) = \frac{\dot{\varphi}_{Mxref}(s)}{x_{Txref}(s) - x_{Tx}(s)} = K_{Px} \quad (6.5.1)$$

The underlying speed controller is realized analogously as a PI-controller with time lag

$$G_{nx}(s) = \frac{\dot{I}_{xref}(s)}{\dot{\varphi}_{Mxref}(s) - \dot{\varphi}_{Mx}(s)} = K_{nx} \left( 1 + \frac{1}{T_{Inx}s} \right) \left( \frac{1}{1 + T_{1nx}s} \right) \quad (6.5.2)$$

Based on the model structure of Figure 6.27b, a state representation can be derived with the seventh order state vector

$$\underline{x}^T = [x_{1n}, x_{2n}, I_x, \varphi_{Mx}, \dot{\varphi}_{Mx}, x_{Tx}, \dot{x}_{Tx}] \quad (6.5.3)$$

$x_{1n}$  and  $x_{2n}$  are state variables of the speed controller. For further details, see Konrad (1997).

## 6.5.2 Identification of the Feed Drive Control System

As several parameters of the feed drive system cannot be determined precisely from data sheets, they were estimated based on measurements of the frequency response  $G_x(i\omega) = \frac{\dot{x}_{Tx}(i\omega)}{\dot{\varphi}_{Mxref}(i\omega)}$  with opened position control but closed speed control, assuming the gear ratios  $v_x$  and  $h_x$  as known. For the experiments, sinusoidal changes of the reference input of the speed controller were applied, with an added linear drift in order to avoid the non-linearities of the dry frictions. As a parameter estimation method, a numerical optimization method for the model output error was used (simplex-algorithm). Figure 6.29 shows a comparison of the directly measured with the estimated frequency response, given the linear model structure with three masses. The agreement is relatively good for  $f \leq 120$  Hz. Figure 6.30 shows the directly measured friction characteristics of the servomotor and the machine table. Finally, an overall model as shown in Figure 6.31 was obtained. It was successfully applied to the reconstruction of the dynamic cutting forces of a

milling process by measuring the positions  $\varphi_{Gx}$  of the pulley and  $x_{Tx}$  of the table, and was used for model-based fault detection of the milling tool.

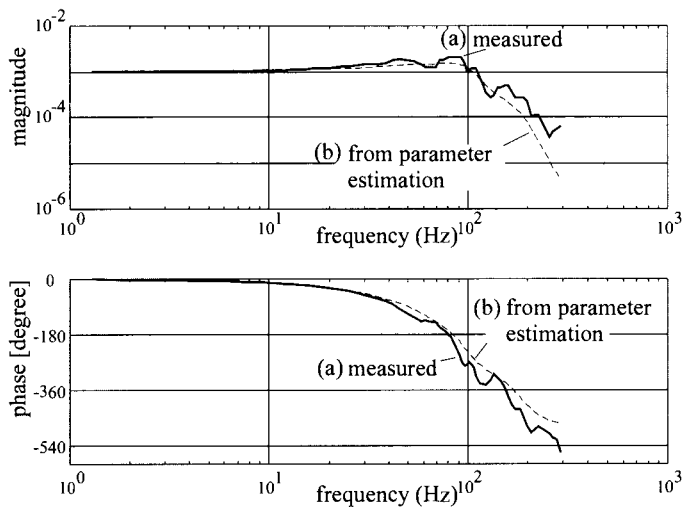


**Figure 6.29.** Directly measured and parameter estimated responses of the feed drive with  $\varphi_{Mxref}$  as input and  $\dot{x}_{Tx}$  as output: (a) directly measured; (b) with parameter estimation

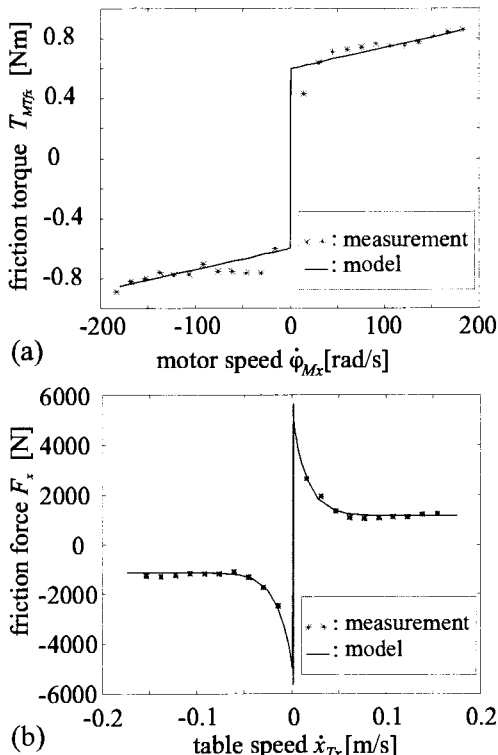


**Figure 6.30.** (a) measured and identified friction characteristic of the servo motor; (b) measured and identified friction characteristic of the machine table

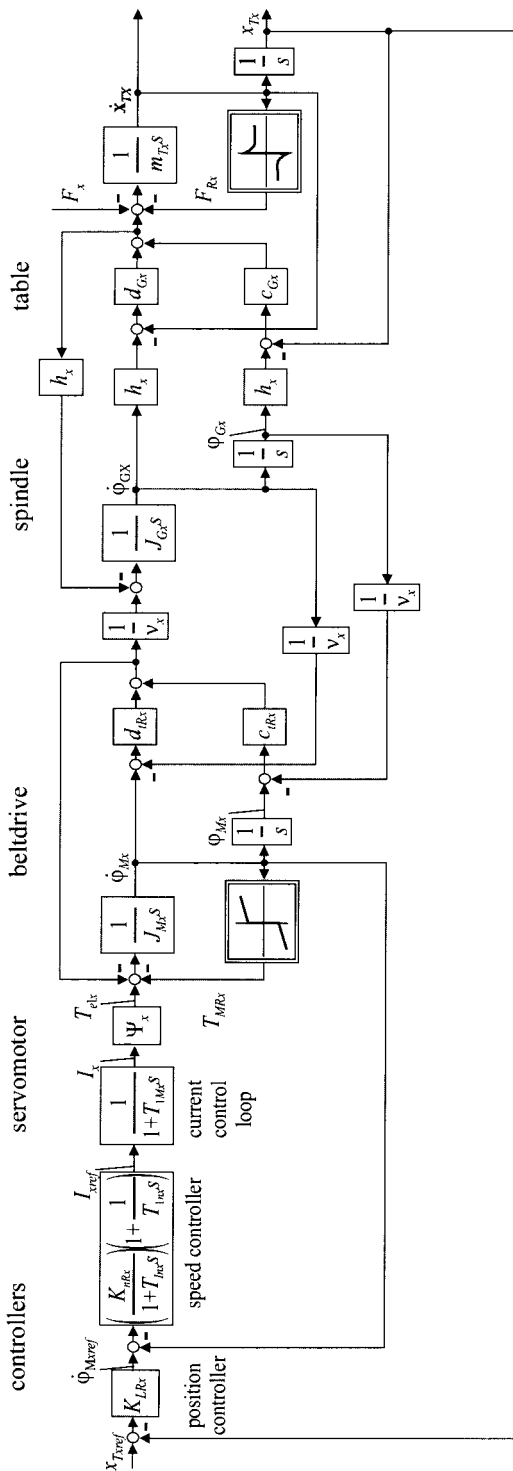


Figure 6.31. Overall model of the feed-drive of a machine tool

## 6.6 DYNAMIC MODEL OF AN AC MOTOR AND CENTRIFUGAL PUMP SYSTEM

As a further example of modeling and identification of machines, a drive unit, consisting of an AC motor and a centrifugal pump, is considered. The dynamic models of AC motors are treated in Section 5.4.1. Here, a speed-controlled AC motor is used together with a radial-flow centrifugal pump.

### 6.6.1 Theoretical Model of Centrifugal Pumps

Centrifugal pumps can be decomposed into a hydraulic subsystem and a mechanical one. First, the hydraulic system consisting of the pump itself and the joined piping is considered.

Centrifugal pumps are characterized by the so-called delivery head  $H(t)$ , which is a measure of the energy difference between inlet and outlet side of the pump. In the case of incompressible fluids, the head is proportional to the pressure difference  $\Delta p_p(t)$

$$H(t) = \frac{p_2(t) - p_1(t)}{\rho g} = \frac{\Delta p_p(t)}{\rho g} \quad (6.6.1)$$

and can be obtained by pressure measurements. Usually, the mass density  $\rho$  of hydraulic media can be assumed to be constant.

Taking Euler's turbine equation and loss terms into account, the pump pressure difference results

$$\Delta p_p(t) = h_{NN}\omega^2(t) - h_{NV}\omega(t)\dot{V}(t) - h_{VV}\dot{V}^2(t) \quad (6.6.2)$$

where  $\dot{V}(t)$  is the volume flow and  $\omega(t)$  is the angular speed. This equation describes the delivery head as well as flow and frictional losses, see Pfleiderer, Petermann (1991), Dixon (1966), Klein *et al.* (1995), Gülich (1999). The pressure difference of the tube system depends on the pressure losses in the different tubes and the height difference between pump and storage, according to Figure 6.32. Assuming turbulent flow, a flow resistance to each tube module can be assigned, see Section 6.10. In the considered plant, the flow resistance is mainly determined by the pipe elbows and the throttle valves. The pressure difference in the tube system can be evaluated by means of the dynamic equation

$$\Delta p_{TS}(t) = a_B \ddot{V}(t) + h_{RR} \dot{V}^2(t), \quad a_B = \frac{\rho l}{A_F} \quad (6.6.3)$$

whereupon the constant  $h_{RR}$  corresponds to the flow resistance of the tube system,  $l$  is the tube length and  $A_F$  its cross-sectional area. The principle of momentum for the mechanical subsystem leads to

$$T_{el}(t) = J_P \dot{\omega}(t) + T_F(t) + T_P(t) \quad (6.6.4)$$

The torque  $T_{el}(t)$  generated by the motor is spent for the acceleration of the overall inertia  $J_p$ , the friction losses summarized in term  $T_F(t)$  and, finally, for the generation of the pressure difference according to the term  $T_H(t)$ . The mechanical friction can be modeled by

$$T_F(t) = T_{Fc} \operatorname{sign}(\omega) + T_{Fv} \dot{\omega} \quad (6.6.5)$$

with the Coulomb friction  $T_{Fc}$  and viscous friction torque  $T_{Fv}$ .

The required power for the pump is

$$P_P = \dot{V} \Delta p_P$$

Further, it holds that

$$P_P = T_P \omega$$

Hence, the required torque for the pump is

$$T_P = \frac{\dot{V}}{\omega} \Delta p_P$$

Introducing (6.6.2) leads to

$$T_P(t) = h_{NN} \omega(t) \dot{V}(t) - h_{NV} \dot{V}^2(t) - h_{VV} \frac{\dot{V}^3(t)}{\omega} \quad (6.6.6)$$

Frequently, the last term can be neglected.

## 6.6.2 Overall Model of the Pumping Plant and Identification

The process under investigation is a centrifugal pump that delivers the fluid to a vessel, see Figure 6.32.

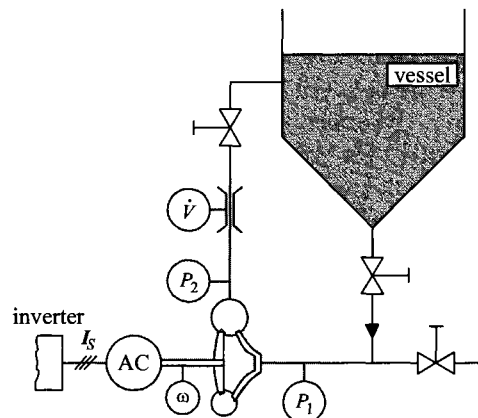


**Figure 6.32.** Scheme of the AC motor and axial-radial centrifugal pump plant

The measured signals are the pressures  $P_1(t)$ ,  $P_2(t)$  at the inlet and outlet side, the flow rate  $\dot{V}(t)$  and the angular speed  $\omega(t)$ . The pump is driven by an inverter-fed, speed-variable AC motor, which is controlled by a

field-oriented closed-loop control. Here, the measured stator current vector ( $\mathbf{I}_S = I_{S\alpha} + iI_{S\beta}$ ) is transformed in the reference-frame defined by the rotor-flux, which is reconstructed by an adequate state observer, see Section 5.4. The advantage of this transformation is that the rotor-flux  $\Psi_{Rd}$  ( $I_{Sd}$ ) as well as the motor torque  $T_{el}$  ( $I_{Sq}$ ) are only dependent on one component of the transformed stator current vector  $\mathbf{I}_S^T = I_{Sd} + iI_{Sq}$ . Hence, the motor torque can be evaluated by applying

$$T_{el} = k_T \Psi_{Rd} I_{Sq} \quad (6.6.7)$$

with a constant  $k_T$ . The investigated motor is a three-phase, 50 Hz, two-pole, 1.5 kW, squirrel-cage induction machine, rated at 400 V, 3.4 A and 2900 rpm.

The basic physical models have to be adapted to the present plant. Due to the slow inductive flow rate sensor (corresponding time constant: 0.48 s), the signal cannot be measured with acceptable dynamics.

In the hydraulic system, according to Figure 6.32, the relationship,  $\Delta p_P = \Delta p_{RL}$  is valid. Thus, the pressure difference in (6.6.2) can be eliminated by means of (6.6.3) and the resulting differential equation only comprises the variables  $\dot{V}$  and  $\omega$ . The idea is therefore to reconstruct the flow rate by the speed. Due to the short length of the piping in the considered plant ( $l < 3$  m), the acceleration constant  $a_B$  is very small and the corresponding term can be neglected. The equalization of (6.6.2) and (6.6.3) results in

$$(h_{RR} + h_{VV})\dot{V}^2(t) + h_{NV}\omega_m(t)\dot{V}(t) - h_{NN}\omega_m^2(t) = 0 \quad (6.6.8a)$$

Solving the quadratic equation gives

$$\dot{V}(t) = \zeta \omega_m(t), \text{ with } \zeta = \frac{+(-)\sqrt{h_{NV}^2 + 4h_{NN}(h_{RR} + h_{VV})} - h_{NV}}{2(h_{RR} + h_{VV})} \quad (6.6.8b)$$

where the flow rate is proportional with reference to the speed.

With this, (6.6.2) can be simplified according to

$$\Delta p_P(t) = \tilde{h}_{NN}\omega_m^2(t) \quad \text{with} \quad \tilde{h}_{NN} = h_{NN} - \zeta h_{NV} - \zeta^2 h_{VV} \quad (6.6.8c)$$

Better approximation results have been achieved by introducing additionally a speed-proportional term according to

$$\Delta p_P(t) = \tilde{h}_{NN}\omega_m^2(t) + \tilde{h}_{NV}\omega_m(t) \quad (6.6.8d)$$

which does not have a direct physical meaning.

The hydraulic model of the tube system can be used as specified in (6.6.3), whereupon the parameter  $a_B$  is mainly determined by the dynamics of the flow rate sensor rather than the dynamics of the process.

Inserting (6.6.5) and (6.6.6) into (6.6.4) leads to

$$T_{el}(t) = J_P \dot{\omega}(t) + T_{Fc} + T_{Fv} \omega(t) + h_{NN} \omega(t) \dot{V}(t) - h_{NV} \dot{V}^2(t) - h_{VV} \frac{\dot{V}^2(t)}{\omega(t)} \quad (6.6.9)$$

Again, the flow rate can be eliminated by (6.6.8b), which yields

$$T_{el}(t) = J_P \dot{\omega}(t) + T_{Fc} + T_{Fv} \omega(t) + h_2 \omega^2(t), \quad \text{with } h_2 = \zeta \tilde{h}_{NN} \quad (6.6.10a)$$

Experiments have shown, Wolfram *et al.* (2001), that for the specific pump station this equation can be satisfactorily approximated by

$$T_{el}(t) = J_P \dot{\omega}(t) + T_{Fc} + h_2 \omega^2(t) \quad (6.6.10b)$$

Based on these equations, the signal flow diagram of the overall system is depicted in Figure 6.33. Here, the pump is driven by a vector-controlled induction motor. The torque is determined by (5.4.18), (5.4.19) and (5.4.24).

On the basis of the models (6.6.3), (6.6.9) and (6.6.10a–b), the dynamic behavior of both the hydraulic and the mechanical subsystem can be identified. For this purpose, the process has to be excited with an appropriate input signal in order to get enough information about the dynamic and static behavior of the process within the operating range. The input signal applied to the plant is the reference value of the controller for the angular speed  $\omega(t) = 2\pi n(t)$ . Good results have been achieved by employing an amplitude-modulated pseudo-random binary signal (APRBS). In contrast to standard PRBS signals with only two discrete values, the amplitudes here are equally distributed within the predefined excitation interval. Thus, the non-linearities of (6.6.3), (6.6.9), (6.6.10a–b) are excited properly within the operating range of interest.

For the following example, a speed interval of  $n \in [2150 \text{ rpm}; 2450 \text{ rpm}]$  was chosen. The motor speed  $n$ , the difference pressure  $\Delta p_p$  and the flow rate  $\dot{V}$  are directly measured and the motor torque  $T_{el}$  is calculated by evaluating the measured currents according to (6.6.7).

As (6.6.3), (6.6.8a–d) and (6.6.9) are linear in the parameters, the physical parameters can be estimated by means of least squares parameter estimation methods, see (7.2.15), whereby the required derivatives are computed with state variable filters, Isermann (1992), or digital FIR-filters (finite impulse response), Wolfram, Moseler (2000).

The obtained parameter estimates are given in Table 6.4.

**Table 6.4.** Estimated parameters of the centrifugal pump system

hydraulic subsystem centrifugal pump		hydraulic subsystem piping		mechanical subsystem		
$\Delta p_p(t) = \tilde{h}_{NN} \omega^2(t) + \tilde{h}_{NV} \omega(t)$		$\Delta p_{TS}(t) = a_B \tilde{V}(t) + h_{RR} \dot{V}^2(t)$		$T_{el}(t) = J_P \dot{\omega}(t) + T_{Fc} + h_2 \omega^2(t)$		
$\tilde{h}_{NN}$	$\tilde{h}_{NV}$	$a_B$	$h_{RR}$	$J_P$	$T_{Fc}$	$h_2$
18.8 $\mu\text{bar}\cdot\text{s}^2$	668 $\mu\text{bar}\cdot\text{s}$	1.36 $\text{bar}\cdot\text{s}^2/\text{l}$	0.692 $\text{bar}\cdot\text{s}^2/\text{l}^2$	$3.01 \cdot 10^{-3}$ $\text{Nm}\cdot\text{s}^2$	$65.3 \cdot 10^{-3}$ $\text{Nm}$	$58.3 \cdot 10^{-6}$ $\text{Nm}\cdot\text{s}^2$

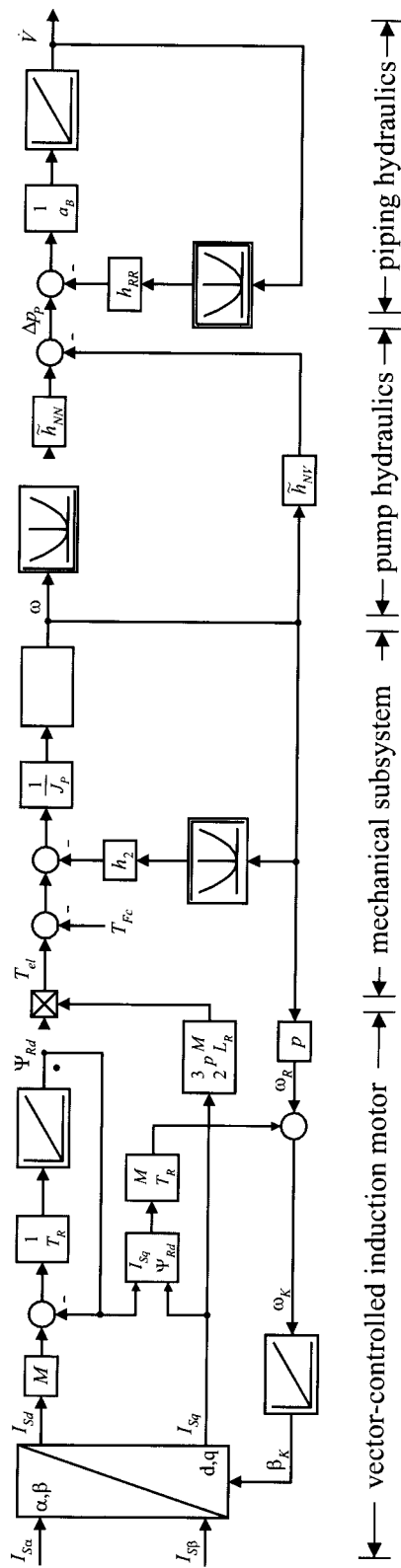
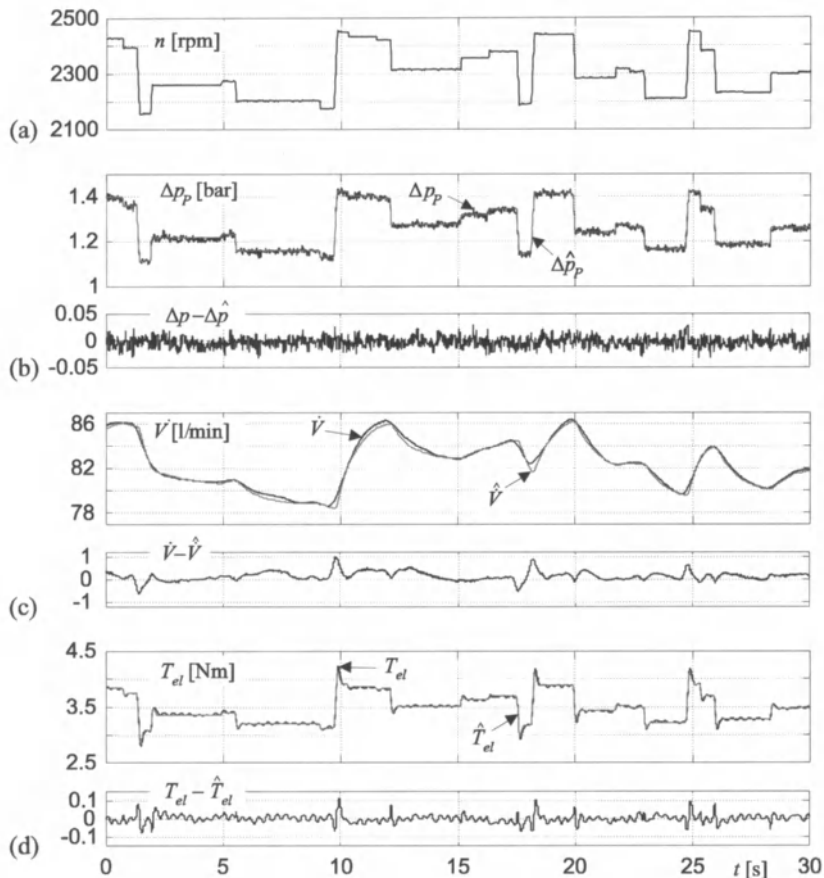


Figure 6.33. Signal flow diagram of the simplified overall motor-pump system

The quality of the estimated models can be seen from the comparison of the measured with the simulated models. As depicted in Figure 6.34, there is good agreement within the considered operating range. The estimated models of this pump system can be either utilized for controller design or for fault detection, Wolfram (2002).



**Figure 6.34.** Measured and simulated signals with model error

## 6.7 DYNAMIC MODEL OF AN AUTOMOBILE DRIVETRAIN

For the simulation of the longitudinal behavior of automobiles, a model of the drivetrain is required. This section describes a simplified drivetrain model with drive shaft elasticity, which is able to capture the major part of the drivetrain dynamics with regard to the speed of the engine and the vehicle.

### 6.7.1 Components of an Automotive Drivetrain

The drivetrain of a rear-driven car is presented in Figure 6.35, Pfeiffer (1997).

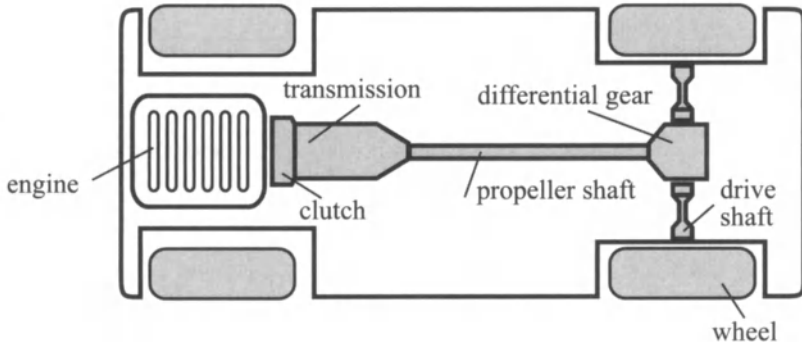


**Figure 6.35.** Parts of an automotive drivetrain of a rear-driven car

It consists of:

- *engine*: the engine generates the driving torque  $T_{eng}$  by combustion. The actual engine speed  $\dot{\alpha}_{cs}$  results from Newton's second law of motion, where  $T_c$  is the external load from the clutch,  $J_{eng}$  is the mass moment of inertia, and  $\alpha_{cs}$  is the crankshaft angle:

$$J_{eng} \ddot{\phi}_{cs}(t) = T_{eng}(t) - T_c(t) \quad (6.7.1)$$

- *clutch*: for vehicles equipped with manual transmission, the clutch allows the interruption of power flow, stationary idling and transition to motion. The clutch slips to compensate for the difference in the rotational speeds of engine and drivetrain when the vehicle is set in motion, Bosch (1996). When the clutch is engaged, no internal friction losses appear and torque oscillations are neglected, the clutch torque is equal to the transmission torque:

$$T_c = T_t$$

- *transmission*: the transmission modifies the engine torque and speed to adapt to the vehicle's momentary requirements. The conversion ratio  $i_t$  is defined as the quotient of the transmission's input  $\dot{\phi}_{t,i}$  and output speed  $\dot{\phi}_{t,o}$ :

$$i_t = \frac{\dot{\phi}_{t,i}}{\dot{\phi}_{t,o}}$$

If internal friction within the gear is neglected, the transmission's output torque  $T_p$  is

$$T_p = i_t T_t$$

- *propeller shaft*: the propeller shaft connects the transmission's output shaft with the differential gear. If stiffness and no internal friction is assumed, the differential gear torque is equal to the propeller shaft torque:

$$T_{dg} = T_p$$

- *differential gear*: the differential gear allows laterally opposed axles and wheels to rotate at varying rates during cornering, while providing uniform distribution of the driving forces. It is characterized by a conversion ratio  $i_{dg}$ :

$$T_{ds} = i_{dg} T_{dg}$$

- *driveshafts*: the driveshafts connect the wheels with the differential gear and transmit the torque to the wheels;
- *wheels*: the wheels are transmitting the torque to the ground. They have moment of inertia  $J_w$ . The driving resistance  $F_{res}$  acting on a vehicle with mass  $m_{veh}$  and driving with the velocity  $v_{veh}$  consists of the *rolling resistance*  $F_r$

$$F_r = k_r \cdot m_{veh} g$$

where  $g$  is the gravitational constant and  $k_r$  is a constant depending on the tire and the tire pressure, *the climbing resistance*  $F_{cli}$

$$F_{cli} = m_{veh} g \sin \alpha_{road}$$

where  $\alpha_{road}$  is the slope of the road, and the *air drag*  $F_{air}$

$$F_{air} = \frac{1}{2} c_{air} A_L \rho_{air} v_{veh}^2$$

where  $c_{air}$  is the drag coefficient,  $A_L$  the maximum vehicle cross-section area, and  $\rho_{air}$  the air density. The resulting torque  $T_{res}$  due to the driving resistance is equal to

$$T_{res} = (F_r + F_{cli} + F_{air}) r_{eff} = F_{res} r_{eff} \quad (6.7.2)$$

where  $r_{eff}$  is the effective wheel radius. In the case of a braking manoeuvre, the brake torque  $T_b$  is acting additionally on the wheels of the vehicle, see Figure 6.36.

### 6.7.2 Drivetrain Model with Driveshaft Elasticity

The most important elasticity of the driveline is located between the output shaft of the transmission and the wheels. For a simplified model, where only one dominating elastic element is taken into consideration, the drive shaft can be described as having damped torsional elasticity. It is shown in Kiencke, Nielsen (2000) that the main contribution to dri-

veline dynamics from driving torque to engine speed and wheel speed is the drive shaft, resulting in the first main eigen-frequency of the driveline. The reason for this is that the driveshaft is subject to the relatively largest torsion, due to the high conversion rates of the transmissions and the differential gear. The clutch and the propeller shaft are assumed to be stiff and the transmission and differential gear multiply the torque by the conversion ratio without losses.

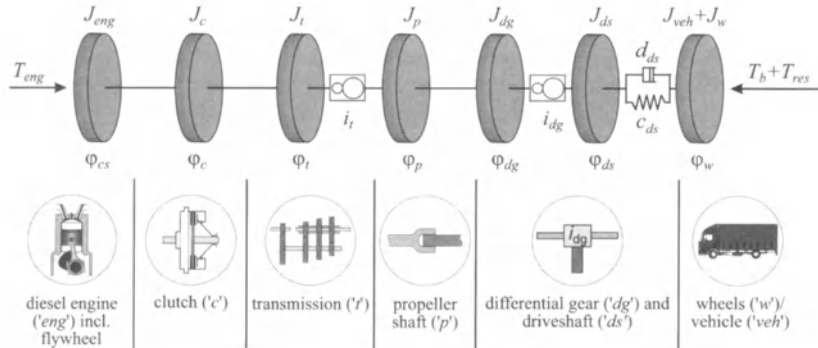


**Figure 6.36.** Simplified drivetrain model with driveshaft elasticity for an engaged clutch

Figure 6.36 shows the complete driveline model for an engaged clutch, Schaffnit (2001). The driveshaft is modeled as having damped torsional elasticity with spring constant  $c_{ds} = c_d$  and damping coefficient  $d_{ds} = d_d$ . Hence, the moments of inertia of the engine, clutch, transmission, propeller shaft, differential gear and driveshaft are lumped together as well as the wheel/vehicle inertia and connected by a damped torsional elasticity, Figure 6.37. The resulting moments of inertia, torques and angular velocities are:

$$\begin{aligned} J_1 &= \left( (J_{eng} + J_c + J_t) i_t^2 + J_p + J_{dg} \right) i_{dg}^2 + J_{ds} \\ J_2 &= J_{veh} = m_{veh} r_{eff}^2 + J_w \end{aligned}$$

$$\begin{aligned} T_1 &= T_{eng} i_t i_{dg} \\ T_2 &= T_{res} + T_b \end{aligned}$$

$$\Phi_1 = \frac{1}{i_t i_{dg}} \Phi_{cs}$$

$$\Phi_2 = \Phi_w$$

The moment of inertia  $J_2$  consists of the moment of inertia of the wheels  $J_w$  and the effect of the vehicle mass  $m_{veh}$  on the driveshaft. Applying Newton's second law of motion gives a simplified drive line model for the two-mass spring-mass-damper system, compare (4.6.1):

$$\begin{aligned} J_1 \ddot{\varphi}_1 &= T_1 - c_d(\dot{\varphi}_1 - \dot{\varphi}_2) - d_d(\dot{\varphi}_1 - \dot{\varphi}_2) \\ J_2 \ddot{\varphi}_2 &= -T_2 + c_d(\dot{\varphi}_1 - \dot{\varphi}_2) + d_d(\dot{\varphi}_1 - \dot{\varphi}_2) \end{aligned} \quad (6.7.3)$$

To transform the model into the state space formulation

$$\begin{aligned} \dot{x}(t) &= Ax(t) + b(t) \\ y(t) &= c^T x(t) \end{aligned} \quad (6.7.4)$$

the input  $u$ , output  $y$  and state variables  $x$  have to be chosen. The inputs to the drivetrain system are the torques  $T_1$  and  $T_2$  and the output variables are the engine speed  $\dot{\varphi}_{cs}$  and wheel speed  $\dot{\varphi}_w$ . Here, the angle difference of the torsional elasticity and the angle velocity of each inertia are used as state variables:

$$u(t) = [T_1(t) \ T_2(t)]^T$$

$$x(t) = [\dot{\varphi}_1(t) \ \dot{\varphi}_2(t) \ (\varphi_1(t) - \varphi_2(t))]^T$$

$$y(t) = [\dot{\varphi}_{cs}(t) \ \dot{\varphi}_w(t)]^T$$

The matrices  $A$ ,  $b$ ,  $c^T$  are defined as:

$$A = \begin{bmatrix} -\frac{d_d}{J_1} & \frac{d_d}{J_1} & \frac{c_d}{J_1} \\ \frac{d_d}{J_2} & -\frac{d_d}{J_2} & \frac{c_d}{J_2} \\ 1 & -1 & 0 \end{bmatrix}, \quad b = \begin{bmatrix} \frac{1}{J_1} & 0 \\ 0 & -\frac{1}{J_2} \\ 0 & 0 \end{bmatrix}, \quad c^T = \begin{bmatrix} i_t \cdot i_f & 0 & 0 \\ 0 & 1 & 0 \end{bmatrix}$$

The resulting linear mass-spring model with driveshafts as the main elasticity captures the major part of the drivetrain dynamics. More detailed drivetrain models are presented, e.g., in Kiencke, Nielsen (2000), Gillespie (1992), Sailer (1996) and Würtenberger (1997).

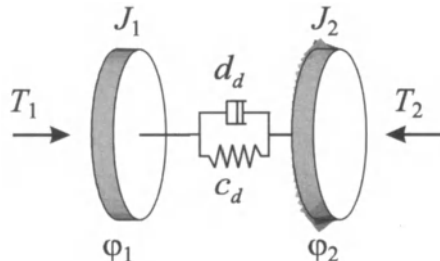


**Figure 6.37.** Reduced drivetrain model

A *simulation example* is given for a heavy truck model (total mass

40 tons) with driveshaft elasticity, Sinsel (1999). It demonstrates the oscillations of the driveline caused by a full-load acceleration, Figure 6.38.

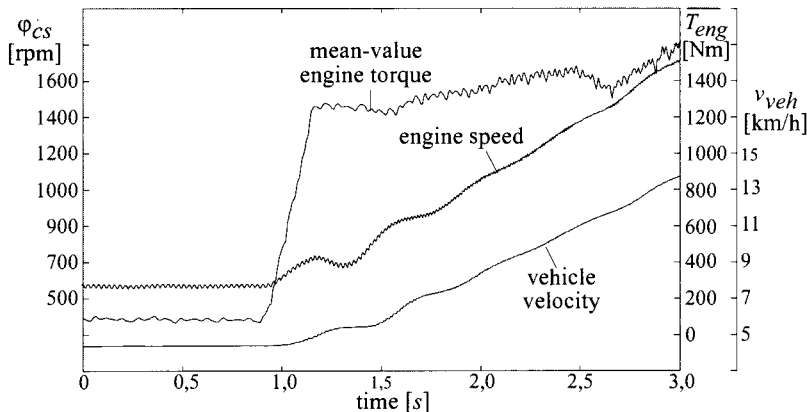


**Figure 6.38.** Simulation of a heavy truck model (40 tons) demonstrating the drivetrain oscillations caused by a full-load acceleration

At the beginning of the simulation, the vehicle drives with constant speed in third gear. The high-frequency oscillations in the engine speed are caused by the variations of the engine torque during the engine cycles. After approximately 0.9 s, a full-load acceleration leads to a strong rise of the engine torque, which is plotted in Figure 6.38 as the mean-value torque for a better graphic representation. One can observe the resulting oscillations in the engine speed and in the vehicle velocity. The oscillations have a frequency of 2.4 Hz.

## 6.8 DEPENDENCY OF SYSTEM BEHAVIOR ON THE OPERATING POINT

The static and dynamic behavior of many technical processes depends on the operating point. For linearized process models, the parameters vary according to the operating point, which often depends on the load (e.g., torque, speed of rotation, heat flow, temperature). For some processes this will be described in the following.

### 6.8.1 Storage with and without Feedback

Figure 6.39 shows the block diagram of an energy storage without feedback. The process has integral behavior without dependency on the operating condition if the stored value  $\Delta E_s(t)$  is the output of the system. For a feedback system, see Figure 6.40, and the feedback

$$\Delta \dot{E}_o = c \Delta E_s \quad (6.8.1)$$

the energy balance results in

$$\Delta \dot{E}_i(t) - c \Delta E_s(t) = \frac{d \Delta E_s(t)}{dt}$$

$$\frac{1}{c} \frac{d E_s(t)}{dt} + \Delta E_s(t) = \frac{1}{c} \Delta \dot{E}_i(t) \quad (6.8.2)$$

which is a first order time delay.

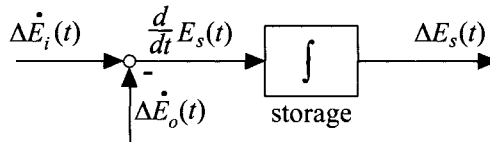


Figure 6.39. Block diagram of energy storage without feedback

The transfer function is given as

$$G(s) = \frac{\Delta E_s(s)}{\Delta \dot{E}_i(s)} = \frac{K}{1 + Ts}$$

with  $T = \frac{1}{c} = \frac{\Delta E_s(\infty)}{\Delta \dot{E}_i(\infty)}$ ,  $K = \frac{1}{c}$  (6.8.3)

A dependency of the parameter  $c$  on the operating condition results in an operating condition-dependent gain  $K$  and time constant  $T$ . This will be illustrated in the following.

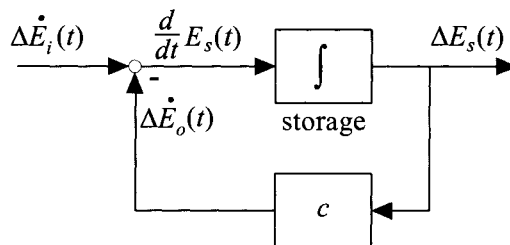


Figure 6.40. Block diagram of an energy storage with feedback

### Example 6.3. Operating point-dependent behavior of an engine

#### a) Motor without friction

Neglecting the frictional torque of a motor during idling, the torque balance can be written as

$$J_M \dot{\omega}_M(t) = T_i(t)$$

$$\omega_M(t) = \frac{1}{J_M} \int T_i(t) dt$$

with  $T_i(t)$  denoting the mean torque at the shaft. Integral action is obtained since feedback is neglected. The system behavior is independent of

the operating point for the considered input signal.

### b) Motor with friction

The load torque of an engine can frequently be approximated as

$$T_F(t) = c_{F0} + c_{F1}\omega_M(t) + c_{F2}\omega_M^2(t).$$

This holds, for example, for a coupled propeller or fan, including bearing friction. After linearization around the operating point  $\omega_{M0}$ , one obtains

$$\frac{dT_F}{d\omega_M} = c_{F1} + c_{F2}\omega_{M0} = c_F(\omega_{M0})$$

Therefore

$$\Delta T_F(t) = c_F(\omega_{M0}) \Delta\omega_M(t)$$

and

$$\frac{J_M}{c_F} \dot{\omega}_M(t) + \Delta\omega_M(t) = \frac{1}{c_F} \Delta T_i(t)$$

The transfer function can then be written as

$$G(s) = \frac{\Delta\omega_M(s)}{\Delta T_i(s)} = \frac{K}{1 + Ts}$$

with

$$K = \frac{1}{c_F(\omega_{M0})} \quad T = \frac{J_M}{c_F(\omega_{M0})}$$

Hence, both the gain  $K$  and the time constant  $T$  depend on the coefficient of  $c_F$  and therefore on the operating point, see Figure 6.41.

For the sake of completeness, it should be mentioned that for simplicity the indicated torque  $T_i$  is considered as the input variable. However, it may depend on the load, too.

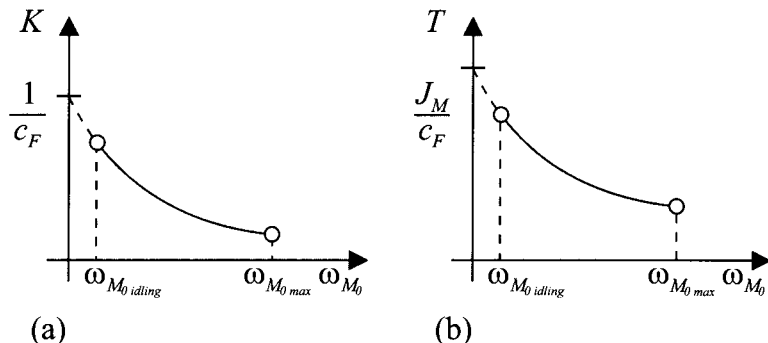


**Figure 6.41.** Dependency of gain  $K$  and time constant  $T$  on the operating point for a motor with load

□

### 6.8.2 Tuning of Controller Parameters

In the following, it is assumed that the dynamic behavior of the plant depends on the operating point. If the gain depends only on the load as shown in Figure 6.42, then for the tuning of the parameters of a linear controller (*e.g.*, PID-controller) the following facts result:

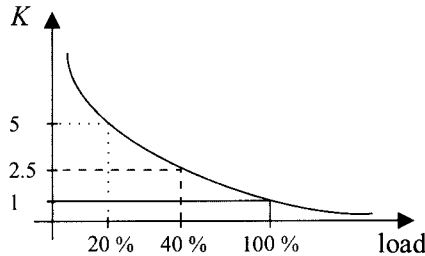


**Figure 6.42.** Dependency of the gain of the plant on the load

- if the controller parameters are optimized for full-load conditions, then the closed-loop system can become unstable at small loads due to an increased control gain;
- if the controller parameters are optimized for small-load conditions, then the transient response of the closed-loop system can be unacceptably slow (due to smaller control gains);
- as a compromise, the controller parameters are often tuned at 30% to 40% load. If the behavior at this condition is sufficiently damped, then the overall performance is usually acceptable. At full load, it has to be verified if an resulting overshoot is still acceptable;
- a performance index for multiple operating conditions allows development of a single controller that optimizes the control performance for various operating conditions. This is often referred to as *robust control*;
- if for all load points a good control performance is required, then a feedforward adaptation of the controller parameters depending on the load is recommended, Isermann *et al.* (1992).

## 6.9 ADVANCED CONTROL OF MECHANICAL SYSTEMS

Because of the integration of various functions, the use of modern tools plays an important rule in the design of the control system if higher performances are required. Herewith, all advantages of digital control can be applied, see, *e.g.*, Isermann (1989). It is proposed to consider the basic control as a knowledge-based multi-level feedback control system, which is shown in Figure 6.43.

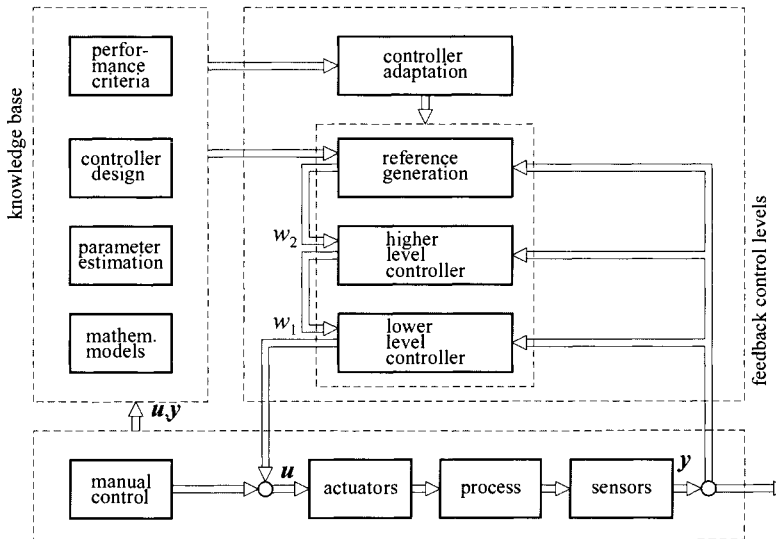


**Figure 6.43.** Knowledge-based multi-level feedback control for mechatronic systems

The knowledge-based multi-level feedback control system is a part of the intelligent system of Figure 1.12. The knowledge base consists of mathematical process models, identification, parameter estimation, controller design methods and control performance criteria. For machines consisting of, *e.g.*, a motor and a working process, the models frequently show the properties stated in Section 6.1.

The feedback control can be organized into lower level and higher level controllers, a reference value generation module and controller parameter adaptation. With this structure, the main control functions of mechatronic systems can be organized. In this section, only some control principles will be considered briefly.

### 6.9.1 Lower Level Feedback Control

The goal of the lower level feedback is to provide a certain dynamic behavior (*e.g.*, enforcement of damping) to compensate for non-linearities like friction, and to reduce parameter sensitivity. Some examples are:

- 1) *damping of high-frequency oscillations*: weakly damped higher frequency oscillations appear, *e.g.*, in multi-mass drivetrains. The damping can generally be improved by high-pass filtering the outputs and using a state variable feedback or PD (proportional-derivative) feedback. Figure 6.44 shows a scheme of an adaptive damping feedback with parameter estimation;
- 2) *compensation of non-linear static characteristics*: non-linear static characteristics are present in many subsystems of mechanical processes. Figure 6.45 shows as an example the position

control for a non-linear actuator. Frequently, a first non-linearity appears in the force- or torque-generating part like an electromagnet or a pneumatic or hydraulic actuator where, e.g., the force  $F_D = f(U)$  follows a nonlinear static characteristic. This non-linearity can now be compensated by an inverse characteristic  $U = f^{-1}(U')$  such that the I/O behavior  $F_D = f(U')$  becomes approximately linear, Isermann, Raab (1993), and a linear (PID-type) controller  $G_{c1}$  can be applied.

- 3) *friction compensation*: for many mechanical systems, the friction can be described approximately by

$$F_{F\pm}(t) = f_{FC\pm} \operatorname{sign} \dot{Y}(t) + f_{Fu\pm} \dot{Y}(t) \quad |\dot{Y}(t)| > 0$$

see (4.7.8) where  $f_{FC}$  is the Coulomb friction and  $f_{Fu}$  the linear viscous friction coefficient which may be dependent on the motion direction, indicated by + or -.

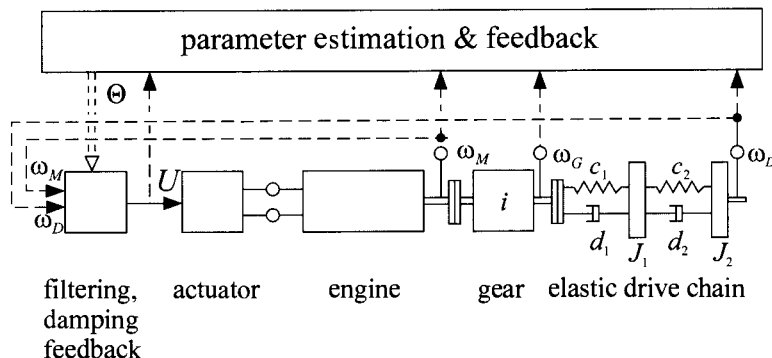


**Figure 6.44.** Adaptive damping feedback of drivetrain oscillations (usually a selection of  $\omega_M, \omega_G, \omega_D$  is fed back)

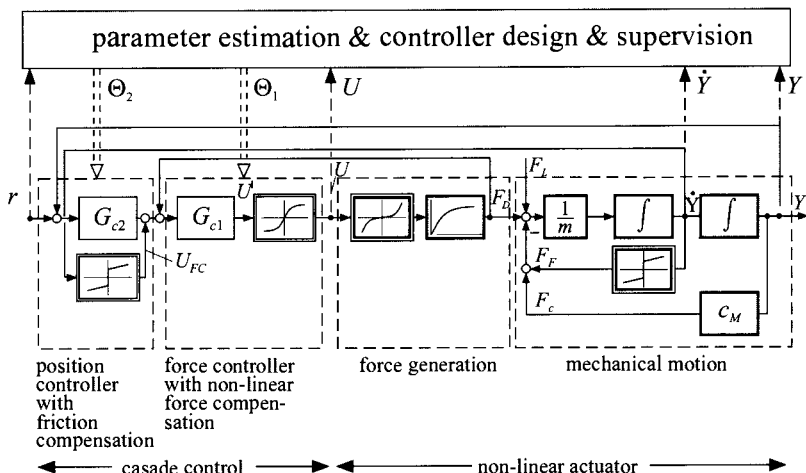


**Figure 6.45.** Adaptive position control of a non-linear actuator

The Coulomb friction has a strongly negative effect on the control performance if a high positioning accuracy is required, because it leads to a hysteresis effect, see Section 4.7. When the process stops within the hysteresis width before the set point is reached, only the integral part of the position controller can compensate for the offset. This may yield a significant loss of control performance and accuracy, especially during small position changes.

The basic idea of friction compensation is to compensate the relay function of the Coulomb friction by adding an adequate compensation signal  $U_{FC}$  to the normal control action. Different methods such as dithering, feedforward compensation and adaptive friction compensation are alternatives, see Section 10.2 and Isermann, Raab (1993), Tomizuka (1995).

After compensating the non-linear friction, the position controller  $G_{C2}$  can be designed for controlling the underlying linearized force control and remaining mechanical process without friction, Figure 4.45. In simple cases, then a linear controller of PID-type or a state controller is sufficient.

An alternative for position control of non-linear actuators is the use of a *sliding mode controller*. It consists of a nominal part for feedback linearization and an additional feedback to compensate for model uncertainties, Utkin (1977), Slotine, Weiping (1991). The resulting chattering by the included switching function hereby generates a dither signal. A comparison of a fixed PID-controller with friction compensation with a sliding mode controller for an electromagnetic actuator is, e.g., shown by Pfeufer *et al.*, 1995. The sliding mode controller resulted in good robustness to changing process parameters at a cost of higher design and computational effort.

## 6.9.2 Higher Level Feedback Control

The task of the higher level controller is to generate a good overall dynamic behavior with regard to the servo dynamics function due to changes of the position reference  $r(t)$  and to compensate for disturbances stemming, e.g., from variations of the load forces  $F_L(t)$ , see Figure 6.45. This high-level controller may be realized as a parameter optimized controller of PID-type or a state controller with or without state observer. A state observer is required only if the position  $Y(t)$  is measurable. If both  $Y(t)$  and  $\dot{Y}(t)$  can be measured,  $\ddot{Y}(t)$  can be obtained by differentiation of  $\dot{Y}(t)$  (if required at all) such that no state observer is needed, see Isermann *et al.* (1995).

The control scheme may be expanded by additional feedback controllers from a load or working process that is coupled with the mechanical process, resulting in a multiple-cascaded control system.

### 6.9.3 Adaptive Control

A prerequisite for the application of advanced control algorithms is the use of well-adapted process models. This then leads to self-tuning or adaptive control systems.

- 1) *parameter scheduling*: parameter scheduling based on the measurement of varying operation conditions is an effective method to deal with known and approximately time-invariant process non-linearities. Supposing measurable auxiliary variables  $V$  that correlate well with the process changes, the adaptation of the controller parameters  $\Gamma$  is performed as functions of  $V$  (parameter schedules, gain scheduling);
- 2) *parameter-adaptive control systems*: parameter-adaptive control systems are characterized by using identification methods for parametric process models. This is indicated in the adaptation level of Figure 6.43. Parameter estimation has proven to be an appropriate basis for the adaptive control of mechanical processes, including the adaptation to non-linear characteristics, Coulomb friction, and the unknown parameters like masses, stiffness, damping, see Isermann, Raab (1993), Isermann *et al.* (1992), Åström, Wittenmark (1997). These digital adaptive control systems work well if the assumptions for their design and convergence are satisfied. This includes, *e.g.*, proper excitation of the process dynamics. For the cases where the assumptions are violated, a supervision level is required which takes appropriate actions.

### 6.9.4 Fuzzy Control

The development of fuzzy logic theory, Zadeh (1972), stimulated alternative ways of solving automatic control problems. Based on these basic ideas, fuzzy controllers were proposed, Mamdani, Assilian (1975), which describe human control in linguistic form. As fuzzy logic provides a systematic framework to treat vague variables and knowledge, it should be applied primarily if sensors yield imprecise outputs, the process behavior is only qualitatively known or the automation functions cannot be described by equations or Boolean logic. The potentials of fuzzy logic approaches in general increase with higher automation levels, because the degree of the qualitative knowledge and the required intelligence in general grow with the hierarchical level.

The static and dynamic behavior of most mechanical systems can be rather precisely described by mathematical process models obtained through theoretical modeling and identification methods. Hence, there is, in many cases, no need to apply fuzzy concepts to the control of mechanical systems in the lower levels. However, fuzzy control concepts may be of interest in:

- 1) fuzzy tuning and adaptation of classical controllers;
- 2) fuzzy quality and comfort control;
- 3) fuzzy control for special (abnormal) operating conditions.

Particularly for the reference value generation of underlying (classical) control systems, Figure 6.43, where the quality or comfort and therefore the human reception plays a role, fuzzy rule-based methods offer interesting possibilities, *i.e.*, for the higher control levels. Examples for such mechatronic systems are:

- 1) the comfort control of suspensions in passenger cars;
- 2) the comfort of start-up of automobiles with clutch manipulation, gear shifting and automatic transmission;
- 3) distance and velocity control of automobiles and elevators.

For a more detailed description see Isermann (1998).

## 6.10 PROBLEMS

- 6.10.1 Sketch the characteristic and stable or unstable operating points for:

- (a) AC motor and centrifugal pump;
- (b) DC motor with field weakening and hot rolling mill;
- (c) diesel engine and piston pump;
- (d) hydromotor and lift.

How do the operating points change for a 10% increase of speed?

- 6.10.2 The dynamic behavior of the DC motor-driven circular pump of Figure 6.5 is considered.

The tube holds:  $d = 50 \text{ mm}$ ;  $l = 100 \text{ m}, 300 \text{ m}$ ;  $q = 1000 \text{ kg/m}^3$ ;  $H = 10 \text{ m}, 100 \text{ m}$ ;  $\zeta = l/D\lambda$  ( $\lambda$ : tube friction coefficient  $\lambda = 2 \cdot 10^{-2}$ ).

The characteristic of the pump is assumed to be

$$\Delta P_p = P_o - k_m \dot{m}^2$$

for constant speed ( $P_o = 10 \text{ kW}$ ;  $k_m = 0.025 \text{ kW s}^2/\text{m}^2$ ).

The water flow velocity is  $v = 5 \text{ m/s}$  at the operating point. Determine the mass flow  $\bar{\dot{m}}$  and  $\bar{P}$  for the operating point. Solve the problem for the given data and their combinations for  $l$  and  $H$ .

- 6.10.3 A centrifugal pump is directly driven by a spark-ignition (SI) engine. The torque characteristic of the pump can be described by (6.6.6). The torque characteristic of the SI engine is given by the diagram in Figure 6.20. Determine the pumped volume flow  $\dot{V}$  depending on the throttle angle  $\alpha$  and draw the corresponding diagram.
- 6.10.4 Determine the acceleration of the car in Example 6.2 for throttle angle  $\alpha = 30^\circ$  in second gear for road gradient 0% and 5% at  $v = 50 \text{ km/h}$ . Use the diagram in Figure 6.20c.
- 6.10.5 The governing equations of a centrifugal pump and a pipe are given in Table 6.4. Determine the steady states of the pump difference pressure  $\overline{\Delta P}$  and the volume flow  $\overline{\dot{V}}$  for the speeds  $n = 500, 1000$  and  $2500 \text{ rpm}$ . How large are power losses of the mechanical subsystem for these speeds according to Table 6.4?
- 6.10.6 A spark-ignition (SI) combustion engine (like in Example 6.2) has to be tested with a dynamometer, as shown in Section 6.4. However, the dynamometer consists of a directly coupled asynchronous motor that can be operated with positive and negative torque (four-quadrant-drive) in order to accelerate or decelerate the SI engine. The torque of the SI engine is manipulated by the throttle angle  $\alpha$  and the power electronics of the AC motor manipulates the current  $I$  or the frequency  $\omega$ .
- Represent the whole system in the form of one- and two-ports like in Figure 6.3a.
  - Draw the signal flow diagrams for the case that the SI engine is torque-controlled or speed-controlled, like in Figures 6.3b and c.
  - Develop a signal flow diagram (block diagram) with all important transfer elements, as in Figure 6.7 or Figure 6.23 and design the torque-control or the speed-control structure.

# 7 Identification of Dynamic Systems

---

By physical (theoretical) modeling of dynamic systems, one usually obtains the structure as well as the parameters of the mathematical model. The model parameters can generally be calculated, based on physical coefficients or other basic data of the process. However, some process properties may not be completely known and consequently the model structure and parameter uncertainties can be large. Therefore, experimental modeling, so-called process or system identification, can be employed additionally or even instead of physical modeling. Herewith, measured signals are used to obtain the temporal behavior of the system within certain classes of mathematical models.

In the following, a brief overview of system identification with regard to mechatronic systems will be given. A more thorough representation can be found in Eykhoff (1974), Young (1984), Ljung (1987) and Isermann (1992).

## 7.1 IDENTIFICATION METHODS

### 7.1.1 General Procedure

A linear process shown in Figure 7.1 is considered. The process is assumed to be stable such that a unique relationship between the input signal  $u(t)$  and the output signal  $y_u(t)$  exists. Usually, disturbances act on the process, which can be seen as a disturbance signal  $y_z(t)$  that is added to the process output  $y_u(t)$ . The task of system identification is to determine a mathematical model of the process  $P$  based on the known in-

put signal  $u(t)$  and the disturbed output signal  $y(t)$ . One can think of this procedure generating an error signal  $e(t)$  between the process and the model, see Figure 7.2, which gradually decreases during the identification procedure. If only the input and output signal are available for system identification, only the input–output behavior of the process can be determined. Also, only the controllable and observable part of the process becomes part of the identified model.

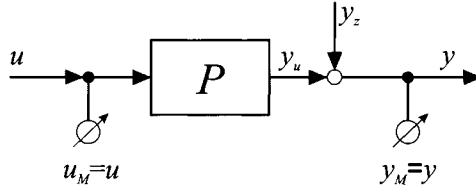


Figure 7.1. Linear process with disturbed output signal

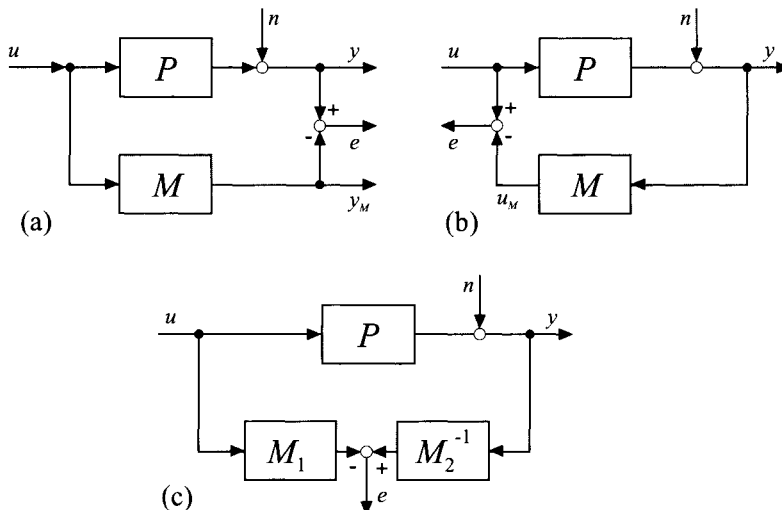


Figure 7.2. Generation of different error signals between the process  $P$  and the model  $M$ : (a) output error  $e = y - Mu$ ; (b) input error  $e = u - M^{-1}y$ ; (c) generalized error  $e = M_2^{-1}y - M_1u$

In principle, there are several restrictions that have to be taken into account during the identification experiment: the measurement time is limited,  $T_M \leq T_{M\max}$ ; the range of the test signal is limited  $u_0 \leq u_{0\max}$ ; the output signal is limited  $y_0 \leq y_{0\max}$ . Additionally, the disturbance signal  $y_z(t)$  usually consists of different components: stochastic, stationary component  $n(t)$ , non-stationary component (drift)  $d(t)$ , and other not clearly defined components  $h(t)$  such as, e.g., steps or pulses.

### 7.1.2 Classification of Identification Methods

During the last 30 years, a variety of different identification methods have been developed, e.g., Eykhoff (1974), Strobel (1975), Leonhard (1973), Young (1984), Ljung, Söderström (1985), such that a general

classification becomes necessary for understanding their differences. Considering linear processes with lumped parameters with one input and one output, the following classification features can be specified:

1. *Type of mathematical model:*

parametric model: equations that explicitly contain the parameters (differential equations, transfer functions);

non-parametric model: functions in the form of look-up tables or plotted curves (impulse responses, frequency responses);

2. *Type of signal used in the model:*

continuous signal: amplitude and time have continuous ranges of values;

discrete time signal: discrete time and continuous amplitude (sampled signal);

3. *Input signal:*

deterministic or stochastic;

4. *Error between model and process:*

input, output, or generalized error (see Figure 7.2);

5. *Connection between process and computer:*

off-line or on-line;

6. *Type of signal processing:*

batch processing or real-time processing;

7. *Type of algorithmic realization:*

non-recursive or recursive.

8. *Type of non-recursive processing:*

direct (one shot) or iterative (multiple shots).

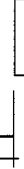
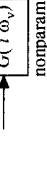
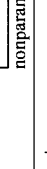
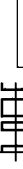
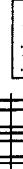
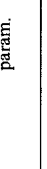
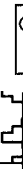
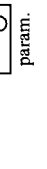
### 7.1.3 Identification Methods

The most important identification methods can be characterized as follows, compare Table 7.1.

#### *Non-parametric models*

The frequency response measurement with periodic test signals directly yields single values of the frequency response. In evaluation of the frequency response, the orthogonal correlation method has proven to yield good results, and is usually implemented in frequency response measurement devices.

Table 7.1. Survey of important identification methods

input signal	model	output signal	identification method	used device	allowable disturbances	digital computer coupling	data processing off-line	on-line	one shot	real-time	reachable accuracy	extendibility	application example
			determination of characteristic valves	recorder	very small	-	-	-	-	-	small	-	rough model, controller tuning
			Fourier analysis	recorder	small	X	-	X	-	medium	-	X	- verification of theoretical models
			frequency response measurement	recorder, F. resp. meas. device	medium	X	X	-	-	very large	-	X	- verification of theoretical models
			correlation	correlator	large	-	-	X	X	large	X	X	detection of signal relations, time delay, identification
			model adjustment parameter estimation	analog computer process computer	small	-	-	X	X	medium	X	-	analog-adaptive control
			adaptation neural net	process computer	large	X	X	X	-	very large	-	X	X design of non-linear controllers, learning controllers, fault detection

The required measurement time is relatively large when several frequencies have to be evaluated. The precision of the obtained result is very high.

*Fourier analysis* is mainly used for linear processes with continuous signals in order to obtain the frequency response from step or impulse responses. It is a simple procedure with a relatively small computational demand, relatively short measurement time and is recommended only for processes with a large signal-to-noise ratio.

*Correlation analysis* is employed in the time domain and can be applied to linear processes with continuous or discrete signals. The input signal can be stochastic as well as periodic. The results are correlation functions or, in special cases, impulse responses. Correlation methods are preferred for processes with a small signal-to-noise ratio. The computational demand is low.

For *spectral analysis*, the requirements are the same as for correlation analysis. The evaluation, however, is performed in the frequency domain by calculation of spectral densities. The results are single values of the frequency response.

The only *a priori* information required for the identification of non-parametric models is that the process has to be linearisable. A certain model structure does not have to be defined. Hence, non-parametric models can be applied to processes with lumped as well as distributed parameters with an arbitrary complex structure. They are favourably used for validation of theoretically derived models since no explicit model structure has to be assumed.

#### *Parametric models*

The identification methods for parametric models require the assumption of a certain model structure. If the assumed model structure matches the process structure, a higher model accuracy can be achieved because of the incorporated *a priori* information combined with statistical regression methods.

The simplest method is the *determination of characteristic values*. Here, certain parameters such as dead-time and dynamic delay times are determined based on measured process responses with respect to non-periodic test signals. The model parameters of simple models can then be determined from look-up tables or diagrams. This method is only applicable to simple processes with small disturbances, especially when the evaluation is performed manually.

*Model reference methods* or *model matching methods* have been developed for models realized on analog computers with continuous signals. They yield the parameters of differential or difference equations based on the assumed model structure. For the input signals, usually the only requirement is that all frequencies of the process that are of interest are sufficiently well excited. Model reference methods have lost their importance in favor of parameter estimation methods.

*Parameter estimation methods* consider differential or difference equations of arbitrary order and dead-time. By applying static regression methods that are especially modified for dynamic processes, functions of certain error signals are minimized. The choice of the input signal is arbitrary and large disturbance signals are admissible. Therefore, parameter estimation methods can be employed with versatility. Even in the presence of a large noise-to-signal ratio, accurate models can be obtained, also in closed-loop configuration.

For identification of non-linear processes without essential *a priori* knowledge about the model structure, *artificial neural networks*, based on mathematically formulated neurons, can be favorably employed.

### 7.1.4 Test Signals

In general, it is recommended to utilize artificially generated test signals, since the signals during regular operation seldom excite the process sufficiently. Usually, the following requirements have to be met by test signals:

- simple to generate and reproducible;
- mathematically simple to describe;
- realizable with the given actuators;
- applicable to the process;
- good excitation of the process dynamics that are of interest.

Figure 7.3 shows commonly used test signals. For correlation and parameter estimation methods, the pseudo-random-binary signal (PRBS) has proven to yield good results. Especially for airplanes, the 3211-Signal has found a large acceptance, which can be interpreted as a combination of rectangular pulses or part of a PRBS.

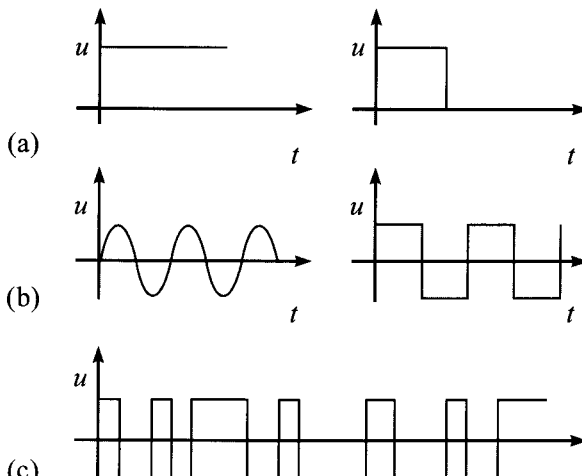


**Figure 7.3.** Commonly used test signals: (a) non-periodic: step- and square-pulse function; (b) periodic: sine- and square-wave; (c) stochastic: discrete binary noise

### 7.1.5 Closed-loop Identification

Proportionally acting processes can, in general, be identified in open-loop configuration. Integrating processes, however, usually do not allow the identification in open loop, because there are either disturbing drift signals acting on the process or the operation in open loop is not admissible for a long period of time since the process drifts out of the current operating point. In these cases and also for unstable processes, the identification has to be performed in closed-loop configuration, see Figure 7.4. If an external signal, e.g., the reference signal  $w$ , is measurable, the process can be identified using correlation or parameter estimation methods. If no measurable signal is acting on the control loop, e.g., only the disturbance signal  $y_z(t)$  is present, parameter estimation methods can be employed provided that the identifiability conditions are satisfied.

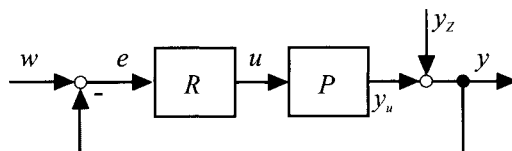


Figure 7.4. Identification in closed-loop configuration

### 7.1.6 Type of Application

The final application of the identified model has the decisive influence on the choice of the mathematical model, the identification method, the required model accuracy and the choice of the employed equipment.

For modern applications, the parameter estimation methods are of special importance because they can be implemented on-line and in real-time. Also, they can be relatively easily transferred to certain classes of non-linear processes. Therefore, these methods will be discussed first in the following.

## 7.2 PARAMETER ESTIMATION FOR DISCRETE TIME SIGNALS

It is assumed that the process can be described by the linear difference equation

$$\begin{aligned} y_u(k) + a_1 y_u(k-1) + \dots + a_m y_u(k-m) \\ = b_1 u(k-d-1) + \dots + b_m u(k-d-m) \end{aligned} \quad (7.2.1)$$

Here,

$$\begin{aligned} u(k) &= U(k) - U_{00} \\ y_u(k) &= Y_u(k) - Y_{00} \end{aligned} \quad (7.2.2)$$

are the deviations of the absolute signals  $U(k)$  and  $Y_u(k)$  from the operating point described by  $U_{00}$  and  $Y_{00}$ ,  $k$  is the discrete time  $k = t/T_0 = 0, 1, 2, \dots$ ,  $T_0$  is the sampling time and  $d = T_0/T_0 = 0, 1, 2, \dots$  is the discrete dead-time of the process. The corresponding transfer function in the  $z$ -domain is

$$\begin{aligned} G_p(z) &= \frac{y_u(z)}{u(z)} = \frac{B(z^{-1})}{A(z^{-1})} z^{-d} \\ &= \frac{b_1 z^{-1} + \dots + b_m z^{-m}}{1 + a_1 z^{-1} + \dots + a_m z^{-m}} z^{-d} \end{aligned} \quad (7.2.3)$$

The measured signal contains a stationary, stochastic disturbance

$$y(k) = y_u(k) + n(k) \quad \text{with} \quad E\{n(k)\} = 0 \quad (7.2.4)$$

The task is to determine the unknown parameters  $a_i$  and  $b_i$  from  $N$  measured input and output signal data points.

### 7.2.1 Method of Least Squares (LS)

Let the model parameters obtained from the data up to the sample ( $k - 1$ ) be denoted by  $\hat{a}_i$  and  $\hat{b}_i$ . Then, (7.2.1) becomes in the presence of a disturbed output signal

$$\begin{aligned} y(k) + \hat{a}_1 y(k-1) + \dots + \hat{a}_m y(k-m) \\ - \hat{b}_1 u(k-d-1) - \dots - \hat{b}_m u(k-d-m) = e(k) \end{aligned} \quad (7.2.5)$$

where the *equation error* (residual)  $e(t)$  is introduced instead of "0". This error corresponds to a generalized error, see Figure 7.2. This can be seen by rewriting (7.2.5), compare Figure 7.5

$$\hat{A}(z^{-1})y(z) - \hat{B}(z^{-1})z^{-d}u(z) = e(z) \quad (7.2.6)$$

$e$  is linearly dependent on the parameters sought for (linear in the parameters).

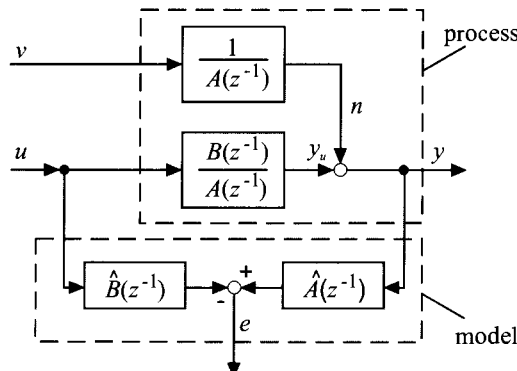


**Figure 7.5.** Model configuration for the least squares method with equation error (generalized error)

From (7.2.5),  $\hat{y}(k|k-1)$  can be interpreted as the one-step-ahead prediction, based on the measurements up to sample  $(k-1)$

$$\hat{y}(k|k-1) = \Psi^T(k)\hat{\Theta} \quad (7.2.7)$$

with the data vector

$$\begin{aligned} \Psi^T(k) = [ -y(k-1) \dots -y(k-m) | & u(k-d-1) \dots \\ & u(k-d-m) ] \end{aligned} \quad (7.2.8)$$

and the parameter vector

$$\hat{\Theta} = [\hat{a}_1 \dots \hat{a}_m | \hat{b}_1 \dots \hat{b}_m]^T \quad (7.2.9)$$

Consequently, (7.2.5) can be written as

$$y(k) = \Psi^T(k)\hat{\Theta} + e(k) \quad (7.2.10)$$

The measured signals for  $k = m+d, \dots, m+d+N$  are written in vectors, e.g.,

$$y^T(m+d+N) = [y(m+d) \dots y(m+d+N)] \quad (7.2.11)$$

Then,

$$y(m+d+n) = \Psi(m+d+N)\hat{\Theta} + e(m+d+N) \quad (7.2.12)$$

where  $\Psi$  is a  $((N+1), 2m)$ -data matrix. Minimizing the sum of errors squared

$$V = \sum_{k=m+d}^{m+d+N} e^2(k) = e^T(m+d+N)e(m+d+N) \quad (7.2.13)$$

yields

$$\frac{dV}{d\Theta} \Big|_{\Theta=\hat{\Theta}} = -2\Psi^T[y - \Psi\hat{\Theta}] = \mathbf{0} \quad (7.2.14)$$

for the unknown parameters. From this, the (non-recursive) estimation equation of the least squares (LS) method can be obtained

$$\hat{\Theta} = [\Psi^T\Psi]^{-1}\Psi^Ty \quad (7.2.15)$$

The matrix

$$P = [\Psi^T\Psi]^{-1} \quad (7.2.16)$$

has the dimension  $(2m, 2m)$ . The inverse exists if and only if

$$\det[\Psi^T\Psi] = \det P^{-1} \neq 0 \quad (7.2.17)$$

Also,

$$\frac{\partial^2 V}{\partial\Theta\partial\Theta^T} = \Psi^T\Psi \quad (7.2.18)$$

has to be positive-definite such that the loss function  $V$  has a minimum. Both requirements are satisfied if and only if

$$\det[\Psi^T \Psi] = \det P^{-1} > 0 \quad (7.2.19)$$

This condition also includes that the input signal is *persistently exciting* the process and that the process is *stable*.

From parameter estimation methods, it is usually required that the estimate is not biased for a finite number of data samples  $N$

$$E\{\Theta(N)\} = \Theta_0 \quad (7.2.20)$$

( $\Theta_0$  denotes the true parameters) and is consistent in the quadratic mean

$$\lim_{N \rightarrow \infty} E\{\hat{\Theta}(N)\} = \Theta_0 \quad (7.2.21)$$

$$\lim_{N \rightarrow \infty} E\{[\hat{\Theta}(N) - \Theta_0][\Theta(N) - \Theta_0]^T\} = \mathbf{0} \quad (7.2.22)$$

For the least squares method, (7.2.21) becomes, by substituting (7.2.12) into (7.2.15)

$$\begin{aligned} E\{\hat{\Theta}(N)\} &= \Theta_0 + E\{[\Psi^T \Psi]^{-1} \Psi^T e\} \\ &= \Theta_0 + b \end{aligned} \quad (7.2.23)$$

In order to have a vanishing bias (systematic estimation error)  $b$ ,  $\Psi^T$  and  $e$  must be uncorrelated. Consequently,  $e(k)$  must not be correlated and  $E\{e(k)\} = 0$ . The estimation is unbiased if the disturbance signal  $n(k)$  is generated by the disturbance filter

$$G_v(z) = \frac{n(z)}{v(z)} = \frac{1}{A(z^{-1})} \quad (7.2.24)$$

where  $v(k)$  is discrete white noise, see Figure 7.5. Since this filter does not exist in practice, the least squares estimation, in general, yields biased estimates. These systematic estimation errors are the larger the greater the variance  $\sigma_n^2$  of the disturbance signal is compared to the output signal  $\sigma_{yu}^2$ .

For the covariance matrix, the following is true if  $\hat{\Theta} = \Theta_0$  (which means  $e = \mathbf{0}$ )

$$\begin{aligned} cov[\Delta \Theta] &= E\{[\hat{\Theta} - \Theta_0][\hat{\Theta} - \Theta_0]^T\} \sigma_e^2 E\{P\} \\ &= \sigma_e^2 E\left\{\left[\frac{1}{N+1} \Psi^T \Psi\right]^{-1}\right\} \frac{1}{N+1} \\ &= \sigma_e^2 \{ \Phi^{-1}(N+1) \} \frac{1}{N+1} \end{aligned} \quad (7.2.25)$$

$\sigma_e^2$  is the variance of  $e(k)$ .  $\Psi$  is a matrix whose elements are correlation functions. For  $N \rightarrow \infty$ , (7.2.22) is satisfied.  $E\{P\}$  is proportional to the covariance matrix of the parameter estimation errors.

Because of the biased estimates for the least squares algorithm, this method can only be used for processes with no or only small disturbance signals. A big advantage of the least squares algorithm, however, is that the parameter vector  $\hat{\Theta}$  can be determined in one batch calculation

and no iterative methods are necessary. This is possible since the employed error measure is linear in the parameters.

### 7.2.2 Recursive Method of Least Squares (RLS)

The least squares method discussed so far has been non-recursive. This means that all measured data has to be stored first before the parameter vector  $\hat{\Theta}(N)$  is calculated in one shot. However, it is required to estimate a parameter vector  $\hat{\Theta}(k)$  in real-time after each measurement of  $u(k)$  and  $y(k)$ . Equation (7.2.15) can be transformed into a recursive formulation and the following recursive least squares (RLS) estimation equation is obtained

$$\hat{\Theta}(k+1) = \hat{\Theta}(k) + \gamma(k) \cdot [y(k+1) - \Psi^T(k+1)\hat{\Theta}(k)] \quad (7.2.26)$$

$$\gamma(k) = \frac{1}{\Psi^T(k+1)\mathbf{P}(k)\Psi(k+1) + 1} \mathbf{P}(k)\Psi(k+1) \quad (7.2.27)$$

$$\mathbf{P}(k+1) = [I - y(k)\Psi^T(k+1)\mathbf{P}(k)] \quad (7.2.28)$$

For initialization, the parameter vector is set to  $\hat{\Theta}(0) = \mathbf{0}$  and large variances are assumed,  $\mathbf{P} = \alpha I$  with  $\alpha=100,\dots,1000$ . Because of a numerically more stable behavior, more sophisticated methods are usually implemented, *e.g.*, square root filtering algorithms such as DSFC, DSFI, or DUDC, see, *e.g.*, Isermann *et al.* (1992).

### 7.2.3 Modifications of the Least Squares Method

In order to cope with coloured disturbance signals, as they usually appear in practice, several modifications of the least squares method have been proposed to obtain unbiased parameter estimates. Some methods are, *e.g.*, the generalized least squares (GLS) method, the extended least squares (ELS) method, or the maximum-likelihood method, see Eykhoff (1974), Isermann (1992).

## 7.3 PARAMETER ESTIMATION FOR CONTINUOUS TIME SIGNALS

Parameter estimation methods for dynamic processes were first developed for process models in discrete time in combination with digital control systems. For some applications, *e.g.*, the validation of theoretical models or for fault diagnosis, however, parameter estimation methods for models with continuous time signals are needed.

### 7.3.1 Method of Least Squares

A stable process with lumped parameters is considered, which can be described by the linear, time-invariant differential equation

$$\begin{aligned} & a_n y_u^{(n)}(t) + a_{n-1} y_u^{n-1}(t) + \dots + a_1 y_u^{(1)}(t) + y_u(t) \\ = & b_m u^{(m)}(t) + b_{m-1} u^{(m-1)}(t) + \dots + b_1 u^{(1)}(t) + b_0 u(t) \quad m < n \end{aligned} \quad (7.3.1)$$

It is assumed that the derivatives of the output signal

$$y^{(j)}(t) = d^j y(t) / dt^j, \quad j = 1, 2, \dots, n \quad (7.3.2)$$

and of the input signal for  $j = 1, 2, \dots, m$  exist.  $u(t)$  and  $y(t)$  are the deviations

$$\begin{aligned} u(t) &= U(t) - U_{00} \\ y(t) &= Y(t) - Y_{00} \end{aligned} \quad (7.3.3)$$

of the absolute signals  $U(t)$  and  $Y(t)$  from the operating point described by  $U_{00}$  and  $Y_{00}$ . The function corresponding transfer to (7.3.1) is

$$\begin{aligned} G_P(s) &= \frac{y_u(s)}{u(s)} = \frac{B(s)}{A(s)} \\ &= \frac{b_0 + b_1 s + \dots + b_{m-1} s^{m-1} + b_m s^m}{1 + a_1 s + \dots + a_{n-1} s^{n-1} + a_n s^n} \end{aligned} \quad (7.3.4)$$

The measurable signal  $y(t)$  contains an additional disturbance signal  $n(t)$

$$y(t) = y_u(t) + n(t) \quad (7.3.5)$$

Substituting (7.3.5) into (7.3.1) and introducing an equation error  $e(t)$  yields (corresponding to (7.2.10))

$$y(t) = \Psi^T(t) \Theta + e(t) \quad (7.3.6)$$

with

$$\Psi^T(t) = [-y^{(1)}(t) \dots -y^{(n)}(t) \mid u(t) \dots u^{(m)}(t)] \quad (7.3.7)$$

$$\Theta = [a_1 \dots a_n \mid b_0 \dots b_m]^T \quad (7.3.8)$$

The input and output signals are measured at discrete time samples  $t = kT_0, k = 0, 1, 2, \dots, N$  with sampling time  $T_0$  and the derivatives are generated. Based on this,  $N+1$  equations can be written down

$$y(k) = \Psi^T(k) \hat{\Theta} + e(k) \quad (7.3.9)$$

This system of equations can be written in matrix notation as

$$\mathbf{y} = \Psi \hat{\Theta} + \mathbf{e} \quad (7.3.10)$$

Minimizing the loss function

$$V = \mathbf{e}^T(N) \mathbf{e}(N) = \sum_{k=0}^N e^2(k) \quad (7.3.11)$$

yields with  $dV/d\hat{\Theta} = \mathbf{0}$  as previously shown in Section 7.2 the vector of parameter estimates for the least squares method

$$\hat{\Theta}(N) = [\Psi^T \Psi]^{-1} \Psi^T y \quad (7.3.12)$$

The existence of a unique solution requires that the matrix  $\Psi^T \Psi$  is positive-definite. After dividing this matrix by the measurement time, the elements of the resulting matrix are the estimates of the correlation functions  $\Phi(\tau)$  of the derivatives of the signals for  $\tau = 0$  with no time shift. It can be seen that the form is very similar to the least squares method for models with discrete time signals. Hence, a lot of the derivations can be directly transferred, such as the recursive formulation and the numerically improved versions. However, particular problems arise concerning the convergence and the evaluation of the needed derivatives of the signals.

A *convergence analysis* shows that the estimates for continuous signals are also biased if the error signal  $e(k)$  is statistically independent. Hence, the estimates in general are biased for disturbed processes.

If the needed derivatives of the signals are directly measurable (e.g., as for vehicle applications), these values can be written in the data matrix  $\Psi$  and the correlation functions in the matrix  $[\Psi^T \Psi]/(N + 1)$  can be directly calculated. However, if the derivatives are not measurable, the derivatives have to be evaluated from the sampled signals  $u(t)$  and  $y(t)$ . For this, there basically exist the following methods. The *numerical differentiation* in combination with interpolation approaches (splines, Newton's method) is usually not able to suppress noise due to disturbance signals. State variable filters (SVF), see Figure 7.6,

$$F(s) = \frac{y_f(s)}{y(s)} = \frac{1}{f_0 + f_1 s + \dots + f_{n-1} s^{n-1} + s^n} \quad (7.3.13)$$

have proven to yield good results. The state variable filter is a low-pass filter that provides the derivatives as well as filters the disturbance signals. With the state variable filter, the input signal  $u(t)$  and the output signal  $y(t)$  is filtered. The choice of the filter parameters  $f_i$  is relatively free. The design of a Butterworth filter is recommended, see Peter (1993). A further possibility is the application of finite impulse response filters (FIR), where the derivations of the impulse response of a low-pass filter are convoluted with the signal, Oppenheim *et al.* (1999), Moseler, Vogt (2000).

For large signal-to-disturbance ratios, this least squares method has been shown to yield good results. For larger disturbance signals, consistent parameter estimation methods should be employed such as the *instrumental variables method*.

Since these parameter estimation methods are based on discrete time estimation methods, a lot of results and estimation methods for discrete time models can be transferred to models for continuous time.

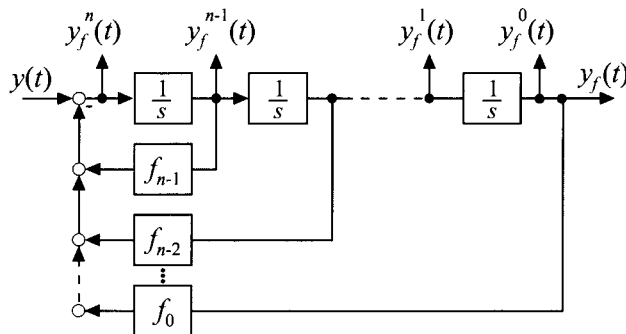


Figure 7.6. State variable filter

## 7.4 TIME-VARYING SYSTEMS

For the identification methods discussed so far, it has been assumed that the parameters are constant. In practice, however, this is seldom true since the parameters change through time due to internal or external influences. Frequently, a linear process behavior can be assumed around an operating point for small deviations of the signals. Changes of the operating points then reveal the overall non-linear behavior of the process. For weakly non-linear behavior, it is then possible to employ linear models with time-varying parameters. Therefore, *recursive estimation methods with forgetting memory*, which will be briefly discussed in the following, are well suited and are based on the recursive least squares method.

In order to weight the latest measurement values stronger than the older values, the squared errors can be multiplied by weights  $w(k)$

$$w(k) = \lambda^{N-k}, \quad 0 < \lambda < 1 \quad (7.4.1)$$

which are exponentially decreasing as can be easily seen

$$w(N) = 1, \quad w(N-1) = \lambda, \quad w(N-2) = \lambda^2, \dots \quad (7.4.2)$$

where  $\lambda$  is the so-called forgetting factor.

The loss function then becomes

$$V = \sum_{k=N-N}^N w(k) e^2(k) = \sum_{k=N-N}^N \lambda^{N-k} e^2(k) \quad (7.4.3)$$

Based on the weighted loss function, the recursive estimation equations for the weighted least squares method become

$$\hat{\Theta}(k+1) = \hat{\Theta}(k) + \gamma(k) [y(k+1) - \Psi^T(k+1)\Theta(k)] \quad (7.4.4)$$

$$\gamma(k) = \frac{1}{\Psi^T(k+1)\mathbf{P}(k)\Psi(k+1) + \lambda} \mathbf{P}(k)\Psi(k+1) \quad (7.4.5)$$

$$\mathbf{P}(k+1) = [\mathbf{I} - \gamma(k)\Psi^T(k+1)] \mathbf{P}(k) \frac{1}{\lambda} \quad (7.4.6)$$

The influence of the forgetting factor can be seen by looking at the inverse of the covariance matrix, which is needed for the derivation of the recursive methods

$$\mathbf{P}^{-1}(k+1) = \lambda \mathbf{P}^{-1}(k) + \Psi(k+1)\Psi^T(k+1) \quad (7.4.7)$$

$\mathbf{P}^{-1}$  is proportional to the information matrix

$$J = \frac{1}{\sigma_e^2} E \{\Psi^T \Psi\} = \frac{1}{\sigma_e^2} E \{\mathbf{P}^{-1}\} \quad (7.4.8)$$

With  $\lambda < 1$ , the information of the previous step is decreased, which means that the covariance values are increased. Consequently, the previous estimates are considered to be worse such that the new measurement data is weighted stronger.

For  $\lambda = 1$  (no exponential forgetting factor)

$$\begin{aligned} \lim_{k \rightarrow \infty} E \{\mathbf{P}(k)\} &= \mathbf{0}, \quad \lim_{k \rightarrow \infty} \mathbf{P}^{-1}(k) = \infty \\ \lim_{k \rightarrow \infty} E \{\gamma(k)\} &= 0 \end{aligned} \quad (7.4.9)$$

with  $\lambda < 1$ , the following limits can be evaluated

$$\begin{aligned} \lim_{k \rightarrow \infty} E \{\mathbf{P}(k)\} &= \mathbf{P}(\infty), \quad \lim_{k \rightarrow \infty} E \{\mathbf{P}^{-1}(k)\} = \mathbf{P}^{-1}(\infty) \\ \lim_{k \rightarrow \infty} E \{\gamma(k)\} &= \gamma(\infty) \end{aligned} \quad (7.4.10)$$

Hence, for large values of  $k$ , the measurement data is weighted with a constant weight and not with a constantly decreasing weight as for  $\lambda = 1$ . Consequently, the estimation algorithm stays sensitive with respect to parameter variations. Because of the decreasing effective number of measurement points for the estimation, the influence of disturbance signals becomes larger. Hence, there is a trade-off for the choice of  $\lambda$  between good parameter tracking (small  $\lambda$ ) and good disturbance suppression (large  $\lambda$ ). The exponential weighting, however, allows only slowly-varying parameters since  $\gamma(k)$  as well as  $\mathbf{P}(k+1)$  only changes slowly (exponential).

Of particular importance to  $\lambda < 1$  is the persistent excitation of the process. Otherwise,  $\mathbf{P}^{-1}(k+1)$  is decreasing because of  $\Psi(k+1) \approx 0$  or  $\mathbf{P}(k+1)$  and  $\gamma(k)$  are constantly increasing and the estimation algorithms becomes more sensitive and will finally diverge. Therefore, it is possible to introduce a variable forgetting factor  $\lambda(k)$ , e.g., based on the actual information content or on the eigenvalue of the parameter estimation algorithm, see Kofahl (1988), Isermann (1992).

## 7.5 NON-LINEAR PROCESSES

Many processes within the area of mechatronic systems show a non-linear static and dynamic behavior, especially if wide areas of operations are considered. Examples are vehicles, aircraft and combustion engines and all processes with Coulomb friction and magnetic hysteresis. Therefore, the identification of non-linear processes is of increasing interest.

Classical non-linear models in combination with parameter estimation methods as well as model architectures originating from the field of artificial neural networks are well suited to the identification of non-linear static and dynamic processes. The next four sections present model architectures for the identification of processes with continuously differentiable non-linearities. The fifth section deals with the experimental modeling of non-continuously differentiable processes.

### 7.5.1 Parameter Estimation with Classical Non-linear Models

Classical methods for the identification of dynamic systems are mostly based on polynomial approximators. One distinguishes between general approaches, *e.g.*, Volterra-series or Kolmogorov-Gabor polynomials, and approaches that involve special structure assumptions such as Hammerstein, Wiener or non-linear difference equation (NDE) models, Eykhoff (1974), Haber, Unbehauen (1990), see also Isermann (1992), Isermann *et al.* (1992).

Static polynomial approximators have the advantage of being *linear in the parameters*. This advantage can be maintained for certain dynamic polynomial models. This way, computationally expensive iterative optimisation methods can be avoided.

In the following, the linear difference equation is written with the shift operator  $q^{-1}$ , where ( $q^{-1}y(k) = y(k - i)$ )

$$A(q^{-1})y(k) = B(q^{-1})q^{-d}u(k) + D(q^{-1})v(k) \quad (7.5.1)$$

according to (7.2.3).

The following examples of classical non-linear dynamic models are based on the representation of the non-linearity by polynomials.

#### *Generalized Hammerstein model*

$$\begin{aligned} A(q^{-1})y(k) = & B_1(q^{-1})u(k) \\ & + B_2(q^{-1})u^2(k) + \dots + D(q^{-1})v(k) \end{aligned} \quad (7.5.2)$$

*Parametric Volterra model*

$$\begin{aligned} A(q^{-1})y(k) = & \quad B_1(q^{-1})u(k) \\ & + \sum_{\alpha} B_2(q^{-1})u(k)[q^{-\alpha}u(k)] \\ & + D(q^{-1})v(k) \end{aligned} \quad (7.5.3)$$

*Non-linear Model, Lachmann (1983)*

$$\begin{aligned} A_1(q^{-1})y(k) + \sum_{\alpha} A_2(q^{-1})y(k)[q^{-\alpha}y(k)] \\ = B(q^{-1})u(k) + D(q^{-1})v(k) \end{aligned} \quad (7.5.4)$$

In the case of an equation error optimization, these models have the advantage of being linear in the parameters. Therefore, linear parameter estimation methods like LS, RLS and RELS can be applied directly, Lachmann (1983), Isermann *et al.* (1992).

## 7.5.2 Artificial Neural Networks

For a general identification approach, methods of interest are those that do not require specific knowledge of the process structure and hence are widely applicable. Artificial neural networks fulfil these requirements. They are composed of mathematically formulated neurons. At first, these neurons were used to describe the behavior of biological neurons, McCulloch, Pitts (1943). The interconnection of neurons in networks allowed the description of relationships between input and output signals, Rosenblatt (1985), Widrow, Hoff (1960). In the sequel, artificial neural networks (ANN) are considered that map input signals  $u$  to output signals  $y$ , Figure 7.7. Usually, the adaptable parameters of neural networks are unknown. As a result, they have to be adapted or “trained” or “learned” by processing measured signals  $u$  and  $y$ , Hecht-Nielson (1990), Haykin (1994). This is a typical system identification problem. If inputs and outputs are gathered into groups or clusters, a classification task in connection with, *e.g.*, pattern recognition is given, Bishop (1995). In the following, the problem of non-linear system identification is considered (supervised learning). Thereby, the capability of ANNs to approximate non-linear relationships to any desired degree of accuracy is utilized. Firstly, ANNs for describing *static transfer behavior*, Hafner *et al.* (1992), Preuss, Tresp (1994), will be investigated, which will then be extended to *dynamic behavior*, Ayoubi (1996), Nelles *et al.* (1997), Isermann *et al.* (1997).

### a) Artificial neural networks for static systems

Neural networks are universal approximators for static non-linearities and are consequently an alternative to polynomial approaches. Their advantages are the need for only little *a priori* knowledge about the process structure and the uniform treatment of single-input and multi-

input processes. In the following, it is assumed that a non-linear system with  $P$  inputs and  $M$  outputs has to be approximated, see Figure 7.7.

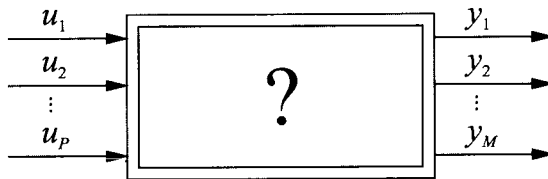


**Figure 7.7.** System with  $P$  inputs and  $M$  outputs, which has to be approximated by an artificial neural network

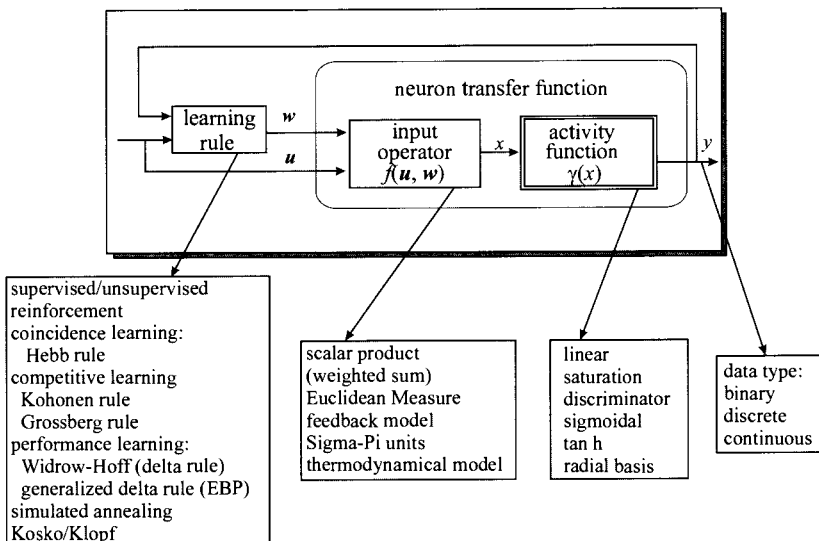
### Neuron model

Figure 7.8 shows the block diagram of a neuron. In the *input operator* (synaptic function), a similarity measure between the input vector  $\mathbf{u}$  and the (stored) weight vector  $\mathbf{w}$  is formed, e.g., by the scalar product

$$x = \mathbf{w}^T \mathbf{u} = \sum_{i=1}^P w_i u_i = \|\mathbf{w}\| \|\mathbf{u}\| \cos \phi \quad (7.5.5)$$

or the Euclidean distance

$$x = \|\mathbf{u} - \mathbf{w}\|^2 = \sum_{i=1}^P (u_i - w_i)^2 \quad (7.5.6)$$



**Figure 7.8.** General neuron model

If  $w$  and  $u$  are similar, the resulting scalar quantity  $x$  will be large in the first case and small in the second case. The quantity  $x$ , also called the *activation of the neuron*, affects the activation function and consequently the output value  $y$

$$y = \gamma(x - c) \quad (7.5.7)$$

Figure 7.9 shows several examples of those in general non-linear functions. The threshold  $c$  is a constant causing a parallel shift in the  $x$ -direction.

a. hyperbolic tangens (Tangens Hyperbolicus)

$$y = \frac{e^{(x-c)} - e^{-(x-c)}}{e^{(x-c)} + e^{-(x-c)}} = 1 - \frac{2}{1 + e^{2(x-c)}}$$

b. Sigmoidal function

$$y = \frac{1}{1 + e^{-(x-c)}}$$

c. limiter

$$y = \begin{cases} 1 & ; x - c \geq 1 \\ x - c & ; |x - c| < 1 \\ -1 & ; x - c \leq -1 \end{cases}$$

d. neutral zone

$$y = \begin{cases} 0 & ; |x - c| \leq 1 \\ x - c - 1 & ; x - c > 1 \\ x - c + 1 & ; x - c \leq -1 \end{cases}$$

e. Gauss-functions  $y = e^{-(x-c)^2}$

f. binary function

$$y = \begin{cases} 0 & ; x - c < 0 \\ 1 & ; x - c > 0 \end{cases}$$

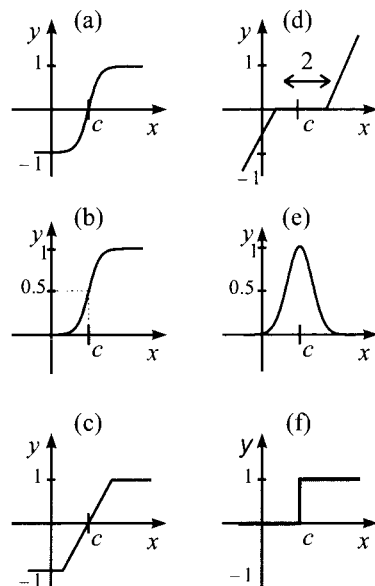


Figure 7.9. Examples of activation functions

### Network structure

The single neurons are interconnected to a network structure, Figure 7.10. Hence, one has to distinguish between different layers with parallel arranged neurons: the input layer, the first, second, ... hidden layer and the output layer. Generally, the input layer is used to scale the input signals and is not often counted as a separate layer. Then, the real network structure begins with the first hidden layer. Figure 7.10 shows the most important types of internal links between neurons: feedforward, backward, lateral and recurrent. With respect to their range of values, the input signals can be either binary, discrete or continuous. Binary and discrete signals are used especially for classification, while continuous signals are used for identification tasks.

### Multi-layer perceptron (MLP) network

The neurons of an MLP network are called perceptrons, Figure 7.11, and follow directly from the general neuron model, shown in Figure 7.8. Typically, the input operator is realized as a scalar product, while

the activation functions are realized by sigmoidal or hyperbolic tangent functions. The latter ones are a multiple of differentiable functions yielding a neuron output with  $y \neq 0$  in a wide range. Therefore, they have a global effect with extrapolation capability. The weights  $w_i$  are assigned to the input operator and lie in the signal flow before the activation function.

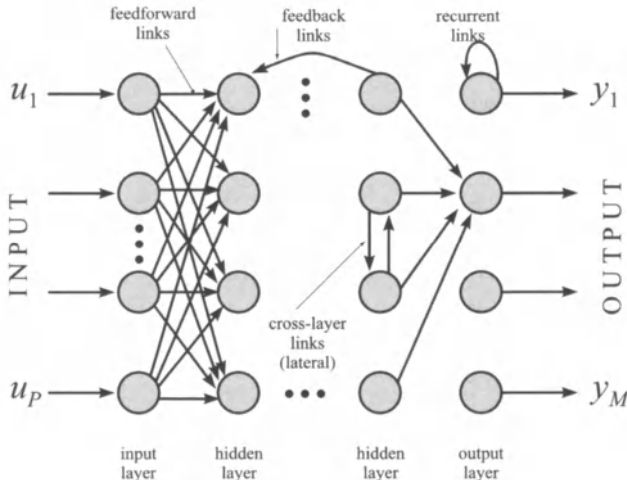


**Figure 7.10.** Network structure: layers and links in a neural network

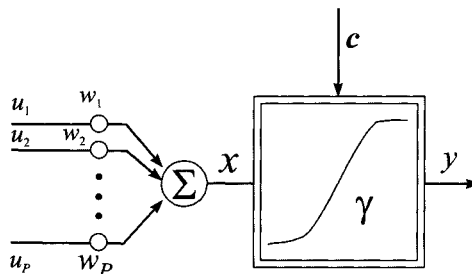


**Figure 7.11.** Perceptron neuron with weights  $w_i$ , summation of input signals (scalar product) and non-linear activation function

The perceptrons are connected in parallel and are arranged in consecutive layers to a feedforward MLP network, Figure 7.12. Each of the  $P$  inputs affects each perceptron in such a way that in a hidden layer with  $K$  perceptrons there exist  $(K \cdot P)$  weights  $w_{kp}$ . The output neuron is most often a perceptron with a linear activation function, Figure 7.13.

The adaptation of the weights  $w_i$  based on measured input and output signals is usually realized by the minimisation of the quadratic loss function.

$$J(\mathbf{w}) = \frac{1}{2} \sum_{n=1}^{N-1} e^2(n) \quad (7.5.8)$$

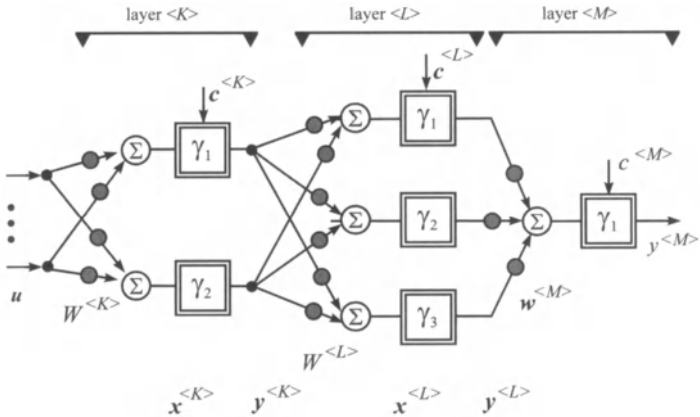


**Figure 7.12.** Feedforward multi-layer perceptron network (MLP network). Three layers with  $(2 \cdot 3 \cdot 1)$  perceptrons.  $\langle K \rangle$  is the first hidden layer

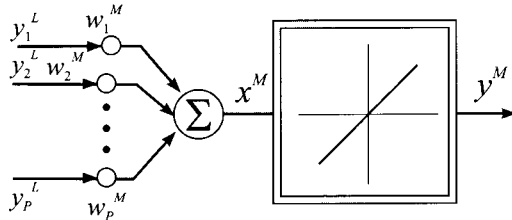


**Figure 7.13.** Output neuron as perceptron with linear activation function

$$e(n) = y(n) - \hat{y}(n)$$

where  $e$  is the model error,  $y$  is the measured output signal and  $\hat{y}$  is the network output.

As in the case of parameter estimation with the least squares method,

$$\frac{dJ(\mathbf{w})}{d\mathbf{w}} = \mathbf{0} \quad (7.5.9)$$

is generated. Due to the non-linear dependency, a direct solution is not possible. Therefore, e.g., gradient methods for numerical optimization are applied. Because of the necessary back-propagation of errors through all hidden layers, the method is called “error back-propagation” or also “delta-rule”. The so-called learning rate  $\eta$  has to be chosen (tested) suitably. In principle, gradient methods allow only slow convergence in the case of a large number of unknown parameters.

### Radial basis function (RBF) Network

The neurons of RBF networks, Figure 7.14, compute the Euclidean distance in the input operator

$$x = \|\mathbf{u} - \mathbf{c}\|^2 \quad (7.5.10)$$

and feed it to the activation function

$$G_m = \gamma_m (\|\mathbf{u} - \mathbf{c}\|^2) \quad (7.5.11)$$

The activation function is given by radial basis functions usually in the form of Gaussian functions with

$$\gamma_m = \exp \left[ -\frac{1}{2} \left( \frac{(u_1 - c_{m1})^2}{\sigma_{m1}^2} + \frac{(u_2 - c_{m2})^2}{\sigma_{m2}^2} + \dots + \frac{(u_P - c_{mP})^2}{\sigma_{mP}^2} \right) \right] \quad (7.5.12)$$

The centres  $c_j$  and the standard deviations  $\sigma_j$  are determined *a priori* so that the Gaussian functions are spread, e.g., uniformly in the input space. The activation function determines the distances of each input signal to the center of the corresponding basis function. However, radial basis functions contribute to the model output only locally, namely in the vicinity of their centers. They possess less extrapolation capability, since their output values tend to go to zero with a growing distance to their centers.

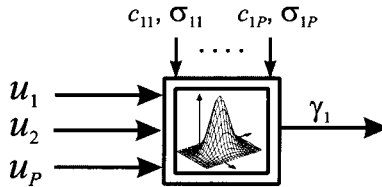


Figure 7.14. Neuron with radial basis function

Usually, radial basis function networks consist of two layers, Figure 7.15. The outputs  $\gamma_i$  are weighted and added up in a neuron of the perceptron type, Figure 7.13, so that

$$y = \sum_{m=1}^M w_m G_m (\|\mathbf{u} - \mathbf{c}\|^2) \quad (7.5.13)$$

Since the output layer weights are located behind the non-linear activation functions in the signal flow, the error signal is linear in these parameters and, consequently, the least squares method in its explicit form can be applied. In comparison to MLP networks with gradient methods, a significantly faster convergence can be obtained. However, if the centers and standard deviations have to be optimized too, non-linear numerical optimization methods are also required.

#### *Local linear model networks*

The local linear model network (LOLIMOT) is an extended radial basis function network, Nelles (1997), Nelles (2001). It is extended by replacing the output layer weights with a linear function of the network inputs (7.5.14). Furthermore, the RBF network is normalized, such that the sum of all basis functions is one. Thus, each neuron represents a local linear model with its corresponding validity function, see Figure 7.16. The validity functions determine the regions of the input space

where each neuron is active. The general architecture of local model networks is extensively discussed in Murray-Smith, Johansen (1997).

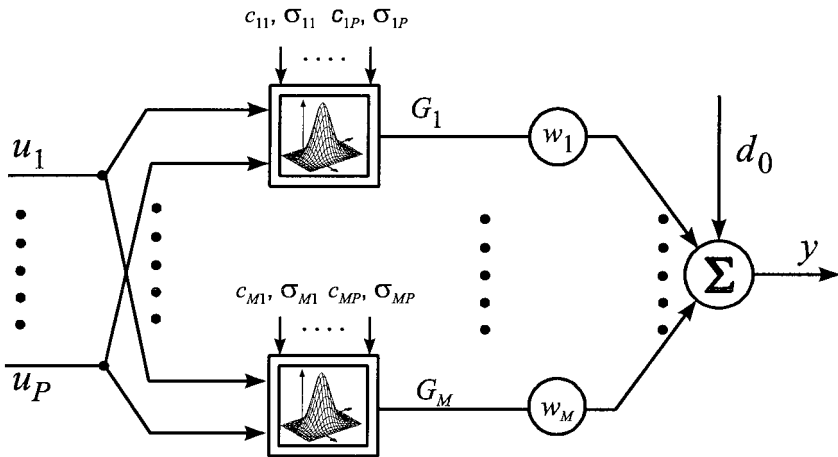


Figure 7.15. Feedforward radial basis function (RBF) network

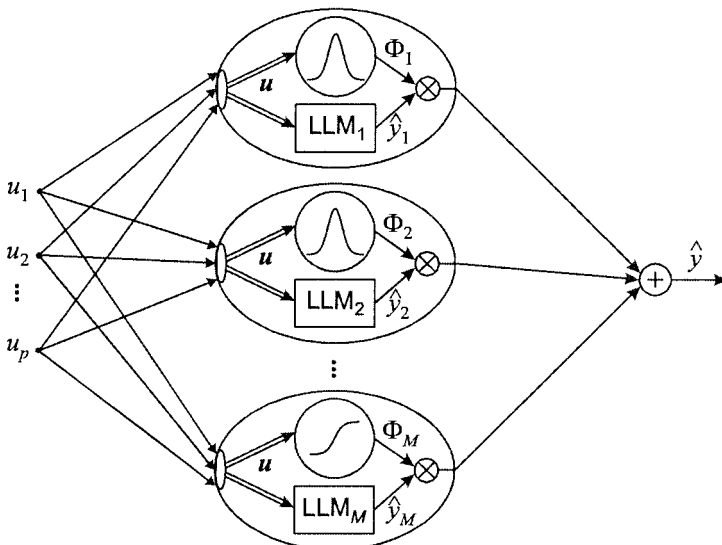


Figure 7.16. Local linear model network (LOLIMOT)

The kind of local model network discussed here utilizes normalized Gaussian validity functions (7.5.15) and an axis-orthogonal partitioning of the input space. Therefore, the validity functions can be composed of one-dimensional membership functions and the network can be interpreted as a Takagi-Sugeno fuzzy model, see Section 7.5.3.

The output of the local linear model is calculated by

$$\hat{y} = \sum_{i=1}^M \Phi_i(\mathbf{u}) (w_{i,p} + w_{i,1}u_1 + \dots + w_{i,p}u_p) \quad (7.5.14)$$

with the normalized Gaussian validity functions

$$\Phi_i(\mathbf{u}) = \frac{\mu_i(\mathbf{u})}{\sum_{j=1}^M \mu_j(\mathbf{u})} \quad (7.5.15)$$

here

$$\mu_i(\mathbf{u}) = \prod_{j=1}^P \exp \left( -\frac{1}{2} \left( \frac{(\mathbf{u}_j - c_{i,j})^2}{\sigma_{i,j}^2} \right) \right) \quad (7.5.16)$$

The centers  $c$  and standard deviations  $\sigma$  are non-linear parameters, while the local model parameters  $w_i$  are linear parameters. The local linear model tree (LOLIMOT) algorithm is applied for the training. It consists of an outer loop, in which the input space is decomposed by determining the parameters of the validity functions, and a nested inner loop in which the parameters of the local linear models are optimized by local-weighted least squares estimation.

The input space is decomposed in an axis-orthogonal manner, yielding hyper-rectangles in whose centers the Gaussian validity functions  $\mu_i(\mathbf{u})$  are placed. The standard deviations of these Gaussians are chosen proportionally to the extension of hyper-rectangles to account for the varying granularity. Thus, the non-linear parameters  $c_{i,j}$  and  $\sigma_{i,j}$  are determined by a heuristic-avoiding explicit non-linear optimization. LOLIMOT starts with a single linear model that is valid for the whole input space. In each iteration, it splits one local linear model into two new sub-models. Only the (locally) worst performing local model is considered for further refinement. Splits along all input axes are compared and the best performing alternative is carried out, see Figure 7.17.

The main advantages of this local model approach are the inherent structure identification and the very fast and robust training algorithm. The model structure is adapted to the complexity of the process. However, explicit application of time-consuming non-linear optimization algorithms can be avoided.

Another local linear model architecture, the so-called hinging hyperplane trees, is presented in Ernst (Töpfer) (1998), Töpfer (2002). These models can be interpreted as an extension of the LOLIMOT networks with respect to the partitioning scheme. While the LOLIMOT algorithm is restricted to axis-orthogonal splits, the hinging hyperplane trees allow an axis-oblique decomposition of the input space. These more complex partitioning strategies lead to an increased effort in model construction. However, this feature is necessary in the case of strong non-linear model behavior and higher-dimensional input spaces.

The fundamental structures of three artificial neural networks have been described. These models are very well suited to the approximation of measured input/output data of *static processes*, compare also Hafner *et al.* (1992), Preuss, Tresp (1994). For this, the training data has to be chosen in such a way that the considered input space is as evenly as possible covered with data. After the training procedure, a parametric

mathematical model of the static process behavior is available. Consequently, direct computation of the output values  $\hat{y}$  for arbitrary input combinations  $u$  is possible.

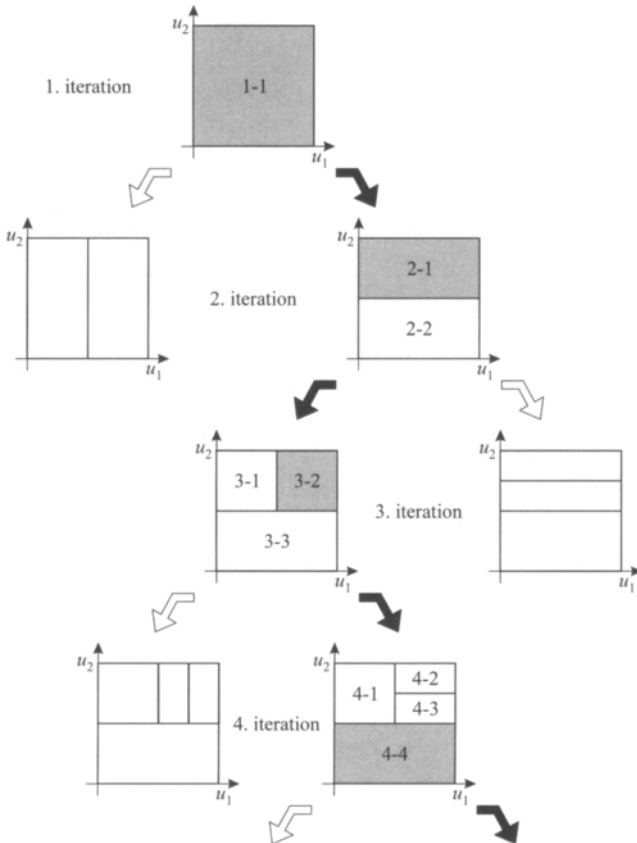


**Figure 7.17.** Tree construction of the LOLIMOT algorithm

An advantage of the automatic training procedure is the possibility of using arbitrarily distributed data in the training data set. There is no necessity to know data at exactly defined positions, as in the case of grid-based look-up table models, see Section 7.5.4. This clearly decreases the effort required for measurements in practical applications.

**Example 7.1.** Artificial neural network for the static behavior of a combustion engine

As an example, the engine characteristics of a six-cylinder SI (spark-ignition) engine is used. Here, the engine torque has to be identified and is dependent on the throttle angle and the engine speed. Figure 7.18 shows the 433 available data points that were measured on an engine test stand.

For the approximation, an MLP network is applied. After the tri-

ning, an approximation for the measurement data shown in Figure 7.19 is given. For that purpose, 31 parameters are required. Obviously, the neural network possesses good interpolation and extrapolation capabilities. This also means that in areas with only few training data, the process behavior can be approximated quite well, Holzmann *et al.* (1997).

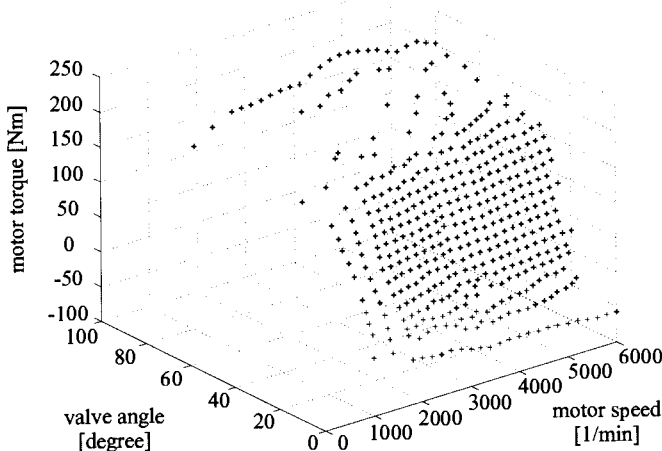


**Figure 7.18.** Measured SI engine data (2.5 l, V6 cyl.): unevenly distributed, 433 measurement data points

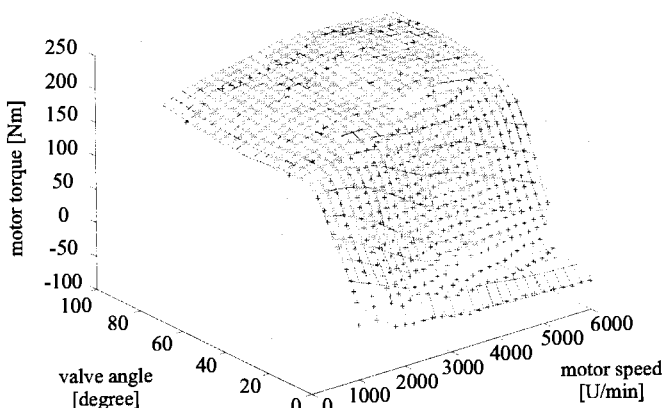


**Figure 7.19.** Approximation of measured engine data (+) with an MLP network ( $2 \cdot 6 \cdot 1$ ): 31 parameters

□

### b) Artificial neural networks for dynamic systems

The memoryless static networks can be extended with dynamic elements to dynamic neural networks. One can distinguish between neural networks with external and internal dynamics, Nelles *et al.* (1997), Isermann *et al.* (1997). ANNs with external dynamics are based

on static networks, e.g., MLP or RBF networks. The discrete time input signals  $u(k)$  are passed to the network through additional filters  $F_i(q^{-1})$ . In the same way, either the measured output signals  $y(k)$  or the NN outputs  $\hat{y}(k)$  are passed to the network through filters  $G_i(q^{-1})$ . The operator  $q^{-1}$  denotes a time shift

$$y(k) \cdot q^{-1} = y(k-1) \quad (7.5.17)$$

In the simplest case, the filters are pure time delays, Figure 7.20a,

$$\hat{y}(k) = f_{NN} [u(k), u(k-1), \dots, \hat{y}(k-1), \hat{y}(k-2), \dots] \quad (7.5.18)$$

where the time-shifted sampled values are the network input signals. The structure in Figure 7.20a shows a parallel model (equivalent to the output error model for parameter estimation of linear models). In Figure 7.20b, the measured output signal is passed to the network input. Then, the series-parallel model is obtained (equivalent to the equation error model for parameter estimation of linear models). One advantage of the external dynamic approach is the possibility of using the same adaptation methods as in the case of static networks. However, the drawbacks are the increased dimensionality of the input space, possible stability problems and an iterative way of computing the static model behavior, namely through simulation of the model. Then, for example, a step function is used as the input signal and one has to wait until the steady state of the model is reached.

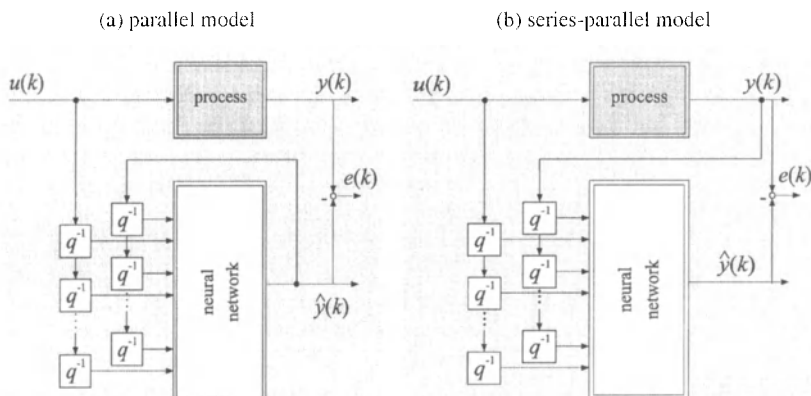


**Figure 7.20.** Artificial neural network with external dynamics: (a) parallel model; (b) series-parallel model

ANNs with internal dynamics realize dynamic elements inside the model structure. According to the kind of included dynamic elements, one can distinguish between recurrent networks, partially recurrent networks and locally recurrent globally feedforward networks (LRGF), Nelles *et al.* (1997). The LRGF networks maintain the structure of static networks except that dynamic neurons are utilized, see Figure 7.21. The following can be distinguished: local synapse feedback, local activation feedback and local output feedback. The simplest case is the lo-

cal activation feedback, Ayoubi (1996). Here, each neuron is extended by a linear transfer function, most often of first or second order, see Figure 7.22. The dynamic parameters  $a_i$  and  $b_i$  are adapted. Static and dynamic behavior can be easily distinguished and stability can be guaranteed.

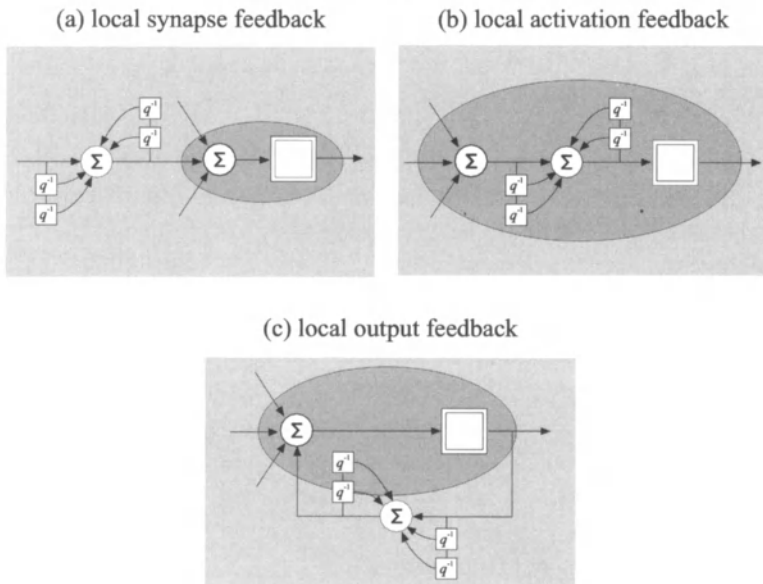


**Figure 7.21.** Dynamic neurons for neural networks with internal dynamics: (a) local synapse feedback; (b) local activation feedback; (c) local output feedback

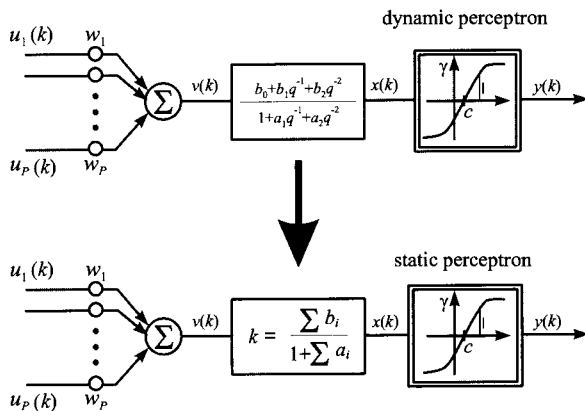


**Figure 7.22.** Dynamic perceptron, Ayoubi (1996)

Usually, MLP networks are used in LRGF structures. However, RBF networks with dynamic elements in the output layer can be applied as well, if a Hammerstein-structure of the process can be assumed, Ayoubi (1996). Usually, the adaptation of these dynamic NNs is based on extended gradient methods, Nelles *et al.* (1997).

Based on the basic structure of ANNs, special structures with particular properties can be built. If, for example, the local linear model networks (LOLIMOT) are combined with the external dynamic approach, a model structure with locally valid linear input/output models result.

**Example 7.2.** Artificial neural networks for the identification of the dynamic behavior of combustion engine emissions

The following example illustrates the application and performance of a dynamic neural network for the identification of combustion engine emissions. Accurate emission models can, *e.g.*, be employed for tasks like the design of controllers, model-based optimization of the engine, model-based fault detection and diagnosis, *etc.* Unfortunately, it is hardly possible to build emission models based on first principles because a lot of complex thermodynamic and chemical reactions underlie combustion and exhaust formation and there is decisive influence by local effects and disturbances. Neural networks, however, are well suited to experimental modeling, *i.e.*, identification of the emission behavior based on measured input–output data, Hafner *et al.* (2000).

In this example, a dynamic  $\text{NO}_x$  model for a VW 1.9 l TDI diesel engine is to be built. The data was collected at a fixed operating point with an engine speed of 1000 rpm and an engine torque of 130 Nm. The manipulated variables for the control of the specific engine were chosen as inputs for the net, *i.e.*, position of the exhaust gas recirculation (EGR) valve, start of injection angle ( $\Theta_{inj}$ ) and position of the variable nozzle turbocharger (VGT). According to Figure 7.23, the model was realized by an internal dynamic multi-layer perceptron (DMLP) network with five hidden neurons and one output neuron. The dynamics of the process were incorporated by means of the chosen order of the filter transfer functions. In this case, the first order polynomials  $A_i$  and  $B_i$  led to quite satisfying results.

The measurements themselves have to be well designed in order to excite the process at its relevant amplitudes and frequencies. The resulting design of the experiment and the measured training data is depicted in Figure 7.24. With the most important time constants of the process being 1–3 s regarding EGR and VTG, the sampling time was set to  $T_0 = 100$  ms.

The training data (approximately 9000 measured points for each of the three model inputs and the output) was then used for the estimation of the specific model parameters. With the DMLP-training algorithm, it took some 45 minutes to generate the dynamic model with a root-mean-square error of 0.08. Figure 7.25a illustrates the performance of the model when generalized at some unknown data. The comparison between the measured and simulated behavior proves the quality of the network.

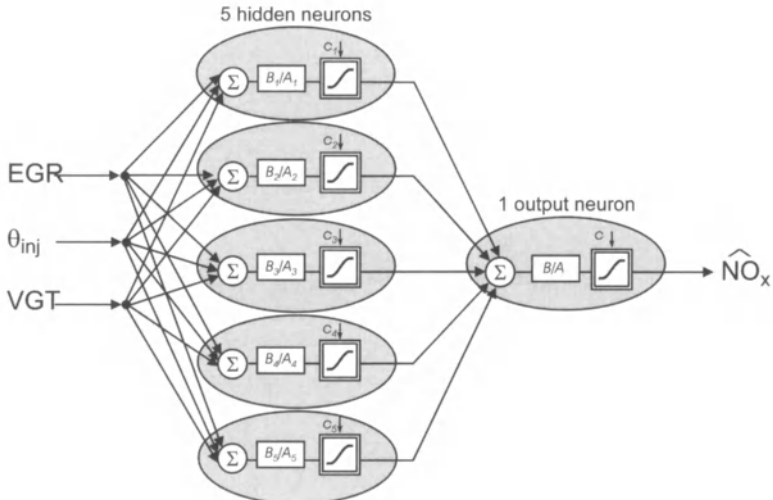


**Figure 7.23.** Structure of the dynamic artificial neural network for modelling the  $NO_x$  emissions with the inputs EGR (exhaust gas recirculation),  $\Theta_{inj}$  (start of injection) and VGT (position of the variable nozzle turbocharger)

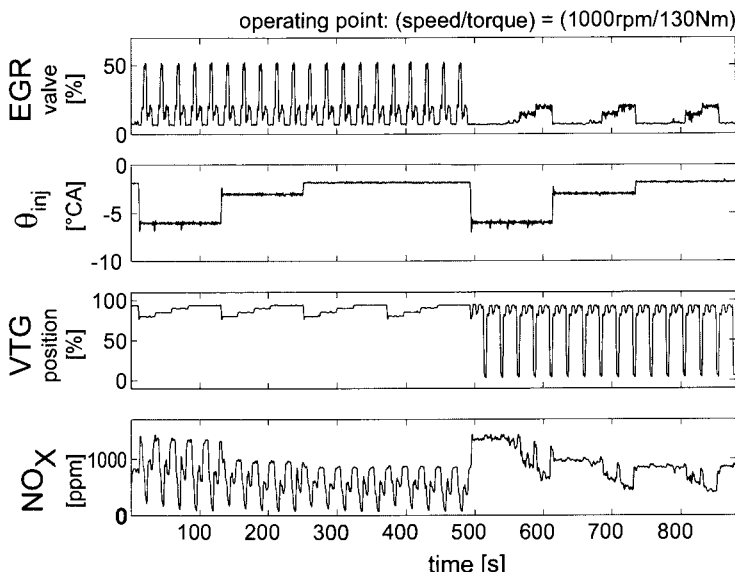


**Figure 7.24.** Dynamically measured data for the training of the ANN that excites the process at different amplitudes and frequencies (1.9 l TDI diesel engine at an engine speed of 1000 rpm and an engine torque of 130 Nm)

An additional benefit in dynamic modeling is the ability to calculate the static non-linearities of the process by means of the dynamic model. The static map in Figure 7.25b was derived by applying static input data to the  $NO_x$  model according to Figure 7.23. As expected, the  $NO_x$  emissions were raised with early injection (smaller numbers in  $\Theta_{inj}$  and low EGR values).

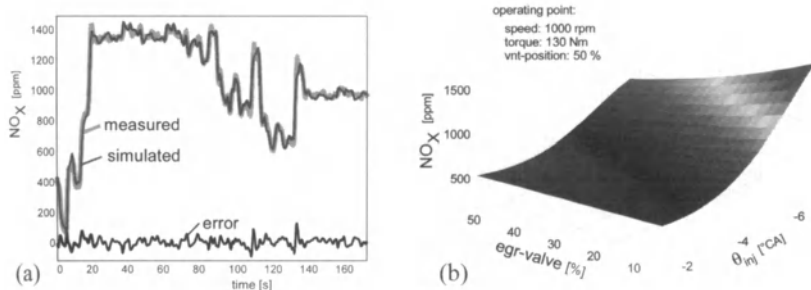


**Figure 7.25.** Approximation results: (a) generalization of the dynamic  $\text{NO}_x$  model; (b) calculation of the static process behavior by means of the dynamic neural network

□

### 7.5.3 Fuzzy-logic Models

A further possibility of approximating a non-linear process behavior is given by fuzzy-logic methods, *e.g.*, Bothe (1993), Kiendl (1996), Preuss (1992), Zadeh (1965). Figure 7.26 illustrates the basic structure of a fuzzy-logic system.

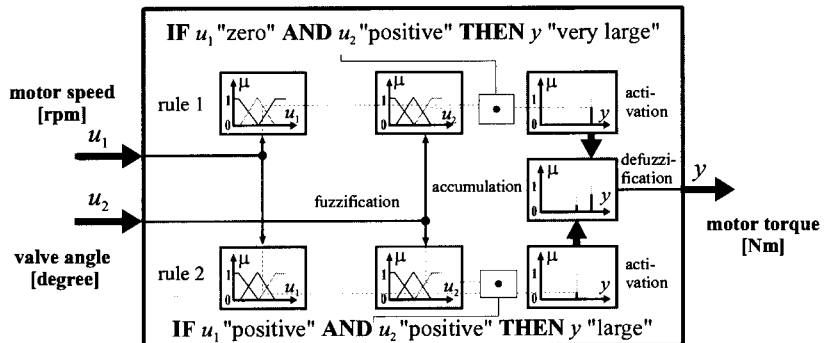


**Figure 7.26.** Basic structure of a fuzzy-logic system

The deterministic input values  $u_1$  and  $u_2$  are transformed by membership functions into “fuzzy” linguistic values. This procedure is called *fuzzification*. The linguistic values are then processed by *fuzzy if-then-rules*. The output of the rules is again given in a linguistic form. These values have to be summed up (accumulation) and finally they have to be transformed into crisp output values  $y$  by *defuzzification*.

Based on the linguistic description of fuzzy values, a fuzzy-logic description of a process with a moderate number of rules becomes transparent and easily modifiable.

In order to find a set of fuzzy rules that approximates a special process input/output behavior, so-called fuzzy identification methods are used. Wide spread methods of that kind are based, *e.g.*, on conventional parameter estimation methods, Pfeiffer (1995), or on the combination

of fuzzy-logic and neural networks, Kosko (1992), Preuss, Tresp (1994), Chiu (1994). These neuro-fuzzy methods allow the combination of the transparency of fuzzy descriptions and the adaptation capability of neural networks. To demonstrate the quality of fuzzy descriptions, Figure 7.27 shows the approximation of the considered non-linear engine characteristic, corresponding to Example 7.1 and Figures 7.18 and 7.19.

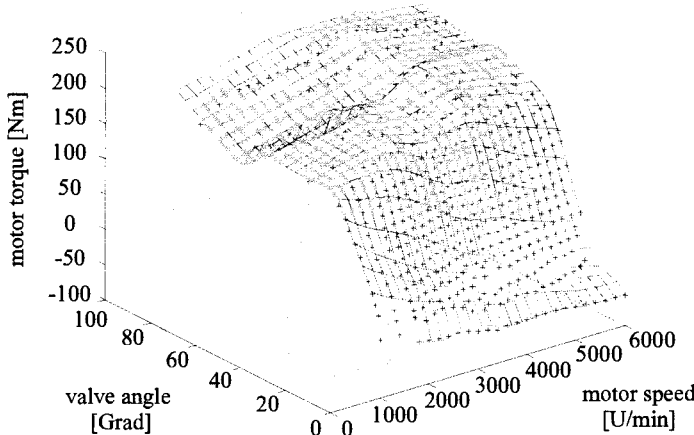


**Figure 7.27.** Fuzzy-logic representation of measured SI engine data (+) (12 fuzzy if-then-rules)

The quality of the approximation decisively depends on the number of membership functions and rules of the fuzzy system. If a relatively simple fuzzy system is chosen, problems, especially with the representation of complex process behavior with strong non-linearities, arise. On the other hand, if the fuzzy system is too complex, the approximated output will show overfitting, *i.e.*, the desirable smoothing effect especially with regard to noisy measurement data is lost. The fuzzy system shown in Figure 7.27 consists of 12 membership functions together for both inputs and 12 fuzzy rules. For identification, a neuro-fuzzy method was applied, Jang (1993).

A direct comparison with the model output of the MLP network (Figure 7.19) shows poorer results for the fuzzy identification method mainly in regions with only few training data. The computational effort for model generation is similar for both neural and neuro-fuzzy methods.

As described for neural networks, fuzzy systems can also be extended with dynamic elements. However, mainly the external dynamic approach is applied in combination with fuzzy systems. The resulting dynamic fuzzy systems possess similar features like the external dynamic neural networks.

### 7.5.4 Grid-based Look-up Tables for Static Systems

In this section, a further non-linear model architecture besides the polynomial-based models, neural networks and fuzzy systems is presented. These grid-based look-up tables are the most common type of non-linear static models used in practice. Especially in the field of non-linear control, look-up tables are widely accepted as they provide a transparent and flexible representation of non-linear relationships. Electronic control units of modern automobiles, for example, contain about 100 such grid-based look-up tables, in particular for engine and emission control, Bosch (1995).

In automotive applications, due to cost reasons computational power and storage capacity are strongly restricted. Furthermore, constraints of real-time operation have to be met. Under these conditions, grid-based look-up tables represent a suitable means of storage of non-linear static mappings. The models consist of a set of data points or nodes positioned on a multidimensional grid. Each node comprises two components. The scalar data point heights are estimates of the approximated non-linear function at their corresponding data point position. All nodes located on grid lines, as shown in Figure 7.28, are stored, *e.g.*, in the ROM of the control unit. For model generation, usually all data point positions are fixed *a priori*. The most widely applied method of obtaining the data point heights is to position measurement data points directly on the grid. Then, an optimization can be avoided.

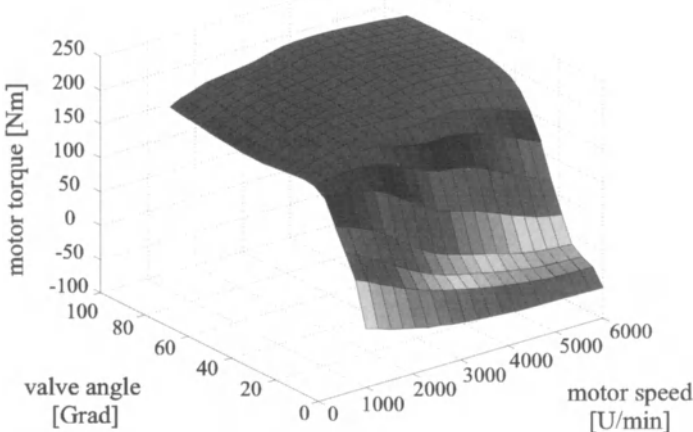


**Figure 7.28.** Grid-based look-up table of a six-cylinder SI engine

In the following, the most common two-dimensional case will be considered. The calculation of the desired output  $Z$  for given input values  $X$  and  $Y$  consists of two steps. In the first step, the indices of the enclosing four data points have to be selected. Then, a bilinear area interpolation is performed, Schmitt (1995). For this, four areas have to be calculated, as shown in Figure 7.29, Schmitt (1995), Töpfer (2002).

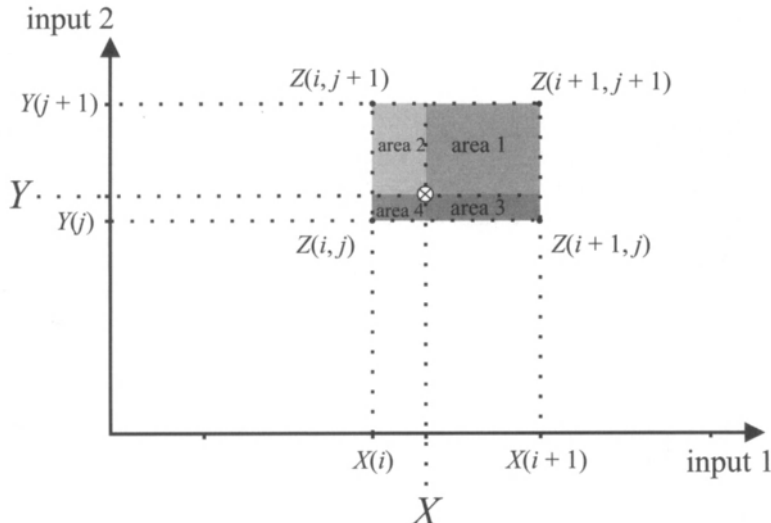


**Figure 7.29.** Areas for interpolation within a look-up table

For the calculation of the desired output  $Z$ , the four selected data point heights are weighted with the opposite areas and added up. Finally, this result has to be divided by the total area, (7.5.19).

$$\begin{aligned}
 Z(X, Y) = & [Z(i,j) \frac{(X(i+j) - X)(Y(j+1) - Y)}{\text{area 1}} \\
 & + [Z(i+1,j) \frac{(X - X(i)) (Y(j+1) - Y)}{\text{area 2}} \\
 & + [Z(i,j+1) \frac{(X(i+1) - X) (Y - Y(j))}{\text{area 3}} \\
 & + [Z(i+1,y+1) \frac{(X - X(i)) (Y - Y(j))}{\text{area 4}}] \\
 & \div [\frac{(X(i+1) - X(i)) (Y(j+1) - Y(j))}{\text{overall area}}]
 \end{aligned} \tag{7.5.19}$$

Because of the relatively simple computational algorithm, area interpolation rules are widely applied, especially in real-time applications. The accuracy of the method depends on the number of grid positions. For the approximation of “smooth” mappings, a small number of data points is sufficient, while for stronger non-linear behavior a finer grid has to be chosen.

The area interpolation is based on the assumption that all data point heights are available in the whole range covered by the grid. However, this condition is often not fulfilled.

Grid-based look-up tables belong to the class of *non-parametric models*. The described model structure has the advantage that a subsequent adaptation of single data point heights due to changing environmental conditions is easy to realize. However, the main disadvantage of this look-up table is the exponential growth of the number of data

points with an increasing number of inputs. Therefore, grid-based look-up tables are restricted to one- and two-dimensional input spaces in practical applications. Determination of the heights of the look-up table based on measurements at arbitrary coordinates with parameter estimation methods is treated by Müller (2002).

Another alternative are *parametric model* representations, like polynomial models, neural networks or fuzzy models, which clearly require less model parameters to approximate a given input–output relationship. Therefore, the storage demand of these models is much lower. However, in contrast to area interpolation, the complexity of the computation of the output is much higher, since complex non-linear functions for each neuron of a fuzzy rule has to be computed. On the other hand, grid-based look-up tables are not suitable for the identification and modeling of dynamic process behavior.

A detailed overview of model structures for non-linear system identification is given in Nelles (2001).

### 7.5.5 Parameter Estimation for Non-continuously Differentiable Non-linear Processes (Friction and Backlash)

Non-continuously differentiable non-linear processes appear in mechanical systems, especially in the form of friction and backlash and in electrical systems with magnetization hysteresis.

#### a) Processes with friction

In Section 4.7, it was specified how to consider dry and viscous friction in differential equations. Here, dry friction appears as a constant with a velocity-dependent sign. In steady state, a hysteresis curve arises from the dynamic relationship.

For the identification of processes with friction, the hysteresis curve can directly be found point-wise by slow continuous or stepwise changes of the input signal  $u(t) = y_1(t)$  and the measurement of  $y(t) = y_2(t)$ .

If the hysteresis curves are described by

$$\begin{aligned} y_+(u) &= K_{0+} + K_{1+} u \\ y_-(u) &= K_{0-} + K_{1-} u \end{aligned} \quad (7.5.20)$$

then the parameters can be estimated from  $v = 1, 2, \dots, N - 1$  measured points with the least squares method

$$\hat{K}_{1\pm} = \frac{N \sum u(v)y_{\pm}(v) - \sum u(v)\sum y_{\pm}(v)}{N \sum u^2(v) - \sum u(v)\sum u(v)} \quad (7.5.21)$$

$$\hat{K}_{0\pm} = \frac{1}{N} \left[ \sum y_{\pm}(v) - \hat{K}_{1\pm} \sum u(v) \right] \quad (7.5.22)$$

As the differential equations are linear in the parameters, direct

methods of parameter estimation can be applied for processes with dry and viscous friction in motion. For this, both differential and difference equations are well-suited process models. In some cases, it is expedient not only to use velocity-dependent dry friction but also velocity direction-dependent dynamic parameters, *e.g.*, in the form of difference equations

$$y(k) = - \sum_{i=1}^m a_{i+} y(k-i) + \sum_{i=1}^m b_{i+} u(k-i) + K_{0+} \quad (7.5.23)$$

$$y(k) = - \sum_{i=1}^m a_{i-} y(k-i) + \sum_{i=1}^m b_{i-} u(k-i) + K_{0-} \quad (7.5.24)$$

$K_{0+}$  and  $K_{0-}$  can be understood as direction-dependent offsets or DC values. Then, the following methods can be applied for the estimation of these offsets:

- implicit estimation of the offset parameters  $K_{0+}$  and  $K_{0-}$ ;
- explicit estimation of the offset parameters  $K_{0+}$  and  $K_{0-}$  with generation of differences  $\Delta y(k)$  and  $\Delta u(k)$  and parameter estimation for

$$\Delta y(k) = - \sum_{i=1}^m \hat{a}_i \Delta y(k-i) + \sum_{i=1}^m \hat{b}_i \Delta u(k-i) \quad (7.5.25)$$

with the assumption of velocity-independent dynamic parameters  $\hat{a}_i$  and  $\hat{b}_i$ . Then, for each direction, the parameters  $\hat{K}_{0+}$  and  $\hat{K}_{0-}$  have to be estimated separately.

For this parameter estimation method with a direction-dependent model, an additional identification requirement has to be considered, which is that the motion takes place in only one direction without reversal. This means it has to satisfy

$$\dot{y}(t) > 0 \quad \text{or} \quad \dot{y}(t) < 0 \quad (7.5.26)$$

which can be tested by

$$\Delta y(k) > \epsilon \quad \text{or} \quad \Delta y(k) < -\epsilon \quad (7.5.27)$$

for all  $k$  with  $\epsilon \geq 0$ .

A test signal for proportional acting processes fulfilling this condition was proposed by Maron (1991), Figure 7.30. The motion in one direction with a certain velocity is generated by a linear ascent. Then, this is followed by a step for the excitation of higher frequencies and a transition to a steady state condition. In the case of a reversal of motion, the parameter estimation has to be stopped (in Figure 7.30 the points 1, 2, 3, ...) and has either to be restarted or continued with values according to the same direction.

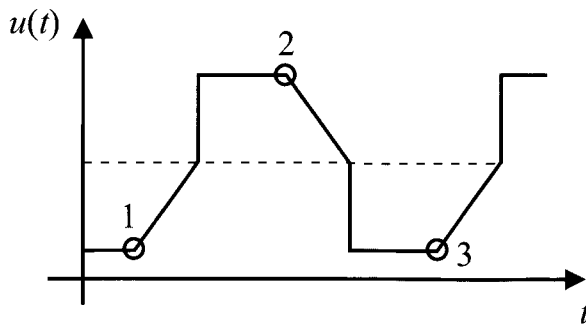


**Figure 7.30.** Test signal for parameter estimation of processes with dry friction

The hysteresis curve can be computed from the static behavior of the model (7.5.23), (7.5.24)

$$y_+(u) = \frac{\hat{K}_{0+}}{1 + \sum \hat{a}_{i+}} + \frac{\sum \hat{b}_{i+}}{1 + \sum \hat{a}_{i+}} u \quad (7.5.28)$$

$$y_-(u) = \frac{\hat{K}_{0-}}{1 + \sum \hat{a}_{i-}} + \frac{\sum \hat{b}_{i-}}{1 + \sum \hat{a}_{i-}} u \quad (7.5.29)$$

For the verification of the parameter estimation based on the dynamic behavior, the computed characteristic curve can be compared with the measured curve resulting directly from the measured static behavior.

For rotary drives, Held, Maron (1988), Held (1991) have developed a special parameter estimation method that correlates the measured torque with the rotational acceleration and estimates the moment of inertia. Following from that, the characteristic curve of the friction torque can be estimated in a non-parametric form.

The methods described above for the identification of processes with friction have been successfully tested in practical applications and applied to digital control with friction compensation, see Maron (1991), Raab (1992). Further treatment is given by Armstrong-Hélouvy (1991), Canudas de Wit (1988).

### b) Processes with backlash (dead zone)

As an example again, an oscillator with backlash or dead zone of width  $2y_t$  is considered, Figure 7.31. For the oscillator without backlash, it is

$$m\ddot{y}_2(t) + d\dot{y}_2(t) + cy_2(t) = cy_3(t) \quad (7.5.30)$$

The backlash can be described as follows

$$y_3(t) = \begin{cases} y_1(t) - y_t & \text{for } y_1(t) > y_t \\ 0 & \text{for } -y_t \leq y_1(t) \leq y_t \\ y_1(t) + y_t & \text{for } y_1(t) < -y_t \end{cases} \quad (7.5.31)$$

This equation leads to the non-linear characteristic shown in Figure 7.31b. In the case where the backlash is at one restriction ( $y_1(t) > y_t$ ), it is

$$m\ddot{y}_2(t) + d\dot{y}_2(t) + cy_2(t) + cy_t = cy_1(t) \quad (7.5.32)$$

and for the other restriction with  $y_1(t) < y_t$

$$m\ddot{y}_2(t) + d\dot{y}_2(t) + cy_2 - cy_t = cy_1(t) \quad (7.5.33)$$

The backlash appears as a constant with a sign depending on the sign of  $y_1(t)$ . For the range inside the backlash, it is  $y_3(t) = 0$  and it holds that the system eigen-behavior

$$m\ddot{y}_2(t) + d\dot{y}_2(t) + cy_2(t) = 0 \quad (7.5.34)$$

if point 3 (for instance, because of a friction not considered) is fixed. If point 3 is not fixed and can move arbitrarily inside the backlash, the spring forces do not apply. Then, one has to set  $y_2 = y_3$  and in (7.5.30)  $c = 0$ .

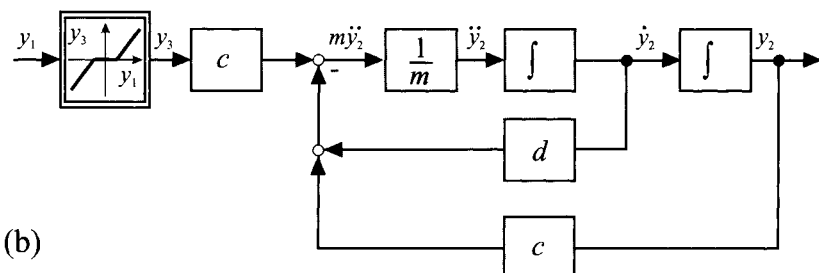
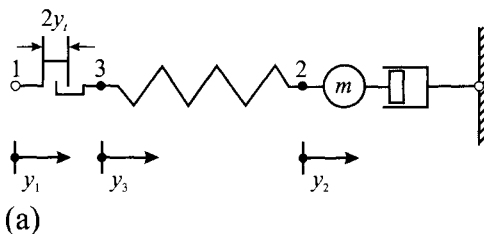


**Figure 7.31.** Mechanical oscillator with backlash (dead zone): (a) schematic set-up; (b) block diagram for the cases  $y_1(t) > y_t$  and  $y_1(t) < y_t$

One obtains a simplified block diagram for the regions outside the backlash shown in Figure 7.32. The effect of the backlash in these regions can be interpreted as an offset shift of the input signal with changing sign.

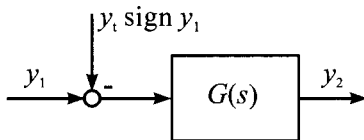


**Figure 7.32.** Simplified block diagram for a linear system with backlash for  $|y_1(t)| > |y_t|$

## 7.6 PROBLEMS

- 7.6.1 The following linear first order difference equation is given  
 $y(k) + a_1 y(k-1) = b_1 u(k - 1)$ .  
 The measured input and output signals  $u(k)$  and  $y(k)$  respectively, with  $k = 1 \dots N$ , are given. What are the estimation equations to calculate the parameters  $a_1$  and  $b_1$  with the least squares method?  
 What has to be changed in the estimation equation if a dead-time of  $d = 5$  is added?
- 7.6.2 Derive the estimation equation for the estimation of the weighting function  $g(k)$ ,  $k = 0 \dots n$  (impulse response) of a linear process using the least squares method given the measured input and output signals  $u(k)$  and  $y(k)$  ( $k = 1 \dots N$ ) respectively?
- 7.6.3. The linear first order system  
 $y(k) + a_1 y(k-1) = b_1 u(k - 1)$   
 is given with the following measurements:
- | $k$    | 0 | 1 | 2  | 3 | 4 | 5 | 6  | 7  | 8 | 9 | 10 |
|--------|---|---|----|---|---|---|----|----|---|---|----|
| $u(k)$ | 0 | 1 | -1 | 1 | 1 | 1 | -1 | -1 | 0 | 0 | 0  |
| $y(k)$ | 0 | 0 | 0  | 0 | 0 | 0 | 1  | 0  | 0 | 0 | 0  |
- Calculate the estimates of the parameters  $a_1$  and  $b_1$ .
- 7.6.4 State the recursive estimation equations for the least squares method for the linear first order process  
 $y(k) + a_1 y(k - 1) = b_1 u(k - 1)$   
 What has to be changed in the estimation equations if a dead-time of  $d = 2$  is added?
- 7.6.5 The first order differential equation  
 $y(t) + a_1 \dot{y}(t) = b_0 u(t)$   
 describes a linear system in continuous time domain. The input

and the output signal  $u(t)$  and  $y(t)$  and its derivative  $\dot{y}(t)$  are measured at discrete time samples  $k = 1 \dots N$ . Determine the equations to estimate the parameters  $a_1$  and  $b_0$  of the differential equation with the least squares method.

- 7.6.6 What are the conditions for the utilization of direct parameter estimation methods (e.g., LS method) for the parameters of polynomial non-linear models?
- 7.6.7 Sketch a neuron of a MLP and a RBF network.
- 7.6.8 The training of MLP networks and the training of the output layer weights of RBF networks should be compared. Which kind of optimization methods are applicable? Characterize the different optimization methods.
- 7.6.9 Consider a two-layer perceptron network with  $P$  inputs,  $K$  hidden neurons and  $M$  output units. Write down an expression for the total number of network weights.
- 7.6.10 Determine the equations for the interpolation of a grid-based look-up table with one input and one output. What kind of interpolation appears in this one-dimensional case?

# 8 Models of Oscillations and their Identification

---

Many technical processes are characterized by oscillating or cyclic behavior (rotary machines, alternating currents, *etc.*) The occurring signals  $y(t)$  are then *periodic* or contain periodic parts.

In mechatronic systems, periodic oscillations play an important role in many parts. For mechanical oscillation generators, which are powered, for instance, with electrical or hydraulic energy, oscillations of a certain form, amplitude and frequency have to be generated. However, in many cases, oscillations of power-generating and power-consuming machines or vehicles must be damped specifically. Changes in the oscillation behavior can also indicate faults such as unbalance or asymmetries in rotary machines making these suitable for supervision.

This chapter deals with the formation and description of harmonic oscillations. It is shown how one can determine and thus model the oscillation components of measured signals by means of the discrete Fourier transform and a special type of parameter estimation, the maximum entropy estimation.

## 8.1 HARMONIC OSCILLATIONS

For undamped periodic signals with cycle duration  $T_p$ , the following expression is generally valid

$$y(t) = y(t + T_p) \quad (8.1.1)$$

### 8.1.1 Single Oscillations

A harmonic steady state oscillation is described by a phase-shifted sine function

$$y(t) = y_0 \sin(2\pi f_0 t + \varphi) = y_0 \sin(\omega_0 t + \varphi) \quad (8.1.2)$$

with amplitude  $y_0$ , frequency  $f_0 = 1/T_p$ , angular frequency  $\omega_0 = 2\pi f_0$  and phase angle  $\varphi$ . A damped harmonic oscillation is denoted by

$$y(t) = y_0 e^{-\delta t} \sin(\omega_0 t + \varphi) \quad (8.1.3)$$

with the damping constant  $\delta$ .

Examples of the formation of such oscillations with mechanical systems have been shown in Chapter 4. In the following, the combination of different harmonic oscillations and their models in the time domain are considered.

### 8.1.2 Superposition

The simplest form of combined oscillations results from the superposition (addition)

$$y(t) = \sum_{v=1}^m y_0 e^{-\delta_v t} \sin(\omega_v t + \varphi_v) \quad (8.1.4)$$

The superposition of two undamped oscillations with the angular frequencies  $\omega_1$  and  $\omega_2$  yields the amplitude spectrum shown in Figure 8.1.

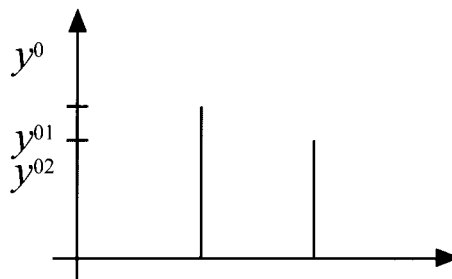


**Figure 8.1.** Amplitude spectrum for the superposition of two oscillations

### 8.1.3 Amplitude Modulation

An amplitude-modulated oscillation is obtained if the amplitude  $y_{01}$  of the carrier signal with angular frequency  $\omega_1$  is altered by a second oscillation, the modulation oscillation, with amplitude  $y_{02}$  and angular frequency  $\omega_2$ . This results in the multiplicative operation

$$y(t) = y_1(t)y_2(t) = y_{01} [y_{02} \sin(\omega_2 t + \varphi_2)] \sin(\omega_1 t + \varphi_1) \quad (8.1.5)$$

Using the trigonometric relation

$$\sin \alpha \sin \beta = \frac{1}{2} [\cos(\alpha - \beta) - \cos(\alpha + \beta)]$$

one obtains

$$y(t) = \frac{1}{2} y_{01} y_{02} [\cos((\omega_1 - \omega_2)t + \varphi_1 - \varphi_2) - \cos((\omega_1 + \omega_2)t + \varphi_1 + \varphi_2)] \quad (8.1.6)$$

Thus, two oscillation components of the same amplitude with the difference and sum frequency appear as shown in Figure 8.2.

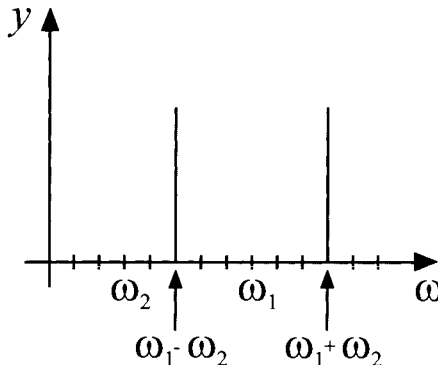


**Figure 8.2.** Amplitude spectrum with amplitude modulation

### 8.1.4 Frequency and Phase Modulation

A frequency modulation of the carrier oscillation is obtained by

$$y(t) = y_{01} \sin[\omega_1(y_{02} \sin(\omega_2 t + \varphi_2))t + \varphi_1] \quad (8.1.7)$$

and a modulation of the phase angle by

$$y(t) = y_{01} \sin(\omega_1 t + y_{02} \sin(\omega_2 t + \varphi_2) + \varphi_1) \quad (8.1.8)$$

These modulations are particularly used in communication engineering, since the useful information is contained in the frequency and phase of the carrier signal. In this case, disturbances of the amplitude  $y_{01}$  have practically no influence on the reconstruction of the useful signal in a receiver (demodulation).

#### Example 8.1

Figure 8.3 shows the results of the amplitude, phase and frequency modulation for a signal composed of two undamped partial oscillations.

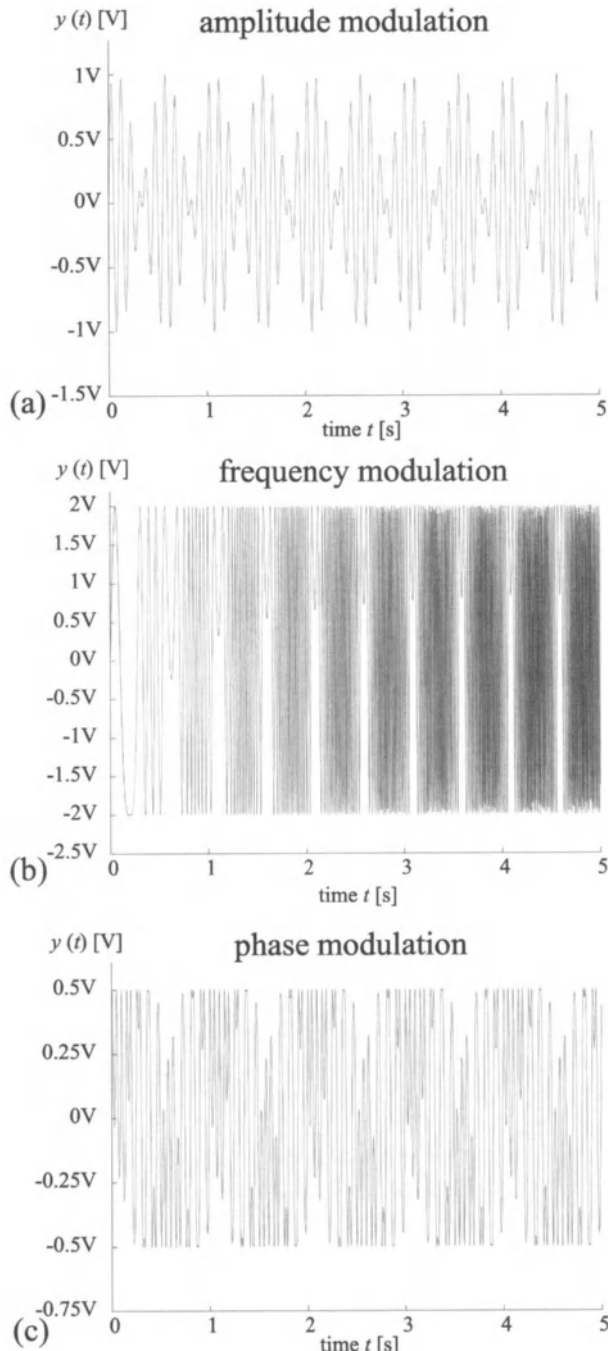


**Figure 8.3.** Time course of an oscillation with:

- (a) amplitude modulation:  $y(t) = \sin(2\pi \cdot 10Hz \cdot t) \cdot \sin(2\pi \cdot 1Hz \cdot t + \pi/3)$
- (b) frequency modulation:  $y(t) = 2\sin[(2\pi \cdot 10Hz \cdot t + 0.5) \cdot \sin(2\pi \cdot 1Hz \cdot t + \pi/3)]$
- (c) phase modulation:  $y(t) = 0.5\sin(2\pi \cdot 1Hz \cdot t + 2 \cdot \sin(2\pi \cdot 10Hz \cdot t) + \pi/3)$

□

### 8.1.5 Beating (Libration)

Now, the superposition of two oscillations, with angular frequencies  $\omega_1$  and  $\omega_2$  with a minor difference of  $\Delta\omega = \omega_2 - \omega_1$  but the same amplitudes, is considered

$$\begin{aligned}y_1(t) &= y_0 \sin(\omega_1 t + \varphi_1) \\y_2(t) &= y_0 \sin[(\omega_1 + \Delta\omega)t + \varphi_2]\end{aligned}$$

Using the trigonometric relation

$$\sin\alpha + \sin\beta = 2 \sin\left(\frac{\alpha + \beta}{2}\right) \cdot \cos\left(\frac{\alpha - \beta}{2}\right)$$

one then obtains

$$\begin{aligned}y(t) &= y_1(t) + y_2(t) \\&= y_0(t) \sin\left[\left(\omega_1 + \frac{\Delta\omega}{2}\right)t + \varphi\right] \\&= y_0(t) \sin\left[\frac{\omega_1 + \omega_2}{2}t + \varphi\right]\end{aligned}\tag{8.1.9}$$

with

$$\begin{aligned}y_0(t) &= 2 \cos\left[\frac{\Delta\omega t - \varphi_1 + \varphi_2}{2}\right] = 2 \cos\left[\frac{\omega_2 - \omega_1}{2} - \frac{\varphi_1 + \varphi_2}{2}\right] \\ \varphi &= \frac{1}{2}(\varphi_1 + \varphi_2)\end{aligned}$$

It yields a sinusoidal oscillation with an averaged frequency  $(\omega_1 + \omega_2)/2$  and an amplitude  $y_0(t)$  that changes sinusoidally with the half difference frequency  $\Delta\omega/2$ , a so-called *beating*. A superposition of oscillations with adjacent frequencies leads to an amplitude-modulated signal, whose carrier signal has the frequency  $(\omega_1 + \omega_2)/2$  and whose modulation signal is the frequency  $(\omega_2 - \omega_1)/2$ .

#### Example 8.2

The superposition of the oscillations

$$y_1(t) = \sin(2\pi \cdot 1 \text{ Hz} \cdot t)$$

$$y_2(t) = \sin(2\pi \cdot 1,01 \text{ Hz} \cdot t)$$

yields a beating with a frequency of  $\Delta f/2 = 0.005 \text{ Hz}$ , as shown in Figure 8.4.

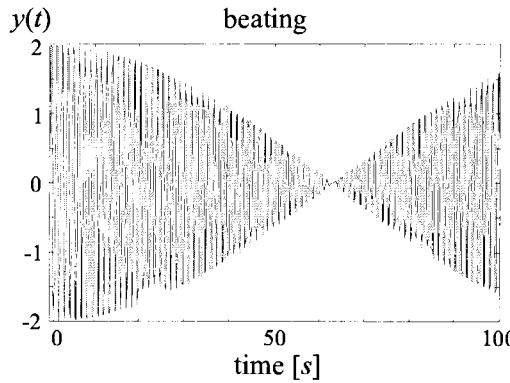


Figure 8.4. Time course of a beating

□

### 8.1.6 Superposition and Non-linear Characteristics

Now, the case of a signal  $y(t)$  composed of two superimposed oscillations is considered

$$\begin{aligned} y(t) &= y_1(t) + y_2(t) \\ y_1(t) &= y_{01}\sin(\omega_1 t + \varphi_1) \\ y_2(t) &= y_{02}\sin(\omega_2 t + \varphi_2) \end{aligned} \quad (8.1.10)$$

is fed into a succeeding non-linear characteristic curve

$$z(y) = y^2 \quad (8.1.11)$$

Then

$$\begin{aligned} z(t) &= y_{01}^2\sin^2(\omega_1 t + \varphi_1) + 2y_{01}y_{02}\sin(\omega_1 t + \varphi_1)\sin(\omega_2 t + \varphi_2) \\ &\quad + y_{02}^2\sin^2(\omega_2 t + \varphi_2) \\ &= y_{01}^2\sin^2(\omega_1 t + \varphi_1) + y_{02}^2\sin^2(\omega_2 t + \varphi_2) + 2y_{01}[y_{02}\sin(\omega_2 t + \varphi_2)] \\ &\quad \cdot \sin(\omega_1 t + \varphi_1) \end{aligned} \quad (8.1.12)$$

applies to the resulting signal. Thus, squared-sinusoidal oscillations for each fundamental frequency and an amplitude-modulated sinusoidal oscillation emerge. A further transformation by means of the trigonometric function

$$\sin^2\alpha = \frac{1}{2}[1 - \cos 2\alpha]$$

yields

$$\begin{aligned} z(t) &= \frac{1}{2}(y_{01}^2 + y_{02}^2) \\ &\quad - \frac{1}{2}y_{01}^2\cos(2\omega_1 t + \varphi_1) - \frac{1}{2}y_{02}^2\cos(2\omega_2 t + \varphi_2) \\ &\quad + y_{01}y_{02}\cos[(\omega_1 - \omega_2)t + \varphi_1 - \varphi_2] \\ &\quad - y_{01}y_{02}\cos[(\omega_1 + \omega_2)t + \varphi_1 + \varphi_2] \end{aligned} \quad (8.1.13)$$

As two oscillations with the angular frequencies  $\omega_1$  and  $\omega_2$  pass through

a squared non-linear characteristic curve, the angular frequencies become

$$2\omega_1, 2\omega_2, \omega_1 - \omega_2, \omega_1 + \omega_2$$

and an additional offset occurs, as shown in Figure 8.5. Thus, non-linear transfer elements lead to oscillations with new frequencies at the output.

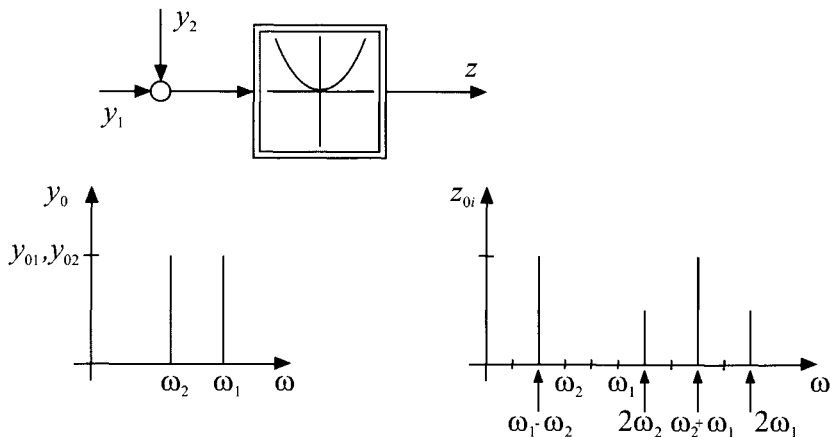


**Figure 8.5.** Effect of a square characteristic curve on the amplitude spectrum of two superimposed oscillations

## 8.2 IDENTIFICATION OF HARMONIC OSCILLATIONS

Measured periodic signals generally consist of a periodic useful signal component  $y_u(t)$  and a disturbing signal component  $n(t)$

$$y(t) = y_u(t) + n(t) \quad (8.2.1)$$

In the case of steady state oscillations, the periodic useful signal components can be represented, as is generally known, by superposition of sinusoidal oscillations

$$y_u(t) = \sum_{v=1}^m y_{0v} \sin(\omega_v t + \varphi_v) \quad (8.2.2)$$

The individual oscillation components can be determined from measurements as follows.

### 8.2.1 Bandpass Filtering

A first possibility for the determination of the amplitudes is the use of narrow-band bandpass filters with variable or fixed mid-band frequencies, Stearns, Hush (1990), Hess (1989). With so-called comb filters,

several graded mid-band frequencies are present.

### 8.2.2 Fourier Analysis

The Fourier series expansion of the phase-shifted sinusoidal oscillations (8.2.2) (without disturbing signals  $n(t) = 0$ ) can be stated in the following form

$$y(t) = \frac{a_0}{2} + \sum_{v=1}^N a_v \cos(v\omega_0 t) + \sum_{v=1}^N b_v \sin(v\omega_0 t) \quad (8.2.3)$$

in which  $a_v, b_v$  represent the Fourier coefficients of the different oscillation components

$$\begin{aligned} a_v &= \frac{2}{T_p} \int_0^{T_p} y(t) \cos(v\omega_0 t) dt \\ b_v &= \frac{2}{T_p} \int_0^{T_p} y(t) \sin(v\omega_0 t) dt \end{aligned} \quad (8.2.4)$$

The Fourier series can be put in the complex form

$$\begin{aligned} y(t) &= c_0 + \sum_{v=1}^N c_v e^{iv\omega_0 t} + \sum_{v=1}^N c_{-v} e^{-iv\omega_0 t} \\ &= \sum_{v=-\infty}^{\infty} c_v e^{iv\omega_0 t} \end{aligned} \quad (8.2.5)$$

with the complex Fourier coefficients

$$c_v(iv\omega_0) = \frac{1}{T_p} \int_0^{T_p} y(t) e^{-iv\omega_0 t} dt \quad (8.2.6)$$

For  $T_p \rightarrow \infty$  and thus  $\omega_0 \rightarrow d\omega$  and  $v\omega_0 = \omega$ , the periodic function becomes a non-periodic function resulting in the Fourier transform  $y(i\omega)$ , (8.2.11).

### 8.2.3 Correlation Functions

The autocorrelation function (ACF) for stationary disturbing and periodic signals is given by the general form

$$R_{yy}(\tau) = \lim_{T \rightarrow \infty} \frac{1}{T} \int_0^T y(t)y(t + \tau) dt \quad (8.2.7a)$$

For periodic signals, it is to average over integral periods. Thus applies

$$R_{yy}(\tau) = \lim_{n \rightarrow \infty} \frac{1}{nT_{pv}} \int_0^{nT_{pv}} y(t)y(t + \tau) dt \quad (8.2.7b)$$

For a sinusoidal phase-shifted oscillation with  $\omega_v = 2\pi/T_{pv}$

$$y_u(t) = y_{0v} \sin(\omega_v t + \varphi_v) + n(t) \quad (8.2.8)$$

the ACF becomes, Isermann (1992),

$$R_{yy}(\tau) = \frac{y_{0v}^2}{2} \cos \omega_v \tau \quad (8.2.9)$$

and thus again a periodic function. The result is independent of the phase shift  $\varphi_v$ . The stationary disturbing signal components  $n(t)$  and oscillations with  $\omega \neq \omega_v$  for  $n \rightarrow \infty$  have no influence on the ACF. Thus, the ACF is suitable for analyzing periodic signals with stochastic disturbing signal components.

For the cross - correlation function between the input signal  $u(t)=u_0 \sin \omega_v t$  of a linear system and the output  $y(t)$  it holds

$$R_{yu}(\tau) = \lim_{n \rightarrow \infty} \frac{u_0}{n T_{pv}} \int_0^{n T_{pv}} y(t) \sin \omega_v (t + \tau) dt \quad (8.2.10)$$

Only oscillation components of  $y(t)$  with  $\omega = \omega_v$  have an influence. One may consider the similarity to the Fourier coefficients  $b_v$  (8.2.4).

## 8.2.4 Fourier Transformation

The Fourier transform of a non-periodic signal  $y(t)$  is defined as

$$y(i\omega) = \mathcal{F} \{y(t)\} = \int_{-\infty}^{\infty} y(t) e^{-i\omega t} dt \quad (8.2.11)$$

To ensure its convergence, the following condition must be fulfilled

$$\int_{-\infty}^{\infty} |y(t)| dt < \infty \quad (8.2.12)$$

Figure 8.6 shows the amplitude densities  $|y(i\omega)|$  for some examples of finite periodic signals, for which the convergence condition is fulfilled, Papoulis (1984).

If the Fourier transform is applied to an oscillation of finite duration  $T$ , one obtains a peak at  $\omega = \omega_v$ , Figure 8.6c. The longer the duration  $T$ , the higher and more narrow the amplitude density  $|y(i\omega)|$  around  $\omega = \omega_v$ . A steady state oscillation with  $T \rightarrow \infty$  yields  $|y(i\omega)| \rightarrow \infty$ . In this case, the convergence condition is no longer fulfilled.

Sampling the continuous time signal  $y(t)$  with the sampling time  $T_0$  results, from (8.2.11) in the case of  $y(t) = 0$  for  $t < 0$ , approximately in

$$y(i\omega) \approx T_0 \sum_{k=0}^{\infty} y(kT_0) e^{-i\omega kT_0} \quad (8.2.13)$$

Omitting the constant  $T_0$  yields the discrete Fourier transform (DFT)

$$y_D(i\omega) = \sum_{k=0}^{\infty} y(kT_0) e^{-i\omega kT_0} \quad (8.2.14)$$

Restricting its application only to a finite measuring interval  $0 \leq k \leq N - 1$ , then applies

$$\begin{aligned}\hat{y}_D(i\omega) &= \sum_{k=0}^{N-1} y(kT_0) e^{-i\omega kT_0} \\ &= \sum_{k=0}^{N-1} y(kT_0) \cos\omega kT_0 - i \sum_{k=0}^{N-1} y(kT_0) \sin\omega kT_0 \\ &= Re(y_D(i\omega)) + i Im(y_D(i\omega))\end{aligned}\quad (8.2.15)$$

whereas the discrete amplitude spectrum can be calculated from

$$|y_D(i\omega)| = \left[ Re^2(y_D(i\omega)) + Im^2(y_D(i\omega)) \right]^{\frac{1}{2}} \quad (8.2.16)$$

and the discrete phase spectrum from

$$\alpha_D(i\omega) = \arctg \left[ Im(y_D(i\omega)) / Re(y_D(i\omega)) \right] \quad (8.2.17)$$

Introducing the abbreviation

$$z = e^{i\omega T_0} \quad (8.2.18)$$

one obtains the  $z$ -transform

$$\hat{y}_D(z) = \sum_{k=0}^{N-1} y(kT_0) z^{-k} \quad (8.2.19)$$

For each angular frequency  $\omega$ ,  $2N$  multiplications and  $2(N - 1)$  additions are necessary. Therefore, the computing effort is relatively high.

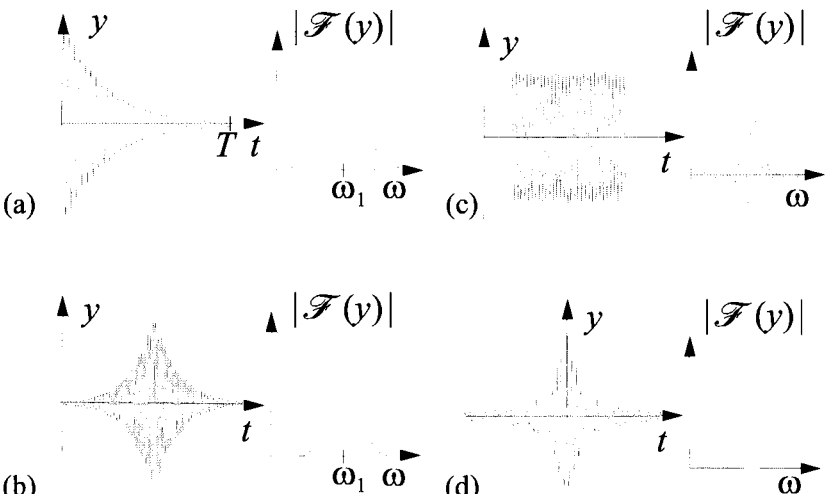


**Figure 8.6.** Amplitude densities of some signals of finite duration: (a) decaying oscillation; (b) growing and decaying oscillation; (c) finite periodic signal; (d) time course of a rectangular Fourier transform

### 8.2.5 Fast Fourier Transformation (FFT)

A reduction of the long computing time of the DFT can be achieved by utilising the cyclic properties of the oscillation pointers in the complex plane, Cooley, Tuckey (1965), Brigham (1974). The analysis is then restricted to re-sorting data and multiplications with precalculated sine and cosine values. The angular frequencies are as well discretized with a spacing of  $\Delta\omega$ . With a finite measuring duration  $T = NT_0$ , the lowest describable angular frequency is  $\omega_{min} = 2\pi/T = 2\pi/NT_0$  and the highest angular frequency is  $\omega_{max} = \pi/T_0$  according to the Shannon sampling theorem. The frequency resolution becomes

$$\omega = n \Delta\omega \text{ with } \Delta\omega = \frac{2\pi}{NT_0} \quad (8.2.20)$$

Using (8.2.15) gives the series

$$\hat{y}_D(in\Delta\omega) = \sum_{k=0}^{N-1} y(kT_0) e^{-ikn\Delta\omega T_0} = \sum_{k=0}^{N-1} y(kT_0) W_N^{kn} \quad (8.2.21)$$

with constant data set-independent complex factors  $W_N$

$$W_N = e^{-i\Delta\omega T_0} = e^{i2\pi/N} = \text{const.} \quad (8.2.22)$$

The analysis of several data of equal length permits the factors  $W_N^{kn}$  to be precalculated and stored as sine/cosine tables for different lengths of data sets  $N$  in order to save computing time, *e.g.*, for real-time processing. In addition, the following symmetry characteristic is valid

$$W_N = e^{-i2\pi/N} = \{e^{-i2\pi/(N/2)}\}^{1/2} = W_{N/2}^{1/2} \quad (8.2.23)$$

A decomposition of the sample set  $y(k)$  into two parts, one containing only even-numbered samples and the second containing odd-numbered samples

$$y_{even} = y(2k); y_{odd} = y(2k+1), k = 0 \dots (\frac{N}{2}-1) \quad (8.2.24)$$

yields two sub-sequences from (8.2.21) and (8.2.23)

$$\hat{y}_{even}(n) = \sum_{k=0}^{N/2-1} y(2k) W_{N/2}^{2kn} = \sum_{k=0}^{N/2-1} y(2k) W_N^{2kn} \quad (8.2.25)$$

$$\hat{y}_{odd}(n) = \sum_{k=0}^{N/2-1} y(2k+1) W_{N/2}^{2kn} = \sum_{k=0}^{N/2-1} y(2k+1) W_N^{2kn} \quad (8.2.26)$$

Thus, the entire series of the signal  $y(k)$  can be denoted

$$\begin{aligned} \hat{y}_D(n) &= \sum_{k=0}^{N/2-1} \{y(2k) W_N^{2kn} + y(2k+1) W_N^{(2k+1)n}\} \\ &= \hat{y}_{even}(n) + W_N^n \hat{y}_{odd}(n) \end{aligned} \quad (8.2.27)$$

in such a way as to permit a calculation by formation of two sub-sequences, each with the half data set length. According to (8.2.27), the decomposition can be proceeded as long as the length of the sub-sequences is even. A perfect utilization of the calculation symmetry is possible if the length of the data set  $N$  represents a power of two,  $N = 2^v$ . In this case, the evaluation of (8.2.21) degenerates into a rearrangement of  $y(k)$  as well as into multiplications of the precalculable complex values  $W_N$ . This corresponds to a computing effort of each  $4N \lg N / \lg 2$  real multiplications and additions for this FFT.

According to the order of the operations, one distinguishes between Cooley-Tuckey algorithms (re-sorting with subsequent multiplication) and Sande-Tuckey algorithms (multiplication of the data with sine/cosine values and subsequent re-sorting, Press *et al.* (1988)).

A comparison of the computing effort between the DFT and FFT with fixed data set length  $N$  shows the strong increase of the DFT versus the FFT with increasing length  $N$ , Table 8.1. Due to the large savings in computing time, the disadvantage of a specific data set length (power of two) required for the FFT is usually accepted.

**Table 8.1.** Comparison of required calculations for DFT and FFT

data set length $N$	required calculations for		
	DFT	FFT	
128	33282	3584	multiplications
	256	3584	additions
1024	2101250	40960	multiplications
	2048	40960	additions
4096	33570818	196608	multiplications
	8192	196608	additions

### Example 8.3

The signal processor DSP32C (AT&T) needs a computing time of 80 ns with a clock frequency of  $f_c = 50$  MHz ( $T_c = 20$  ns) for one calculation step (floating-point addition and/or multiplication). Due to its specific architecture (multiplier-adder cascade), both an addition and a multiplication operation can be executed together within one calculation step. Regarding the calculation of the FFT, with the same number of both operations half of the computing time can be saved. However, with the DFT only minor effects are noticeable, see Table 8.2.

**Table 8.2.** Comparison of the required computing time of a signal processor for DFT and FFT

$N$	DFT	FFT	Factor DFT/FFT
128	26.8 ms	2.85 ms	94
1024	1.68 s	32.75 ms	513
4096	26.86 s	0.1575 s	1705

Table 8.2 shows that the factor of time-saving becomes larger with increasing data set length.

□

Regarding the successive utilization of symmetries with the FFT, the data set length  $N$  is limited to a power of two numbers ( $N = 2^v$ ). Often,  $N = 1024 = 2^{10}$  is used. Whenever a data set does not meet these requirements, it must be either truncated or padded with zeros (“zero padding”) up to the next power of two numbers, which means a corruption of the raw data.

Another disadvantage of the DFT and FFT of a discrete spectrum arises from the selected representation of a discrete spectrum. Due to its finite curvature behavior, sharp spectral lines (“Peaks”), which may arise from discrete sinusoidal oscillation components, cannot be modeled accurately. A finite data set length in the time domain ( $k = 0 \dots N - 1$ ) can be generated from an infinitely long data set length by a rectangular windowing function  $f_{rec}$ , with

$$f_{rec}(kT_0) = \begin{cases} 1 & \text{for } 0 \leq k \leq N \\ 0 & \text{else} \end{cases} \quad (8.2.28)$$

see Figure 8.7. Instead of a sequence  $y(k)$  of the real measured signal, a sequence of finite duration  $y_{tr}(k)$  is transformed into the frequency domain, which results from the multiplication of the signal and the windowing function

$$y_{tr}(k) = f_{rec}(k)y(k) \quad (8.2.29)$$

In the frequency domain, this operation leads to a convolution of the spectrum of the measured signal and the Fourier transform of the rectangular window, which forms the sinc-function dependent on the data set length  $N$ . The amplitudes of all discrete frequency components smear over by such a convolution performed over the entire frequency range (*leakage effect*), see, e.g., Kammeyer, Kroschel (1992).

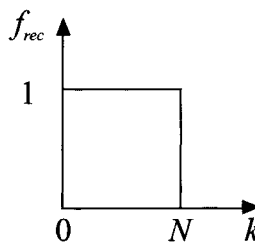
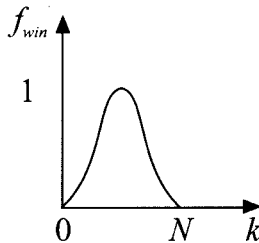


Figure 8.7. Rectangular windowing function  $f_{rec}(k)$

A reduction of the leakage effect can often be achieved by introducing specific windowing functions  $f_{win}(k)$ , which are multiplied with the measured signal prior to the transformation, as shown in Figure 8.8,

$$y_{tr}(k) = f_{win}(k)y(k) \quad (8.2.30)$$



**Figure 8.8.** Generalized windowing function  $f_{win}(k)$

These windowing functions  $f_{win}(k)$  continuously change their values from 1 in the middle of the measuring interval to 0 on the edges. Besides the reduction of the leakage effect, however, the disadvantage of a diminished resolution of the resulting spectrum due to the corruption of the signal values on the edges occurs.

#### Example 8.4

The sinusoidal oscillation

$$y(t) = 1V \sin(2\pi \cdot 1Hz \cdot t)$$

is sampled ( $T_0 = 200$  ms) within the measuring interval  $k = 0 \dots N - 1$ . The amplitude spectrum is estimated by means of the FFT from the appropriate sampled sequence  $y(k)$ :

a) *Without additional windowing function  $f_{win}$*

$$y(n\Delta\omega) = FFT\{f_{rec}(k) y(k)\}$$

From Figure 8.9, it becomes evident that the limitation of the measuring interval to  $N$  samples, particularly for small values of  $N$  ( $N = 128$ ), leads to a significant estimation error of the signal amplitude and signal frequency.

b) *With additional windowing function (Hanning-window)*

$$y(n\Delta\omega) = FFT\{f_{win}(k) f_{rec}(k) y(k)\}$$

$$f_{win}(k) = 0.5 \left\{ 1 - \cos\left(\frac{2\pi k}{n}\right) \right\}$$

The additional Hanning-window causes an improvement of the frequency and amplitude estimation for small values  $N$  ( $N = 128$ ), as illustrated in Figure 8.10. The influence of the leakage effect on the estimation results decreases with increasing data set length  $N$ .

For complete details on using the FFT, refer, for instance, to Akaike (1974), Brigham (1974), Nussbaumer (1981), Schüssler (1988), Stearns, Hush (1990), Kammeyer, Kroschel (1992).

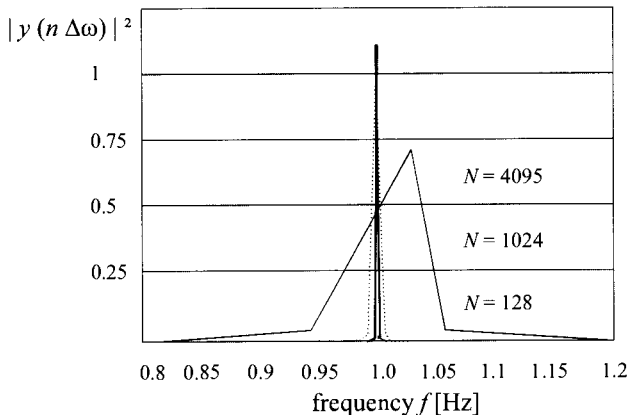


**Figure 8.9.** FFT of a sinusoidal oscillation with 1 Hz,  $y(k)$  for different data set lengths  $N$

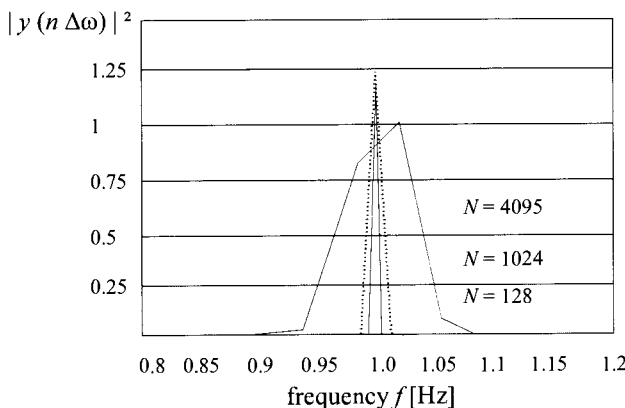


**Figure 8.10.** FFT of a sinusoidal oscillation with 1 Hz or different data set length  $N$  and additional Hanning-window

□

### 8.2.6 Maximum Entropy Spectral Estimation

Most problems of the FFT could be solved if the course of the measured signal outside of the measuring interval was known. For this reason, Burg (1968) searched for an approach to predict the unknown signal course from the well-known measured values, whereby no *a priori* assumptions concerning the signal course should be made. This estimation of the values with maximum uncertainty concerning the signal course led to the term *maximum entropy* and to a substantially improved spectral estimation.

#### a) Parametric signal models in the frequency domain

As an approach for a parametric signal model in the frequency domain, a fictitious form filter  $F(z)$  resp.  $F(i\omega)$  is used, which is stimulated by

the Kronecker-Delta impulse

$$\delta(k) = \begin{cases} 1 & \text{for } k=0 \\ 0 & \text{else} \end{cases} \Rightarrow \delta(z) = 1 \quad (8.2.31)$$

to generate steady state oscillations  $y(k)$ , Figure 8.11.

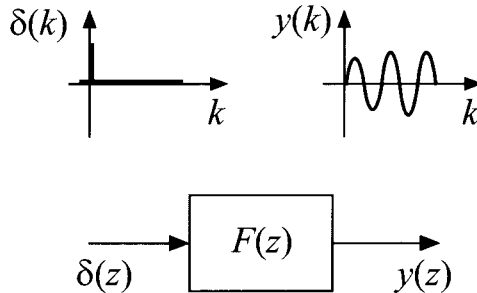


**Figure 8.11.** Generation of steady state oscillations  $y(k)$  by means of a fictitious form filter  $F(z)$  and stimulation with a  $\delta$ -impulse

The dynamic system behavior of the form filter is to be determined in such a way that it yields

$$y(z) = F(z) \delta(z) = F(z) \quad \text{with } \delta(z) = 1 \quad (8.2.32)$$

to give an identical frequency response of the form filter  $F(z)$  and amplitude spectrum of the measured signal  $y(z)$ . This applies similarly to the power spectral density

$$S_{yy}(\omega) = |F(i\omega)|^2 S_{\delta\delta}(\omega) = |F(i\omega)|^2 \quad \text{with } S_{\delta\delta}(\omega) = 1 \quad \forall \omega \quad (8.2.33)$$

Three possible parametric model approaches of such filters can be distinguished, Box, Jenkins (1970). The MA (moving average) model is

$$F_{MA}(z) = \beta_0 + \beta_1 z^{-1} + \dots + \beta_n z^{-n} \quad (8.2.34)$$

Here, the signal spectrum is approximated by a polynomial of limited order  $m$ . Thus, the spectrum can only represent limited variations of the amplitude and is unsuitable for the modeling of periodic signals, whose amplitude spectrum only consists of discrete peaks. In the time domain, an MA approach corresponds to the filter-difference equation

$$y(k) = \beta \delta(k) + \beta_1 \delta(k-1) + \dots + \beta_n \delta(k-n) \quad (8.2.35)$$

A pure autoregressive (AR) model

$$F_{AR}(z) = \frac{\beta_0}{1 + \alpha_1 z^{-1} + \dots + \alpha_n z^{-n}} \quad (8.2.36)$$

is able to approximate sharp spectral lines of periodic signals according to the poles of the denominator polynomial. Thus, it is particularly suitable for estimating the spectra of harmonic oscillations, Tong (1975, 1977), Pandit, Wu (1983). The corresponding filter-difference equation is

$$\beta_0 \delta(k) = y(k) + \alpha_1 y(k-1) + \dots + \alpha_n y(k-n) \quad (8.2.37)$$

After a single stimulation by a  $\delta$ -pulse, the following course of  $y(k)$  is only dependent on its passed values  $y(k-i)$ .

The mixed (ARMA)-filter model approach

$$F_{ARMA}(z) = \frac{\beta_0 + \beta_1 z^{-1} + \dots + \beta_p z^{-p}}{1 + \alpha_1 z^{-1} + \dots + \alpha_n z^{-n}} \quad (8.2.38)$$

is given by the ARMA-difference equation

$$y(k) + \alpha_1 y(k-1) + \dots + \alpha_n y(k-n) = \beta_0 \delta(k) + \dots + \beta_p \delta(k-p) \quad (8.2.39)$$

and is composed of both the MA and AR model approach.

However, strong convergence problems arise with regard to the estimation as the consequence of doubling the number of parameters ( $\beta_j$ ,  $\alpha_i$ ). Regarding this type of model, more complex and more special estimation procedures are described in the literature, see Makhoul (1975), which, however, yield worse results for periodic signals (mainly autoregressive signal components) compared to an AR model approach.

A model structure of the form filter  $F(z)$  can generally be derived also for periodic signals by the method of maximizing the entropy in the form of a pure AR model for the power spectral density  $S_{yy}(z)$ , Edward, Fitelson (1973), Ulrych, Bishop (1975)

$$S_{yy}(z) = F(z)F(z^{-1}) \cdot S_{\delta\delta}(z) = \frac{\beta_0^2}{|1 + \sum_{i=1}^n \alpha_i z^{-i}|^2} \quad (8.2.40)$$

By estimating the coefficients  $\alpha_i$  and  $\beta_0$  from the measured signal  $y(k)$ , one obtains a *parametric, autoregressive model in the frequency domain* for the power spectral density  $S_{yy}(\omega)$ , which is characterized by  $(n+1)$  parameters (typically:  $n = 4 \dots 30$ ).

### b) Determination of the coefficients

A suppression of stochastic signal components with respect to the estimation can be achieved, if instead of the signal  $y(t)$

$$y(t) = \sum_{v=1}^m y_{0v} e^{-d_v t} \sin(\omega_v t + \varphi_v) \quad (8.2.41)$$

its autocorrelation function  $R_{yy}(\tau)$  is used

$$R_{yy}(\tau) = E\{y(t) y(t+\tau)\} = \sum_{v=1}^m \frac{y_{0v}^2}{2} e^{-d_v \tau} \cos(\omega_v \tau) \quad (8.2.42)$$

Since the autocorrelation function  $R_{yy}(\tau)$  of a periodic signal  $y(t)$  yields again a periodic function in  $\tau$  of the type (8.2.41), for this function a form filter model given by (8.2.32) can be assumed as well.

$$R_{yy}(z) = F(z) \delta(z) \quad (8.2.43)$$

The eigen-behavior of  $y(t)$ , represented by its  $m$  characteristic frequencies  $\omega_v$  and damping coefficients  $d_v$ , is also contained in  $R_{yy}(\tau)$ . However, the phase information gets lost and the amplitudes of the ACF become

$$R_{0v} = 0.5 y_{0v}^2 \quad (8.2.44)$$

The approach of a general form filter model of the ARMA-type (8.2.39) yields a filter-difference equation for the ACF of the measured signal with  $m$  eigenfrequencies and thus of the order  $n = 2m$

$$\begin{aligned} R_{yy}(\tau) &= -\alpha_1 R_{yy}(\tau-1) - \alpha_2 R_{yy}(\tau-2) - \dots - \alpha_n R_{yy}(\tau-2m) \\ &\quad + \beta_0 R_{\delta\delta}(\tau) + \beta_1 R_{\delta\delta}(\tau-1) + \dots + \beta_{2m-1} R_{\delta\delta}(\tau-2m+1) \\ &\quad + R_{nn}(\tau) \end{aligned} \quad (8.2.45)$$

if an additive-affecting, uncorrelated disturbing signal  $n(t)$  of zero-mean value is taken into account. Its autocorrelation function  $R_{nn}(\tau)$

$$R_{nn}(\tau) = \begin{cases} n_0 & \text{for } \tau=0 \\ 0 & \text{else} \end{cases} \quad (8.2.46)$$

gives only a constant contribution for  $\tau = 0$ .

The ARMA-signal model (8.2.45) reaches the steady state after  $\tau = 2m$  steps. In the model (8.2.45), all  $\beta$ -parameters are then omitted. From this time, the ACF  $R_{yy}(\tau)$  proceeds in the form of a stationary steady state oscillation and can be exclusively described by the AR-part of (8.2.45).

In the case of the AR model, the eigen-behavior of the autocorrelation function can be expressed by

$$R_{nn}(\tau) = R_{yy}(\tau) + \alpha_1 R_{yy}(\tau-1) + \alpha_2 R_{yy}(\tau-2) + \dots + \alpha_n R_{yy}(\tau-2m) \quad (8.2.47)$$

This relationship yields a system of equations for different shifts  $\tau$  for the determination of the coefficients  $\alpha_j$  and  $n_0$ .

$$\begin{bmatrix} R_{yy}(0) & R_{yy}(1) & \dots & R_{yy}(2m) \\ R_{yy}(1) & R_{yy}(0) & \dots & R_{yy}(2m-1) \\ \dots & \dots & \dots & \dots \\ R_{yy}(2m) & R_{yy}(2m-1) & \dots & R_{yy}(0) \end{bmatrix} \begin{bmatrix} 1 \\ \alpha_1 \\ \vdots \\ \alpha_{2m} \end{bmatrix} = \begin{bmatrix} n_0 \\ 0 \\ \vdots \\ 0 \end{bmatrix} \quad (8.2.48)$$

The coefficient  $n_0$  is a measure for the mean-square model error

$$R_{nn}(0) = n_0 = E\{n^2(k)\} = E\{\{y(k) - \hat{y}(k)\}^2\} \quad (8.2.49)$$

with  $\hat{y}(k)$  as the model prediction for  $y(k)$ , (8.2.37). To resolve the system of equations (8.2.47), (8.2.48), estimates of the ACF  $R_{yy}(\tau)$  for  $\tau = 0 \dots 2m$  have to be determined from the measured signal sequence  $y(k)$ ,  $k = 0 \dots N-1$ .

$$R_{yy}(\tau) = \frac{1}{N-|\tau|+1} \sum_{k=0}^{N-|\tau|} y(k) y(k+\tau) \quad (8.2.50)$$

For an efficient solution of the equation system (8.2.48), the Burg algorithm, Press *et al.* (1988), is recommended. Here, the signal model (8.2.47) is interpreted as a predictor filter for the unknown autocorrelation values  $R_{yy}(\tau)$ . Starting from the order of  $m = 1$ , the coefficients and values of the autocorrelation function are estimated alternately up to the final order of  $2m$ , Burg (1968).

The eigenfrequencies of significant discrete oscillation components in  $y(t)$  are calculated by pole decomposition of the denominator polynomial in the AR-signal model (8.2.36)

$$\begin{aligned} A^*(z) &= z^{2m}A(z^{-1}) = z^{2m}\left\{1 + \alpha_1 z^{-1} + \alpha_2 z^{-2} + \dots + \alpha_{2m} z^{-2m}\right\} \\ &= \prod_{v=1}^m (1 + \alpha_{1v} z + \alpha_{2v} z^2) \end{aligned} \quad (8.2.51)$$

or by searching the maximum in  $A^*(z)$ . The resulting conjugate-complex poles  $z_v$  permit a factorization into square parts, (8.2.51)

$$\alpha_{2v} z^2 + \alpha_{1v} z + 1 = \alpha_{2v}(z - z_{v1})(z - z_{v2}) = 0 \quad (8.2.52)$$

From a corresponding table of the  $z$ -transform, e.g., Isermann (1988), one obtains for each conjugate-complex pair of poles ( $z_{v1}, z_{v2}$  from (8.2.51)) the angular frequency  $\omega_v$  of the appropriate sinusoidal partial oscillation  $y_v(t)$  in  $y(t)$

$$\omega_v = \frac{1}{T_0} \arccos \left[ \frac{-\alpha_{1v}}{2\sqrt{\alpha_{2v}}} \right] \quad (8.2.53)$$

In this way all significant partial oscillation frequencies  $\omega_v$  of the measured signal  $y(t)$  are calculable.

#### *Estimation of the amplitudes*

A determination of the amplitudes from the AR-signal model (8.2.47), (8.2.48) is only inaccurately possible. The amplitudes  $y_{0v}$  of each partial oscillation of a significant eigenfrequency  $z_v$  result with (8.2.40) from

$$S_{yy}(z_v) = \frac{\beta_0^2}{|A(z_v)|^2} \quad (8.2.54)$$

with  $A(z_v) = A^*(z_v)$  given by (8.2.51). They are dependent on the denominator coefficient  $\alpha_i$  and the constant numerator coefficient  $\beta_0$ . Here, the slightest estimation errors of the coefficients result in large variations of the amplitudes. For this reason, a second estimation level is particularly performed to determine the amplitudes, Neumann, Janik (1990), Neumann (1991).

In the autocorrelation function of periodic oscillations

$$R_{yy}(\tau) = E\{y(t) y(t+\tau)\} = \sum_{v=1}^m \frac{y_{0v}^2}{2} e^{-d_v \tau} \cos(\omega_v \tau) \quad (8.2.55)$$

the damping term can be neglected for small damping values

$$R_{yy}(\tau) = E\{y(t) y(t+\tau)\} = \sum_{v=1}^m \frac{y_{0v}^2}{2} \cos(\omega_v \tau) \quad (8.2.56)$$

without obtaining a noticeable influence on the accuracy of the estimation result. With known eigenfrequencies  $\omega_v$  provided by the first estimation level, one obtains a system of equations for determination of the appropriately demanded amplitudes of the autocorrelation  $R_{0v}$

$$\begin{bmatrix} R_{yy}(1) \\ R_{yy}(2) \\ \dots \\ R_{yy}(m) \end{bmatrix} = \begin{bmatrix} \cos(\omega_1 T_0) & \cos(\omega_2 T_0) & \dots & \cos(\omega_m T_0) \\ \cos(\omega_1 2T_0) & \cos(\omega_2 2T_0) & \dots & \cos(\omega_m 2T_0) \\ \dots & \dots & \dots & \dots \\ \cos(\omega_1 mT_0) & \cos(\omega_2 mT_0) & \dots & \cos(\omega_m mT_0) \end{bmatrix} \begin{bmatrix} R_{01} \\ R_{02} \\ \dots \\ R_{0m} \end{bmatrix} \quad (8.2.57)$$

In consideration of (8.2.44), the signal amplitudes can be evaluated by means of the amplitudes of autocorrelation with

$$y_{0v} = \sqrt{2 R_{0v}} \quad (8.2.58)$$

by inverting the (non-singular) matrix (8.2.57).

Thus, a parametric model representation for the demanded power spectral density  $S_{yy}(\omega)$  of the measured signal  $y(kT_0)$  was found, which represents the spectrum by a parametric AR model respectively by frequencies of significant sinusoidal oscillation components with appropriate amplitudes. For applications only the sampling time  $T_0$ , the data set length  $N$  and the order  $m$  of the expected significant partial oscillations must be given.

Figure 8.12 shows the amplitude spectrum of the current of an asynchronous motor of a hacksawing machine for nine frequencies. Further examples are given in Neumann (1994).

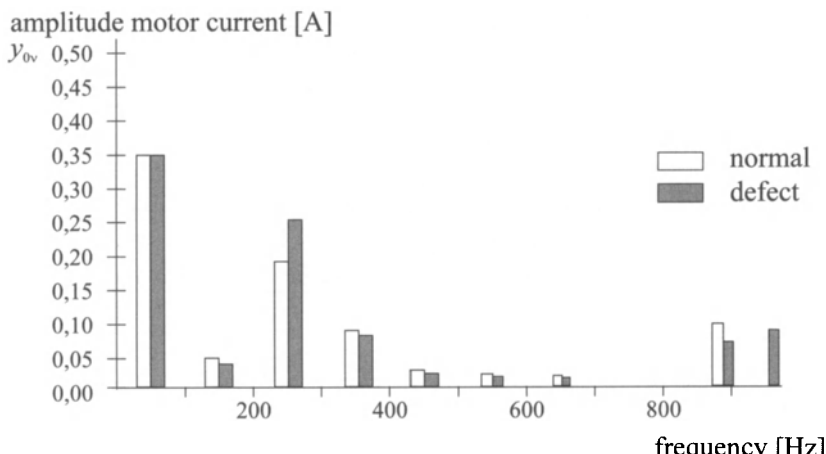


**Figure 8.12.** Estimated amplitudes  $y_{0v}$  of the current of an asynchronous motor of a hacksawing machine for an intact and worn-out saw blade,  $m = 0$ ,  $N = 100$

### 8.2.7 Speed Signal Analysis of Combustion Engines

Increasing demands on economy, reliability and particularly the reduction of exhaust gas emissions is forcing vehicle manufacturers to develop suitable detection and diagnosis functions for combustion engines. Legal regulations, such as the On Board Diagnosis II (OBD II) introduced by the California Air Resources Board (CARB) in 1996 (California's OBD-II Requirements) or the European On Board Diagnosis (EOBD) introduced by the European Union in 1998, have promoted the development of supervision methods of all components in a passenger car that cause an increase of exhaust gas emissions in the case of faults. Statistics, Muffert (1980), have shown that an increase in exhaust gas emissions and decrease in engine performance is, in most cases, caused by faults in the injection or mixture preparation. Regarding spark-ignition engines, misfire detection is a very demanding task. When a cylinder misfires, e.g., due to faults in the mixture preparation or ignition system with the effect that no combustion or incomplete combustion occurs, unburned fuel enters the exhaust system, which then burns in the hot catalytic converter. The released heat may damage or destroy the catalytic converter by thermal overloading. If a given misfire ratio is exceeded, the fuel supply for the misfiring cylinders can be cut off in order to protect the catalytic converter from damage and to avoid exceeding the emission standard. One way to detect misfiring cylinders is to evaluate the engine speed signal at the engine flywheel.

The signal characteristics of a combustion engine are determined by the batch behavior of the combustion, which depends on the crankshaft angle CA. Each cylinder of a four-stroke engine fires every  $720^\circ\text{CA}$ . This corresponds to one working cycle and specifies the engine base period. All relevant signal components are multiples of this base frequency. During a working cycle, each cylinder fires one time so that a combustion every  $180^\circ\text{CA}$  results for a four-cylinder engine. If the engine angular speed, measured at the flywheel, is denoted by  $\omega_E$ , the frequency of this oscillation corresponds to the ignition frequency  $f_1$  by

$$f_1 = \frac{\omega_E}{4\pi} i_c, \quad i_c : \text{number of cylinders} \quad (8.2.59)$$

In Figure 8.13, a typical engine speed signal of a spark-ignition (SI) engine measured at idle speed without misfiring is depicted showing speed oscillations with the ignition frequency around the engine speed mean value (approx. 800 rpm).

If misfires or faults in the injection mass occur, the engine speed decreases significantly. Figure 8.14 shows the measured engine speed of a four-cylinder engine in the case of continuous misfiring of one cylinder. Then, additional low-frequency oscillations arise, as can be clearly seen from the low-pass filtered engine speed signal. The appearing frequency components are harmonics of the engine base frequency. Depending on the misfiring cylinders, different frequency patterns result.

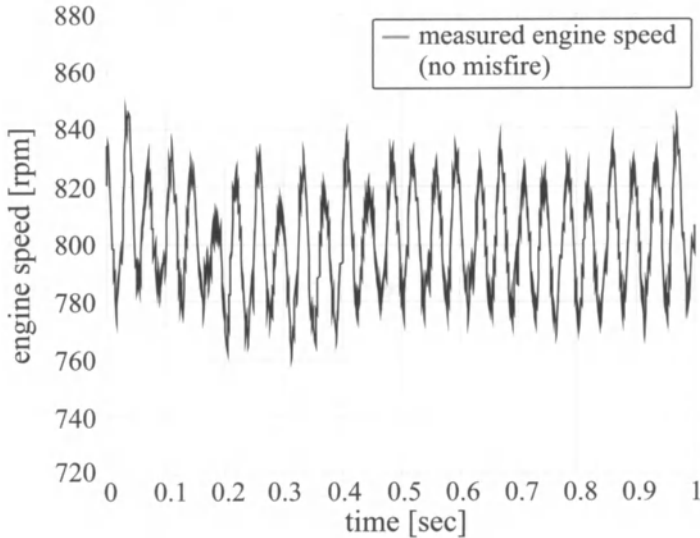


**Figure 8.13.** Measured engine speed signal at idle speed of an SI engine (no misfires)

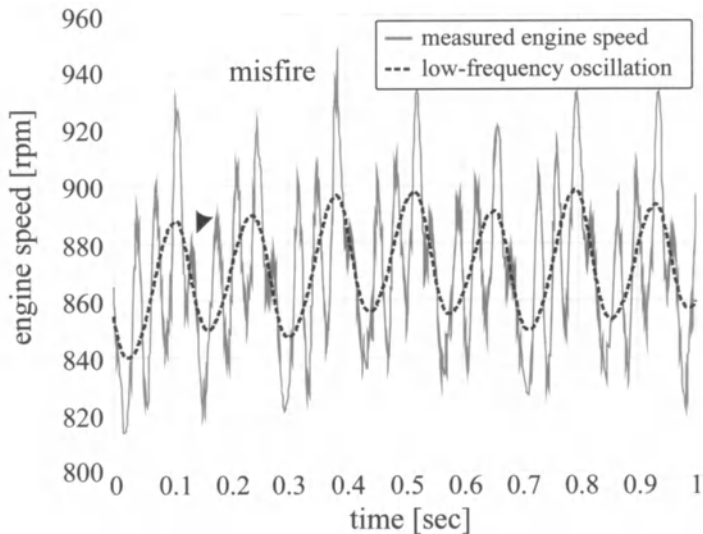


**Figure 8.14.** Measured engine speed signal and low-pass filtered signal at idle speed with misfires in cylinder 1

In the past few years, methods have been investigated using the Fourier and the fast Fourier analysis to evaluate these frequency components, see Ribbens, Rizzoni (1990). Figure 8.15 shows the Fourier transforms of both engine speed signals (no misfire and misfire in cylinder 1). Without misfire, the ignition frequency means that only the fourth engine harmonic appears in the spectrum. In the case of misfires, additional frequency components arise. Evaluating these frequency components means that not only misfires, but also the misfiring cylinder, can be detected and located.

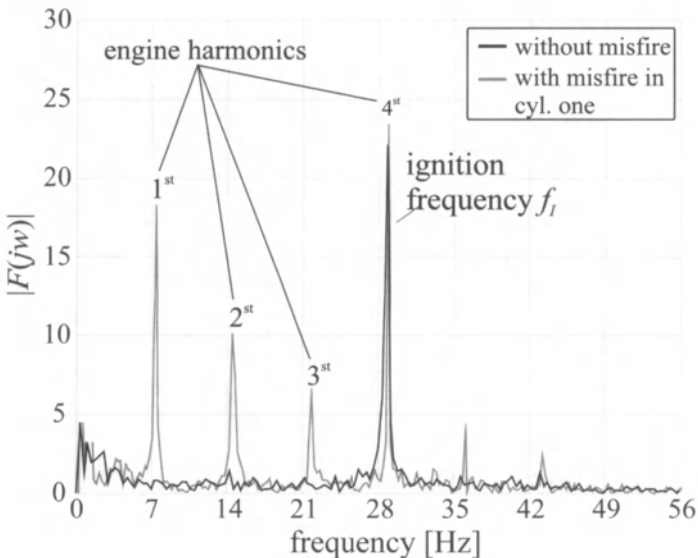


**Figure 8.15.** Fourier transform of the engine speed signal without and with misfires in cylinder 1

Another method to be considered, Führer *et al.* (1993), uses the real and imaginary components of the discrete Fourier transformation (DFT) applied to the engine speed signal. Thereby, a four-stroke four-cylinder engine shall be considered, whereas the principle of the method was also successfully implemented in a six-cylinder spark-ignition engine up to 6000 rpm and for loads higher than 20%.

Since the engine is time-variant, the data acquisition is performed crank angle synchronously so that no sampling time adaptation is necessary. For calculation of the DFT, the data is sampled all at 90°CA. This corresponds to the double ignition frequency, so satisfying the Shannon sampling theorem. The resulting speed-dependent sampling time for a four-stroke engine then follows from the ignition frequency:

$$T_o = 2\pi f_1 = \frac{\omega_E}{2} \quad (8.2.60)$$

The DFT evaluation can now be determined by using only eight sampling points per combustion cycle. Only a few sampling points  $N$  have to be taken into account, which is an easy real-time application. To compute the DFT, the amplitudes and the phase angle can be calculated as follows:

$$A_m = \sqrt{\left( \sum_{i=1}^{N-1} \omega_i \cos\left(\frac{2\pi m i}{N}\right) \right)^2 + \left( \sum_{i=1}^{N-1} \omega_i \sin\left(\frac{2\pi m i}{N}\right) \right)^2} \quad (8.2.61)$$

$$\varphi_m = \arctan \frac{\sum_{i=1}^{N-1} \omega_i \sin\left(\frac{2\pi m i}{N}\right)}{\sum_{i=1}^{N-1} \omega_i \cos\left(\frac{2\pi m i}{N}\right)} \quad (8.2.62)$$

whereas  $m$  denotes the order. Because of the usually non-cyclic combustion variations, an average value for several working cycles can be calculated from the measured data.

Faults to be taken into consideration are misfires or combustion differences in one or two cylinders. Six different patterns  $P$  have to be distinguished for the relative location of the misfiring cylinders to each other:

- $P_0$ : no fault;
- $P_1$ : one cylinder oversupplies;
- $P_2$ : one cylinder undersupplies;
- $P_3$ : two subsequent cylinders undersupply;
- $P_4$ : two oppositely cylinders undersupply;
- $P_X$ : undetectable.

To locate the misfiring cylinders, only the first and second engine harmonics ( $m = 1$  and  $m = 2$ ) have to be evaluated, see also Figure 8.15. Representing the real and imaginary components of these two frequencies, values equal to zero for no misfires and unequal to zero for misfires appear. For pattern recognition and misfire detection respectively, comparisons of the amplitude values and the real and imaginary components have to be performed. Also, two thresholds  $T_1$ ,  $T_2$ , which are dependent on engine speed and load, have to be determined. The flowchart in Figure 8.16 shows the signal flow of monitoring and diagnosis of the possible fault patterns. Depending on the fault case, different vector patterns arise, with which the defective cylinders can be detected. Thus, the fault diagnosis is executed by a pattern recognition method of the amplitudes and phases of the DFT.

The performance of the proposed method is, on the one hand, limited by faults in the data acquisition (for example, error in measurements) and, on the other hand, by overlaid disturbances on the measured signal. It can be used for misfire detection as well as for monitoring smooth engine operation for the whole operation area, except for too-low loads and high speeds. A similar approach was developed by Willimowski *et al.* (1999) for measuring the exhaust gas pressure.

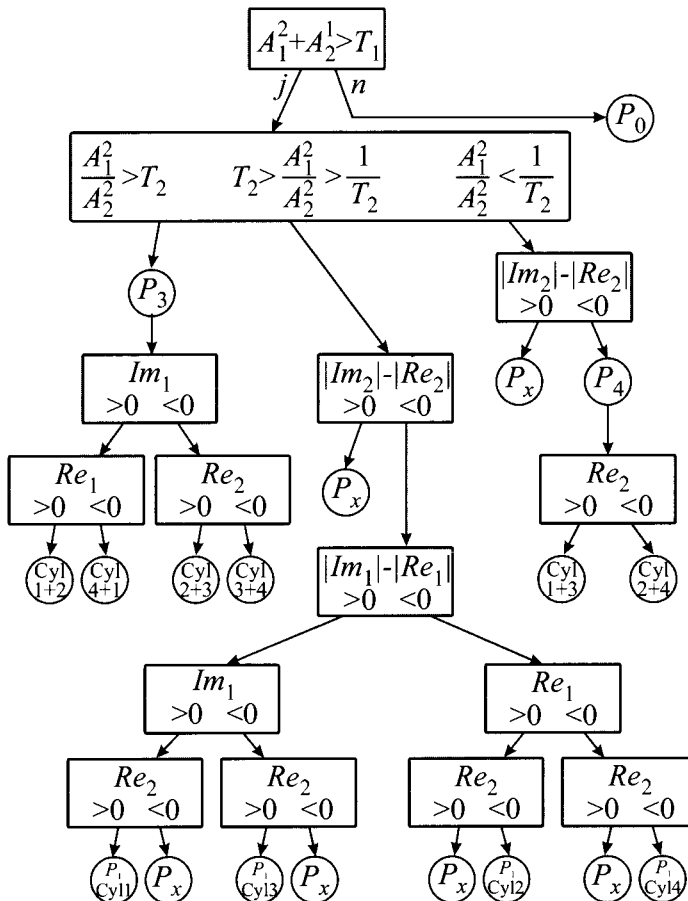


**Figure 8.16.** Scheme for detection of misfires and diagnosis of the faulty cylinders

## 8.3 PROBLEMS

- 8.3.1 An acoustic harmonic signal with  $f_1 = 1000$  Hz is amplitude-modulated with  $f_2 = 50$  Hz. Determine the frequencies of the resulting oscillations.
- 8.3.2 The amplitude  $y_{01} = 1$  of a harmonic signal with frequency  $f_1 = 100$  Hz is modulated with  $f_2 = 20$  Hz and amplitude  $y_{02} = 0.5$ . Determine the resulting frequencies and show them in a diagram for the amplitude spectrum.
- 8.3.3 The two engines of an aircraft run at 2500 and 2510 rpm. It is assumed that the six-cylinder four-stroke engines generate a noise with the ignition frequency. Which frequencies will be heard?

8.3.4 The electromagnetic force on the armature in a solenoid is proportional to the square of the magnetomotance and the current respectively, see Section 5.2.5. Which frequencies arise in the magnetic force for an alternative current of 50 Hz?

8.3.5 State the advantage of the FFT compared to DFT.

# 9 Sensors

---

Sensors and the associated measuring systems provide the required measurable information about the process in mechatronic systems. They represent an essential link between the process and the information-processing part, *i.e.*, microcomputers, see Figure 9.1. Sensors that measure mechanical or thermal quantities and transform them into an electrical signal are of special importance for mechatronic systems. This chapter gives a brief overview of some of the characteristic features, signal types and measurement principles. A more detailed description of the broad field of metrology is given in, *e.g.*, Jones (1977), Schrüfer (1983), Jüttemann (1988), Czichos (1989), Juckenack (1990), Thiel (1990), Profos, Pfeifer (1992), Schaumburg (1992), Tränkler (1992), Beckwith *et al.* (1995), Bauer (1996), Christiansen (1996), Jurgen (1997).

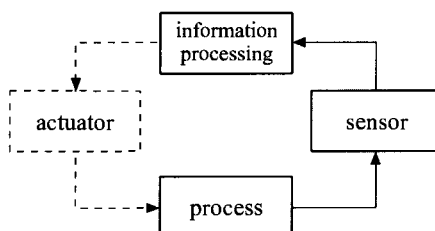


**Figure 9.1.** Sensors as links between a process and the information-processing unit

## 9.1 MEASURING SYSTEM

The purpose of a measuring system is to observe and quantify a variable physical quantity (called a measurand) and to process the obtained information. The first element of this system is the sensor or sensing element (increasingly used instead of “pickup”). Its primary function is to detect the measurand and transform it into a suitable signal, see Figure 9.2. Mechatronic systems generally rely on sensors with an electrical output signal. The characteristics of the output signal depends on the measurement principle of the sensor. Transducers and amplifiers transform the electric sensor output signal into a standardized electrical signal, *e.g.*, 0...20 mA or 4...20 mA or 0...10 V, which is more suitable for further processing. If high-frequency disturbances contaminate the usable signal, a low-pass filter is applied in order to decrease the influence. A sample and hold device and an analog-to-digital converter are necessary if the sensor signal is to be processed by a microcomputer.

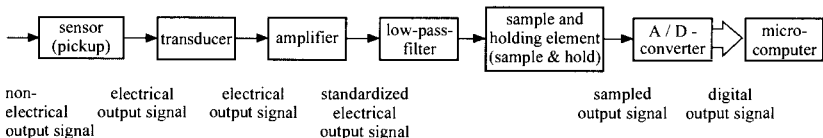


**Figure 9.2.** Measuring system

Consumer goods and low-cost appliances do not require high-precision measurement and a modular arrangement of the measuring system. Therefore, simplifications may be made in order to reduce costs, *e.g.*, by omitting the generation of standardized electrical signals.

## 9.2 CLASSIFICATION OF SENSORS

Because of the broad spectrum of metrology, it is difficult to classify sensors and the corresponding signal processing devices. A survey entitled “Technical Sensors” (1983) proposed a hierarchical division consisting of five levels and 75 subdivisions. Important features for the classification of sensors are:

- measured quantity;
- sensor-principle;
- manufacturing technology;
- signal types and interfaces;
- fields of application;
- properties, features;
- quality class;
- cost.

Table 9.1 gives an overview of the classification of some important measurands. A rough classification might be:

- mechanical quantities;
- thermal/caloric quantities;
- electrical quantities;
- chemical and physical quantities.

**Table 9.1.** Survey of the classification of important measuring quantities

class	measuring quantity
mechanical quantities	geometrical quantities
	kinematic quantities
	stress quantities
	material characteristics
	acoustic quantities
thermal quantities	temperature
electrical quantities	electrical state variable
	electrical parameter
	field variable
chemical and physical quantities	concentration
	size of particle
	kind of molecule
	optical quantities

The following sections will deal with properties and features of sensors, as well as different kinds of signal types. In addition, the principles of some sensors with an electrical output signal will be

described.

### 9.3 SENSOR PROPERTIES

The transformation of non-electrical quantities into electrical ones depends on physical or chemical effects. These may be divided into *main* and *side* effects. The main effect is responsible for generating the desired measuring signal, *e.g.*, the electrical voltage of a piezoelectric pressure sensor. However, disturbing side effects are frequently superimposed, *e.g.*, the influence of temperature changes. The design process for sensors needs to take these side effects (sometimes called “cross sensitivity”) into account. Their influence should have only little effect or should be compensated by appropriate measures.

The most important criteria for evaluating sensors are:

- static behavior;
- dynamic behavior;
- quality class, measuring range;
- overload capacity;
- compatibility with associated components;
- environmental influences;
- reliability.

A sensor’s static behavior is described by the characteristics of the sensor. It defines the sensitivity of a sensor, *i.e.*, the ratio of the change of the electrical output signal to the change of the measured variable. Other important properties of a sensor are linearity, hysteresis and repeatability (reproducibility).

The dynamic behavior is described by a sensor’s frequency response or simple characteristic values, *e.g.*, cut-off frequencies or time constants. The sensor dynamics have to be adjusted to the process and the measuring task.

The quality class gives a basic measure about a sensor’s accuracy. It is the percentage maximum error of a measurement with reference to the full scale. Applications for consumer goods don’t need a high accuracy (2% to 5% is sufficient). Industrial applications, on the other hand, require a much higher precision (0.05% to 1%). Equipment for high-precision measurements, *e.g.*, calibration and test equipment, have to meet very strict requirements. The measuring range describes the range in which the sensor’s specifications are met.

The overload capacity specifies the range in which a sensor may be operated without changes in the sensor’s characteristics or damage to itself. Typical overload capacities are between 200% and 500%.

A sensor’s compatibility depends on the output signal type (see next section). Environmental influences, *e.g.*, temperature, acceleration, corrosion, contamination, wear and tear, are especially important.

The reliability of a sensor is described by characteristic parameters, e.g., the “mean time between failures” (MTBF in [h] or its reciprocal value the mean failure rate ( $[h^{-1}]$ )).

## 9.4 SIGNAL TYPES, TRANSDUCERS, MEASURING AMPLIFIERS

The type of signal supplied by the sensor depends on both the measuring principle and on the associated signal transmission and signal processing devices. Signal types may be subdivided into the following categories:

- amplitude-modulated signals;
- frequency-modulated signals;
- digital signals.

Amplitude-modulated signals are characterized by a proportional relationship between the signal amplitude and the measured quantity. If the signal frequency is proportional to the measured quantity, the signal is called a frequency-modulated signal. Digital signals encode a measured quantity using serial or parallel binary signals.

Table 9.2 describes some of the properties of these signal types, cf., Schrüfer (1983) and Tränkler (1992).

**Table 9.2.** Some properties of signal types for measuring signals

signal type properties \	amplitude- modulated	frequency- modulated	digital
static accuracy	large	large	limited by word length
dynamic behavior	very fast	limited through transducer	limited through sampling
noise sensitivity	medium/large	small	small
galvanic separation	costly	simple (transducer)	simple (optical coupling)
interfacing to a digital computer	analog-digital converter	simple (frequency counter)	simple
computational operation	very limited	limited	simple, if microcomputer

Transducers convert the amplitude-modulated signal into another appropriate electrical signal. Examples of transducer circuits without amplification are:

- voltage-current transducer with precision resistor;
- voltage divider, current divider;

- resistance-current transducer;
- compensation network for measuring voltage, current or resistance (resistance bridge).

Measuring amplifiers raise low-power sensor output signals to a higher power level or generate more powerful standardized signals (0 ... 10 V, 0 ... 20 mA). High-power sensor output signals are needed for associated components of the measuring chain, *e.g.*, transmission links, filters and displays. Measuring amplifiers often consist of operational amplifiers made out of resistors and transistors in the form of analog integrated circuits. Operational amplifiers possess high gains, which may vary considerably due to aging and dependence on temperature. Without additional circuitry, operational amplifiers may only be used as zero gains for comparator or compensator circuits. By adding a negative feedback, one observes that the gain of the entire circuit depends mainly on the resistors of the negative feedback for the case of high feedforward gains of the operational amplifier. Measuring amplifiers with negative feedback are divided into four basic types of circuits:

- voltage amplifiers;
- voltage amplifiers with current output;
- current amplifiers;
- current amplifiers with voltage output.

The following sections give a short description of some important sensor principles. For a more detailed description, refer to the references given in the bibliography.

## 9.5 DISPLACEMENT MEASUREMENT

### a) Resistive sensing elements

Resistive pick-ups exploit the proportional relationship between the length of a wire or film resistor and its electrical resistance, see Table 9.3. They are potentiometers made of electrically conductive plastics or metal wire. Potentiometers are wired as voltage dividers and are offered as linear or rotational sensing elements, in the latter form as multiplex potentiometers (*e.g.*, 10 revolutions). The measuring range of linear sensing elements starts at a few millimeters and goes up to about two meters. Encapsulation of the sensor housing enables the deployment of the sensor in rough environments. Safety rails ensure a movement of the brush free of lateral forces. Sensing elements made out of electrically conductive plastics have a very high resolution, *e.g.*, measurement of 100 mm with a resolution of 0.01 mm. However, a high accuracy requires a very precise voltage source.

Table 9.3. Displacement sensors (linear)

sensor principle (example)	resistive sensors	inductive sensors	capacitive sensors	strain gauge	code sensors	incremental sensors	Hall sensor
material	metal, semiconductors, conductive plastics	ferrromagnetic metal	capacitor	metal, semiconductor	optical encoders	glass, metals	Hall semiconductor
output signal	analog voltage	analog voltage	analog voltage	analog voltage	binary signal	binary signal	binary signal
measurement range	1 cm...2 m 300° (angular displacement)	±100 µm...±50 cm	0.1 cm...10 cm			10 mm...3 m	360°
maximum sensitivity	0.2 V/° or 2 V/cm	0.1 V/cm...40 mV/µm		$k = \frac{\Delta R/R}{\Delta I/I} = 2(\text{metal})$ $k = 100 (\text{semiconductor})$	4096 pulses/rev		4000 pulses per revolution
accuracy, resolution	max. 40 µm or 0.1°	0.1 µm	<0.1 nm		1 LSB	0.1 µm 0.00005°	10 <sup>-5</sup> revs
temperature range	-50°C...+250°C	-40°C...+100°C	up to 800°C	-270°C...+1000°C	-50°C...+100°C	0°C...+50°C	-200°C...150°C

### b) Inductive sensing elements

Inductive sensing elements rely on the dependence of the change in the self and mutual inductance on the element's position. The inductance of coil arrays is changed by variation of the air gap. A lattice network consisting of differential coils ensures an almost linear characteristic.

Differential transformers exploit the relationship of the mutual inductance between the primary and secondary coil and a displacement of the iron core. The primary coil is subjected to a carrier frequency. The difference in the voltage of the secondary coil acts as a displacement-dependent output signal. Inductive sensors are non-contact sensing elements. Their measuring range starts at a few millimeters and goes up to about one meter. Other designs are displacement angle sensing elements.

### c) Capacitive sensing elements

A change in plate distance, plate area or of the dielectric material between plates influences the capacitance of a capacitor. The signal processing circuits consist of AC lattice networks (capacitive bridge). They have to be operated with a high carrier frequency (0.5 ... 1 MHz) because of small capacitances.

### d) Strain gauge

Strain gauges (SG) transform small linear deformations into electrical signals. They are based on the effect that a change in the length of an electrical conductor results in a change in the electrical resistance. If one expands a wire of length  $L$  by  $\Delta L$ , the electrical resistance of the wire changes due to changes in the specific electrical resistance (because of structural deformations), the length and the cross-sectional area.

*Metal wire* and *film SG* consist of thin constantan wires or films. Changes in the length and cross-sectional area lead to a change in the electrical resistance, while the specific electrical resistance is not affected. For *semiconductor SG*, the main effect is the change in the specific resistance due to the structural deformation by elongation. Semiconductor SG are much more sensitive to elongation (about 40 to 80 times more sensitive than constantan) but have non-linear characteristics at large elongations and are much more expensive than metal SG. Embedded between thin films, SG are pasted directly onto the measuring object. This could directly be the constructive component whose elongation is to be measured. SG in conjunction with special spring elements and diaphragms serve as force, torque and pressure sensors. The change in the electrical resistance is evaluated with lattice networks (bridge circuits). A temperature compensation is often provided.

### e) Encoders

Encoders use code rulers or code discs on which the discrete displacement data is encoded. The allocation is absolute because they do not need an external reference. Unit-distance codes, e.g., Gray code, are

often used for coding. The sampling is performed optically. In order to distinguish between  $2^n$  different discrete positions, one needs  $n$  sampling tracks. This makes this kind of sensing element relatively complicated. Coded sensing elements are mainly used in industrial metrology, *e.g.*, for numerically controlled machine tools and robots.

#### **f) Incremental sensing elements**

Incremental position and angle sensors count the number of so-called notches or slots, *i.e.*, *increments*, relative to an initial point. Sampling is performed either by optical (*e.g.*, diodes) or inductive methods, resulting in pulse trains that are counted. The initial point can be chosen arbitrarily. If a failure (*e.g.*, power failure) occurs, the initial point gets lost and must therefore be reset by moving to a reference position. A fault while counting the increments influences all the following readings. Additional circuitry with two samplers per scale enables detection of movement direction and a pulse multiplication.

The sensor housing often contains a pulse-shaping circuitry. Incremental sensors are mainly used in industrial metrology, *e.g.*, manufacturing. Linear scales with a range of up to 3 m and a graduation of 1  $\mu\text{m}$  are available. Shaft encoders with up to 36.000 slots are used for precision applications. Using pulse multiplication (interpolation), a resolution of about 0.00005° is achievable.

#### **g) Hall effect sensors**

If a voltage is applied to a conductor or semiconductor located in a magnetic field perpendicular (right angled with the current flow) to the applied voltage, the Hall voltage is generated, which is perpendicular to both the current flow and the magnetic field. The dependence of the Hall voltage on the magnetization is now used for proximity or position measurement. If the semiconductor is a silicon Hall plate, the voltage has to be amplified. Integrated Hall ICs exist, which incorporate amplification, stabilization and temperature compensation. A rotational position sensor now consists of a permanent magnet and a soft magnetic tooth wheel moving through a gap between the magnet and the Hall IC (*e.g.*, bipolar technology). Hence, by interruption of the magnetic field, a pulse train is generated whose frequency is proportional to the rotational velocity. The Hall IC requires a supply voltage (*e.g.*, 12 V). This type of sensor is used, for example, for rotor position sensing of brushless DC motors and for ignition triggering of SI engines (Bauer 1996).

#### **h) Further measuring methods**

*Ultrasonic distance sensors* are used for level measurement (bulk material, fluids) or as distance meters (park assistance for an automobile). They rely on the time interval between transmission and echo-return of the ultrasonic signal. *Laser interferometers* are based on the phase comparison of coherent light and are used for contactless precision displacement measurement.

All of the above-mentioned measuring methods may also be used for the measurement of force or pressure. They detect displacement of springs or membranes and transform it into an electrical signal.

## 9.6 VELOCITY MEASUREMENT

One possibility of measuring velocities is to differentiate the signal of displacement or angular sensors. However, this has the disadvantage of amplifying the noise relative to the usable signal. Therefore, direct measuring methods for velocity measuring are more suitable. Angular velocity sensors especially are of practical significance. Translational velocities are often converted into rotational velocities for measurement purposes (speedometer).

### a) Active electrodynamic sensing elements

Active electrodynamic sensing elements operate like generators, see Table 9.4. If  $N$  electrical conductors move through a magnetic field with magnetic flux  $\Phi$ , this induces a voltage

$$V = -Nd\Phi/dt$$

in the conductors according to the law of induction, see Section 5.2.4. As Table 9.4 shows, one can distinguish:

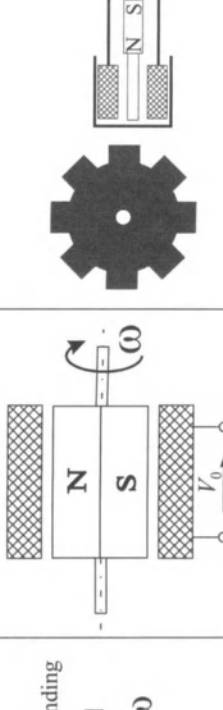
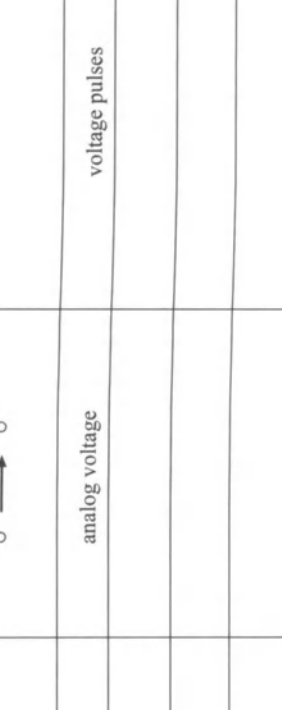
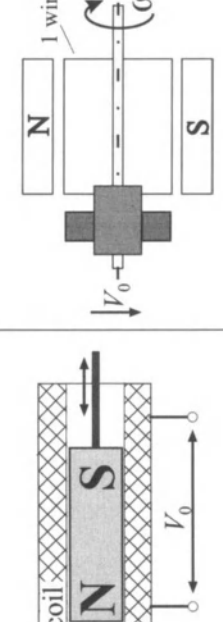
*Sensors for translation:* a permanent magnet moves inside a coil and induces a voltage that is proportional to the velocity.

*Sensors for rotation:* AC generators use a permanent magnetic rotor and a stator winding. In order to measure the rotational speed, both the output signal's frequency and voltage may be used. A linear voltage characteristic results. DC tacho generators consist of a commutator and a coil rotating in a constant magnetic field derived from a permanent magnet. The generated voltages are then proportional to the rotational speed. The polarity of the voltage depends on the sense of rotation. This sort of sensing element has a linear characteristic but a rippled voltage signal because of the commutation.

### b) Incremental inductive sensors

These sensing elements correspond to incremental displacement sensors. A ferromagnetic ring gear with rectangular teeth passes an inductive sensor, Table 9.4. This sensor consists of a bar magnet with a soft magnetic pole pin and an induction coil. The voltage in the coil is proportional to the periodic variation in the magnetic flux. The output signal therefore is a pulse sequence and its frequency is related to the rotational speed. A frequency-voltage converter transforms the pulse frequency into a voltage. Discrete evaluation is performed by counting the number of pulses during a certain time-span or by measuring the time interval between two pulses.

Table 9.4. Velocity sensors

sensor principle (example)	translational velocity sensor	DC generator (tacho-generator)	AC generator	incremental velocity sensors												
 		<table border="1"> <tr> <td data-bbox="563 179 622 889">output signal</td><td data-bbox="563 889 622 1511">analog voltage</td><td data-bbox="563 1511 622 1674">analog voltage</td></tr> <tr> <td data-bbox="622 179 680 889">measurement range</td><td data-bbox="622 889 680 1511"><math>\pm 6000 \text{ rev/min}</math></td><td data-bbox="622 1511 680 1674">voltage pulses</td></tr> <tr> <td data-bbox="680 179 739 889">sensitivity</td><td data-bbox="680 889 739 1511">10 mV/mm/s</td><td data-bbox="680 1511 739 1674">5 V per 1000 rev/min</td></tr> <tr> <td data-bbox="739 179 775 889">accuracy, resolution</td><td data-bbox="739 889 775 1511"></td><td data-bbox="739 1511 775 1674"></td></tr> </table>	output signal	analog voltage	analog voltage	measurement range	$\pm 6000 \text{ rev/min}$	voltage pulses	sensitivity	10 mV/mm/s	5 V per 1000 rev/min	accuracy, resolution				
output signal	analog voltage	analog voltage														
measurement range	$\pm 6000 \text{ rev/min}$	voltage pulses														
sensitivity	10 mV/mm/s	5 V per 1000 rev/min														
accuracy, resolution																

The number of pulses per rotation depends on the specific application and ranges from one to several thousand pulses. This sensor is, for example, used for engine crankshafts and wheels for ABS (anti-lock braking system) functions. It does not need an electrical power supply.

### c) Other methods

Another method of measuring translational velocity exploits the *Doppler effect*. A velocity-dependent frequency shift between a transmitted and a reflected signal by a moving object occurs. Well-known examples for these kinds of sensors are the Doppler radar (traffic radar) and the laser Doppler for high precision, contactless measurement, but these are at a high cost.

Yet another method utilizes *cross-correlation* between two stochastic or periodic signals. Two identical sensing elements are placed at distance  $l$  and the measurement of the time delay  $\tau$  between the transmitted and received signal enables the determination of the velocity  $v = l/\tau$ . This is, for example, used with optical sensors for rough surfaces or for fluids.

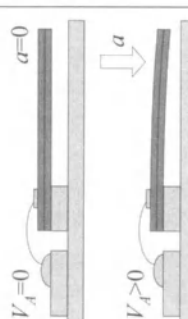
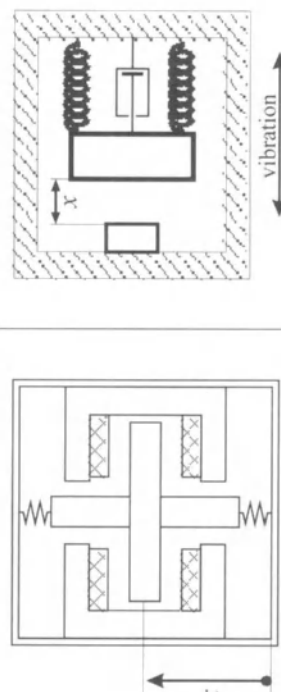
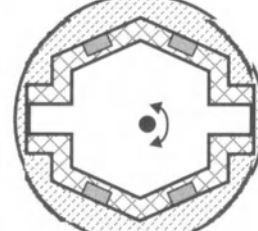
## 9.7 ACCELERATION MEASUREMENT

Measurement of acceleration is frequently based on force measurement using the relationship between the acceleration  $a$  of a mass  $m$  and the inertial force  $F$ :  $a = F/m$ . For direct measurement of the force  $F$  *piezoelectric force sensors* may be used, see Table 9.5. Due to the large spring stiffness and small masses of these transducers, it is possible to achieve high natural frequencies (100 kHz).

Spring-mass systems consist of a seismic mass connected to the sensor casing with springs and dampers. The acceleration is determined by measuring the displacement of the spring (e.g., inductively). There are many different kinds of acceleration sensors that are capable of measuring accelerations of, e.g.,  $10^{-6}$  g for inertial navigation purposes or up to  $10^5$  g for measuring explosions. Masses, springs and dampers are chosen such that high natural frequencies (15 Hz to over 100 kHz) are achieved. The utilizable measurement frequency reaches about half of the natural frequency. Sensors for angular acceleration use equivalent arrangements. Table 9.5 shows some examples.

An acceleration may also be determined by differentiating the signal of a velocity sensor once or by differentiating the signal of a displacement sensor twice. However, this leads to an increase in high-frequency noise and makes low-pass filtering inevitable.

Table 9.5. Acceleration and vibration sensors

sensor principle (example)	piezoelectric acceleration sensor	acceleration sensor with seismic mass	vibration sensor with seismic mass	angular vibration sensor
				
material		seismic mass with large natural frequencies	seismic mass with small natural frequencies	seismic mass with small natural frequencies
output signal	analog voltage	amplitude-modulated analog voltage	amplitude-modulated analog voltage	amplitude-modulated analog voltage
measurement range	$\pm 500 \text{ g}$	$5 \text{ Hz} - 50 \text{ kHz}$	$\pm 2000 \text{ g}$	
sensitivity	$0.1 \text{ mV/(m/s}^2\text{)}$			
accuracy, resolution	$0.01 \text{ g}$		$0.1 \text{ g}$	

## 9.8 VIBRATION AND OSCILLATION MEASUREMENT

The measurement of relative vibrations is based on the displacement between two reference points, which is measured by displacement sensors. For measuring absolute vibrations, the missing second reference point has to be replaced by a seismic mass, see Table 9.5. Measurement of the oscillation amplitude requires a large seismic mass and a small spring constant of the suspension (small natural frequency). This leads to a motionless seismic mass and an oscillating sensor housing. A displacement sensor (*e.g.*, inductive sensor) measures the displacement between the seismic mass and the sensor housing. The same applies to electrodynamic velocity sensors, which measure the vibration velocity. Vibration acceleration is measured with acceleration sensors calibrated for high natural frequencies.

## 9.9 FORCE AND PRESSURE MEASUREMENT

Measurement of pressure and force is performed indirectly by measuring the spring or diaphragm deflection with displacement sensors like those described in Section 9.5 (especially strain gauges, used for so-called load cells, and inductive sensing elements).

Piezo-sensing elements are of special importance for pressure and force gauging. Piezoelectric sensing elements exploit the piezoelectric effect: a displacement results in an electrical charge at the surface of a crystal lattice. The arising displacement is very small (a few  $\mu\text{m}$ ). The electrical charge charges the artificial capacitance (consisting of the sensing element, wire and amplifier input). The resulting voltage  $V$  decays with the time constant  $T = RL$ . This is the reason why piezoelectric sensing elements are suitable for dynamic measurement only.

The subsequent measuring amplifier has to have a very high input resistance ( $R > 10^{13} \Omega$ ) in order to obtain a large time constant. Charge amplifiers are used with time constants of up to several hours. The maximum measuring frequency is about 100 kHz.

*Piezoresistive* sensing elements exploit the piezoresistive effect. In this case, a crystal subjected to mechanical forces changes its electrical resistance due to a dislocation in the crystal lattice structure. This also allows static measurements.

## 9.10 TORQUE MEASUREMENT

Torque is measured by gauging the torsion of a shaft section using angular, displacement or elongation sensors. For this purpose, special *torquemeters* may be attached to the shaft using flanges with or without bearings. Another possibility is to base the measurement of torque on the torsion of the shaft due to a load. The signal transmission depends on whether the shaft is rotating or not. If the shaft is rotating, the revolving sensors transmit their signals to the stationary electronic signal-processing unit via a slip-ring or without direct electrical contact, *e.g.*, through inductive coupling.

Measurements of a shaft's torsion can be obtained by employing either of the two following methods. The first method uses wire strain gauges, which are placed on the shaft with an inclination of 45° to its longitudinal axis, interconnected to a Wheatstone network, see Table 9.6. The second method measures the change of permeability by measuring the voltage induced in coils. Both measurement principles may be applied directly to the shaft or in conjunction with special torque-meters. In many cases, *torque-gauge heads* are necessary, which are easily incorporable, do not require much space and do not introduce too much elasticity. Additional requirements include the possibility of connecting a sensor via, *e.g.*, a flange to the shaft or integration of the sensor into pulleys.

The rotational angle between two twisted discs or axial dislocation of discs due to kinematic transmission may be measured inductively. Another measurement principle uses disc- or sleeve-like parts that consist of electrically conductive and non-conductive zones. Twisting of the shaft leads to a shift of the zones against each other and results in a change of the eddy current. This yields a change in the impedance of a stationary measuring coil. Additional possibilities for measuring torque include the use of surface-resonators and piezoelectric sensors, which are placed into the force flux. Pahl (1992) gives an overview of different torque sensors.

## 9.11 TEMPERATURE MEASUREMENT

### a) Resistance thermometers

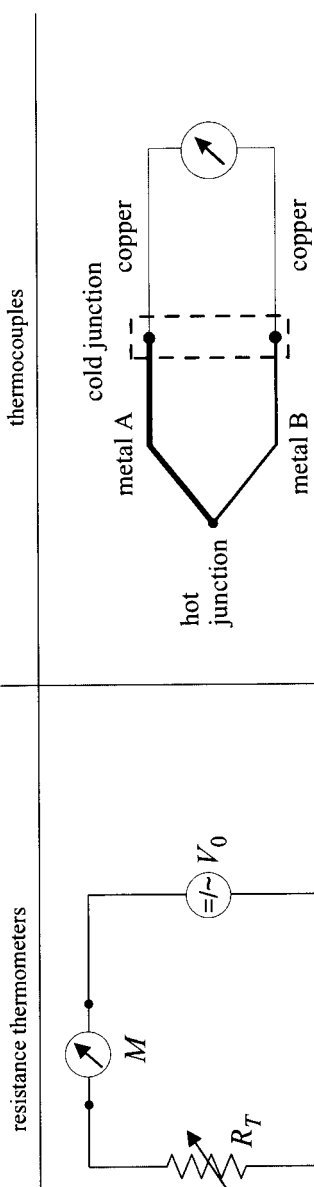
Passive resistance thermometers exploit the sensitivity of electrical resistors to temperature variation, compare Table 9.7. Metal resistance thermometers consist of nickel or platinum wire wound in the form of a free spiral around thin mica or laminated paper strips or embedded in glass. The resistance-temperature sensitivity is 0.358 Ω/K for platinum (Pt100) and 0.612 Ω/K for nickel (Ni100). The nominal resistance in each case is 100 Ω and the maximum measuring temperature is 150°C for Ni and 500°C for Pt.

Table 9.6. Force, torque and pressure sensors

sensor principle (example)	piezoelectric force sensor	torque measurement using strain gauges	force spring deflection sensor	pressure diaphragm sensor
material	piezoelectric material	strain gauges on surface	spring in a casing	flexible diaphragm
output signal	analog voltage	analog voltage	analog displacement	analog displacement
measurement range	1 N...1 MN	0.05 Nm...50 kNm		0.1 bar...10000 bar
sensitivity	125 V/kN	.		
temperature	-80°C...+150°C	+10°C...+60°C	-40°C...+60°C	-25°C...+100°C

Table 9.7. Temperature sensors

sensor principle (example)	resistance thermometers		thermocouples	
	material	metal resistor	semiconductor resistor	
Principle example	Pt	Ni	NTC	PTC
Output signal		analog voltage		analog voltage
Measurement range	-250°C...+1000°C	-40°C...+850°C	-200°C...+850°C	-180°C...+760°C
Sensitivity		<5 mV/°C		53 µV/°C
Accuracy, resolution		0.3% ... 0.25% of measured temperature		0.25% ... 0.75% of measured temperature
			Pt-Rh	0°C...+1750°C



A thermistor is a resistance thermometer consisting of a metal oxide semiconductor material. It is about 10 times as sensitive as metal resistance thermometers, has a strong non-linear characteristic and is less accurate. Commercial forms are very small (< 0.5 mm) and thus possess a low heat capacity. This makes thermistors suitable for measuring surface temperatures and for the measurement of dynamic processes. If the semiconductor possesses a negative temperature coefficient (electrical conductivity increases if temperature rises), it is called an NTC thermistor, while a semiconductor with a positive temperature coefficient (electrical conductivity decreases if temperature rises) is called a PTC thermistor. These metallic resistors can be produced as thin-film or thick-film sensors and are then integrated upon a single substrate wafer with neutral trimming resistors for precision manufacturing, Bauer (1996). Maximum temperatures range from 100°C to 1000°C for NTC thermistors and from -10°C to 500°C for PTC thermistors.

### b) Thermocouples

The arrangement of two lengths of dissimilar wire, insulated from each other but joined at one end, is known as a thermocouple, Jones (1977). Thermocouples are active temperature sensors. Exposing the junction of the two metals to heat generates an EMF that depends on the temperature at the junction. This is called the *Seebeck effect*. When the junction between two dissimilar metals is heated or cooled relative to a second reference junction, the resulting overall voltage is a function of the difference temperature of the two junctions. The performance of a thermocouple is usually specified in relation to a reference temperature of 0°C (ice water). In many practical arrangements, the reference junction is located in a controlled environment with a non-zero reference temperature.

The temperature-voltage characteristic is non-linear but a linearization is possible for a wide range of operation. The advantages of thermocouples are their small dimension, which leads to small measuring points, and that they do not need a power supply. However, they have low sensitivities and the output signal level is small. Thermocouples enclosed in protective tubes with a diameter of 0.25 mm to 3 mm have a wide measuring range of 220°C to 2400°C. Due to the small heat capacities of such sensors, it is possible to measure even rapid temperature changes.

## 9.12 ANALOG-TO-DIGITAL CONVERSION

The discussed sensing elements transform a physical quantity into a change of electrical resistance, capacitance or inductance. DC or AC lattice networks transform these changes of electrical properties into a voltage signal and amplify it. Other sensing elements produce low-

power voltage or current signals that need to be amplified by special circuits, *e.g.*, voltage or current amplifiers, electrometer or charge amplifiers.

If a microcomputer is used for data acquisition purposes, analog-to-digital conversion is necessary. A low-pass filter limits the measurement signal bandwidth if necessary in order to achieve compliance with the sampling theorem. The filter is followed by a sample and hold device and finally the analog-to-digital converter (ADC), see Section 11.3. The precision of the ADC is chosen depending on the application. Standard ADCs have an 8-, 10- or 12-bit precision, while high-precision applications need 16-bit. Converters that use time interval or frequency as intermediate quantity (charge-balancing or dual-slope converters) integrate the input voltage over a fixed input sample time (the measuring interval). An example is the digital voltmeter. This kind of conversion method is very precise but the measured quantity may not change rapidly. Often, low-pass filters and sample and hold devices are not used in this conversion process. ADCs that use the principle of compensation, *e.g.*, successive-approximation converters, operate by comparing the input voltage with the output of a digital-to-analog converter (DAC). The ADC employs the DAC in a feedback loop, Jones (1977). In conjunction with sample and hold devices, this type of converter makes conversion rates of up to 1 MHz possible. Parallel ADC (flash converters) reach even higher conversion rates (up to 100 MHz with a 10-bit precision).

## 9.13 ELECTROMAGNETIC COMPATIBILITY (EMC)

The surroundings in which a sensor system is applied influences the selection of a sensor type. The environmental conditions are of a mechanical (vibration, shock), thermal and chemical (water, salt, oil, solvents) nature. Electromagnetic radiation from the surrounding environment poses another important influence on sensor systems. A sensor system's property of remaining neutral to this influence is called *electromagnetic compatibility* (EMC). The sources of this sort of interference are manifold and cover a wide range of frequencies, *e.g.*, from 16 2/3 Hz (power supply of trains) to several GHz (radar installations). The power supply of trains, electrical substations, transmission lines, radio, television and communication transmissions, radar installations, welding tools, lightning, *etc.*, all emit electro-magnetic energy that influences a system from a distance. Other interferences are due to wire-bound influences from the power supply. Examples of this are peak loads of other electrical consumers, commutator sparking of electric motors, variations of the power supply level, *e.g.*, in a 12 V vehicle electrical system, or spikes and collapses in the power supply due to a breakdown

of other systems. In addition to this electrical and electronic devices influence each other. This so-called near-field influence has to be taken into account, too. This is especially the case if the devices are mounted in a confined space. Examples for near-field influence include crosstalk between wires in a cable tree, emission of interference by electrical drives, the clock rate of microprocessors and other digital devices, thyristor circuits and ignition systems. In addition to these effects, one has to take into account static charges, accidental earths and handling errors, *e.g.*, faulty connections or short circuits. There are a lot of problems of this sort, especially in automotive applications.

Suppression or reduction of the interference emission at its source is an important countermeasure. There are several methods for achieving this, *e.g.*, appropriate housing or use of interference suppressor coils in supply lines. Limits for noise field intensities are given in the appropriate regulations like VDE 0874 and VDE 0871.

Sufficient space between devices, especially between wires, helps to reduce the noise level. Instrumentation and power cables should always be installed separately. The use of radio shielding (metal casing) is one possibility to shield devices and components. Transmission lines configured as twisted pairs are less susceptible to inductive influences and may be shielded from capacitive (and high-frequency magnetic) influences. A proper connection of the shielding to earth is essential, Lauber (1989). An effective method for avoiding problems with EMC is reducing the length of wires needed for interconnecting devices. This is achievable by integrating the sensor, measuring amplifier and signal conditioning device into a single unit. Using signal transmission that is safe from interference (use of high signal levels, current transmission 4–20 mA, encoded transmission with error detection) further improves the EMC. Optical transmission using fibre cables in conjunction with measuring principles that are insensitive to electromagnetic influences (optical, digital) leads to even less susceptibility to interference.

Examining the EMC properties of parts of a system or of an entire system (EMC/EMP tests) is very expensive and difficult. A complete examination of all interactions in a complex system is usually impossible. Therefore, it is necessary to consider EMC aspects during the design of a system or component. Both emission of interference and susceptibility to interference of all components has to be minimized.

## 9.14 INTEGRATED AND INTELLIGENT SENSORS

Sensors are designed with two goals in mind. The desired signal should be the dominating signal a sensor measures and the measured signal must correspond to the actual physical quantity unambiguously. In reality, these goals cannot be fulfilled entirely. Sensors are subjected to

side effects, *e.g.*, cross-sensitivity, perturbations, non-linear transmission (non-linear characteristics, hysteresis, responsiveness, null drift), drift, aging, slow dynamic behavior and individual manufacturing tolerances. Disregarding these non-ideal properties during signal processing leads to faulty measurements. This is why steps have to be taken to compensate for some of these side effects, even when using analog evaluation circuits. These steps include the use of filters, signal differences of two identical sensors or special circuits to suppress the null drift, Tränkler, Böttcher (1992). However, many additional and new possibilities arise with the use of *digital signal processing*.

Figure 9.3a shows a conventional measuring chain with associated analog-to-digital converter and a microcomputer or microcontroller. If, for example, the non-linear characteristics of the sensor do not change over time, it is possible to linearize or adjust them by using the microcomputer. This enables calibration of each individual sensor during its manufacturing and decreases the necessary measures on the analog part of the sensor. The use of microcontrollers makes frequency-modulated and incremental sensors economic because of the built-in counters that are able to measure frequencies easily.

Further improvement is possible by *integration* of sensor, signal processing, ADC and microcomputer with a bus interface into one single unit, Figure 9.3b. This integration (possibly onto one single chip) has several important advantages: reduction of costs for large-scale manufacturing, reduction of space requirements, higher precision, decrease of susceptibility to noise. Because of this integration, however, the requirements for robustness and reliability increase because a sensor is often subject to a rough environment.

*Integrated sensor components* allow the realization of additional functions. This leads to so-called “smart sensors” or “intelligent sensors”, Figure 9.4. One example is the use of a second sensor to measure a parasitic quantity, *e.g.*, temperature, and using this measurement to compensate for an unwanted side effect. Other examples result from the use of special algorithms built into the microcomputer. These algorithms serve as noise filters, for compensation and linearization purposes, for compensating for hysteresis effects (due to magnetic properties, friction, responsiveness), dynamic delays and drift and aging effects. It is possible to introduce self-calibration for all algorithms during manufacturing and maintenance, and even fault detection and fault diagnosis schemes are possible. The fact that all of these algorithms may be programmed individually for each sensor is also very important. Manufacturing tolerances for the sensors need not be as small as in the conventional case. One way of realizing the digital processing chip is through an application-specific integrated circuit or ASIC. Kleinschmidt (1990), Tränkler (1992) and Kiencke (1992) describe the development of intelligent sensors.

It is interesting to see that sensor technology development follows a path similar to that of mechatronic system development, *i.e.*, by reducing the requirements on the sensor elements and to shift certain functio-

ns into microelectronics by including even more intelligent functions as described in Chapter 1.

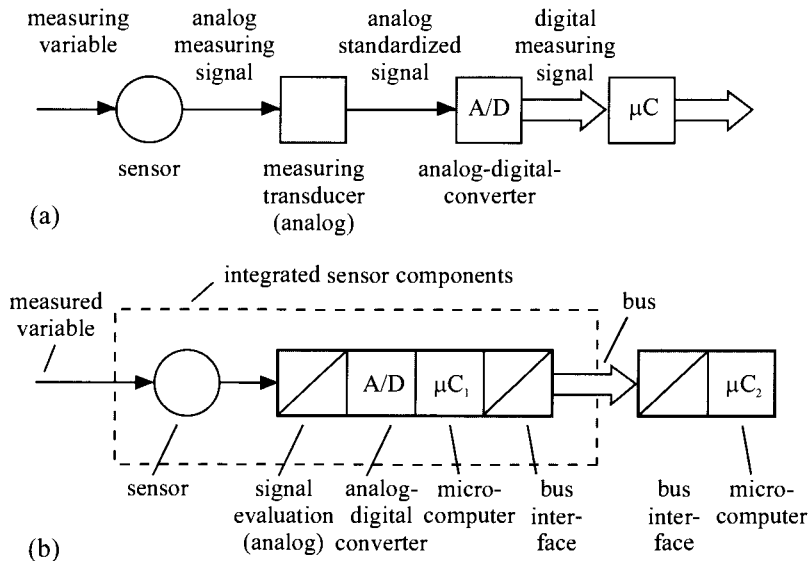


**Figure 9.3.** Integration of sensor technology: (a) conventional measuring chain with digital-processing unit; (b) integrated sensor components with digital-processing unit

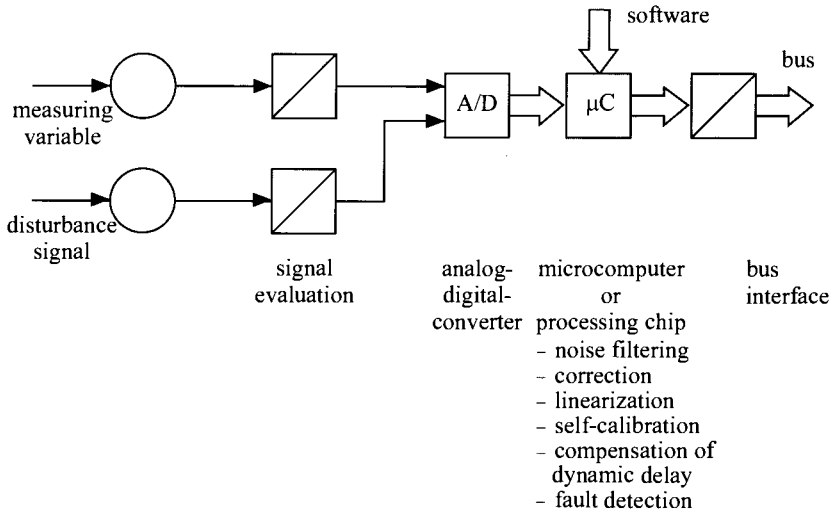


**Figure 9.4.** Integrated sensor components with “intelligent” functions

Further possibilities arise with the use of multi-sensor technology, *i.e.*, a combination of similar or different types of sensors, and the many developments that are emerging through micromechanics.

## 9.15 PROBLEMS

- 9.15.1 Compare the merits of a platinum resistance thermometer, a thermistor and a thermocouple for temperature measurement.
- 9.15.2 Consider a capacitive displacement transducer to be governed by the relationship  $C = 0.225A d$ , where  $A$  is the cross-sectional area of the transducer tip (in  $\text{cm}^2$ ) and  $d$  is the air gap distance (in mm). Determine the change in voltage when the air gap changes from 2 mm to 3 mm.
- 9.15.3 A choice of an incremental shaft encoder or an absolute shaft encoder is offered for the measurement of an angular displacement. What is the main difference between the results that can be obtained?
- 9.15.4 A pressure sensor consisting of a diaphragm with strain gauges bonded to its surface has the following information in its specification:  
 Ranges: 0 to 1400 kPa.  
 Non-linearity error:  $\pm 0.15\%$  of full range  
 Hysteresis error:  $\pm 0.05\%$  of full range.  
 What is the total error due to non-linearity and hysteresis for a reading of 1000 kPa?
- 9.15.5 A vibration measuring system indicates an overshoot of 37% when subjected to a step input. Calculate the damping ratio of the system. If the damping ratio of the system in question was changed to 0.9, determine the percentage overshoot to be expected when a step input signal is applied.
- 9.15.6 A sensor gives a maximum analog output of 5 V. What word length is required for an analog-to-digital converter for a resolution of 10 mV?
- 9.15.7 Digital signals from a sensor are often polluted by noise typically of the order of 100 V or more. Explain how protection can be afforded for a following microprocessor.
- 9.15.8 A rotary variable differential transformer (RVDT) has a specification that includes the following information:  
 Ranges:  $\pm 30^\circ$ , linearity error  $\pm 0.5\%$  full range  
 $\pm 60^\circ$ , linearity error  $\pm 2.0\%$  full range  
 Sensitivity: 1.1 (mV/V input)/degree  
 Impedance: Primary 750  $\Omega$ , Secondary 2000  $\Omega$ .
- What will be the error in a reading of  $40^\circ$  due to non-linearity

- when the RVDT is used on the  $\pm 60^\circ$  range and the output voltage change that occurs per degree if there is an input voltage of 3 V?
- 9.15.9 It is desired to construct a dynamic compression force cell capable of measuring forces in the range of  $\pm 1000\text{ N}$ . If a quartz disc 1.0 mm thick and 10 mm in diameter is used as the sensing element, determine the force cell sensitivity (mV/N).
- 9.15.10 Describe the methods for decreasing the influences of electromagnetic radiation on a measurement system.

# 10 Actuators

---

Technical processes are usually influenced or manipulated by actuators, which affect certain input variables. In most cases, electrical, hydraulic or pneumatic auxiliary power is required. The actuator's input variables, the manipulated variables, can be adjusted by feedforward or feedback control or by an operator. Actuators therefore act on the matter or energy flow of the process by means of information processing and are an important link between the signal level of the automation device and the technical process, Figure 10.1.

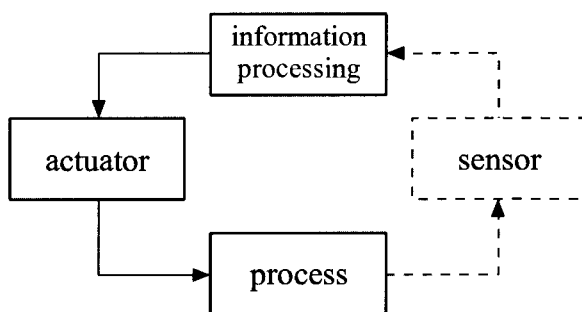


**Figure 10.1.** Actuator as connection between information processing and process

Actuators are applied in all fields of technology. Because of the manifold requirements, there exists a great variety of designs. This chapter deals with actuators for mechatronic systems. They normally have an electrical input and a mechanical output, e.g., way, velocity or force, and use different kinds of auxiliary energies from electrical, pneumatic or hydraulic supplies. After a description of the basic structure, an overview of different actuator principles will be given. Actuators with different

auxiliary energies will be presented and their properties and fields of application with regard to their selection will be compared. Mathematical models of electromagnets and electrical motors are already described in Chapter 5 and are not repeated here. However, detailed models will be derived for hydraulic and pneumatic actuators. After a comparison of the application areas of actuators, the design of fault-tolerant components as actuators and sensors is considered.

## 10.1 BASIC STRUCTURES OF ACTUATORS

Actuators usually transform low-power manipulated variables (e.g., analog voltages 0...10V, applied currents 0...20mA or 4...20mA) into process input variables of a much higher power level. In mechatronic systems, the process input variable is often a flow of energy or matter. The power needed for actuating is provided by an auxiliary energy supply, which feeds the power amplifier integrated in the actuator. The auxiliary energy can be electrical, pneumatic or hydraulic. Many actuators have one of the basic structures shown in Figure 10.2. In most cases, the manipulated variable  $U_i$  is an electrical variable that is transformed into a controlled variable  $U_1$  suitable for controlling the actuator drive by means of a *signal transformer*, Figure 10.2a. For an electrical actuator drive, this control variable could be another voltage or a voltage clock signal. For a pneumatic drive, it could be an air flow and for a hydraulic system an oil flow. The low-power-controlled variable  $U_1$  is used as an input into the subsequent *actuator servo-drive* and is amplified into a higher power output signal  $U_2$  by means of the auxiliary energy. For translational motions, the variable  $U_2$  can be a force, a displacement or a velocity, for rotational motions it can be a torque, a rotational angle or a rotational speed.

Consequently, using the terminology of Chapter 2, this servo-drive is an active transformer or an active converter. The actuator drive's output variable  $U_2$  often has to be transformed into a suitable range for the subsequent component. The corresponding element is called an *actuator transformer* with output variable  $U_3$ . It could be a lever transformer for displacements, a gear for angles and torques, or it can transform rotational motion into translational motion, like a spindle. Thus, a controlled actuator with an input variable  $U_i$  and an output variable  $U_3$  is created, Figure 10.2a.

The relation between  $U_i$  and  $U_3$  can be influenced by disturbances or by properties like friction, backlash, electromagnetic hysteresis or changes of the gain because of aging and wear. For this reason, the output variable  $U_3$  is sometimes *feedback-controlled* if actuators of higher precision are required, Figure 10.2b. This requires an additional sensor in the actuator, which measures displacements, velocities or forces. An analog or digital position controller  $R_1$  changes the manipulated variable  $U_i$  in such a way that the output variable  $U_3$  conforms with the new input variable, the

reference input variable  $U_{3r}$ . Hereby, it is possible to achieve a better static correspondence between  $U_{3r}$  and  $U_3$  and a better dynamic behavior.

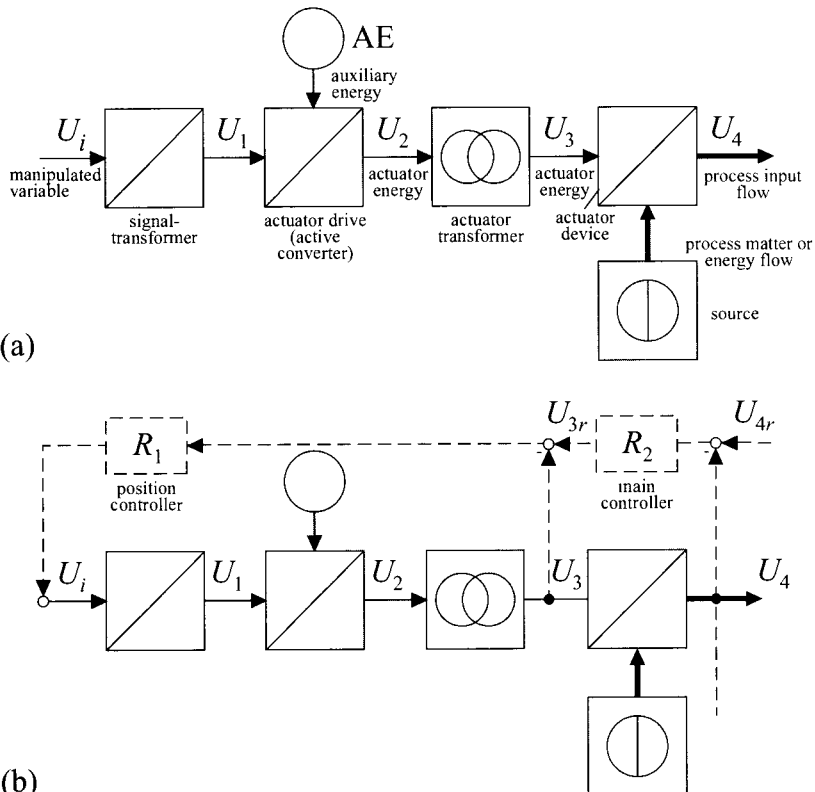


**Figure 10.2.** Basic structures of actuators: (a) open-loop-controlled actuator; (b) closed-loop-controlled actuator

In many cases, the variable that actsuates on the technical process is not the output variable  $U_3$  of the actuator drive but the matter or energy flow of a subsequent actuating device or valve, Figure 10.2a. This could be the air flow (throttle valve) or the fuel flow (injection valve) of a spark-ignition engine, the oil flow into a hydraulic work cylinder (main valve), the momentum flow (force) of the rudder of an airplane, the warm water flow of a heat exchanger (regulating valve) or the electrical current of an electrical motor (thyristor-current converter). The matter or energy flow provided by the actuating device lies in the power level of the process input and is usually significantly higher than the power level of the auxiliary energy. Therefore, the actuating mechanism is a second power amplifier and thus a second active element (transformer or transducer), so that the whole actuator (or the actuator system) contains at least two power amplifiers.

1. actuator: the manipulated variable controls the actuator power;
2. actuator device: the actuator power controls the power flow.

It is also possible to speak of a “primary actuator” and a “secondary actuator”. Between them, there might be an additional energy or power amplifier, called an *actuator transformer* or converter. Because of the disturbances and non-linearities in the actuating mechanism, the output variable  $U_4$  can be controlled by a second controller  $R_2$ . This actuator main controller (matter or energy flow controller) operates on the reference input of the position controller, which leads to a *cascade control system*, Figure 10.2b.

Hence, Figure 10.2 shows that actuators consist of a chain of energy or power amplifiers, Oppelt (1980, 1986), and that they can have several feedbacks. One can distinguish between the actuator drive, the mechanical actuator device and sensors, as shown in Figure 10.3, with an energy flow in the forward direction and an information flow in the backward direction. A comparison with Figure 1.1 shows that actuators are mechatronic systems themselves.

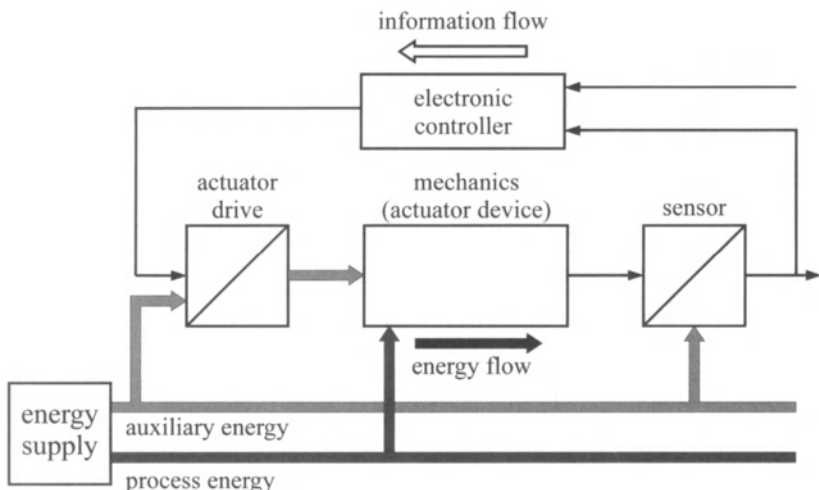


**Figure 10.3.** Electromechanical actuator as mechatronic system

In the following section, the technical implementations of actuators will be discussed. The descriptions will be limited to actuator drives and actuator devices with an electrical input, a mechanical output and powers up to about 5 kW.

## 10.2 GENERAL SURVEY OF ACTUATORS

To obtain a general view of the different types of actuator principles, this section will present the most important kinds of auxiliary energy and the basic transient responses, Raab (1990).

### 10.2.1 Types of Auxiliary Energy

Figure 10.4 schematically shows different kinds of auxiliary energies and force generation.

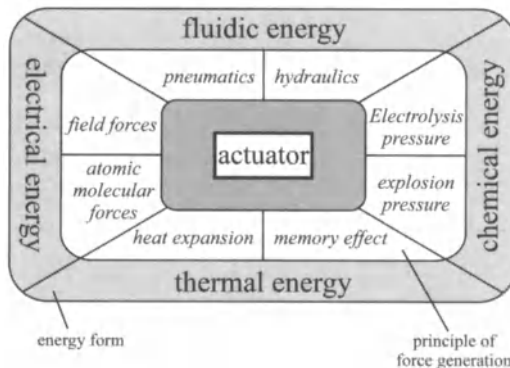


**Figure 10.4.** Auxiliary energies and forces to generate mechanical output variables

#### a) Electricity

In most cases, electrical energy already exists and is decentrally available. Its unproblematic generation and battery storage in combination with good conversion and transmission capability provides high flexibility. This is supported by an easy manipulation of energy flows with relatively low-priced semiconductor elements. The signal conversion and the actuator drive can be operated with the same kind of energy and maybe even with the same potential. Because of these advantages, the electrical auxiliary energy is usually given preference over other kinds of energy. Exceptions are made in the case of too-high actuating forces, high temperatures or for safety reasons.

#### b) Hydraulics

The oil flow of a hydraulic circuit usually has to be provided by an additional auxiliary energy supply. The operation pressures are relatively high (100 to 400 bar). The resulting advantages are high positioning forces and robust and compact actuator drives with a very high power-weight ratio.

#### c) Pneumatics

Pneumatic systems are realized both with vacuum (especially in automobiles) as well as with over-pressure relative to atmospheric pressure. The

supply pressures are limited to 6–8 bar, in the process automation to 1.4 bar, which leads to larger devices compared to hydraulics. Furthermore, careful air conditioning is indispensable. Nevertheless, pneumatics provide a series of advantages such as a robust design and a reliable and safe operation, especially in a warm and explosive environment.

Table 10.1 shows different properties and characteristics of actuators used in automobiles for the discussed types of auxiliary energies.

Depending on these three main auxiliary energies, the following actuator principles can be distinguished:

- electromechanical actuators;
- fluid energy actuators;
- unconventional actuators.

**Table 10.1.** Properties and characteristics of auxiliary energies for actuators in vehicles, Raab (1990)

auxiliary energy	potential	average rated power	power/weight ratio*	suitable for translational motion	suitable for rotational motion
		W	W/kg		
electricity battery generator	12–24 V 14–26 V	< 100 < 500	40–130	medium	good
hydraulics engine pressure hydr. system	1–5 bar 30–200 bar	< 100 > 1000	1000–2500	good	medium
pneumatics vacuum over pressure	0.1–0.8 bar 6–8 bar	< 100 > 1000	5–25 200–400	good	medium

\* without power supply

Figure 10.5 shows another classification into different realizations, Raab, Isermann (1990). Their characteristic properties and typical ranges of application will be described in the following subsections.

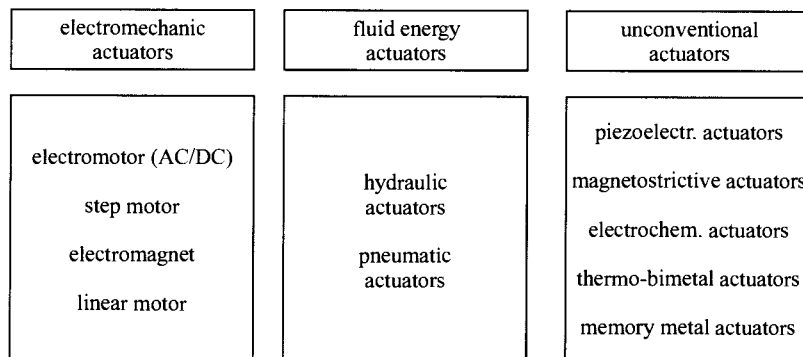


**Figure 10.5.** Classification of different actuator principles

### 10.2.2 Actuator Time Behavior and Control

The different actuator drives or complete actuators can also be distinguished by their transient behavior. If for a step increase of the controlled variable  $\Delta U_1$  the output variable  $\Delta U_2$  of the actuator drive, Figure 10.2a, changes proportionally to  $\Delta U_1$ , such that

$$\Delta U_2(t) = K_p \Delta U_1(t) \quad (10.2.1)$$

the transient behavior is called *proportional action* (Figure 10.6a). If the output variable changes with a constant rate

$$\frac{dU_2(t)}{dt} = K_I \Delta U_1(t) \text{ or } \Delta U_2(t) = K_I \int_0^t \Delta U_1(t') dt' \quad (10.2.2)$$

then the transient behavior is called *integral action*, Figure 10.6b. The static behavior of proportional action actuator drives is represented by characteristic curves. Figure 10.7a gives examples of unique linear and non-linear characteristics. An example of an ambiguous characteristic is the hysteresis, Figure 10.7b, which is generated by dry friction or backlash. If  $\Delta \dot{U}_2(t)$  is drawn above  $U_1(t)$ , one gets corresponding characteristics for integral action actuators.

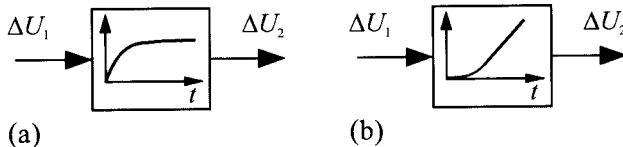


**Figure 10.6.** Transfer behavior of actuator drives: (a) proportional acting; (b) integral acting

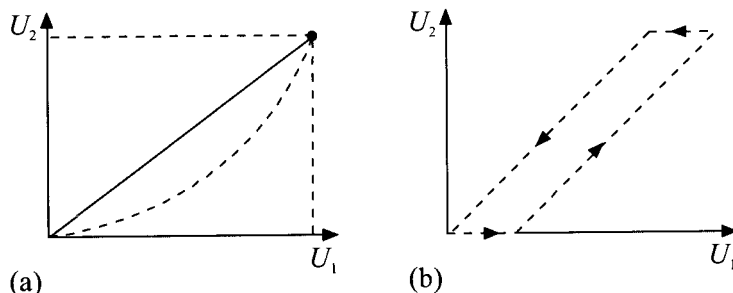


**Figure 10.7.** Static behavior of proportional acting actuator drives: (a) unique characteristics; (b) ambiguous characteristic (hysteresis)

Table 10.2 shows the typical static behavior of some actuator drives. In Figure 10.8, the block diagram of an actuator drive is shown, which is typical for several designs. The actuator force generation often follows a non-linear characteristic (e.g., electromagnetic, pneumatic or hydraulic cylinder) with a dynamic behavior of low order (often almost linear and

of first order). In this case, the positioning force acts on the mechanical converter (e.g., guide bar with bearing and return spring). This mechanical part includes a mass  $m$ , a return spring constant  $c$  and a viscous and dry friction. The dry friction leads to another non-linearity, which is ambiguous (hysteresis).

Therefore, high-quality actuator drives are supplied with a cascade control like in Figure 10.9, with an underlying force control (current control for electromagnets, differential pressure control for fluidic cylinders) and an overlying positioning control. The non-linear characteristic of the force generation can be compensated for by an inverse characteristic, resulting in an approximately linear behavior of the force control. Furthermore, the non-linear behavior of the mechanical converter for the positioning control can be cancelled by compensation of the dry friction. With these possibilities of a software-based influence, the negative properties of actuator drives can be significantly improved, see Isermann, Keller (1993) and Section 10.5.3.

**Table 10.2.** Static transfer behavior of some actuators

actuator principle	proportional acting			integral acting		
	characteristic			characteristic		
	unique		non-unique	unique		non-unique
	linear	non-linear	non-linear (hysteresis)	linear	nonlinear	non-linear (hysteresis)
electro-mechanical actuators	stepper motors		electro-magnets	DC motors	AC motors (with switch)	electrical drives with friction or backlash
fluidic actuators			pneumatic diaphragm with return spring		hydraulic actuators	pneumatic cylinders
unconventional actuators			piezoceramic actuator magnetostriuctive actuators memory metal actuators			

The actuator device following the actuator drive, Figure 10.2, which frequently manipulates a matter or energy flow and often has proportional behavior. The layout of the static characteristic of this actuator device depends on the static behavior of the subsequent process, such that the combined action of actuator and process defines a certain *overall operating characteristic*.

This operating characteristic should be approximately linear in closed-loop control, if this leads to stability with constant control parameters over

the whole operating range. If the process has a linear characteristic, then the characteristic of the actuator also has to be designed as linear. For a non-linear process characteristic, a linear operating characteristic can be achieved by a corresponding inverse non-linear actuator characteristic (e.g., for a flow valve). The adaptation to an operator sometimes makes non-linear actuator characteristics necessary, e.g., the non-linear drive characteristic for combustion engines in automobiles and the adjustment of stick-slip behavior in airplanes.

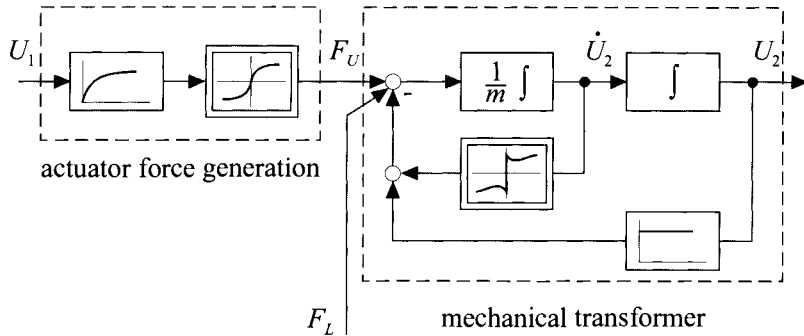


**Figure 10.8.** Block diagram of a proportional acting actuator drive with non-linear force generation (electrical, hydraulic, pneumatic) and mechanical transformer with viscous and dry friction for generating a speed and displacement:  $U_1$ : input of the actuator;  $U_2$ : output (displacement) of the actuator;  $F_U$ : actuation force;  $F_L$ : load force (from subsequent actuator device)

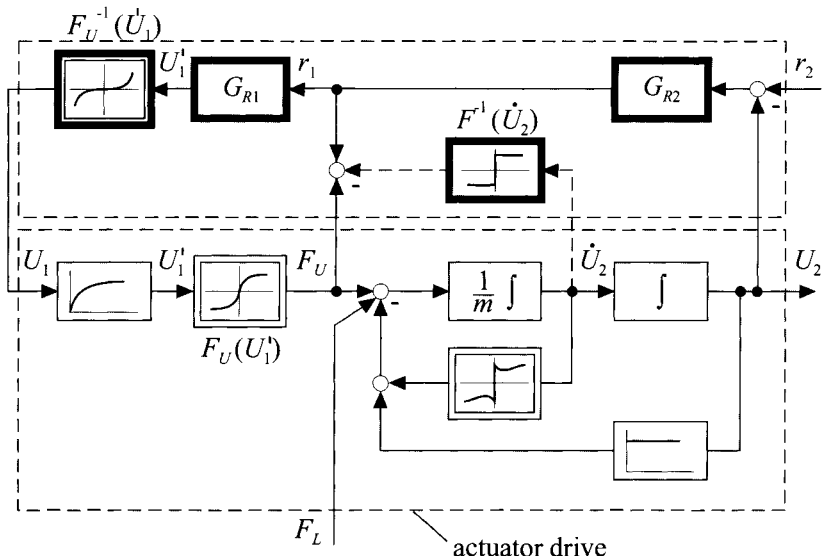


**Figure 10.9.** Block diagram of the cascade control of an actuator drive as Figure 10.8 with  $G_{R1}$ : force controller;  $G_{R2}$ : position controller;  $F_U^{-1}(U_1^*)$ : compensation of static non-linearity;  $F^{-1}(\dot{U}_2)$ : compensation of dry friction

### 10.2.3 Requirements for Actuators and Servo-drives

Unlike power-generating or power-consuming machines, the drives of actuators are not operated continuously but only for short periods of time, and have to be exact in positioning. Therefore, special drives were developed for this task, so-called *servo-drives*. They have to fulfil the following requirements:

- functioning in the four-quadrant operation (drive and brake in both directions);
- high overload capability;
- high resolution for exact positioning;
- good static transfer properties (as linear as possible, little friction, no backlash);
- fast, well-damped dynamic properties (little time constants, no overshoot);
- high range of longitudinal speed and rotational speed;
- high force generation or torque generation and little wear in standstill (breaking-off and holding);
- appropriate interfaces to the signal transformer of the manipulated variable.

## 10.3 ELECTROMECHANICAL ACTUATOR DRIVES

Electromechanical actuating units are widely used and are characterized by a large variety of different designs. The variety of types, especially of motor-driven actuators, permits a flexible customization for a wide range of applications, as can be seen in Table 10.3.

**Table 10.3.** General features of electromechanical (in particular electromotive) actuators

advantages	disadvantages
<ul style="list-style-type: none"> <li>• good response characteristics;</li> <li>• highly dynamic;</li> <li>• flexible drive concepts;</li> <li>• high overall efficiency;</li> <li>• condition can be monitored well.</li> </ul>	<ul style="list-style-type: none"> <li>• restricted power density;</li> <li>• energy consumption during static operation;</li> <li>• restricted thermal range of operation;</li> <li>• high percentage of moving mechanics.</li> </ul>

Electrical drives play a predominant role if small to medium actuating power must be provided. This fact can, in part, be attributed to the high availability of electric power and the number of ways to convert it. Additionally, electrical drives deliver a high degree of positioning accuracy and good dynamic performance. The high efficiency of the total system surpasses the efficiency of comparable pneumatic or hydraulic systems.

However, high dynamic requirements combined with a demand for higher actuating power impose limits on the applicability of electromechanical actuators. Demanding high actuating power results in large drives since the power density is physically limited by saturation effects of the magnetic materials.

Major disadvantages arise from the mechanical construction. If mounted directly onto other machines, electrical drives can be subject to severe strain due to shaking, which might necessitate extensive constructive countermeasures. High ambient temperatures can also affect the operation from effects such as degaussing or impairing the isolation of the windings. The utilization and lifespan of electromechanical systems is thus limited in the presence of high ambient temperatures or vibrational strain, Wetschirke, v. Willich (1986).

Electromechanical drives can primarily be divided into translatory (electromagnets, linear motors) and rotary (electrical motors) transformers. The latter will usually be used in conjunction with a gear or feeding mechanism (actuation transformer) in order to generate a different rotary or linear motion. In the following, the different types of actuator drives will be discussed in detail. Based on the general description of electrical motors as well as their mathematical models in Chapter 5, here only the special properties for actuator drives are outlined and compared.

### 10.3.1 Electrical Motors

A large number of the actuators employed in mechatronic systems are electrical motors. The general structure of the different classes of electrical motors along with their primary features has already been presented in Chapter 5. In contrast to the electrical drives used in power-generating or power-consuming machines, the electrical motors employed as actuators are running neither continuously nor in a preferred rotational direction. Actuators are used as positioning devices, which results in requirements different from those for prime movers. These different requirements include the capability to sustain larger electrical and mechanical overloads, high positioning accuracy, very good dynamic behavior and therefore a small moment of inertia, low-wear generation of a certain holding torque, and a large region of acceptable rotational velocities. The power output ranges from a few watts for sub-miniature motors up to several kilowatts.

Since, for most applications, different types of motors can be taken into consideration, a comparison of the different constructional principles will be presented in the following. The interested reader is also referred to the survey articles by Jung, Schneider (1984), Weck (1989), (1990), Henneberger (1989), von Bechen (1989), and Janocha (1992) among others.

With regard to their key features, electrical motors can be divided into self-commutated and externally commutated machines, compare Section 5.7. For the former, the windings will be energized as controlled by the angular position of the rotor, whereas for the latter, the windings will be

energized as determined by either the phase sequence of the feeding power supply system or an external control circuit.

### a) Self-commutated motors

Self-commutated motors with a mechanical commutator are characterized by two features. First, the torque-generating stator field is created by permanent magnets or by a field coil. Secondly, the torque-producing current in the rotor windings is supplied to the rotor via brushes and a commutator. These brushes and the commutator form a switch, which toggles the current in the armature windings such that the torque is always created under the most favorable conditions. Table 10.4 presents a survey of the most common commutator motors with a power output of up to 1 kW, see also Chapter 5.

#### *Mechanically commutated (brush) DC motors*

For permanently excited DC motors with mechanical commutation, the stator will consist of permanent magnets while the rotor is made up of a winding connected to a commutator. These motors typically have a voltage rating below 42 V and for battery-powered applications their use is widespread due to their high efficiency. These areas of application include road vehicles, household appliances, garden tools, medical and laboratory equipment as well as office equipment.

If the permanent magnets are replaced by a stator winding, the resulting motor will be an electrically excited DC motor. For series-wound motors, the stator winding and the armature winding are connected in series. The rotational velocity drops disproportionately to the load torque, but, on the other hand, the break-away torque can be two to six times larger than the nominal torque. Since series-wound motors can also be supplied with alternating current, they are also referred to as *universal motors*. However, their efficiency is higher if they are fed with direct current.

For shunt-wound motors, the field coil and the armature coil are connected in parallel, which causes the rotational velocity-torque relation to be as stiff and as linear as that of the permanent-magnet excited machines. Shunt motors can only be fed with direct current. Operation with an AC supply is only possible if the voltage is rectified prior to being supplied to the motor.

Compound motors consist of both a shunt winding and a series winding, thereby combining the advantages of both types of winding, namely the high break-away torque and the stiff rotational velocity behavior. These motors can only be supplied with direct current and are quite expensive due to the elaborate stator winding.

Table 10.4. Survey of self-commutated motors with power ratings up to 1 kW

type of power supply	DC					AC (single phase)	
	brushless DC motor	permanent magnet motor	shunt-wound motor	compound motor	series-wound motor	universal motor	repulsion motor
type of motor	electronically	mechanically	mechanically	mechanically	mechanically	mechanically	mechanically
type of commutation	basic circuit diagram	rotational speed versus torque	rotational speed versus torque	rotational speed versus torque	rotational speed versus torque	rotational speed versus torque	rotational speed versus torque
nominal speed	rpm	< 60000	< 30000	< 12000	< 6000	< 15000	< 30000
power rating	W	1–1100	0.001–1000	0.2–1000	20–1000	8–1100	5–1000
voltage rating	V	< 400	< 250	< 600	< 220	< 600	< 220
efficiency	$\eta$	0.4–0.7	0.4–0.8	0.3–0.7	0.3–0.7	0.3–0.7	0.3–0.6
max. torque/ rated torque		< 10	< 6	< 6	< 5	< 5	< 2.5
speed control	electronically	series resistor or third brush			resistor in parallel with armature winding series resistor phase control	pulse width modulation	'variation of brush angle $\alpha$
legend		■ permanent magnet stator ● permanent magnet rotor ➤ rotor with cage or commutator winding			○ reluctance rotor ○ hysteresis rotor ➤ transistor		

The key features of mechanically commutated DC motors are summarized in Table 10.5. The main disadvantages compared to other types of electrical drives emanate from the primary structure. The heat developing in the armature windings cannot be carried off well. Therefore, thermal aspects must be considered even if the motor is in overload for only a short amount of time. Furthermore, the mechanical commutation also limits the maximum motor current during standstill (“burn through”) as well as at high rotational velocities (“brushfire”). Since the coal brushes wear out over time, low-cost drives require a certain amount of maintenance work.

**Table 10.5.** Characteristics of mechanically commutated DC motors

advantages	disadvantages
<ul style="list-style-type: none"> <li>• good response characteristics;</li> <li>• small volume and weight;</li> <li>• good dynamic behavior;</li> <li>• very high degree of synchronism;</li> <li>• large speed range.</li> </ul>	<ul style="list-style-type: none"> <li>• wear of commutator and brushes (- short lifetime → maintenance);</li> <li>• dynamics and standstill torque are restricted by commutator;</li> <li>• bad heat discharge.</li> </ul>
Scope of application: <ul style="list-style-type: none"> <li>• small to medium actuating torque/force;</li> <li>• precise positioning tasks;</li> <li>• standard applications (areas of application include auxiliary drives for road vehicles, laboratory equipment, office equipment).</li> </ul>	

#### *Mechanically commutated (brush) AC motors*

In contrast to the repulsion motor, whose use is hampered by both the complicated speed control (by means of a variation of the angular position of the brush) and the limited speed range, the universal motor plays an important role as an electrical drive. Due to the high maximum rotational velocity, these motors can be designed such that they offer a good power–weight ratio. The speed control for universal motors is less complicated and allows for a wider range of rotational velocities than any other type of electrical motor. This makes the universal motor the predominant choice for household appliances and machines tools, Table 10.6.

**Table 10.6.** Characteristics of mechanically commutated AC motors

advantages	disadvantages
<ul style="list-style-type: none"> <li>• good response characteristics;</li> <li>• very high power–weight ratio;</li> <li>• large speed range;</li> <li>• high maximum speed.</li> </ul>	<ul style="list-style-type: none"> <li>• wear of commutator and brushes (- short lifetime → maintenance);</li> <li>• bad heat discharge.</li> </ul>
Scope of application: <ul style="list-style-type: none"> <li>• small to medium actuating torque/force;</li> <li>• standard applications (areas of application include household appliances and machine tool drives).</li> </ul>	

### *Electronically commutated (brushless) motor*

Until a few years ago, mainly mechanically commutated DC motors were chosen as highly dynamic servo-drives. In the range of small to medium actuating powers, they are increasingly being replaced by electronically commutated brushless DC motors. These consist of a permanent magnet rotor, multiple stator windings and an electronic control circuit, which cyclically energizes the stator windings depending on the angular position of the rotor. This working principle makes these motors as robust and as quiet-running as asynchronous drives. Further advantages are the maintenance-free operation and the higher overload capacity due to the absence of a mechanical commutator, Table 10.7.

**Table 10.7.** Characteristics of electronically commutated DC motors

advantages	disadvantages
<ul style="list-style-type: none"> <li>• as robust and as quiet-running as asynchronous drives;</li> <li>• good response characteristics due to linear current-torque relation;</li> <li>• high overload capacity;</li> <li>• maintenance-free;</li> <li>• smaller moment of inertia and better power-weight ratio than mechanically commutated DC motors.</li> </ul>	<ul style="list-style-type: none"> <li>• sensor system and complex control circuitry;</li> <li>• higher cost of system than for normal DC drive;</li> <li>• typically: restricted degree of synchronism (torque ripple).</li> </ul>

Scope of application:

- small to medium actuating torque/force;
- high-value applications.

The big advantage of brushless motors is that the heat, solely originating in the stator windings, can be carried off well. This also results in a better performance-to-weight ratio compared to the corresponding traditionally commutated drives. On the other hand, these beneficial effects are at the expense of both more complex control circuitry and a more comprehensive sensor system. Moreover, the rotor speed and generated torque exhibit ripples, an effect that could be reduced by employing modern control concepts such as a sinusoidal current control, Wilke (1988). Due to these ripples, the degree of synchronism is limited, a problem that is especially severe at low rotational velocities.

### *Servo-motors*

The lower end of the power range of servo-motors allows for the use of servo-motors as small actuators. These servo-motors are used for positioning tasks with a specified time-frame and accuracy. Quite often, several motors have to operate with a high degree of synchronism. These requirements are typical for machine tool drives, robots and flap- and valve-drives. Thus, restrictive requirements are imposed on the dynamics, positioning accuracy, maximum torque, degree of synchronism, and efficiency to name a few (see Section 10.2.3). In the lower power range, electrical servo-drives have prevailed against hydraulic and pneumatic actuators. The reasons have been listed in Table 10.8.

**Table 10.8.** Comparison of hydraulic and electrical servo-drives

hydraulic servo-drives	electrical servo-drives
<ul style="list-style-type: none"> <li>• higher energy density;</li> <li>• lower power-weight ratio;</li> <li>• smaller installation space;</li> <li>• faster acceleration;</li> <li>• lower cost;</li> <li>• simple generation of a linear motion (cylinders);</li> <li>• very robust.</li> </ul>	<ul style="list-style-type: none"> <li>• better control behavior;</li> <li>• better accuracy;</li> <li>• higher efficiency;</li> <li>• simple diagnosis and maintenance;</li> <li>• matching to different applications quite simple;</li> <li>• electrical energy used for sensors, controller and actuator.</li> </ul>

### b) Externally commutated asynchronous drives

Asynchronous drives are employed for household appliances, garden tools, laboratory and medical equipment, and machine tool drives among other areas of application. A survey of commonly used asynchronous drives for small power output is shown in Table 10.9. The *three-phase asynchronous drive* exhibits the most favorable power-weight ratio of all asynchronous drives. This is exploited for drives for portable tools, where the motor is supplied with alternating current of a frequency of between 200 and 300 Hz. Here, rotational velocities between 12000 and 18000 rpm can be reached. This speed range is comparable to that of universal motors. It is possible to connect a three-phase asynchronous machine to a single-phase power supply system. In this case, two terminals are connected directly to the power supply system, whereas the third is connected to a capacitor which in turn is connected to the power supply system. This design is called a *three-phase capacitor motor*.

However, two windings are sufficient to generate a rotary field, provided they carry phase-shifted currents. This phase shift is generated with the help of a capacitor (*two-phase capacitor motor*), by increasing the ohmic resistance of one winding (*resistance-start AC induction motor*) or by shortening one of the windings. In the last case, an induced current will flow in the shortened winding (*shaded-pole motor*). *Resistance-start AC induction motors* are even more robust than capacitor motors and are typically used when the motor is switched on and off frequently (e.g., cooling units). *Shaded-pole motors* are very cheap to build, but have a very bad efficiency and are solely used for very simple appliances.

### c) Externally commutated synchronous motors

For synchronous motors, the stator field is generated the same way as for asynchronous motors. For the latter, the rotor always has a smaller rotational velocity than the rotary field. On the other hand, for synchronous motors, the rotor is turning at the synchronous speed of the rotating field. Due to this characteristic, synchronous motors are predominantly used as drives for high-precision speed control. Because of their simple design, they are also used in household appliances.

**Table 10.9.** Survey of externally commutated asynchronous motors with small power range

type of power supply	three-phase		single-phase		resistance-start AC induction motor	shaded-pole motor	Ferraris motor
	brushless DC motor	capacity motor $C_A$ = starting capacitor $C_B$ = running capacitor	2	2			
number of phases in the motor	3	3	2	2			
basic circuit diagram							
rotational speed versus torque							
nominal speed rpm	< 6000		< 3600			3000–30000	< 3000
power rating W	0.06–1100		0.2–1100			5–1000	< 500
voltage rating V	12–800		0.2–500				
efficiency $\eta$	0.5–0.8	0.3–0.7	0.4–0.7	0.4–0.7	0.3–0.7	0.05–0.4	0.2–0.5
break-away torque / rated torque	1–3	1–2	$C_A$ : 2–4 $C_B$ : 1–2	2–4	0.2–1	0.2–1	< 2
max. torque / rated torque	1.5–7	< 1.50	< 1.56	< 1.5	< 1.5	< 1.2	< 1.2
speed control		reduced stator voltage change of number of poles	reduced stator voltage change of number of poles	tapped winding	choke coil	change of control voltage $V_S$	
legend		■ permanent magnet stator permanent magnet rotor rotor with cage or commutator winding	○ reluctance rotor ○ hysteresis rotor ✖ transistor				

Synchronous motors can be constructed with two or three independent coils. If connected to a single-phase power supply system, capacitors or resistors can be used to generate a phase-shifted current, see Table 10.10. These are the same working principles that are also used for single-phase asynchronous motors.

**Table 10.10.** Survey of externally commutated synchronous motors

type of power supply	three-phase alternating current	single-phase alternating current
type of motor	permanent magnet motor	reluctance motor
number of phases in the motor	3	3
basic circuit diagram		
rotational speed versus torque		
nominal speed	< 33000 rpm	< 6600 rpm
power rating	W	1-1100 W
voltage rating	V	1-800 V
efficiency	$\eta$	0.3-0.6
break-away torque / rated torque		< 0.05-0.6
max. torque / rated torque	< 1.5	< 1.3
speed control	change of number of poles	choke coil
legend	 permanent magnet stator  permanent magnet rotor  rotor with cage or commutator winding  transistor	 reluctance rotor  hysteresis rotor

Typical for synchronous motors is their run-up behavior. Permanently excited synchronous motors can only be run up by gradually increasing the frequency until the nominal frequency has been reached or by means of a pole-changed winding. In contrast to this, the hysteresis motor runs up autonomously. The magnetization of the hysteretic material is constantly reversed, thereby softly accelerating the rotor. For the reluctance motor, the magnetic resistance of the rotor (reluctance) changes along the circumference of the rotor according to the pole number. Table 10.11 lists some of the typical advantages and disadvantages of externally excited synchronous motors.

**Table 10.11.** Characteristics of synchronous motors

advantages	disadvantages
<ul style="list-style-type: none"> <li>• cost-effective drive concept;</li> <li>• maintenance-free;</li> <li>• speed is in proportion to the power supply system's frequency.</li> </ul>	<ul style="list-style-type: none"> <li>• run-up issues;</li> <li>• stall under overload;</li> <li>• susceptible to oscillation build-up under load changes.</li> </ul>
Scope of application:	<ul style="list-style-type: none"> <li>• mostly small actuating torque/force;</li> <li>• standard tasks (e.g., household appliances);</li> <li>• control engineering.</li> </ul>

Many positioning tasks demand stepwise rotating motors instead of continuously turning motors. For small actuating power (< 500 W) *stepper motors* represent a cost-effective alternative compared with electronically commutated DC motors. Stepper motors also commutate electronically, but with a constant frequency determined by the external control logic. Stepper motors are thus synchronous motors and exhibit all their characteristic features.

There exists a vast number of stepper motor types, which in conjunction with the integration of control circuitry allows for an easy design of controlled positioning devices, see Section 5.3.7 and, e.g., Traeger (1979), Kreuth (1988). The feedforward-controlled stepper motor is limited in its application as a positioning drive, since reliable operation necessitates good knowledge about the applied load. The assumption that load variations, break-away forces and vibrations do not cause stepping errors can only be justified up to certain maximum loads. To account for this, stepper motors are most of the times overrated. If stepping errors cannot be accepted, the motor must be controlled in closed-loop, Gfröer (1988). However, this annuls the principal advantages over other types of motors. It must also be pointed out that the efficiency of stepper motors is lower and that they are not capable of withstanding large overload. Also, the stepper motor must constantly be supplied with the maximum current, which means that the power consumption is unnecessarily high, Höfer (1991). However, the stepper motor offers a very high degree of reliability for a known load and maintenance-free operation and Table 10.12 shows some specifications for stepper motors. Table 10.13 summarizes the key aspects of stepper motors.

**Table 10.12.** Some characteristic values of stepper motors and linear motors

type of motor		stepper motor			linear motor / electrical cylinder				
current type		DC	AC, single phase	AC, three phase	DC	AC, single phase	AC, three phase		
holding torque	Nm	0.001–30	0.2–7	0.015–5	---	---	---		
nominal torque	Nm	0.003–20	0.2–7	0.23–28	---	---	---		
stepping angle	°	0.003–400	0.03–2	0.03–120	---	---	---		
stepping frequency	Hz	0–250000	0–250000	0–400000	---	---	---		
supply voltage	V	1–310	0–310	3–310	12–750				
efficiency									
power rating	W	< 500			up to 10000				
maximum stroke	mm	---	---	---	< 5000	linear motor: < 20000 electrical cylinder: < 5000			
maximum force	kN	---	---	---	linear motor: < 1000 electrical cylinder: < 600				
lifting speed	mm/s	---	---	---	linear motor: < 20000 electrical cylinder: < 2000				

**Table 10.13.** Characteristics of stepper motors

advantages	disadvantages
<ul style="list-style-type: none"> <li>direct digital control via integrated control circuitry and drives;</li> <li>maintenance free;</li> <li>cost-effective drive concept;</li> <li>feedforward-controlled operation.</li> </ul>	<ul style="list-style-type: none"> <li>load range must be known → overrating necessary;</li> <li>rather small power density;</li> <li>danger of stepping errors on feedforward-controlled operation;</li> <li>comparatively small actuating dynamics.</li> </ul>
Scope of application:	<ul style="list-style-type: none"> <li>small actuating torque/force;</li> <li>simple positioning task provided load is known.</li> </ul>

### *Subsequent mechanical converters (matching gears)*

Electrical motors are primarily generating a rotary motion, which in general will not match the rotational velocity and torque requirements of the downstream actuator devices. In many cases, the motion must also be converted into linear motion. These demands can be satisfied by matching gears, which can perform the desired conversion. The use of these gears will also alter the system characteristics significantly. Details of these implications are pointed out in Table 10.14.

Among the gears employed in mechatronic systems, *gear drives* or *transmissions*, Tables 4.1 and 4.2, play a predominant role. Due to the form-locked force transmission, they are predestined for large power/large torque applications. Gear drives are built as gears with fixed ratio or step-

wise variable ratio. They can also be combined with continuously changeable gearboxes.

**Table 10.14.** Characteristics of mechanical matching gears

advantages	disadvantages
<ul style="list-style-type: none"> <li>• match rotary motion to load and rotational velocity requirements;</li> <li>• mediate generation of linear motion;</li> <li>• self-locking gears reduce the power consumption during holding phases;</li> <li>• expands connection possibilities.</li> </ul>	<ul style="list-style-type: none"> <li>• time-invariant friction and gear play (backlash);</li> <li>• increased total moment of inertia;</li> <li>• power loss in gear necessitates stronger drive and reduced overall efficiency;</li> <li>• increases overall size.</li> </ul>

The most simple design of a gear drive is the *spur gear*. This gear type is characterized by the teeth, which are perpendicular to the face of the gear. The two meshed gears are termed gear and pinion. The shafts are supported by friction bearings or rolling bearings. A V drive, that is, a gear where the driving shaft and the driven shaft intersect, is typically realized as a *bevel gear* or *worm gear*. The latter have a higher share of viscous friction than spur gears or bevel gears. Due to this, they are quiet-running, but they also operate at a lower efficiency and will thus heat up more extensively for the same power throughput. One important property of worm gears is the irreversibility. When a worm gear is driven, the meshing spur gear will turn, but turning the spur gear will not turn the worm gear. Thus, the resulting gear is self-locking.

A special form of the spur gear is the *planetary gear*, which offers one additional degree of freedom. It is in general constructed such that a central sun gear is surrounded by a number of planetary gears, see Table 4.1. These are mounted on a plate, the planet carrier. This carrier has the same center of rotation as the sun gear. All the planetary gears also engage the inside of the ring. The ring also has the same center of rotation as the sun and the planet carrier. The input and the output of this gear can be chosen arbitrarily, thus different gear ratios can be realized with the same gear.

If a very high gear ratio must be realized with few gearbox stages, a special and quite expensive design, the *harmonic drive*, comes into play. In general, these gears consist of an internal gear and an eccentrically positioned gear. This gear can rotate freely and is mounted on an eccentric carrier, which itself is mounted coaxially with the internal gear. Despite the high gear ratio, which is determined by the difference in teeth of the two gear wheels, harmonic drives are compactly built and have a coaxial arrangement of the driving and the driven shafts. The rotational motion of the driven shaft is homogenous.

One application that is quite common is the conversion of rotary into translatory motion. This task is accomplished by *straight gears*, which include *rack and pinion gears*, *toothed belt drives* and the *recirculating ball spindle*.

*Transmission belts* are used if a certain distance between the driving shaft and the driven shaft must be bridged. They can also be used to drive

multiple shafts in the same or even in the opposite sense of rotation (e.g., the internal combustion engine). They outperform gear drives with their simple and thus cheap design and only a little amount of maintenance is required.

*Hydraulic transmissions* can be divided into *hydrostatic* and *hydrodynamic transmissions*. The former are arbitrarily changeable in their gear ratio, whereas for the latter, the gear ratio will usually depend on the load and torque. Hydrostatic transmissions are composed of a pump P, a hydraulic motor M, and some sort of control unit, see Table 10.22. This transmission system can be controlled by either manipulating the geometry of the pump or of the motor (primary or secondary control) or by controlling both. Compared to continuously changeable mechanical gears, they have a lower efficiency, but offer tremendous overload capacities and a high power density.

Hydrodynamic transmissions are based on the Föttinger principle. In contrast to the original design, they nowadays consist of an additional reactor that can support part of the torque delivered, thereby allowing adjustment of the torque transmitted through the unit. Different geometries of the impeller I, reactor R and turbine T allow the overall behavior adjustment of the hydrostatic transmission, see Table 4.2.

### 10.3.2 Electromagnets

Electromagnets are electrical–magnetic–mechanical converters. They convert electrical energy into mechanical energy via the intermediate form of magnetic energy. They are paramountly used for the generation of limited, alternating and latching, translatory or rotary motion. The latching positions correspond to the stable positions, the magnet settles in if the coil is energized and switched off. Because of the energy conversion principle of electromagnets, the reluctance principle, it is characteristic for electromagnets that the magnet armature can only be displaced in one direction (active direction of motion). An external force (e.g., spring load) must be used to return the magnet armature to its initial position if the magnet is switched off, see Chapter 5.

Because of their operating principle, electromagnets are directly acting actuators, which means that there is no mechanical converter or transmission element. This also requires that the electromagnet's specifications are matched to each particular application. The best adaptation can be accomplished if the electromagnet and the actuated element form one functional unit (e.g., magnetic valves, relay, magnetic clutch). Hereby, elements arise that offer superior characteristics (smaller unit volume, faster switching times, longer lifespan) and at the same time allow for cost savings. The vast majority of electromagnets that are produced today are specialized designs. A classification scheme for electromagnets is suggested in Table 10.15. For this scheme, the electromagnet has been considered both as a separate unit and as part of a functional group.

**Table 10.15.** Classification criteria for electromagnets, Kallenbach *et al.* (1994)

function	actuating magnets (operating magnets)	lifting magnet pull-type electromagnet rotary magnet valve magnets: – switching valve magnets – proportional valve magnets
	holding magnets (armature-free magnets)	clamping magnet lifting magnet magnetic separator
	force transmission magnets	electromagnetic clutch electromagnetic brake
iron	basic shape	pot shape (axially symmetric) U-shape E-shape
	assembly	solid laminated sintered
type of excitation	mode of operation power-on time	AC DC DC with permanent pre-magnetization
field coil	shape	cylindrical coil rectangular coil shaped coil
	assembly	wire-wound coil: – orthocyclical-wound – random-wound thin film coil
	number of coils	single coil multiple coils
magnet gap	position of magnet gap	within coil outside coil
	number of gaps	one magnet gap multiple magnet gaps
	size	short stroke magnet medium stroke magnet long stroke magnet
type of motion	translatory	pull-type push-type alternating
	rotary	single-acting double-acting double-acting with center position

Further adaption possibilities arise from the application of electronic driver circuits, by which the static and dynamic behavior of electromagnets can be influenced to a high degree. These circuits allow for the adjustment of the non-linear magnetic-force curve, Raab (1993), compensation of friction, Maron (1990), and fast positioning even under the demand for relatively large actuation forces, all by means of optimal control strategies, see Section 5.2.

## 10.4 HYDRAULIC ACTUATORS

The next two sections discuss hydraulic and pneumatic actuators, which both belong to the class of *fluidic actuators*. They are characterized by their rugged design and their high power-to-weight ratio. In addition, they also offer the opportunity to generate linear motion easily and directly by employing hydraulic cylinders and diaphragm drives. Further, fluidic actuators can be designed such that they only dissipate energy during dynamic operation. Thus, during static phases, high reaction forces can be generated with little energy consumption. The ongoing fusion of fluidic and (micro-)electronic components (“*fluidtronics*”) allows the design of actuators that offer both precise positioning and fast dynamics, Backé (1992), Anders (1986).

Besides these advantages, there are also some drawbacks. The efficiency of the overall systems is below that of electrical drives and the required auxiliary energy may not be available. Furthermore, the maximum positioning accuracy is limited to some 10 µm. The major advantages and disadvantages are summarized in Table 10.16.

**Table 10.16.** Characteristics of fluidic actuators

advantages	disadvantages
<ul style="list-style-type: none"> <li>• high actuating force;</li> <li>• large displacement;</li> <li>• high power density;</li> <li>• direct generation of linear motion;</li> <li>• no power consumption during standstill;</li> <li>• rugged design.</li> </ul>	<ul style="list-style-type: none"> <li>• (additional) auxiliary power unit necessary;</li> <li>• requires complex system structure;</li> <li>• partly expensive servo-components (e.g., valves)</li> <li>• limited positioning accuracy;</li> <li>• noise.</li> </ul>

Table 10.17 shows a classification of fluidic actuators. Mainly, they can be divided into two groups. The first comprises the pneumatic actuators and is further divided into pressure actuators and vacuum actuators. The second group contains the hydraulic actuators with the typical translational and rotary drives.

**Table 10.17.** Overview of important fluidic actuators (standard: translatory motion, italic: rotary, angular motion)

force generation	energy conversion	implementation
pneumatic	pressure actuator	cylinder diaphragm drive
	vacuum actuator	<i>air motor</i> diaphragm drive
hydraulic	pressure actuator	cylinder <i>hydraulic motor</i>

### 10.4.1 Hydraulic Actuation Systems

Hydraulic actuators are usually applied to very large actuation forces and actuation power respectively. However, they require a special hydraulic power supply. Therefore, they are an interesting option if several servo-axes for medium actuation forces can be replaced simultaneously. Hydraulic actuators outperform comparable electrical drives with respect to their system dynamics. The fact that the moving mass of hydraulic actuators is rather small despite the large actuation power facilitates dynamically fast positioning. Hydraulic actuators surpass pneumatic actuators in their high stiffness and shock resistance. The major advantages and disadvantages of hydraulic actuators are listed in Table 10.18.

**Table 10.18.** Characteristics of hydraulic actuators

advantages	disadvantages
<ul style="list-style-type: none"> <li>• small dimensions;</li> <li>• fast dynamics and high power density;</li> <li>• high stiffness;</li> <li>• high working capacity.</li> </ul>	<ul style="list-style-type: none"> <li>• possibly high system cost;</li> <li>• two line system;</li> <li>• possibly oil conditioning necessary;</li> <li>• friction and complex dynamics exacerbate control.</li> </ul>
scope of application:	<ul style="list-style-type: none"> <li>• medium to high actuating force;</li> <li>• medium to high displacement range;</li> <li>• limited space available;</li> <li>• highly dynamic systems.</li> </ul>

The dynamic behavior of hydraulic control circuits is, above all, characterized by the weak damping, which is furthermore dependent on both the piston displacement and the external load. Nevertheless, in conjunction with modern control concepts, one can design servo-hydraulic actuators that offer both good positioning accuracy and good dynamic behavior, Saffee (1986), Scheffel (1989), Glotzbach (1996).

Figure 10.10 shows a typical hydraulic actuator for linear motion. The hydraulic power supply consists of an oil tank and an electrically-driven piston pump connected to a proportional acting electro-hydraulic servo-valve. Depending on the position of the servo-valve, the cylinder moves with the corresponding direction and speed. The connection pipe between the pump and the servo-valve usually contains a directional (non-return) valve, avoiding back-flow of the oil, a pressure relief valve as a safeguard against excessive pressures, and a hydraulic accumulator to dampen pressure oscillations from the pump.

The next section will describe the principles and modeling of these hydraulic components. At the end of this section, a hydraulic servo-axis will be considered in detail.

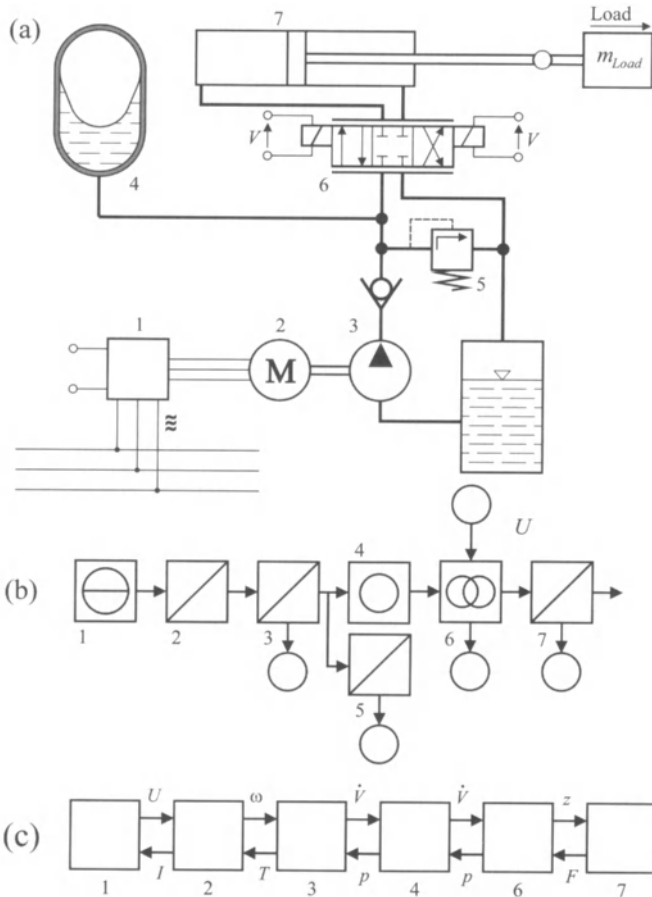


**Figure 10.10.** Hydraulic actuator for linear motion with power supply: (a) schematic; (b) energy flow scheme; (c) two-port representation. 1 power electronics; 2 AC motor; 3 radial piston pump; 4 accumulator; 5 check valve; 6 proportional valve; 7 cylinder

### 10.4.2 Hydraulic Components and their Models

For modeling of hydraulic components, a short summary of fluid dynamic principles is presented. Then, some material properties of the hydraulic fluid will be discussed. Next, hydraulic components will be considered. These include solenoid valves, as well as locking valves, throttle valves and check valves. Further on, hydraulic transmission lines, accumulators and motors are considered.

#### a) Some fluid dynamic properties

Hydraulic systems use fluids to transmit power between different components. In this section, some laws are considered for hydraulic power systems in the one-dimensional form.

The *mass balance* of a fluid mass  $m_s = \rho V_s$  becomes, according to (2.3.4)

$$\frac{\partial}{\partial t} m_s(t) = \frac{\partial}{\partial t} [V_s(t) \rho(t)] = \frac{\partial V_s(t)}{\partial t} \rho(t) + \frac{\partial \rho(t)}{\partial t} V_s(t) = \sum_i \rho_i \dot{V}_i(t) \quad (10.4.1)$$

where  $\dot{V}_i(t)$  are the inward volume flows across the volume surface. If the density can be assumed to be constant, the mass balance reads

$$\frac{\partial V_s(t)}{\partial t} = - \sum_i \dot{V}_i(t) \quad (10.4.2)$$

and if the volume is constant, it holds that

$$\frac{\partial \rho(t)}{\partial t} V_s = - \sum_i \rho_i \dot{V}_i(t) \quad (10.4.3)$$

Applying the momentum theorem to a fluid element of length  $dz$ , constant cross-sectional area  $A_F$ , density  $\rho(z,t)$  and friction force  $F_f(z,t)$  leads to

$$F_1(t) + g \rho dz \sin \alpha - dF_f = F_2(t) = \frac{d}{dt} (A_F \rho v_z dz) \quad (10.4.4)$$

See Figure 10.11.

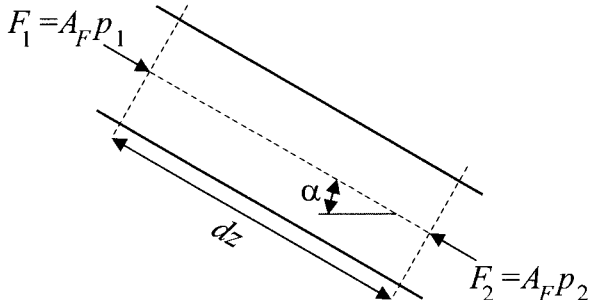


**Figure 10.11.** Fluid element in a tube

Using the pressure, this equation becomes

$$\begin{aligned} p_1(t) + g \rho dz \sin \alpha - \frac{1}{A_F} dF_f & \left( p_1(t) + \frac{\partial p}{\partial z} dz \right) = \frac{d}{dt} (\rho v_z dz) \\ - \frac{\partial p}{\partial z} + \rho g \sin \alpha - \frac{1}{A_F} \frac{\partial F_f}{\partial z} & = v_z \left( \frac{\partial \rho}{\partial t} + v_z \frac{\partial \rho}{\partial z} \right) + \rho \left( \frac{\partial v_z}{\partial t} + v_z \frac{\partial v_z}{\partial z} \right) \\ & = \frac{D(\rho v_z)}{Dt} \end{aligned} \quad (10.4.5)$$

For laminar flow, this is known as the *Navier-Stokes equation*. This equation can be simplified for an ideal fluid with  $\rho = \text{const.}$  and  $\alpha = 0$

$$\frac{Dv(z,t)}{Dt} = \frac{\partial v}{\partial t} + v \frac{\partial v}{\partial z} = - \frac{1}{\rho} \frac{\partial p}{\partial z} \quad (10.4.6)$$

which is known as the *Euler differential equation*.

Now, a prismatic fluid column of length  $l$  is considered and lumped parameters are assumed (like a rigid body). Then, it follows that

$$\rho l \frac{dv(t)}{dt} = -\Delta p(t) = -(p_1(t) - p_2(t)) \quad (10.4.7)$$

If the flow is stationary and the fluid incompressible, see Figure 10.12, integration of (10.4.6) leads to Bernoulli's equation

$$\left( p_1 + \frac{\rho v_1^2}{2} \right) - \left( p_2 + \frac{\rho v_2^2}{2} \right) = \Delta p_{Loss} \quad (10.4.8)$$

where  $\Delta p_{Loss}$  denotes the pressure loss due to friction effects.

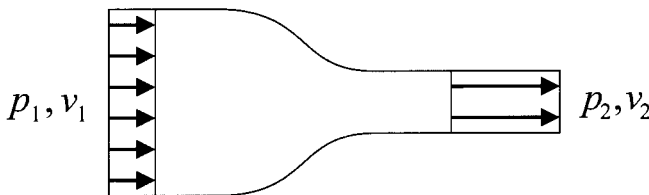


**Figure 10.12.** Fluid with changing tube area (contraction)

With regard to the friction in the pipe, two different types of flow can be distinguished, laminar and turbulent flow, see also Section 2.3.

*Laminar flow* is characterized by an orderly movement of the individual fluid layers, which slide on one another. Laminar flow losses can be described by the linear relationship

$$\Delta p = \frac{1}{G} \dot{V} = f \dot{V} \quad (10.4.9)$$

compare (2.3.62).  $G$  is termed the hydraulic conductance and  $f$  the friction factor. For a pipe with a circular cross-section,  $G$  evaluates to

$$G = \frac{\pi D^4}{128 \nu \rho l} \quad (10.4.10)$$

which can be derived from the circular Poiseuille flow. In this equation,  $l$  denotes the length of the pipe with diameter  $D$ . For a rectangular cross-section, the hydraulic conductance is given by

$$G = \frac{b h^3}{10 \rho v l} \left[ 1 - \frac{192 h}{\pi^5 b} \tanh \frac{\pi b}{2 h} \right] \quad (10.4.11)$$

where  $b$  and  $h$  describe the geometry of the rectangle. Other hydraulic conductances can be found in Merritt (1967).

*Turbulent flow* is composed of both a general movement in direction of the pipe and a superposed, inordinate, orthogonal movement. Therefore, the path of fluid particles is not known in advance for a turbulent flow field. The motion of individual particles is random and can only be des-

cribed by statistical parameters such as the mean velocity  $\bar{v}$ . Experiments show that the pressure loss is

$$\Delta p = f \frac{l}{D} \frac{\rho \bar{v}^2}{2} \quad (10.4.12)$$

In general, the friction factor  $f$  depends on the surface roughness and the Reynolds number  $Re$ , which is defined as

$$Re = \frac{D\bar{v}}{v} \quad (10.4.13)$$

where  $v_f$  is the kinematic viscosity.

For smooth pipes and  $Re \leq 80000$ , *Blasius' law* can be used to calculate the friction factor as

$$f = \frac{0.3164}{Re^{0.25}} \quad (10.4.14)$$

Laminar flow can also be covered by (10.4.12) if the friction factor for the laminar regime is set to

$$f = \frac{64}{Re} \quad (10.4.15)$$

In the transition area between laminar and turbulent flow, a third relationship is defined to avoid discontinuities. One possible set of equations is given as

$$f = \left\{ \begin{array}{lll} \frac{64}{Re} & \text{for} & Re < 1404 & \text{(Poiseulle)} \\ 0.0456 & \text{for} & 1404 \leq Re < 2320 & \text{(transition)} \\ \frac{0.3164}{Re^{0.25}} & \text{for} & 2320 \leq Re & \text{(Blasius)} \end{array} \right\} \quad (10.4.16)$$

For lumped losses, it is reasonable to assume turbulent flow in most cases, also because of elements with higher resistances like orifices or tube bends.

For turbulent flow, the pressure loss-volume flow rate relation at the orifices is given by

$$\dot{V} = \alpha_D A \sqrt{\frac{2}{\rho} |\Delta p|} \text{sign}(\Delta p) \quad (10.4.17)$$

where  $\alpha_D$  incorporates the contraction of the jet upon passing through the orifice. The point along the jet where the cross-sectional area of the jet reaches its minimum is called *vena contracta*.  $\alpha_D$  and  $A$  are combined into one parameter, which is obtained by experiments.

Turbulent flow losses are also evoked by sudden changes in the flow's cross-sectional area, by bends and other obstacles. For these cases, the pressure loss is defined by

$$\Delta p = \zeta \frac{\rho}{2} \left( \frac{\dot{V}}{A} \right)^2 \quad (10.4.18)$$

where  $\zeta$  is the loss coefficient, which depends on the geometry, see Table 10.19.

**Table 10.19.** Loss coefficients for typical orifices, Merritt (1967)

	type of entrance	$\zeta$
	inward projecting pipe entrance	1–1.3
	sharp edged entrance	0.3–0.4
	rounded entrance	0.012–0.2
	perfectly rounded entrance	approximately 0

*Material properties* of the hydraulic oil and surrounding vessels play an important role in the overall performance of hydraulic control systems. The equation of state relates by definition the pressure, temperature and density of any solid, liquid or gaseous phase. While the equation of state for an ideal gas can be derived by applying first principles, it is not possible to do so for a liquid fluid. In general, the density increases with an increase in pressure or a decrease in temperature. The density increase due to pressure, the so-termed compressibility, is more than 100 times larger than that of steel. Therefore, this effect cannot be neglected. The *bulk modulus* or *compressibility module* is defined as

$$\beta = -V \left( \frac{\partial p}{\partial V} \right)_{T=\text{const.}} \quad (10.4.19)$$

The compressibility  $\kappa$  of a liquid is defined by

$$\kappa = \frac{1}{\beta} = -\frac{1}{V} \left( \frac{\partial V}{\partial p} \right)_{T=\text{const.}} \quad (10.4.20)$$

The relative change of length  $l$  of a liquid column becomes, for constant cross-sectional area  $A$

$$\frac{dl}{l} = -\frac{dV}{V} = \frac{1}{\beta} dp = \frac{1}{\beta} \frac{dF}{A} \quad (10.4.21)$$

This corresponds to the elasticity  $\epsilon$  of a solid material and a comparison with (4.1.1) and (4.1.3) shows that  $\beta$  is equivalent to the modulus of elasticity  $E$ . Therefore, the stiffness of a liquid column of length  $l$  becomes,

$$c_l = \frac{dF}{dl} = \beta \frac{A}{l} \quad (10.4.22)$$

The compressibility is not only affected by the fluid itself. It is also altered by air trapped in the liquid. Further, if thin-walled vessels are pressurized, then these vessels will expand as their walls give way. This increases the volume that the enclosed liquid can fill and thus causes a decrease in both pressure and density of the encompassed fluid. This interaction also effectively changes the bulk modulus. All these influences are combined into one parameter, the effective bulk modulus, usually denoted by  $\beta'$ .

One point that divides solids from fluids is the fact that the latter deform unlimitedly if subject to a shear force. Different material-specific laws have been formulated to capture this behavior. Hydraulic fluids are most often modeled as Newtonian fluids, for which the shear stress on the surfaces is in proportion to the velocity gradient

$$\tau = \mu \frac{\partial v}{\partial y} \quad (10.4.23)$$

with the absolute viscosity  $\mu$  being the proportional constant. Depending on the experimental set-up used to measure the viscosity, two different parameters can be acquired: The absolute viscosity  $\mu$  and the kinematic viscosity  $v_f$ . They can be converted into one another by

$$v_f = \frac{\mu}{\rho} \quad (10.4.24)$$

Some properties of standard hydraulic oil have been collected in Table 10.20 to give an idea of the magnitude of the respective values.

**Table 10.20.** Characteristic properties of standard hydraulic oil

variable	density	specific volume	specific heat	bulk modulus	kinematic viscosity	thermal expansion coefficient	vapor pressure
symbol		$v$	$c_p$	$\beta$	$v_f$	$\epsilon_T$	$p$
dimension	$\frac{kg}{m^3}$	$\frac{m^3}{kg}$	$\frac{J}{kgK}$	$\frac{N}{m^2}$	$\frac{mm}{s^2}$	$\frac{1}{K}$	bar
defined at	15°C	15°C	20°C		40°C		50°C
value	870	$1.15 \cdot 10^{-3}$	1885	$2 \cdot 10^9$	15...70	$7 \cdot 10^{-4}$	37536

Hydraulic control systems consist of different components, which will now be modeled. As has already been stated in Chapter 2 (Table 2.3), the pressure  $p$  (effort variable) and volume flow rate  $\dot{V}$  (flow variable) are usually chosen as power variables for hydraulic systems.

### b) Hydraulic control valves

For manipulating the oil flow in tubes, hydraulic control valves are used. Based on their task, valves can be divided into four classes: solenoid valves, locking valves, pressure control valves and flow valves.

A schematic view of a spool valve is shown in Figure 10.13. Here, the spool is driven by a combination of two electromagnets, each coil being responsible for displacing the spool in one direction.

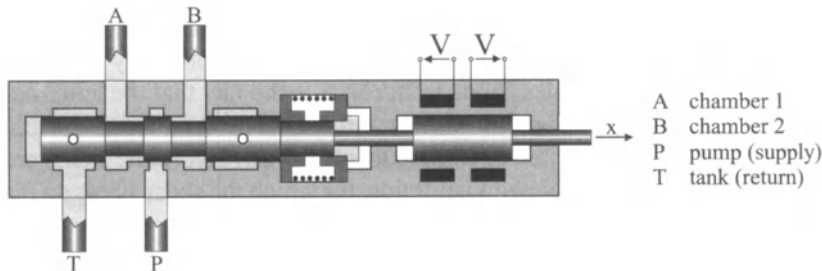


**Figure 10.13.** Schematic view of a hydraulic spool valve

In proportional valves, the spool is driven by one or more electromagnets. Electromagnets have been discussed in detail in Section 5.2. Here, only the most important equations will be repeated. The electromagnet can be modeled using (5.2.42)

$$V(t) = RI(t) + L_d \frac{dI(t)}{dt} + c_y \frac{dY}{dt} \quad (10.4.25)$$

The force exerted by the electromagnet is given as (5.2.43)

$$F_M(t) = c_y I(t) \quad (10.4.26)$$

The position dependency is neglected. Under this assumption, one can combine the equations (10.4.20) and (10.4.21), yielding

$$\dot{F}_M(t) + \alpha_M F_M(t) = k_M V(t) \quad (10.4.27)$$

The quantity  $V$  denotes the terminal voltage,  $\alpha_M$  and  $k_M$  designate the time constant and gain respectively. This magnet exerts a force  $F_M$  on the spool. The spool is modeled as a second order system

$$m_s \ddot{z}(t) + d_s \dot{z}(t) + c_s z(t) = F_M(t) + F_{Ext}(t) \quad (10.4.28)$$

where the coefficients  $m_s$ ,  $d_s$  and  $c_s$  denote the mass, damping and spring constant respectively, and  $F_{Ext}$  is the resultant of all external forces acting on the spool. These forces could stem from friction as well as from the fluid flow inside the valve. Most often, these forces are neglected, mainly because their influence is relatively small.

Flow through the valve orifices is modeled as turbulent flow, described by (10.4.15). The area of the orifice is a function of the spool displacement and is given by

$$A = \begin{cases} A_V'(z - z_0) & \text{for } z \geq z_0 \\ 0 & \text{for } z < z_0 \end{cases} \quad (10.4.29)$$

$A_V'$  denotes the cross-sectional area of the valve opening per unit displacement of the spool and is called the opening or area gradient of the valve. The function in (10.4.24) depends on the geometry of the valve and will vary with different designs. The parameter  $z_0$  is determined by the valve lapping, *i.e.*,  $z_0 < 0$  for an underlapped valve,  $z_0 = 0$  for a zero-lapped valve and  $z_0 > 0$  for an overlapped valve. Figure 10.14 presents the different configurations along with the characteristic curves for the flow. For the underlapped valve, two flow paths can be open at the same time. This is indicated by the characteristic curve having two branches.

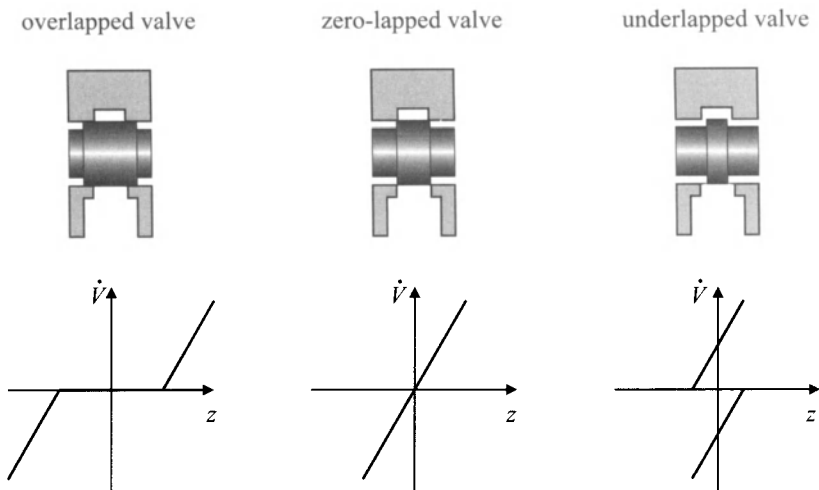
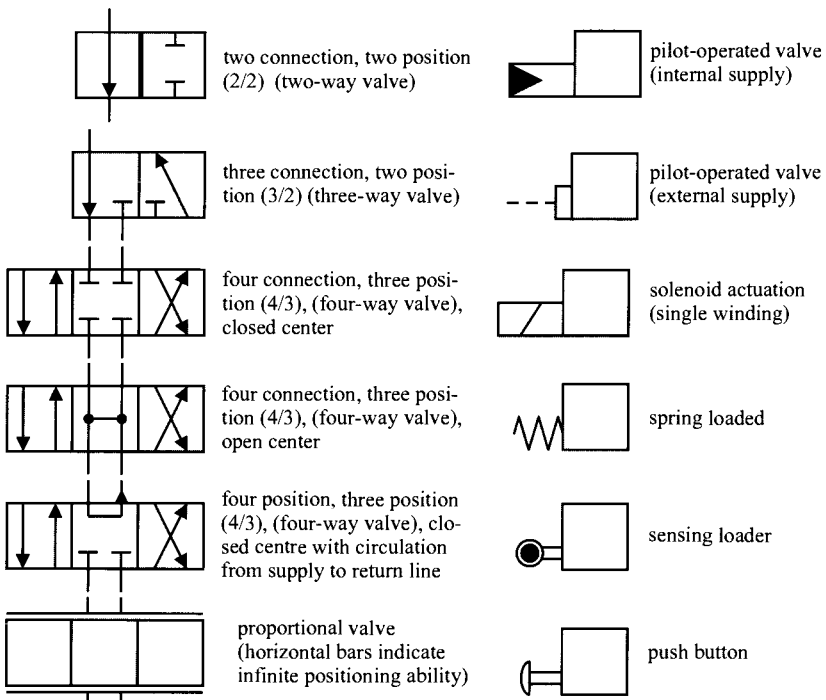


**Figure 10.14.** Spool displacement flow curves for differently lapped proportional valves

There exists a wide variety of different control valves, differing in the number of hydraulic connectors, arrangement of the flow paths and actuation principle. Some examples are given in Figure 10.15 along with the graphical representation used in hydraulic circuit diagrams. In the case of switching valves, a segment is used for each switching position. Finite switching valves are specified in terms of the number of connections and the number of positions they have. Thus, a 4/2 valve is one with four ports and two positions. Two-way valves can be constructed as seat valves, which offer superior (leakage-free) sealing. The other valves are typically constructed as sliding valves, with the spool type being the predominant construction principle.

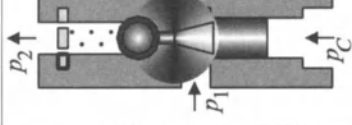
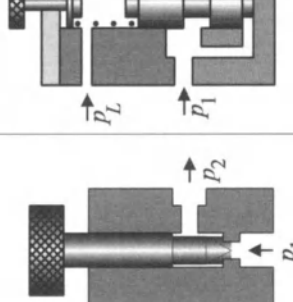
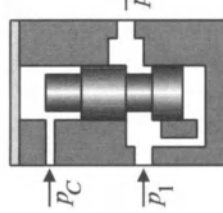
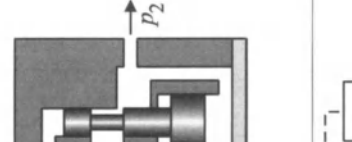
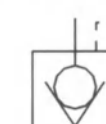
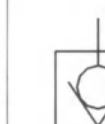
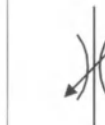
Two-way valves are also manufactured with internal, mechanical control circuits, controlling the pressure or flow through the valve. Examples for these types of valves are given in Table 10.21. The locking valves are constructed as seating valves with a ball being used to tightly

seal the opening. The check valves shown in Table 10.21 are constructed as spool-type valves. The simple non-return valve can be used to bypass a throttle valve in one flow direction. Thus, the dynamics of the pressure build-up and pressure release can be influenced independently. This technique is exploited for hydraulic braking systems of road vehicles. Pilot-operated non-return valves are typically used in conjunction with solenoid valves, where they tightly seal the cylinder chambers whenever the spool is in its center position. Throttle valves change the pressure-flow relation as they dissipate hydraulic power. Pressure relief valves are safety devices that limit the maximum level of the hydraulic pressure in a system. Their construction is almost identical to that of sequence valves. The latter only pressurize their secondary hydraulic port if the pressure at the primary port exceeds a certain threshold. The pressure threshold can also be set by means of an external control pressure. Other valves are used to maintain a certain pressure ratio between the primary and the secondary port. The functional principle is the force balance at the piston. The piston is constructed such that the areas on which the primary and secondary pressure act are different. Since the force is the product of pressure and area, the pressure ratio required for a balance of forces will be the reciprocal of the active piston areas.



**Figure 10.15.** Valve types and symbols: a segment is used for each switching position

Table 10.21. Construction and symbols of different hydraulic valves

class	type	locking valves	throttle valves	pressure relief valve/sequence valve	check valves	
constructional principle	simple non-return valve	pilot-operated non-return valve	needle valve	externally controlled pressure control valve	counterbalance valve with fixed pressure ratio	
	$p_2$					
graphical representation	$p_2$					keeps the pressure ratio of $p_1 / p_2$ constant
	$p_1$					keeps the pressure ratio of $p_1 / p_2$ constant
function						reduces the pressure such that $p_1$ is equal to or less than the control pressure $p_C$

The dynamics of the internal mechanical control loops are typically much faster than those of the other hydraulic components used in the hydraulic system. Thus, one does not need to model the individual components of the internal control loop, such as masses, springs, pistons, *etc.* Instead, these valves are typically represented by a static model that describes the pressure-flow characteristic of the valve.

### c) Hydraulic transmission lines

Depending on the length of the pipe, different effects must be modeled. Very short pipes are usually not modeled, especially if they have a relatively large cross-sectional area. For longer pipes, the compressibility must be taken into account. The inertia of the fluid has to be considered if the fluid is subject to an oscillatory excitation or if segments of the line have a small cross-sectional area. The flow resistance plays an important role for long lines or those with small cross-sectional areas.

A section of a prismatic tube of length  $l$  and cross-sectional area  $A$  has the mass

$$m_l = A l \rho \quad (10.4.30)$$

It is assumed that the compressibility of the fluid requires a force

$$F_c = c_l(z_1 - z_2) \quad (10.4.31)$$

with  $c_l$  being the oil-spring constant and  $z_1$  and  $z_2$  being the displacement of the two ends, see Figure 10.16. The damping force through liquid motion is

$$F_d = d \dot{v} \quad (10.4.32)$$

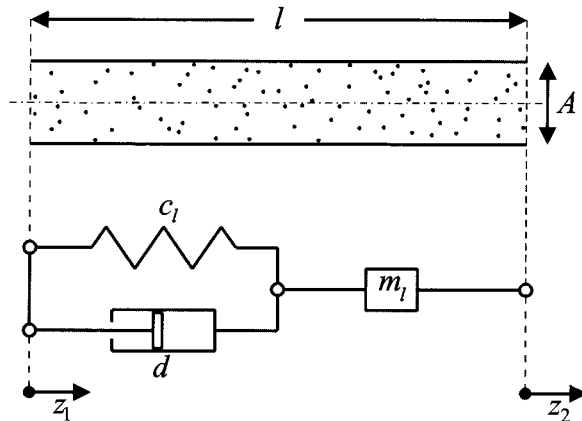


**Figure 10.16.** Mechanical equivalent model of a hydraulic transmission tube section

Applying the law of momentum yields

$$m_l \ddot{z}_2(t) + d \dot{z}_2(t) + c_l z_2(t) = c_l z_1(t) \quad (10.4.33)$$

or in terms of volume  $V$  and pressure  $p$

$$m_l \ddot{V}_2(t) + d \dot{V}_2(t) + c_l V_2(t) = A^2 \Delta p_1(t) \quad (10.4.34)$$

Hence, the second order oscillatory model of an oil column shows the following characteristic values, compare (4.5.5)

$$\omega_0 = \sqrt{\frac{c_l}{m}} = \frac{1}{l} \sqrt{\frac{\beta}{\rho}} \quad (\text{undamped natural frequency}) \quad (10.4.35)$$

$$\zeta = \frac{d}{2\sqrt{c_l m}} = \frac{d}{2A\sqrt{\beta\rho}} \quad (\text{damping factor}) \quad (10.4.36)$$

#### d) Hydraulic pressure storages (hydraulic accumulators)

The task of hydraulic accumulators is to ingest a certain quantity of pressurized hydraulic fluid, which can be fed back into the hydraulic circuit. These storage devices can supply hydraulic fluid to satisfy the peak demand, compensate for temperature-related variations, supply energy during emergency conditions (power loss) or dampen pump-induced pressure oscillations.

There are three basic constructional principles, *piston-type accumulators*, *bladder-type accumulators* and *diaphragm-type accumulators*, see Figure 10.17. For the piston type accumulator, two chambers are separated by a piston assembly. One chamber is filled with a gas, typically nitrogen ( $N_2$ ). The other chamber is connected to the hydraulic system and thus filled with oil. This accumulator type is primarily used if a high storage capacity at a high system pressure is required. Due to the comparably large mass of the piston, the piston-type accumulator is much slower in its dynamics than the bladder and diaphragm type accumulators. The latter use elastomeric elements to separate gas and liquid. Piston-type accumulators seal the two chambers in an almost hermetical way, whereas the other two designs are impaired in that the nitrogen may diffuse through the divider element over time.

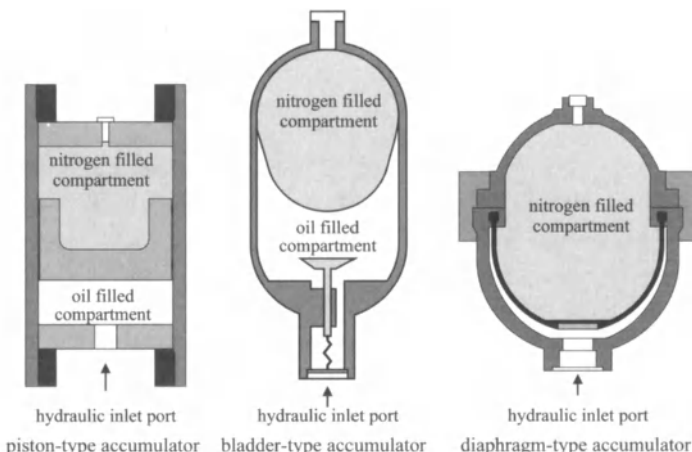


Figure 10.17. Hydraulic accumulators

The behavior of these fluid storage devices is mainly determined by the behavior of the charge gas. For simple calculations, nitrogen can be treated as an ideal gas, thus obeying the equation of state of the ideal gas, given as

$$pV = mRT \quad (10.4.37)$$

This equation models the behavior of the charge gas sufficiently precisely for system pressures up to 10 bar. For higher pressures, one must use experimentally derived equations, such as the Beattie and Bridgman equation, e.g., Korkmaz (1982), see Section 10.5,

$$p = \frac{RT(1-\varepsilon)}{V^2} (V + B) - \frac{A}{V^2}$$

$$A = A_0 \left(1 - \frac{\alpha}{V}\right), \quad B = B_0 \left(1 - \frac{b}{V}\right), \quad \varepsilon = \frac{C}{VT^3} \quad (10.4.38)$$

for system pressures up to 250 bar.

Upon compression and expansion of the charge gas, the internal energy of the filling gas will change and heat will be exchanged with other components. The simplest model of this process assumes polytropic expansion of the gas with a constant polytropic coefficient,

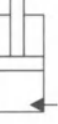
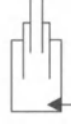
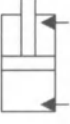
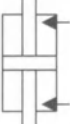
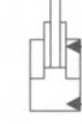
$$p_0 V_0^n = p V^n \quad (10.4.39)$$

The choice of the polytropic coefficient  $n$  depends on the general nature of volume changes. For a slow charging process, one can assume an isothermal change of state ( $n = 1$ ). Theoretically, the polytropic coefficient is limited by  $n \leq 1.4$ , where the limiting case is the adiabatic expansion. This would be the case for a fast discharge, for example, to cover the peak demand. However, in reality, the heat exchange is much more complex and cannot be governed by (10.4.39). For the simulation of hydraulic accumulators, it is thus necessary to model the temperature exchange with the surroundings and to introduce the temperature as a new state.

### e) Hydraulic translatory motors

Depending on the motion to be generated, one differentiates between rotary motors (hydraulic motors) and translatory motors (hydraulic cylinders). Translatory motion is generated by hydraulic cylinders, which – based on the type of piston support – can be classified as cylinders with low-friction sealing and cylinders with hydrostatic bearings. They can be constructed as single-acting and double-acting cylinders, see Table 10.22. For single-acting cylinders (plunger cylinders, telescopic cylinders), which have only one hydraulic connector, the rod is extended by means of a hydraulic force while it is retracted by means of some external force (gravity, return spring, counter cylinder). Double-acting cylinders have two hydraulic connectors, thus the piston can be both extended and retracted by a hydraulic force.

Table 10.22. Construction principles and key features of hydraulic translatory motors

hydraulic cylinder type	construction principle	graphical symbol	maximum stroke	minimum stroke	features
single-acting plunger cylinder	single rod cylinder				- lower weight than plunger cylinder; - more friction than plunger cylinder; - more sophisticated design.
	plunger cylinder				- simple design; - low initial cost; - low friction; - good efficiency; - stroke limited due to weight of plunger.
	telescopic cylinder		8 m	130 kN	- large stroke at small installation volume; - complicated design; - without compensation methods, the velocity and force generated by the cylinder are position-dependent.
double-acting	single rod cylinder				- unequal active piston areas; - generated force and velocity are direction-dependent; - hydraulic retraction possible.
	double rod cylinder				- equal active piston areas; - force and velocity are not direction-dependent; - transfer function parameters are identical for both chambers provided piston is centered
	telescopic cylinder		2.5 m		- complicated design; - large stroke at small installation volume; - hydraulic retraction possible.

The double-acting cylinder can be employed as a pull-type or push-type cylinder. The single-rod piston is the most widespread type, available with many different piston-area ratios, different types of mounting and different types of connections. Compared to double rod cylinders, they need less installation space for the same piston stroke. Due to the different piston areas, the differential cylinder has a direction-dependent piston speed and actuation force in the case of constant supply pressure and volume flow rate.

For most applications, servo-cylinders with special contact sealing can meet the imposed requirements. However, this puts demanding constraints on the surface quality of the cylinder tube, piston rod and piston support. With this special contact sealing, undesired friction and stick-slip effects can be reduced noticeably, Backé (1986b).

For modeling a double-acting cylinder, a scheme like in Figure 10.18 is considered. The displacement of the piston is  $z$ . Both chambers are parameterized by the initial volume  $V_0$  for  $z = 0$  and the effective cross-sectional area of the piston  $A$ . The volume flow rate into the chamber is designated as  $\dot{V}$  and the pressure inside the cylinder chamber as  $p$ .

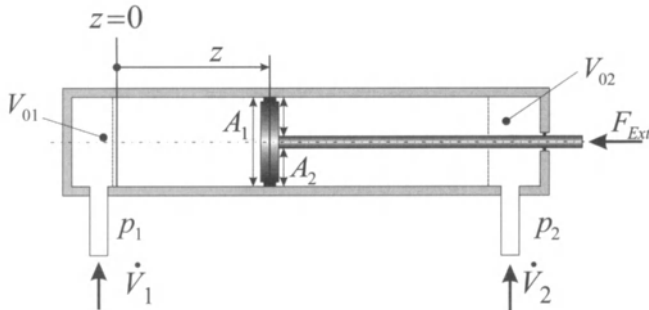


**Figure 10.18.** Schematic view of a hydraulic cylinder

Applying the mass balance equation (2.3.7) to the left cylinder chamber leads to

$$\begin{aligned}\dot{m}_1(t) &= \frac{d}{dt}(V_1(t)\rho_1(t)) = \dot{V}_1(t)\rho_1(t) + V_1(t)\dot{\rho}_1(t) \\ &= A_1\rho_1(t)\dot{z}(t) + (V_{01} + A_1z(t))\dot{\rho}_1(t)\end{aligned}\quad (10.4.40a)$$

and, for the right chamber, one obtains correspondingly

$$\begin{aligned}\dot{m}_2(t) &= \frac{d}{dt}(V_2(t)\rho_2(t)) = \dot{V}_2(t)\rho_2(t) + V_2(t)\dot{\rho}_2(t) \\ &= -A_2\rho_2(t)\dot{z}(t) + (V_{02} - A_2z(t))\dot{\rho}_2(t)\end{aligned}\quad (10.4.40b)$$

In order to eliminate the density from the above equations, a relation between the pressure and the density must be established. Applying  $V = m/\rho$  and  $\partial V/\partial \rho = -V/\rho$  leads to

$$\frac{\partial p}{\partial \rho} = \left( \frac{\partial p}{\partial V} \right) \left( \frac{\partial V}{\partial \rho} \right) = \left( -\frac{V}{\rho} \right) \left( \frac{\partial p}{\partial V} \right) \quad (10.4.41)$$

which can also be written in the form

$$\frac{\partial p}{\partial \rho} = \left[ \left( -\frac{1}{V} \right) \left( \frac{\partial V}{\partial \rho} \right) \right] \rho \frac{\partial p}{\partial \rho} \quad (10.4.42)$$

Inserting the bulk modulus  $\beta$  (10.4.19) yields

$$\dot{\rho} = \frac{\rho}{\beta} \dot{p} \quad (10.4.43)$$

This equation can be used to rewrite the equations in (10.4.40) independent of the density as

$$\begin{aligned} \dot{p}_1(t) &= \frac{V_{01} + A_1 z(t)}{\beta} + A_1 \dot{z}(t) = \dot{V}_1(t) \\ \dot{p}_2(t) &= \frac{V_{02} - A_2 z(t)}{\beta} - A_2 \dot{z}(t) = \dot{V}_2(t) \end{aligned} \quad (10.4.44)$$

For double-acting cylinders, one must also model the cross-port leakage flow between the two chambers, which is assumed to be laminar. The pressure-flow relation is

$$\dot{V}_{1-2}(t) = C_{1-2} (p_1(t) - p_2(t)) \quad (10.4.45)$$

for a flow from chamber 1 to chamber 2. The cross-port leakage coefficient  $C_{1-2}$  is found to be

$$C_{1-2} = \frac{\pi}{96 \nu \rho} \frac{(D_o + D_i)}{2} \frac{(D_o - D_i)^3}{l} \quad (10.4.46)$$

where the inner diameter of the housing is assigned to  $D_o$  and the diameter of the piston to  $D_i$ . Once the pressure build-up in the chambers is known, the dynamic behavior of the piston rod can be calculated. Other forces acting on the piston besides the hydraulic forces are friction forces, inertia forces due to the mass of the piston and external forces. The balance of forces for the piston rod is finally given by

$$m_p \ddot{z}(t) + d_p \dot{z}(t) + c_p z(t) + f_C \operatorname{sign}(\dot{z}(t)) = p_1(t) A_1 - p_2(t) A_2 - F_{Ext}(t) \quad (10.4.47)$$

where  $F_{Ext}$  is the sum of all external forces,  $m_p$  is the mass of rod and piston,  $d_p$  and  $c_p$  are the damping coefficient and spring stiffness respectively and  $f_C$  is the friction coefficient for dry friction. An overall cylinder model is derived in Section 10.4.3.

## f) Hydraulic rotary motors

In contrast to their pneumatic counterparts, hydraulic motors play a more important role since they offer high torque at small size (the power density of a hydraulic motor is 20–25 times greater than that of an electric motor) and have a small moment of inertia. This results in very small time constants and permits a highly dynamic manipulation of the rotational speed.

Hydraulic rotary motors are based on the positive displacement principle. They must have some mechanical element on which the pressure acts and which recurrently increases and decreases the size of an enclosed volume. Based on the shape and kinematics of this element, one can classify hydraulic motors as axial- and radial-piston motors, external and internal gear types, and sliding vane and rolling vane types. An overview of the different construction principles is given in Table 10.23. Each principle has its distinct features, which makes it suited to certain applications.

Despite this wide variety of engineering designs for hydrostatic motors, all motors work on the same positive displacement principle and can thus be modeled using the same equations. Furthermore, most functional principles can be utilized as both pumps and motors. Thus, the term "hydraulic machine" is used in the following.

First, an ideal hydraulic machine will be modeled. This model is based on the assumption that there are no losses and that the fluid is incompressible. Under these presumptions, the volume flow rate is proportional to the active volume per revolution of the machine chamber  $V_M$  and the rotational speed  $\omega$  as

$$\dot{V}_{\text{theo}} = \frac{\omega}{2\pi} V_M \quad (10.4.48)$$

For both modes of operation, *i.e.*, pump and motor, the power consumed and then emitted by the ideal machine is given by

$$P = \Delta p \dot{V} \quad (10.4.49)$$

The indicator diagram for the ideal hydraulic machine is shown in Figure 10.19. Between points A and B, the chamber is connected to the intake. For an ideal pump, the chamber is filled with fluid as the volume grows from  $V_{\min}$  to  $V_{\max}$ . During this phase, the pressure in the chamber is identical to the pressure at the inlet  $p_1$ . Then, the connection to the intake is closed and the connection to the outlet is opened. For an ideal pump, the pressure in the chamber rises to the pressure at the outlet  $p_2$ . Between points C and D, the fluid is pushed out of the chamber through the outlet as the volume shrinks from  $V_{\max}$  to  $V_{\min}$ . Finally, the connection to the outlet is closed and the chamber is coupled again to the inlet. For an ideal motor, this work cycle is executed in the reverse order.

Two effects influence the shape of the indicator diagram. The first effect is the *compressibility* of the fluid. Upon pressurization, the volume will shrink. It will expand again as the pressure level decreases. This effect is considered in the indicator diagram shown in Figure 10.19 and is governed according to (10.4.19) by

$$\frac{\Delta V}{(p_2 - p_1)} = - \frac{V}{\beta'} \quad (10.4.50)$$

Table 10.23. Characteristics of hydraulic rotary motors (hydraulic motors), Nordmann, Isermann (1999), Matthies (1995), Bauer (1998)

hydraulic rotary type	construction principle (example)	operation pressure/bar	rotational velocity / min	displacement per rev./cm <sup>3</sup>	overall efficiency	advantages	disadvantages
axial piston motor		100–500	5–8000	2–4000	0.85–0.9	- high operating pressure; - high power density; - adjustable displacement; - good efficiency; - low operational cost.	- complicated manufacturing; - high initial cost; - possibly long construction length.
radial piston motor		120–750	5–3000	2–35000	0.85–0.9	- high operating pressure; - high power density; - good efficiency; - generation of high torque and rotational velocities	- complicated manufacturing; - less compactly built than axial piston pumps.
external gear motor (spur gear)		80–300	200–8000	1–1000	0.6–0.9	- small unit volume; - high power density; - simple design; - rugged.	- constant displacement; - change of flow only by means of a throttle valve, thus heating-up of the oil; - high operational cost.
internal gear motor (generator)		< 260	10–2000	10–900	0.6–0.8	- small unit volume; - high power density; - simple design; - high torque at low rotational velocity.	- constant displacement; - bad efficiency; - high operational cost.
sliding vane motor		50–200	10–4000	2–2000	0.7–0.8	- small unit volume; - low noise level; - adjustable displacement; - low flow pulsation.	- sensitive to pressure spikes; - bad efficiency.
rolling vane and swinging vane motors		< 280	1–3000	8–1600	0.7–0.9	- small unit volume; - low noise level; - hydraulically balanced.	- sensitive to pressure spikes; - bad efficiency; - constant displacement for rolling vane motors.

This effect requires that the connections to the intake and outlet are not changed instantaneously. The shape of the indicator diagram is also affected by the flow-induced pressure losses. The indicator diagram of an ideal pump, considering the aforementioned effects, is shown in Figure 10.19. It can be seen that during the suction phase, the pressure in the pump chamber falls below the pressure at the intake. This is a critical point in the design of hydraulic pumps. If the pressure in the chambers drops below the vapor pressure, part of the fluid will vaporize. Thus, the chamber will only be partially filled with hydraulic fluid. This effect may also lead to "cavitation". On the other hand, while the fluid is pushed out of the chamber, the pressure will rise above the pressure at the outlet port. For the hydraulic motor, a similar indicator diagram is plotted in Figure 10.19. For a hydraulic motor, the pressure in the chamber will never drop below the pressure at the low pressure port. Therefore, hydraulic motors are not susceptible to cavitation.

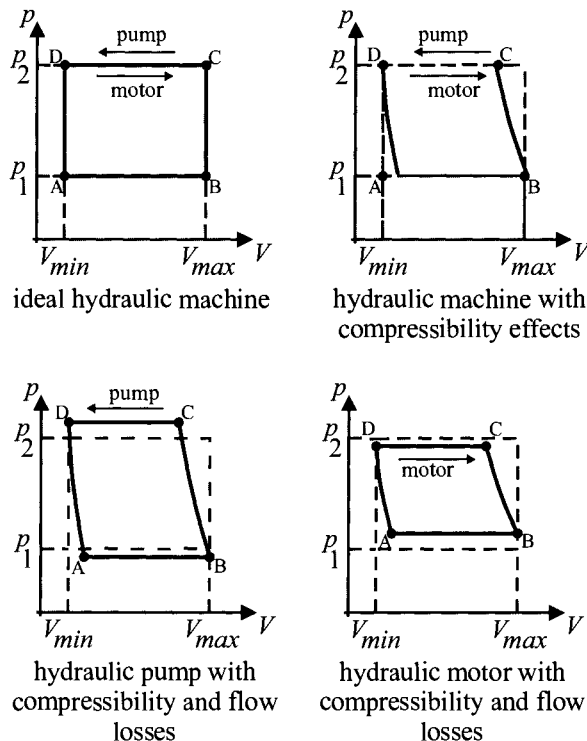


Figure 10.19. Indicator diagrams for hydraulic machines

In contrast to an ideal hydraulic machine, the performance of a real hydraulic machine is impaired by a couple of losses, which are largely divided into volumetric and hydraulic-mechanical losses. The former cause a difference between the volume flow rate of an ideal machine and a real machine. Several factors affect the volume flow rate. The first effect that induces *volumetric losses* is the compressibility of the fluid, because the volume will shrink upon pressurization in the hydraulic pump by

$$\dot{V}_{vol} = \frac{\omega}{2\pi} \frac{V_M}{\beta'} \Delta p \quad (10.4.51)$$

It may be noted that as far as the energy flow is concerned, this effect cannot be called a loss, since the energy consumed during the compression of the fluid in the pump is stored in the fluid itself and can thus be regained in the hydraulic motor. Another effect is the incomplete charge of the pump chamber if the pressure in the intake drops below the vapor pressure (cavitation), which is characteristic of hydraulic pumps. Cavitation typically occurs at higher rotational velocities, since the volume flow rate increases with the rotational velocity as does the flow-induced pressure loss. Both of these effects, compressibility of the oil and cavitation, are usually not modeled, since they are negligible compared to the internal and external leakage flows, the biggest source of volumetric losses. Since most machines are constructed such that fluid leaking from the machine is directed to the port with the lower pressure level, external leakage flows can also be treated as being internal. The exact nature of the leakage flows cannot be determined in most cases, therefore this flow is modeled as being partially laminar and partially turbulent

$$\dot{V}_{Leak} = k_{Lam} \Delta p + k_{Turb} \sqrt{\frac{\Delta p}{\rho}} \quad (10.4.52)$$

where  $k_{Lam}$  and  $k_{Turb}$  are the corresponding coefficients. This model is well suited to lower pressure levels. For higher pressure, the losses increase noticeably as the gaps expand and as the energy dissipation and thus the temperature of the fluid increases.

*Hydro-mechanical losses* stem from friction within the fluid, on friction surfaces and in bearings. The change in the momentum of the enclosed fluid also uses up part of the torque.

Taking all of these effects into account, the volume flow rate is given by

$$\begin{aligned} \dot{V} &= \dot{V}_{theo} - \dot{V}_{Vol} - \dot{V}_{Leak} \\ &= -\dot{V}_{theo} \left( 1 - \frac{\dot{V}_{Vol}}{\dot{V}_{theo}} - \frac{\dot{V}_{Leak}}{\dot{V}_{theo}} \right) = \dot{V}_{theo} \eta_{Vol} \end{aligned} \quad (10.4.53)$$

the output power of a hydraulic pump is therefore

$$P_1 = \dot{V}_1 \Delta p_1 = \dot{V}_{1theo} \eta_{1Vol} \Delta p_1 = \frac{\omega_1}{2\pi} V_{1M} \Delta p_1 \eta_{1Vol} \quad (10.4.54)$$

and its input power

$$P_1 = \frac{\omega_1}{2\pi} V_{1M} \Delta p_1 \frac{1}{\eta_{1m}} \quad (10.4.55)$$

where the mathematical efficiency takes into account mechanical losses. The driving torque then becomes

$$T_1 = \frac{P_1}{\omega_1} = \frac{1}{2\pi} V_{1M} \Delta p_1 \frac{1}{\eta_{1m}} \quad (10.4.56)$$

A hydraulic rotary motor receives volume flow  $\dot{V}_1$ , which results in an effective motor volume flow

$$\dot{V}_2 = \dot{V}_1 \eta_{2Vol} \quad (10.4.57)$$

and generates the output power of the motor

$$P_2 = \dot{V}_1 \eta_{2Vol} \eta_{2m} \Delta p_2 = \frac{\omega_2}{2\pi} V_{2M} \Delta p_2 \eta_{2Vol} \eta_{2m} \quad (10.4.58)$$

and the output torque

$$T_2 = \frac{P_2}{\omega_2} = \frac{1}{2\pi} V_{2M} \Delta p_2 \eta_{2Vol} \eta_{2m} \quad (10.4.59)$$

Figure 10.20 shows the torque-volume flow characteristics of a hydraulic motor.

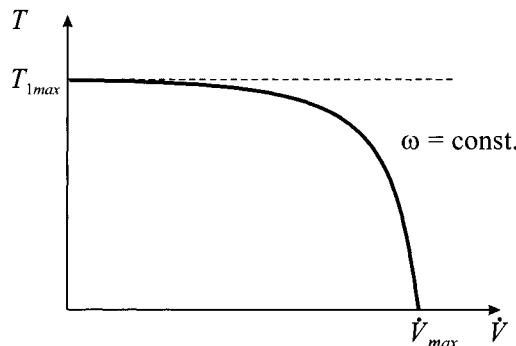


**Figure 10.20.** Characteristic torque-curve for a hydraulic motor

Almost all positive displacement machines have a finite number of displacing bodies. Therefore, they are not able to provide a continuous supply of pressurized hydraulic fluid. Rather, the flow is pulsating, which is a major issue in the design of hydraulic power systems as this causes pressure oscillations that might excite oscillations in subsequent hydraulic elements and can be a major source of noise emitted by the hydraulic system.

For a *variable displacement machine*, the volume flow rate is multiplied with a factor  $\kappa$ ,

$$\dot{V} = \kappa n V_M \quad (10.4.60)$$

which lies between 0 and 1 for a normal machine or -1 to 1 for a reversing machine. This factor captures the change in output due to the variation of the machine geometry. Most variable displacement machines, in particular wash plate and bent-axis machines, are controlled by the angular displacement  $\alpha$  of some part of the set-up. For these machines,  $\kappa$  is given by

$$\kappa = \tan \alpha = f(U) \quad (10.4.61)$$

A schematic cross-sectional view of a wash plate machine is shown in Figure 10.21. The figure is meant to illustrate the basic principle. In real designs, typically an odd number of pistons is chosen since this will reduce pressure oscillations in the high-pressure line connected to the pump outlet.

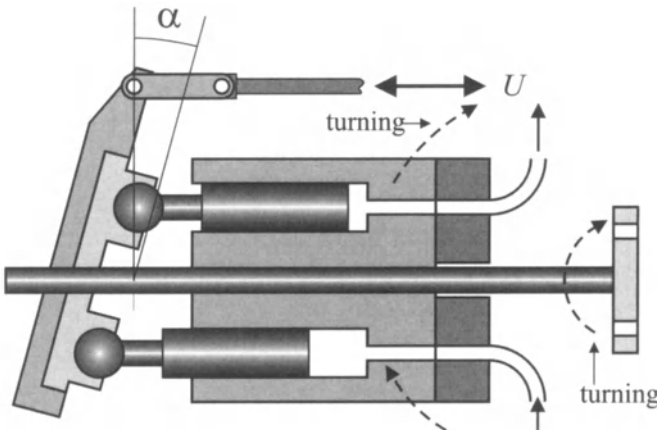


Figure 10.21. Schematic view of a wash plate machine

### 10.4.3 Models of a Hydraulic Servo-axis: An Example

An example for modeling a hydrodynamic overall system, the hydraulic servo-axis of Figure 10.10 is considered. The system consists of an axial piston pump, a proportional valve and a hydraulic cylinder, which will work against a mass  $m_{Load}$ . This set-up represents the work-table drive of a CNC drilling machine. For machine tools, linear hydraulic actuators can be used to replace the traditional ball bearing spindle-servomotor combination. It is assumed that the hydraulic actuator is supplied by a piston pump that is operated at a constant speed. The input of the actuator model will be the voltage  $V$  applied at the proportional valve and the output will be the position  $z$  of the cylinder and the work-table respectively.

#### a) Non-linear model

It will be assumed that the supply pressure  $p_s$  is constant and that the pump can always deliver the required amount of hydraulic fluid to the cylinder. Thus, the behavior of the pump does not need to be modeled. The connection pipes will not be modeled either. It is presumed that their contribution to the dynamics of the overall system is negligible.

The first subsystem under consideration is the proportional valve. The degree of valve opening  $H$  will be defined as the ratio between the actual and the maximum spool displacement,

$$H = \frac{z_s}{z_{s,\max}} \quad (10.4.62)$$

For the control of the double-acting cylinder, a four-way (4/3) valve will be used. There are four orifices, whose geometry can be controlled. For each orifice, the pressure-flow relation will be modeled using the equation

$$\Delta p = \frac{R_{\min}}{H^2} \dot{V}^2 \operatorname{sign}(\dot{V}) = \frac{R_{\min}}{H^2} \dot{V} |\dot{V}| \quad (10.4.63)$$

where  $R_{\min}$  denotes the minimum hydraulic resistance, *i.e.*, the hydraulic resistance of the fully open valve. It is assumed that the valve is zero-lapped. For  $z_s = 0$ , all four orifices will be closed. Two orifices will open if  $z_s > 0$ . For  $z_s < 0$ , the other two orifices will conduct the hydraulic flow. The pressure at the outlet will be set to zero. Under normal operating conditions, it is assumed that the flow into one cylinder chamber is equal to the flow out of the opposite chamber (this assumption is referred to as “matched and symmetric orifices”), thus

$$\dot{V}_{Load} = \dot{V}_1 = -\dot{V}_2 \quad (10.4.64)$$

If the volume flow rate through two identical orifices is the same, the resulting pressure loss across the apertures will also be the same. Thus, the pressure loss across one orifice, denoted by  $\Delta p$ , can be expressed as

$$\Delta p = \frac{1}{2} (p_s - p_{Load}) \quad (10.4.65)$$

where  $p_{Load}$  is the pressure difference between the two cylinder chambers. These equations can be combined into

$$\dot{V}_{Load} = \frac{|H|}{\sqrt{2 R_{\min}}} \sqrt{|p_s \operatorname{sign}(H) - p_{Load}|} \operatorname{sign}(p_s \operatorname{sign}(H) - p_{Load}) \quad (10.4.66)$$

which results in the block diagram shown in Figure 10.22. Usually, proportional valves contain an inner control loop, which controls the spool positioning. The control loop is modeled as a first order system.

The valve is connected to a hydraulic cylinder, which will be supplied with the load flows  $\dot{V}_1$  and  $\dot{V}_2$ . According to the equation of continuity, the flow into the cylinder chamber will lead to a change in the density of the fluid contained in the cylinder or to a change in the displacement of the piston, which effectively changes the volume of the cylinder chamber. For the following derivation, the zero reference point of the piston displacement will be the cylinder mid-point. The volume of the two cylinder chambers is then given by

$$\begin{aligned} V_1 &= V_{01} + A_1 z_p \\ V_2 &= V_{02} - A_2 z_p \end{aligned} \quad (10.4.67)$$

In these equations,  $V_{01}$  and  $V_{02}$  denote the initial volume of the two chambers. The increase in pressure due to compression of the fluid is governed by

$$\Delta p = \frac{\beta}{V} \Delta V \quad (10.4.68)$$

These lead to the block diagram shown in Figure 10.22. For the mechanical subsystem, the force acting on the piston rod is the difference between the two hydraulic forces less any frictional forces. Friction will be modeled as a combination of Coulomb and viscous friction, see Figure 10.22.

Two simulations running with parameters according to Table 10.24 show the behavior of the hydraulic servo-axes. The first simulation run, shown in Figure 10.23, depicts the system response due to a step input applied at the control input of the valve, *i.e.*, at the terminals of the electromagnet. One can see the time lag of the step response due to the pressure build-up in the chambers and the inertia effects of the connected mass. Later, the system comes to a point where the acceleration gets more and more determined by the flow resistance in the valve.

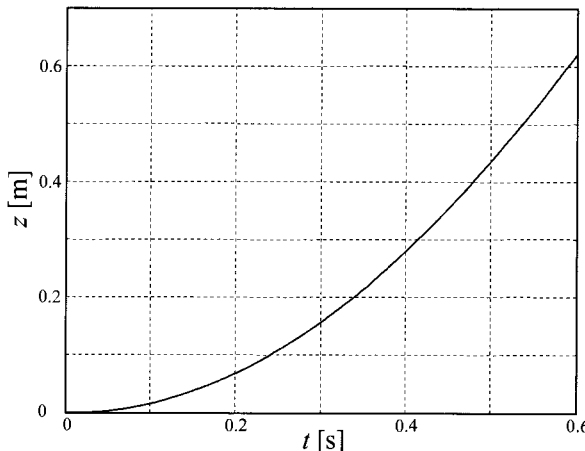


Figure 10.23. Simulated transient function of the position

The second simulation run, Figure 10.24, describes the system behavior if an external force is applied at the piston rod at  $t = 0.1$  s. As the piston moves in the negative  $x$  direction, the volume enclosed by one chamber shrinks, whereas the volume enclosed by the other chamber grows. The chamber whose volume decreases is tightly sealed.

Therefore, the encompassed fluid acts like a spring, the so-termed oil spring. The oscillations of the piston can be seen in the diagram. The dotted horizontal line denotes the theoretically expected displacement of the piston rod as calculated using (10.4.19). The difference of the theoretically derived and the effectively reached volume can be explained by Coulomb friction effects.

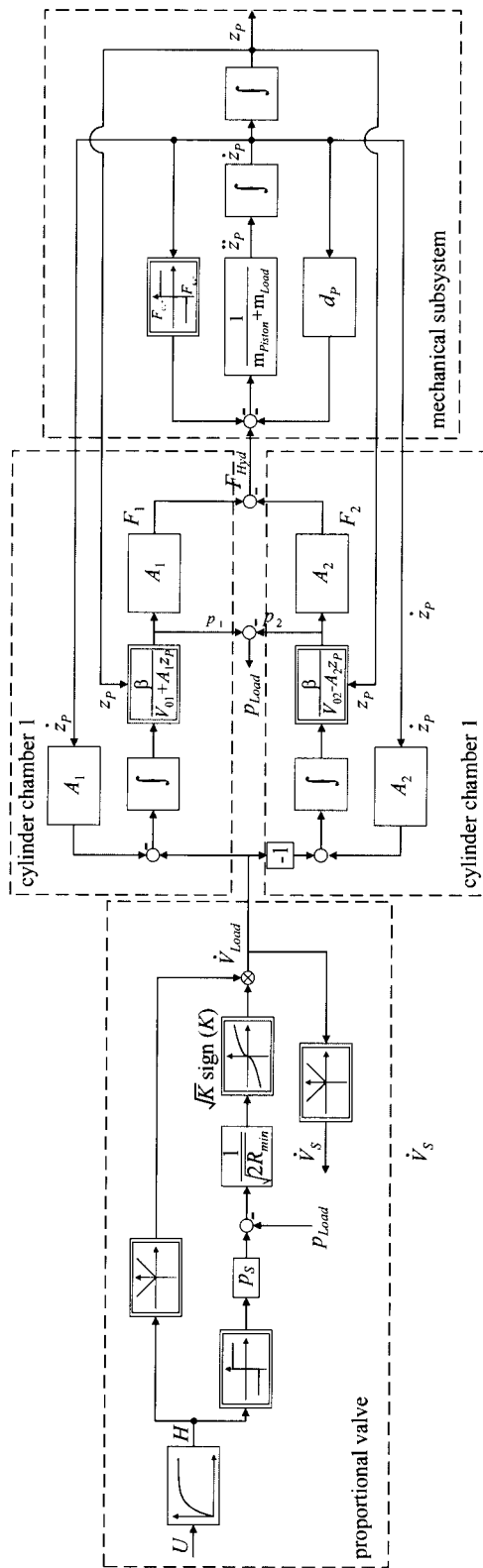
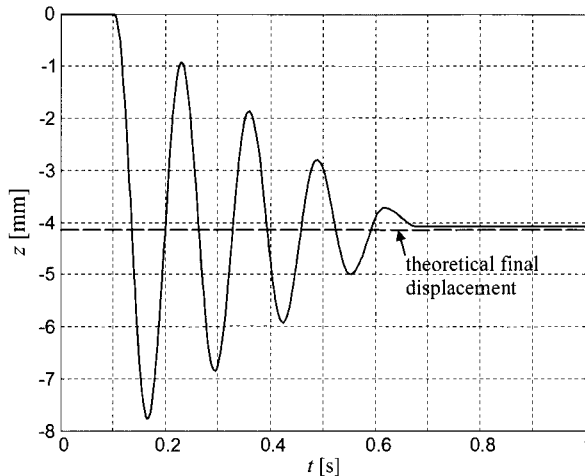


Figure 10.22. Block diagram of the hydraulic servo-axis;  $K = |p_s| \text{ sign}(H) - p_{load}|$ ; see (10.4.66)



**Figure 10.24.** Simulated transient function of the position for a stepwise external force input

The parameters for the simulation runs are listed in Table 10.24. The value for Coulomb friction for simulation 1 resembles a low friction (servo) cylinder, whereas the value for simulation 2 was chosen rather high to illustrate the problems associated with Coulomb friction.

**Table 10.24.** Parameters for the simulation of an hydraulic servo-axis

	simulation 1 valve-controlled	simulation 2 external force		
time constant of the servo-valve (critically-damped system)	$T_{Valve,1} = T_{Valve,2} = 0.01$	s	-	
minimum hydraulic resistance	$R_{min} = 250000$	$\frac{Pas^2}{m^6}$	-	
supply pressure	$p_s = 50 \cdot 10$	Pa	-	
piston area left and right	$d = 765.76 \cdot 10^{-6}$	$m^2$	$d = 765.76 \cdot 10^{-6}$	$m^2$
maximum displacement of cylinder	$l = 0.6$	m	$l = 0.6$	m
dead volume left	$V_{01} = 3.2182 \cdot 10^{-4}$	$m^3$	$V_{01} = 3.2182 \cdot 10^{-4}$	$m^3$
dead volume right	$V_{02} = 7.047 \cdot 10^{-4}$	$m^3$	$V_{02} = 7.047 \cdot 10^{-4}$	$m^3$
total weight of mechanical system and moving parts of hydraulic cylinder	$m_{Load} = 1000$	kg	$m_{Load} = 1000$	kg
Coulomb friction	$F_C = 100$	N	$F_C = 500$	N

### b) Linearized model

For some tasks, it is possible to work with a linear system model. This is especially true for problems such as stability analysis and controller design. Therefore, linear models of valves and hydraulic cylinders are presented.

In order to derive a linear valve model, the flow through the valve is expressed as a Taylor-series expansion around the operating point,

$$\dot{V}_{Load} = \dot{V}_{Load,0} + \frac{\partial \dot{V}_{Load}}{\partial z_s} \Big|_{O.P.} \Delta z_s + \frac{\partial \dot{V}_{Load}}{\partial p_{Load}} \Big|_{O.P.} \Delta p_{Load} + \dots \quad (10.4.69)$$

The quantity

$$K_{\dot{V}} = \frac{\partial \dot{V}_{Load}}{\partial z_s} \quad (10.4.70)$$

is called the flow gain. The flow-pressure coefficient is defined as

$$K_C = \frac{\partial \dot{V}_{Load}}{\partial p_{Load}} \quad (10.4.71)$$

One can also define the pressure sensitivity

$$K_P = \frac{\partial p_{Load}}{\partial z_s} = \frac{K_C}{K_{\dot{V}}} \quad (10.4.72)$$

These three parameters are termed valve coefficients. With these coefficients, (10.4.64) can be written as

$$\dot{V}_{Load} = K_{\dot{V}} z_s - K_C p_{Load} \quad (10.4.73)$$

which is the valve equation linearized around a certain operating point. The resulting block diagram is shown in Figure 10.25.

The most important point is  $\dot{V}_{Load} = p_{Load} = z_s = 0$ , because all normal operating points will be in the close vicinity of this point. In addition, this operating point is of special importance for the investigation of stability. Here, the flow gain is largest, resulting in a large overall system gain. Furthermore, the flow-pressure coefficient is the smallest, yielding a small damping ratio. Therefore, this is usually the most critical point as far as stability of the system is concerned. The valve coefficients evaluated at this point are called the null valve coefficients.

In most servo-hydraulic applications, zero-lapped valves, also referred to as critical center valves, are used. For them, the values of the valve coefficients will now be determined analytically by differentiating the pressure-flow relation (10.4.17), which for the case at hand can be written as

$$\dot{V}_{Load} = \alpha_D A' z_s \sqrt{\left| \frac{1}{\rho} (p_s - \text{sign}(z_s) p_{Load}) \right|} \text{sign}(p_s - \text{sign}(z_s) p_{Load}) \text{sign}(z_s) \quad (10.4.74)$$

where the direction of the flow is determined by both the spool stroke and the pressure gradient across the orifice. For the following analysis, a positive pressure gradient and a positive spool displacement is assumed. Due to the symmetry assumptions, this can be done without a loss of generality. Taking the partial derivatives results in

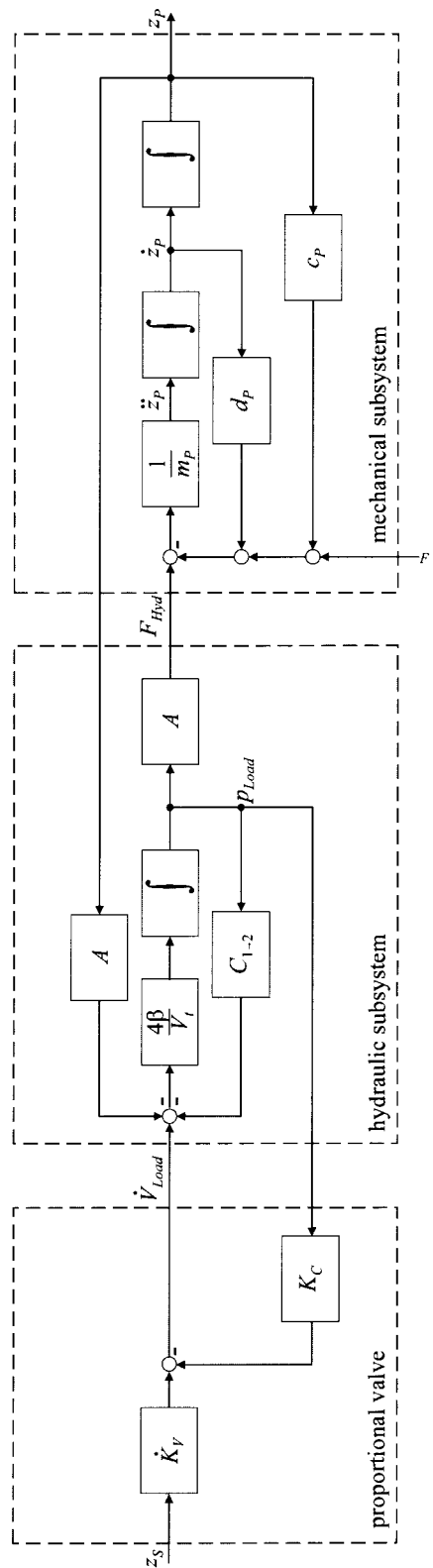


Figure 10.25. Block diagram of the total linearized system of a hydraulic actuator

$$\begin{aligned}
K_{\dot{V}} &= \frac{\partial \dot{V}_{Load}}{\partial z_S} = \alpha_D A' \sqrt{\frac{1}{\rho}} \sqrt{p_S - p_{Load}} \\
K_C &= -\frac{\partial \dot{V}_{Load}}{\partial p_{Load}} = \alpha_D A' z_S \sqrt{\frac{1}{\rho}} \sqrt{p_S - p_{Load}} \frac{1}{2(p_S - p_{Load})} \\
K_p &= \frac{K_{\dot{V}}}{K_C} = \frac{2(p_S - p_{Load})}{z_S}
\end{aligned} \tag{10.4.75}$$

Evaluating these coefficients at the point  $\dot{V}_{Load} = p_{Load} = z_S = 0$  results in

$$\begin{aligned}
K_{\dot{V},0} &= \alpha_D A' \sqrt{\frac{1}{\rho}} \sqrt{p_S} \\
K_{C,0} &= 0 \\
K_{p,0} &\rightarrow \infty
\end{aligned} \tag{10.4.76}$$

For the flow gain, the value matches well with experimental results, Merrit (1967), whereas the other two coefficients should be determined using a different method that determines these coefficients by looking at the center flow curve. The curve is a recording of the leakage flow for a centered spool and blocked load ports. For this experimental configuration, a leakage flow inside the valve can be observed upon pressurization. The slope of the curve at the particular operating pressure can be used as the null flow-pressure coefficient.

Now, the piston dynamics will be linearized. The volume flow into the two chambers can be calculated by evaluating the equation of continuity (10.4.2), which evaluates to

$$\begin{aligned}
\dot{V}_1 - C_{1-2}(p_1 - p_2) &= \frac{\partial V_1}{\partial t} + \frac{V_1}{\beta} \frac{\partial p_1}{\partial t} \\
\dot{V}_2 - C_{1-2}(p_1 - p_2) &= \frac{\partial V_2}{\partial t} + \frac{V_2}{\beta} \frac{\partial p_2}{\partial t}
\end{aligned} \tag{10.4.77}$$

The volume of the two chambers can be calculated as shown in (10.4.67). Here, it is assumed that both piston areas are identical, hence

$$\begin{aligned}
V_1 &= V_{01} + A z_P \\
V_2 &= V_{02} - A z_P
\end{aligned} \tag{10.4.78}$$

The total volume of the cylinder will be denoted  $V_{tot}$ . It is called the *total compressed volume* (or also total contained volume) and is given by

$$V_{tot} = V_{01} + V_{02} = V_1 + V_2 \tag{10.4.79}$$

Equations (10.4.78) and (10.4.79) will now be combined into one equation. Substituting the total compressed volume and the volume flow rate yields

$$\dot{V}_{Load} - 2C_{1-2}p_{Load} = 2A\dot{z}_P + \frac{A\dot{z}_P}{\beta}(\dot{p}_1 + \dot{p}_2) + \frac{V_{01}}{\beta}\dot{p}_1 - \frac{V_{02}}{\beta}\dot{p}_2 \tag{10.4.80}$$

It will be assumed that the initial volume of both chambers is identical,  $V_{01} = V_{02} = V_0$ . Then, the equation simplifies to

$$\dot{V}_{Load} - C_{1-2} p_{Load} + A \dot{z}_P + \frac{V_{tot}}{4\beta} p_{Load} \quad (10.4.81)$$

Since the supply pressure is assumed to be constant, the term

$$\frac{\partial p_1}{\partial t} + \frac{\partial p_2}{\partial t} = \frac{\partial}{\partial t} \left( \frac{p_S - p_V}{2} \right) + \frac{\partial}{\partial t} \left( \frac{p_S + p_V}{2} \right) = \frac{\partial}{\partial t} p_S = 0 \quad (10.4.82)$$

vanishes. The block diagram based on the linearized equations for the pressure build-up in the cylinder chambers is shown in Figure 10.25.

This equation is supplemented by Newton's second equation, which governs the dynamics of the piston

$$A p_{Load} - F_L = m_p \ddot{z}_P + d_p \dot{z}_P + c_p z_P \quad (10.4.83)$$

where  $F_L$  denotes an arbitrary load force on the piston. The block diagram of the mechanical subsystem is illustrated in Figure 10.25.

Equations (10.4.73), (10.4.80) and (10.4.83) are linear and can now be Laplace-transformed to derive the transfer functions of the overall system. The complete transfer function is given by

$$z_p(s) = \frac{\frac{K \dot{V}}{A} z_S(s) - \frac{K^*}{A^2} \left( 1 + \frac{V_t}{4\beta K^*} s \right) F_L(s)}{\frac{m_p V_t}{4\beta A^2} s^3 + \left( \frac{V_t d_p}{4\beta A^2} + \frac{m_p K^*}{A^2} \right) s^2 + \left( \frac{d_p K^*}{A^2} + 1 + \frac{c_p V_t}{4\beta A^2} \right) s + \frac{c_p K^*}{A^2}} \quad (10.4.84)$$

Here,  $m_p$  denotes the driven mass, i.e., piston and load.  $V_t$  is the total compressed volume. A special case can now be considered. Usually, the stiffness of the entire set-up can be neglected. For many systems, the term

$\frac{d_p K^*}{A^2}$  is negligible compared to 1. Then, the transfer function is given

by

$$z_p(s) = \frac{\frac{K \dot{V}}{A} z_S(s) - \frac{K^*}{A^2} \left( 1 + \frac{V_t}{4\beta K^*} s \right) F_L(s)}{s \left( \frac{m_p V_t}{4\beta A^2} s^2 + \left( \frac{V_t d_p}{4\beta A^2} + \frac{m_p K^*}{A^2} \right) s + 1 \right)} \quad (10.4.85)$$

with

$$K^* = K_C + C_{1-2} \quad (10.4.86)$$

Comparing the denominator with a second order system yields a natural frequency of

$$\omega_0 = \sqrt{\frac{4\beta A^2}{m_p V_t}} \quad (10.4.87)$$

and a damping ratio of

$$\zeta = \frac{d_p}{4A} \sqrt{\frac{V_t}{\beta m_p}} + \frac{K^*}{A} \sqrt{\frac{m_p \beta}{V_t}} \quad (10.4.88)$$

These two equations also give hints to the designer on how to reach good system performance. First, (10.4.88) will be discussed. The damping ratio is, in general, influenced by viscous friction as well as flow losses evoked by the leakage flow between the two cylinder chambers. Many hydraulic cylinders are designed as low-friction cylinders. For these, the latter term in (10.4.88) is predominantly influencing the damping ratio. It will now be investigated in detail how different parameters change the system performance.

The parameter  $K^*$  can be increased by increasing the leakage flow between the two chambers. However, this goes along with a decrease in stiffness of the servo-axis. The total mass also influences the damping ratio. Unfortunately, this quantity is most of the time beyond the control of the engineer designing the hydraulic system. It is worthwhile mentioning that for hydraulic systems – as opposed to mechanical spring-mass systems – an increase in mass also increases the damping ratio.

The other variable quantities of the cylinder, namely the active cross-sectional area  $A$  and the total compressed volume in the cylinder, are determined by the required maximum force and displacement and can therefore not be varied. The total compressed volume is given as the sum of the compressed volume of the cylinder and that of the connection lines. One way to reduce the total compressed volume is to shorten the connection lines. It would be best to eliminate the connection lines totally, thus the valve should be mounted right on top of the hydraulic cylinder. The natural frequency (10.4.87) can also be varied by changing the driven mass  $m_p$  or the total compressed volume  $V_t$ . This fact emphasizes the importance of having short connection lines as a means of reducing the total compressed volume.

There are some non-linearities in hydraulic circuits that have not been captured by the linearized model. In the development of the transfer function, a zero-lapped valve was assumed. An underlapped valve increases the leakage flow between the chambers for small or zero spool displacement. In contrast, an overlapped valve introduces a dead band into the control circuit and thus tends to destabilize the entire system. If the spool is displaced, then the valve coefficients will also vary drastically. Upon opening the valve, the load pressure will increase due to the dynamic forces. The inter-chamber leakage will also increase.

During operation of the hydraulic cylinder, the displacement of the piston will vary. This means that the amount of fluid contained in the two cylinder chambers will vary. This causes a change in the stiffness of the so-called oil springs and will thus alter the natural frequency of the system.

## 10.5 PNEUMATIC ACTUATORS

### 10.5.1 Pneumatic Actuating Systems

Pneumatic actuators exploit the physical characteristics of compressed air. The high compressibility of air, along with the capability of storing a larger amount of energy and the low viscosity of the transmission medium, permit the design of efficient and fast drives. Offering a rugged and simple design (only one supply line necessary), these pneumatic drives are well suited to applications where typical forces of a few kN must be supplied by the actuators. They can move at high velocities and over long ranges. Besides these features, they are characterized by very safe operation even under extreme ambient conditions (temperature resistance, contamination resistance, overload capability, explosion-proof construction). The system is immune against interference caused by electric and magnetic fields, as well as radiation, Heinbach *et al.* (1977), Backé (1986a), Schriek, Sonemann (1988), Table 10.25.

**Table 10.25.** Characteristics of pneumatic actuators

advantages	disadvantages
<ul style="list-style-type: none"> <li>• good working capacity;</li> <li>• good thermal operating range;</li> <li>• good power-weight ratio;</li> <li>• high reliability and operating safety;</li> <li>• good price-performance ratio;</li> <li>• one supply line.</li> </ul>	<ul style="list-style-type: none"> <li>• conditioning of compressed air necessary;</li> <li>• to some extent: large dimensions;</li> <li>• friction and compressibility complicate control;</li> <li>• limited positioning accuracy.</li> </ul>
Scope of application:	<ul style="list-style-type: none"> <li>• medium to high actuating force;</li> <li>• medium to high displacement range;</li> <li>• hazardous-duty and high-temperature applications;</li> <li>• high movement speed;</li> <li>• low positioning accuracy.</li> </ul>

Pneumatic actuators basically consist of a valve and an actuating device, which transforms the pneumatic energy into mechanical energy, Figure 10.26. The valve is connected to the pneumatic pressure line, which is supplied by an air compressor and controls the pressurized air flow to the actuating device. Different to hydraulic systems, pneumatic systems require only one forward line and no closed fluid circuit, as the air flows into the environment after expansion.

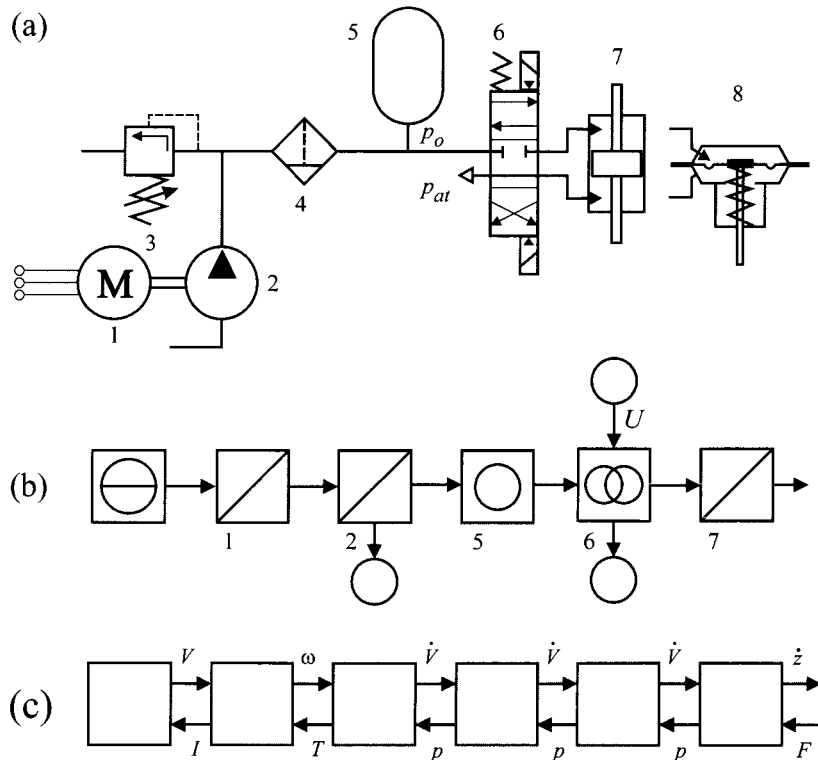


**Figure 10.26.** Pneumatic actuator for linear motion with power supply: (a) schematic; (b) energy flow scheme; (c) two-port representation 1: AC motor; 2: air compressor; 3: pressure relief valve; 4: air filter with water trap; 5: air storage (accumulator); 6: 4/3 proportional valve, solenoid actuation, spring return; 7: double rod cylinder; 8: diaphragm drive

The valves are either switching valves or proportional acting valves. In the case of switching valves, they have usually either two positions for both movement directions of the actuator or three positions for both directions and a holding position. The used symbols for the valves are the same as for hydraulic systems, see Figure 10.15. These switching valves are usually moved by on/off electromagnets.

Proportional acting valves allow a continuous manipulation of the air flow and need a proportional acting electromagnet, frequently with position feedback control.

Pneumatic actuating devices can largely be divided into pneumatic cylinders or diaphragms generating a translatory motion, and air motors generating a rotary motion. Figure 10.27 shows some schemes of pneumatic cylinders. The cylinders consist of a hollow cylindrical tube along which a piston and a ram can slide. The piston with seals or piston rings separates the two chambers. Single-acting cylinders are used when the pressure is applied on one side of the piston and the external force or a return spring is used to provide the opposition of the motion. In the case of double-acting cylinders, the controlled pressures are applied to each

side of the piston and the pressure difference then results in a force and motion of the piston being able to move in either direction. Magnetic coupling between the piston and an outer ring allow a rodless construction. Larger travelways are possible by telescope arrangements.

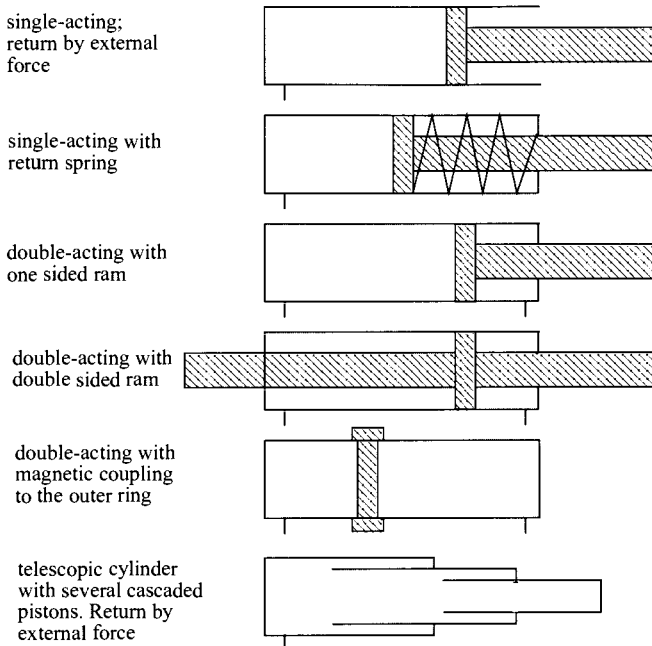


**Figure 10.27.** Schemes of pneumatic cylinders

*Pneumatic diaphragm* actuators are mainly used for flow control valves in the process industries, especially in explosive surroundings or as position control valves as, e.g., for exhaust gas turbochargers or brake force amplifiers in automobiles. Figure 10.28a shows a schematic diagram. It consists of a diaphragm with the controlled pressure on one side and another pressure, most frequently atmospheric pressure, on the other side. The diaphragm is made of rubber, which is centered between two steel discs such that the control part of the diaphragm results in the motion of a shaft. The shaft then acts on a valve or lever construction. Usually, the diaphragm acts against a return spring. In the case of pressure loss, the return spring then closes or opens, e.g., the control valve, dependent on which side of the diaphragm the working pressure is applied and an intended fail-safe position of the valve. This is also referred to as a “closing valve” or “opening valve”.

For both arrangements, the cylinder and the diaphragm, changes in the external force on the ram or shaft result in displacement of the actuator. In addition, the relatively large friction forces of the piston or the shaft have an effect on the precision of positioning. Therefore, a position controller is frequently used to compensate for these negative effects.

For relatively light loads and small displacements, pneumatic *bellows*

can be used, Figure 10.28b. Most commonly they are used as pressure-sensing devices, like in pneumatic controllers.

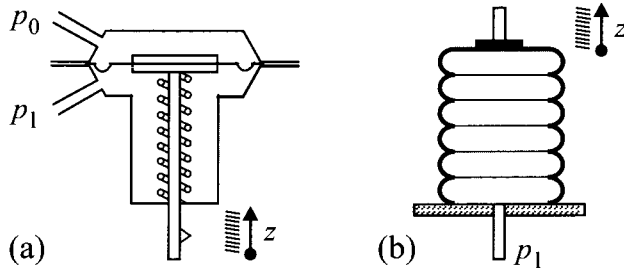


Figure 10.28. (a) pneumatic diaphragm actuator; (b) pneumatic bellow actuator

To generate a continuous rotation, pneumatic motors are available, e.g., as vane types, see Figure 10.29, or piston types. They are intrinsically safe (explosive areas) and robust, but have relatively low efficiency and are noisy. Pneumatic rotary motors are used for tools in manufacturing or on ships or as starters for combustion engines, see Atlas-Copco (1977).

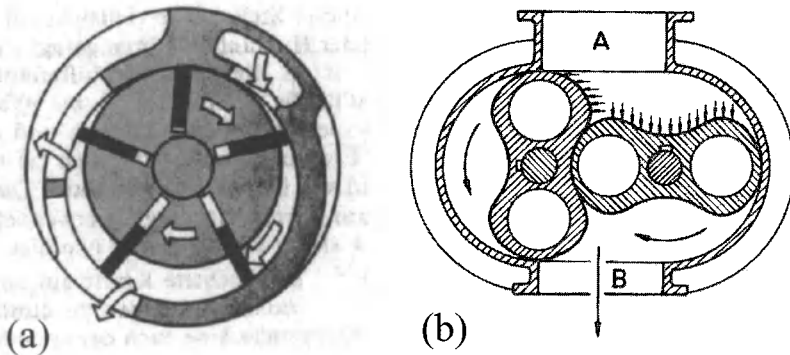


Figure 10.29. Pneumatic rotary motors: (a) vane motor; (b) roots motor

## 10.5.2 Pneumatic Components and their Models

### a) Some gas dynamic properties

Like hydraulic systems, pneumatic systems use a fluid to transmit power between different components. However, the fluid here is the air and is therefore a compressible gas. As the compressibility of fluids is not the dominating property of a hydraulic system and can be neglected in many cases, it is dominating for pneumatic systems. On the other hand, the effect of accelerated masses can be neglected in many cases of pneumatic system behavior.

The principle of linear momentum for a pneumatic line is like for general fluids described by (10.4.1). Also, the flow dynamic equations like Bernouilli's equation (10.4.8) to (10.4.16) dependent on the Reynolds number hold for pneumatic pipes.

The physical states of air, consisting of 79.09% N<sub>2</sub>, 20.25% O<sub>2</sub>, 0.92% Ar, 0.03% CO<sub>2</sub>, 0.002% Ne, 0.0005% He, the pressure, volume, density and temperature follow the constitutive equation of gas, the *gas law* for an ideal gas

$$pV = nR_m T \quad (10.5.1a)$$

or

$$pV = mRT \quad (10.5.1b)$$

or

$$pV = RT \quad (10.5.2)$$

with the specific volume  $v = 1/\rho$ , absolute temperature  $T$  and the gas constant  $R$ . If in (10.5.1a)  $n$  is the quantity in mol, then  $R_m$  is the universal gas constant

$$R_m = 8.314510 \text{ J/mol}\cdot\text{K}$$

and is valid for any ideal gas. However, with  $m$  as the mass of the gas in (10.5.1b),  $R$  is called the specific gas constant and becomes dependent on the type of gas, Table 10.26. The state of the gas is defined if three of the four variables in (10.5.1) or two of the three variables in (10.5.2) are given.

**Table 10.26.** Specific gas constant  $R$  of some gases

Gas	N <sub>2</sub>	O <sub>2</sub>	CO <sub>2</sub>	H <sub>2</sub> O	CO	H <sub>2</sub>	air
R	296.8	259.8	188.9	461.5	296.8	4124.4	286.9

Using (10.5.2), the gas constant  $R$  can be interpreted as the required energy to change the volume of  $m = 1 \text{ kg}$  gas for constant pressure  $p$  through heating by  $\Delta T = 1 \text{ K}$ .

The gas law is valid for ideal gases, which are all gases that are far away from condensation. This holds for all real gases if  $p \leq 1 \text{ bar}$ . For  $p \approx 20 \text{ bar}$ , errors of the gas law are smaller than 1%.

*Caloric equations* of state describe the relation between one caloric state variable and two thermal states. Thus, the specific inner energy of an ideal gas is

$$u = c_v T \quad (10.5.3)$$

with  $c_v$  the specific heat capacity for constant volume. For the enthalpy, it is valid that

$$h = c_p T \quad (10.5.4)$$

where  $c_p$  is the specific heat capacity for constant pressure. Further, it holds that

$$R = c_p - c_v \quad (10.5.5)$$

The isentropic exponent (adiabatic coefficient) is defined as

$$\kappa = c_p / c_v \quad (10.5.6)$$

and is for one atomic gas  $\kappa = 1.66$ , for two atomic gases  $\kappa = 1.4$  and for three atomic gases  $\kappa = 1.3$ . Some characteristic properties of air are given in Table 10.27.

Changes of state of gases are usually represented in  $p$ - $v$  diagrams or  $T$ - $s$  diagrams ( $s$ : entropy). According to the gas law, the state of one variable depends for a certain mass of gas on two other variables as, e.g.,  $p = f(v, T)$ . Therefore, generally three-dimensional trajectories result.

**Table 10.27.** Characteristic properties of air

variable	density	specific volume	specific heat $p = \text{const.}$	specific heat $v = \text{const.}$	gas constant		heat conduction coefficient
symbol	$\rho$	$v$	$c_p$	$c_v$	$R$	$\kappa = \frac{c_p}{c_v}$	$\lambda$
dimension	$\frac{\text{kg}}{\text{m}^3}$	$\frac{\text{m}^3}{\text{kg}}$	$\frac{\text{J}}{\text{kg K}}$	$\frac{\text{J}}{\text{kg K}}$	$\frac{\text{J}}{\text{kg K}}$	-	$\frac{\text{W}}{\text{m K}}$
defined at	273 K 1.013 bar	273 K 1.013 bar			ideal gas		293 K 1.013 bar
value	1.293	0.773	1005	718	287	1.4	0.026

To simplify the graphic representation and calculation, special assumptions are made to obtain two-dimensional state equations or family of curves. They are called isobaric if  $p = \text{const.}$ , isochoric if  $v = \text{const.}$ , isothermal if  $T = \text{const.}$  and isentropic if  $s = \text{const.}$  (or no heat loss). Real changes of gas state are polytropic and are characterized by the polytropic state equation between two states

$$p_1 v_1^n = p_2 v_2^n \quad (1 \leq n \leq \kappa) \quad (10.5.7)$$

Then, the special changes of state follow with  $n = 0$  for isobaric,  $n = \infty$  for isochoric,  $n = 1$  for isothermal and  $n = \kappa$  for isentropic state changes. Applying the specific gas law (10.5.2) yields

$$\frac{v_1}{v_2} = \left( \frac{P_2}{P_1} \right)^{\frac{1}{n}} = \left( \frac{T_2}{T_1} \right)^{\frac{1}{n-1}} \quad (10.5.8)$$

and the external work becomes

$$\begin{aligned} W_{12} &= m \int_{1}^{2} p \, dv = m(T_1 - T_2)R/(n-1) \\ &= mp_1 v_1 \left[ 1 - (p_2/p_1)^{(n-1)/n} \right] / (n-1) \end{aligned} \quad (10.5.9)$$

and the technical work

$$W_t = m \int_1^2 v dp = n W_{12} \quad (10.5.10)$$

Now, a certain closed air volume  $V$  is considered (like on one side of a cylinder with piston). If the compressibility module or elasticity module is defined as for hydraulic oil, (10.4.19)

$$E_{\text{gas}} = -V \left( \frac{\partial p}{\partial V} \right) \quad (10.5.11)$$

then it follows from the polytropic state equation

$$\begin{aligned} pV^n &= K_{\text{pol}} \\ \frac{\partial p}{\partial V} &= -\frac{K_{\text{pol}}n}{V^{n+1}} \\ E_{\text{gas}} &= \frac{K_{\text{pol}}n}{V^n} = np \end{aligned} \quad (10.5.12)$$

Hence, the compressibility module only depends on the pressure  $p$  and the polytropic exponent  $n$ .

The stiffness of the closed air volume in a cylinder with area A results in

$$c_{\text{gas}} = \frac{dF}{dz} = A \frac{dp}{dz} = A \frac{dp}{dV} \frac{dV}{dz}$$

The volume is

$$V = V_0 - Az$$

and with  $dV/dz = -A$ , it holds that

$$c_{\text{gas}} = -A^2 \frac{dp}{dV}$$

Introducing (10.5.11) leads to

$$c_{\text{gas}} = -A^2 \frac{E_{\text{gas}}}{V} = A^2 \frac{np}{V} = \frac{A}{z} np \quad (10.5.13)$$

Therefore the stiffness is inverse proportional to the deflection  $z$  and proportional to the pressure  $p$  at the operating point.

### b) Pneumatic control valves

For manipulating the air flow, pneumatic control valves are used. The various types are the same or at least similar to those of Figures 10.13 to 10.15 and 10.17 for hydraulic systems. However, the flow characteristic through a valve is different, due to the compressibility of the air and sound velocity.

A gas flow from a container with pressure  $p_1$  and temperature  $T_1$  through a nozzle with rounded shape into a container with pressure  $p_2$  and

temperature  $T_2$  is considered, see Figure 10.30. It is assumed that the flow is without friction and without heat exchange with the environment, hence an isentropic flow. Then it follows from the energy balance that

$$h_1 + \frac{v_1^2}{2} = h_2 + \frac{v_2^2}{2} \quad (10.5.14)$$

With the assumption for the velocities  $v_1 \ll v_2$ , it holds that

$$\frac{v_2^2}{2} = h_1 - h_2 = c_p(T_1 - T_2)$$

Introducing the gas equation, specific heat capacity and isentropic state equation

$$T_1 = \frac{p_1}{R\rho_1}; \quad \frac{c_p}{R} = \frac{\kappa}{\kappa-1}; \quad \left(\frac{T_2}{T_1}\right) = \left(\frac{p_2}{p_1}\right)^{\frac{\kappa-1}{\kappa}}$$

leads to the outflow velocity

$$v_2 = \sqrt{2 \frac{\kappa}{\kappa-1} \frac{p_1}{\rho_1} \left[ 1 - \left( \frac{p_2}{p_1} \right)^{\frac{\kappa-1}{\kappa}} \right]} \quad (10.5.15)$$

The mass flow follows with  $\dot{m} = A\rho_2 v_2$  (10.5.8)

$$\dot{m} = A\Psi \sqrt{2p_1\rho_1} = A\Psi p_1 \sqrt{\frac{2}{RT_1}} \quad (10.5.16)$$

where the outflow function is

$$\Psi = \sqrt{\frac{k}{\kappa-1} \left[ \left( \frac{p_2}{p_1} \right)^{\frac{2}{\kappa}} - \left( \frac{p_2}{p_1} \right)^{\frac{\kappa+1}{\kappa}} \right]} \quad (10.5.17)$$

$\Psi$  depends on  $p_2/p_1$  and has a maximum at

$$d\Psi/d(p_2/p_1) = 0$$

The pressure ratio  $p_2/p_1$  at the maximum outflow function is called the critical pressure ratio and is

$$\left( \frac{p_2}{p_1} \right)_{crit} = \left( \frac{2}{\kappa+1} \right)^{\frac{k}{\kappa-1}} = 0.53 \quad (10.5.18)$$

for air. Then, the maximum of the outflow function becomes

$$\Psi_{max} = 0.484$$

Figure 10.31 shows the outflow function  $\Psi(p_2/p_1)$ . For constant  $p_1$  and decreasing  $p_2$ , the outflow function increases until  $\Psi_{max}$  and holds this value also for smaller  $p_2$  because the sound velocity

$$v_{2crit} = a = \sqrt{\frac{2\kappa}{\kappa+1} \frac{p_1}{p_1}} = \sqrt{\frac{2\kappa}{\kappa+1} R T_1} \quad (10.5.19)$$

is reached. Hence, for overcritical  $p_2/p_1 > 0.53$ , the mass flow  $\dot{m}$  only depends on  $p_1$  and  $T_1$ , see Backé (1986a).

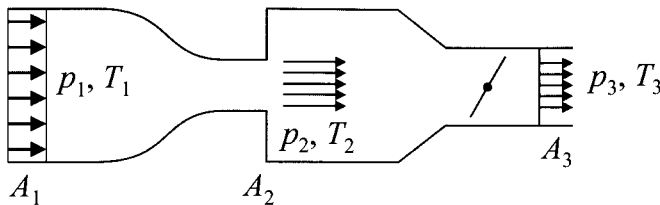


Figure 10.30. Gas flow through a contraction (nozzle)

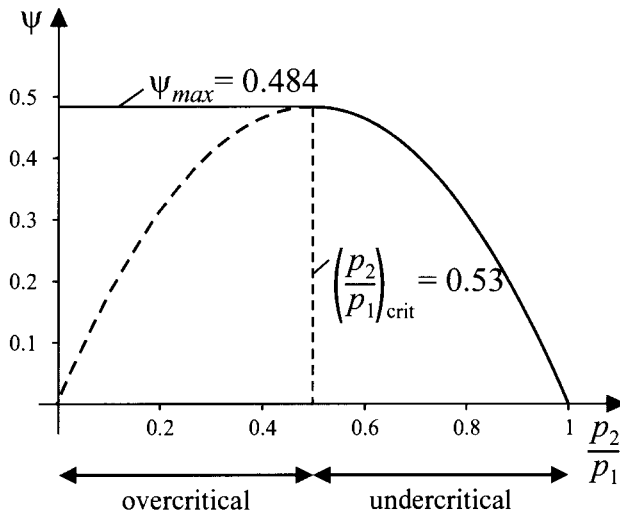
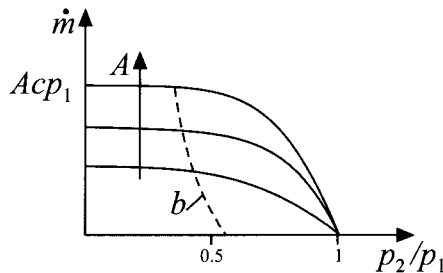


Figure 10.31. Outflow function for air with  $\kappa = 1.4$

For practical use, an approximation of (10.5.16) can be used, ISO/DIN 6358

$$\dot{m} = \begin{cases} Ac p_1 & \frac{p_2}{p_1} < b \\ Ac p_1 \sqrt{1 - \left( \frac{p_2/p_1 - b}{1-b} \right)^2} & b \leq \frac{p_2}{p_1} \leq 1 \end{cases} \quad (10.5.20)$$

With this equation, pneumatic resistances can be described, where the parameters  $c$  and  $b$  are determined experimentally, Minxue *et al.* (1986). Figure 10.32 shows the resulting characteristics for a flow valve. The cross-sectional area  $A$  of the valve depends on the manipulated variable  $U$ .

**Figure 10.32.** Flow characteristic of a pneumatic valve**c) Pneumatic pressure storages (accumulators)**

A gas storage with volume  $V_s$  according to Figure 10.33 with a gas mass flow  $\dot{m}_1(t)$  at the inlet and  $\dot{m}_2(t)$  at the outlet is considered. It is assumed that no flow resistance occurs, *i.e.*,  $p_1(t) = p_2(t) = p_s(t)$ . The mass flow balance then yields

$$\dot{m}_1(t) - \dot{m}_2(t) = \frac{d}{dt} m_s(t) = \frac{d}{dt} V_s \rho(t) = V_s \frac{d\rho(t)}{dt} \quad (10.5.21)$$

If a polytropic gas equation holds

$$p v^n = p \left( \frac{1}{\rho} \right)^n = k_{pol}$$

then

$$\rho_s = \left( \frac{1}{k_{pol}} p_s \right)^{\frac{1}{n}}$$

and

$$\frac{dp_s}{dt} = \frac{1}{nk_{pol}^{\frac{1}{n}}} p_s(t)^{\frac{1}{n}-1} \frac{dp_s}{dt}$$

Thus, it leads to

$$\dot{m}_1(t) - \dot{m}_2(t) = \frac{V_s}{nk_{pol}^{\frac{1}{n}}} p_s(t)^{\frac{1}{n}-1} \frac{dp_s}{dt}$$

and with

$$m_s(t) = V_s \rho_s(t) = V_s \left( \frac{1}{k_{pol}} p_s(t) \right)^{\frac{1}{n}}$$

it becomes

$$\dot{m}_1(t) - \dot{m}_2(t) = \frac{m_s(p)}{n} \frac{1}{p_S(t)} \frac{dp_S(t)}{dt} \quad (10.5.22)$$

The gas volume therefore has non-linear integral behavior with a pressure-dependent integration time

$$T_I(p_S) = \frac{m_s(p_S)}{np_S} = \frac{V_S}{nk_{pol}} p_S^{\frac{1}{n}-1} \quad (10.5.23)$$

Only for isothermal state with  $n = 1$  the mass balance becomes linear with  $T_I = V_S k_{pol}^{-1}$

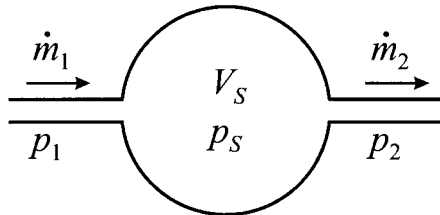


Figure 10.33. Schematic of a gas storage (accumulator)

#### d) Pneumatic valve-accumulator elements and transmission lines

A valve and a storage are now connected to a *valve-accumulator element* as shown in Figure 10.34a. The cross-sectional area  $A$  of the valve can be changed by the manipulated variable  $U$ . Figure 10.34b represents a two-port representation, assuming that the valve is supplied by a pressurized tank source. (Here, the volume flows  $\dot{V} = \dot{m}/\rho$  are used according to the power variable definitions of Table 2.3.) Assuming  $\dot{m}_2 = \dot{m}_1$  and  $p_2 = p_S = p_3$ , it follows that with (10.5.16) and (10.5.22)

$$\dot{m}_1 = A(U) \Psi \left( \frac{p_3}{p_1} \right) p_1 \sqrt{\frac{2}{RT_1}} \quad (10.5.24)$$

$$\dot{m}_1(t) - \dot{m}_3(t) = \frac{1}{T_I(p_3)} \frac{dp_3(t)}{dt} \quad (10.5.25)$$

This leads to the block diagram shown in Figure 10.35 showing several non-linearities through multiplications and characteristics.

A simplification of the non-linear relation can be made for small changes around a certain operation point. This leads to the valve equation

$$\begin{aligned} \Delta \dot{m}_1 &= \frac{\partial \dot{m}_1}{\partial p_1} \Delta p_1 + \frac{\partial \dot{m}_1}{\partial p_2} \Delta p_2 \\ &= A [c_1 \Delta p_1 + c_2 \Delta p_2] \end{aligned} \quad (10.5.26)$$

Another, simpler approach is to use the pressure loss equation (10.4.18) for the turbulent flow of orifices in the case of undercritical pressure ratio.

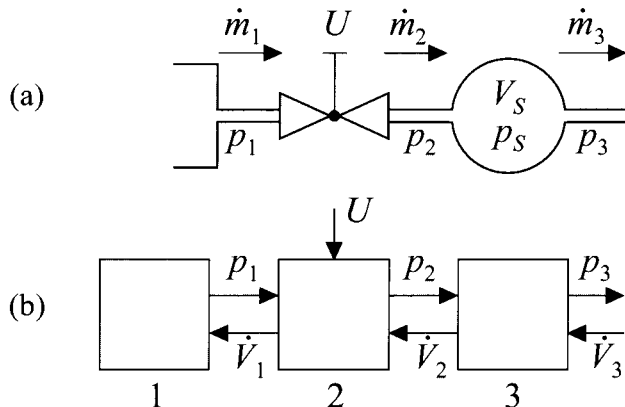


**Figure 10.34.** Pneumatic valve-accumulator element: (a) schematic; (b) two-port representation. 1: source; 2: valve; 3: accumulator

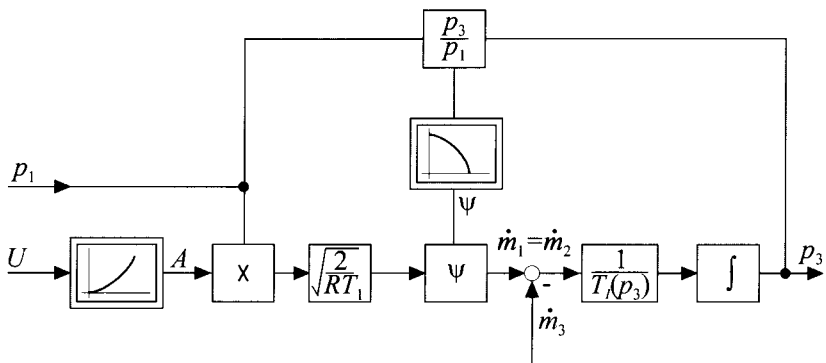


**Figure 10.35.** Signal flow diagram of the valve-accumulator element of Figure 10.34

Then, it holds that

$$\dot{m}_1 = A \sqrt{\frac{2\rho}{\zeta}} \sqrt{p_1 - p_2} \quad (10.5.27)$$

Linearization of this equation around a certain operation point  $(A, p_1, p_2, \dot{m}_1)$  leads to

$$\Delta \dot{m}_1 = \frac{\partial \dot{m}}{\partial p_1} \Delta p_1 + \frac{\partial \dot{m}_1}{\partial p_2} \Delta p_2 - \Delta p_2 + \frac{\partial \dot{m}_1}{\partial A} \Delta A \quad (10.5.28)$$

with

$$\frac{\partial \dot{m}_1}{\partial p_1} = - \frac{\partial \dot{m}_2}{\partial p_2} = A c_3 = A \sqrt{\frac{\rho}{2\xi}} (p_1 - p_2)^{\frac{1}{2}}$$

$$\frac{\partial \dot{m}_1}{\partial A} = c_4 = \sqrt{\frac{2\rho}{\xi}} \sqrt{p_1 - p_2}$$

Finally, with linearization of the valve characteristics

$$\frac{\partial A}{\partial U} = c_5$$

and  $\Delta p_2 = \Delta p_3$ , a linearized signal flow diagram as given in Figure 10.36 results. After Laplace transformation, one obtains

$$\Delta p_3 = \frac{1}{Ts + 1} \left[ \frac{c_4 c_5}{A c_3} \Delta U(s) + \Delta p_1(s) - \frac{1}{A c_3} \Delta \dot{m}_3(s) \right] \quad (10.5.29)$$

Hence, first order transfer functions with time constant

$$T = \frac{1}{A c_3} T_I = \frac{m_s}{p_3 A c_3} \quad (10.5.30)$$

result, assuming an isothermal state change with  $n = 1$ . Therefore, a valve-accumulator can be roughly described by a first order lag element if only small deviations are considered and undercritical pressure ratio across the valve applies.

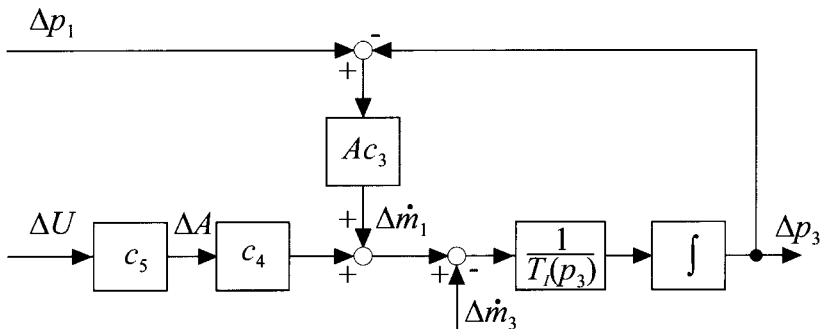


**Figure 10.36.** Signal flow diagram of the linearized behavior of the valve-accumulator element of Figure 10.34 for an undercritical pressure ratio

For an overcritical pressure ratio, the mass flow through the valve does not depend on the pressure  $p_3$  in the storage and the transfer behavior becomes

$$\Delta p_3(s) = \frac{1}{T_I s} \left[ c_4 c_5 \Delta U(s) + A c_3 \Delta p_1(s) - \Delta \dot{m}_3(s) \right] \quad (10.5.31)$$

which means integral behavior.

*Pneumatic transmission lines* can be considered as distributed resistance-volume elements. For not-too-long lines, a lumped parameter approach is applicable as shown in Figure 10.35 and the linearized model (10.5.29) with  $\Delta U = 0$  can be used.

### e) Pneumatic translatory motors

Pneumatic translatory motors have the same construction principle as shown in Figure 10.18 for hydraulic cylinders. Also, the same equations (10.4.45) for the volume flows hold if the compressibility module  $\beta$  of oil is replaced by the compressibility module of gas  $E_{gas} = np$ , (10.5.12)

$$\begin{aligned}\dot{p}_1(t) \frac{\frac{V_{01} + A_1 z(t)}{np_1(t)}}{np_1(t)} + A_1 \dot{z}(t) &= \dot{V}_1(t) \\ \dot{p}_2(t) \frac{\frac{V_{02} - A_2 z(t)}{np_1(t)}}{np_1(t)} - A_2 \dot{z}(t) &= \dot{V}_2(t)\end{aligned}\quad (10.5.32)$$

If the mass flow  $\dot{m}(t)$  is used instead of the volume flow  $\dot{V}$ , one obtains with  $m = V\rho$  and the gas equation (10.5.1b)

$$\begin{aligned}\dot{p}_1(t) \left[ \frac{V_{01} + A_1 z(t)}{np_1(t)} \right] + np_1(t) A_1 \dot{z}(t) &= nRT_0 \dot{m}_1(t) \\ \dot{p}_2(t) \left[ \frac{V_{02} - A_2 z(t)}{np_1(t)} \right] - np_2(t) A_2 \dot{z}(t) &= nRT_0 \dot{m}_2(t)\end{aligned}\quad (10.5.33)$$

where  $T_0$  is a reference temperature, e.g., the supply air temperature. For isothermic state changes,  $n = 1$  can be assumed, and the dynamic behavior of the pressure in chamber 1 becomes

$$\dot{p}_1(t) + \frac{A_1}{V_{01} + A_1 z(t)} \dot{z}(t) p_1 = \frac{RT_0}{V_{01} + A_1 z(t)} \dot{m}_1(t) \quad (10.5.34)$$

Hence, the parameters of this pressure differential equation are time-variant and depend on the mechanical motion of the piston. The resulting signal flow for this pneumatic part is shown in Figure 10.37, left cylinder chamber.

The pressures in both cylinder chambers generate the force on the piston. The balance of forces on the piston rod is the same as for hydraulic cylinders and follows (10.4.48). Finally, a complete signal flow diagram can be drawn as in Figure 10.37, Keller (1994). The servo-valve with position controller can be approximated by a first order lag with time constant  $T_{valve}$ .

### 10.5.3 Model-based Control of a Pneumatic Servo-axis

Pneumatic cylinder-piston actuators are mainly used for transportation and assembling tasks. Due to their non-linear behavior, they operate predominantly with limit stops or brakes. The non-linear static and dynamic behavior results from the compressibility of the air, the friction of the piston and the characteristics of the electromechanical proportional control valves. Therefore, precise motion control is rather involved and does not result in sufficient control performance with linear controllers only.

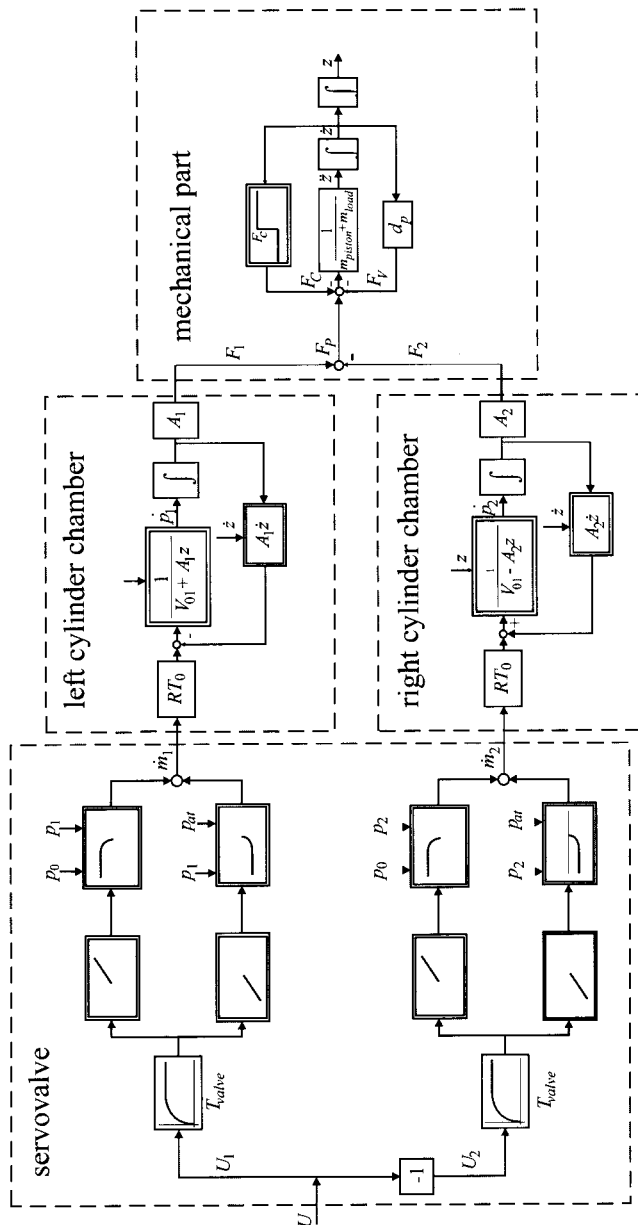
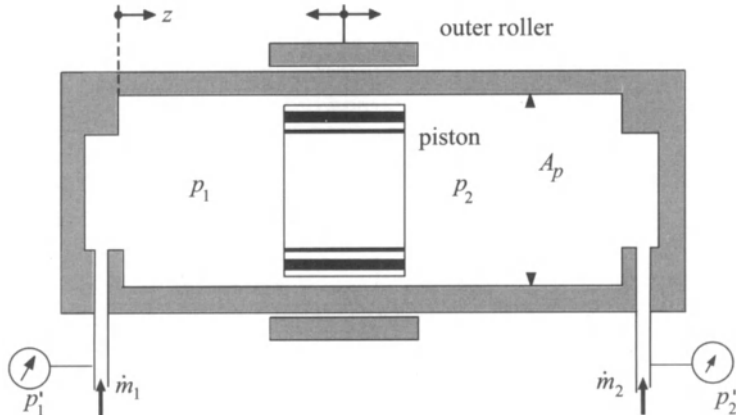


Figure 10.37. Signal flow diagram of a pneumatic servo-axis, Keller (1994).  $p_0$ : supply pressure;  $p_{at}$ : atmospheric pressure

In the following, it will be shown how through a non-linear model-based adaptive control system it becomes possible to obtain a relatively high position accuracy, Keller (1994).

The investigated pneumatic actuator is a standard pneumatic cylinder as shown in Figure 10.38. The motion transmission of the outer roller is obtained by magnetic coupling. The positioning range is 200 mm and the piston diameter is 25 mm, which leads to a force of 213 N by applying a pressure of 6 bar.



**Figure 10.38.** Scheme of the investigated pneumatic cylinder

Process input is a voltage  $V$  that manipulates the mass flows, either  $\dot{m}_1$  or  $\dot{m}_2$ , into the cylinder chambers through a control valve. Then, either chamber 2 or 1 is connected to atmospheric air. The position  $z$  can be measured by a linear potentiometer. In addition, the pressures  $p_1'$  and  $p_2'$  at the cylinder tube connections are available.

Theoretical modeling leads to a model with several dynamic non-linearities as is shown in Figure 10.37. Here,  $A_1 = A_2 = A_p$ . Therefore, a static non-linear correction only will not work. However, the implementation of an underlying differential pressure control loop with a simple P-controller is able to generate an adjustable input force  $F_p$  to the piston. This control then requires the knowledge of the difference pressure  $\Delta p = p_1 - p_2$ .

A further significant non-linearity of this actuator is the friction. The typical stiction force is roughly 45 N (21% of the nominal input force) and values of about 30 N have been estimated for Coulomb friction via system identification. Therefore, friction compensation is required. Further, because the friction force changes with time, the friction compensation should be adaptive.

Figure 10.39 depicts the implemented overall control strategy with state controller, underlying differential pressure control and adaptive feedforward friction compensation. The pressure difference control of  $\Delta p = p_1 - p_2$  is based on the model-based reconstruction of the chamber pressure  $p_1$  and  $p_2$  based on the measurements of  $p_1'$  and  $p_2'$ . Furthermore, the position of  $z$  is measured and the speed  $\dot{z}$  and acceleration  $\ddot{z}$  are determined by numerical differentiation.

Feedforward friction compensation, as is shown in Figure 10.9, yields continuous oscillations with an amplitude of at least 0.5 mm. This occurs due to the non-negligible dynamics of the underlying difference pressure loop. Therefore, the compensation has to be switched off if the control variable  $z$  lies within a tolerance band ( $\pm 0.05$  mm) of the set point  $r$ .

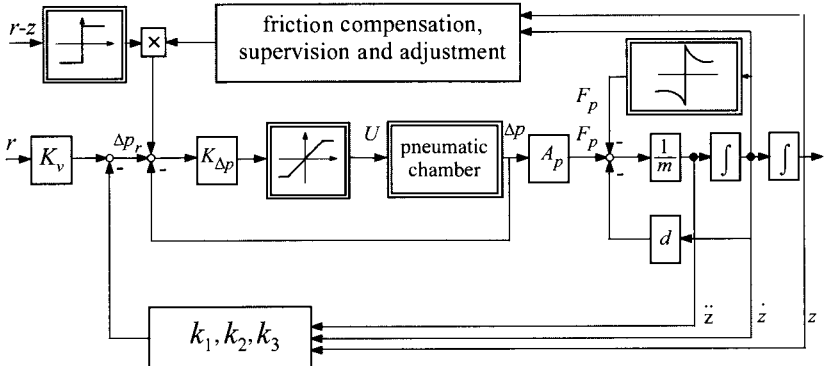


**Figure 10.39.** Overall structure for the adaptive non-linear positioning control of a pneumatic actuator with friction compensation

As several investigations have shown, *e.g.*, Rusterholz (1985), Chen, Leufgen (1987), friction forces of pneumatic cylinders are highly position-dependent and vary with the applied pressure as well as with the time period of standstill. Therefore, under- and overcompensation is very likely and supervision of the steady state control behavior must take place in order to adapt the amplitude of the compensation values. The amplitude will be reduced if oscillations are detected and increased if the control value does not lie in the set point tolerance band. This is done by “friction compensation supervision and adjustment” (FCSA), Keller (1994). Figure 10.40 shows the improvement by friction compensation.

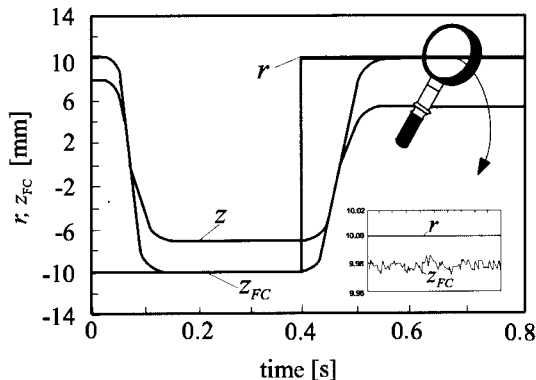


**Figure 10.40.** Comparison of the position control performance without and with (index<sub>FC</sub>) adaptive friction compensation,  $T_0 = 1 \text{ ms}$ ,  $m = 3.5 \text{ kg}$

The state controller values ( $k_1, k_2, k_3$ ) are obtained by numerical optimization of a quadratic loss function using a non-linear system model. Without friction compensation, an offset of about 3 mm is obtained. Applying friction compensation, the positioning accuracy is significantly improved to about 0.05 mm.

This is an example where the negative properties of the pneumatic

actuator are compensated for a considerable degree by model-based control. Hence, integration by information processing takes place to result in an appropriate overall behavior of the pneumatic mechatronic actuator.

#### 10.5.4 Models of a Pneumatic Valve

Fluid flow is frequently controlled by means of pneumatically driven valves. These pneumatic valves are composed of two units: a pneumatic and a mechanical subsystem, Figure 10.41. The pneumatic subsystem comprises a chamber sealed by a diaphragm that is acting on the valve stem. At the tip of the valve stem, a body is mounted which, in conjunction with its counterpart, the valve seat, controls the hydraulic flow. Depending on the precision accuracy and the kind of fluid, different geometries are used. For very precise control tasks, usually needle-shaped bodies are used, whereas disc- or ball-shaped bodies are commonly chosen for fully opening and closing valves. The stem passes through a gland in order to seal the hydraulic system. Figure 10.41 shows a cross-sectional view of such a valve. A position controller is mounted directly on the valve.

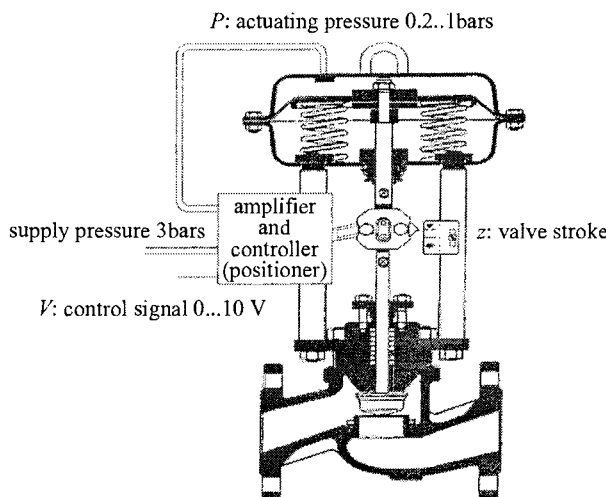


**Figure 10.41.** Cross-sectional view of a pneumatic valve

The valve contains an inner pneumatic control loop, which varies the displacement of the valve stem in accordance with the input voltage. By means of a nozzle-flapper arrangement, the control error between the valve stem position and its reference value is sensed and the pressure supplied to the diaphragm chamber is varied accordingly. Since the nozzle-flapper arrangement would not be able to supply a sufficient air flow, an air amplifier is connected in between the nozzle-flapper arrangement and the working chamber.

For modeling of the valve, the same equation as for the pneumatic cylinder can be used if  $A_D$  is the area of the diaphragm,  $z$  the position of

the valve stem and  $c_s$  the constant of the return spring. Figure 10.42 shows the resulting signal flow diagram. For more details see Deibert (1997).

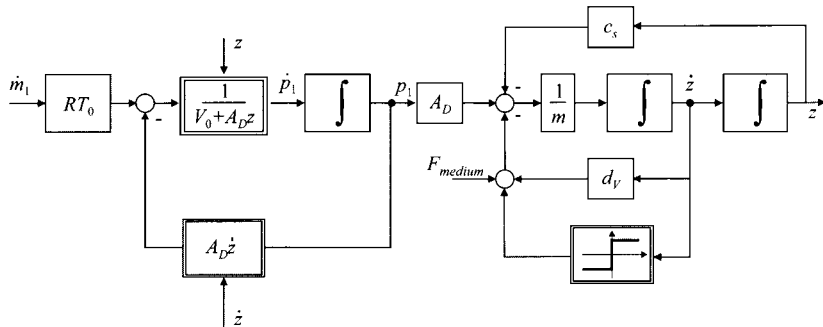


**Figure 10.42.** Signal flow diagram of a pneumatic flow valve

Usually, the hysteresis effect of the friction of the gland is compensated for by a position controller. However, if no position controller can be applied, limit cycles can appear in the closed-loop flow control. In this case, an adaptive friction compensation as shown in the last Section 10.5.4 can improve the control behavior considerably. This was demonstrated by Schaffnit (2002) for the position control of a pneumatic actuator for a variable geometry turbocharger of a diesel engine.

## 10.6 UNCONVENTIONAL ACTUATORS

Over the past few years, a number of new concepts for “unconventional actuators” have been developed and existing designs have been improved, which can be attributed to both the on-going research in the area of materials science and the application of modern manufacturing technologies. The commonality of these actuators is the fact that they use certain physical phenomena. However, the different technical realizations exhibit a large degree of specialization, which leads to a limited scope of application. The high cost of these materials further limits the spread of these actuators. Presently, especially the development of piezoelectric actuators or traveling-wave motors show an interesting prospect for the future.

A survey of unconventional actuating principles is summarized in Table 10.28. The first main group consists of the so-called direct energy converters, such as piezoelectric, electroviscous and magnetostrictive actuators. They generate a force by changes in the atomic/molecular structure upon energization by an electric input signal. Their main area of application is for fast and highly precise positioning tasks with a very small stroke.

**Table 10.28.** Overview of unconventional actuators (normal: translatory motion; *italic*: rotary motion)

generation of force	actuator	technical realization
molecular forces (direct energy converters)	piezoelectric actuator	stack design <i>bending actuator</i> <i>traveling-wave motor</i> <i>inchworm motor</i>
	magnetostrictive actuator	linear actuator <i>inchworm motor</i>
	electroviscous fluid	adjustable dampers <i>clutches</i>
shape memory effect	shape memory alloys	<i>bending actuator</i> <i>torsional actuator</i>
thermal expansion	thermo-bimetal	<i>bending actuator</i>
	thermal expansion elements	membrane actuator elastomer actuator
chemical reaction forces	electromechanical actuators	pyrotechnic actuator
	electrochemical actuator	membrane actuator

Shape memory alloys and thermal expansion actuators do not necessarily need an auxiliary power supply. The actuation energy can be gathered from the surroundings (e.g., ambient heat for the control of a radiator).

In the following, some concepts for unconventional actuators will be examined in more detail. The interested reader is also referred to survey articles by Janocha (1992), Lenz *et al.* (1990), Tautzenberger (1989). Introductions to smart materials are given by Srinivasan, McFarland (2000) and Culshaw (1996). The technology field of smart materials refers to active materials. Upon one or more input stimuli, these materials change their shape or exchange energy with the surroundings. This characterizes these materials as energy converters. In the literature, these materials are referred to as smart materials, active materials, as well as adaptive materials interchangeably. Typically, the group of active materials encompasses piezoelectric actuators, magnetostrictive actuators, electrostrictive actuators, shape memory alloys and thermo-bimetals. Since the area of unconventional actuators is fairly new, the aforementioned definitions are still evolving.

### 10.6.1 Thermo-bimetals

Thermal expansion describes the effect of materials changing their length if subject to a temperature change. This effect can be exploited for thermo-bimetals. If two materials with different coefficients of thermal expansion are joined together and the temperature changes, one metallic strip will contract or expand more than the other and thus the beam starts to bend. If the beam is encumbered in its bending motion, it can be used as a “force actuator”. Instead of the motion, tension inside the thermo-bimetal starts to build up. Thus, the thermo-bimetal can store energy, comparable to a spring. The functional principle of thermo-bimetal actuators is shown in Figure 10.43.

The change in temperature of the thermo-bimetal may not only be

caused by a change in the ambient temperature, but can also be evoked by means of heat radiation or convection as well as electrical heating. For the latter, one differentiates indirect heating by an electrical heating element, mounted close by the thermo-bimetal, and direct heating, where the current is conducted by the thermo-bimetal itself (*e.g.*, thermal fuses for all kinds of electrical machinery). A summary of the material properties, the areas of application as well as the major features of thermo-bimetals is given in Table 10.29.

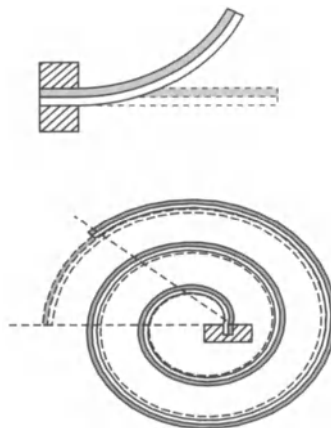


**Figure 10.43.** Thermo-bimetal actuators

**Table 10.29.** Main features of thermo-bimetals, Rau (1974)

design principle	change of shape due to different thermal expansion of two metals
advantages	disadvantages
<ul style="list-style-type: none"> <li>available in different sizes and shapes;</li> <li>inexpensive;</li> <li>linear temperature-displacement relationship over a wide range of temperatures.</li> </ul>	<ul style="list-style-type: none"> <li>small actuation forces;</li> <li>only bending motion can be realized directly;</li> <li>small energy density.</li> </ul>
areas of application	<ul style="list-style-type: none"> <li>electric toaster;</li> <li>fuse.</li> </ul>
physical properties (according to DIN 1715, <i>e.g.</i> , for TB 1425)	applicable up to 450°C specific curvature $26.1 \cdot 10^{-6}$ 1/K Young's modulus $170 \cdot 10^3$ N/mm <sup>2</sup> maximum bending stress 200 N/mm <sup>2</sup> specific resistance $0.26 \cdot 10^{-6}$ Ω m density $8.3 \cdot 10^3$ kg/m <sup>3</sup> linear range -20°C to 200°C

## 10.6.2 Shape Memory Alloys

Shape memory alloys are materials that can “remember” shapes, *i.e.*, they can return to some previously defined shape when subject to a certain thermal procedure. This behavior is known as the *shape memory effect* and

arises from a change in phases. The change is between two solid phases and embraces a rearrangement of the atoms in the crystal lattice. Depending on the ambient temperature or applied stress and strain, the shaped memory alloy takes up one of two different crystalline configurations. *Martensite* is the low-temperature phase and shows a highly twinned crystalline structure, whereas *austenite* is the phase that exists at higher temperatures and is based upon a body-centered cubic structure. By applying external forces in the martensitic phase, the highly twinned structure can be de-twinned. The entire process is depicted in Figure 10.44.

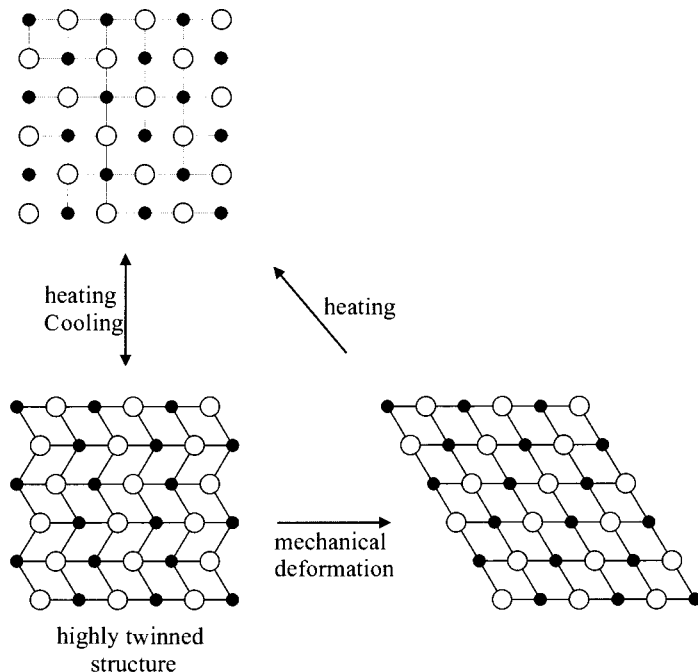


**Figure 10.44.** Crystal lattice of a shape memory alloy (one-way effect)

The shape memory alloy (SMA) can react to its cooling down in two different ways. With the so-termed one-way shape memory effect, elements just remain in the shape they had while being in the austenitic configuration. In contrast, the two-way shape memory elements assume their old shape again, thus they have been taught two different shapes, which can be recalled unlimitedly just by changing the temperature of the shape memory alloy. While both the one-way and the two-way elements can generate rather large forces during heating up, the force exerted by the two-way element during cooling down is rather limited.

The applicability of SMAs will be determined mainly by their transformation time and characteristic temperature. There are a magnitude of different shape memory alloys available today with transition temperatures between  $-100^{\circ}\text{C}$  and  $+100^{\circ}\text{C}$ . Most alloys are nickel-titanium or copper-zinc-aluminum alloys. A summary of the features of shape memory alloys is given in Table 10.30. This table also lists material properties

of nickel-titanium alloys. The temperature change of the shape memory alloy can be evoked by different means. First of all, an electric heater can be mounted on the elements. The element may also be heated up by a current flowing through the element itself. Also, the element can dissipate heat from the surroundings, such as, *e.g.*, from a fluid the shape memory element is immersed into. More problematic, however, is the cooling down of the material. Here, one has two competing design goals. During static phases, the energy consumption should be minimized, which mandates good insulation of the SMA. During the cooling down, however, the heat energy should be purged as fast as possible, which is hindered by the insulation. Another possibility would be the introduction of an active cooling element. This, however, makes the actuator more bulky.

**Table 10.30.** Main features of shape memory alloys

actuating principle	change of shape during transitions from and to martensitic/austenitic crystal configuration in certain alloys
advantages	disadvantages
<ul style="list-style-type: none"> <li>good temperature response – full transformation over temperature range as small as 10°C;</li> <li>can exert high forces during heating up;</li> <li>shape can change in many ways (expansion, contraction, bending motion, ...);</li> <li>large number of different SMAs with transition temperatures between -100C and +100C available.</li> </ul>	<ul style="list-style-type: none"> <li>very sensitive to composition variations and fabrication;</li> <li>Ni-Ti alloys are expensive (Cu-based alloys are much cheaper);</li> <li>two-way elements can only exert small forces during cooling down;</li> <li>slow dynamics;</li> <li>strong hysteresis.</li> </ul>
areas of application	actuation of safety-related devices valve and flap actuation clamping and locking
physical properties (given for NiTi alloys) Hodgson (1989)	melting point 1300°C density 6.4 kg/m <sup>3</sup> Young's modulus austenite 82×10 <sup>9</sup> N/m <sup>2</sup> martensite 31×10 <sup>9</sup> N/m <sup>2</sup> yield strength austenite 690×10 <sup>6</sup> N/m <sup>2</sup> martensite 150×10 <sup>6</sup> N/m <sup>2</sup> ultimate strength 900×10 <sup>6</sup> N/m <sup>2</sup> transformation temperature - 200...100 °C maximum shape memory strain one-way 8.4% maximum shape memory strain two-way 3%

Due to their behavior, SMAs are well suited to switching applications. Here, their capability of creating large actuation forces and their temperature response characteristics come into favor. On the other hand, SMAs are rather unsuitable for applications where a continuous motion or fast response times are required. Although the heat-up cycle can be expedited

by using a larger heating element, the cool-down cycle remains unchanged, leading to long manoeuvre times. Also, the strong hysteresis contradicts the use as a continuously variable actuator.

The first practical applications of SMAs as switching type actuators date back to the 1970s. Nowadays, areas of application include actuators for vanes that control the flow of air through jet engines and window latches that open and close automatically. Another interesting application is as a blood clot filter. This opens up when inserted into the blood vein and heated up to body temperature.

The most important characteristics of SMAs are outlined in Table 10.30. More detailed information can be found in Waram (1993).

### 10.6.3 Thermal Expansion Elements

These actuators, just like thermo-bimetals, are based on thermal expansion. While the latter exploit the change in length due to a change in temperature, thermal expansion elements rely on the change in volume associated with high thermal coefficients of certain solid and fluid materials. Upon an increase in temperature, the volume of an enclosed material amount will grow. The material is usually contained in some sort of cylinder and gives rise to the movement of a piston upon expansion. The functional principle is depicted in Figure 10.45. Depending on the material used, these thermal expansion elements have different temperature displacement characteristics. In general, fluids show a better linearity in the temperature-displacement characteristics than solids. Expansion elements are typically controlled by the ambient temperature only. However, there also exist versions with an attached electric heating element. A typical area of application is the actuation of valves (*e.g.*, radiators). The major advantages and disadvantages are listed in Table 10.31.

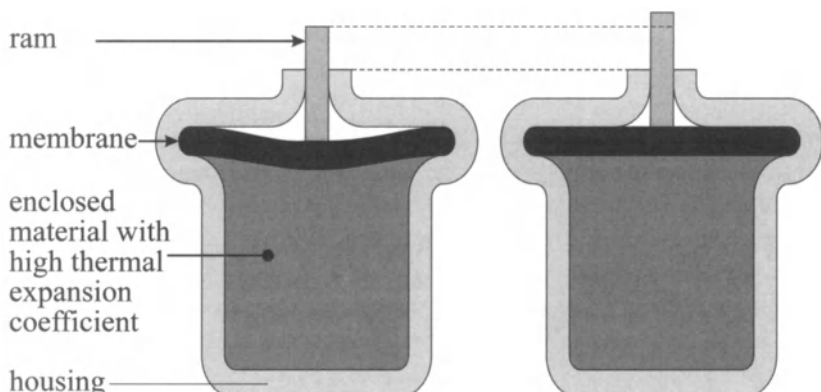


**Figure 10.45.** Cross-sectional view of thermal expansion elements (membrane actuator)

**Table 10.31.** Main features of thermal expansion elements, Janocha (1992)

actuating principle	movement of a piston due to thermal expansion of an enclosed material
advantages	disadvantages
<ul style="list-style-type: none"> <li>• mechanically robust;</li> <li>• inexpensive;</li> <li>• large displacement and actuation force.</li> </ul>	<ul style="list-style-type: none"> <li>• mediocre dynamic behavior;</li> <li>• limited thermal range of application (-20°C to +150°C).</li> </ul>
areas of application	actuation of valves
physical properties	displacement 5...15 mm maximum actuation force 250...1500 N

#### 10.6.4 Electrochemical Actuators

The electrochemical actuator exploits certain electrochemical reactions, which, evoked by a direct current, lead to the development of gas. This gas is contained within an enclosed volume and exerts a force on a membrane. By either reversing the current flow or shortening the cathode and the anode, the chemical reaction can be reversed and the gas will be dissolved again, resulting in a reduction of the pressure inside the sealed volume. This actuator is still at an experimental stage, nevertheless it has been included to show the variety of possible actuation principles that can be employed for mechatronic systems. Due to this multifariousness, the designer of a mechatronic system will experience a great latitude of different actuators to choose from. Some expected features of these newly proposed electrochemical actuators are listed in Table 10.32.

**Table 10.32.** Main features of electrochemical actuators, Gevatter (2000)

actuating principle	gas generated by electro-chemical reaction displaces a membrane
advantages	disadvantages
<ul style="list-style-type: none"> <li>• no energy consumption during static phases;</li> <li>• no moving parts;</li> <li>• retraction possible without external power (fail-safe);</li> <li>• noiseless.</li> </ul>	<ul style="list-style-type: none"> <li>• slow;</li> <li>• strong variations in the time-displacement behavior necessitate closed-loop control;</li> <li>• not much experience with this actuation principle available so far.</li> </ul>
areas of application	still at experimental status
physical properties	displacement 5...16 mm actuation force 300...3000 N response time ...150 s rated voltage 12...36 V rated current 0.3 ... 1 A operating temperature -5...60 °C

#### 10.6.5 Electro-rheological and Magneto-rheological Fluids

The fluids considered in this section change their rheological properties in response to an applied electric or magnetic field. The main focus of this section will be on electro-rheological (ER) fluids, but, due to their close

resemblance, magneto-rheological (MR) fluids will also be considered. From their chemical composition, ER fluids are suspensions of non-metallic hydrophilic solid particles (around 1 to 10  $\mu\text{m}$  in size) along with adsorbed water in an inert carrier liquid. Typically, certain additives are also added as to improve the stability of the structure or to adjust the physical properties. From an engineering point of view, however, these additives need not be considered.

In the case of zero-field, ER and MR fluids are modeled as ordinary Newtonian fluids, with the shear stress increasing proportionally to the strain rate. In reality, this assumption may not be true. The deviation from the ideal Newtonian model can be attributed to the heavy particles suspended in the fluid. More interesting than their behavior in the absence of electrical fields, however, is their behavior if subject to an electric or magnetic field. Then, the shear strain-velocity characteristics change remarkably. The underlying physical principle is still not thoroughly understood. It is believed that the electric field induces the almost instantaneous formation of chains – so-called *fibrils* – in the fluid, see Figure 10.46. Upon relative movement between the fluid and the walls of the enclosing vessel or upon a relative movement within the fluid, the fibrils will break and reform continuously, thus resisting such movements. This resistance gives rise to an offset of the shear-strain-velocity curve, resulting in a non-zero flow limit, also referred to as the *yield stress*. The physical model of ER and MR fluids, is for most applications, based on the Bingham plastic model. The shear stress is often modeled as increasing linearly with the field strength. Measurements indicate that the growth is normally proportional to the field strength raised to a power between 1 and 2. The upper limit of the electric field is typically given by a value of 4 kV/mm, above which the insulation of the fluid breaks down. For MR fluids, the yield stress is limited by saturation, typically occurring at a field strength of about 250 A/mm.

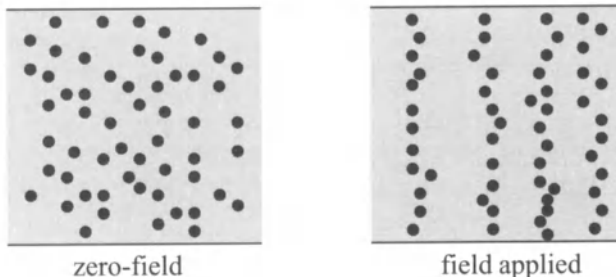


**Figure 10.46.** Formation of fibrils

For the technical realization, one can differentiate between two types of ER applications. Either the electrodes move relative to each other as is the case for ER clutches and some ER shock absorbers, or the fluid flows through the rigidly connected pair of electrodes. This set-up can also be used for shock absorbers, where the pair of electrodes, shaped as an orifice, represent a bypass valve. Since the electro-rheological effect is inde-

pendent of the polarity of the external electrical field, electro-rheological fluids can be controlled by either a DC or an AC excitation. For AC excitation, however, the viscosity also becomes a function of the frequency of the applied electric field. For MR fluids, similar areas of application emerge, *e.g.*, magneto-clutch. Table 10.33 summarizes the features of ER and MR fluids. Information about electro-rheology can be found in Block, Kelly (1998) and Duclos *et al.* (1992). Applications of the magneto-rheological effect are described in Kpordonsky (1993).

**Table 10.33.** Main features of electro-rheological and magneto-rheological fluids  
actuating principle

	change of viscosity of certain fluids if subjected to an electric or magnetic field
advantages	disadvantages
<ul style="list-style-type: none"> <li>• viscosity easily controllable;</li> <li>• fast response time.</li> </ul>	<ul style="list-style-type: none"> <li>• ER fluids in particular sensitive to water enclosures;</li> <li>• temperature-dependent properties;</li> <li>• sedimentation can become problematic;</li> <li>• not highly available;</li> <li>• can only evoke reaction forces and cannot generate primary actuation forces → semi-active actuators.</li> </ul>
areas of application	adjustable shock absorber clutch
physical properties	electro-rheological fluids zero-field viscosity 100...1000 mPa/s maximum yield stress 2...5 kPa density 1...2·10 <sup>3</sup> kg/m <sup>3</sup> magneto-rheological fluids zero-field viscosity 100...1000 mPa/s maximum yield stress 50...100 kPa density 3...4·10 <sup>3</sup> kg/m <sup>3</sup>

### 10.6.6 Piezoelectric Actuators

Certain crystals, *e.g.*, quartz, show a physical relationship between the mechanical stress and their electric charge. If the ions of the crystal lattice are displaced due to an externally applied mechanical stress, this displacement manifests itself as an electrical polarization of the crystal. The polarization can be measured by electrodes mounted on the crystal surface. The effect is termed the *direct piezoelectric effect* and is used, *e.g.*, for pressure and force transducers. The piezoelectric effect can also be reversed. Upon applying an electric voltage to a piezoelectric crystal, the crystal will change its thickness. This is termed the *reciprocal piezoelectric effect* and allows for the design of piezoelectric actuators. The best-known material that exhibits this effect is lead-zirconate-titanium (PZT), in fact, the term “PZT” is commonly used to refer to piezoelectric materials regardless of their actual chemical composition.

When first manufactured, the piezoelectric material has a random arrangement of the electric dipoles. It is not until the *poling* that the material exhibits the piezoelectric effect. In the process termed *poling*, the dipoles are permanently aligned. For this to happen, the material must first be heated above its Curie temperature, which typically lies between 120°C and 350°C. Above this temperature level, the dipoles can change their orientation in the solid phase material. If, in this state, the dipoles are subjected to a strong electric field, they will align themselves with this external field. If this field is maintained during the cooling down of the material, this alignment will be retained permanently. In the subsequent operation, special attention must be paid to the operating conditions, in particular to the ambient temperature, the compressible stress and the field strength of the electric field. If heated above the Curie temperature, the dipoles can again change their alignment and thus the crystal might lose its piezoelectric effect. Typically, the operating temperature is limited to 50–75% of the Curie temperature in Kelvin. Furthermore, the polarization can also vanish due to a strong electric field if this field is applied opposite to the direction of polarization. As a general rule, the electric field strength may not exceed 500 V/mm. Finally, polarization can also fade due to excessive compressible strain. Here, a limit is given as 100...150 N/mm<sup>2</sup>.

There exists a variety of different shapes of piezoelectric actuators, which makes them well suited to different applications. Different PZT actuators, along with their respective specifications, are shown in Table 10.34. A few of them will be described in the following. A basic PZT actuator can only cover a very small range of realizable displacements. In order to make PZT-based actuators more appealing, the realizable displacement must be increased, which is accomplished by different means, such as stacking PZT actuators or using a lever arrangement.

The most commonly used type is the *stack design actuator*. Here, stacks of small ceramic discs (0.3–1 mm high) are stacked on top of each other and glued together. From a mechanical point of view, the individual actuators are thus connected in series. Their electrodes are connected in parallel. In order to avoid a current flow, which could be evoked from the applied electric field, the entire column is covered with highly insulating material. To achieve an even larger range of realizable displacements, the motion of the PZT can be amplified by means of a lever arrangement. Another constructional principle is the *laminar design*. For this kind of actuator, small stripes of PZT material are stacked. These actuators exploit the transversal piezoelectric effect, which means that the electric field is applied orthogonal to the desired change in length. These actuators are usually very flat, since the piezoelectric effect is more prominent with a larger ratio of length to thickness. Upon application of an electric voltage, this class of actuators actually shortens. There is also another constructional principle exploiting the longitudinal effect, the *bender-type actuator*.

**Table 10.34.** Technical designs of piezoelectric actuators, Jendritz (1998)

design	transversal	stack design stack design with integrated lever motion amplifier	longitudinal
		laminar design	tube design bender-type design
displacement	20...200 $\mu\text{m}$	...1000 $\mu\text{m}$	...50 $\mu\text{m}$ ...1000 $\mu\text{m}$
actuating force	...30000 N	...3500 N	...1000 N ...5 N
actuating force	60...200 V 200...500 V 500...1000 V	60...200 V 200...500 V 500...1000 V	120...10000 V 10...400 V

Somewhat similar to the thermo-bimets, the design consists of two small beams that are joined together such that they cannot move independently of each other. If the two beams expand or contract differently, the entire structure will start to bend. For the unimorph design, a piezoceramic strip and a normal metallic strip are joined together, whereas for the bimorph design, two PZT strips are linked together. The PZT effect then induces a change in length of the ceramic strips.

For most applications, PZTs will be bonded to or embedded in a passive base structure. The piezoelectric effect can also be used for the design of linear motors, such as the inchworm motor.

The inchworm motor consists of three piezoelectric actuators. Two of these are clamping elements that can hold an axle that runs through these two clamping elements. A third PZT is used to displace these two clamping elements. It is rigidly supported in the middle. The motion of this motor is coordinated by an electronic control circuit and is shown in Figure 10.47. There, the behavior of the inch worm motor is detailed for movement of the rod to the right. At the beginning of one motion cycle (1), the middle element is relaxed and the left clamping element holds the beam. Then (2), an electric field is applied to the middle element, which contracts due to this input stimulus. The rod, which was tightly clamped by the left element, moves in accordance with the left clamping element. After the right clamping element has got hold of the rod, the left clamp is disengaged (3). Next, the electric field applied to the middle element is shut off (4). While the middle element expands to its original length, the clamping elements move back to their home positions. Since the right clamp moves to the right, the tightly attached rod will also move further to the right. Now, the whole cycle can be repeated (5). Due to the frictionally engaged connection of the clamping elements and the rod, the entire set-up must typically be operated in closed-loop control. The characteristics of piezoelectric actuators are listed into Table 10.35.

A detailed description of piezoelectric materials can be found in Cady (1964) and Jaffe *et al.* (1971). An outline is also given in Takuro (1996).

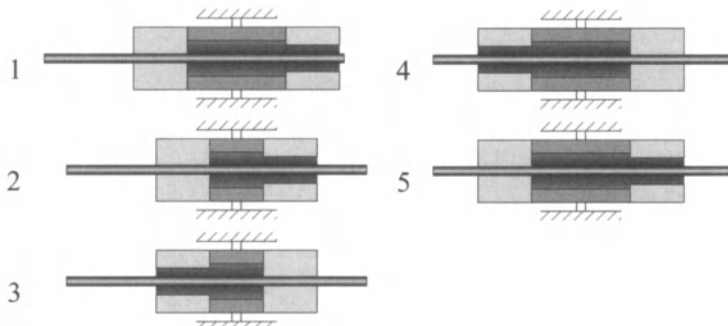


**Figure 10.47.** Operating principle of the inchworm motor, see description in text (not drawn to scale)

**Table 10.35.** Main features of piezoelectric actuators, Raab (1993)

actuating principle	displacement of ions in certain crystals upon application of an electric field
advantages	disadvantages
<ul style="list-style-type: none"> <li>large actuation forces;</li> <li>high power-weight ratio;</li> <li>fast response time;</li> <li>negligible energy consumption during static phases;</li> <li>linear field-strain characteristic;</li> <li>ceramics can be configured in many shapes and are highly available;</li> <li>almost no wear-out.</li> </ul>	<ul style="list-style-type: none"> <li>characteristics vary with temperature changes and aging;</li> <li>piezoeffect can be lost if crystal is subject to high temperatures, strong electric fields or mechanical shock;</li> <li>high voltage supply necessary which must be able to drive capacitive loads;</li> <li>open D-E loop implies high hysteresis and high losses, material-heat up.</li> </ul>
areas of application	fuel injection valves
physical properties	maximum displacement 20...1000 $\mu\text{m}$ static large-signal stiffness 75...1800 N/ $\mu\text{m}$ natural frequency 3.5...60 kHz maximum compressive strain ...800 N/mm <sup>2</sup> maximum tensile strain ...55 N/mm <sup>2</sup> rated voltage ...1500 V capacity ...6500 nF

### 10.6.7 Electrostrictive and Magnetostrictive Actuators

Similar to piezoelectric materials, *electrostrictive materials* are also predominantly made of ceramics, typically lead manganese niobate: lead titanate (PMN:PT) and lead lanthanum zirconate titanate (PLZT). In contrast to PZTs, no poling is necessary, since electrostriction occurs in virtually any material – although the effect is not strongly developed in some materials. Upon application of an electric field, the electric charges in the material attract each other, resulting in compression along the axis of the electric field but independent of the polarization of the applied field.

The strain is typically modeled as being proportional to the square of the applied field. Electrostrictive materials outperform PZTs in the smaller hysteresis loop of the strain-electric field relation. They exhibit less losses and can be operated at higher frequencies. Their major drawback is the quadratic dependency between strain and electric field. Their area of application will be the same as that of piezoelectric actuators.

Similar to the electrostrictive effect, *magnetostrictive materials* shrink in the presence of a magnetic field. This is caused by rotation of the magnetic domains and a shift of the Bloch walls. Magnetostrictives are made of alloys of iron, nickel and cobalt doped with rare earths. The complicated production process restricts the available sizes and shapes of magnetostrictives and also makes them very expensive. The main advantage of magnetostrictive actuators is their high energy density, which allows for higher actuation forces. However, only a very limited number of applications justify the use of these expensive materials. Typically, these are defence-related, e.g., sonar “pingers”. Typical material properties of mag-

netostrictive and electrostrictive actuators can be found in Table 10.36.

**Table 10.36.** Main features of electrostrictive and magnetostrictive actuators, Raab (1993)

actuating principle	change in length of certain materials if subject to an electric or magnetic field
advantages	disadvantages
<ul style="list-style-type: none"> <li>high actuation forces;</li> <li>electrostrictives: high efficiency due to closed D-E loop, can be operated at higher frequencies than PZTs;</li> <li>high energy density;</li> <li>fast response times;</li> <li>actuator can be made of single piece of material;</li> <li>electrostrictives: ceramics can be produced in many forms/shapes;</li> <li>almost no wear.</li> </ul>	<ul style="list-style-type: none"> <li>magnetostrictives: expensive and restricted availability (military applications);</li> <li>energy consumption during static phases;</li> <li>material properties are temperature-dependent;</li> <li>non-linear strain-field characteristics.</li> </ul>
areas of application	<ul style="list-style-type: none"> <li>sonar;</li> <li>other applications still at experimental stage.</li> </ul>
physical properties (given for magnetostrictive material TERFENOL-D)	maximum elongation ... $1200 \cdot 10^{-6} \text{ m/m}$ Young's modulus $25 \dots 30 \cdot 10^3 \text{ N/mm}^2$ specific electric resistance $0.6 \cdot 10^{-6} \Omega \text{ m}$ maximum compressive strain $700 \text{ N/mm}^2$ maximum tensile strain $28 \text{ N/mm}^2$ density $9.25 \cdot 10^3 \text{ kg/m}^3$

### 10.6.8 Micro-actuators

Micro-actuators are those actuators whose functional components are manufactured employing production processes used in the area of micro-technology, such as etching and lithography. The functional principle of micro-actuators can be based on any of the physical effects that have been described in this chapter so far, such as electromagnetism, thermal expansion, piezoelectricity, electrostriction or magnetostriction. One physical effect that has been found to be extremely well suited to micro-actuators is electrostatic force. At the small scale of micro-actuators, the distance between the electrodes is in the range of micrometers, and so even normal transistor comparative voltages of less than 5 V can generate a field strength in the area of a few kV/mm. Secondly, the disruptive strength of isolators grows with a decrease in thickness, thus the maximum allowable electric field strength increases.

Most micro-actuators are manufactured from silicon, which has already been used extensively for the production of integrated circuits and is thus well researched. Furthermore, since silicon is also used for the production of integrated circuits, the actuator and the control circuitry can be combined and manufactured together, leading to so-called MEMS (micro-electrical-mechanical systems). Detailed information about MEMS can also be found in Gad-El-Hak (2002).

Micro-actuators are still at an experimental stage, so typical properties and areas of application have not yet been determined clearly, but a few advantages and disadvantages are given in Table 10.37.

**Table 10.37.** Main features of micro-actuators

actuating principle	very small-scale actuators using different actuation principles (predominantly electrostatic forces)
advantages	disadvantages
<ul style="list-style-type: none"> <li>• inexpensive production using techniques well known from the manufacture of integrated circuits;</li> <li>• microelectronic-compatible voltage levels allow integration of actuator and controller on one wafer;</li> <li>• reliable;</li> <li>• cheap.</li> </ul>	<ul style="list-style-type: none"> <li>• due to the size of the actuator: only very small displacement and actuation forces realizable.</li> </ul>
areas of application	still at experimental stage
physical properties	still at experimental stage

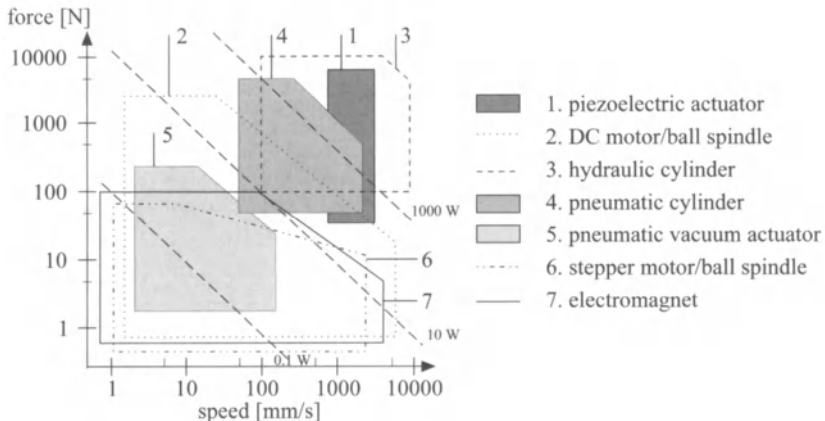
## 10.7. COMPARISON OF APPLICATION AREAS

In this section, diagrams are presented that allow the graphical comparison of the different actuators introduced in the preceding sections. These diagrams will focus on the following actuators:

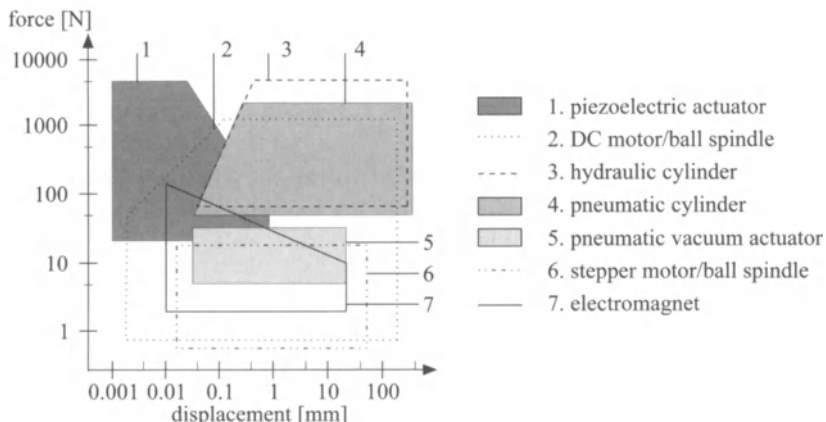
- electric motors and stepper motors with matching gear;
- electromagnets;
- pneumatic and hydraulic cylinders;
- piezoelectric stack actuators.

The specifications have been taken from company data sheets and publications, Raab (1990,1993). They refer to translatory actuators for small to medium actuation power. The diagrams compare typical properties. The actuation force has been chosen as the common ordinate for all diagrams.

Figure 10.48 illustrates the maximum speed of the different actuators, which also allows for a comparison of the power output (product of speed and force). The maximum displacement is plotted in Figure 10.49. The lower limit is determined either by the smallest possible displacement or by the positioning accuracy. The upper limit represents the upper bound for the maximum displacement that can be reached by a certain kind of actuator. The product of force and maximum displacement determines the working capacity of the actuator. One can see that electric motors cover a large range of realizable displacements. Piezoelectric actuators offer the best positioning accuracy.



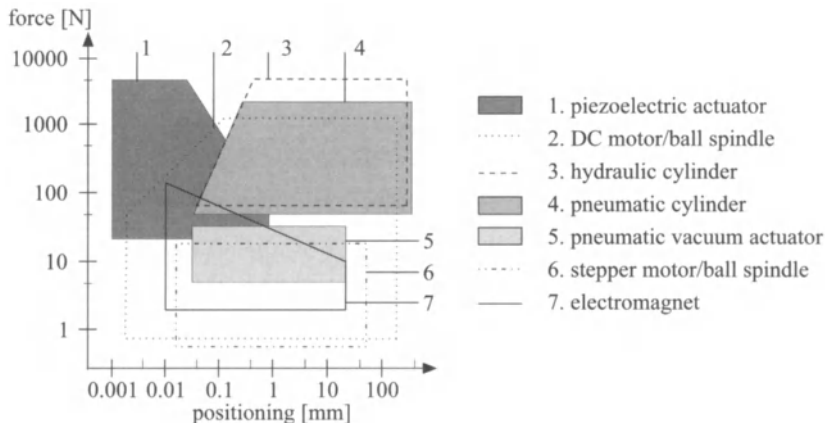
**Figure 10.48.** Actuating force versus speed range of selected actuators



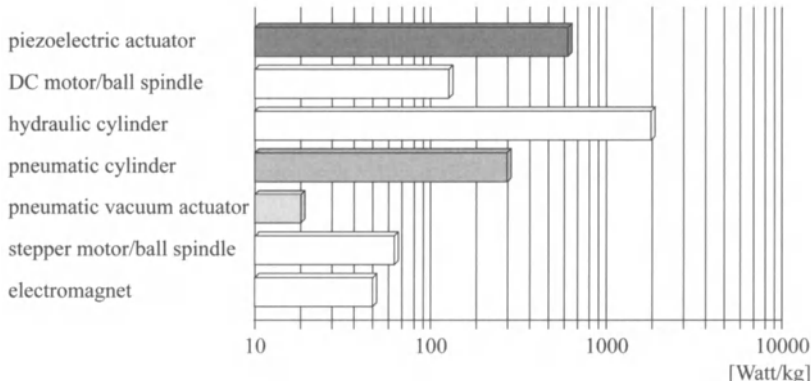
**Figure 10.49.** Actuating force versus displacement range of selected actuators

Figure 10.50 plots the positioning time for feedback-controlled operation. In this diagram, the smaller times represent small stroke manoeuvres whereas the longer times are representative of a full stroke, *e.g.*, traversing the total control range. Small positioning times can be reached by employing electric actuators. However, piezoelectric actuators (and magnetostrictive actuators, which have not been considered in this comparison), stepper motors and electromagnets also allow for fast positioning.

The power-weight ratio [W/kg] is plotted in Figure 10.51. Hydraulic actuators surpass other actuators in their power-weight ratio provided that the generation of the hydraulic (auxiliary) energy is not considered in the computation of the ratio.



**Figure 10.50.** Actuating force versus positioning time of selected actuators (feedback-controlled operation)



**Figure 10.51.** Power density of selected actuators (without consideration of auxiliary energy generation)

The demand for high positioning accuracy and good dynamic behavior necessitates feedback-controlled operation of the actuators. Effects such as:

- friction and backlash in mechanical gears and guidance elements;
- hysteresis and saturation effects of certain materials;
- static non-linearities;
- deviation of plant parameters due to operating point dependencies of the parameters or external influences such as aging, wear-and-tear, temperature, auxiliary energy fluctuation

limit the maximum positioning accuracy, Raab, Isermann (1990).

An assessment of the input/output behavior of selected actuators has been summarized in Table 10.38. This table proves the good control characteristics of electric motors, which are to some extent degraded by the subsequent matching gears and feeding drives. Electromagnets exhibit

distinct friction and hysteresis effects and have static non-linearities (magnetic force curve). Piezoelectric stack actuators are impaired by hysteresis and backlash. Pneumatic and hydraulic actuators suffer from distinctive friction and non-linearities in the control valves. Their parameters are both direction- and position-dependent and vary with temperature.

To summarize, it can be noted that all actuators are hampered by similar, undesired effects. They play a more dominant role for simple actuator designs. Control approaches that record and compensate these unwanted effects can be used to increase the performance of all actuator systems. Consequently, the mechanism and the microelectronic control circuit must be developed as an “integrated mechatronic actuator system”. Fluidic and electromagnetic actuators show a high potential for improvement, since one can integrate both a model-based control system and an automatic fault detection system, Isermann, Raab (1993), Isermann, Keller (1993).

**Table 10.38.** Assessment of the input/output behavior of selected actuators

actuator type \ properties	linearity of force-torque generation	special non-linearities			deviation of plant parameters	
		friction	backlash	electric hysteresis	internal	external
electric motor with gear	+	O	O			O
stepper motor with gear	O	O	O			O
electromagnet	-	-	+	-	O	-
pneumatic cylinder	-	-			-	O
hydraulic cylinder	-	O	+		-	O
PZT-stacked actuator	O	-	-	-		O

symbols: + good, negligible; o mediocre, existing; - bad, distinctly noticeable

## 10.8 ACTUATORS AS SYSTEM COMPONENTS

In the face of the application of actuators as a part of mechatronic systems, the interfacing becomes more important. The term “interfacing” refers to all the properties that allow or obstruct the integration of an actuator in a total system. These are:

- type of auxiliary power;
- input-output behavior;
- ports;
- integration of actuator and process;
- implemented functionality, degree of “intelligence”, and smartness;
- measures to increase the reliability.

The first two characteristics have been treated in the preceding chapters.

### 10.8.1 Ports

In the case of analog signals, the transmitted signals should conform to the standardized current ranges  $0 \dots 20 \text{ mA}$ ,  $4 \dots 20 \text{ mA}$  or to the standardized voltage ranges  $-10 \text{ V} \dots 0 \dots +10 \text{ V}$ . For connection to a digital bus system, interfaces for serial or parallel data transmission must be used as described in Chapter 11.

### 10.8.2 Integration of Actuator and Process

There exist a vast variety of ways to connect an actuator to a process. For a small number of units, it is best to resort to standardized flanges, terminals, screw joints and scaled families of actuators (*e.g.*, solenoid valves). For mass production, proprietary constructions will be employed (*e.g.*, fuel-injection pumps, throttle-valve actuators). Actuators are typically available as standardized products.

### 10.8.3 Implemented Functionality

If control of the actuator, Figure 10.2, is delegated to an integrated microcomputer, then it is possible to implement model-based non-linear adaptive control algorithms, which significantly increase the control performance. Integration of advanced control algorithms can also lead to a reduction of the unit cost. The electromechanical design can be simplified, leading to a simplified and thus cheaper manufacturing process. Then, the induced loss in performance is compensated by the more sophisticated control concepts. Since actuators will increasingly turn into mechatronic components, one can apply the ideas developed in Chapter 1. This will result in "intelligent actuators", so-called *smart* actuators, which can offer the following functions:

- model-based, non-linear adaptive control;
- model-based fault detection (parameter estimation, parity methods, state observer);
- fault diagnosis which informs about the type of fault and the required maintenance;
- energy-optimal and reduced-wear control strategies.

The underlying methods are described in Isermann, Raab (1993), Isermann, Keller (1993).

## 10.9 FAULT-TOLERANT COMPONENTS

The improvement of reliability can be increased by two different approaches, *perfectness* or *tolerance*, Lauber (1988). Perfectness refers to the idea of avoiding faults and failures by means of an improved mechanical design. This includes the continued technical advancement of actuator components that increase the service life. During operation of the component, the intactness of the component must be maintained by regular maintenance and replacement of wearing parts. Methods that facilitate fault detection at an early stage allow for replacing the regular maintenance schedule with a maintenance-on-demand scheme.

Tolerance describes the notion of trying to contain the consequences of faults and failures thus that the components remain functional. This can be reached by the principle of *fault-tolerance*. Herewith, faults are compensated in such a way that they do not lead to system failures. The most obvious way to reach this goal is *redundancy* in components, units or subsystems. However, the overall systems then become more complex and costly. In the following, various types of fault-tolerant methods are reviewed briefly, see Isermann *et al.* (2000)

### 10.9.1 Fault-tolerance for Components

Fault-tolerance methods generally use *redundancy*. This means that in addition to the considered module, one or more modules are connected, usually in parallel. These redundant modules are either *identical* or *diverse*. Such redundant schemes can be designed for hardware, software, information processing, and mechanical and electrical components like sensors, actuators, microcomputers, buses, power supplies, *etc.*

#### *Basic redundant structures*

There exist mainly two basic approaches for fault-tolerance, static redundancy and dynamic redundancy. The corresponding configurations are first considered for *electronic hardware* and then for other components. Figure 10.52a shows a scheme for *static redundancy*. It uses three or more parallel modules that have the same input signal and are all active. Their outputs are connected to a voter, who compares these signals and decides by majority which signal value is the correct one. If a triple modular-redundant system is applied, and the fault in one of the modules generates a wrong output, this faulty module is masked (*i.e.*, not taken into account) by the two-out-of-three voting. Hence, a single faulty module is tolerated without any effort for specific fault detection,  $n$  redundant modules can tolerate  $(n - 1)/2$  faults ( $n$  odd).

*Dynamic redundancy* needs less modules at the cost of more information processing. A minimal configuration consists of two modules, Figure 10.52b and c. One module is usually in operation and, if it fails, the stand-by or back-up unit takes over. This requires fault detection to observe if

the operation modules become faulty. Simple fault-detection methods only use the output signal for, *e.g.*, consistency checking (range of the signal), comparison with redundant modules or use of information redundancy in computers like parity checking or watchdog timers. After fault detection, it is the task of the reconfiguration to switch to the standby module and to remove the faulty one.

In the arrangement of Figure 10.52b, the standby module is continuously operating, called “*hot standby*”. Then, the transfer time is small at the cost of operational aging (wear-out) of the standby module.

Dynamic redundancy, where the standby system is out of function and does not wear, is shown in Figure 10.52c, called “*cold standby*”. This arrangement needs two more switches at the input and more transfer time due to a start-up procedure. For both schemes, the performance of the fault detection is essential.

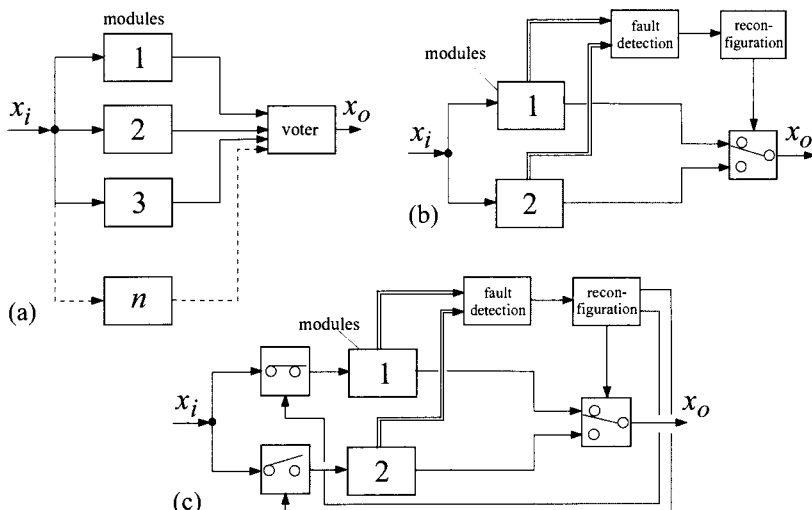


**Figure 10.52.** Fault-tolerant schemes for electronic hardware: (a) static redundancy: multiple-redundant modules with majority voting and fault masking,  $m$  out of  $n$  systems (all modules are active); (b) dynamic redundancy: standby module that is continuously active, “*hot standby*”; (c) dynamic redundancy: standby module that is inactive, “*cold standby*”

Similar redundant schemes as for electronic hardware exist for *software fault-tolerance*, *i.e.*, tolerance against mistakes in coding or errors of calculations. The simplest form of static redundancy is repeated running ( $n \geq 3$ ) of the same software and majority voting for the result. However, this only helps for some transient faults. As software faults in general are systematic and not random, a duplication of the same software does not help. Therefore, the redundancy must include diversity of software, like other programming teams, other languages, or other compilers. With  $n \geq 3$  diverse programs, a multiple-redundant system can be established followed by majority voting as in Figure 10.52a. However, if only one processor is used, calculation time is increased and using  $n$  processors may be too costly.

Dynamic redundancy by using standby software with diverse programs can be realized by using recovering blocks. This means that in addition to the main software module, other diverse software modules exist, Storey (1996), Leveson (1995).

Fault-tolerance can also be designed for purely mechanical and electrical systems. Static redundancy is very often used in all kinds of homogeneous and inhomogeneous materials (*e.g.*, metals and fibers) and in special mechanical constructions like lattice-structures, spoke-wheels, dual tires or in electrical components with multiple wiring, multiple coil windings, multiple brushes for DC motors and multiple contacts for potentiometers. This quite natural built-in fault-tolerance is generally characterized by a parallel configuration. However, the inputs and outputs are not signals but, *e.g.*, forces, electrical currents or energy flows, and a voter does not exist. All elements operate in parallel and if one element fails (*e.g.*, by breakage) the others take over a higher force or current, following the physical laws of compatibility or continuity. Hence, this is a kind of “stressful degradation”. Mechanical and electrical systems with dynamic redundancy as depicted in Figure 10.52b, c can also be built. Mostly, only cold standby is meaningful.

Fault tolerance with dynamic redundancy and cold standby is especially attractive for mechatronic systems where more measured signals and embedded computers are already available and therefore fault detection can be improved considerably by applying process model-based approaches. Table 10.39 summarizes the appropriate fault-tolerance methods for the case of electronic hardware.

**Table 10.39.** Fail behavior of electronic hardware for different redundant structures. FO: fail-operational; F: fail; (FS: fail-safe not considered)

structures	number of elements	static redundancy		dynamic redundancy		
		tolerated faults	fail behavior	tolerated failures	fault behavior	discrepancy detection
duplex	2	0	F	0	F	two comparators
				1	FO-F	fault detection
triplex	3	1	FO-F	2	FO-FO-F	fault detection
quadruplex	4	1	FO-F	3	FO-FO-FO-F	fault detection
duo-duplex	4	1	FO-F	-	-	-

#### *Redundant structures for mechatronic systems*

Mainly because of costs, space and weight, a suitable compromise between the degree of fault tolerance and the number of redundant components has to be found for mechatronic systems. In contrast to fly-by-wire systems, only one single or two failures can be tolerated for hazardous cases, mainly because a safe state can be reached easier and faster. This means that not all components need very stringent fault-tolerance requirements. The following steps of degradation are distinguished:

- *fail-operational* (FO): one failure is tolerated, *i.e.*, the component stays operational after one failure. This is required if no safe state exists immediately after the component fails;
- *fail-safe* (FS): after one (or several) failure(s), the component directly possesses a safe state (passive fail-safe, without external power) or is brought to a safe state by a special action (active fail-safe, with external power);
- *fail-silent* (FSIL): after one (or several) failure(s), the component is quiet externally, *i.e.*, stays passive by switching off and therefore does not influence other components in a wrong way.

For vehicles, it is proposed to subdivide FO into “long time” and “short time”. Considering these degradation steps for various components, one has to check first if a safe state exists. For automobiles, (usually) a safe state is stand still (or low speed) at a non-hazardous place. For components of automobiles, a fail-safe status is (usually) a mechanical back-up (*i.e.*, a mechanical or hydraulic linkage) for direct manipulation by the driver. Passive fail-safe is then reached, *e.g.*, after failure of electronics if the vehicle comes to a stop independently of the electronics, *e.g.*, by a closing spring in the throttle or by actions of the driver via mechanical backup. However, if no mechanical back-up exists after failure of electronics, only an action by other electronics (switch to a still operating module) can bring the vehicle (in motion) to a safe state, *i.e.*, to reach a stop through active fail-safe. This requires the availability of electric power.

Generally, a *graceful degradation* is envisaged, where less critical functions are dropped to maintain the more critical functions available, using priorities, IEC 61508 (1997). Table 10.39 shows degradation steps to fail-operational for different redundant structures of electronic hardware. As the fail-safe status depends on the controlled system and the kind of components, it is not considered here.

For flight-control computers, usually a triplex structure with dynamic redundancy (hot standby) is used, which leads to FO-FO-FS, such that two failures are tolerated and a third one allows the pilot to operate manually. If the fault tolerance has to cover only one fault to stay fail-operational (FO-F), a triplex system with static redundancy or a duplex system with dynamic redundancy is appropriate. If fail-safe can be reached after one failure (FS), a duplex system with two comparators is sufficient. However, if one fault has to be tolerated to continue fail-operational and after a next fault it is possible to switch to a fail-safe (FO-FS), either a triplex system with static redundancy or a duo-duplex system may be used. The duo-duplex system has the advantages of simpler failure detection and modularity.

### 10.9.2 Fault-tolerance for Control Systems

For automatically controlled systems, the appearance of faults and failures in the actuators, the process and the sensors will usually affect the operating behavior. With feedforward control, generally all small or large faults influence the output variables and therefore more or less the operation.

If the system operates with feedback control, small additive or multiplicative faults in the actuator or process are in general covered by the controller, because of the usual robustness properties. This property is therefore *passive controller fault-tolerance*. However, additive and gain sensor faults will immediately lead to deviations from the reference values. For large changes in actuators, process and sensors, the dynamic control behavior becomes either too sluggish or too less damped or even unstable. Then either a very robust control system or an *active fault-tolerant* control system is required to save the operation. In the last case, it consists of fault-detection methods and reconfiguration mechanisms, which modify the controller. Depending on the kind of faults, the reconfiguration may change the structure and/or parameters of the controller. This can also include the change to other manipulated variables or actuators or sensors, if available.

Examples are fault-tolerant flight control with reconfiguration to other control surfaces after failure of actuators or ailerons, elevators and rudders, see, e.g., Rauch (1995), Chandler (1997), Patton (1997), Chen *et al.* (1999). For failures in the satellite altitude control system, see Blanke *et al.* (1997). Failures in heat exchangers are treated in Ballé *et al.* (1998) and fault-tolerant control for lateral vehicle control in Suryanaryanan, Tomizuka (2000).

### 10.9.3 Fault Detection for Sensors, Actuators and Mechatronic Servo-systems

Fault-detection methods based on measured signals can be classified as:

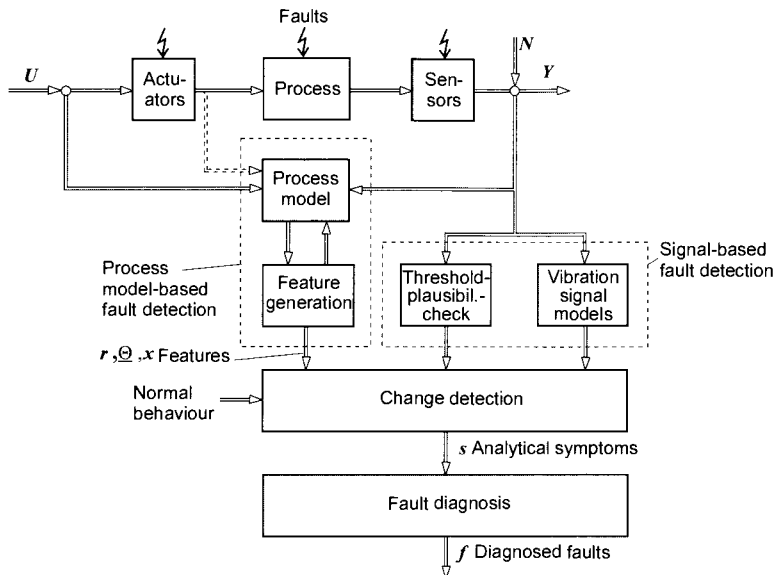
- *limit value checking* (thresholds) and *plausibility checks* (ranges) of single signals;
- *signal model-based methods* for single periodic or stochastic signals;
- *process model-based methods* for two or more related signals.

Figure 10.53 shows a scheme for these methods.

For a description of the various method, refer to the literature, e.g., the special section in IFAC Journal Control Engineering Practice (1996) or the books Chen, Patton (1999), Gertler (1999), Isermann (1994a).

In order to obtain specific symptoms it is necessary to have more than one input and one output signal for parity equations or output observers. For parameter estimation, one input and one output may be sufficient. Because of the various properties, it is recommended to combine different

methods in order to have a large fault detection coverage, Isermann (1994b), Pfeufer (1997).



**Figure 10.53.** General scheme of process model-based and signal-based fault detection

#### 10.9.4 Fault-tolerant Components for Mechatronic Systems

High-integrity systems require a comprehensive overall fault-tolerance by fault-tolerant components and corresponding control. This means the design of fault-tolerant sensors, actuators, process parts, computers, communication (bus systems), and control algorithms. Examples of components with multiple redundancy are known for aircraft, space and nuclear power systems. However, lower cost components with built-in fault tolerance have to be developed. In the following, some examples are given for sensors and actuators.

#### 10.9.5 Fault-tolerant Sensors

A fault-tolerant sensor configuration should be at least fail-operational (FO) for one sensor fault. This can be obtained by applying hardware redundancy with the same type of sensors or by analytical redundancy with different sensors and process models.

##### *Hardware sensor redundancy*

Sensor systems with static redundancy are realized, for example, with a triplex system and a voter, Figure 10.54a. A configuration with dynamic redundancy needs at least two sensors and fault detection for each sensor, Figure 10.54b. Usually, only hot standby is feasible. Another less powerful possibility is plausibility checks for two sensors, also by using signal

models (e.g., variance) to select the more plausible one, Figure 10.54c.

The fault detection can be performed by *self-tests*, e.g., by applying a known measurement value to the sensor. Another way uses *self-validating sensors*, Henry, Clarke (1993), Clarke (1995), where the sensor, transducer and a microprocessor form an integrated, decentralized unit with self-diagnostic capability. The self-diagnosis takes place within the sensor or transducer and uses several internal measurements. The output consists of the sensor's best estimate of the measurement and a validity status, like good, suspect, impaired, bad and critical.

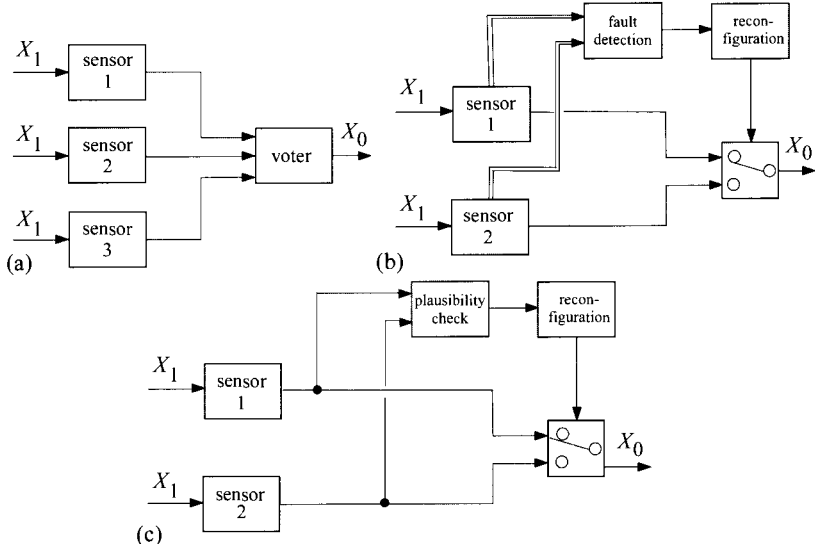


**Figure 10.54.** Fault-tolerant sensors with hardware redundancy: (a) triplex system with static redundancy and hot standby; (b) duplex system with dynamic redundancy, hot standby; (c) duplex system with dynamic redundancy, hot standby and plausibility checks

#### Analytical sensor redundancy

As a simple example, a process with one input and one main output  $y_1$  and an auxiliary output  $y_2$  is considered, see Figure 10.55a. Assuming the process input signal  $u$  is not available but two output signals  $y_1$  and  $y_2$ , which both depend on  $u$ , one of the signals, e.g.,  $\hat{y}_1$  can be reconstructed and used as a redundant signal if process models  $G_{M1}$  and  $G_{M2}$  are known and considerable disturbances do not appear (ideal cases).

For a process with only one output sensor  $y_1$  and one input sensor  $u$ , the output  $\hat{y}_1$  can be reconstructed if the process model  $G_{M1}$  is known, Figure 10.55b. In both cases, the relationship between the signals of the process are used and expressed in the form of analytical models.

To obtain one usable fault-tolerant measurement value  $y_{1FT}$ , at least three different values for  $y$ , e.g., the measured one and two reconstructed ones, must be available. This can be obtained by combining the schemes of Figure 10.55a and b as shown in Figure 10.56a. A sensor fault  $y_1$  is then detected and masked by a majority voter and either  $\hat{y}_1$  or  $\hat{y}_{1u}$  is used as a

replacement depending on a further decision. (Also, single sensor faults in  $y_2$  or  $u$  are tolerated with this scheme.)

One example for this combined analytical redundancy is the yaw rate sensor for the ESP (electronic stability program) of vehicles, where additionally the steering wheel angle as input is used to reconstruct the yaw rate through a vehicle model as in Figure 10.55b, and the lateral acceleration and the wheel speed difference of the right and left wheel (no slip) are used to reconstruct the yaw rate according to Figure 10.55a.

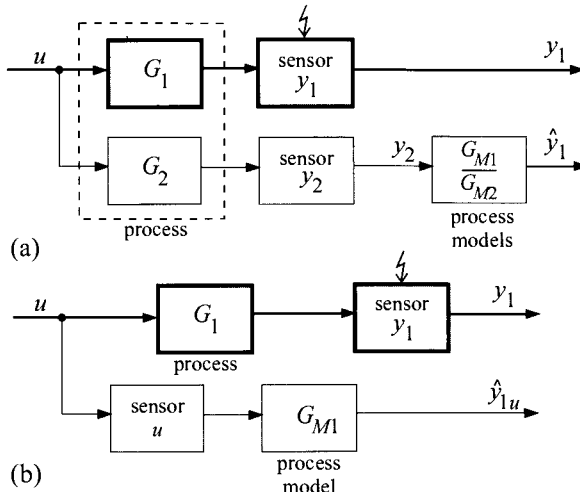


**Figure 10.55.** Sensor fault-tolerance for one output signal  $y_1$  (main sensor) through analytical redundancy by process models (basic schemes): (a) two measured outputs, no measured input; (b) one measured input and one measured output

A more general sensor fault-tolerant system can be designed if two output sensors and one input sensor yield measurements of the same quality. Then, by a scheme as shown in Figure 10.56b, three residuals can be generated and by a decision logic, fault-tolerant outputs can be obtained in the case of single faults of any of the three sensors. The residuals are generated based on parity equations. In this case, state observers can also be used for residual generation, compare, *e.g.*, the dedicated observers by Clark (1989). (Note that all schemes assume ideal cases. For the realizability, constraints and additional filters have to be considered.)

If possible, a faulty sensor should be fail-silent, *i.e.*, should be switched off. However, this needs additional switches that lower the reliability. For both hardware and analytical sensor redundancy without fault detection for individual sensors, at least three measurements must be available to make one sensor fail-operational. However, if the sensor (system) has in-built fault detection (integrated self-test or self-validating), two measurements are enough and a scheme like Figure 10.54b can be applied. (This means that by methods of fault detection, one element can be saved).

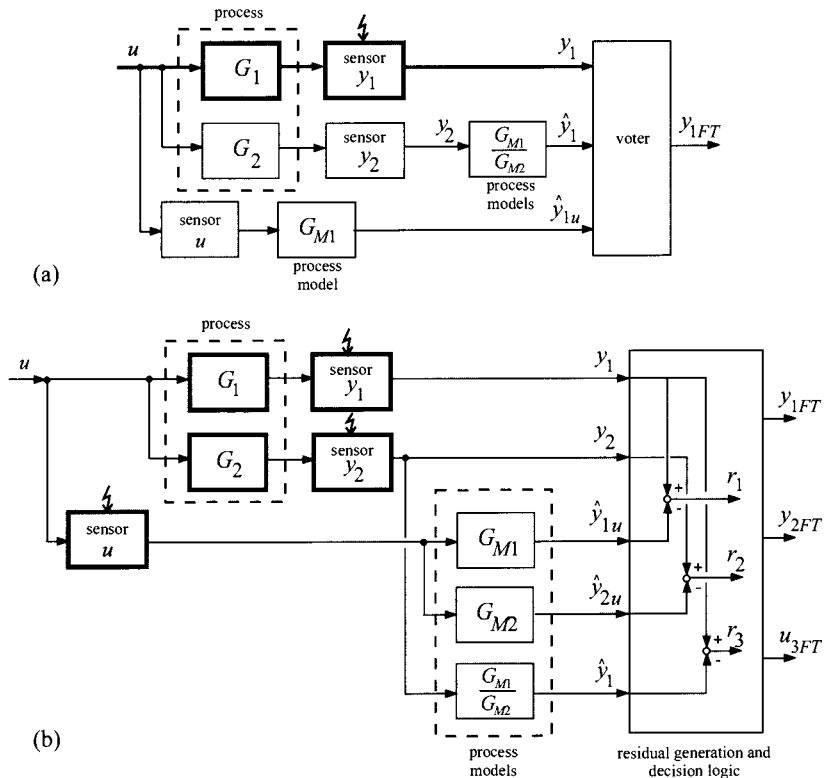


**Figure 10.56.** Fault-tolerant sensors with combined analytical redundancy for two measured outputs and one measured input through (analytical) process models: (a)  $y_1$  is main measurement,  $y_2, u$  are auxiliary measurements (combination of Figure 10.55a and b); (b)  $y_1, y_2$  and  $u$  are measurements of same quality (parity equation approach)

### 10.9.6 Fault-tolerant Actuators

Actuators generally consist of different parts: input transformer, actuation converter, actuation transformer and actuation element (e.g., a set of DC amplifier, DC motor, gear and valve, as shown in Figure 10.57a). The actuation converter converts one form of energy (e.g., electrical or pneumatic) into another form (e.g., mechanical or hydraulic). Available measurements are frequently the input signal  $U_i$ , the manipulated variable  $U_0$  and an intermediate signal  $U_3$ .

Fault-tolerant actuators can be designed by using *multiple complete actuators* in parallel, either with static redundancy or dynamic redundancy with cold or hot standby (Figure 10.52). One example of static redundancy are hydraulic actuators for fly-by-wire aircraft where at least two independent actuators operate with two independent hydraulic energy circuits.

Another possibility is to limit the redundancy to parts of the actuator that have the lowest reliability. Figure 10.57b shows a scheme where the actuation converter (motor) is split into separate parallel parts. Examples with static redundancy are two servo-valves for hydraulic actuators, Oeh-

ler *et al.* (1997) or three windings of an electrical motor (including power electronics), Krautstrunk, Mutschler (1999). Within electromotor-driven throttles for SI engines, only the slider is doubled to make the potentiometer position sensor static-redundant.

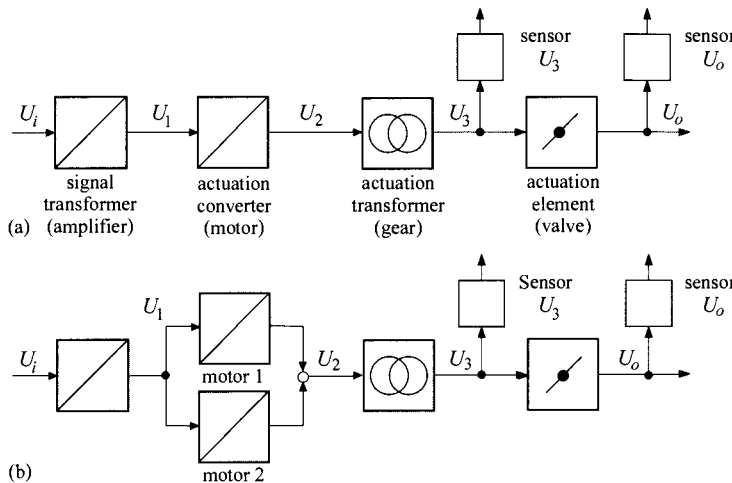


**Figure 10.57.** Fault-tolerant actuator: (a) common actuator; (b) actuator with duplex drive

One example for dynamic redundancy with cold standby is the cabin pressure flap actuator in aircraft, where two independent DC motors exist and act on one planetary gear, Moseler *et al.* (1999).

As cost and weight generally are higher than for sensors, actuators with fail-operational duplex configuration are to be preferred. Then, either static-redundant structures, where both parts operate continuously, Figure 10.52a, or dynamic redundant structures with hot standby, Figure 10.52b, or cold standby, Figure 10.52c, can be chosen. For dynamic redundancy fault-detection methods of the actuator parts are required, Isermann, Raab (1993). One goal should always be that the faulty part of the actuator fails silent, *i.e.*, has no influence on the redundant parts.

## 10.10 PROBLEMS

- 10.10.1 Describe the different components of an AC motor-driven flow valve by drawings according to Figure 10.2. Include a position controller for the valve shaft.
- 10.10.2 In which cases are linear or non-linear characteristics of flow valves selected?
- 10.10.3 State the advantages and disadvantages of electromotors, pneumatic membrane drives and hydraulic cylinder drives for:

- a) flow control of steam flow for a 500 MW steam turbine;
  - b) position control for a machine tool feed drive;
  - c) ailerons of an aircraft.
- 10.10.4 Compare the properties of DC electrical brush and brushless motor.
- 10.10.5 Which actuator drives and subsequent gears need or do not need power for position holding under load?
- 10.10.6 How can the non-linear current-position behavior of electromagnets be improved for position control of the armature by constructive means or by algorithmic ways?
- 10.10.7 Which actuator drives should be preferred for the following requirements for
- a) displacement 1 m and very large speed and force;
  - b) displacement 10mm, force 5N and cheap mass production;
  - c) displacement 0.01 mm and force 100 N;
  - d) displacement 0.1 m, force 1000 N and explosive environment;
  - e) displacement 0.2 m, force 1000 N and high power-weight ratio.
- 10.10.8 How large are approximately the smallest time constants of pneumatic, hydraulic, electromotoric, electro magnets and piezoelectric actuator drives?
- 10.10.9 Determine the time constant of a pneumatic diaphragm valve with diameter  $D = 0.1 \text{ m}$ , air volume  $V = 1 \cdot 10^{-3} \text{ m}^3$ , inflow  $\dot{V}_{\max} = 0.5 \text{ l/s}$ ,  $p_i = 1 \text{ bar}$ . It is assumed that friction can be neglected.
- 10.10.10 What types of linear controllers can be used for precise and fast position control of an electromagnet, pneumatic diaphragm and hydraulic cylinder drive?
- 10.10.11 Describe the possibilities for the construction of fault-tolerant drives with two electrical motors.
- 10.10.12 How can a fault-tolerant temperature measurement system be built with two sensors (thermocouple and resistance thermometer) and three sensors of the same type?

# 11 Microcomputers

---

In general, the processing of information in mechatronic systems takes place in a microcomputer or in a system of microcomputers. These microcomputers are primarily used as process computers, meaning they should process the information in real-time and feature interfaces for input and output process signals. In the following, a short overview of microcomputers, specific processors, bus systems and architectures used in control engineering applications as well as in mechatronic systems will be given.

The crucial steps in microelectronics development were the discovery of the transistor (1948), the first silicon-integrated circuits in bipolar (1959) and MOS (metal oxide semiconductor, field-effect transistors) technology (1969). The first UV light-erasable permanent memory (EPROM, 1969) and the first 4-bit Intel microprocessor 4004 (1971), with central processing unit (CPU), permanent memory (ROM), and write/read memory (RAM) came shortly thereafter.

Since then, progress in microcomputer development can be characterized by the number of elements per chip, Figure 11.1, and the computing power in MIPS (million instructions per second), Figure 11.2.

A summary of current as well as future trends is given, for example, in Gibson (1994), Carter (1995), Patterson (1995), Wieder (1996), Meierau (1996). The following tendencies may be derived from these sources:

- the number of functional components per chip doubles with each IC generation, meaning every 18 months (Moore's law) (the package density quadruples every three years);
- investments in manufacturing facilities double with each generation (due to miniaturization of dimensions, clean-room technology, larger wafer diameters, increasing number of process steps, reliance on automation);

- nevertheless, the price of electronic equipment has remained constant, often fundamentally reduced per computer function;
- the typical microelectronics product is presently characterized by: 16-Mbit DRAM with 40ns access time,  $10^7$  components per chip, 0.5  $\mu\text{m}$  CMOS technology, computing capacity of 200 MIPS;
- future development is likely to be characterized by a drastic increase in the number of functional components per chip, CMOS technology, transition from logic, arithmetic, and memory on a chip to a whole system on a chip with parallelism in time and space, less power consumption (portable devices), higher clock frequencies, simultaneous hardware and software design.

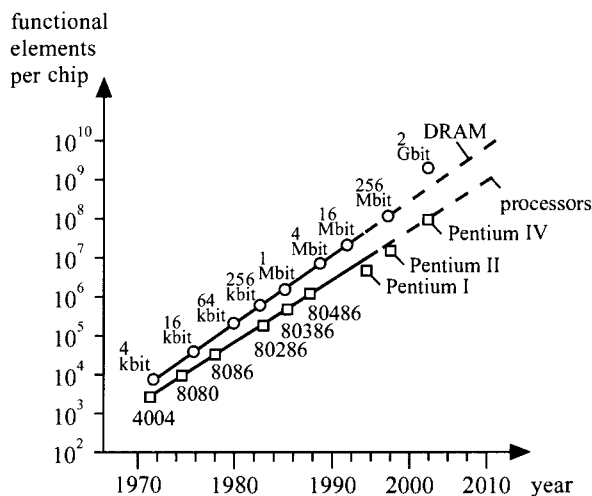


**Figure 11.1.** Number of functional elements per chip at time of market launch for dynamic memory (DRAM) and processors in silicon technology, Wieder (1996)

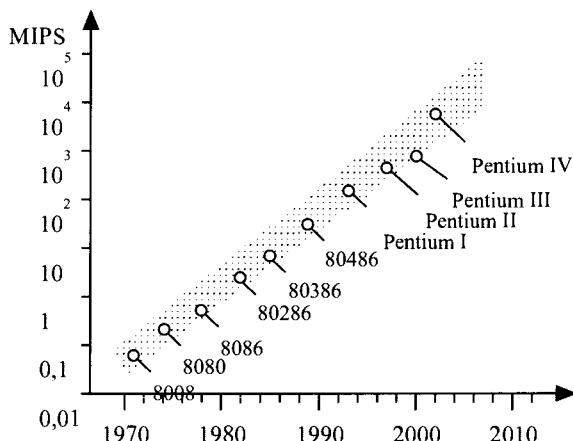


**Figure 11.2.** Computing performance of microprocessors in MIPS (million instructions per second) at time of market launch (RISC and CISC processors), Wieder (1996)

These trends applied to mechatronic systems design indicate that information processing continues to become more extensive, faster and more reliable despite no significant increase in production costs.

## 11.1 MICROCOMPUTER STRUCTURE

One distinguishes between two basic construction principles of microcomputer systems: *modular microcomputer systems*, which are built from discrete functional components, and *one-chip microcomputers*.

Figure 11.3 shows a general design of a modular microcomputer system.

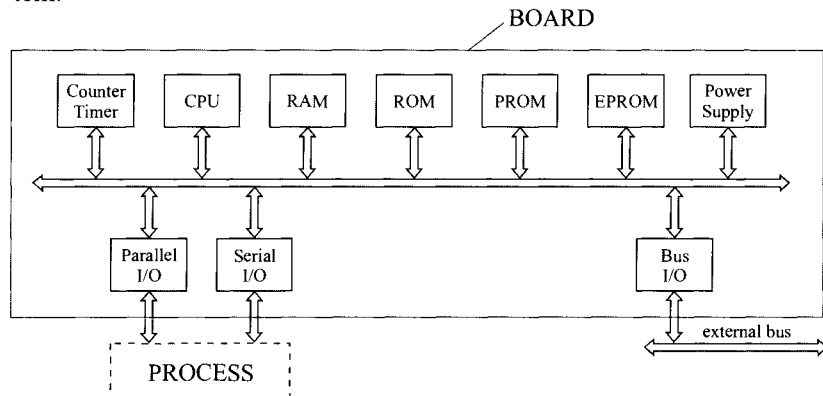


**Figure 11.3.** General design of a modular microcomputer system

The microcomputer consists of the following components, which are assembled as integrated circuits (IC) on the main board:

- CPU (central processing unit): microprocessor (central unit) for arithmetical and logical data operations;
- Counter/timer: clock generator, timing circuits;
- RAM (random access memory): memory blocks with read and write access;
- ROM (read only memory): read only memory programmed by fabrication;
- PROM (programmable ROM), OTP (one time programmable), EPROM (erasable PROM), EEPROM (electrical erasable PROM), FLASH ROM: read only memory programmed by the user, erasable in the case of EPROM/EEPROM/FLASH memory;
- Parallel I/O: inputs and outputs with several parallel bits;
- Serial I/O: input and output ports for serial bits usually used for peripheral devices;
- Bus I/O: communication with external bus systems.

Due to the modularity, such systems are easily adapted to particular applications, for instance, by the addition of more RAM, ROM, external memory (floppy disk, hard disk), arithmetic processors for rapid floating point calculation or other specialized components.

On the contrary, in a one-chip microcomputer system, CPU, RAM, ROM, I/O channels are integrated into a single block and the whole system is functional without external components. For some terms and units, see Table 11.1.

## 11.2 STANDARD PROCESSORS

Microprocessors are the central units of digital computers (CPU) and consist of several million transistors, resistances and capacities. These are implemented on a single chip – a crystal silicon surface of a few square millimeters. The power consumption is between 0.5 and 25 Watt.

Figure 11.4 shows the four main components of a microprocessor (CPU):

- control unit: decodes the control information of commands and drives the execution of commands;
- arithmetic unit: executes logical and arithmetic data operations;
- memory unit: determines the memory address of commands and operands. It serves as a fast temporary memory buffer during the execution of a command;
- bus interface: link unit into the internal microcomputer bus, which connects to RAM, ROM, and I/O. It serves as a temporary buffering memory for address information.

The signal transmission in the microprocessor consists of a bus system with up to three specific buses:

- data bus: transfers data (commands, operands, results) between components, bi-directional;
- address bus: activates or selects certain components by the use of addresses, single direction;
- control bus: time coordination of signals, connects data and address information.

The structures presented in Figure 11.4 correspond to a von Neumann computer, namely, a central processor that consists of a control unit and an arithmetic unit, main memory for programs and data, I/O processor (bus interface), and a main system bus, consisting of data, address and control bus.

The operating sequence of a *Princeton structure* computer, Figure 11.4 a, can be described as follows:

- command address: the control unit determines the address of the command in the main memory using the address bus;
- command fetch: the control unit fetches and interprets the command from the data bus;
- operand addresses: the control unit determines the operand address in the main memory using the address bus;
- operand fetch: the arithmetic unit fetches the operand from the data bus.
- execute command: the arithmetic unit executes the command and stores the result in the register unit of the CPU;
- next command address: the control unit incrementally increases the command counter by one.

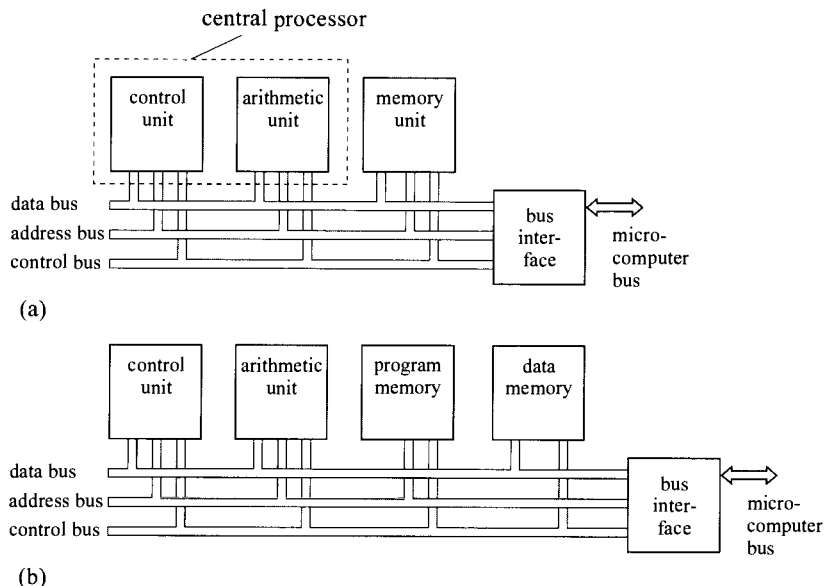


**Figure 11.4.** The main components of a microprocessor (CPU) based upon the von Neumann computer principle: (a) Princeton structure: one memory area for data and programs (b) Harvard structure: different memory areas for data and programs

Another structure with reference to the memory is illustrated in Figure 11.4b. In this case, there are distinct memory areas for programs and data. This design is called a *Harvard structure*. It enables a parallel transfer of data and commands through separate buses. It is the basic design principle of digital signal processors (DSP), see Section 11.6.

**Table 11.1.** Several terms and units used in computer science**information contents**

bit (binary digit): memory element of a register or a memory cell, binary value of a data word or address. Possible values: 0 or 1.

$$\begin{array}{llll} 1 \text{ kbit (kilobit)} & = & 2^{10} \text{ bit} & = 1024 \text{ bit} \\ 1 \text{ Mbit (megabit)} & = & 2^{20} \text{ bit} & = 1048576 \text{ bit} \\ 1 \text{ Gbit (gigabit)} & = & 2^{30} \text{ bit} & = 1073741824 \text{ bit} \end{array}$$

byte: 8 connected bits

<b>frequencies</b>		<b>period of oscillation</b>		
1 Hz	:	1 period/s	1 s	
1 kHz	=	$10^3$ Hz	1 ms	$= 10^{-3}$ s
1 MHz	=	$10^6$ Hz	1 $\mu$ s	$= 10^{-6}$ s
1 GHz	=	$10^9$ Hz	1 ns	$= 10^{-9}$ s
1 THz	=	$10^{12}$ Hz	1 ps	$= 10^{-12}$ s

<b>transfer rate</b>				
1 bit/s	=	1 bps (baud)		
1 kbit/s	=	1 kbps	$= 10^3$ bps	
1 Mbit/s	=	1 Mbps	$= 10^6$ bps	
1 Gbit/s	=	1 Gbps	$= 10^9$ bps	

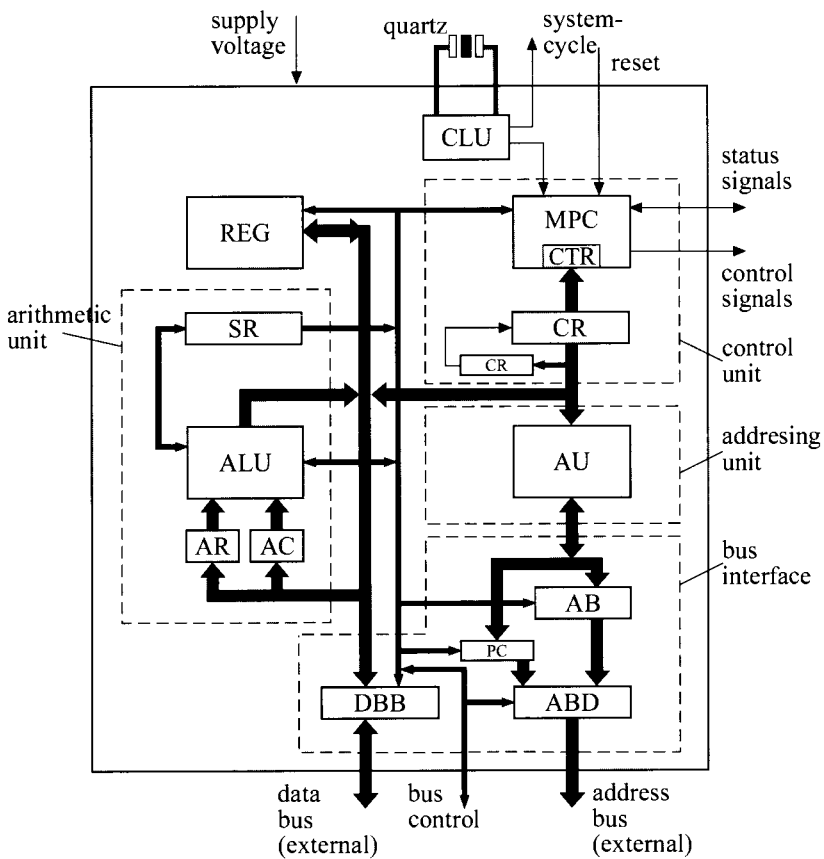
<b>computer performance</b>				
1 MIPS	=	1 millions instructions per second		

### 11.2.1 Standard Processor Architecture

The main components of a microprocessor are illustrated in more detail in Figure 11.5, see, e.g., Bähring (1994), Gilmore (1987), Whitacker (2000).

The *control unit* consists of a command register, a command encoder, microprogram control and a control register. The control unit works at a clock frequency between 1 MHz and 1 GHz. The clock unit will either be external or incorporated into the unit by means of an internal square generator utilizing external quartz synchronization. The control unit delivers control signals corresponding to a command given by a program (sequence of commands, located in the memory) to other components of the microprocessor and external components. It will be also driven from other components (interrupt). The microprocessor program consists of a sequence of machine commands (macros). Those machine commands that contain operations and components will be loaded into the command register (operational code).

The control register influences the operating mode of the processor. In writing special control words into the register (e.g., interrupts), the program specifies user or system mode, single-step mode or BCD(binary coded decimals) mode .



ABD	address bus driver	MPC	microprogram control
AC	accumulator	DBB	data bus buffer
ALU	arithmetic logic unit	AR	auxiliary register (latches)
AB	address buffer	PC	program counter
AU	addressing unit	REG	registers
CE	command encoder	SR	status register
CTR	control register	CLU	clock unit
CR	command register		

Figure 11.5. General construction of a microprocessor

The *arithmetic unit* of a microprocessor contains the arithmetic logical unit (ALU), auxiliary and status registers. Each input of the ALU is equipped with *auxiliary registers* (latches) or accumulators, which temporarily save the operands. The ALU only executes logical and arithmetic operations and therefore does not store the data. The results of the operations are transferred into a register of the microprocessor or to an ALU auxiliary register using the output bus.

The status register of the ALU is modified to indicate the state of the arithmetic unit after an operation using independent bits (flags). The main functions of the ALU consist of arithmetic operations for all numbers (e.g., addition, subtraction, multiplication, division, increment), logical

operations such as AND, OR, negation, XOR, shift and rotation operations and transport operations. More complex mathematical operations (*e.g.*, floating point arithmetics) are executed in special arithmetic processors.

A microprocessor requires several *registers* as *cache memory* with fast access time. These registers are connected either directly to the control or the arithmetic unit or are part of a special set of registers. There are data registers for operands of the ALU, address registers for selecting an operand in memory, an index register for the distance of an address to a basis address and special registers (*e.g.*, stack register).

The *addressing unit* determines the address of an operand based upon the contents of memory and registers. In modern microprocessors, the address component works in parallel with the arithmetic unit. Virtual memory is also used (MMU: memory management unit). The addressing unit consists primarily of a summation counter. The input is obtained from an internal register or from the data bus buffer. The results are stored in the program counter or in the address buffer.

A schematic diagram of a microprocessor's *internal bus system* is shown in Figure 11.5. The internal data bus connects the components: arithmetic unit, control unit, register set and addressing unit, while the address bus connects the addressing unit with the program counter. Both end in buffers and bus drivers to connect peripheral components to the internal bus system (*system bus interface*).

Addresses and data are temporarily stored and internal and external signal voltage levels are adapted. In order to connect several external devices, bus drivers are used. The registers of the system bus interface are the data bus buffer, a program counter, and an address buffer. The *data bus buffer* saves all external or internal data. It is possible to read and write data in both directions (bi-directional data bus driver). The *program counter* holds the memory address of the next command. During normal program execution, the program counter is increased by +1. In the case of jump or branch commands, the program counter is loaded directly from the addressing unit. The *address buffer* receives operand addresses from the addressing unit. The program counter and address buffer are connected to the external bus via the address bus drivers and are switched alternatively.

In order to extend the functions of the microprocessor, *auxiliary processors* are connected to the system bus interface. The control of peripheral devices or the execution of floating point arithmetics are typical tasks.

So far, universally applicable microprogrammed standard microprocessors have been described. They are capable of more than 100 commands in different formats and addressing methods. They are called CISC (complex instruction set computer) processors. In addition to their versatility and vast applicability, they are also very complex in terms of manufacturing. To reduce complexity, RISC(reduced instruction set computer) processors were developed. RISC processors feature a small set of commands (30–100) and addressing modes, so the control unit can be implemented in hardware without the need of microprograms. In general,

they feature wide data and addressing buses (at least 32 bit). All commands can be executed in only a few clock cycles (1...3) such that lower clock frequencies are required and power consumption can be reduced. Such microprocessors are predominantly used with higher-level programming languages using compilers and less often with assembly languages.

A comparison of computing times for some CISC and RISC microprocessors shows that RISC processors are somewhat faster, but newer CISC processors feature similar elements to RISC processors (*e.g.*, wide data and addressing bus, hardware-implemented microprograms) and thus reach approximately the same computing times, see Stiller (1995, 1996).

The microprocessor chip is encapsulated in a plastic or ceramic package in order to enable fixed mechanical connections, dissipate the heat and to mount the connectors. There are packages with plug-in terminal pins on the base of the socket (on two sides: dual in-line package (DIP)), or on four sides: quad-pack) or with direct solder pins (in matrix form: pin grid arrays (PGA)) for surface-mounted devices (SMD). The connections inside the package between chip and connectors are established through small gold-plated wires (bond wires). The choice of the proper package type and material depends on the operating conditions. Climatic and mechanical requirements are very important. For instance, in the automotive field, temperatures between  $-40^{\circ}$  and  $+90^{\circ}$  C are typically encountered. Failure rates of single-integrated circuits are approximately between  $10^{-4}$  and  $10^{-9}$  1/h and dependent mainly on temperature, see, *e.g.*, Schrüfer (1992). Depending on the application, demands concerning humidity, condensation, water jets, oil, fuel and dust should be taken into consideration as well. The mechanical requirements regarding accelerations (during operation, transport or production) are also important. However, due to the small masses and by casting of chips and board in plastic, this problem is not problematic, see, *e.g.*, Conzelmann, Kiencke (1995).

Table 11.2 shows a comparison of characteristic values for typical microprocessors since 1970. From this figure, we can observe a general trend of increase in clock frequency, internal memory and computing power.

### 11.2.2 Software for Standard Processors

The development of software programs for microprocessors is usually performed by development systems on the target computer or applied to other host computers. *Development systems* are used in order to design programs, to translate (compile) source programs into object programs (assembler, compiler), to find errors in programs (debugger), or to load the programs into PROM or EPROM or EEPROM simulators. The development systems consist of extensive system software and all necessary peripherals that connect the microprocessor to the development system.

**Table 11.2.** Characteristic values and properties of some standard microprocessors

	unit	Intel 8008	Intel 8080	MC 6800	Intel 8086	Z 8001	MC 68000	Intel 80286	Intel 80386	Intel 80486	Intel Pentium I	Intel Pentium II	Intel Pentium III	Athlon
year or market		1971	1974	1978	1979	1979	1982	1985	1989	1993	1995	1999	1999	2001
data bus width	bit	4	8	8	16	16	16	32	32	64	64			
cycle frequency	MHz	0.75	1	2	10	10	8	25	33	252240	60	450	733	2000
addressable memory	byte	640	64 k	64 k	1 M	8 M	16 M	16 M	4 G	4 G	4 G			
number of transistors		2300	5000	29 k		68 k	134 k	275 k	1.2 M	3.1 M	7.5 M	9.5 M	22 M	
register		16 × 4 bit	2	2 × 8 bit 2 × 16 bit	14	14	16	19	19	31				
pins		16		40						168 PGA	296 PGA			
computing power	MIPS	0.06	0.29	0.33						20	112	366	1616	2500
feature size	µm	8		6			4			1	0.28			
internal cache memory		-	-	-	-	-	-	-	-	+	+	+	+	+
internal floating point arithmetic		-	-	-	-	-	-	-	-	-	+	+	+	+

Software design by means of *host computers* uses specialized cross-software (cross-compilers).

## 11.3 MEMORY

Microprocessors usually require external memory. Modern semiconductor memory components are based on highly integrated circuits consisting of diodes, transistors, and capacitors. Figure 11.6 shows the general structure. A memory unit consists of  $n$  memory cells with  $m$  memory elements. A memory element is formed using a circuit that can take and hold a binary value (0 or 1). Memory cells consist of  $m = 8$  bit (1 byte), 16 bit (1 word) or 32 bit (1 double word).

The *capacity* of a memory unit therefore results from  $1\text{ k} \times 8\text{ bit} \triangleq 2^{10}$  bit = 1024 memory cells.

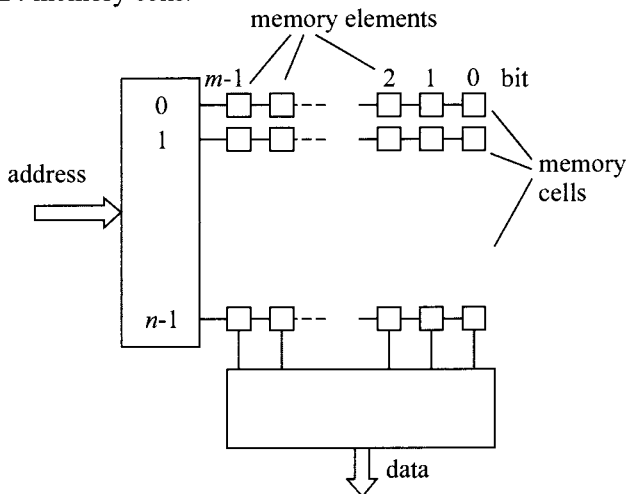


**Figure 11.6.** General structure of a main memory of  $n \times m$  bit capacity

An additional characteristic of memory is the *cycle time*, known as the time between two subsequent memory accesses. The cycle time consists of the access time (address input – data output), settling time and possible latency time (so-called wait states).

Semiconductor memory elements consists of the following components, Figure 11.7:

- semiconductor diode: only permits the passage of a current from anode to cathode if the diode voltage exceeds a specified threshold voltage (e.g., 0.5 V), working similar to a current valve;
- bipolar transistor: if the control voltage between base and emitter exceeds a threshold voltage (e.g., 0.5 V), a small base current flows. The transistor becomes conductive between collector and

emitter, so an external voltage drives a collector current, with a voltage drop on an external resistor (pull-up resistor). In this case, the transistor output voltage becomes zero. In the other case, it is equal to the external voltage. The transistor works as a binary inverter;

- MOS transistor: A MOS (metal oxide semiconductor) transistor is produced by diffusion of foreign atoms into a mono-crystal silicon layer (so called n- and p-zone with an excess of negative or positive charge carriers respectively). The connectors for drain (D) and source (S) electrodes are etched into the  $\text{SiO}_2$  isolation layer. The gate (G) electrode is connected to the isolation in between drain and source electrode. Applying a control voltage between G and S above a threshold limit creates an electrical field between G and the silicon substrate (field effect transistor), which makes the transistor conductive between D and S. Thus, a low-power switch is created. A positive external voltage between D and S generates the current. In exchanging the dotation of the zones, a complimentary MOS transistor is obtained. Connecting both transistor types, one obtains an inverter in CMOS (complimentary MOS) technology. In this case, only power is needed for changing the switching state, thus creating an element that has less power consumption.

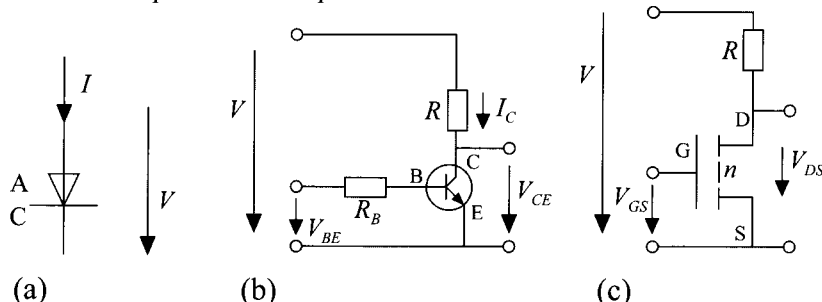


**Figure 11.7.** Components of semiconductor memory elements: (a) diode; (b) bipolar transistor; (c) MOS transistor. A: anode; B: base; D: drain; K: cathode; C: collector; S: source; E: emitter; G: gate (control electrode)

Memory elements are constituted from these components, which are located at an intersecting point of a selection and a data line (row and column of a matrix structure).

Semiconductor memory can be subdivided into two main groups: read only memory and write-read memory. In the case of ROM (read only memory), the memory content, once written, remains after disconnection from the power supply (non-volatile memory). On the contrary, RAM (write/read memory-random access memory) can be changed during normal operation, but loses its content once power is cut off (volatile memory).

The following section describes the construction of different memory types, their properties are summarized in Table 11.3.

**Table 11.3.** Overview of different semiconductor memory types

classification	semiconductor elements	capacity	access time	power	remarks
read only memories	ROM diode bipol. trans. MOS / CMOS	≤ 16 Mbit	200–350 ns	75–300 mW	mask programmed during production; large series production
	PROM diode bipol. trans.	≤ 1 Mbit	≥ 35 ns	100 mW	
EPROM	MOS CMOS	≤ 1 Mbit	150–450 ns	100 mW	5 μW programming by current pulses with user devices
EEPROM	MOS CMOS	≤ 256 kbit	55–450 ns	300 mW	125 mW programming by current pulses; erasing with UV
write-read memories	SRAM bipol. trans. MOS / CMOS	≤ 1 Mbit	15–150 ns	300 mW – 1 W	programming and erasing by current pulses with microprocessor
	DRAM MOS CMOS	≤ 16 Mbit	100–250 ns	190–350 mW	
NVRAM	MOS	16 kbit	150–300 ns		150 mW volatile memory memory refreshing; low power consumption
					non-volatile memory

The most important read only memory types are ROM, PROM, EPROM and EEPROM.

ROM (read only memory) is “mask” programmed during the manufacturing process. Depending on the working principle of the memory elements, this can be achieved by different means. In the case of a diode array, the diodes connecting a selection and a data line are either provided or not. If bipolar transistors are used, their basis connection is either wired or not. In MOS transistors, this effect is achieved by a different thickness of the gate insulation layer.

PROM (programmable ROM) is a user programmable read only memory, which may be programmed only once (OTP, one time programmable). Using specialized programming devices, the connections between selector and data lines can be destroyed (melting of a resistor) or their characteristic can be changed (conversion of a diode into a resistor). ROM and PROM cannot be changed after programming.

EPROM (erasable and programmable read only memory) is programmed by the user and can be erased by UV radiation. This type of memory uses MOS transistors, which have a supplementary control electrode in the isolation layer (floating gate) (FAMOS). By applying a programming voltage, the control electrode is charged and the characteristic of the field effect transistors changes so the transistor does not conduct at normal operating voltage. UV radiation discharges the load of the control electrode.

EEPROM (electrically erasable and programmable read only memory) is programmable read only memory that can be reset by electronic inputs. It consists of MOS memory transistors with an additional control electrode (like FAMOS transistors) and a switching transistor. Hence, the discharge of the control electrode can be initiated electrically.

Write/read memories belong to the RAM (random access memory) group. SRAM and DRAM can be distinguished between.

SRAM (static random access memory) features flip-flop circuits consisting of two feedback bipolar transistors with two emitters, MOS transistors or CMOS-inverter transistors. In order to write the memory content, for example, one of the transistors is brought into a locked state and the other into a conductive state in connecting selector and data line to high potential.

In order to read, the data lines are put on low potential while the emitter is put on high potential using the selector line. In this case, the conductive transistor allows current flow into the data lines, providing the information through a read amplifier. Static MOS or CMOS memory cells are built using several transistors. SRAM retains the information until it is overwritten, or the power supply is cut off.

DRAM (dynamic random access memory) consists of a MOS or CMOS transistor and a capacitor. In order to write, the gate electrode is put on high potential. The transistor becomes conductive and charges the capacitor, which is integrated into the drain zone. In order to read, the gate electrode is put on high potential and the discharge current through the

data line is measured by a read amplifier.

Current flow only occurs during read or write operations, resulting in a low power consumption. However, the memory content must be rewritten after reading and after certain time intervals to compensate for the self-discharge of the capacitor.

NVRAM (non-volatile random access memory) consists of both a static RAM memory cell and a EEPROM cell. During normal operation, the static RAM is active. When needed (*e.g.*, shortly before power is cut off), the memory content is transferred into the EEPROM cell.

As shown above, several additional circuits are needed for the operation of a memory unit. Examples are: read and write amplifiers, line and column selectors, data bus interfaces, and the control logic of the entire memory, see Bähring (1994), Christiansen (1996), Whitacker (2000), Chen (2000) for details.

In addition to main memory, *cache memory* has become increasingly necessary. Cache memory is utilized as buffer memory between microprocessor and main memory. To reduce costs, cheaper DRAM cells with relatively large access times are used for large main memory requirements. As clock frequencies increase with each processor generation, cache memory consisting of fast SRAM cells is interconnected. Applying intelligent strategies (*e.g.*, buffer data most frequently used, or intelligent data read ahead), the fast cache memory can provide the necessary data without the need to access the slow DRAM cells, Bähring (1994), Rembold, Levi (1994).

## 11.4 INTERFACES TO THE PROCESS (PERIPHERALS)

The connection between the physical process and the microprocessor is achieved by the use of special interface components. These interfaces process the analog, binary or digital input signals, save them, and transmit them as digital signals to the microprocessor. On the output side, the interface components save, process and convert the digital signals of the microprocessor to analog, digital and binary outputs, see Figure 11.8.

Examples of input interface components are, *e.g.*, sensors or a keyboard, output components are actuators and displays. Therefore, one can distinguish between:

- analog inputs;
- digital and binary inputs;
- analog outputs;
- digital and binary outputs.

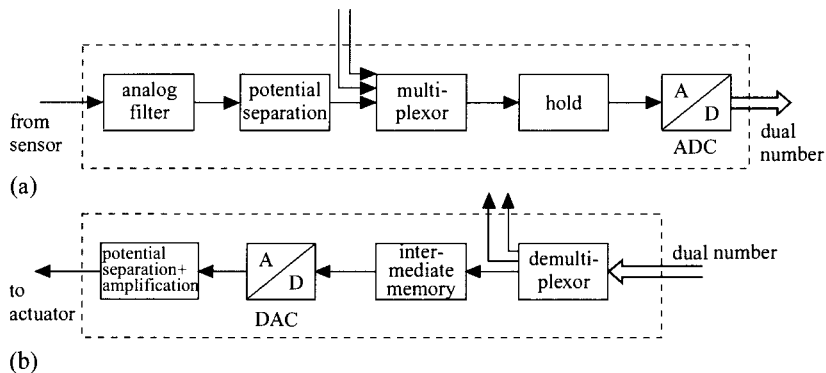


**Figure 11.8.** The general scheme of an analog/digital interface: (a) analog input (ADC: analog digital converter); (b) analog output (DAC: digital analog converter)

### 11.4.1 Analog Inputs

Figure 11.8a shows the general design of an analog input interface. It consists of the following components:

- analog filter: as analog signals are sampled at discrete time intervals  $T_0$ , signal components above the Shannon frequency ( $\omega_0/2 = \pi/T_0$ ) cause low-frequency errors in the measured signal, which cannot be corrected by subsequent digital signal processing. To prevent these errors, each analog input should feature an analog filter with a cut-off frequency less than the Shannon frequency  $\omega_f < \omega_0/2$  (anti-aliasing filter);
- potential separation: a galvanic separation between the microprocessor and its periphery is recommended, since both may have different voltage potentials that could damage the electronic components. This is achieved by the use of optoelectronic couplers or isolation amplifiers;
- multiplexor: in the case a single A/D converter being used for multiple channels, the measuring signals have to be connected successively. This is achieved by an array of electronic switches (e.g., field effect transistors);
- hold element: at the beginning of each sampling interval, the analog value is set into a hold element for the duration of the conversion process. The hold element is an analog memory element, for instance, a capacitor (zero order hold element);
- analog-to-digital converter (ADC): the analog signal is converted into a digitally coded output signal. Thereby, the analog signal is quantized utilizing the word length  $WL = n$  bit (without sign bit). The binary code is valid for the number range

$$NR = 2^{WL} - 1 \quad (11.4.1)$$

Based upon this, the resolution (quantifying unit) is

$$\Delta = \frac{1}{NR} = \frac{1}{2^{WL}-1} \approx \frac{1}{2^{WL}} = \frac{1}{2^n} \quad (11.4.2)$$

Table 11.4 contains some numerical values.

**Table 11.4.** Quantifying unit in dependence of word length

word length (in bits)	8	10	12	15
number range	255	1023	4095	32767
quantization unit $\Delta$	0.00392	0.00098	0.00024	0.00003
quantization unit $\Delta$ [%]	0.392	0.098	0.024	0.003

The digital signal is represented by a binary number, a sum of base 2 powers.

$$N = a_{n-1} 2^{n-1} + \dots + a_1 2^1 + a_0 2^0 \quad (11.4.3)$$

The coefficients  $a_i$  are binary variables with value 0 or 1. In short notation the powers of 2 are omitted (as in the decimal system). For example, the binary number 10101101 with a word length of 8 bit = 1 byte corresponds to the decimal number 173. The digital number is transmitted to the microprocessor via parallel or serial interfaces.

According to their working principle, analog-to-digital converters can be subdivided into:

#### *ADC with potential reference input element*

In parallel ADCs, the input signal is compared simultaneously with  $2^n - 1$  reference signals. Thus, the conversion is very fast (< 100 ns). However, the expenditure in circuitry is certainly high (flash converter). Serial ADCs require only a single comparator. In incremental ADCs, the reference voltage is incrementally increased until it exceeds the input voltage. The number of increments is counted (approximately 4 ms conversion time at 12 bit, 1 MHz). If the principle of successive approximation is used, at each step one bit of the result is determined, leaving an analog remainder for the next step (approximately 1...10  $\mu$ s conversion time at 8...16 bit).

#### *ADCs with time or frequency counter*

In the first stage, the input voltage is converted into a time interval or frequency. The resulting oscillator impulses are counted. Sawtooth ADCs work with a ramp generator and the impulses are counted until the input voltage is reached (single-slope converter). If a potential-frequency converter is used, the input potential is integrated and the time is counted until a reference potential is reached. Dual-slope ADCs integrate the input potential. Subsequently, the integrator is discharged with a constant negative reference potential. The discharge time is counted. This procedure limits the influence of component tolerances.

All of the described ADCs are instantaneous-value converters. Disturbing signal components can be reduced by the averaging of a given time interval. By integration of 20 ms periods, net frequency 50 Hz-disturbance signals are completely eliminated, for instance, using an integrated two-slope ADC.

A detailed design of different ADCs is described in Färber (1994), Lauber (1989), Profos, Pfeifer (1992), Schrüfer (1983), Christiansen (1996), van den Plassche (1994).

Analog input units consisting of a multiplexor, hold element and ADC are obtainable as hybrid elements or integrated circuits.

### 11.4.2 Digital and Binary Inputs

Usually, digital inputs are acquired word-wise, meaning that a group of  $m$  digital inputs with  $n$  bit word length is moved into the microprocessor simultaneously. The digital signals may either have pre-defined logic voltage levels (e.g., TTL (transistor-transistor-logic) levels: low-level: 0 – 0.8 V; high-level: 2.0 – 5.5 V) or the signal levels have to be adapted (e.g., by optoelectronic couplers or resistance networks). Special circuits exist with high sensitivity to signal changes (slope detectors). If the number of slope changes is of interest (incremental, or frequency-analog sensors), specialized counting circuits are used.

### 11.4.3 Analog Outputs

In order to operate analog components such as servo-motors, indicating instruments, chart recorders or analog controllers by a microprocessor, a digital value of length 8 to 16 bit has to be converted into an analog voltage or an analog current.

The overall structure of an analog output is shown in Figure 11.8b. In general, the following components can be distinguished:

#### *Demultiplexer*

The output value arrives from the data bus as a binary number of word length  $n$  and is distributed to the appropriate output line according to the information on the address bus.

#### *Temporary memory*

Stores the output data until it is overwritten.

#### *Digital-to-analog converter (DAC)*

The DAC converts the digital word into an analog value. A DAC may be seen as a controllable voltage source. This can be realized by a constant current source, which feeds a resistor network. The resistor network consists of a series connection of  $n$  resistors, whose values decrease by a factor of 2 ( $R_i = \frac{1}{2} * R_{i-1}$ ). Each resistor features an electronic switch (bipolar or FET transistor) connected in parallel, which is closed at 0 input

and opened at 1 input according to the respective bit of the digital input value. The voltage on the resultant resistor of the series connection corresponds to the digital value. An alternative approach is a parallel resistor network, which is fed by a reference voltage source. The resistors are graded in relations of powers of 2. Each resistor has a switch connected in series. The cumulative current is equivalent to the digital value. To convert the current into a voltage, the current is fed into a simple inverting operational amplifier stage.

Disadvantage of these DACs is the large domain of resistance values that are needed at larger word lengths (for instance,  $1 : 2^{12}$  or  $1 : 4096$  at 12 bit). In order to reduce the number of resistance values needed, a  $R/2R$  series/parallel resistor network is used. Although the number of resistors doubles, only resistors of value  $R$  and  $2R$  are needed. Independent of their absolute value, only their relation is of importance.

Voltage output can be unipolar (*e.g.*, 0...10 V) or bipolar (*e.g.*, -5...+5 V). Current outputs with 0...10 mA or 4...20 mA are commonly used. The minimum allowance of the load resistance, where the current can be provided, has to be taken into account.

The conversion time of DACs is relatively small (*e.g.*, 1  $\mu$ s).  $2^n$  different voltage levels can be realized with  $n$  bits. An  $n = 8, 12, 16$  bit resolution results in an output signal quantization of 1:255, 4095, 65535 respectively. DACs are available as integrated circuits featuring several analog outputs, which can be selected by an address input. Demultiplexer, temporary memory (buffer) and DACs are typically combined in a single-integrated circuit. For details see Tietze, Schenk (1989), Christiansen (196), van den Plasschke (1994).

#### *Potential separation and power amplifier*

For the same reasons as for analog inputs the outputs should feature a galvanic separation between microprocessor and analog output signal. This can be achieved by optoelectronic couplers on the digital side of the DAC. In this case, the DAC has the same potential as the analog outputs. If the potential separation is on the analog side of the DAC, isolation amplifiers or analog optoelectronic couplers can be used. A power amplifier provides the required power for the analog outputs, *e.g.*, operating a servo-motor.

#### **11.4.4 Digital and Binary Outputs**

Digital outputs can be used to control external relays or binary indicators, to transmit digital signals to accessory equipment or to generate special binary pulse sequences. Similar to analog outputs, a digital output port consists of an  $n$ -bit array of switching elements, each connected to an output pin. The data bus information is connected directly to the switching elements according to the address present at the address bus. The output is only valid as long as the address of the respective output is present on the address bus. Some external components (*e.g.*, relays) require continu-

ous output levels. In this case a latch register is interconnected, which stores the state of the output port until it is accessed again.

Digital outputs may produce specified voltage levels (*e.g.*, TTL levels) or operate an electronic switch (*e.g.*, bipolar transistors or optoelectronic couplers) for control of external voltages or currents. Potential separation is achieved by the use of optoelectronic couplers.

Electronic displays are also controlled using the digital outputs. For the numerals 0–9, at least four binary variables are needed. In this case, different binary codes such as BCD (binary coded decimals), Aiken code, Gray code or other fault-tolerant codes are used, see Schrüfer (1992), Christiansen (1996).

Several types of displays can be distinguished: cathode-ray tubes (CRT) or flat displays (*e.g.*, matrix displays) and static displays. Matrix displays consist of an  $n \cdot m$  matrix of indicating elements, segment displays of at least seven segments. The indicators may be light-emitting diodes (LED) or liquid crystal displays (LCD). Flat panel displays are mostly based on LCD displays, where liquid crystal molecules align themselves parallel to an electrical field and lie flat when no field is applied. Typically, displays are driven by specialized integrated circuits.

## 11.5 MICROCONTROLLERS

Microcontrollers are highly integrated circuits that integrate microprocessor memory, data memory, input and output interfaces, and additional peripheral functions (for instance, timer, bus controller, *etc.*) on a chip.

When the production number for on-line applications became large enough as, for example, for digital control, microcontrollers were produced that integrated the separated circuits of one-board computers into one chip. Through higher integration of microcontrollers, the number of elements and the error sources can be further reduced.

Newer developments in the field of mechanic-electronic systems show a trend towards integration of decentralized control of components. Through this integration, decentralized information is accessible for real-time applications of the entire system (*e.g.*, wheel speed information of anti-lock brake systems in automobiles used for gear control). Generally, the integration of decentralized microcontroller structures are achieved through the use of a data bus system (for instance, CAN bus) or of a number of smaller microcontrollers in a central, highly integrated microcontroller (one-ship solution).

The widespread use of microcontrollers in modern systems increases substantially in all fields of investment and consumer goods.

### 11.5.1 Architecture of Microcontrollers

The construction of a microcontroller is characterized by its modular structure. This provides a fast adaptation of a standard controller to customer requirements with a specially adapted configuration, for instance, power electronics for engine control, CAN bus interface, PWM generator, *etc.* Construction and design of individual modules are characterized by special real-time requirements within the microcontroller. A description of the construction of microcontrollers, using the example of a 16-bit standard controller Siemens (Infineon) 80C166, is found in Figure 11.9.

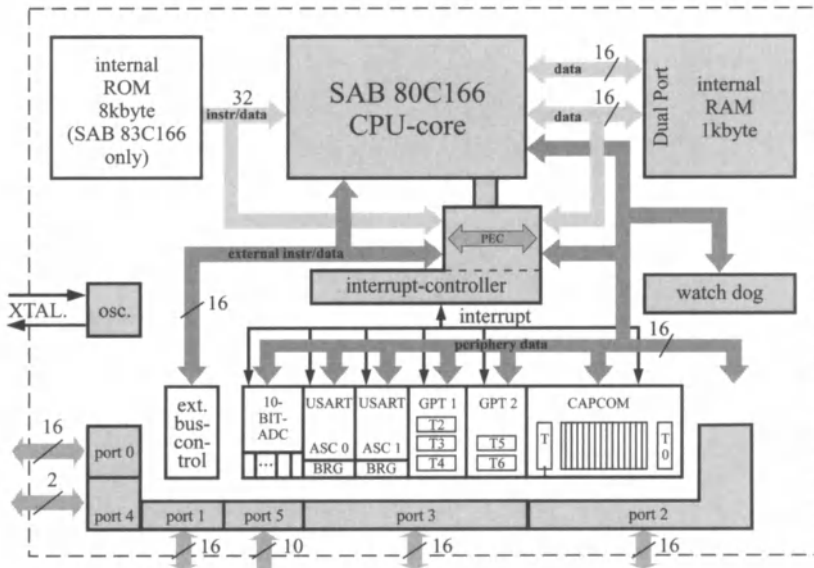


**Figure 11.9.** Block circuit diagram of the standard controller 80C166, Fleck, Bauer (1989)

- CPU: the CPU is the main part of the entire data processing within the microcontroller. Important components of the CPU are the flow control with address management and the command decoder as well as the ALU (algorithmic logic unit). Processing of most commands happens in one cycle ( $100\text{ ns}$  at  $f_{CPU} = 20\text{ MHz}$ ) for exclusively internal memory access;
- ROM: all information (programs, data, *etc.*) that will not change during the processing activity of the controller is stored into the ROM. Controllers with mask-programmed ROMs are useful only for large series ( $>1000$  pieces) as the prices are high for mask production. EPROMS are used during the development phase for a small number of pieces in order to store programs and constants. They are preferably applied when the number of items does not warrant the expenditure of a mask but the program has a mature status. When using an EEPROM memory, one needs considerably more space than with an EPROM version and is more expensive.

Due to ease of use and their partially erasable property, EEPROMSs are used in all applications where data should be preserved in the case of power supply failure. An example is the storage of adapted process parameters, *e.g.*, process-specific calibration data. There are also microcontrollers with various ROM variants available on the market;

- RAM: the RAM in microcontrollers is implemented primarily as static memory. Comparing with dynamic memory, this kind of memory has the advantage that it does not have to be refreshed. The internal RAM is designed, depending on periphery, as a dual-port RAM that enables the periphery to directly access the data. In the case of the 80C166, this access is controlled through a peripheral event controller (PEC);
- interrupt controller: the interrupt controller enables the interrupt-controlled program through interruption sources of integrated periphery as well as through external interrupts at the port pins;
- EBC: the EBC (external bus controller) is responsible for the access to an external memory. Depending on addressed memory cells, the EBC activates the pre-selected bus configuration and takes over the selection of signals;
- serial I/O interface: most microcontrollers have one or two serial interfaces at their disposal that work with various synchronization modes (asynchronous and synchronous) between transmitter and receiver. The asynchronous transfer mode is used for communication with standard periphery (for instance, printers, monitors, *etc.*) and the synchronous mode is used for transferring special periphery electric circuits and by coupling more controllers. The 80C166 is equipped with two identical synchronous/asynchronous serial interfaces (ASC0 and ASC1) (USART: universal synchronous/asynchronous receiver/transmitter);
- timer and capture-compare unit: in most cases, the timer units (GPT1 and GPT2 of 80C166) are laid out very flexibly. They can be connected in parallel as well as serial, and enable functions like pulse counting, time measurements and time-difference measurements. Furthermore, they form the basis of cyclic processing. The capture-compare unit is used to generate the digital-to-analog conversion of PWM-signal generation and the time measurement of external events;
- analog-to-digital converter: ADCs exist on most microcontrollers. They are differentiated by the number of quantifying levels as well as by the conversion modes (for instance, one-channel conversion, continuous one-channel conversion, autoscan mode, *etc.*) The converter can be externally triggered depending on the inputs of the CAPCOM unit. The 80C166 uses a 10-channel ADC with a 10-bit wide quantifier;
- WDT: using the WDT (watch dog timer), the right processing of the programs are monitored. When processing errors are encoun-

- tered, the WDT reset is achieved by resetting the on-chip periphery and changing the instruction pointer (IP) value zero (0);
- other modules: in addition to the above-mentioned modules found in almost all microcontrollers, customer modules can easily be implemented using the modular concept of microcontrollers. Examples of such periphery units can be found in the automotive field, audio field, telecommunications, and so on.

Table 11.5 shows a classification of microcontrollers based upon data bus width. Certainly, the lower performance class of 4-bit controllers not discussed here still have a great impact on the market. However, due to low arithmetic performance, these controllers find less application in the area of mechatronic systems. In the meantime, while market interest has shifted to the 8-bit microcontrollers.

**Table 11.5.** Parameters of microcontrollers with various internal data bus width (compare also market overview N.N. (1994, 1995) and Morgenroth (1995)).

data bus width	8 bit	16 bit	32 bit
cycle frequency	4–33 MHz	8–40 MHz	8–66 MHz
chip size (pins)	16–128	40–160	–240
basis functions	memory universal timer or counter units interrupt logic serial and parallel interfaces		
additional function	memory (EPROM, EEPROM, Flash, DRAM interface) DMA channel, RTC interfaces: A/D, PWM, I <sup>2</sup> C, USB, Firewire, Bluetooth PCMCIA interface, LCD controller, video controller, audio interface CAN controller fuzzy hardware		
examples of products	Intel 80C51 Motorola 68HC05 TI cMCU370	Siemens 80C16X Intel 80C196 Motorola 68HC16	Intel i960 Motorola 68332 Motorola 68328
application examples	heating control washing machine  automobile (I/O, supervision)	automobile (engine, transmission control, ABS) drive controller  field devices	PDA, telecommunications, laser printer, plotter

The computational capacity of this type of microcontroller is enough for many sequence-control applications and for the control of slow processes (*e.g.*, heating). For intensive computation application with fast processes (*e.g.*, automotive), 16-bit controllers are usually used. Because of high costs, solutions involving 32-bit controllers remain an exception within the field of automation. However, a gradual transition from 16-bit controllers to 32-bit controllers is expected.

A further classification of performance characteristics of particular architectures is difficult because almost each customer uses modular design techniques. Therefore, great flexibility exists in the design of microcontrollers. Shipped variations of many producers reach the hundreds, Höfling (1994).

Herewith, the widespread 8-bit controller exhibits the largest variety in periphery function. Examples for customer variants are the integration of a motor full bridge circuit and a 8-bit microcontroller on one chip presented in Sax (1993), as well as the VeCon chip that contains a C165 microcontroller core and additional functions for field-oriented control of AC drives in Kiel, Schumacher (1994).

### 11.5.2 Software for Microcontrollers

Different development systems exist for the software development of microcontrollers. In many cases, the programming is done in a high-level programming language such as C, Pascal, or Forth. With the help of a cross-compiler that generally runs on a host computer (PC), the program code for the target system is translated into machine code and loaded onto the microcontroller using a monitor program. The cross-compilers are often designed for the entire microcontroller family. There are also consumer-friendly graphical user interfaces (GUI) for DOS or Windows. Integrated development environments (IDE) with a combination of an editor, compiler, and debugger represent another possibility. For a large number of pieces where the performance and the memory capacity of microcontrollers are low primarily due to cost prohibitions, the programs are generally written in assembler or directly in machine code. Debugging represents a problem with the programming of microcontrollers. For simple applications, simulators that emulate the microcontrollers on the development computer are offered. The professional systems function with so-called in-circuit emulators (ICEs) that replace the microcontroller directly in a circuit using an emulator. The emulators are differentiated through real-time capability and non-real-time capability variants. Another approach to debugging microcontrollers is offered by using powerful microcontrollers for bond-out chips where the internal values are accessible through extra pins.

## 11.6 SIGNAL PROCESSORS

Digital signal processors (DSP) are microprocessors specially designed for digital signal processing. Although there are many different DSP manufacturers, they are mostly designed with the same basic features in mind: specialized, efficient and high-speed arithmetic, interfaces for data transfer to the real world and memory architectures that allow multiple and fast access. Therefore, DSPs are especially efficient in computing digital fil-

ters, correlation functions or Fourier transformations. They are usually based on an advanced Harvard architecture, which has separate buses for reading program memory, reading and writing data memory, allowing parallel command and data transfer. The available multipliers and adders can also be used in parallel within a single instruction cycle. To increase the efficiency of arithmetic operations, intermediate values can be held in the numerous registers, which may be of fixed-point or floating-point format. Another characteristic feature of DSPs is the ability to generate efficiently the new addresses for program or data access. By using special address registers, the next address can be generated with no overhead. Beside the mentioned registers, several other special memory registers, *e.g.*, program cache, embedded flash memory and boot ROM are often available on chip. DSPs not only possess multiple internal communication routes but also a variety of ways of receiving and transmitting data in real-time from and to the connected hardware. This includes a set of analog-to-digital converters, timers, high-speed synchronous serial I/O ports, asynchronous serial ports, CAN bus interfaces and powerful interrupt-handling systems with a quick response to interrupt events. For data exchange at high rates, most DSPs are equipped with a DMA (direct memory access) controller, which can read from and write to DSP memory simultaneously without stopping the DSP. These DMA communication ports are used to communicate with a host processor, for example, to download new software or parameters to the DSP or to set up a multiprocessor system for additional computational power.

DSPs are traditionally used in telecom applications like speech synthesis, error-correction coding, baseband modulation and demodulation. They are also widely used in the field of digital control. The TMS320F2X family is specially designed for digital control applications. Figure 11.10 shows the core block diagram of the 32-bit control DSP TMS320F28XX. Its performance is extensible up to 400 MIPS. With on-board flash memory and the fact that system and math code may be developed completely in C/C++, the development time for DSP applications can be remarkably reduced. Besides a high-performance CPU with an advanced Harvard structure, there are several peripherals included that are needed in digital control applications: up to 45 peripheral interrupts, two event managers with general purpose 16-bit timers, compare/capture PWM units and quadrature-encoders, three 32-bit timers, a 12-bit A/D-converter with a conversion time (sample and hold and conversion) of 200 ns that can convert up to 16 multiplexed analog input signals, enhanced CAN module compliant with CAN protocol 2.0B and data rates up to 1 Mbps.

Since the introduction of the first programmable signal processor i2920 from Intel (1979), a very rapid development has been recorded in the field of integrated digital processors. Today, there exist a large variety of DSP chips that can be classified as universal signal processors (for instance, TMS320FX from Texas Instruments and DSP5601 from Motorola) that exhibit no special design and specialized signal processors (for instance, BDSP91V24 from Sharp that performs FFT, AD9844A for Ima-

ging and CCD processing). Table 11.6 contains a comparison of several spread signal processors.

The programming of DSPs is often accomplished in assembler language or in C. An example of an application of a high programming language to hardware-in-the-loop simulation with DSP is described in Hanselmann (1996). Numerous application notes and code samples for DSPs can be found on the web and in the home pages of the DSP manufacturer. For further literature see Lane and Martinez (2001), Rorabaugh (1998), Morgan (1996), Grant (1996), El-Sharkawy (1997).

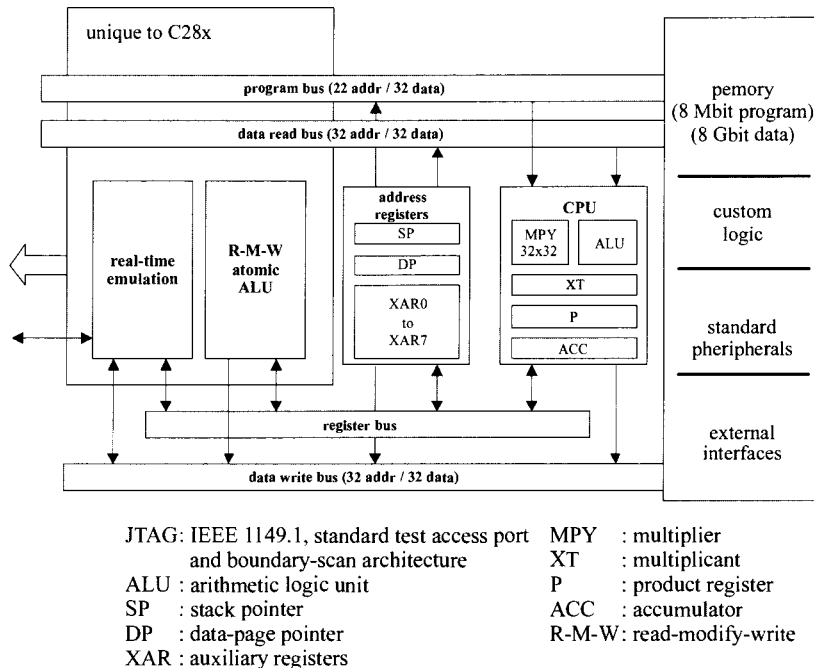


**Figure 11.10.** Core block diagram of the 32-bit digital signal processor DSP TMS320RF28XX

## 11.7 APPLICATION-SPECIFIC PROCESSORS (ASICS)

The design and production of microelectronic circuits is accomplished through numerous methods and techniques utilizing VLSI (very large scale integration) circuits. Therefore, the complexity of highly integrated circuits can only be controlled using special principles, see Rammig (1989), Post (1989), Wunderlich (1991), Bleck *et al.* (1996). These principles include the hierarchical structuring in transparent circuit parts, local (capsulated) module circuits, only few standard circuits, spatial structure

after the signal flow with minimal connection lengths and testability during the design and after production. Herewith, scientific criteria take priority, meaning that a favorable compromise can be achieved by varying chip area, design and production costs, design and production times depending on production numbers.

**Table 11.6.** Data of several digital signal processors

device	cycle time	width of the data bus	
		floating point	fixed point
<b>Texas Instruments</b>			
TMS320C64X	2.5–1.67	–	32/40
TMS320C67X	7–6	32/32	–
TMS320VC5502	5	–	32/40
TMS320F2810	6.67	32/64	–
<b>Analog Devices</b>			
ADSP-2191M	6.25	–	16/40
ADSP-21161	10	32/40	–
ADSP-TS101S	5.56	32/80	–
ADSP-21532	3.33–1.66	–	16/40
<b>NEC</b>			
$\mu$ PD77018A	16.6	–	16/40
$\mu$ PD77112	13.3	–	16/40
<b>Motorola</b>			
DSP5630	10	–	24/56
DSP56824	14.28	–	16/36
DSP56852	8.33	–	16/36

In addition to the standard VLSI circuits, application-specific circuits are also necessary for smaller piece numbers. In the case of so-called ASIC (application-specific integrated circuits), continuously new features are offered. Using suitable design software (for instance, with hardware-description language VHDL) and prepared basis circuits, individual VLSI circuits are available to the user, without necessitating an in-depth knowledge of semiconductor production technology. See, for example, Glesner *et al.* (1993), Herpel (1995), Bleck *et al.* (1996).

In order to design VLSI circuits, two approaches have been developed: the full custom-specific design and the semi-custom-specific design. In full custom-specific design, the VLSI circuits are optimized down to the lowest level, in order to achieve the smallest chip, the highest circuit speeds and the lowest power losses. However, this design is expensive and implies a great effort. Therefore, this way is usually only recommended for standard circuits produced in large numbers as for microprocessors. A

semi-custom-specific design uses existing components and circuits based upon given libraries. Therefore, the design and production costs are lower as a result of the inherent optimal properties. This procedure is suitable for a small to medium production number. The following methods are applicable in this semi-custom design:

- cell design: prefabricated *standard cells* (logic cells) in optimal form are placed in line-order by the manufacturer, and wired in accordance to the problem. Another possibility is the use of *macro-cells* in the form of function blocks. In this case, standard cells are placed in macro-cells conveniently arranged on the chips surface, such that microprocessor kernels, RAM or ROM can be built in. As in the case of full custom design, the production steps have to be followed completely such that production costs can be saved;
- mask-programmed circuits: prefabricated *wafers* (silicon discs) are used, in which a large number of various cells such as transistors, gates, drivers and so on already exist (semi-fabricated products in large number of pieces). In this way, only the wiring level has to be designed and produced. In the case of *gate-arrays*, the cells have the form of an unwired matrix and are wired through the design of channels. In the case of *sea-of-gates*, no fixed wire channels are available and the wiring space (two metallic levels) is gained by not using transistors. The design in this case is certainly more complex than that of gate-arrays;
- reconfigurable mask-programmable circuits: here, the prefabrication goes a bit further because a prefabricated component with function cells is used. The user can wire this component electrically using a programmable device (such as for EPROM). The FPGA (field-programmable gate-array) falls into this category. The wiring can even be changed afterwards. Because of low fixed costs and also reusability, this procedure can also be applied in the case of small production numbers.

## 11.8 FIELD BUS SYSTEMS

Buses are common connections to exchange information among several participants. Therefore, communication handling has to follow certain transfer rules. Especially for different participants, it is important that not only the electrical data, but also the mechanical connections are specified and standardized.

Depending on the method of bit transfer, in parallel in different ways or one after another on one wire, parallel and serial buses are distinguished. In process automation, parallel buses are used for short distances (max. 20 m) and serial buses for larger distances (20 m up to max. 15 km).

Various levels are differentiated. The lowest automation level close to the process is indicated as a “field”.

In the following, field buses that are part of a *local network* (LAN: local area network) connecting individual components such as microcomputers, sensors, actuators and switches, are briefly considered, see Figure 11.11. One distinguishes between *universal field buses*, with real-time computers connecting decentralized digital controllers and sensors and actuators with digital outputs, and special *actuator-sensor field buses*, with simple sensor and actuator connections, eventually with auxiliary power supply.

The following description gives a short overview. Detailed descriptions of bus systems are found in Färber (1987, 1994), Bender (1990), Rembold, Levi (1994), Kriesel, Madelung (1995), Reissenweber (2002).

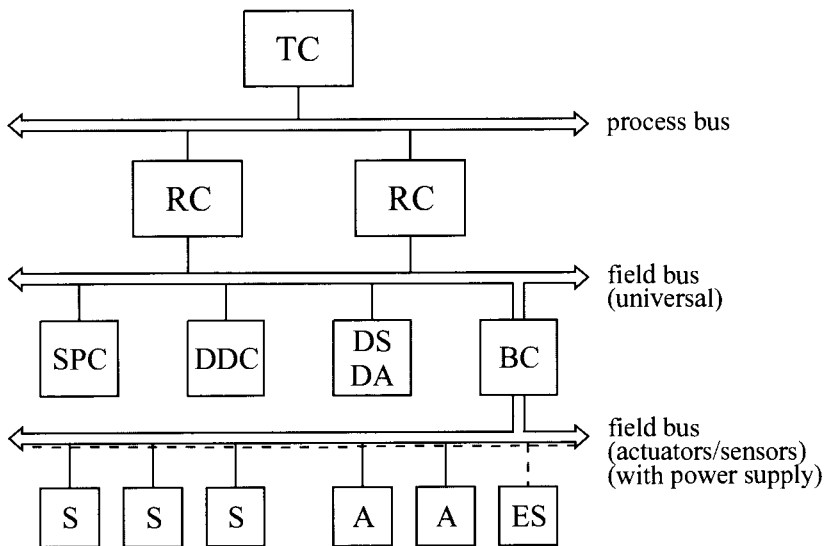


**Figure 11.11.** Structure of buses in a process automation system; TC: top computer, RC: real-time computer (control in the higher level), SPC: storage-programmable control, DDC: digital control (lower level), DS/DA: sensor and actuator with digital output, BC: bus converter (bridge), S: sensors; A: actuators; ES: auxiliary energy supply

### 11.8.1 Net Topologies

The most important basic structures of local nets are depicted in Figure 11.12. One differentiates between:

- star structure: the participants are connected to the central unit through individual lines. The advantages of this structure are a fast real-time operation and increased reliability in the case of line disturbances. The disadvantages are the expensive cable costs and the potential of an overall failure when the central unit fails;
- ring structure: the participants are serially connected through a

- bus ring with information transfer to its neighbor. Cable costs are low, but disturbances of one participant or the bus have an effect on all participants. Furthermore, only relatively slow operation is possible;
- bus structure: the participants are connected in parallel through a common bus. Cable costs are relatively low, the transfer structure is simple and semi-rapid real-time operation is possible. However, disturbances of the bus have an effect on all participants.

Generally, for field buses, the used bus structure is the one depicted in Figure 11.12c. If then connections are made using bus converters, see Figure 11.11, tree structures develop. In order to ensure a low cable effort and to achieve a semi-rapid real-time operation, field buses are usually defined as serial buses. The signal transfer is realized for electrical buses through one wire, twisted pair wires, or shielded coaxial wires. Partially for pair lines, electrical energy for field devices (direct current or 50 Hz-alternative current) is also transferred. The bus connection is implemented galvanically through optical-decoupled bus drives or inductively through transformers. Another possibility is the use of optical buses in the form of light wave conductors as glass fibers or plastic fibers. They cannot be electromagnetically disturbed but have a relatively high damping for great distances and at each participant. For this reason, a ring structure is preferred, Figure 11.12b.

Wireless field buses were also developed using infrared or microwave transfer, Färber (1994).

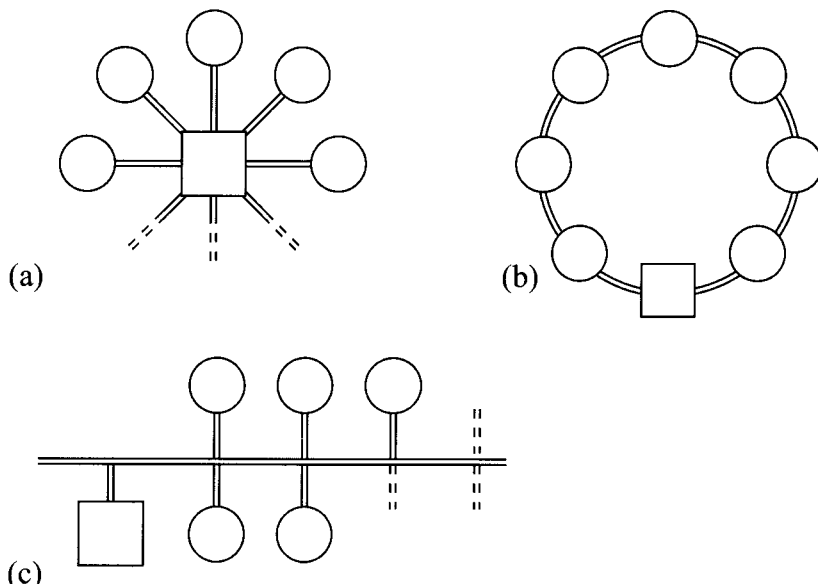


**Figure 11.12.** Basic structures of local nets: (a) star structure; (b) ring structure; (c) bus structure

### 11.8.2 Basic Bus Functions

The basic functions that must be carried out in bus systems are the bus assignment or bus arbitration, the synchronization, the reaction in the case of faults and alarming.

The *bus arbitration* is realized either centrally or decentrally by the participants. In the case of central bus arbitration, the bus requirement is assigned by the participant to the central arbitration logic, for instance, through status inquiry (polling) or after a fixed time (TDMA (time division multiple access) method). The decentralized arbitration shifts the decision to the participant. The arbitration is achieved cyclically from participant to participant (token-passing), based on the highest address or by utilizing the CSMA (carrier sense multiple access) method by first testing if the bus is free or not.

The *synchronization* of bus participants with the passing of signals by the transmitter and signal transfer of the receiver is done either in synchronous or asynchronous mode. In *synchronous transfer*, the data transfer instants are set using a fixed central clock. The *asynchronous transfer* reaches synchronization through special signs with or without feedback from the receiver.

A detailed description of various bus functions can be found in Färber (1987, 1994), Rembold, Levi (1994), Reissenweber (2002).

### 11.8.3 OSI (Open System Interconnection) Reference Model

The communication among network participants requires a multitude of functions and agreements. In order to classify and compare networks and transfer systems and to allow inter-operable network implementations (*e.g.*, bus systems), their functionality is subdivided into a maximum of seven layers built one on top of the other. From a logical perspective, two instances exist on each layer to carry out communication through a *layer protocol* to each communication partner. In this protocol, the specific functions of one layer are summarized. The interface between individual layers are described using standards. The individual instances exchange information using services and functions of the lower layers, while offering their services for the higher levels, Bender (1990). Figure 11.13 shows the general construction of the OSI reference model, which was released in 1984 by ISO (International Standards Organization), compare Stallings (1994), Bradley *et al.* (1991), Christiansen (1996).

In the following section, the functions of individual layers from the lowest layer up to the highest layer are explained.

- physical layer: this layer is the lowest layer and is concerned with all aspects of the physical interconnection of the communications interface to the cable. For example, the standards will define the electrical levels of signals or bits transmitted and received via the cable, *e.g.*, V24 or RS485;

- data link layer: this layer is concerned with the functional and procedural means of data transfer over the network. The layer therefore defines several aspects, such as the way the serial data, consisting of the protocol data bus arbitration such as CSMA/CD, master/slave, token-passing, polling and application data, is organized and the detection and possible correction of errors that occur at the physical layer;

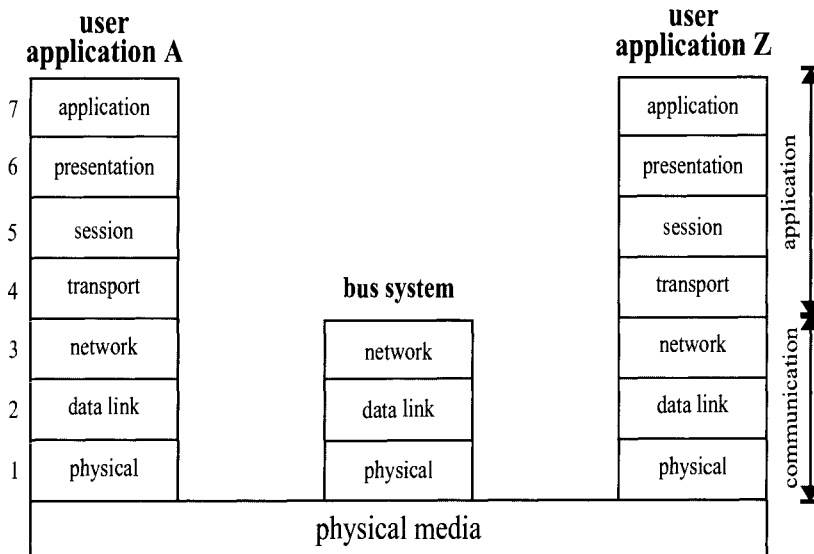


Figure 11.13. The OSI reference model

- network layer: this layer has the task of masking from the transport layer all of the characteristics of the transfer medium. In the cases where several networks are interconnected, the network layer ensures that the data is routed correctly in order for the data to arrive at its destination;
- transport layer: this layer provides a transparent data transfer service between systems connected to the network. It relies on those services provided by the network layer to give a reliable and efficient service to the higher protocol layers, ensuring that the data is transferred error-free and in the right sequence. This is because two user applications must first establish a connection via the network and then interact with one another. The session layer thus establishes, manages and terminates sessions between applications;
- session layer: this layer is involved with establishing the interactions between two user applications on different systems connected to each other by the network. This is because two user applications must first establish a connection via the network and then interact with one another. The session layer thus establishes,

- manages and terminates sessions between applications;
- presentation layer: the function of the presentation layer is to ensure that the formal and data representation of one system is translated into another system, if required. Hence, differences in the way that computers communicate with one another (the syntax) and in the actual data can be adapted;
- application layer: this layer provides a set of services that can be directly called by user application programs, like file transfer and terminal operation.

The first three layers of the seven-layer reference model determine the specific details of operation of the communication system technology from the higher layers. Therefore, the transport layer (layer 4), for example, is unaware of the type of the network employed or if errors have occurred during the transmission of data. Layers 1 to 3 of the reference model are therefore dependent on the communications system's technology, while the operation of the upper layers 4 to 7 depends on the application program running on the system connected to the networks. The layers 1, 2, 3 and 7 are the most important for field buses while layers 4 to 6 are typically not used.

Field bus systems can be roughly subdivided into three application classes: the *standard field buses* (e.g., PROFIBUS, FIP, INTERBUS-S) carry out the general functional and time requirements for communication in the field. Beyond that, *fast bus systems* have been developed that are adequate for special time requirements (e.g., SERCOS, TTP) or can be assigned to special *application domains* (e.g., intrinsic safety field buses for the ex-protection domain or CAN for the safety-critical automotive domain. Table 11.7 gives an overview of the data of several field bus systems. In the following section, the PROFIBUS (process field bus) and the CAN-bus (controller area network) representing typical structures are explained.

#### 11.8.4 PROFIBUS

The PROFIBUS was developed in 1987 as part of a project supported by BMBF (Germany Ministry of Research and Education). Fifteen companies and five research institutes took part in this project. The main goal of this project was twofold: on the one hand the development and dissemination of a serial bit bus concept for the lower layers of process automation systems, and on the other hand the creation of a homogenous norm for field bus systems, DIN 19245 (1988). The PROFIBUS and its further developments (PROFIBUS-DP, PROFIBUS-PA or PROFIBUS-FMS) are today predominantly used in highly complex, multi-layered process automation systems of industrial processes.

**Table 11.7.** Data for field bus systems

bus name	transfer media	min. wire number	max. participants	min/max bit rate	response time	max. length	access principle	priorities	remarks
Bitbus	RS 485	2	28	62.5–2400 kbit/s	> 1 ms	1200 m	MS	-	Intel (1984)
PDV-bus	TP, Koax	2	255	~1000		1000	MST/T		DIN (1984)
PROFIBUS	RS 485	2	127	93.75–5000	> 1	4800	MST/T/P	2	
PROFIBUS-DP	RS 485, LWC	2	32	93.75–1500		9600	MST/T/P	1	
FIP	TP, LWC	5	256	31 / 1000	> 1.5	2000	MS	-	
INTERBUS-S	RS 485, LWC	2	258	300	> 2	400	TDMA	2	unidir. ring
SERCOS	RS 485, LWC	2	256	2000–4000		250	TDMA	-	drive systems
CAN	RS 485 2 wires	2	64	10–1000	> 1	40–1000	CSMA/CA	2032	bus structure automotive vehicles
ASI	2 wires	2	31	150	5	100	MS	-	actuator-sensor bus with power supply

### a) PROFIBUS in OSI reference model

Only the layers 1, 2 and 7 of the OSI reference model are filled out in the PROFIBUS protocol. Layer 1 is realized as hardware, while layer 2 and the two subdivisions of layer 7 are software. The functions of the individual layers are controlled through a parallel, ordered, structured management layer.

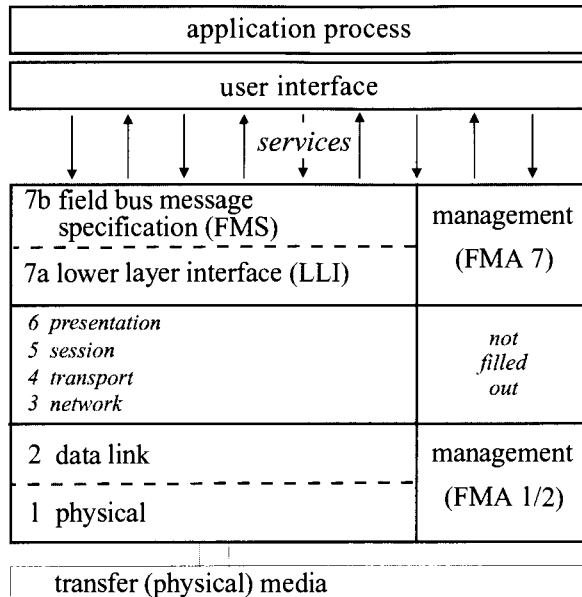


Figure 11.14. PROFIBUS in the OSI reference model

- transfer medium and the physical structure: the data transfer in the PROFIBUS concept is done through a protected, twisted two-wired cable with a terminal resistance. From a topological perspective, this cable forms a line without a branch. The physical interfaces correspond to the norm RS 485. Using PROFIBUS, 32 active (master) and 95 passive participants (slaves) can communicate together at maximum. Therefore, the maximal transfer rate varies from 500 kbit/s, when the bus is 800 m long to a rate of 93.74 kbit/s, when the bus is at the maximum length of 4800 m. In order to process the signals, up to three bi-directional line amplifiers can be used;
- bus arbitration method: the PROFIBUS is a multimaster-multislave-system. From the logical point of view, the active stations are ordered into a ring, the passive ones are grouped in a star formation around a master, where a slave can also be directed to a number of different masters. In each case, a master occupies the transmission authorization and may send exclusively for a given amount of time. Within this time segment, the master asks the other masters or slaves (polling, central). Afterwards, the master

- passes the other transmission authorization onto the next active station (token-passing, decentralized). Hence, a hybrid bus access method is utilized. The PROFIBUS protocol is connection-orientated. Each master holds the addresses of the recognized objects, master and slaves in its object directory, which is fixed during the configuration of the network. Addressing certain instances of objects (e.g., a measured value with data type, value domain, commentary, etc.) is done using indices;
- data transfer: the PROFIBUS possesses services whose data can be transferred either cyclically or acyclically. Herewith, broad or multi-cast information is transferred or information broadcasting is done through receipt replies or data replies. When a number of messages are in the queue at the same time waiting to be transferred, the highest priority message is sent first, then the cyclical and finally the lowest priority, the acyclical data, are sent. The synchronization of the bus participants is reached through a cyclical broadcast of a message with high priority. Seven telegram formats are available. Their format as well as their length can differentiate between the format of the fields (maximally 249 bytes). The optimal speed of data transfer is ensured through the use of a suitable telegram format;
  - functions of application layer: in the PROFIBUS concept, the interface-to-application process is twofold. The highest part layer (FMS) maps the communication requirements (construction and exploitation of connections, read and write of data, alarm treatment) of the application process based upon the services necessary for the PROFIBUS protocol, while layers 3 to 6 of the OSI reference model are not explicitly filled out. Therefore, it forms an independent, bi-directional interface layer between the lower part layer and the higher user services.

### b) Data security, failure security and error treatment

Since the PROFIBUS-hardware is built up, without exception, from tested standard components, and the interfaces correspond to norm RS 485, the physical failure security of the bus is generally high. The security and the checking of data transfer occurs through broadcasting of a monitoring control byte and a test byte. After cycling block testing of the message (CRC: cycle redundancy check), the expected errors are detected. When an error is detected during a master–slave communication, the broadcast of a faulty telegram is repeated up to a defined maximum number of trials. The information contained in a faulty telegram is not used. When an error is encountered during the forwarding of tokens, the master attempts four trials (at max.) in order to pass the token on to the next master. When this fails, the token is then passed on to the next following master. In the case that a token is lost, the master with the lowest address generates a new token. When a passive bus participant fails, the “silent” station is removed from the participants’ list. Meanwhile, the bus proceeds and asks the re-

maining slaves. A detailed description of the PROFIBUS can be found in Bender (1990), Volz (1993).

### 11.8.5 CAN Bus

The CAN (controller area network) bus is a serial bus system, whose development was initiated in 1983 while considering its application in the automotive field, Bosch (1995). The necessity of such a system became evident with the increased number of electronic modules – particularly existent in high-performance vehicles – requiring effective data exchange between individual control devices, which could not be realized with customary cabling techniques.

Except the reduction in cabling, the CAN bus can be used in vehicles for mobile communication as well as for on-board diagnosis. An increasing number of applications of the CAN bus system is also found in the industrial application field. This tendency is evident because of the relative simplicity of the bus protocol, its coherent disturbance reliability and certainly because of the availability of low-cost CAN-controllers on the market.

#### a) The CAN bus within the OSI-reference model

Just like the PROFIBUS, the CAN bus only utilizes the first, second and seventh layer of the OSI reference model. Herewith, the bit transfer layer and data link layer are realized directly as hardware and standardized in the frame of ISO.

In the application layer, a connection of the bus systems to other special applications is possible by using appropriate software.

- transfer medium and the physical structure: the CAN bus works with the “multi-master principle”, in which multiple components having equal rights are connected through a linear bus structure. This structure has the advantage, since the bus system remains available to other participants even if one participant breaks down.

The maximal possible network extension is limited by the required bus signal running time. The higher the speed requirements of the system (e.g., to guarantee the real-time behavior for the communication between vehicle control systems), the smaller the maximal possible bus length. Typical transfer rates are 80 kbit/s to 1 Mbit/s for cable length of 1000 m to 40 m.

The number of participants per network is not limited by the protocol, but depends on the performance of the used bus drivers. Repeater nodes enable an additional expansion of the number of participants;

- bus arbitration method: the CAN protocol is based on a data exchange by marking the message with an identifier. All network participants check if the actual message is a relevant one. This

principle of so-called acceptance filtering has, compared to the principle of station addressing with messages for only one participant, the advantage that messages can be accepted by several stations (multi-casting). The identifier determines, besides the contents of a message simultaneously, also its priority. Herewith, identifiers with a low binary number possess a high priority and *vice versa*. The allocation of the bus arbitration for the CAN bus is not realized by a special station in the network. Each participant can start with transmitting information if the bus is given as free. If several stations begin simultaneously to transmit information, a “wired-and” arbitration scheme is applied to the resolution of the bus arbitration conflict. The information with the highest priority wins without losing time or bits. As soon as a transmitting participant loses the arbitration, it automatically becomes a receiver and repeats the transmission trial after the information with the highest priority is processed;

- message format: the information transfer within the CAN bus is based on four different message frames:
  - data frame;
  - remote frame;
  - error frame;
  - overload frame.

A data message has a maximal length of 130 bits, distributed over seven succeeding fields, see Figure 11.15.

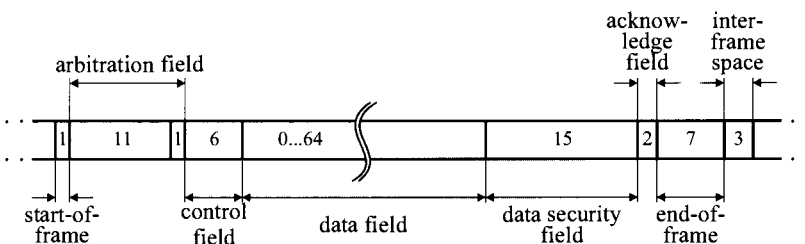


**Figure 11.15.** Format of a CAN data message. Field length in bits

The *start-of-frame* marks the beginning of a message and synchronizes all bus stations. The following *arbitration field* consists of the identifier of the message and an additional check bit. During transferring of this field, the transmitter checks for each bit if it has the transmitting right or if a station with higher priority is transmitting. For the standard CAN specification, the identifier comprises 11 bits, enabling a differentiation of  $2^{11} = 2048$  messages. Based on the check bit, it is decided if it concerns a data frame or a remote frame. The 6-bit *control field* has four lower valued bits that determine the data length of the following

*data field*. This data field contains the very user information of the CAN message and can have from 0 to 8 bytes. To detect transmission disturbances, the *data security field* uses a 15-bit checking sequence (CRC: cyclic redundancy check). The *acknowledge field* contains an acknowledge signal of all receivers that received the message error free.

Each frame is closed by a 7-bit *end-of-frame*. The space between two frames comprises an *interframe-space* of three bits. An error frame results in a break of disturbed data or remote frame through a controlled code damage. This is realized by a sequence of six equal bits, which does not occur in normal operation. An *overload-frame* is transmitted if a data or remote frame can be read by a participant only with delay;

- function of the OSI application layer: because of the separation of levels 1 and 2 of the OSI model, realized by hardware, and its software application layer in level 7, a complete decoupling of the communication and application is reached. The realization of the application distributed over the network follows through service elements of the application layer. A detailed description can be found in Etschberger (1994) and Etschberger, Suters (1993).

### b) Data security and error treatment

Because of the original application of the CAN bus system for automobiles, especially high requirements are posed with regard to the security of the data transmission. Therefore, the CAN protocol is provided with several measures for error detection. Hereto belongs, e.g., the *bit-monitoring*, where each bus participant directly compares the transmitted and the sampled bit. Additionally, each receiver compares in the frame of the cyclic redundancy check (CRC) the received CRC-check sequence with an internally calculated one. This checking method supplements the detection of global acting errors through bit monitoring by the detection of errors, which appear only locally in the receiver. If one bus participant detects the appearance of an error, this will be signaled to all other participants through an error flag, which interrupts the present transmission. Also, already received messages by the participants are cancelled. This mechanism guarantees a network-wide consistency of messages. As defective stations may strongly influence the functionality of the bus system, modern CAN-controllers possess methods that can distinguish between occasionally appearing disturbances and station breakdowns. This is reached by error detection based on statistic methods.

To obtain a measure for data security, a so-called residual error probability is defined. This is a probability for the data that are erroneous and remain undetected. For safety-critical applications as in, e.g., the automotive area, the residual error probability should be so small that it is smaller than one for the whole operation time period of a vehicle. For the application of CAN bus systems in vehicles, this residual probability is in the range of  $10^{12}$  1/h. The CAN bus is described comprehensively in Dais,

Unruh (1992), Embacher (1995), Etschberger (1994), Etschberger, Suters (1993), ISO-DIS 11989, 11591-1, Unruh *et al.* (1990).

# **12 Examples for the Design of Mechatronic Systems: Modeling, Control and Diagnosis**

---

This last chapter presents some examples for mechatronic systems, based on the results of the previous chapters. For an electromagnetic actuator, it is shown how the control performance can be considerably improved by the compensation of non-linearities like friction. This is followed by modeling an electrical throttle valve for spark-ignition engines and its use in controller tuning and model-based fault detection. Then, an overview of the various possibilities for semi-active vehicle suspensions is given and the resulting improvements for drive safety and ride comfort are discussed. A further example for mechatronic developments is the electromechanical disc brake. The control prototyping and hardware-in-the-loop simulation of combustion engines shows the use of modern design tools for engine control. Finally, Lagrange equations are used to model the dynamics of an industrial robot and its use in the design of position control.

## **12.1 ELECTROMAGNETIC ACTUATOR: NON-LINEAR CONTROL AND FAULT DETECTION**

### **12.1.1 Model-based Compensation of Non-linearities**

The compensation of non-linearities plays an important role in high-precision actuators. Therefore, an example is given for an electromagnetic position actuator. The main principle for the compensation of non-linearities is the use of a model-based approach. This means that a mathematical model of the system is used to predict its behavior under different operating conditions. The model is then used to calculate the required control signals to compensate for the non-linearities. This approach is particularly useful for high-precision actuators where small errors can have a significant impact on the final output. The model-based approach also allows for the rapid prototyping and testing of different control strategies, which can help to optimize the performance of the actuator. In addition, the model-based approach can help to identify potential faults or anomalies in the system, which can be addressed before they become serious problems. Overall, the model-based approach is a powerful tool for the design and optimization of mechatronic systems.

ties was already discussed in Section 6.9.1. Here, some more details are given.

### a) Correction of non-linear static characteristics

Non-linear static characteristics are present in many actuators. The objective is to compensate the main static non-linearity  $F_U$  by an approximate inverse function  $F_U^{-1}$ , which can be implemented in the microprocessor. According to Figure 12.1, the regular actuator input  $U$  is substituted by the “corrected” value

$$U'_1 = F_U^{-1}(U, Z) \quad (12.1.1)$$

such that the I/O behavior  $U-Z$  becomes approximately linear.  $G_{P1}$  and  $G_{P2}$  represent linear process parts, compare Section 10.2.2.

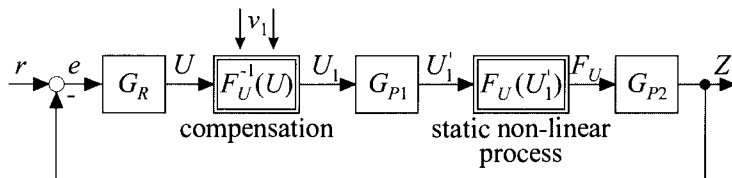


**Figure 12.1.** General structure of a series correction (compensation) for non-linear process statics, compare Figure 10.9.

### b) Friction compensation

Control problems with friction arise if high positioning accuracy is required. If the process stops within the hysteresis width before the set point is reached, only the integral part of the control algorithm can compensate for the offset. This leads to a significant loss of control performance and accuracy, especially during small position changes.

The basic idea of friction compensation is to compensate the relay function of the Coulomb friction by adding an adequate compensation voltage  $U_{comp}$  to the normal control action  $U$ , see Figure 12.2. Different methods such as dithering, compensation and adaptive friction compensation will be described briefly.

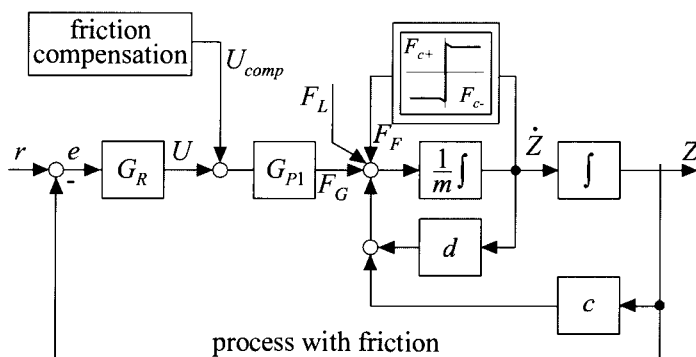


**Figure 12.2.** General structure for friction compensation

### Dithering

Dynamic linearization or so-called *dithering* is the classical way of analog and even digital friction compensation. By adding a high-frequency, periodic signal to the control action  $U$ , the friction is compensated for during half the period, whereas during the second half friction is under-compensated for. The method is quite robust with regard to the amplitude and frequency of the dither signal. However, if the amplitude is too large, the control performance deteriorates.

### Feedforward compensation

From the theoretical point of view, this approach is the ideal control strategy for friction compensation. By adding the compensation value

$$U_{comp}(k) = -\frac{F_{c\pm}}{K_{P1}} \text{sign}[e(k)] \quad (12.1.2)$$

( $F_{c\pm}$  Coulomb friction,  $K_{P1}$  gain of  $G_{P1}$ )

to the controller action  $U$ , an optimal inverse function of the Coulomb relay characteristic is obtained, see Figure 12.2. Note that instead of the unknown velocity  $dZ/dt$  the control error  $e$  is used for the sign of  $U_{comp}$ .

### Adaptive friction compensation

In the preceding methods, the friction compensation was realized by a feedforward control strategy. Better results may be expected if the actual friction value can be adapted in an additional feedback friction control loop. Therefore, an adaptive friction compensation was developed, which interprets the deviation between the measured output  $Z(k)$  and a linear reference model  $Z_M(k)$  as friction effect, Isermann, Keller (1993).

## 12.1.2 Electromagnetic Actuator

A simple electromechanical low-cost component was used to show the development of a high-performance actuating system, with model-based non-linear control and on-line fault detection.

### a) Model-based non-linear control

Electromagnetic actuators play an important role as linear motion elements in, for example, hydraulic/pneumatic valves or fuel-injection pumps. A precise position control is a challenging task as there are severe non-linearities in the system. These include friction forces, magnetic hysteresis and non-linear force-current characteristics that limit the closed-loop control performance in terms of accuracy and dynamics.

The specific DC solenoid drive, Figure 12.3, has a positioning range of 25 mm and shows a non-linear force characteristic as shown in Figure 12.4. The displacement of the armature is working against a spring and can be measured by an inductive position sensor. Process input is thereby

a pulse width-modulated (PWM) and amplified voltage  $V$ , which manipulates the coil current  $I$ .

The objective is to design a robust position control loop, which includes the correction of the non-linear static characteristic in Figure 12.4 and compensation of dominant frictional forces. The low-cost solenoid, which usually performs only simple mechanical switching tasks, then offers similar features as a sophisticated magnet with proportional I/O behavior.

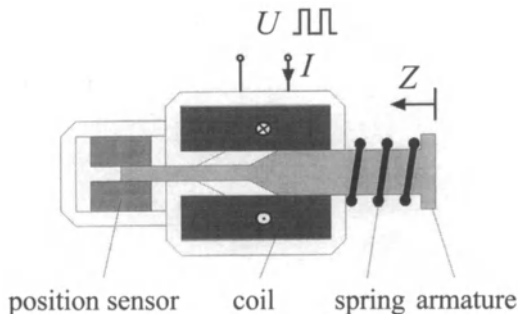


**Figure 12.3.** Scheme of the investigated low-cost DC solenoid drive

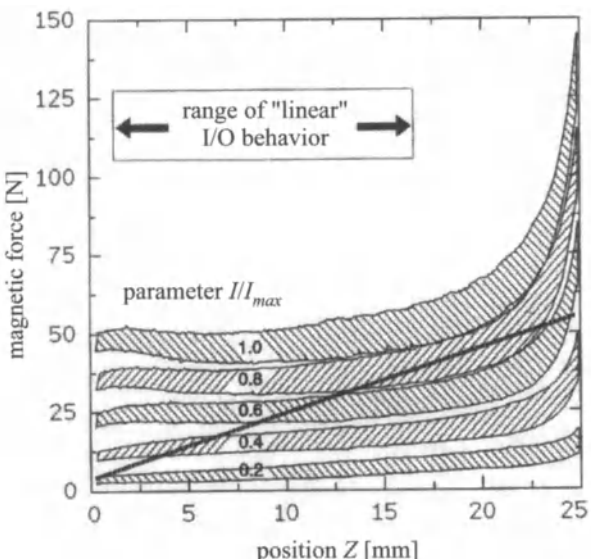


**Figure 12.4.** Position-dependent non-linear force-current characteristic of the solenoid drive. The straight line represents the linear spring characteristic

Therefore, the static force-current position dependency has to be linearized by a non-linear correction as shown in Figure 12.1. An appropriate function for describing the non-linear characteristic is the polynomial approximation

$$f(I, Z) = I \sum_{i=0}^2 \frac{K_i}{(Z_0 - Z)^i} \quad \text{with } Z_0 = 26 \text{ mm} \quad (12.1.3)$$

The resulting statics of the linearized actuator are shown in Figure 12.5 where a typical hysteresis characteristic becomes obvious. Its gradient represents the local gain  $K_p$  of the actuator, which can now be assumed as constant. The position-dependent width of the hysteresis characteristic is a measure for frictional forces and magnetic hysteresis.

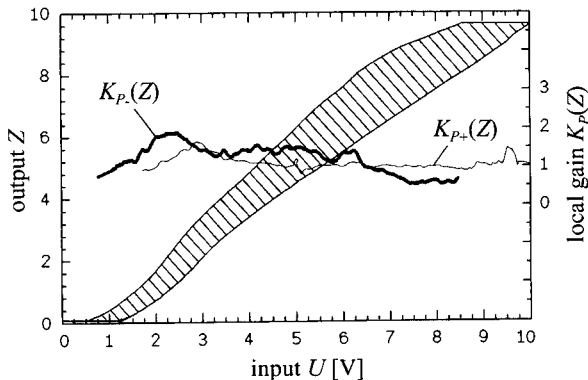


**Figure 12.5.** Hysteresis characteristic and position-dependent local gain of the *linearized* solenoid drive ( $1 \text{ V} \triangleq 2.5 \text{ mm}$ )

According to the linearized system and the equations for the inner current loop

$$T_I \dot{I}(t) + I(t) = K_I U(t) \quad (12.1.4)$$

and the mechanical subsystem

$$m \ddot{Z}(t) + d \dot{Z}(t) + c Z(t) = K_{Mag} I(t) - F_C \text{sign}(\dot{Z}) + F_L(t) \quad (12.1.5)$$

the I/O behavior of the actuator can be modeled as a third order system. The unknown parameters are obtained during a pre-identification phase, exciting the actuator with a special input signal with sampling time  $T_0 = 2.5 \text{ ms}$ . Considering the effect of Coulomb friction, the output error parameter estimation leads to the following direction-dependent transfer functions

$$G_+(s) = \frac{Z(s)}{U(s)} = \frac{382.4}{(s + 116.4)(s^2 + 40.4s + 3329.4)} e^{0.0025s} \quad (12.1.6)$$

$$G_-(s) = \frac{Z(s)}{U(s)} = \frac{220.1}{(s + 47.9)(s^2 + 47.9s + 3444.5)} e^{0.0025s} \quad (12.1.7)$$

Index  $+-$  denotes the direction of the armature motion and the additional

deadtime describes the effect of asynchronous PWM generation.

Figure 12.6 shows the obtained control performance, using a numerically optimized position controller

$$G_R(q^{-1}) = \frac{u(k)}{r(k)} = \frac{2.231 - 4.204q^{-1} + 2.000q^{-2}}{(1 - q^{-1})(1 - 0.616q^{-1})} \quad (12.1.8)$$

(PID-T1-type,  $T_0 = 2.5$  ms) where  $q^{-1}$  is a shift operator for one sampling time ( $u(k)q^{-1} = u(k-1)$ ). Although there is a change in the actuator's dynamic behavior, the controller designed for the slower negative motion (worst case) is robust enough for positive motions. The dynamic features are suitable and stability is obtained even in the positioning range ( $17\text{ mm} < Z < 25\text{ mm}$ ), which is unstable with linear control.

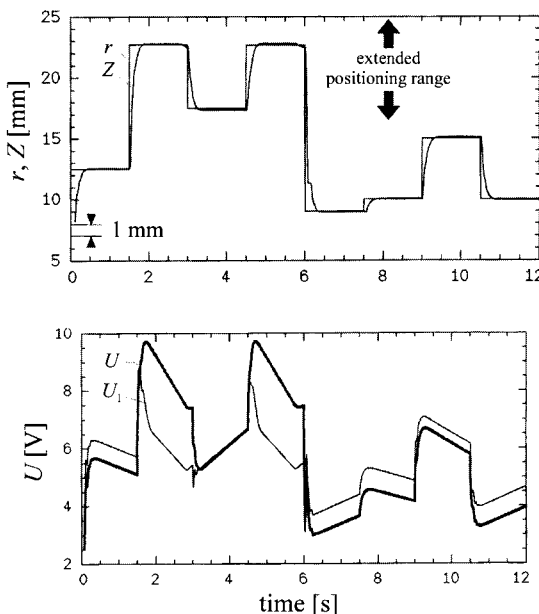


**Figure 12.6.** Closed-loop position control of the solenoid with correction of the non-linear actuator characteristic, but without friction compensation,  $T_0 = 2.5\text{ ms}$

Using the same linear algorithm for small setpoint changes, typical effects by Coulomb friction and hysteresis can be observed. Figure 12.7 shows the unsatisfactory positioning and dynamics. The control variable has considerable delay to the reference value and in steady state an offset of about  $110\text{-}140\text{ }\mu\text{m}$  remains. The improved control performance with adaptive friction compensation is obvious as a positioning accuracy up to  $25\text{-}50\text{ }\mu\text{m}$  could be achieved. At the same time, an adaptation of the actual compensation value to the present hysteresis width is performed. The course of the control action  $U$  shows an automatically generated *dither signal*, which adapts its amplitude and frequency with regard to the control performance, Isermann, Raab (1993), Raab (1993).

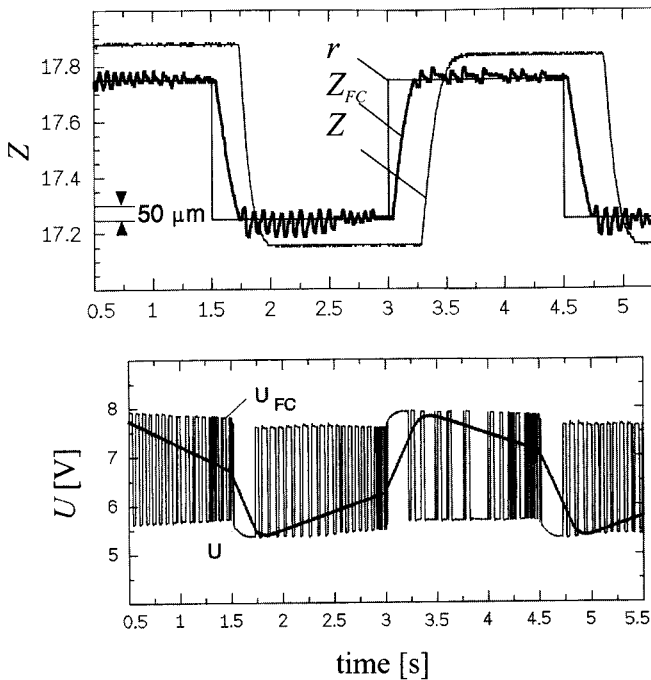


**Figure 12.7.** Comparison of the position control performance for small setpoint changes without/with adaptive friction compensation ((index<sub>FC</sub>),  $T_0 = 2.5 \text{ ms}$ )

### b) Model-based fault detection

An important feature of an “intelligent” actuator is the automatic supervision and fault diagnosis of its components.

The electromagnetic actuator is now considered for the *linearized* operation range from 0–25 mm. From the equations for the current circuit (12.1.4) and the mechanical subsystem (12.1.5), a third order differential equation follows

$$Z^{(3)}(t) + a_2^* \ddot{Z}(t) + a_1^* \dot{Z}(t) + a_0^* Z(t) = b_0^* V(t) + c_0^*(t) \quad (12.1.9)$$

The parameters of the continuous time representation

$$\Theta^T(t) = [a_2^* \ a_1^* \ a_0^* \ b_0^* \ c_0^*] \quad (12.1.10)$$

depend thereby on the physical process coefficients

$$\boldsymbol{p}^T = [T_1, D, \omega_0, K_p, c_0^*] \quad (12.1.11)$$

with, for example,

$$D = \frac{d}{2\sqrt{mc}}, \quad \omega_0 = \sqrt{\frac{c}{m}} \quad (12.1.12)$$

These process coefficients can be expressed in terms of the parameter

estimates  $\Theta$ . Hence, after estimation of the model parameters  $\Theta$  by measuring the voltage  $U$  and the position  $Z$ , all process coefficients  $p$  can be calculated.

In the following, some experimental results are shown for artificially generated actuator faults:

- F1: too-large pretension of the spring;
- F2: decrease of the spring constant (by breaking or aging, change from  $c = 1650$  to  $1200 \text{ Nm}^{-1}$ );
- F3: increase of friction (increase of surface roughness and jamming);
- F4: fault in the current circuit (weak controller gain).

The parameters were estimated by output error minimization using specific excitation signals. Sampling time was  $T_0 = 0.2 \text{ ms}$ . Figure 12.8 and Table 12.1 show the results for different faults. Based on the deviations (symptoms), all faults can be identified. This can be performed by a pattern recognition or a systematic treatment of fault-symptom trees. In all cases, different patterns of coefficient changes result. This enables a unique diagnosis of the four faults.

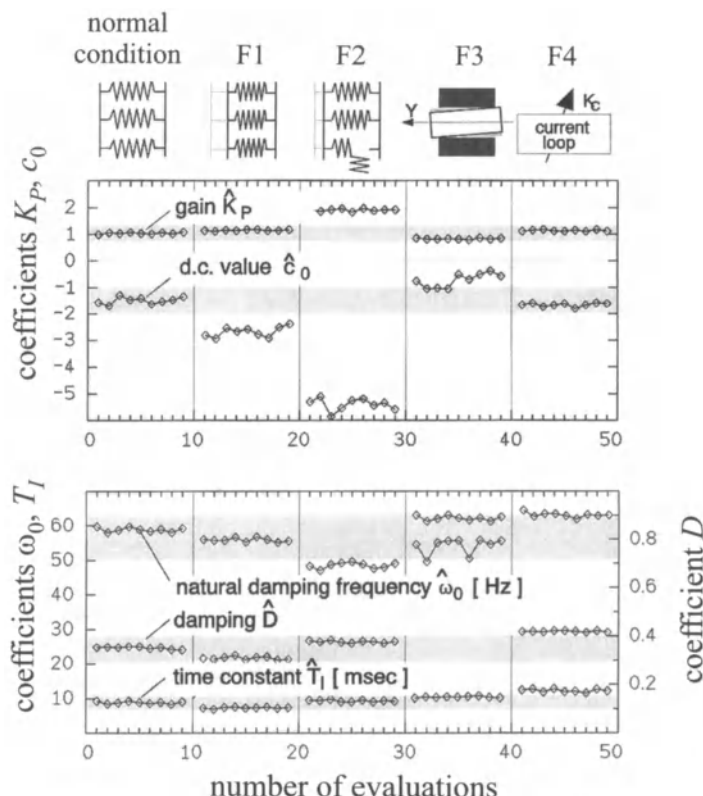


**Figure 12.8.** Parameter estimates for an electromechanical drive with different faults (positive motion direction)

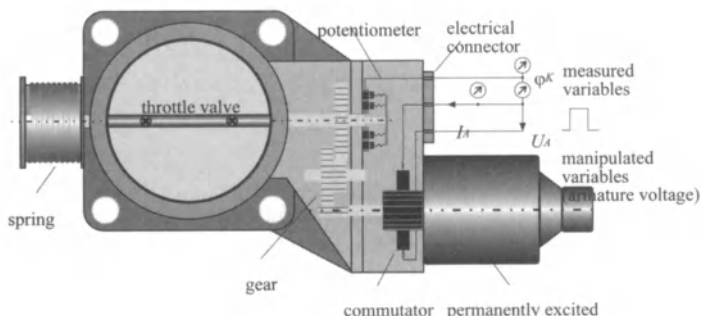
**Table 12.1.** Changes of process coefficients for an electromechanical drive depending on different faults

Fault type	static coefficients		dynamic coefficients		
	$K_{P+}$	$c_{0+}$	$\omega_{0+}$	$D_+$	$T_1$
F1	0	--	0	0	0
F2	++	--	-	0	0
F3	0	+	0	++	0
F4	0	0	+	+	++

## 12.2 ELECTRICAL THROTTLE VALVE FOR SI ENGINES: MODELING AND FAULT DIAGNOSIS

Automobile actuators have to operate very reliably under hard ambient conditions such as a wide temperature range, vibrations and disturbances in signals and power supply. Friction and time-varying process parameters, which are mainly caused by temperature influences, make it difficult to fulfil fast and precise positioning with conventional linear control algorithms. The given throttle-valve actuator is used in an ignition combustion engine to control the air mass flow through the intake manifold into the cylinders. This automotive actuator is embedded in various control systems such as traction control and velocity control, which require fast and precise operation.

Figure 12.9 shows the mechanical function of the actuator. A permanently excited DC motor with a gear turns the throttle valve against the closing torque of a spring. The motor is driven by pulse width-modulated (PWM) armature voltage  $U_A$ , which is measured as well as the resulting armature current  $I_A$ . The angular deflection  $\varphi$  is redundantly measured in the range  $[0\dots 90^\circ]$  by two potentiometers.

**Figure 12.9.** Function scheme of the throttle-valve actuator

Theoretical modeling and measurements have shown that the model

structure illustrated in Figure 12.10 is a sufficient base for control design and fault detection. The gear was modeled as proportional factor with the reduction ratio  $v$ .

The inductance was also neglected because the electrical time constant is much smaller than the mechanical one. Other parameters are the armature resistance  $R_A$ , the magnetic flux linkage  $\Psi$ , the inertia constant  $J$ , the viscous friction coefficients  $T_{F1}$  and the spring constant  $c_F$ . The signal  $T_{ext}$  includes the spring pretension and external load torques.

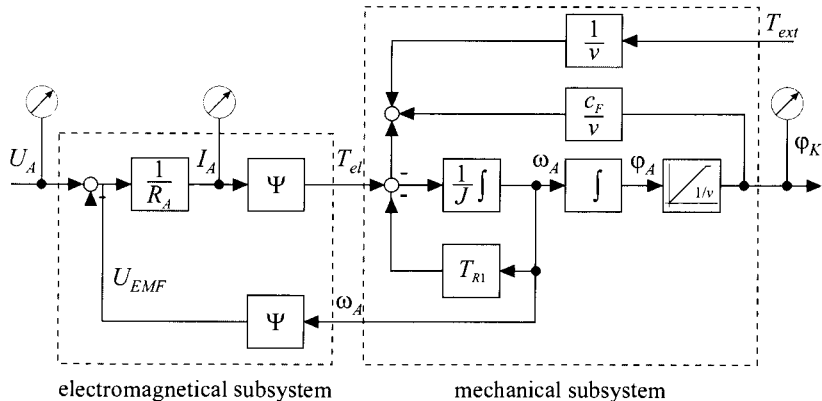


**Figure 12.10.** Mathematical model of the throttle-valve actuator

### *Self-tuning control*

Theoretical modeling and parameter estimation has shown that the process behavior can be described by two linear differential equations with the physical process coefficients

$$\mathbf{p} = [R_A, \Psi, c_{0e}, J, c_F, T_{F1}, T_{ext}]^T \quad (12.2.1)$$

with  $c_{0e}$  the DC value of the electromagnetical subsystem. The developed control algorithm consists of a linear PID- $T_1$ -controller with an additional friction compensator. The parameters of the linear part of the controller are tuned automatically and on-line by evaluation of a loss function and minimization with the downhill-simplex algorithm, while the non-linear friction compensation is based on parameter estimation. The obtained control performance is shown in Figure 12.11. It satisfies the requirements for dynamic and precise positioning over the whole operation range.

### *Fault detection*

Based on the same process model as for controller design, a model-based fault detection and diagnosis was developed using only the voltage, the current and the throttle position as measurements. The deviations of the physical coefficients of the actuator from their normal values  $\mathbf{p}_0$  were used as analytical symptoms for fault detection. These parameters were determined by a recursive parameter estimation.

Fourteen different faults have been generated in the real actuator. The obtained patterns of changes are shown in Table 12.2. All faults cause a

unique symptom pattern. Additionally, a set of four structured discrete time *parity equations* was developed, where each parity equation was decoupled from another process input and output variable respectively ( $r_1: [\varphi_K]$ ,  $r_2: [I_A]$ ,  $r_3: [U_A]$ ,  $r_4: [T_{ext}]$ ). The application leads to the residual pattern also shown in Table 12.2. The residual changes show a direct connection to the offset and scale faults in the sensors of  $U_A$ ,  $I_A$  and  $\varphi_K$  but no unique relations to the actuator faults. Hence, the parity equations can only be used for fast detection of some of the faults, but with little computational effort.

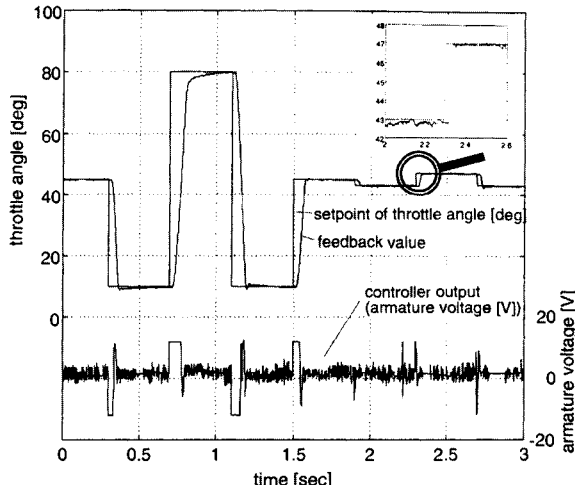


Figure 12.11. Control results with PID- $T_1$ -controller and friction compensation

**Table 12.2.** Process parameter deviations and parity equation residuals for different actuator faults (0 → no significant change, + → increase, ++ → large increase, - → decrease, -- → large decrease)

↓ Faults	features--	parameter estimation							parity equations			
		$R_A$	$\Psi$	$c_{0e}$	$J$	$c_F$	$T_{Fl}$	$T_{ext}$	$r_1$	$r_2$	$r_3$	$r_4$
incr. spring pretension		0	0	0	0	0	0	--	+	-	+	-
decr. spring pretension		0	0	0	0	0	0	++	0	+	-	0
commutator shortcut		--	--	0	+	+	++	0	+	-	+	-
arm. winding shortcut		0	--	0	+	+	++	0	+	0	+	-
arm. winding break		++	-	0	0	+	++	+	-	-	+	+
add. serial resistance		++	0	0	0	0	0	0	-	-	+	+
add. parallel resistance		--	--	0	0	+	++	0	+	+	+	-
increased gear friction		0	0	0	+	+	++	0	+	-	+	-
offset fault $U_A$		0	0	+	0	0	0	0	-	-	0	+
offset fault $I_A$		0	0	-	0	0	0	+	+	0	+	-
offset fault $\varphi_K$		0	0	0	0	0	0	-	0	+	-	0
scale fault $U_A$		+	+	+	+	+	+	+	-	-	0	+
scale fault $I_A$		-	0	0	+	+	+	+	+	0	+	-
scale fault $\varphi_K$		0	-	0	-	-	-	-	0	+	-	0

### *Fault diagnosis*

For fault diagnosis, the information of symptom generation by parameter estimation was used. Fourteen parallel *neuro-fuzzy networks* were implemented and each of them was made sensitive to one fault. The network consists of an antecedent layer, a relation layer and a conclusion layer, which models fuzzy reasoning. The relations of the causal net are identified with adjustable ANDOR connectives of the symptoms. The subsets of the input variables are automatically determined, the most significant rules are extracted and finally the extracted rule base is optimized.

This application example has shown that the integration of different methods leads to a rather complete fault detection and diagnosis by:

- fast fault detection with little computational effort by parity equations;
- fault detection with detailed and deeper information by parameter estimation;
- fault diagnosis by an adaptive neuro-fuzzy reasoning.

More details are given in Pfeufer (1996), Pfeufer, Isermann (1996).

## 12.3 SEMI-ACTIVE VEHICLE SUSPENSIONS

### 12.3.1 Passive Vehicle Suspensions

The vehicle suspension system is responsible for driving comfort and safety. Semi-active and active suspension systems enable the suspension system to adapt to various driving conditions. However, to improve comfort and safety compared to suspensions with fixed properties, the adaptation requires that the control behavior of the damper and the spring is known and that laws are known on how to adapt the free parameters depending on the driving situation.

#### a) Vehicle suspensions

The suspension carries the vehicle body and transmits all vertical forces between body and road. Therefore, the suspension system is responsible for the ride quality and influences considerably the driving stability, Reimpell, Stoll (1989). The task of the spring is to carry the body mass and to isolate the body from road disturbances. The damper contributes to both driving safety and quality. Its task is the damping of body and wheel oscillations. A non-bouncing wheel is the condition for transferring road-contact forces.

Considering the vertical dynamics and taking into account the vehicle's symmetry, a suspension can in the first step be reduced to the so-called quarter-car model as shown in Figure 12.12.

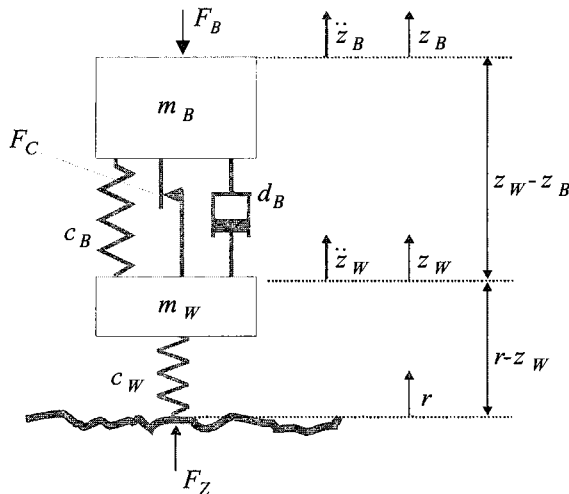


**Figure 12.12.** One-dimensional vertical vehicle representation – the quarter-car model

In its simplest form, the suspension system is comprised of the spring and the damper. A single spring models the tire. Modeling the tire damping is usually negligible. This basic model satisfies the most common control applications, Bußhardt (1995).

*Driving safety* is the result of harmonious suspension design in terms of wheel suspension, springing, steering and braking, and is reflected in optimum vehicle dynamics.

*Conditional safety* results from keeping the physiological stress that the vehicle occupants are subjected to by vibrations, noise and climatic conditions down to as low a level as possible. It is a significant factor in reducing the possibility of misactions in traffic. Consequently, conditional safety refers to the driving comfort. In order to describe driving comfort and safety mathematically, quantitative values are introduced:

The acceleration of a body  $\ddot{z}_B$  is an obvious quantity for the motion and vibration of the car body and therefore the passenger's comfort. Thus, the effective value of the normalized body acceleration for a quarter-car model is chosen as

$$\ddot{z}_{B,rel,eff} = \sqrt{\frac{1}{T} \int_{t=0}^T \left( \frac{\ddot{z}_B}{g} \right)^2 dt} \quad (12.3.1)$$

The tire load determines the road contact. So, the changes of the forces between tire and road describe a quantity for the driving safety. Therefore, the effective value of the *normalized dynamic tire load* is applied

$$\ddot{z}_{zdyn,rel,eff} = \sqrt{\frac{1}{T} \int_{t=0}^T \left( \frac{F_{zdyn}}{F_{zstat}} \right)^2 dt} \quad (12.3.2)$$

In order to improve the ride quality, it is important to isolate the body, also called sprung mass, from the road disturbances and to decrease the resonance peak of the sprung mass near 1 Hz, which is known to be a frequency to which the human body is sensitive. In order to improve the ride stability, it is important to keep the tire in contact with the road surface and therefore to decrease the resonance peak near 10 Hz, which is the resonance frequency of the wheel, also called unsprung mass. For a given suspension spring, the better isolation of the sprung mass from road disturbances can be achieved with soft damping by allowing a larger suspension deflection. However, the better road contact can be achieved with a hard damping, preventing unnecessary suspension deflections. Therefore, the ride quality and the drive stability are two conflicting criteria. Figure 12.13 illustrates this conflict, showing the variation in driving safety and comfort with the changing vehicle parameters body mass, stiffness and damping in the “conflict diagram”.

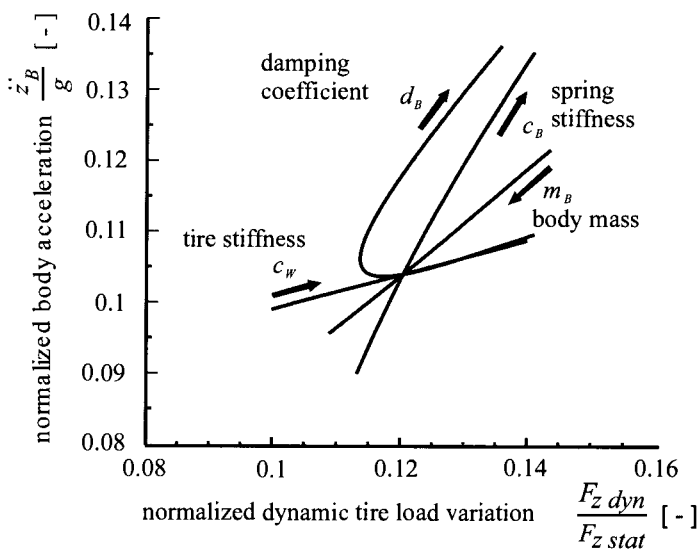


Figure 12.13. Influence of vehicle parameters, quarter-car simulations

The conflict diagram presents the vehicles properties – driving comfort and safety – for a defined manoeuvre as a point in the  $\dot{z}_B - F_{zdyn}$  diagram. Varying set-ups lead to curves that elucidate the respective tendencies.

The fixed setting of a passive suspension system is a compromise between comfort and safety for any given input set of road conditions and a specific stress. In contrast, semi-active and active suspension systems provide modulation or an extra force between the sprung and unsprung

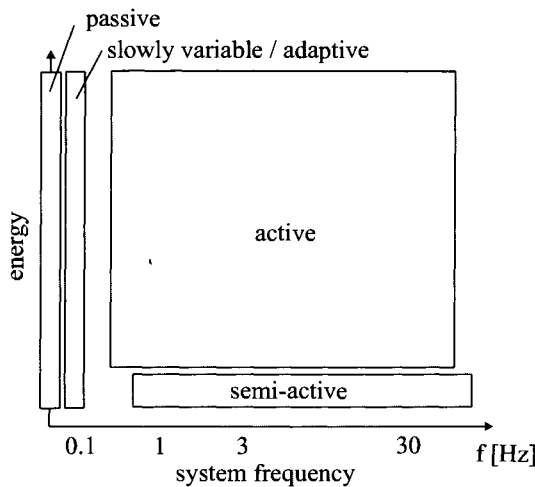
mass, aiming at an increase in driving comfort and safety. The mechanism of semi-active suspension systems is the adaptation of the damping and/or the stiffness of the spring to the actual demands. Active suspension systems provide an extra force input in addition to possible existing passive systems and therefore need much more power.

### b) Adaptive systems

In the case of suspension systems, the changes of the damper and spring parameters as a result of temperature, deflection and wear and tear have to be considered. These changes must be taken into account when designing a controller for an active or semi-active suspension system, to avoid unnecessary performance loss. In order to prevent this a robust or an adaptive controller has to be implemented. This leads to a *parameter-adaptive* suspension system. Generally, a parameter-adaptive system is a control system that adapts its behavior to the changing settings of the systems to be controlled and its signals, Isermann *et al.* (1992), see also Chapter 1. Thus, a parameter-adaptive suspension is distinguished by parameter-estimation and the feedback of these estimated parameters in order to adapt a controller or to influence the system parameters directly.

### c) Semi-active and active systems

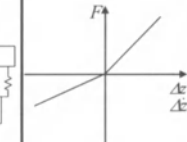
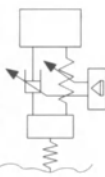
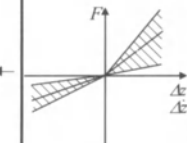
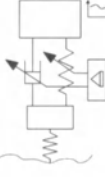
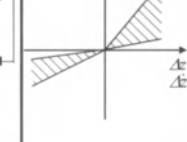
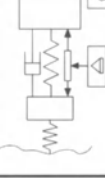
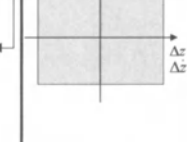
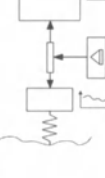
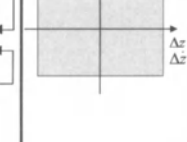
Suspension systems are classified as passive, semi-active, active and various in-between systems. Typical features are the required energy and the characteristic frequency of the actuator. This fact visualizes Figure 12.14, according to Streiter (1996).



**Figure 12.14.** Energy vs. frequency for various suspension systems

The properties of the various systems are summarized in Table 12.3. *Passive systems* consist of invariable components with fixed parameters. Extensions with extra spring, damper or mass systems in order to absorb further energy are possible. However, all systems are only tuned for one fixed frequency or a set of frequencies and vehicle mass and tire pressure.

**Table 12.3.** Classification of suspension systems, Bußhardt (1995). Natural frequencies:  $f_B$  body and  $f_w$  wheel

system	system representation	force range	operation range (frequency)	actuator/sensor demand	max. energy demand	improvements compared to passive system	
						comfort	safety
passive			-	-	-	-	-
slowly variable adaptive			$< f_B$	$4 - 8 / \geq 1$	c. 50 W	15 – 20 %	10 – 25 %
semi-active			$f_B - f_w$	$4 - 8 / \geq 8$	c. 50 W	20 – 30 %	10 – 25 %
active partially loaded			$0 - f_B$	$4 - 8 / \geq 12$	1 – 2 kW	> 30 %	-
active fully loaded			$0 - f_w$	$4 / \geq 12$	1.5 – 7 kW	> 30 %	> 25 %

If the system or its parameters are *slowly variable/adaptive*, an adaptation of the system is possible. Examples of these systems are load-leveling systems. Here, the initial deflection of the spring is varied by changing the air volume of air springs or the oil volume of hydraulic cylinders, which are installed in series to the actual spring. This can be achieved by manual manipulation or by electromechanic/electrohydraulic/electropneumatic systems. However, the manipulation frequency is still very low.

Increasing the manipulation frequency of the above-mentioned slowly variable passive or adaptive systems leads to *semi-active* systems. Semi-active systems do not generate forces out of their own. Therefore, they require less control energy. Here, the mode of operation is the variation of the system's parameters. For instance, the mechanism of semi-active suspension systems is adaptation of the stiffness of the spring and/or damping to the actual demands. Therefore, external energy is only required to adjust parameter changes, but not to influence the motion of the sprung or unsprung mass directly. One distinguishes between fast and slow semi-active systems. A slow system adapts to various car settings, *e.g.*, mass or driving modes, whereas a fast system is able to adapt directly to road disturbances.

*Active* systems provide active forces with usually higher control frequencies, intervening directly in the system dynamics. As a result, the energy demand is relatively high and increasing quadratically with the frequency. Active suspension systems provide an extra force in addition to possible existing passive systems. This extra force is used for compensating road disturbances and roll and pitch motions of the body. Depending on the system's frequency, partially and fully active systems can be distinguished. Furthermore, there are non-, partially- and fully loaded suspension systems, depending on whether the controlled system contributes to carrying the body.

*Parameter-adaptive* systems concern the control engineering approach of how to adjust the free parameters of semi-active or active systems based on measured suspension signals.

For the sake of completeness Figure 12.15 gives a short survey of active suspension systems. Various control strategies exist for these active systems. For example, Streiter (1996) describes the control of a hydro-pneumatic system, in which a hydraulic cylinder is implemented in series into a conventional steel spring. In 2001, such systems have gone into production (*e.g.*, Mercedes CL-Class).

### 12.3.2 Semi-active Suspensions

The basic principles of suspension systems are presented in order to give an insight into the function and the related restrictions for the application in a controlled system.

#### a) Automotive damper elements

Basically, one distinguishes between *single-tube* and *twin-tube* shock absorbers, Figure 12.16.

**Active suspension**

- a) Hydraulic cylinder, b) Hydropneumatic suspension,  
 c) Air suspension.  
 1 Vehicle body, 2 Wheel-load sensor,  
 3 Travel sensor, 4 Accumulator,  
 5 Pumping circuit, 6 Servo valve,  
 7 Actuating cylinder, 8 Acceleration sensor,  
 9 Damper, 10 Valve, 11 Tank,  
 12 Compressor, 13 Solenoid valve.

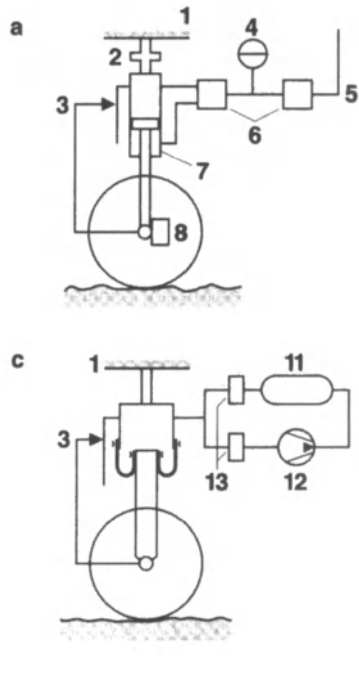


Figure 12.15. Active suspension systems, Bosch (1996)

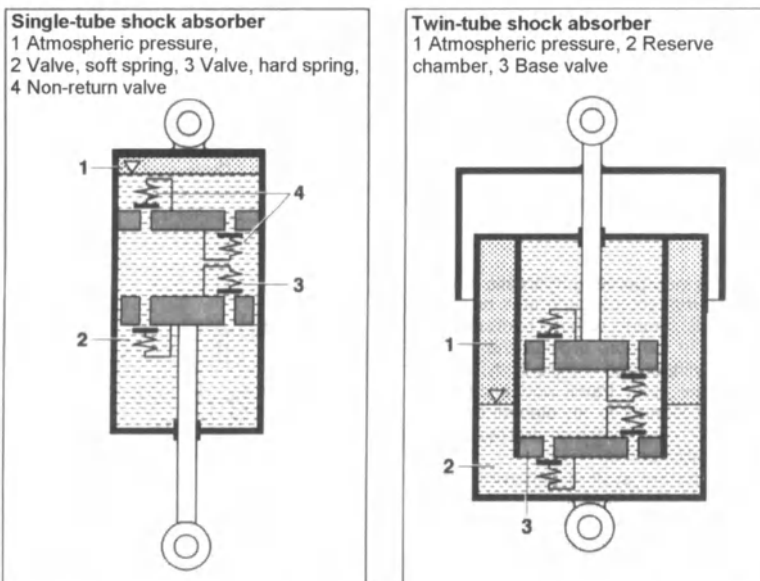


Figure 12.16. Schematic of a single-tube and double-tube absorber, Bosch (1996)

In the case of single-tube shock absorbers, a sliding separating-piston and gas cushion form the gas-pressure damper. Its advantage is the fact that it is easy to tailor to specific applications, as the large piston diameter allows low working pressures and sufficient room for valves and passages. Further advantages are that the heat is dissipated directly via the outer tube and that the shock absorber can be installed in any position. The disadvantages are the length and the sensitivity of the outer tube to damages from stone throw, etc., as it acts as a guide cylinder for the piston. Also, the piston-rod seal is subjected to the damping pressure.

Twin-tube shock absorbers are available as atmospheric or low-pressure twin-tube type. The advantages are firstly insensitivity to external damage, so supplementary mechanical measures can be taken at the outer tube in restricted bodywork areas. Secondly, this shock absorber type is short, as the balance chamber is next to the working cylinder. Disadvantages include sensitivity to overloading, which results in damping ceasing and restricted installation positions.

The damping characteristics are the result of the cumulative function of orifice damping and of the spring-loaded valves, which closes the passage. The spring responds to pressure by increasing the free aperture of the outlet orifice. The piston bore and spring can be specifically tailored to provide linear to mildly degressive damping curves. The decompression forces are frequently only 30...50% of those for the compression mode, Bosch (1996).

### b) Automotive spring elements

In the field of passenger vehicles, four main types of spring elements are used; conventional steel springs in the form of coil springs, torsion bars, air springs and hydropneumatic suspensions, see Figure 12.17.

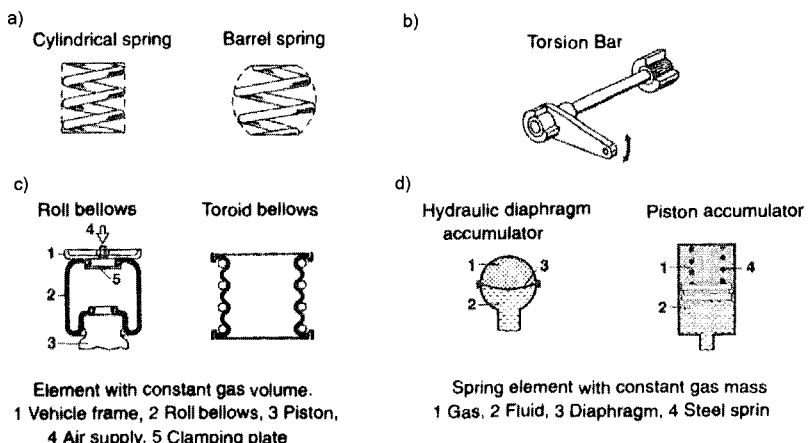


**Figure 12.17.** Spring systems: steel spring, torsion bar, air spring, hydropneumatic spring, Bosch (1996)

*Coil springs* are simple springs without self-damping. On account of their simplicity, they have low weight and are maintenance-free. Only limited space is required and dampers can be mounted within the spring. Their characteristic is linear, but can also be designed progressively. *Torsion bars* are made of round bar stock or flat steel. They are wear-and maintenance-free. *Air springs* provide high driving comfort and enable load-leveling. It is the only spring concept where the natural frequency of the body remains constant under load, but the force characteristics are non-linear due to the gas properties, see Section 4.2. The springing air volume is captured in roll or toroid bellows. Therefore, the wheel travel must be defined by separate mechanical guidance systems. In the case of hydropneumatic suspension, a gas volume in an accumulator determines the response characteristics. The fluid compresses the gas according to the wheel load. The connection between the spring strut and the accumulator contains additional valves for the control of the damping function. The performance curves are non-linear due to the gas properties. This system is favored by Citroën.

### c) Adjustable dampers

The simplest adaptive dampers are *manually adjustable dampers*. The aim is the adaptation of the damping to various long-distance driving situations with varying loads or road windings (e.g., holiday trip, mountain courses). The most common adjustment method is the twisting of the piston or the piston shell resulting in a change of the throttle's properties. The so-called *load-dependent damping variation* is based on the alteration of the deflection in the case of body mass changes. This effect is used to vary the damping coefficient in order to achieve a nearly constant body – damping ratio. In the case of load-leveling systems, the static deflection does not change. In this case the increased pressure of the leveling air spring or hydraulic system can be used as a manipulation variable for damper adjustment. This pressure directs a control valve through a barometric cell, changing the damping.

For the sake of completeness, the *deflection-dependent dampers* are mentioned. These variable dampers increase their damping ratio for deflections near the limit stops. This aims to produce a soft stop at the limits of the deflection and lead to a termination of the energy in contrast to steel spring stops. Thus, this system is not an adaptive system in the sense of an adaptation to driving situations and excitations.

### d) Semi-active dampers

The common function of conventional semi-active shock absorbers is the variation of the throttle cross-sectional area either in fixed steps or continuously in order to obtain multiple performance curves from a single shock absorber. In the continuous case, a continuous valve controls the liquid resistance and in the discrete case various throttles or throttle systems are switched on or off. The active throttle can either be integrated in the damper or in an external bypass, which often is constructed in the form

of a ring channel. The throttle's adjustment is achieved using an electric motor or by means of a magnet valve. The latter provides high switching times and a continuous adjustment, Reimpell, Stoll (1996). The fundamental function is demonstrated in Figure 12.18.

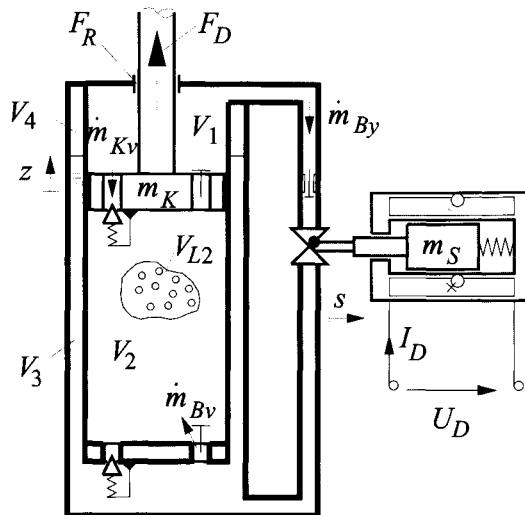


**Figure 12.18.** Schematic of a semi-active damper

During the pull cycle, the oil of the upper chamber ( $V_1$ ) flows through the bypass and the spring-weighted piston valve. The rectifier valve in the piston bottom compensates for a possible additional deficiency of oil in chamber two  $V_2$ . Therefore, the pressure losses in the bypass and at the spring-weighted piston valve determine the damping forces. For the duration of the push cycle, the volume being taken up by the piston generates an oil stream through the bottom spring-weighted valve and the bypass. Consequently, these valves determine the damping forces for the push part of the cycle. On account of the role of the bypass in both the push and pull cycles, the variation in the resistance of the bypass influences the damper characteristics. As demonstrated by Figure 12.18, an electromagnetic valve controls the cross-sectional area of the bypass, but other actuators such as electric motors are also common. The air volume  $V_{L2}$  is the effect of aging or damage and results in fading effects of the damping. Figure 12.19 illustrates the performance characteristics. The manipulated variable is the current applied to an electromagnetic valve.

An extension to this principle is the variation of the working volume. An additional chamber with a controllable pressure is connected through additional valves. In the case of high pressures in the piston, these valves open depending on the pressure in the additional chamber. This supplementary variable influences the damper characteristics.

An important property for the potential of a semi-active suspension is the time constant, or rather response time of the actuators. The response time determines the achievable performance of suspension controllers in

reacting directly to road excitations.

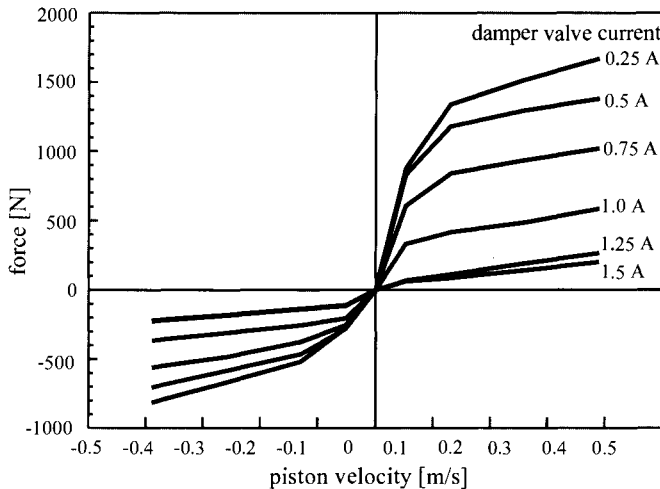


**Figure 12.19.** Family of characteristics of a continuous variable damper, manufacturer's specification

In the last few years, a new development has arisen in the form of dampers taking advantage of the electro-rheological or magneto-rheological property of liquids. Both principles are based on the alteration of the damping medium's viscosity depending on an applied electric or magnetic field. Commonly, these fields are applied in the duct connecting the upper and lower chambers of a damper, for details see, e.g., Choi *et al.* (1998), Choi *et al.* (2001), Fees (2001), Moosheimer, Waller (1999).

One of the salient properties of electro-rheological fluid is that it has a fast response to an electric field and hence a wide control bandwidth, Choi *et al.* (2001). Magneto-rheological shock absorbers have many attractive features such as high yield strength and stable hysteretic behavior over a broad temperature range, Yokoyama *et al.* (2001). In order to achieve the damping forces required for a semi-active electro-rheological vehicle suspension system, a high electric field, about  $E = 3 \dots 5 \text{ kV/mm}$ , has to be applied, Kim, Choi (1999). Obviously, this requirement and the long-term stability of the fluid properties are presently obstacles to application in common vehicle systems.

### e) Load-leveling system

A comfortable suspension is achieved by means of soft springs. However, this increases spring displacement. In order to maintain the vehicle-body height at an acceptable level and have soft springs, air springs or hydro-pneumatic springs are employed.

The advantages of these systems are a velocity-dependent reduction of the ride height, resulting in lower aerodynamic resistance and fuel savings, an increase in vehicle height on poor road surfaces, and enhanced stability in curves achieved through lateral blocking of the suspension elements on a single axle, Bosch (1996).

A serial connection of a conventional steel spring with a hydraulic piston is also possible, for example, the Active-Body-Control System of DaimlerChrysler (2001). However, these systems are in principle active suspension systems, which include a leveling function as part of their design.

Beyond this, self-pumping dampers exist, being able to regulate their level automatically. This is achieved by taking energy out of the body motion. The damper uses this energy to pump itself to a constant mean level.

#### f) Semi-active spring

To begin with, all load-leveling systems can be used in a semi-active purpose, in so far as they provide the required manipulation dynamics.

The common semi-active spring is based on a system containing an air spring or hydropneumatic system. The stiffness of an air spring can be approximated according to Reimpell, Stoll (1989) by the following equation, see also Section 4.2

$$c = n \frac{pA^2}{V} \quad (12.3.3)$$

As a result, the pneumatic systems are based on the alteration of the air volume  $V$  by adding or removing air, resulting in a change of the stiffness. This leads to a continuously adjustable stiffness. Unfortunately, this procedure leads directly to a changing initial deflection.

In order to prevent a varying initial deflection, hydropneumatic systems can be implemented that replace the removed air by oil or *vice versa*, see Bußhardt (1995).

Switchable air volumes are another possibility. This attempts to alter the total volume of air, and thereby the stiffness without significant change of the mean deflection. The common systems, compare Reimpell, Stoll (1989), consist of two connected volumes. By cutting off or opening the pneumatic connection between these volumes, two different stiffness values are achievable.

Often, the air or hydropneumatic spring is arranged in parallel to a conventional steel spring, in order to reduce the forces and stress on these systems.

Also, variable steel spring systems exist. Their principle of operation is based upon the alteration of the point of application. This is attained either by the direct shifting of the point of application at one spring or the bypassing of several springs in a system of serially arranged springs, *e.g.*, Venhovens *et al.* (1992). However, the dynamic response of these mechanical solutions is small.

### 12.3.3 Dynamic Models of a Quarter-car

Physical models for the investigation of vertical dynamics of suspension systems are most commonly built around the quarter-car model. Greater

accuracy is achieved by extensions to a half-, e.g., Krtolica, Hrovat (1990) or full-car model, e.g., Weispfenning (1996). This aims to describe correctly the roll and pitch motion of the car and the connected inertia forces. The stabilizers can also be involved in the modeling. In addition, the lever arm of the wishbones and the related forces can be considered, Streiter (1996).

In the following, a quarter-car model is applied, because it could be shown, e.g., Bußhardt (1995), that it meets the required demands for the investigated topics. A schematic of the quarter-car model is shown in Figure 12.12.

The sprung and unsprung mass displacements are  $z_B$  and  $z_W$  respectively. The damper generates the force  $F_D$  and the spring generates the force  $F_S$ . The dynamic tire load is  $F_{zdyn}$ .  $F_c$  describes the friction of the damper. Body mass  $m_B$ , tire stiffness  $c_W$  and damping coefficient  $d_B$  are commonly not constant. Apart from semi-active changes of spring and damper, the wheel mass  $m_W$  and the body spring coefficient  $c_B$  can be considered to be constant.

Using the road displacement  $r$  and the force  $F_B$ , which describes the body weight and the forces resulting from driving maneuvers as inputs, and using the body acceleration  $\ddot{z}_B$ , the tire acceleration  $\ddot{z}_W$  and the suspension deflection ( $z_W - z_B$ ) as outputs, the following equations can be derived.

$$m_B \ddot{z}_B = F_S + F_D - F_B \quad (12.3.4)$$

$$m_W \ddot{z}_W = F_{zdyn} - F_S - F_D \quad (12.3.5)$$

The characteristic operating curve of steel springs shows a smooth progressive relationship. However, they can be approximated by a linear curve in their operating point. This leads to:

$$F_S = (z_W - z_B) c_B \quad (12.3.6)$$

The tire is assumed to behave as a linear spring. As a result, the dynamic tire force  $F_{zdyn}$  is given by

$$F_{zdyn} = c_W (r - z_W). \quad (12.3.7)$$

The strongly degressive course of the damper's characteristic curve, see Figure 12.19, is usually divided up into a constant, a linear and a non-linear square component. Kraus, Dantle (1970) explains this fact by a complex hydraulic analysis of a damper: the non-linearity results from the opening of the piston valve and the stiffness of its spring. The damper characteristic can be approximated using the linear and non-linear damping parameters  $d_{Bl}$  and  $d_{Bnl}$  and a constant force  $F_0$ . These parameters reflect the constructive parameters of the damper:

$$F_D = d_{Bl} (\dot{z}_W - \dot{z}_B) + F_0 \operatorname{sign}(\dot{z}_W - \dot{z}_B) + d_{Bnl} |\dot{z}_W + \dot{z}_B|^{\frac{2}{1+2n}} \operatorname{sign}(\dot{z}_W - \dot{z}_B) \quad (12.3.8)$$

The constant  $n$  is usually set to  $n = 1.5$ , e.g., Majjad (1997).

Another representation of  $F_D$  is a piecewise linearization of the curve into the segments  $i$

$$F_{Di} = d_{Bi}(\dot{z}_W - \dot{z}_B) + F_{gli} \quad (12.3.9)$$

where  $F_{gli}$  is a parameter needed for the bumpless segmentation of the function.

Another method of handling the non-linear characteristic of the damper is the application of neural networks. For more details see, e.g., Halfmann (2001). However, this procedure does not comprise physical parameters.

(12.3.8) inserted in (12.3.4) and (12.3.5) leads to the non-linear model of a quarter-car

$$\begin{aligned} m_B \ddot{z}_B &= c_B(z_W - z_B) + d_{Bl}(\dot{z}_W - \dot{z}_B) + d_{Bnl} \sqrt{|\dot{z}_W - \dot{z}_B|} \operatorname{sign}(\dot{z}_W - \dot{z}_B) \\ &\quad + F_0 \operatorname{sign}(\dot{z}_W - \dot{z}_B) - F_B \end{aligned} \quad (12.3.10)$$

$$\begin{aligned} m_W \ddot{z}_W &= c_W(r - z_W) - c_B(z_W - z_B) + d_{Bl}(\dot{z}_W - \dot{z}_B) \\ &\quad + d_{Bnl} \sqrt{|\dot{z}_W - \dot{z}_B|} \operatorname{sign}(\dot{z}_W - \dot{z}_B) - F_0 \operatorname{sign}(\dot{z}_W - \dot{z}_B) \end{aligned} \quad (12.3.11)$$

The application of the piecewise linear curve results in:

$$m_B \ddot{z}_B = c_B(z_W - z_B) + d_{Bi}(\dot{z}_W - \dot{z}_B) + F_{gli} - F_B \quad i = 1 \dots N \quad (12.3.12)$$

$$m_B \ddot{z}_B = c_W(r - z_W) + c_B(z_W - z_B) + d_{Bi}(\dot{z}_W - \dot{z}_B) - F_{gli} \quad i = 1 \dots N \quad (12.3.13)$$

The validity of these models could be verified by comparing simulations with accompanying measurements on a test rig, Bußhardt (1995).

### 12.3.4 Identification of a Quarter-car Model

Because only very few measured variables will be available in suspensions, it is not possible to estimate all six parameters of the quarter-car model. Hence, some parameters must be set as known fixed values. Through simple conversion of (12.3.4) and (12.3.5), various estimation equations and sensor set-ups can be found. The resulting arrangements for the different estimation equations are given below, see also Table 12.4.

$$(z_W - z_B) = -\frac{d_B}{c_B}(\dot{z}_W - \dot{z}_B) + \frac{m_B}{c_B} \ddot{z}_B - \frac{1}{c_B} F_{gl} \quad (12.3.14)$$

$$(z_W - z_B) = -\frac{d_B}{c_B}(\dot{z}_W - \dot{z}_B) - \frac{m_W}{c_B} \ddot{z}_W + \frac{c_W}{c_B} (r - z_W) - \frac{1}{c_B} F_{gl} \quad (12.3.15)$$

$$\begin{aligned} (z_w - z_B) &= -\frac{d_B}{c_B}(\dot{z}_w - \dot{z}_B) - \frac{m_w m_B}{c_B(m_w + m_B)} F_{gl} - \frac{m_w m_B}{c_B(m_w + m_B)} (\ddot{z}_w - \ddot{z}_B) \\ &\quad + \frac{c_w m_B}{c_B(m_w + m_B)} (r - z_w) \end{aligned} \quad (12.3.16)$$

$$(z_w - z_B) = -\frac{d_B}{c_B}(\dot{z}_w - \dot{z}_B) - \frac{m_w}{c_B}(\ddot{z}_w - \ddot{z}_B) + \frac{m_B}{c_B} \ddot{z}_w - \frac{1}{c_B} F_{gl} \quad (12.3.17)$$

$$F_S = \frac{d_B}{c_B} \dot{F}_S - \frac{m_B}{c_B} (\ddot{z}_w - \ddot{z}_B) + m_B \ddot{z}_w - F_{gl} \quad (12.3.18)$$

$$F_D = \frac{d_B}{c_B} \dot{F}_D - \frac{m_B}{c_B} \ddot{F}_D + \frac{m_B d_B}{c_B} \ddot{z}_w - F_{gl} \quad (12.3.19)$$

**Table 12.4.** Various estimation equations for the quarter-car parameters

equation	measurable sensor signals	known parameters	parameter estimation	properties
(12.3.14)	$z_w - z_B$ $\ddot{z}_B$	$c_B$	$d_B, m_B, F_{gl}$	+ easily measurable quantities + $c_B$ is practically constant
(12.3.15)	$z_w - z_B$ $\ddot{z}_w,$ $r - z_w$	$m_w$	$d_B, c_B,$ $c_w, F_{gl}$	+ $c_w$ is estimated - road deflection is hardly measurable
(12.3.16)	$z_w - z_B$ $r - z_w$	$c_B, c_w$	$d_B, m_B,$ $c_w, F_{gl}$	+ $c_B$ and $m_w$ are practically constant + $c_w$ is estimated - road deflection is hardly measurable
(12.3.17)	$z_w - z_B$ $\ddot{z}_w$	$c_B$	$d_B, m_B, F_{gl}$	+ easily measurable quantities + $c_B$ is practically constant
(12.3.18) (12.3.19)	$F_S / F_D$ $\ddot{z}_w$	-	$d_B, m_B,$ $c_B, F_{gl}$	+ no pre-information is necessary + all parameters are measurable - $F_S, F_D$ are generally not measurable, except for air springs

Practically, at most only the body acceleration and the deflection are measured. However, measuring instruments for the road/wheel distance have also been discussed, e.g., Nomura, Takeshita (1993) and measurement of wheel acceleration may be used in the future. Therefore, (12.3.14) and eventually (12.3.17) are suitable for the identification. Moreover, the values of the wheel mass and the body mass can be assumed to be constant. Additionally, the variable body mass can be estimated out of the

static spring deflection.

In order to compensate for the non-linearity of damper characteristics, a piecewise estimation of the damper force is assumed. This division is dependent on the actual values of  $(\dot{z}_W - \dot{z}_B)$  and results in a structure-variable system. For the valid range of each single model, a set of parameters can be identified. The estimation equation for each model arises in analogy to (12.3.14) and (12.3.9) to

$$(\ddot{z}_W - \ddot{z}_B) = -\frac{d_{Bi}}{c_B}(\dot{z}_W - \dot{z}_B) + \frac{m_B}{c_B}\ddot{z}_B - \frac{1}{c_B}F_{gli} \quad \text{for } i = 1 \dots N \quad (12.3.20)$$

or in a general form to

$$y(t) = -a_{1i}\dot{y}(t) + b_0 u(t) + c_{gli} \quad \text{for } i = 1 \dots N$$

with  $y(t) = z_W(t) - z_B(t)$  and  $u(t) = \ddot{z}_B(t)$  (12.3.21)

Based on the measurements of  $y(t)$  and  $u(t)$ , the unknown parameters can be estimated by recursive least squares algorithms (RLS or DSFI), see Chapter 7. Alternatively, the identification can be based on the non-linear equation (12.3.10).

The identification methods were applied to a test rig, shown in Figure 12.20, which is equipped with a continuously adjustable damper. The damping is controlled by a magnetic valve, which opens or closes a bypass continuously. The test rig was constructed primarily for investigations on semi-active, parameter-adaptive suspension control, Bußhardt, (1995).

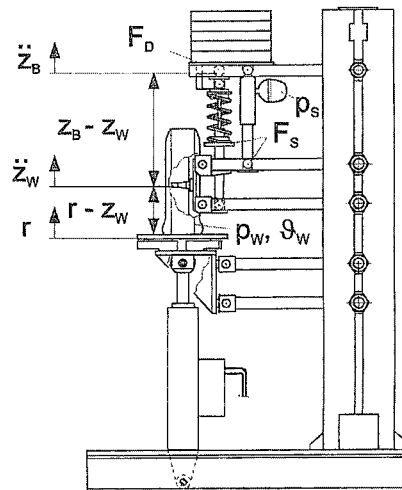
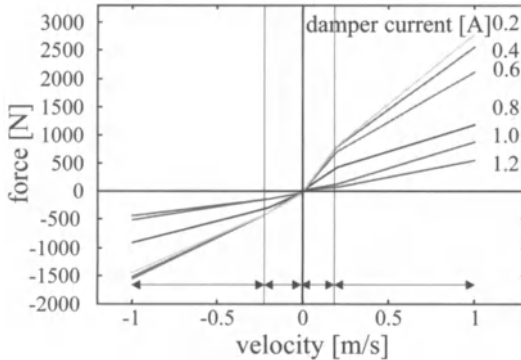


Figure 12.20. Quarter-car test rig

Figure 12.21 shows the estimated damping curve for different damper magnetic valve currents. Because rising damper current opens the bypass, the damping sinks. The damping curve was divided into four sections, two for each direction of motion. It can be seen that the damping curves at different damper currents can be clearly distinguished. Application of

parameter estimation with the non-linear equations led to approximately the same results.



**Figure 12.21.** Estimated damping characteristics of the adjustable damper

### 12.3.5 Suspension Control

#### a) Control principles

The suspension feedback control in general has been investigated extensively in the last 10 years for active and semi-active suspension concepts. Some of these controllers are called *skyhook-controllers*, as their intended use is to hang up the vehicle body on a virtual sky completely uncoupled from road excitations. Active control concepts can also be partly transferred to semi-active systems, leading to a suboptimal solution compared to the active system, Butsuen (1989). There exist various control concepts like the linear-quadratic (LQ) state-vector feedback, e.g., Salman (1988), Yue *et al.* (1989), Krtolica, Hrovat (1990), Ursu *et al.* (1997) or the minimal-variance (MV) principle, Bußhardt (1995). Non-linear robust control techniques such as sliding mode control are also applied, Alleyne, Hedrick (1995), Roukieh, Titli (1993), mostly as a consequence of non-linear actuators.

Semi-active systems are not critical regarding the stability except for resonance effects, as no forces can be generated and the system is always damped. Active systems by contrast can become unstable, so many robust controllers have been developed.  $H^\infty$ -controllers are increasingly applied to this problem, Hayakawa *et al.* (1999), Wang *et al.* (2001).

Many concepts additionally take into consideration preview information for the excitation. This preview information is either measured or estimated mostly using Kalman techniques, Oya *et al.* (1998), Yue *et al.* (1989), Bußhardt (1995), Karlsson *et al.* (2001).

Now, two different control concepts are distinguished between, as demonstrated by Figure 12.22, Bußhardt (1995). Firstly, the *suspension feedback control* is characterized by the feedback of process signals using, for example, a state-vector-controller. This aims to control the states of the vehicle, such as body and wheel acceleration, to specific values. Secondly,

the *feedback of estimated parameters* via a parameter-controller intends to maintain the suspension's parameters to specific values, in order to compensate for fading effects of the damper or to adjust different set-points, so that a certain performance of the suspension system is controlled.

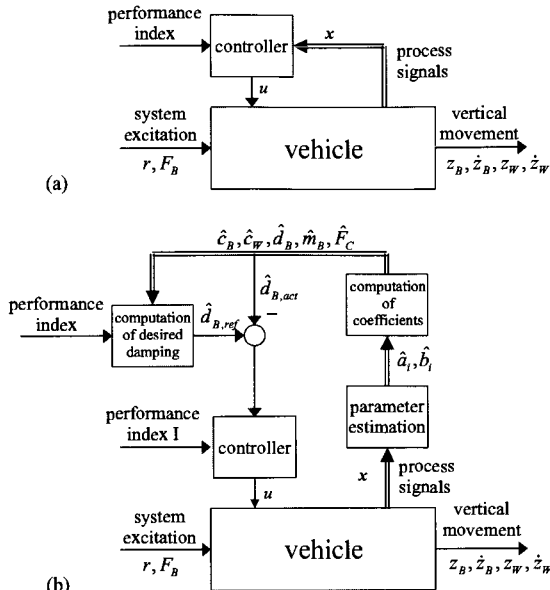


**Figure 12.22.** Suspension control principles: (a) suspension feedback control (state feedback); b. feedback of estimated parameters (parameter feedback)

The combination of these two control concepts results in a parameter-adaptive suspension control system, as shown in Figure 12.23. The “fast” feedback level of the suspension control is extended by the “slow” adaptation level, in order to adapt the controller to the actual system parameters. This enables an optimal control performance despite of altering parameters.

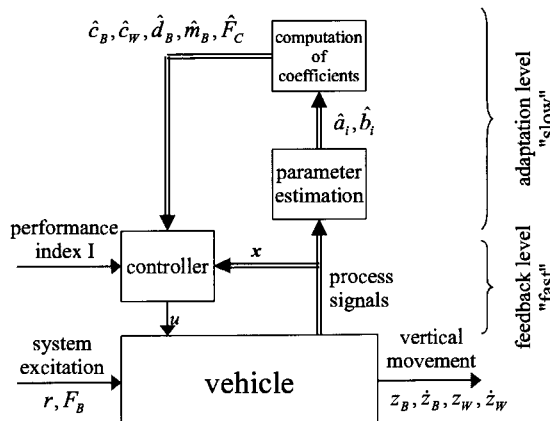


**Figure 12.23.** Parameter-adaptive suspension control

Considering linear damper and spring and an active force  $\Delta F_u$  between body and wheel mass, which can be introduced by a semi-active or active damper, the following quarter-car model can be assumed for the ensuing controller design

$$m_B \ddot{z}_B = c_B(z_W - z_B) + d_B(\dot{z}_W - \dot{z}_B) + \Delta F_u - F_B \quad (12.3.22)$$

$$\begin{aligned} m_W \ddot{z}_W &= c_W(r - z_W) - c_B(z_W - z_B) \\ &\quad - d_B(\dot{z}_W - \dot{z}_B) - \Delta F_u \end{aligned} \quad (12.3.23)$$

(12.3.22) and (12.3.23) directly enable the transformation to a state space representation. As input quantities, the measurable body wheel deflection  $z_W - z_B$  and its derivative  $\dot{z}_W - \dot{z}_B$  estimated by numerical differentiation or using a state variable filter are suitable. The absolute values of the body and wheel position  $z_B$  and  $r$  are also suitable. These quantities can be estimated using a Kalman filter, e.g., Bußhardt (1995). The body acceleration and the dynamic tire loads are chosen as outputs, because they are needed to describe the driving safety and quality. For more details see Bußhardt (1995) and Isermann *et al.* (2002).

### b) Spring and damper as semi-active force generators

In the case of semi-active systems, the force  $\Delta F_u$  has to be generated by the adjustment of the suspension parameters  $c_B$  and  $d_B$ . For the linearized system, the following expressions can be determined:

$$F_S(k) = c_B(k)(z_W(k) - z_B(k)) \quad (12.3.24)$$

$$F_D(k) = d_B(k)(\dot{z}_W(k) - \dot{z}_B(k)) \quad (12.3.25)$$

By dividing the parameters  $c_B$  and  $d_B$  in a constant value ( $c_{B0}$  and  $d_{B0}$ ) and a changing part, (12.3.24) and (12.3.25) can be converted to

$$c_B(k) = \frac{F_S(k)}{z_W(k) - z_B(k)} = c_{B0} + \frac{\Delta F_{Su}(k)}{z_W(k) - z_B(k)} \quad (12.3.26)$$

$$d_B(k) = \frac{F_D(k)}{\dot{z}_W(k) - \dot{z}_B(k)} = d_{B0} + \frac{\Delta F_{Du}(k)}{(\dot{z}_W(k) - \dot{z}_B(k))} \quad (12.3.27)$$

Here, the force  $\Delta F_u$  is divided into the additive parts  $\Delta F_{Su}$  and  $\Delta F_{Du}$  for the spring and damper respectively. Another possibility for the division of the activating force to damper and spring is the differentiation between sprung and unsprung mass forces. Independent of the control scheme, the high-frequency motion of the unsprung mass results in high-frequency manipulating forces, while the low-frequency body motion results in low-frequency manipulating forces. As real semi-active dampers provide higher switching times than semi-active springs, the unsprung mass forces

control is given to the damper and the sprung mass forces control is given to the spring, see Figure 12.24.

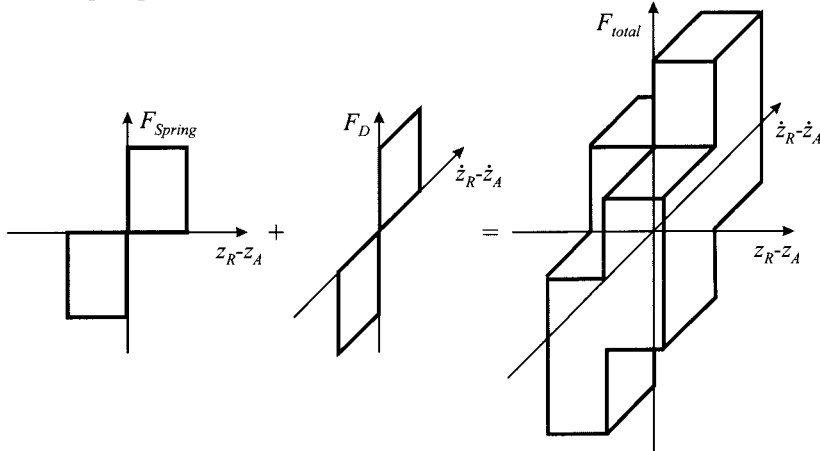


**Figure 12.24.** Force ranges of spring, damper and their combination

### c) Feedback control of estimated coefficients

The characteristic of this method is the successive parameter estimation and parameter control in one loop, see Figure 12.22b. Due to the restricted identification speed, this method is applicable to relatively slowly changing conditions like damping fluid temperature, tire pressure or changing load. In addition, the variable damper or spring has to be adjusted continuously, in order to perform the required fine-tuning of its properties. Due to the feedback of estimated coefficients, the controlled process is the suspension and the parameter estimation.

The feedback control of estimated coefficients prevents wear and fading effects and ensures a constant optimized adjustment of the suspension. Additionally, there is the possibility of controlling the body-damping coefficient to constant optimal values.

The mechanism and the good function of this scheme could be shown in various simulations and could be proved by experimental results on the test rig, Büßhardt (1995).

### d) Suspension feedback control

The objective of a control design for a vehicle's suspension is the maximization of drive safety *and* driving comfort. Fundamental research, Mitschke (1997) and Darenberg *et al.* (1984) shows that, on the one hand, a complete zero-regulation of the dynamic tire load, or, on the other hand, a complete zero-regulation of the body acceleration is only attainable using an optimal force generator ( $c_B = d_B = 0$ ). However, both are not feasible simultaneously. A complete decoupling of the body from the road disturbances would lead to a wheel springing on the road. Correspondingly, the complete minimization of the dynamic tire loads would result in an unacceptable loss of comfort. Thus, a compromise of these properties has to be found.

Consequently, the previously mentioned objectives are equivalent to the minimization of the performance quantities (12.3.1) and (12.3.2). Using a quadratic performance criterion including  $z_B, \dot{z}_B, \ddot{z}_B, z_W$  and  $\dot{z}_W$  an optimal state feedback-controller results.

Simulation results using the minimum-variance (MV) state vector feedback-controller are summarized in Table 12.5. The excitation for all simulation is a street profile with realistic noise characteristics, for details see Bußhardt (1995). The percent quantities refer to the reference point of the underlying passive suspension, Mitschke (1997) and a specific excitation. The application of an ideal variable damper and spring results in a reduction of the mean body acceleration of up to about 46%. This is nearly the same dimension as an active suspension system (60%). The sole application of a variable damper provides only a reduction of up to 23% for the mean body acceleration. This elucidates the effect of the combination of a variable damper and a variable spring.

In the case of body acceleration, a reduction of nearly 20% is achievable. This smaller result compared to the road excitation is explained by the restricted operation range of the semi-active elements.

**Table 12.5.** Mean body acceleration of active/semi-active suspension systems compared to a standard passive system, Bußhardt (1995), simulation, relative quantities

	road excitation %	body excitation %
variable damper	23	20
variable spring	30	12
variable spring and damper	46	22
active	60	55

Applying this control scheme to the test rig causes a reduction of the body acceleration of about approximately 10%. This smaller result compared to the simulations is explainable by the time delays of low-pass filtering and the real magnetic damper actuator.

### e) Influence of the variable damper's time constant and regulation range

An important result of the experiments on the test rig is that the damper's time constant  $T_{mech}$ , the remaining time delay of the low-pass filter  $T_{LP}$  and the microprocessor's dead-time  $T_t$  play an important role in obtaining the best achievable performance. The various time constants are typically added to the sum time constant

$$T_{\Sigma} = T_{mech} + T_{LP} + T_t \quad (12.3.28)$$

Therefore, simulations with various time constants and filter cut-off frequencies have been carried out with the minimal-variance feedback-controller and a variable damper in the case of road excitation. As Figure 12.25a shows, a larger sum time constant  $T_{\Sigma}$  generally deteriorates the

performance. For example, the available reduction of the mean body acceleration with  $T_{\Sigma} = 30$  s, 20 s, 10 s, 0 s is 11%, 14%, 20%, 32% respectively.

According to these results, the time constant  $T_{\Sigma}$  should be less than 10 ms. Nowadays, the time constant lies in the order of 30 ms.

Another limiting aspect for the performance of a semi-active damper is the regulation range. Case one simulations are based on a damper with  $100 \text{ Ns/m} < d_B < 2000 \text{ Ns/m}$ . While smaller damping rates are not achievable, higher damping rates are possible with an adequate damper design. In order to investigate the extension of the regulation range, damping of  $100 \text{ Ns/m} < d_B < 5000 \text{ Ns/m}$  is assumed. The results obtained are shown in Figure 12.25b.

The extension of the regulation range leads to a significant increase in performance. While the small regulation range reduces body acceleration and tire load variation by about 25% and 10%, the large regulation range achieves a reduction of about 35% and 17% respectively. This clearly shows the potential of an extension of the damper's regulation range.

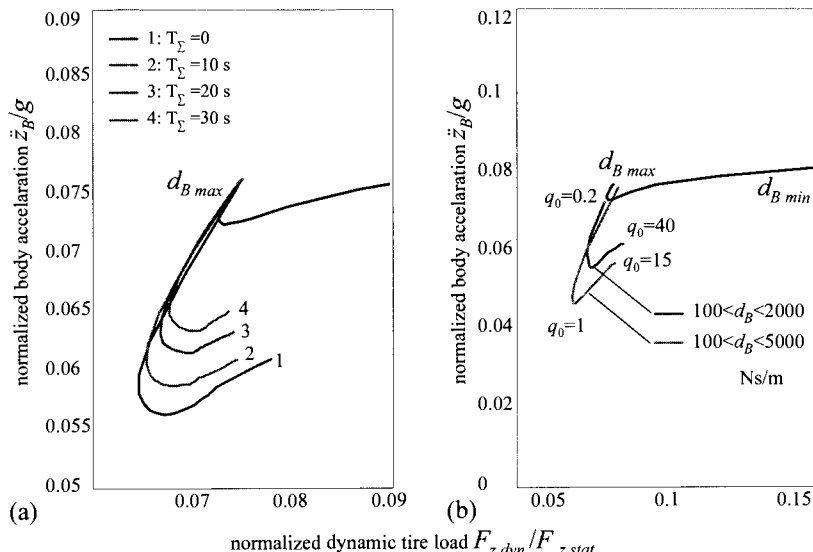


**Figure 12.25.** Effects of the damper actuator properties (simulation): (a) comparison between different sum time constants, variable damper with relative MV state feedback; (b) comparison between passive and semi-active damper with various regulation ranges, relative state vector feedback.

### 12.3.6 Simulations of a Semi-active Two-chamber Air Spring

As previously described, a real semi-active, continuously and fast controllable spring is not commercially available presently. However, air springs with two switchable chambers are possible, Reimpell, Stoll (1989). High switching times are also possible because of the simple valve between the chambers. This provides two different stiffness values for the air spring. The results of such a semi-active spring are illustrated in Figure 12.26.

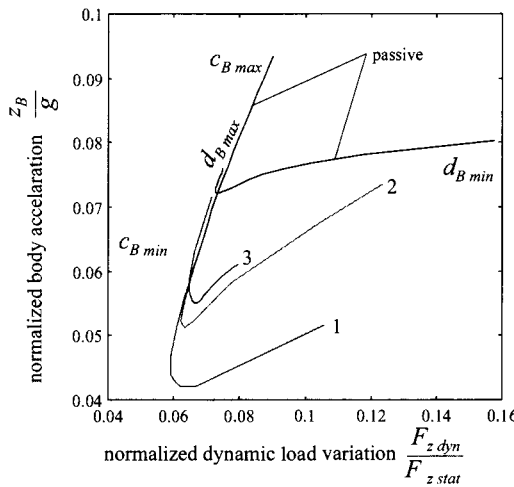


**Figure 12.26.** Comparison of variable damper with: (1) ideal variable spring, (2) two-stage spring, (3) invariable spring

As expected, the two-stage spring achieves a worse result than the continuous variable spring. However, the mean body acceleration can be reduced to nearly 30%. Considering the minor successful experimental results with a single variable damper, this relatively simple semi-active system has interesting potential.

The modeling and parameter estimation of suspension systems can further be favorably used for fault detection, see Weispfenning (1996), Isermann *et al.* (2002).

The discussion of semi-active vehicle suspension system as a typical mechatronic component has shown that modeling and simulation of different actuation principles for variable dampers and springs gives valuable hints for the selection and design of final suspension configuration. It further shows the potential of different sensor and control arrangements for the adaptation of otherwise changing suspension parameters and setting of definite parameters according to commands from higher-level driving controllers.

## 12.4 ELECTROMECHANICAL DISC BRAKE (EMB)

### 12.4.1 Introduction

The number of first registered cars being equipped with modern electronic driver-assisting brake control systems such as anti-lock braking (ABS), traction control system (TCS), and electronic stability program (ESP) is increasing steadily. However, to embed such functionality in conventional hydraulic brake systems, a large number of electrohydraulic components

are required. In recent years, the automotive industry and their suppliers have therefore started to develop brake-by-wire systems as typical mechatronic solutions. There are two concepts currently favored, the electrohydraulic system (EHB) and the fully electromechanical system (EMB). The electrohydraulic brake-by-wire system still uses brake fluid and conventional brake actuators but proportional valves. This system came on the market in 2001.

However, with the disadvantages of the electrohydraulic system (brake fluid, brake lines, proportional valves, *etc.*) the fully electromechanical brake system is a promising concept and is therefore also investigated. Figure 12.27 shows an electromechanical brake actuator, Rieth (1999). An electromechanically actuated brake system provides an ideal basis for converting electrical command signals into clamping forces, or rather peripheral forces, at the brakes. Standard and advanced braking functions can then be realized with uniform hardware and software. The software modules of the control unit and the sensor equipment determine the functionality of the brake-by-wire system.



**Figure 12.27.** Electromechanical disc brake (Continental Teves)

The reduction of vehicle hardware and entire system weight are not the only motivational factors contributing to the development of a fully electromechanical brake-by-wire system. The system is environmentally friendly due to the lack of brake fluid and requires little maintenance (only pads and discs). Its decoupled brake pedal can be mounted in a crash-compatible and space-saving manner for the passenger compartment. There are no restraints to the design of the pedal characteristics, so ergonomic and safety aspects are easy to consider. This “plug and play” concept with a minimized number of parts also reduces production and logistics costs.

However, brake-by-wire systems also entail disadvantages. One of these is the varying efficiency of the brake actuator due to changing rough environmental conditions and wear, see Figure 12.28. The transmission characteristics of each subsystem, such as the electromechanical actuator, the gear unit, the friction brake and the tire/road/vehicle system, is subject to large parameter variations. Therefore, the individual wheel brakes need to be operated in a closed control loop. For disc brakes, an obvious physical quantity to control is the clamping force. Yet, a force sensor is difficult to integrate in the electric brake. Therefore, it can be tried to estimate their force based on easier measurable variables.

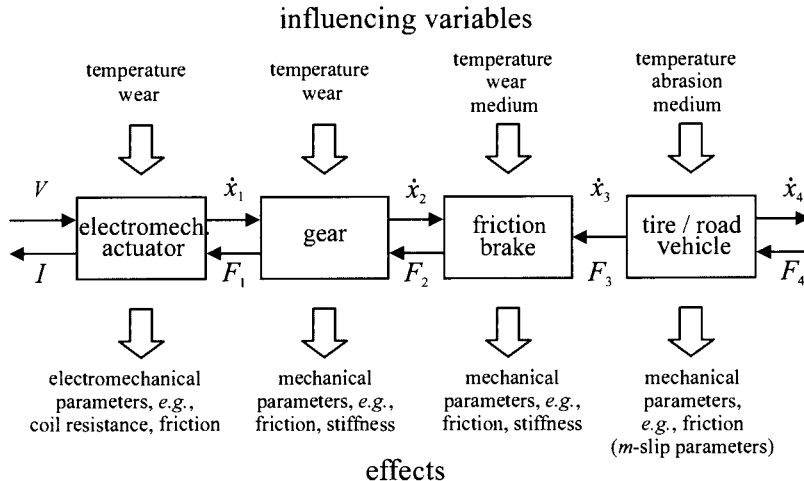


**Figure 12.28.** Two-port representation of a brake-by-wire actuator with influencing variables and their effects

### 12.4.2 Wheel Module

A wheel module consists of an electromechanical brake with servo-amplifier and microcontroller unit, see Figure 12.29, Schwarz (1999).

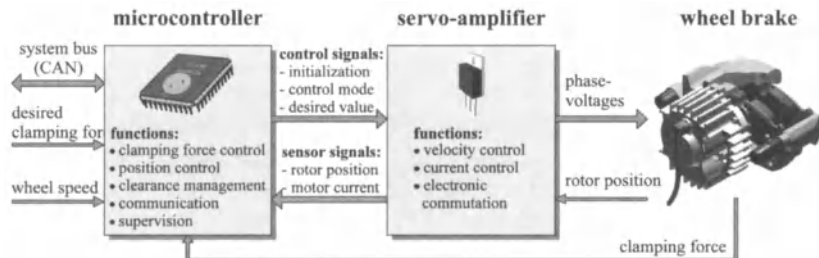


**Figure 12.29.** Block diagram of a wheel module

With the aim of using components that are suitable for large volume production, a standard 16-bit microcontroller was chosen as the program-

ming platform for the digital control algorithms. The microcontroller performs the clamping force and position control as well as the clearance management, the communication and the supervision of the wheel module.

To drive the DC brushless motor of the wheel brake, a compact and powerful servo-amplifier is used. It processes the motor rotor position, which is provided by a resolver, for electronic commutation. Additionally, the servo-amplifier is equipped with two analog-controllers, a motor current-controller, and a rotor velocity-controller.

The design of an “intelligent disc brake” consisting of an electromechanical converter, gear, friction brake, and sensors is mainly driven by the demand for minimized space and lightweight construction. Based on a reliable and well-proven caliper, a very compact electric brake was developed. Figure 12.30 depicts the third-generation actuator with an additional planetary gear, a clamping-force sensor and other modifications.

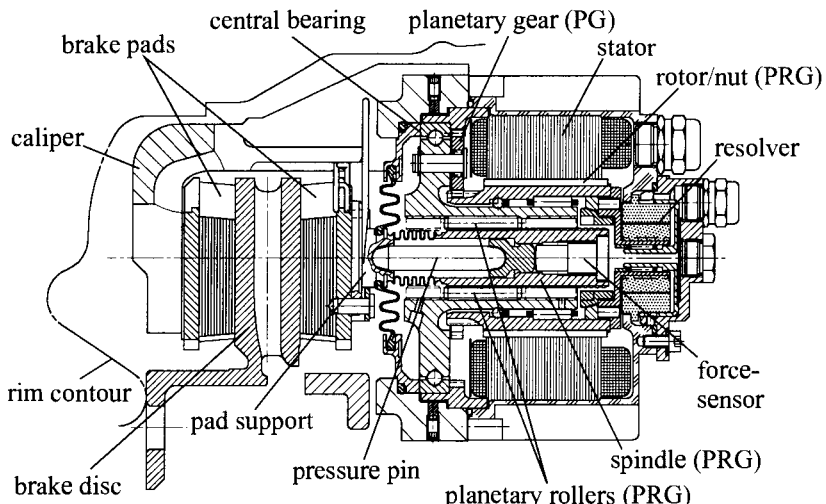


**Figure 12.30.** Sectional drawing of the EMB (Continental Teves), Schwarz (1999)

Instead of the piston in hydraulic brakes, the inner brake pad is actuated by a spindle. The nut of the planetary roller gear (PRG) is driven by the rotor of a brushless torque motor via a planetary gear (PG). By integrating the coil of the servo-motor directly into the brake housing and by supporting the gear unit with one central bearing only, the compact design was made possible. However, the central bearing has to absorb both radial and axial forces. A resolver measures the position of the rotor for electronic commutation.

### 12.4.3 Brake Model

Figure 12.31 shows a block diagram of the EMB, Schwarz (1999). The microcontroller block contains the force- and position-controller, both having proportional behavior. In the analog-controller block, the velocity and the current controller of the servo-amplifier are considered. The velocity controller is a PI-controller and the current controller is a PI-controller with a series-connected first order lag ( $PT_1$ ) element. They are cascaded with the velocity controller in the outer loop.

The next block in the model structure is the motor, Figure 12.31. For simplification, the DC brushless motor was modeled as a standard DC motor with its output torque  $T_m$  being proportional to the motor current  $I_m$ :

$$T_m = I_m \Psi \quad (12.4.1)$$

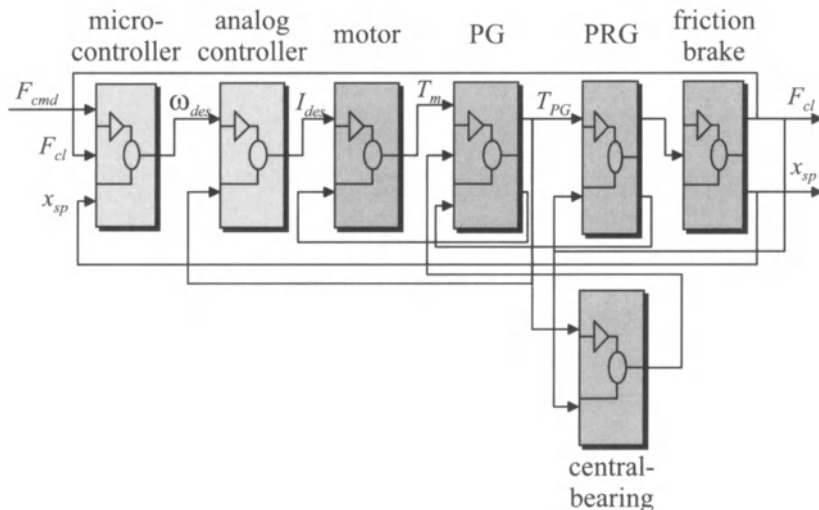


**Figure 12.31.** Matlab®/Simulink™ block diagram or EMB brake control

The planetary gear (PG), Figure 12.32, is modeled as two series-connected gear units. The first gear unit is the sun-planet wheel unit, the second is the planet-carrier wheel unit. Each of the gear units considers friction torque due to bearing friction  $T_{FB1}$  and  $T_{FB2}$  and due to tooth friction  $T_{FT}$ . The stiffnesses and dampings of one gear unit are lumped together as  $c_G$  and  $d_G$ . For the calculation of the inertias and friction losses, special attention has to be paid to the speed ratios of the components. With the support of the component supplier, all parameters could either be evaluated or measured. Figure 12.33 depicts the two-mass model of one gear unit.

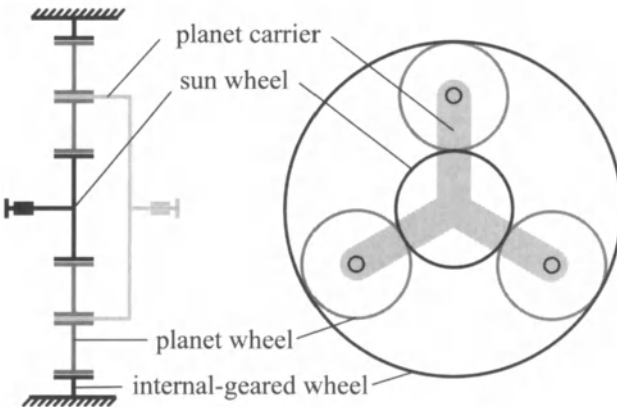


**Figure 12.32.** Principle and components of the planetary gear

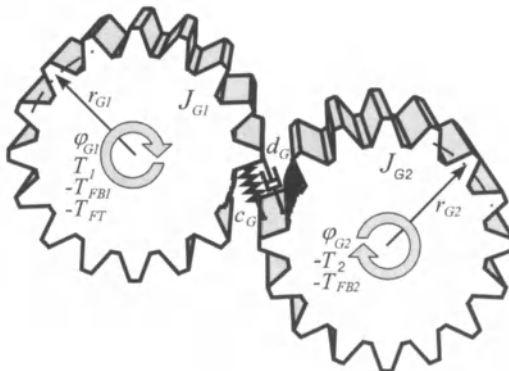


**Figure 12.33.** Two-mass model of one gear unit

One of the most challenging tasks in the modeling process was the design of the planetary roller gear (PRG) subsystem. The PRG was also modeled as a two-mass oscillator with friction due to the bearing mounting as well as the nut-roller and roller-spindle contact. Since the thread-face contact contour of a planetary roller gear is identical to the contact contour of an angular ball bearing the models could be derived from such bearing models. The final PRG subsystem includes, see Figure 12.34:

- stiffness of the nut, spindle, and rollers (lumped together as one stiffness and one damping);
- Coulomb friction of the PRG with axial load dependency  $T_{FR}$ ;
- dead zone of the PRG;
- moments of inertia of the nut  $J_R$ , the rollers  $J_W$ , and the roller cage  $J_K$  as well as the mass of the spindle  $m_S$  and the rollers  $m_W$  (lumped together as one inertia and one mass).

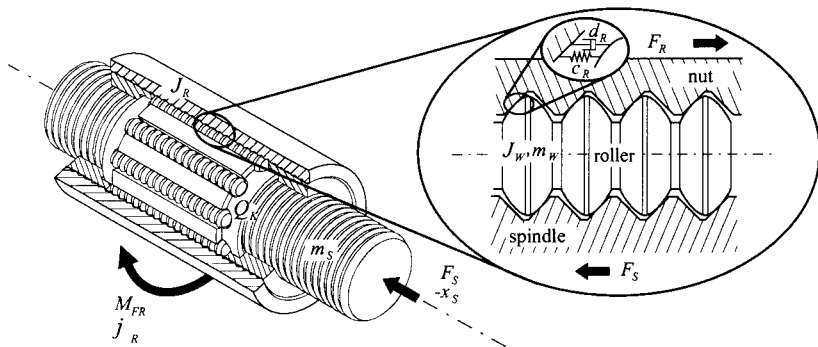


Figure 12.34. Planetary roller gear

In the friction brake subsystem, Figure 12.35, the static and dynamic behavior of the caliper, the brake pads and the brake disc are modeled. The stiffness of the caliper and the brake pads were determined with a specifically designed test unit.

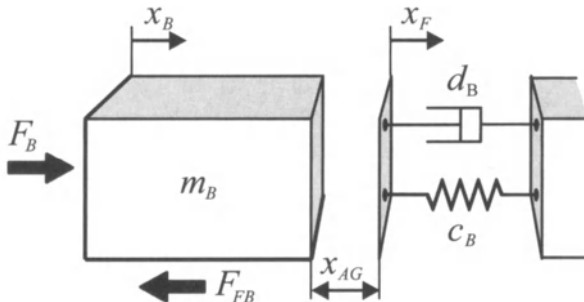


Figure 12.35. Model of friction brake

Two states of the friction brake have to be distinguished:

- the brake pads do not touch the brake disc – clearance (air gap) has to be taken into account ( $x_{AG} > 0$ );
- the brake pads touch the brake disc – no clearance ( $x_{AG} = 0$ )

For each state, the mass  $m_B$ , the translatory friction force  $F_{FB}$ , the stiffness  $c_B$ , and the damping  $d_B$  must be calculated individually. Based on the value of the clearance  $x_{AG}$ , the model is switched between the two states.

A bearing test bench served to identify the parameters of the central bearing subsystem. The moment of friction could be measured for different axial forces and rotational velocities. By means of an easy-to-operate graphical user interface, artificial excitation signals and measurements can be loaded for simulation. The interface allows changing of simulation parameters and the integrating method.

External and internal model signals can be selected for display. Figure 12.36 shows the Windows desktop of the graphical user interface.

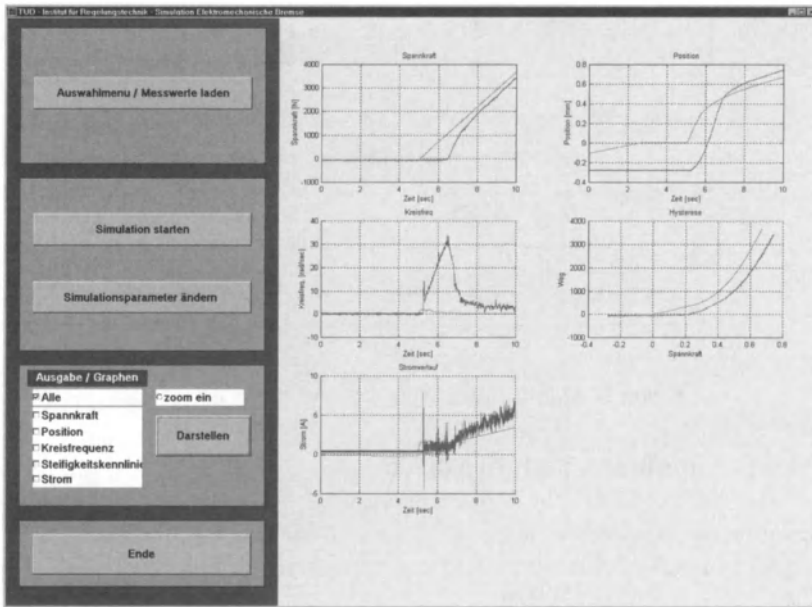


**Figure 12.36.** Graphical user interface

#### 12.4.4 Simplified Brake Model

In the development of the reduced model, Figure 12.37, the different physical parameters were lumped together.  $J_{tot}$  includes all inertias as well as all translatory accelerated masses. The parameter  $d_{tot}$  comprises the viscous friction torques of the individual brake components. With the parameter  $g_{tot}$ , the load-dependent friction is considered. The gear ratio  $n_{tot}$  results from the series connection of the planetary gear ratio and the planetary roller gear ratio. This results in

$$J_{tot} \dot{\omega}_m = T_m - T_{Fv} - T_{Fc} - T_{use} = T_m - d_{tot} \omega_m - \text{sign}(\omega_m)(T_{F0} + g_{tot} F_{cl}) - v_{tot} F_{cl} \quad (12.4.2)$$

The clamping force  $F_{cl}$  is modeled as a characteristic curve, depending on the spindle travel  $x_{sp}$  with the non-linear equation

$$F_{cl} = \alpha_B \sqrt{\beta_B + x_{sp}^2} + \chi_B \quad (\chi_B: \text{offset parameter}) \quad (12.4.3)$$

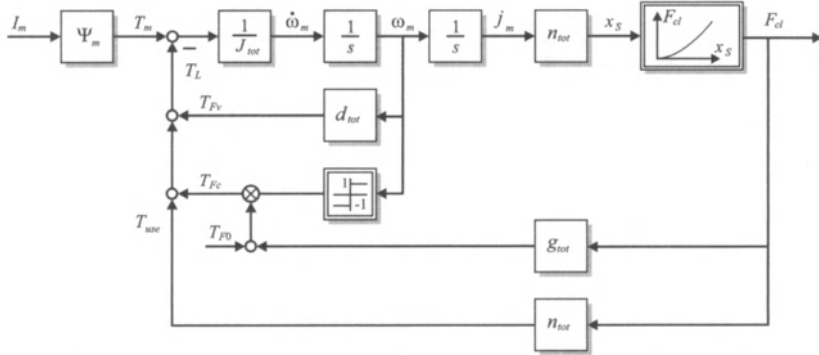


**Figure 12.37.** Block diagram of the simplified brake model

### 12.4.5 Simulation and Measurement

In order to validate the brake model mentioned above, the same input signal is used both for simulation and measurement. Figure 12.38 shows the results, Schwarz (1999).

The output signals of the brake model correspond with the output signals obtained from the physical brake. Minor differences in clamping force, angle of the motor shaft, angular velocity of the motor shaft, and motor current between model and brake can be traced back due to the fact that the variation of the friction parameters due to the transverse forces are neglected here.

By using these models, a complete brake control system could be developed and tested on special test rigs and vehicles.

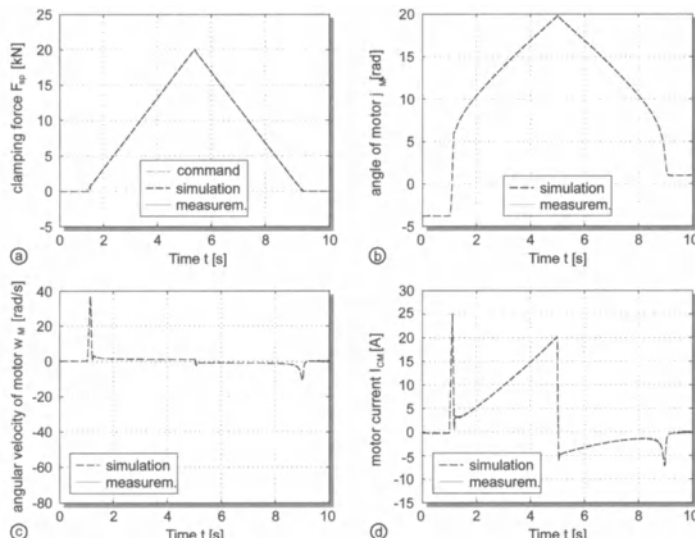


**Figure 12.38.** Simulation and measurement results: (a) clamping force; (b) angle of motor shaft; (c) rotational velocity of motor shaft; (d) motor current

## 12.5 CONTROL PROTOTYPING AND HARDWARE-IN-THE-LOOP SIMULATION

The integration of automatic control functions and general automation functions in mechatronic systems requires appropriate design tools. This holds especially for simultaneous engineering and short time to market. Therefore, development tools like control prototyping, software-in-the-loop and hardware-in-the-loop simulation are increasingly applied, e.g., in the area of automotive systems, enabling an integrated hardware and software environment and a rapid implementation and testing of the algorithms. In the following, a brief description of these tools is given and some application examples are shown for the case of combustion engine control systems.

### 12.5.1 Simulation Methods

A systematic control design for mechatronic systems requires different kind of simulation methods, Hanselmann (1996). Figure 12.39 shows simulation methods that are increasingly used for the design and testing of combustion engine control units (ECU), arranged in the form of a V, sometimes called “V-model”.

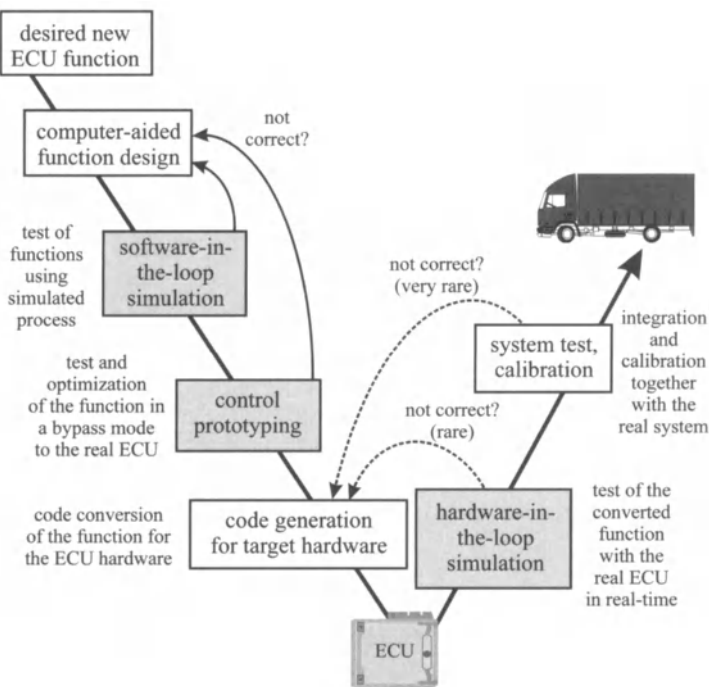


**Figure 12.39.** Design and simulation steps for ECU function development of internal combustion engines, V-arrangement (V-model)

1. software-in-the-loop simulation (SiL): in the first step of the function development, some basic analysis may be performed to develop the control structure and actuator configuration. Software-in-the-loop simulation means that a software version of the control function is tested with the simulated process. Real-time functions are not required in this case;
2. rapid control prototyping (RCP): the control prototyping is used to test the new control function together with the real already existing control unit and the simulated or the real process. In contrast to the software-in-the-loop simulation, only a selected subset of the ECU functions is realized as a special software implementation. Only these interesting parts are calculated on a real-time computer system in a bypass mode to the real ECU, Figure 12.40;
3. hardware-in-the-loop simulation (HiL): after the target code generation of the control functions, the hardware-in-the-loop simulation is employed for testing the implemented ECU functionality. In this configuration, the real ECU hardware operates together with the simulated process in real-time, Isermann *et al.* (1999). To couple the real-time computer system with the engine control unit, it is necessary to generate the required sensor signals (*e.g.*, pulses of the crankshaft and camshaft inductive speed sensors, temperatures and pressures) and to process the actuator signals, Sinsel (1999).

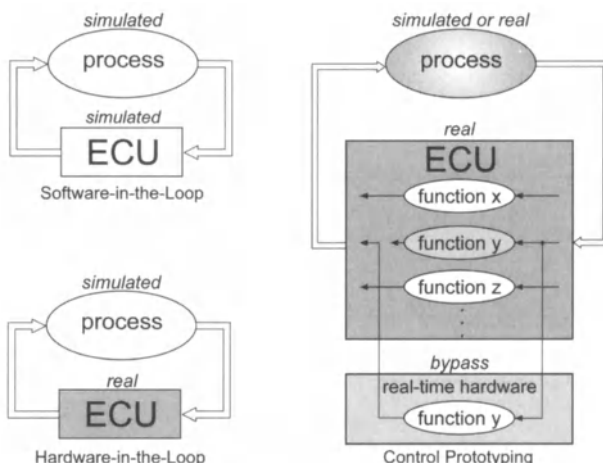


**Figure 12.40.** Simulation methods for the development of electronic control unit (ECU) functions

Figure 12.41 shows a simulation family system for all three simulation categories, SiL, RCP and HiL, Schaffnit, Isermann (2000). In this case, the HiL simulation also includes the real injection pumps.

The following sections describe RCP and HiL in more detail.

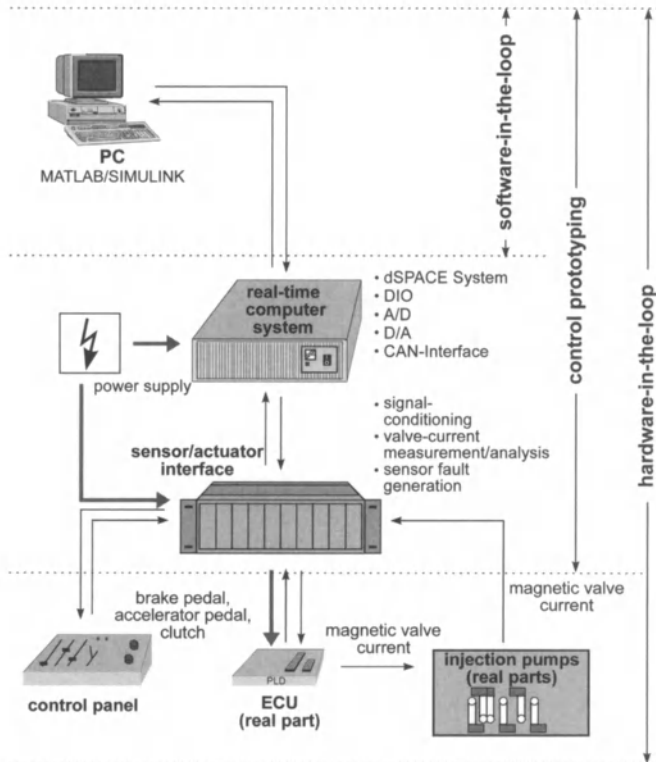


**Figure 12.41.** Simulation system family for software-in-the-loop, control prototyping and hardware-in-the-loop

## 12.5.2 Rapid Control Prototyping for Engine Control

In order to allow development and testing of new control functions on-line in conjunction with the real engine in an efficient manner, powerful real-time computer systems are required. RCP systems allow the implementation and testing of new algorithms together with the already-existing ECU. Thus, programming and modifications of the production ECU are avoided.

The RCP system is capable of fast measurement signal evaluation and advanced engine control algorithms, as it is required, for instance, in the case of combustion pressure-based engine control. It consists of two subsystems, the RCP and a pressure indication system, see Figure 12.42. Both systems operate in parallel to the production car's ECU, and are based on PowerPCs, type Motorola MPC 750, 480 MHz, which are designed for real-time use and are programmed in high-level language.

The indicating system allows evaluation of cylinder pressure signals in real-time at a resolution of 1° crankshaft angle (CA) for four cylinders. Thus, it operates in a crank-synchronous manner. Thermodynamic and signal-based cylinder pressure features, like mean indicated pressure, crank angle of the center of combustion, and location of peak pressure, are

calculated by the indicating system and are transmitted to the RCP system.

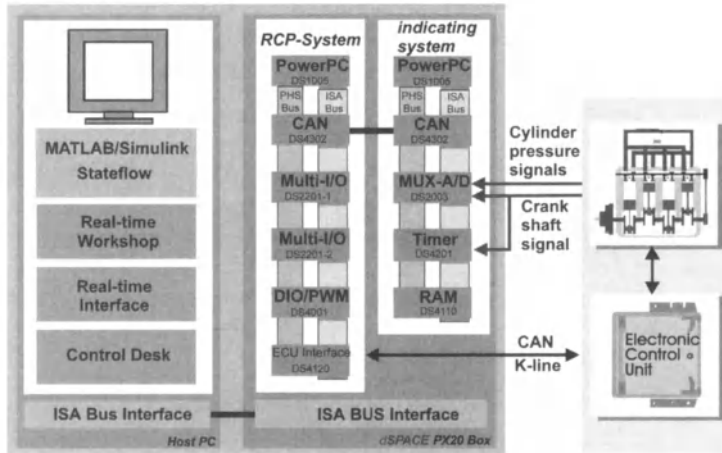


**Figure 12.42.** Rapid control prototyping system configuration with dSPACE units

The RCP system allows very fast and easy implementation and testing of new control concepts on real-time hardware. It computes the control and optimization algorithms and operates in a time-synchronous manner, at a sampling rate of 1 kHz. The user is enabled to code newly-developed algorithms from block diagrams (*e.g.*, MATLAB/Simulink) and download the code by means of an automatic code generation software to the real-time hardware with a mouse click. A complete design iteration can thus be accomplished within a few minutes, Hanselmann (1996).

The RCP system uses the production car sensors, additional test stand sensors and the output signals and messages of the ECU. By evaluating the production car sensor information, the standard ECU control settings can be investigated and then be modified, also independent own control strategies can be implemented. The actuator signals, which are calculated in real-time, are then sent to the actuators or the ECU by means of a CAN bus or by PWM (pulse width-modulated) signal.

The described real-time hardware system enables very fast and easy implementation and testing of complex algorithms, including extensive data preprocessing for the cylinder pressure, even under the hard real-time conditions of combustion engines.

### 12.5.3 Hardware-in-the-loop Simulation for Diesel Engines

After the evaluation of new control functions by using RCP systems or testing new algorithms, the program code is implemented on the real ECU hardware and tested with the real ECU in real-time. The control system of a modern diesel engine has an overall structure as in Figure 12.43.

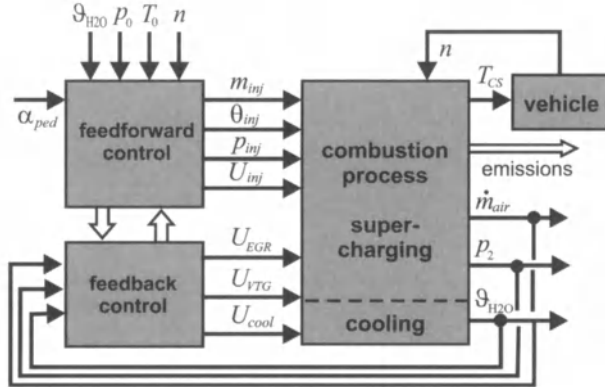


**Figure 12.43.** Simplified control structure of a diesel engine with turbocharger

Feedback control is applied to the air mass flow  $\dot{m}_{air}$  through the exhaust gas recirculation valve  $U_{EGR}$ , the charging pressure  $p_2$  through the vane position of the variable geometry turbocharger  $U_{VTG}$  and coolant temperature  $\theta_{H2O}$  by the cooling flow valve  $U_{cool}$ . All other variables are feedforward-controlled via look-up tables. Figure 12.44 shows the set-up of a HiL simulation test bench for testing new control functions of the real engine control unit of a truck's diesel engine together with the simulated engine. It may be subdivided into the following parts, Isermann *et al.* (1999):

- real-time computer system including I/O modules;
- periphery, consisting of the sensor and actuator interface;
- PLD control unit including real actuator, components, stand-alone or in combination with the real FMR control unit;
- PC with graphical user interface;
- control panel.

### a) The HiL simulator

The real-time computer system for this simulator is based on a dSPACE system equipped with digital signal processors and a DEC Alpha processor. This system has the advantage of high computing power, which makes parallel calculation unnecessary. It also offers the possibility of realizing all the models in MATLAB/SIMULINK and to use all the benefits of a graphical simulation environment. Special I/O modules (digital-I/O module, D/A converter, A/D converter and CAN interface) are used for communication with the periphery. The coupling of the simulator and the control unit is implemented with a special periphery, which can be subdivided into a sensor and an actuator interface.

The *sensor interface* generates the necessary sensor signals like temperatures and pressures. The pulses of the camshaft and crankshaft inductive speed sensors are generated with a board specifically designed for high-speed signal generation.

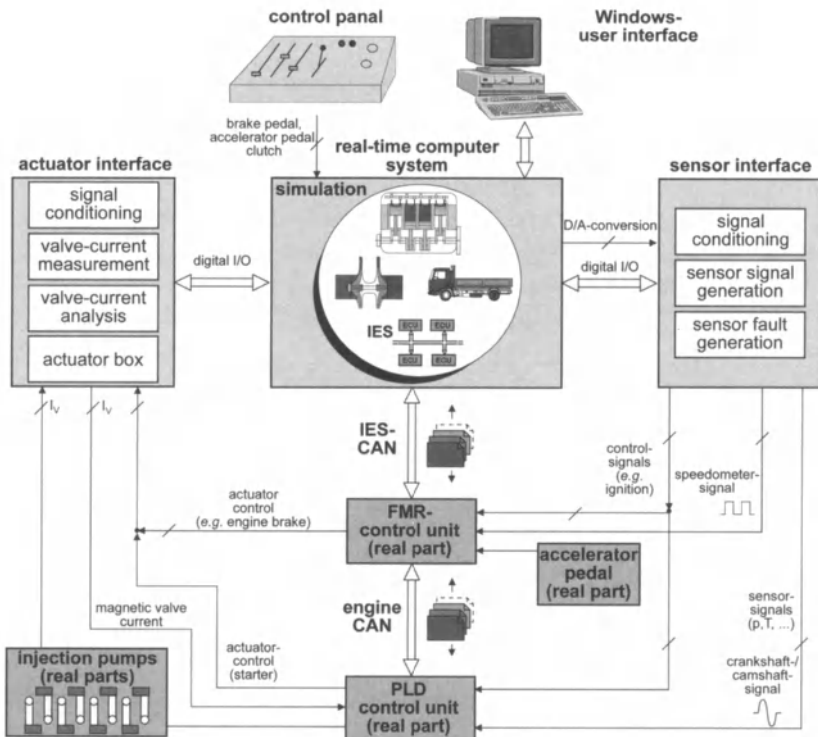


**Figure 12.44.** Hardware-in-the-loop test bench with simulated engine and vehicle and with real engine and vehicle and with real engine control unit and real injection actuators. FMR: vehicle management system; PLD: pump-line-nozzle injection system.

For this purpose a look-up table with the pulse signals versus the crankshaft angle is stored off-line in memory. During the simulation, the signals are periodically read out, synchronous to the simulated engine speed. This realization guarantees a high flexibility in forming the pulses and adapting different gear wheels. The sensor interface also contains an electronic relay to simulate sensor faults like interruptions and short circuits.

The *actuator interface* mainly consists of the injection pumps (pump-line-nozzle injection system), which are integrated in the simulation test bench as real components because the combination of the PLD control unit and the injection pumps represent a mechatronic unit that is difficult to model. A special electronic device measures the magnetic valve currents to reconstruct the real valve opening time and to determine the pulse width and the beginning of injection. These quantities are transferred to the real-time computer system for engine simulation. In this way, the real behavior of the injection pumps is included.

The simulator test bench was set up with the objective of testing the PLD control unit stand-alone or in combination with the FMR control unit. In the first case, the necessary FMR functions are simulated by the

computer system. The data transfer is done via the engine CAN bus. In the second case, the PLD and the FMR control units are connected directly via the engine CAN bus. The computer system emulates other IES (integrated electronic systems) units in this operation mode by transmitting the data via the IES-CAN bus to the FMR. For an efficient use of the simulator, a comfortable experimental environment is needed.

The simulator operation is performed with a Windows user interface on the host PC, which copies the functionality of a real truck cockpit. All relevant simulation quantities can be visualized on-line or be recorded for off-line analysis. To ensure reproducible results, a driver simulation is implemented, which can automatically follow a given speed cycle by operating the accelerate pedal, brake, clutch and gear. As alternative, an interactive “driving” of the simulator can be performed manually with a control panel, where the most important cockpit functionalities are realized.

### b) Simulation results

In the following, three HiL simulation examples for an eight-cylinder truck engine (420kW) are represented in order to document the applicability and the performance of the simulator. Figure 12.45 demonstrates the effect of switching off a single injection pump valve. The gearbox is in neutral position and at the beginning the engine runs with idle speed. The cyclic decrease of the engine torque and the engine speed after the fuel shut-off can directly be seen. The control unit gradually compensates for the missing torque of one cylinder by increasing the pulse width in order to keep the desired idle speed.

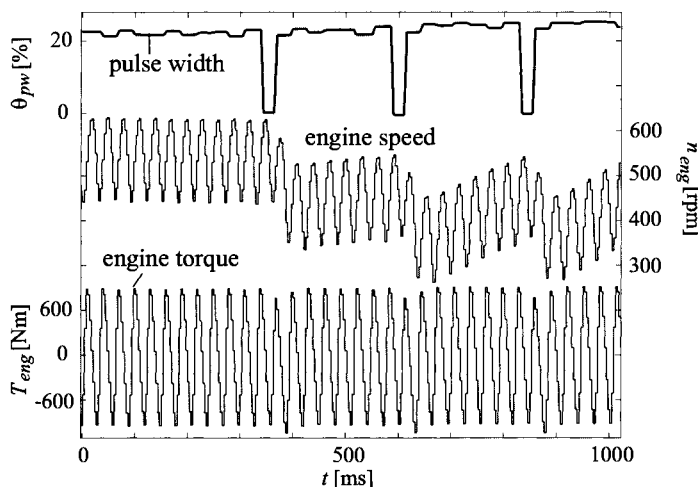


**Figure 12.45.** HiL-simulation of a single injection pump valve cut-off

A full power acceleration of a 40 ton truck including two gear shifts (1) is depicted in Figure 12.46. The following effects can be observed:

- oscillations in the drivetrain (2);

- maximum speed limit regulation (4);
- limitation of soot (3);
- lagged reaction of the turbo-charging pressure (5).

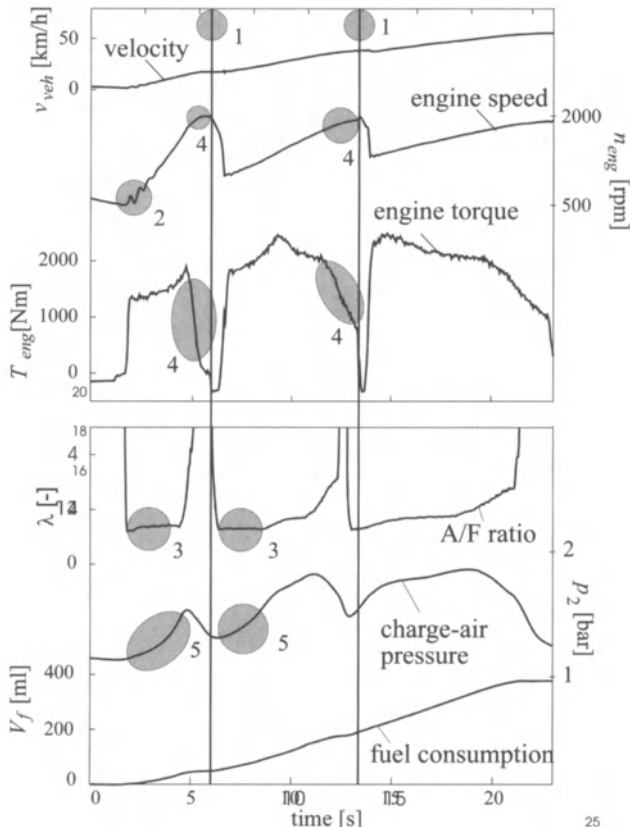


**Figure 12.46.** HiL simulation of the full power acceleration of a 40 ton truck

Figure 12.47 shows the simulation results evaluating the cruise control function. The 40 ton truck runs at a constant speed of  $v_{veh} = 60 \text{ km/h}$ . After a road slope of  $\alpha_R = -2\%$ , the engine control unit reduces engine torque  $T_{eng}$  until all injection pumps are switched off (at 10 s). After the change of the road slope to  $+4\%$ , engine torque is increased in order to compensate for the deviation between desired vehicle speed and simulated vehicle speed.

The various simulation results illustrate the performance of the HiL simulator. It allows repeatable testing of engine control units and control algorithms under various conditions. Thus, expensive engine experiments and driving maneuvers are avoided to a good part. In addition, the behavior of the ECU during sensor or actuator faults can be easily studied.

Several of these HiL systems have been developed for Daimler-Chrysler AG, Stuttgart, Germany.

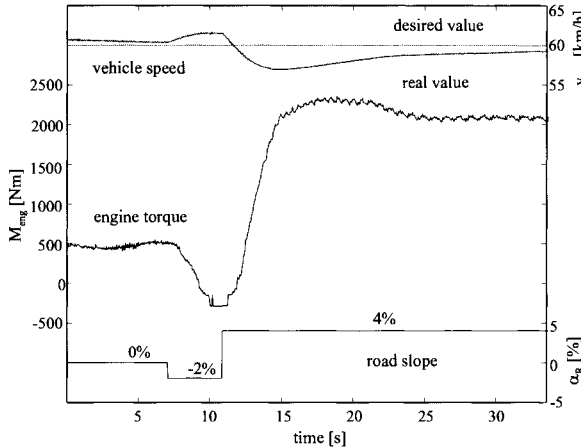


**Figure 12.47.** HiL simulation, evaluating the cruise control function of a 40 ton truck

## 12.6 INDUSTRIAL ROBOT

Industrial robots (IR) are characterized by versatility and flexibility. According to the widely accepted definition of the Robot Institute of America, a robot is a *reprogrammable multifunctional manipulator designed to move materials, parts, tools or specialized devices through variable programmed motions for the performance of a variety of tasks*. Such a definition, dating to 1980, reflects the current status of robotics technology. The IR is frequently a component of linked production lines. Generally, robots can be:

- the number of axes (= number of independent drives);
- the kinematics/geometry of the axis (e.g., SCARA, cartesian, anthropomorphic);
- the type of drives (electric, hydraulic, pneumatic).

Widely used types are of a six-joint anthropomorphic structure with six degrees of freedom, resulting in a spherical workspace. The joint actuators are usually DC motors with electronic servo-drives. Figure 12.48 shows an example of such a type together with the control unit.

### 12.6.1 Modeling

Mathematical modeling of an IR comprises both the kinematics and the dynamics of the whole system. The kinematic equations describe the analytical relationship between the joint positions  $\varphi = [\varphi_1 \dots \varphi_6]^T$  and the cartesian end-effector position and orientation relative to a world coordi-

nate frame

$$T_6 = \Lambda(\varphi) \quad (12.6.1)$$

$$\varphi = \Lambda^{-1}(T_6) \quad (12.6.2)$$

$T_6$  represents the position and orientation of the manipulator as a homogeneous  $4 \times 4$  transformation matrix. It consists of four vectors describing the position ( $p$ ) and orientation ( $n, o, a$ ) of the end-effector reference frame, compare Figure 12.49, according to the kinematic function  $\Lambda$ .

$$T_6 = \begin{bmatrix} n & o & a & p \\ 0 & 0 & 0 & 1 \end{bmatrix} \quad (12.6.3)$$

More information about finding the kinematic equations can be found in Denavit, Hartenberg (1955), Paul (1989), Scialvicio, Siciliano (2000).

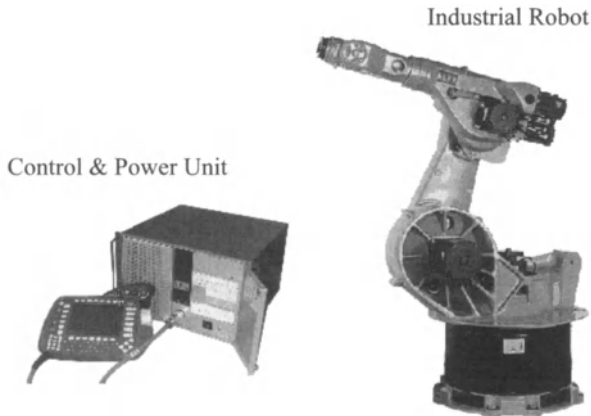


Figure 12.48. Industrial robot with control/power unit (KUKA)

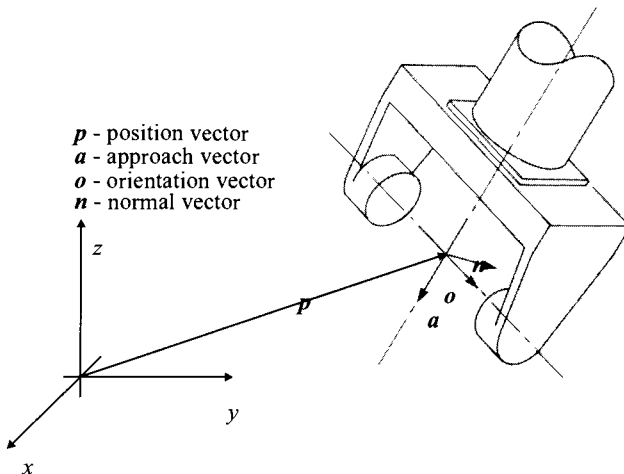


Figure 12.49. Position and orientation vectors

The kinematics of a manipulator represent the basis of a systematic, general derivation of its dynamics, *i.e.*, the equations of motion of the manipulator as a function of the forces and moments acting on it. The availability of the dynamic model is very useful in the mechanical design of the structure, choice of actuators, determination of control strategies and computer simulation of manipulator motion.

Frequently used methods for deriving the dynamic equations of motion of a manipulator are the Lagrange formulation and the Newton-Euler formulation. In the following, the Lagrangian equations are derived for a rigidly coupled two-mass system as depicted in Figure 12.50 and in simplified form in Figure 12.51. The example shows the method in principle, for more information refer to Denavit, Hartenberg (1955), Paul (1989) and Scialvicio, Siciliano (2000).

In Chapter 3, the Lagrangian  $L$  is defined as the difference between the kinetic energy  $E_K$  and the potential energy  $E_P$  of the system within an arbitrarily chosen stationary potential field (here: the gravitational field of the earth) (3.2.32)

$$L = E_K - E_P \quad (12.6.4)$$

As generalized coordinates, the joint angles  $\varphi_i$  are used. The dynamics equations, in terms of the coordinates used to express the kinetic and potential energy, are obtained as (3.2.34)

$$T_i = \frac{d}{dt} \frac{\partial L}{\partial \dot{\varphi}_i} - \frac{\partial L}{\partial \varphi_i} \quad i=1 \dots 2 \quad (12.6.5)$$

where  $\varphi_i$  is the joint angle of joint  $i$  and  $T_i$  are the applied torque, friction and external torques, not caused by the potential field, compare also (12.6.15), *i.e.*, non-conservative generalized forces, *e.g.*, contact forces. The kinetic and potential energy for joint 1 is followed by

$$E_{K_1} = \frac{1}{2} m_1 r_1^2 \dot{\varphi}_1^2 \quad (12.6.6)$$

$$E_{P_1} = m_1 g r_1 \cos(\varphi_1) \quad (12.6.7)$$

The kinetic and potential energy for joint 2 is

$$E_{K_2} = \frac{1}{2} m_2 \left[ l_1^2 \dot{\varphi}_1^2 + r_2^2 (\dot{\varphi}_1 + \dot{\varphi}_2)^2 + 2 l_1 r_2 \dot{\varphi}_1 (\dot{\varphi}_1 + \dot{\varphi}_2) \cos(\varphi_2) \right] \quad (12.6.8)$$

$$E_{P_2} = m_2 g [l_1 \cos(\varphi_1) + r_2 \cos(\varphi_1 + \varphi_2)] \quad (12.6.9)$$

The Lagrangian  $L$  is then obtained from (12.6.4) and (12.6.6)–(12.7.9) by

$$\begin{aligned}
 L &= \sum E_{K_i} - \sum E_{P_i} \\
 &= \frac{1}{2}(m_1 r_1^2 + m_2 l_1^2) \dot{\varphi}_1^2 + \frac{1}{2}m_2 r_2^2 (\dot{\varphi}_1 + \dot{\varphi}_2)^2 \\
 &\quad + m_2 l_1 r_2 (\dot{\varphi}_1 + \dot{\varphi}_2) \varphi_1 \cos(\varphi_2) \\
 &\quad - g[(m_1 r_1 + m_2 l_2) \cos(\varphi_1) + m_2 r_2 \cos(\varphi_1 + \varphi_2)]
 \end{aligned} \tag{12.6.10}$$

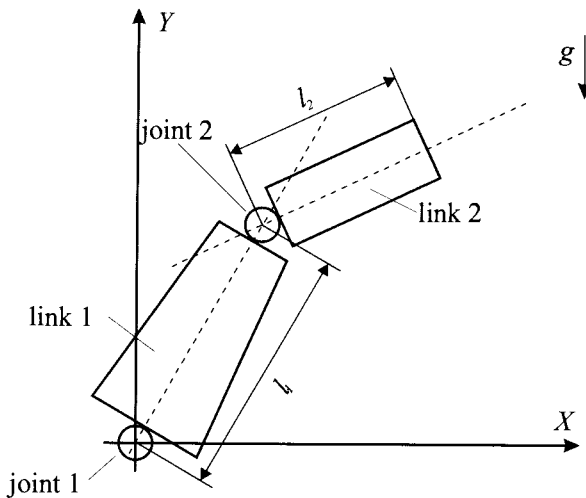


**Figure 12.50.** Rigidly coupled two-mass system

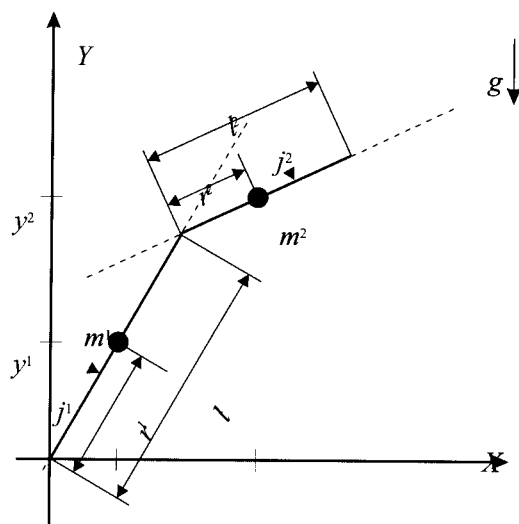


**Figure 12.51.** Simplified representation of Figure 12.50

In order to obtain the dynamics equations, the Lagrangian  $L$  is differentiated according to (12.6.5). This yields for joint 1

$$\begin{aligned} T_1 = & [m_1 r_1^2 + m_2(l_1^2 + r_2^2 + 2l_1r_2 \cos(\varphi_2))] \ddot{\varphi}_1 \\ & + m_2(r_2^2 + l_1r_2 \cos(\varphi_2)) \ddot{\varphi}_2 \\ & - 2m_2l_1r_2 \sin(\varphi_2) \dot{\varphi}_1 \dot{\varphi}_2 \\ & - m_2l_1r_2 \sin(\varphi_2) \dot{\varphi}_2^2 \\ & - g[(m_1r_1 + m_2l_1)\sin(\varphi_1) + m_2r_2\sin(\varphi_1 + \varphi_2)] \end{aligned} \quad (12.6.11)$$

and for joint 2

$$\begin{aligned} T_2 = & m_2[r_2^2 + l_1r_2 \cos(\varphi_2)] \ddot{\varphi}_1 \\ & + m_2r_2^2 \ddot{\varphi}_2 + m_2l_1r_2 \sin(\varphi_2) \dot{\varphi}_1^2 \\ & - g m_2r_2 \sin(\varphi_1 + \varphi_2) \end{aligned} \quad (12.6.12)$$

The dynamic equations of the mechanical system in matrix form are given by

$$\begin{bmatrix} T_1 \\ T_2 \end{bmatrix} = \begin{bmatrix} m_1r_1^2 + m_2(l_1^2 + r_2^2 + 2l_1r_2 \cos(\varphi_2)) & m_2(r_2^2 + l_1r_2 \cos(\varphi_2)) \\ m_2(r_2^2 + l_1r_2 \cos(\varphi_2)) & m_2r_2^2 \\ -2m_2l_1r_2 \sin(\varphi_2) & \dot{\varphi}_1 \dot{\varphi}_2 \\ 0 & 0 \\ 0 & -m_2l_1r_2 \sin(\varphi_2) \\ m_2l_1r_2 \sin(\varphi_2) & 0 \\ -g(m_1r_1 + m_2l_1)\sin(\varphi_1) - g m_2r_2 \sin(\varphi_1 + \varphi_2) \\ -g m_2r_2 \sin(\varphi_1 + \varphi_2) \end{bmatrix} \begin{bmatrix} \ddot{\varphi}_1 \\ \ddot{\varphi}_2 \end{bmatrix} \quad (12.6.13)$$

or in short form, which is the general form of the dynamic equations of an  $n$ -axis industrial robot

$$\mathbf{T} = \mathbf{D}(\varphi) \ddot{\varphi} + \mathbf{T}_K(\dot{\varphi}, \varphi) + \mathbf{T}_G(\varphi) \quad (12.6.14)$$

with

$\mathbf{T}$	$n \cdot 1$	applied forces/torques
$\mathbf{D}$	$n \cdot n$	inertia matrix
$\mathbf{T}_K$	$n \cdot n$	coriolis forces vector
$\mathbf{T}_G$	$n \cdot 1$	gravitational torque vector
$\varphi$	$n \cdot 1$	vector of joint angles.

Figures 12.52 and Figure 12.53 show the torques induced by the gravitational force at joint 1 and 2 of the robot in Figure 12.50. The figures have been calculated with the following values:

Joint 1:  $m_1 = 100 \text{ kg}$ ,  $l_1 = 1.0 \text{ m}$ ,  $r_1 = 0.3 \text{ m}$

Joint 2:  $m_2 = 60 \text{ kg}$ ,  $l_2 = 1.2 \text{ m}$ ,  $r_2 = 0.5 \text{ m}$

Further investigations show that the static coupling (gravity influence) dominates over the centrifugal and coriolis torques.

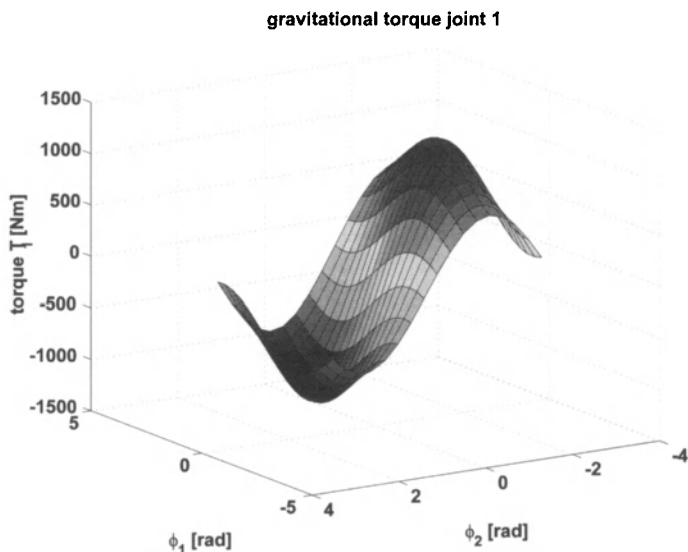


**Figure 12.52.** Gravitational torque at joint 1

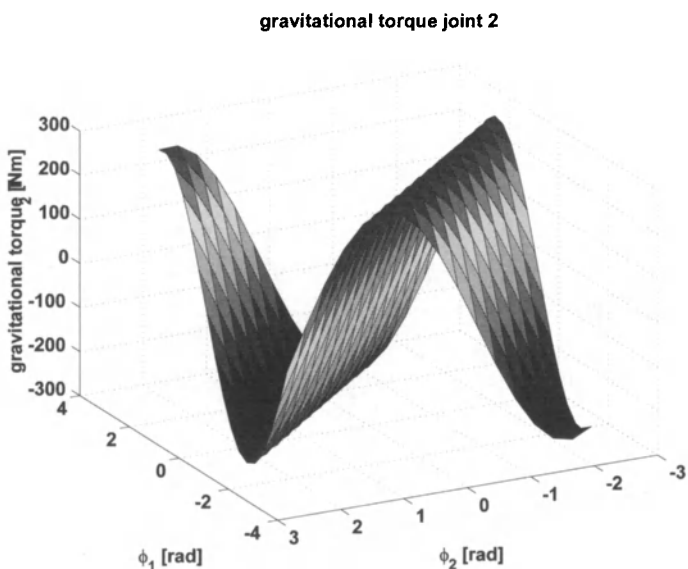


**Figure 12.53.** Gravitational torque at joint 2

So far, only conservative forces/torques depending only on the potential field have been considered. However, there are also dissipative forces/torques, *e.g.*, friction or dynamics in the drives including gear units that have to be taken into account, Held, Maron (1988). Further simplifying assumptions (neglecting drive dynamics and dynamic couplings between axes) lead to the following equation for a decoupled single-link manipulator (based on the principle of momentum balance)

$$J_G \dot{\omega}(t) = \sum_j T_j(t) = T_A(t) - T_{ext}(t) - T_f(t) \quad (12.6.15)$$

where  $\omega$  is the motor speed,  $T_f$  the speed-dependent friction characteristic,  $T_A$  the actuating torque and  $T_{ext}$  takes external torques, such as gravity, into account.  $J = J_A + v^2 J_L$  is the effective link inertia, a sum of the actuator inertia  $J_A$  and the effective link inertia  $J_L$  multiplied by  $v^2$  (the gear reduction factor, typically 1:100...200). Therefore, the term  $v^2 J_L$  is frequently neglected. The resulting block diagram for a decoupled rigid single-link manipulator is depicted in Figure 12.54.

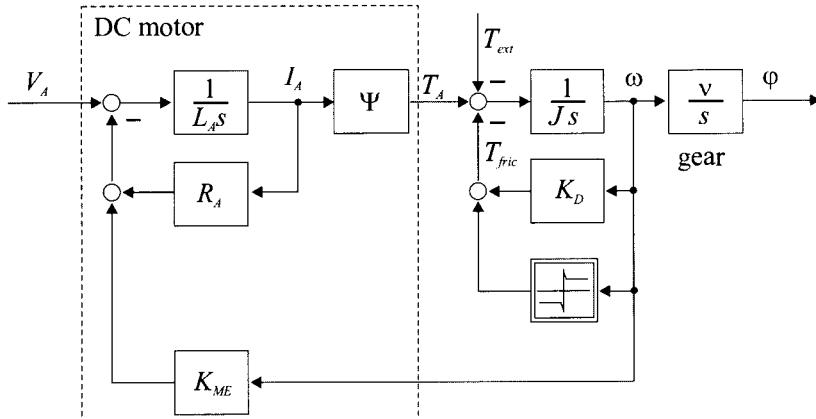


Figure 12.54. Block diagram of a decoupled single manipulator drive

## 12.6.2 Control

The problem of manipulator control is to find the time behavior of the forces and torques to be delivered by the joint actuators so as to ensure the execution of pre-planned end-effector reference trajectories. A number of joint space control techniques have been developed so far. These can be distinguished by *decentralized control schemes*, *i.e.*, when the single manipulator joint is controlled independently of the others, and *centralized control schemes*, *i.e.*, when the dynamic interaction effects between the joints are taken into account. Finally, there is *operational space control* as an approach to interaction control. Here, the first two approaches only are outlined. More elaborate information on these topics can be found in Scialicchio, Siciliano (2000), Craig (1989).

### a) Independent joint control

Figure 12.55 shows a conventional decentralized control structure, developed independently for each axis of the robot. It consists of a cascaded structure comprising the following control loops:

- analog PI motor current/acceleration feedback control;
- analog/digital PI motor speed/velocity feedback control;
- digital P position feedback control.

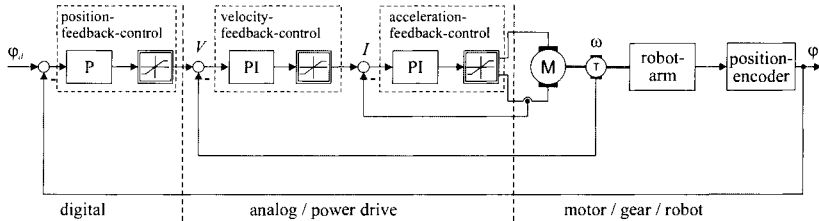


Figure 12.55. Cascaded feedback control of a single link servo

The acceleration control loop mainly deals with the compensation of the electromotive force. The velocity control loop is optimized according to the symmetrical optimum. Finally, the proportional gain of the position controller is tuned such that the final position is reached within the shortest possible time without overshoot and without excitation of the structural resonant frequencies. Unfortunately, the position controller introduces a dynamic tracking error. This could not be overcome by a PI-controller, which would cause limit cycles around a steady state position value due to friction and backlash in the gear units.

If the robot is required to track reference trajectories with high values of speed and acceleration, the tracking capabilities of the control loop in Figure 12.55 are considerably degraded. The introduction of various forms of decentralized feedforward compensation terms reduces the tracking error. The most elaborate control scheme regarding this problem is the cascaded feedback loop from Figure 12.55 modified by velocity and acceleration feedforward inputs. However, it is worth recalling that perfect tracking can be obtained only on the assumption of exact matching of the controller and feedforward compensation parameters with the process parameters, as well as of exact modeling and linearity of the physical system.

### b) Centralized robot control

In the previous section, the independent joint controller has been discussed, which is based on a single-input/single-output approach, where interaction and coupling effects between joints have been treated as disturbances acting on each single joint drive system. However, the robot is not a set of  $n$  decoupled systems, but a multi-variable system with  $n$  inputs (joint torques) and  $n$  outputs (joint positions) interacting between them by means of non-linear relations. Thus, model-based control concepts have

been developed to account for them, which leads to improved manipulator dynamic performance.

Figure 12.56 shows the structure of a feedback decoupling loop. Based on the measured joint angles, velocities and accelerations as well as their reference, values the necessary torques  $T$  are computed by the inverse system model. A drawback, however, is the increased sensitivity to model and parameter uncertainties.

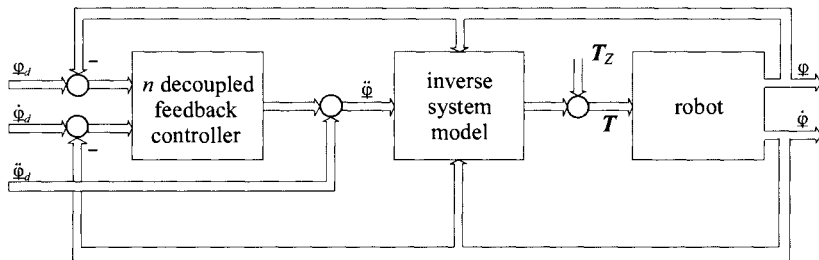


Figure 12.56. Position control by feedback decoupling

In contrast, the feedforward decoupling, shown in Figure 12.57, combines the quickness of a feedforward control with the precision of a feedback control. For this type of decoupling, it is not necessary to have a precise process model if the feedback controller has been designed robust enough.

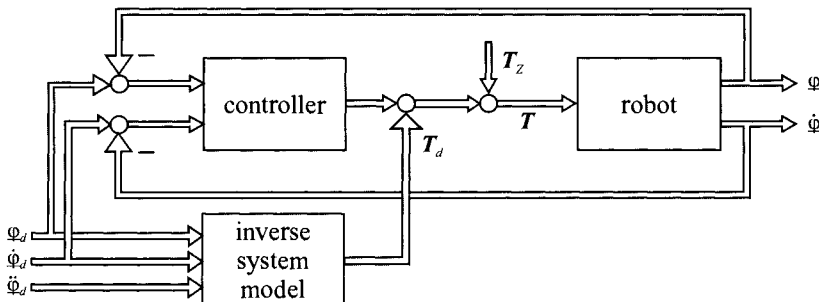


Figure 12.57. Position control by feedforward decoupling

The third possibility is the adaptive controller, which identifies the time-variant parameters of the model on-line recursively. Based on the estimation of these physical parameters, see Freyermuth (1993), Held (1992), Böhm (1994) and Abou-El-Ela (1995), the controller parameters are tuned accordingly. However, due to the adaptation, the stability of the algorithm is not guaranteed, which makes supervision for the adaption necessary, compare also Isermann *et al.* (1992).

### 12.6.3 System Structure

The basic tasks of the robot control unit is the generation of the desired trajectories as well as security-relevant supervision of the overall system.

Usually, robot control is hierarchically structured as can be seen in Figure 12.58.

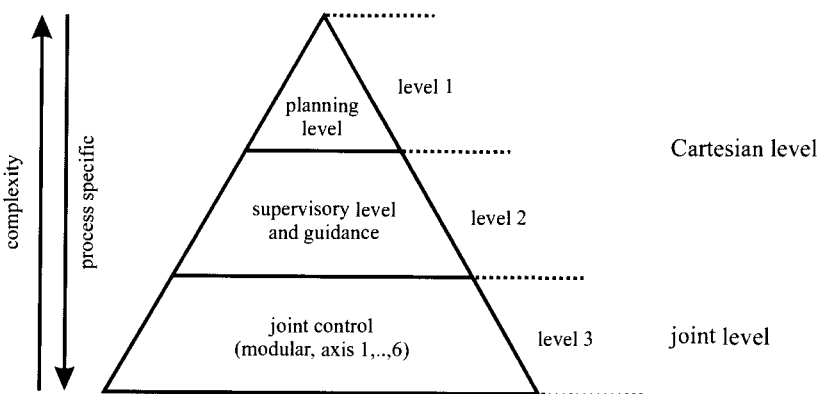


**Figure 12.58.** Hierarchical robot control

The planning level defines the handling task. A motion generation program defines the Cartesian trajectory, the end-effector velocity, orientation of the tool and maybe other switching information. The supervisory and guidance level performs the calculation of the joint trajectories, coordinate transformations and includes optional external sensors. It runs at the sample time of the coarse interpolation cycle of 10 to 50 ms. The lowest level is the joint control level, which performs the – in general linear – fine interpolation of the desired joint trajectories. This level runs at a sampling period of about 1 to 5 ms.

## Outlook

---

As mentioned in Chapter 1, the area of mechatronic systems comprises several disciplines of engineering sciences. Therefore, it is hardly possible to represent mechatronic systems in a comprehensive context in only one book. Hence, this book is restricted to give, on one side, an overview of some principles and, on the other side, to represent some properties of the static and dynamic behavior of components and some mechatronic products and machines. This is oriented towards the construction (design, simulation, experimental test) of integrated overall systems. The resulting *mechatronic overall systems* have to be treated in special books, because of the large variety and very special process knowledge. Some of these rather process-oriented areas are, for example:

- mechatronic machine elements (couplings, dampers);
- magnetic bearings;
- mechatronic hydraulics and pneumatics (fluidtronics);
- mechatronic actuators (electromagnets, piezostacks, electro-rheological fluids);
- robotics (multi-axis, mobile, walking machines);
- power electronics and drives;
- mechatronic combustion engines;
- mechatronic fluid power machines (pumps, compressors, gas turbines);
- mechatronic vehicle components (active brake systems, like ABS, TCS, ESP, active suspensions, electronic power steering);
- mechatronic automobiles (brake-by-wire, steer-by-wire, global

- chassis control, autopilots);
- mechatronic production machines (active tools, flexible machine tools, forming machines, printing machines);
- mechatronic precision devices (cameras, disk storages, fax machines, optical instruments);
- mechatronic medical devices (implants, artificial hearts, active shunts, dialysis machines);
- micromechatronic systems (MEMS, sensors, actuators, micromotors).

Throughout the book, only some of these mechatronic components and systems could be described. The above listing shows that some areas have used mechatronic principles for many years, but don't express this explicitly.

A large significance for the design of mechatronic overall systems has, in addition to the hardware integration, the integration through the software for the on-line, real-time information processing tasks like control, supervision, on-line optimization, fault diagnosis and fault-tolerance. These fields are described in other books and are not restricted to mechatronic systems only.

Another supporting technology is the use of computers in the design of mechatronic systems. Here, in addition to the well-known computer-aided constructive design (CAD) techniques, dynamic modeling, simulation and experimental testing is becoming increasingly important. Related tools such as object-oriented modeling software, control prototyping computers and hardware-in-the-loop simulators are presently being developed and increasingly used in the framework of simultaneous engineering as summarized by the so-called V-model (Figures 12.39 and 12.40).

The development towards the integration of computer-based information processing into the products and their manufacturing comprises large areas of engineering. Therefore, a suitable education in modern engineering and also trade is fundamental for the technological progress, by taking into account multi-disciplinary solutions and method-oriented procedures. The development of curricula for mechatronics as a proper combination of electrical and mechanical engineering and computer science during the last decade shows this tendency.

# References

---

## CHAPTER 1

- AIM IEEE/ASME Conference on Advanced Intelligent Mechatronics.  
Atlanta (1999), Como (2001), Kobe (2003).
- Antsaklis P (1994). Defining intelligent control. *IEEE Control Systems* 1994: 4-66
- Åström KJ (1991). Intelligent control. *Proceedings of the European Control Conference*, Grenoble.
- Åström KJ, Wittenmark B (1994). Adaptive Control. Addison-Wesley, Reading.
- Beitz W (1989). Entwicklung und Konstruktion. In Hütte, 29th edn., part K. Springer, Berlin.
- Beitz W, Küttner KH (ed) (1994). Dubbel. Handbook of Mechanical Engineering, 14th edn. Springer, Berlin.
- Bishop, RH (ed) (2002). The mechatronics handbook. CRC-Press, Boca Raton.
- Bradley DA, Dawson D, Burd D, Loader AJ (1991). Mechatronics-electronics in Products and Processes. Chapman and Hall, London.
- Bröhl AP (ed) (1995). Das V-Modell - Der Standard für Softwareentwicklung, 2nd edn. Oldenbourg, München.
- Chen J, Patton RJ (1999). Robust Model-based Fault Diagnosis for Dynamic Systems. Kluwer Academic Publishers, Boston.
- Davidson A (ed) (1968). Handbook of Precision Engineering, vol.1, no. 8. Macmillan Press, London.
- Dorf RC, Bishop RH (2000). Modern Control Systems, 9th edn. Prentice Hall, Englewood Cliffs.
- DUIS (1993). Mechatronics and Robotics. Hiller M, Fink B (eds). 2nd Conference, Duisburg/Moers, September 27–29.
- Ehrfeld W, Ehrfeld U, Kieswalter S (2000). Progress and profit through microtechnologies. In: Proc. MICRO.tec 2000, VDE World Micro-

- technology Congress, Hannover, September 25–27, 1: 9–17. VDE-Verlag, Berlin.
- Elmqvist H (1993). Object-oriented modeling and automatic formula manipulation in Dymola. Scandinavian Simul. Society SIMS, Kongsvinger.
- Föllinger O (1992). Control Theory (in German), 7th edn. Hüthig Buch Verlag, Heidelberg.
- Franklin GF, Powell JD, Workman D (1998). Digital Control of Dynamic systems, 3rd edn. Addison-Wesley, Menlo Park.
- Gad-el-Hak M (ed) (2000). MEMS Handbook. CRC Press, Boca Raton.
- Gausemeier J, Brexel D, Frank T, Humpert A (1995). Integrated product development. In: 3rd Conference on Mechatronics and Robotics, Paderborn, Germany, October 4–6, Teubner, Stuttgart.
- Gertler JJ (1999). Fault Detection and Diagnosis in Engineering Systems. Marcel Dekker, New York.
- Goodall R, Kortüm W (2000). Mechatronic development for railway vehicles of the future. Proc. 1<sup>st</sup> IFAC Conference on Mechatronic Systems, Darmstadt, September 18–20, Elsevier, Oxford
- Green RE (ed) (1992). Machinery's Handbook, 24th edn. Industrial Press, New York.
- Gupta MM, Sinha NK (1996). Intelligent Control Systems. IEEE Press, New York.
- Harashima F, Tomizuka M (1996). Mechatronics – “What is it, why and how?” IEEE/ASME Trans. on Mechatronics 1: 1–2
- Harris CJ (ed) (1994). Advances in Intelligent Control. Taylor and Francis, London.
- Heimann B, Gerth W, Popp K (1998). Mechatronik-Komponenten-Methoden Beispiele. Hanser Verlag, München.
- Hiller M (1995). Modelling, simulation and control design for large and heavy manipulators, Proceedings of International Conference on Recent Advances in Mechatronics, Istanbul, August 14–16.
- Hupka V (1973). Theory of Machines (in German). Springer, Berlin.
- ICRAM (1995). Recent Advances in Mechatronics. Kaynak O, Özkan M, Bekiroglu N, Tunay I (eds), Proceedings of International Conference ICRAM'95, Istanbul, August 14–16.
- IEEE/ASME (1996). Transactions on Mechatronics vol. 1, no. 1.
- IFAC-Conference on Mechatronic Systems: Darmstadt (2000), Berkeley (2002), Sydney (2004). Preprints Elsevier, Oxford
- IFAC-T.C. 4.2. (2000). IFAC Technical Committee on Mechatronic Systems. <http://rumi.newcastle.edu.au/reza/TCM/>
- IMES (1993). Integrated Mechanical Electronic Systems (in German) Conference TH Darmstadt, March 2–3. Fortschr.-Ber. VDI Reihe 12 no. 179. VDI-Verlag, Düsseldorf.
- Isermann R (1996). Modeling and design methodology of mechatronic systems. IEEE/ASME-Trans. on Mechatronics 1: 16–28.
- Isermann R (1997). Supervision, fault detection and fault diagnosis methods – an introduction. Special section on supervision, fault

- detection and diagnosis. CEP – Control Engineering Practice 5: 639–652.
- Isermann R (1999). Mechatronische Systeme. Springer, Berlin.
- Isermann R (2000). Mechatronic systems: concepts and applications. Trans. of the Institute of Measurement and Control 22: 29–55.
- Isermann R (2005) Supervision, diagnosis and fault-tolerance. Springer Verlag, Berlin.
- Isermann R, Lachmann K-H, Matko D (1992). Adaptive Control Systems. Prentice Hall, New York.
- James J, Cellier F, Pang G, Gray J, Mattson SE (1995). The state of computer-aided control system design (CACSD). IEEE Trans. on Control Systems, Special Issue: 6–7.
- Janocha H (2000). Microactuators - principles, applications, trends. In: Proc. MICRO.tec 2000, VDE World Microtechnology Congress. Hannover, September 25–27, 1: 61–67. VDE-Verlag, Berlin.
- Kitaura K (1986). Industrial Mechatronics (in Japanese). New East Business Ltd.
- Koller R (1985). Design Methodology for Mechanical Engineering (in German). Springer, Berlin.
- Kreith F (ed) (1998). The CRC Handbook of Mechanical Engineering. CRC, Boca Raton.
- Kutz M (ed) (1998). Mechanical engineers' Handbook, 2nd edn. J. Wiley, New York.
- Kyura N, Oho H (1996). Mechatronics - an industrial perspective. IEEE/ASME Trans. on Mechatronics 1: 10–15
- Lückel J (ed) (1995). Third Conference on Mechatronics and Robotics. Paderborn, October 4–6. Teubner, Stuttgart
- Lyshevski SE (2001). Nano- and Micro-electro-mechanical Systems. CRC Press, Boca Raton
- Madon M (2001). Fundamentals of Microfabrication. CRC Press, Boca Raton.
- McConaill PA, Drews P, Robrock K-H (eds) (1991). Mechatronics and Robotics I. ICS Press, Amsterdam.
- Mechatronics (1991). An International Journal. Aims and Scope. Pergamon Press, Oxford.
- Mechatronics System Engineering (1993). International Journal on Design and Application of Integrated Electromechanical Systems. Kluwer Academic Publ. Netherlands.
- Ogata K (1997). Modern Control Engineering, 3rd edn. Prentice Hall, Upper Saddle River.
- Oppelt W (1953, 1972). Kleines Handbuch technischer Regelvorgänge. VerlagChemie, Weinheim.
- Otter M, Gruebel G (1993). Direct physical modeling and automatic code generation for mechatronics simulation. In: 2nd Conference on Mechatronics and Robotics, Duisburg, September 27–29, IMECH, Moers.
- Pahl W, Beitz W (2001). Engineering Design. A Systematic Approach.

- Springer, Berlin.
- Roth K (1982). Design with Catalogues (in German). Springer, Berlin.
- Saridis GN (1977). Self-organizing Control of Stochastic Systems. Marcel Dekker, New York.
- Saridis GN, Valavanis KP (1988). Analytical design of intelligent machines. *Automatica* 24: 123–133.
- Sato K (2000). Micromachining – a survey of the state of the art. In: Proc. MICRO.tec 2000, VDE World Microtechnology Congress. Hannover, September 25–27, 2: 1–6. VDE-Verlag, Berlin.
- Schweitzer G (1992). Mechatronics – a concepts with examples in active magnetic bearings. *Mechatronics* 2: 65–74.
- Smith, H (1994). Mechatronic Engineer's Reference Book, 12th edn. SAE, Warrendale.
- Starts Guide, The. (1989). A guide to methods and software tools for the construction of large real-time systems. NCC Publishers, Manchester
- Tomizuka M (2000). Mechatronics: from the 20th to the 21th century. Proc. 1st IFAC Conference on Mechatronic Systems, Darmstadt, September 18-20, Elsevier, Oxford.
- Töpfer H, Kriesel W (1977, 1983). Funktionseinheiten der Automatisierungstechnik. VEB-Verlag Technik, Berlin.
- UK Mechatronics Forum. Conferences in Cambridge (1990), Dundee (1992), Budapest (1994), Guimaraes (1996), Skovde (1998), Atlanta (2000), Twente (2002).
- VDI 2006 (2003). Design methodology for mechatronic systems. VDI-Richtlinie (in German). VDI-Handbuch Konstruktion. Beuth Verlag, Berlin.
- Walsh, RA (1999). Electromechanical Design Handbook, 3rd edn. McGraw- Hill, New York.
- Whitaker J (ed) (1997). The Electronics Handbook. CRC Press, Boca Raton.
- White DA, Sofge DA (eds) (1992). Handbook of Intelligent Control. Van Norstrand Reinhold, New York.
- van Zanten A (2000). Improvement of road vehicles handling by mechatronic systems. Proc. 1st IFAC Conference on Mechatronic Systems, Darmstadt, September 18-20, Elsevier, Oxford

## CHAPTER 2

- Ahrendts I (1989). Technische Thermodynamik. In Hütte, 14th edn., part F. Springer, Berlin.
- Campbell DP (1958). Process Dynamics. J. Wiley, New York.
- Cellier FE (1991). Continuous System Modelling. Springer, Berlin.
- Crandall SH, Karnopp DC, Kurtz EF, Pridemore-Brown DC (1968). Dynamics of Mechanical and Electromechanical Systems.

- McGraw-Hill, New York.
- Eykhoff P (1974). System Identification. J. Wiley & Sons, London.
- Firestone FA (1957). The Mobility and Classical Impedance Analogies. In: American Institute of Physics Handbook. McGraw-Hill, New York.
- Gawthrop FE, Smith L (1996). Metamodelling: Bond Graphs and Dynamic Systems. Prentice Hall, London.
- Gilles ED (1973). Systeme mit verteilten Parametern. R. Oldenbourg, München.
- Isermann R (1971). Theoretische Analyse der Dynamik industrieller Prozesse. Bibliograph. Inst. Mannheim. Hochschulskript Nr. 764/764a.
- Isermann R (1974). Results on the simplification of dynamic process models. Int. J. Control 19: 149–159.
- Isermann R (1984). Einige Grundlagen der Prozeßdynamik - eine kurze Einführung. Techn. Mitt. Krupp. Forschungsberichte, vol. 42. H3.
- Isermann R (1992). Identifikation dynamischer Systeme vols. 1 and 2. Springer, Berlin.
- Karnopp DC, Rosenberg RC (1970). System Dynamics: A Unified Approach. Wiley, New York.
- Karnopp DC, Margolis DL, Rosenberg RC (1990). System Dynamics. A Unified Approach. Wiley, New York.
- Kecman VV (1988). State-space Models of Lumped and Distributed Systems. Springer, Berlin.
- Ljung L (1987). System Identification – Theory for the User. Prentice Hall, Englewood Cliffs.
- MacFarlane AGJ (1964). Engineering Systems Analysis. GG Harrop, Cambridge.
- MacFarlane AGJ (1967). Analyse technischer Systeme. Bibliograph. Institut, Mannheim.
- MacFarlane AGJ (1970). Dynamical System Models. GG Harrop, London.
- Olsen HF (1958). Dynamical Analogies. Van Nostrand, Princeton.
- Oppelt W (1972). Kleines Handbuch technischer Regelvorgänge. Verlag Chemie, Weinheim.
- Pahl W, Beitz W (2001). Engineering Design. A Systematic Approach. Springer, Berlin.
- Paynter HM (1961). Analysis and Design of Engineering Systems. MIT Press, Cambridge.
- Profos P (1962). Die Regelung von Dampfanlagen. Springer, Berlin.
- Shearer IL, Murphy AT, Richardson HM (1967). Introduction to System Dynamics. Addison Wesley, Reading.
- Takahashi Y, Rabins MJ, Auslander DM (1972). Control and Dynamic Systems. Addison Wesley, Menlo Park.
- Thoma JU (1990). Simulation by Bondgraphs. Springer, Berlin.
- Wellstead PE (1979) Introduction to Physical System Modelling. Academic Press, London.

## CHAPTER 3

- Hagedorn P (1990). Technische Mechanik, vol. 1, 2, 3. Harri Deutsch, Frankfurt.
- Hauger W, Schnell W, Gross D. (1989). Technische Mechanik, 3rd edn., vol. 3. Springer, Berlin.
- Kessel S, Fröhling D (1998). Technische Mechanik: Fachbegriffe im deutschen und englischen Kontext = Technical Mechanics. Teubner, Stuttgart.
- MacFarlane AGJ (1970). Dynamical System Models. GG Harrop, London.
- Meriam JL, Kraige LG (1997). Engineering Mechanics, 4th edn., vol. 1 Statics, 2. Dynamics. Wiley, New York.
- Pfeiffer F (1989). Einführung in die Dynamik. Teubner Studienbücher. Teubner, Stuttgart.
- Schiehlen W (1986). Technische Mechanik. Teubner, Stuttgart.
- Sneck HJ (1991). Machine Dynamics. Prentice Hall, Englewood Cliffs.
- Wells DA (1967). Lagrangian Dynamics. Schaum's Outline Series. McGraw-Hill, New York.

## CHAPTER 4

- Armstrong-Hélouvry B (1991). Control of Machines with Friction. Kluwer Academic Publishers, Boston.
- Bolton V (1996). Mechatronics, Electronic Control Systems in Mechanical Engineering. Addison Wesley Longman Ltd., Harlow.
- Braess HH, Seiffert U (2000). Vieweg Handbuch der Kraftfahrzeugtechnik. Vieweg, Braunschweig and Wiesbaden.
- Bradley DA, Dawson D, Burd D, Loader AJ (1991). Mechatronics-electronics in Products and Processes. Chapman and Hall, London.
- Bremer H (1988). Dynamik und Regelung mechanischer Systeme. Teubner, Stuttgart.
- Bremer H, Pfeiffer P (1993). Elastische Mehrkörpersysteme. Teubner, Stuttgart.
- Canudas de Wit C, Olsson, H, Åström KJ (1995). A new model for control of systems with friction. IEEE Trans. on Automatic Control 40: 419–425.
- Czichos H (ed) (1989). Hütte: die Grundlagen der Ingenieurwissenschaften, 29th edn. Springer, Berlin.
- Ellis G (2000). Control System Design Guide, 2nd edn. Academic Press, San Diego.
- Erxleben S (1984). Untersuchungen zum Betriebsverhalten von Riemengetrieben unter Berücksichtigung des elastischen Materialverhaltens. Dissertation RWTH Aachen.

- Föllinger O (1992). Regelungstechnik, 7th edn. Hüthig, Heidelberg.
- Freyermuth B (1990). Modellgestützte Fehlerdiagnose von Industrierobotern mittels Parameterschätzung. Robotersysteme 6: 202–210.
- FVA (1992). Mess- und Prüfverfahren für eine Wirkungsgradbestimmung von stufenlos verstellbaren Umschlingungsgetrieben (CVT). H. Fansl. FVA-Report No. 367, Frankfurt.
- Göbel EF (1969). Gummifedern, 3rd edn, Konstruktionsbücher, vol. 7. Springer, Berlin.
- Hein K (1973). Getriebebeispiel – Altas. VDI-Verlag, Düsseldorf.
- He X (1993). Modellgestützte Fehlererkennung mittels Parameterschätzung zur wissensbasierten Fehlerdiagnose an einem Vorschubantrieb. Dissertation TH Darmstadt. Fortschr-Ber. VDI Reihe 8, no. 354. VDI-Verlag, Düsseldorf.
- Holzweißig F, Dresig H (1992). Lehrbuch der Maschinendynamik, 3rd edn. Fachbuchverlag, Leipzig and Köln.
- Isermann R (1989). Digital Control Systems, vol. 1, 2. Springer, Berlin.
- Jensen PW (1991). Classical and Modern Mechanisms for Engineers and Inventors. Marcel Dekker, New York.
- Kessel S, Fröhling D (1998). Technische Mechanik: Fachbegriffe im deutschen und englischen Kontext = Technical Mechanics. Teubner, Stuttgart.
- Klingenber R (1978). Experimentelle und analytische Untersuchungen des dynamischen Verhaltens drehnachgiebiger Kupplungen. Dissertation TU Berlin.
- Krämer E (1984). Maschinendynamik. Springer, Berlin.
- Kutz M (ed) (1998). Mechanical Engineers' Handbook, 2nd edn. Wiley, New York.
- Meriam JL, Kraige LG (1997). Engineering Mechanics, 4th edn., vol. 1 Statics, 2. Dynamics. Wiley, New York.
- Ogata K (1997). Modern Control Engineering, 3rd edn. Prentice Hall, Upper Saddle River.
- Palmgren A (1964). Grundlagen der Wälzlagertechnik. Franckh, Stuttgart.
- Paul PR (1989). Robot Manipulators. MIT Press, London.
- Pfeiffer F (1989). Einführung in die Dynamik. Teubner Studienbücher Mechanik. Teubner, Stuttgart.
- Shetty D, Kolk RA (1997). Mechatronics System Design. PWS Publishing Company, Boston.
- Smith H (1994). Mechatronic Engineer's Reference Book, 12th edn. SAE, Warrendale.
- Sneck HJ (1991). Machine Dynamics of Planar Machinery. Prentice-Hall, Englewood Cliffs.
- Stribeck R (1902). Die wesentlichen Eigenschaften der Gleit- und Rollenlager. Zeitschrift des VDI, no. 36.
- Tustin A (1947). The effects of backlash and of speed-dependent friction on the stability of closed cycle control systems. IEE Journal 94, Part 2A: 143–151.

- VDI-Handbuch Getriebetechnik I u. II (1978/79). VDI-Verlag, Düsseldorf.
- Walsh RA (1999). Electromechanical Design Handbook, 3rd edn. McGraw-Hill, New York.

## CHAPTER 5

- Acarnley PP (1985). Stepping Motors. Peter Peregrinus, London.
- Beitz W, Küttner KH (1981). Dubbel-Taschenbuch für den Maschinenbau, 14th edn. Springer, Berlin.
- Bödefeld T, Sequenz H (1971). Elektrische Maschinen. Springer, Wien.
- Bose BK (ed) (1997). Power Electronics and Variable Frequency Drives – Technology and Applications. IEEE Press, New York.
- Clausert W, Wiesemann G (1986). Grundgebiete der Elektronentechnik I, 2nd edn. Oldenbourg, München.
- Dietrich D, Kinhäuser W (1986). Mikrocomputer geregelte Asynchronmaschinen. Oldenbourg, Berlin.
- DIN 42027 (1984). Stellmotoren, Einteilung und Übersicht. Beuth Verlag, Berlin.
- Erickson RW (1997). Fundamentals of Power Electronics. Chapman & Hall, London.
- Fraser C, Milne J (1994). Electro-mechanical Engineering – an Integrated Approach. IEEE Press, Piscataway.
- Freyermuth B (1993). Wissensbasierte Fehlerdiagnose am Beispiel eines Industrieroboters. Dissertation TH Darmstadt. Fortschr.-Ber. VDI Reihe 8 no. 315. VDI-Verlag, Düsseldorf.
- Gray CB (1989). Electrical Machines and Drive Systems. Longmans Scientific and Technical, Harlow.
- Hendershot JR, Miller T (1994). Design of Brushless Permanent Magnet Motors. Magna physics, Clarendon, Oxford.
- Höfling T (1996). Methoden zur Fehlererkennung mit Parameterschätzung und Paritätsgleichungen. Dissertation. Dissertation TH Darmstadt. Fortschr.-Ber. VDI Reihe 8 no. 546. VDI-Verlag, Düsseldorf.
- Holtz J (1992). Pulsewidth modulation - a survey. IEEE Trans. On Industrial Electronics 39: 410–420.
- Huber L, Borojevic D (1995). Space vector modulated three-phase to three-phase matrix converter with input power factor correction. IEEE Trans. on Industrial Applications 31, 6.
- Janocha H (ed) (1992). Aktoren-Grundlagen und Anwendungen. Springer, Berlin.
- Jung R, Schneider J (1984). Elektrische Kleinmotoren. Konstruktionskatalog und Marktübersicht. Feinwerktechnik und Meßtechnik, 92: 153–165.
- Kallenbach E *et al.* (1994). Elektromagnete: Grundlagen, Berechnung,

- Konstruktion, Anwendung. Teubner, Stuttgart.
- Kenjo T (1984). Stepping Motors and their Microprocessor Controls. Scientific, Oxford.
- Krause PC (1986). Analysis of Electrical Machinery. McGraw-Hill, New York.
- Kreuth HP *et al.* (1985). Elektrische Schrittmotoren. Expert-Verlag, Sindelfingen.
- Krein PT (1998). Elements of Power Electronics. Oxford University Press, Oxford.
- Kuo BC (1974). Theory and Applications of Step Motors. West Publishing Co, St. Pauli.
- Leonhard W (1974). Regelung in der elektrischen Antriebstechnik. Teubner Studienbücher, Stuttgart.
- Leonhard W (1996). Control of Electrical Drives, 2nd edn. Springer, Berlin.
- Lindsay FJ, Rashid MH (1986). Electromechanics and Electrical Machines. Prentice Hall, Englewood Cliffs.
- Lyshevski SE (2000). Electromechanical Systems, Electric Machines, and Applied Mechatronics. CRC Press, Boca Raton.
- Meyer M (1985). Elektrische Antriebstechnik vol. 1. Springer, Berlin.
- Moczala H *et al.* (1993). Elektrische Kleinstmotoren. Expert-Verlag, Sindelfingen.
- Moseler O, Isermann R (2000). Application of model-based fault detection to a brushless dc motor. IEEE Trans. on Ind. Electron. 47: 1015–1020.
- Novotny DW, Lipo TA (1996). Vector Control and Dynamics of AC Drives. Clarendon Press, Oxford.
- Nürnberg W, Hanitsch R (1987). Die Prüfung elektrischer Maschinen. Springer, Berlin.
- Pfaff G (1994). Regelung elektrischer Antriebe, 5th edn. Oldenbourg, München.
- Philippow E (1976). Taschenbuch Elektrotechnik. Hanser, München.
- Pillay PR, Krishnan R (1987). Modeling of permanent magnet motor drives. IEEE Trans. Industrial Electronics 35: 537–541.
- Pressman AI (1997). Switching Power Supply Design, 2nd edn. McGraw-Hill, New York.
- Quang NP (1993). Praxis der feldorientierten Drehstromantriebsregelungen. Expert-Verlag, Sindelfingen.
- Raab U (1993). Modellgestützte digitale Regelung und Überwachung von Kraftfahrzeugaktoren. Dissertation TH Darmstadt. Fortschr.-Ber. VDI Reihe 8 no. 313. VDI-Verlag, Düsseldorf.
- Ramminger P (1992). Neue Verfahren zur Prädiktion des Betriebsverhaltens und Fehlererkennung bei Käfigläufermotoren kleiner Leistung. Fortschr.-Ber. VDI Reihe 21 no. 125. VDI-Verlag, Düsseldorf.
- Richter R (1949). Kurzes Lehrbuch der elektrischen Maschinen. Springer, Berlin.

- Sarma MS (1996). Electric Machines. Steady-State Theory and Dynamic Performance. PWS Press, New York.
- Schröder D (1995). Elektrische Antriebe 1. Springer, Berlin.
- Sen PC (1989). Principle of Electrical Machines and Power Electronics. Wiley, Chichester.
- Stadler W (1995). Analytical Robotics and Mechatronics. McGraw-Hill, New York.
- Störling HD (1996). Stand der Technik und Entwicklungstendenzen konventioneller Antriebe. VDI-Bericht no. 1269. VDI-Verlag, Düsseldorf.
- Störling HD, Beisse A (1987). Elektrische Kleinmaschinen. Teubner, Stuttgart.
- Töpfer H, Kriesel W (1983). Funktionseinheiten der Automatisierungs-technik. VEB-Verlag Technik, Berlin.
- Trzynadlowski AM, Legowski S (1998). Introduction to Modern Power Electronics. Wiley, New York.
- Vas P (ed) (1990). Vector Control of AC Machines. Clarendon Press, Oxford.
- Vogt K (1988). Elektrische Maschinen - Berechnung rotierender elektrischer Maschinen. VEB Verlag Technik, Berlin.
- Weißmantel H (1991). Elektrische Kleinantriebe. Lecture TH Darmstadt. Institut für Elektromechanische Konstruktionen.
- Wildi T (1981). Electrical power technology. Wiley, New York.

## CHAPTER 6

- Åström KJ, Wittenmark B (1997). Computer-controlled Systems. Theory and Design. Prentice Hall, Upper Saddle River.
- Bosch (1996). Automotive Handbook, Robert Bosch GmbH.
- Böhm J (1994). Kraft- und Positionsregelung von Industrierobotern mit Hilfe von Motorsignalen. Dissertation TU Darmstadt. Fortschr.-Ber. VDI Reihe 8 no. 405. VDI-Verlag, Düsseldorf.
- Dixon SL (1966). Fluid Mechanics, Thermodynamic of Turbomachinery. Pergamon Press, Oxford.
- Freyermuth B (1993). Wissensbasierte Fehlerdiagnose am Beispiel eines Industrieroboters. Dissertation TH Darmstadt. Fortschr.-Ber. VDI Reihe 8 no. 315. VDI-Verlag, Düsseldorf.
- Fuchs A (1992). Parameteradaptive Regelung des Außenrund-Einstellschleifens. Dissertation TH Darmstadt. Fortschr.-Ber. VDI Reihe 2 no. 266. VDI-Verlag, Düsseldorf.
- Gasch R, Nordmann R, Pfützner H (2001). Rotordynamik. Springer, Berlin.
- Germann S (1997). Modellbildung und modellgestützte Regelung der Fahrzeuggängsdynamik. Dissertation TH Darmstadt. Fortschr.-Ber. VDI Reihe 12 no. 309. VDI-Verlag, Düsseldorf.

- Gillespie TD (1992). Fundamentals of Vehicles Dynamics. SAE, Warrendale.
- Gülich JF (1999). Kreiselpumpen. Springer, Berlin.
- Held V (1992). Parameterschätzung und Reglersynthese für Industrieroboter. Dissertation TH Darmstadt. Fortschr.-Ber. VDI Reihe 8 no. 275. VDI-Verlag, Düsseldorf.
- Isermann R (1984). Einige Grundlagen der Prozeßdynamik – eine kurze Einführung. Techn. Mitt. Krupp. Forschungsberichte 42, 3.
- Isermann R (1989). Digital Control Systems, 2nd edn. Springer, Berlin.
- Isermann R (1992). Identifikation dynamischer Systeme, 2nd edn., vol. 1 and 2. Springer, Berlin.
- Isermann R (1997). Supervision, fault detection and fault diagnosis methods – an introduction. Special section on supervision, fault detection and diagnosis, Control Engineering Practice.
- Isermann R (1998). On fuzzy logic applications for automatic control, supervision, and fault diagnosis. IEEE Transactions on System, Men, and Cybernetics – Part A 28: 221–235.
- Isermann R (1999). Mechatronische Systeme. Springer, Berlin.
- Isermann R, Keller H, Raab U (1995). Intelligent actuators. Chapter 21: In: Gupta NN, Sinha NK (eds) (1995) Intelligent Control Systems. IEEE Press Book, Piscataway.
- Isermann R, Lachmann K-H, Matko D (1992). Adaptive Control Systems. Prentice Hall, New York.
- Isermann R, Raab U (1993). Intelligent actuators. Automatica 29: 1315–1331.
- Janik W (1993). Fehlerdiagnose des Außenrund-Einstechschleifens mit Prozeß- und Signalmodellen. Dissertation TH Darmstadt. Fortschr.-Ber. VDI Reihe 8 no. 288. VDI-Verlag, Düsseldorf.
- Kiencke U, Nielsen L (2000). Automotive Control Systems. Springer, Berlin.
- Klein, Schanzlin, Becker (1995). Kreiselpumpenlexikon, 3rd edn. KSB, Frankenthal.
- Konrad H (1997). Modellbasierte Methoden zur sensorarmen Fehlerdiagnose beim Fräsen. Dissertation TH Darmstadt. Fortschr.-Ber. VDI Reihe 2 no. 449. VDI-Verlag, Düsseldorf.
- Laschet A (1988). Simulation von Antriebssystemen. Fachberichte Simulation. Springer, Berlin.
- Leonhard W (1996). Control of Electrical Drives, 2nd edn. Springer, Berlin.
- Mamdani EH, Assilian S (1995). An experiment in linguistic synthesis with a fuzzy logic controller. International Journal Man-Machine-Studies 7: 1–13.
- Maron C (1991). Methoden zur Identifikation und Lageregelung mechanischer Prozesse mit Reibung. Dissertation TH Darmstadt. Fortschr.-Ber. VDI Reihe 8 no. 246. VDI-Verlag, Düsseldorf.
- Meyer M (1985). Elektrische Antriebstechnik, vol.1. Springer, Berlin.
- Nolzen H (1997). Parameteradaptive Regelung von Fräsprozessen. Dis-

- sertation TH Darmstadt. Fortschr.-Ber. VDI Reihe 8 no. 623. VDI-Verlag, Düsseldorf.
- Pfeiffer K (1997). Fahrsimulation eines Kraftfahrzeuges mit einem dynamischen Motorenprüfstand. Dissertation TH Darmstadt. Fortschr.-Ber. VDI Reihe 12 no. 336. VDI-Verlag, Düsseldorf.
- Pfeuffer T, Landsiedel T, Isermann R (1995) Identification and model-based nonlinear control of electro-mechanical actuators with friction. In: IFAC-Workshop Motion Control. München, Germany, October.
- Pfleiderer C, Petermann H (1991). Strömungsmaschinen, 5th edn. Springer, Berlin.
- Profos P (1982). Untersuchung stabilitätsgefährdeter technischer Prozesse. VGB-Kraftwerkstechnik 62: 144–150.
- Raab U (1993). Modellgestützte digitale Regelung und Überwachung von Kraftfahrzeug-aktoren. Dissertation TH Darmstadt. Fortschr.-Ber. VDI Reihe 8 no. 313. VDI-Verlag, Düsseldorf.
- Reiß T (1993). Fehlerfrüherkennung an Bearbeitungszentren mit den Meßsignalen des Vorschubantriebs. Dissertation TH Darmstadt. Fortschr.-Ber. VDI Reihe 2 no. 286. VDI-Verlag, Düsseldorf.
- Sailer U (1997). Nutzfahrzeug-Simulation auf Parallelrechnern mit Hardware-in-the-Loop. Expert Verlag, Renningen-Malmsheim.
- Schaffnit J (2002). Simulation und Control Prototyping zur Entwicklung von Nutzfahrzeug Motorsteuergerätefunktionen. Dissertation TU Darmstadt. Fortschr.-Ber. VDI Reihe 12 no. 473. VDI-Verlag, Düsseldorf.
- Schwibinger P, Nordmann R (1990). Torsional vibrations in turbogenerators due to network disturbances. Journal of Vibrations and Acoustics, Trans. ASME 112: 312–320.
- Sinsel S (1999). Echtzeitsimulation von Nutzfahrzeug-Dieselmotoren mit Turbolader zur Entwicklung von Motormanagementsystemen. Dissertation TU Darmstadt. Logos-Verlag, Aachen.
- Slotine JJE, Weiping L (1991). Applied nonlinear control, Chapter 7: Sliding Control. Prentice Hall, Englewood Cliffs.
- Specht R (1989). Parameterschätzung und digitale adaptive Regelung eines Industrieroboters. Dissertation TH Darmstadt.
- Spur G, Stöferle T (eds) (1979). Handbuch der Fertigungstechnik, vol. 3/1 Spanen. Hanser, München.
- Stute G (ed) (1981). Regelung an Werkzeugmaschinen. Hanser, München.
- Tomizuka M (1995). Robust digital motion controller for mechanical systems. In: Proceedings of Int. Conf. on Recent Advances in Mechatronics. Istanbul, August 14–16.
- Utkin VI (1977). Variable structure systems with sliding mode: a survey. IEEE Transactions on Automatic Control 22: 212–222.
- Voigt KU (1991). Regelung und Steuerung eines dynamischen Motorprüfstandes. 36. Internationales Wissenschaftliches Kolloquium. TH Ilmenau, October 21–24.

- Wanke P (1993). Modellgestützte Fehlerfrüherkennung am Hauptantrieb von Bearbeitungszentren. Dissertation TH Darmstadt. Fortschr.-Ber. VDI Reihe 2 no. 291. VDI-Verlag, Düsseldorf.
- Weck M (1982). Werkzeugmaschinen, vol. 3. VDI-Verlag, Düsseldorf.
- Wolfram A, Füssel D, Brune, T, Isermann R (2001). Component-based multi-model approach for fault detection and diagnosis of a centrifugal pump. In: Proc. ACC '2001. USA, June 2001.
- Wolfram A, Moseler O (2000), Design and application of digital FIR differentiators using modulating functions. In: Proc. SYSID 2000. Santa Barbara, California. USA, June.
- Würtenberger M (1997). Modellgestützte Verfahren zur Überwachung des Fahrzustandes eines Pkw. Dissertation TH Darmstadt. Fortschr.-Ber. VDI Reihe 12 no. 314. VDI-Verlag, Düsseldorf.
- Zadeh L (1972). A rationale for a fuzzy control. Journal Dynamic Systems, Measurement and Control 94 Series G: 3–4.

## CHAPTER 7

- Armstrong-Hélouvy B (1991). Control of Machines with Friction. Kluwer, Boston.
- Ayoubi M (1996). Nonlinear system identification based on neural networks with locally distributed dynamics and application to technical processes. Dissertation TH Darmstadt. Fortschr.Ber. VDI Reihe 8 no. 591. VDI-Verlag, Düsseldorf.
- Bishop CM (1995). Neural Networks for Pattern Recognition. Clarendon-Press, Oxford.
- Bosch (ed) (1995). Kraftfahrtechnisches Taschenbuch. VDI-Verlag, Düsseldorf.
- Bothe H-H (1993). Fuzzy Logic. Springer, Berlin.
- Canudas de Wit CA (1988). Adaptive Control for Partially Known Systems. Elsevier, Amsterdam.
- Chiu S (1994). Fuzzy model identification based on cluster estimation. Journal of Intelligent and Fuzzy Systems 2: 267–278.
- Ernst (Töpfer) S (1998). Hinging hyperplane trees for approximation and identification. In: IEEE Conference on Decision and Control (CDC). Tampa, USA: 1266–1271.
- Eykhoff P (1974). System Identification. Wiley, London.
- Haber R, Unbehauen H (1990). Structure identification of nonlinear dynamic systems – a survey on input/output approaches. Automatica 26: 651–677.
- Hafner M, Schüler M, Nelles O, Isermann R (2000). Fast neural networks for diesel engine control design. CEP – Control Engineering Practice 8: 1211–1221.
- Hafner S, Geiger H, Kreßel U (1992). Anwendung Künstlicher Neuronaler Netze in der Automatisierungstechnik. Part 1: Eine Einfüh-

- rung. atp – Automatisierungstechnische Praxis 34: 592–645.
- Haykin S (1994). Neural Networks. MacMillan, New York.
- Hecht-Nielsen R (1990). Neurocomputing. Addison Wesley, Reading.
- Held V (1991). Parameterschätzung und Reglersynthese für Industrieroboter. Dissertation TH Darmstadt. Fortschr.-Ber. VDI Reihe 8 no. 275. VDI-Verlag, Düsseldorf.
- Held V, Maron C (1988). Estimation of friction characteristics, inertial and coupling coefficients in robotic joints based on current and speed measurements. In: IFAC Symposium on Robot Control, Karlsruhe. Elsevier, Oxford.
- Holzmann H, Halfmann C, Isermann R (1997). Representation of 3-D mappings for automotive control applications using neural networks and fuzzy logic. In: 6th IEEE Conference on Control Applications, Hartford, Connecticut, USA.
- Isermann R (1992). Identifikation dynamischer Systeme, 2nd edn., vol. 1 and vol. 2. Springer, Berlin.
- Isermann R, Lachmann K-H, Matko D (1992). Adaptive Control Systems. Prentice Hall, New York.
- Isermann R, Ernst S, Nelles O (1997). Identification with dynamic neural networks – architectures, comparisons, applications –. In: 11th IFAC Symposium on System Identification, Fukuoka, Japan. Preprints 3: 997–1022.
- Jang J-S (1993). ANFIS: adaptive-network-based fuzzy inference system. IEEE Trans. on Systems, Man and Cybernetics 23: 665–685.
- Kiendl H (1996). Fuzzy Control methodenorientiert. Oldenbourg, München.
- Kofahl R (1988). Robuste Parameteradaptive Regelungen. Dissertation TH Darmstadt. Springer, Berlin.
- Kosko B (1992). Neural Networks and Fuzzy Systems. Prentice Hall, London.
- Lachmann K-H (1983). Parameteradaptive Regelalgorithmen für bestimmte Klassen nichtlinearer Prozesse mit eindeutigen Nichtlinearitäten. Dissertation TH Darmstadt. Fortschr.-Ber. VDI Reihe 8 no. 66. VDI-Verlag, Düsseldorf.
- Leonhard W (1973). Statistische Analyse linearer Regelsysteme. Teubner, Stuttgart.
- Ljung L (1987). System Identification: Theory for the User. Prentice Hall, New York.
- Ljung L, Söderström T (1985). Theory and Practice of Recursive Identification. MIT Press, Cambridge.
- Maron C (1991). Methoden zur Identifikation und Lageregelung mechanischer Prozesse mit Reibung. Dissertation TH Darmstadt. Fortschr.-Ber. VDI Reihe 8 no. 246. VDI-Verlag, Düsseldorf.
- McCulloch W, Pitts W (1943). A logical calculus of the ideas immanent in nervous activity. Bulletin of Math. Bio. 5: 115–133.
- Moseler O, Vogt M (2000). FIT - filtering and identification. In: 12th IFAC Symposium on System Identification. Santa Barbara, CA,

- USA, June 21-23.
- Müller N (2002). Adaptive Motorregelung beim Ottomotor unter Verwendung von Brennraumdruck-Sensoren. Interner Bericht, Institut für Automatisierungstechnik, TU Darmstadt.
- Murray-Smith R, Johansen TA (1997). Multiple Model Approaches to Modelling and Control. Taylor and Francis, London.
- Nelles O (2001). Nonlinear System Identification. Springer, Berlin.
- Nelles O (1997). LOLIMOT – Lokale, lineare Modelle zur Identifikation nichtlinearer, dynamischer Systeme. *at – Automatisierungstechnik* 45: 163–174.
- Nelles O, Ernst S, Isermann R (1997). Neuronale Netze zur Identifikation nichtlinearer dynamischer Systeme: ein Überblick. *at – Automatisierungstechnik*, 45: 251–262.
- Oppenheim AV, Schafer RW, Buck JR (1999). Discrete-time Signal Processing, reissued 2nd edn. Prentice Hall, Englewood Cliffs.
- Peter K-H (1993). Parameteradaptive Regelalgorithmen auf der Basis zeitkontinuierlicher Prozeßmodelle. Dissertation TH Darmstadt. Fortschr.-Ber. VDI Reihe 8 no. 348. VDI-Verlag, Düsseldorf.
- Pfeiffer B-M (1995). Einsatz von Fuzzy-Logik in lernfähigen digitalen Regelsystemen. Dissertation TH Darmstadt. Fortschr.-Ber. VDI Reihe 8 no. 500. VDI-Verlag, Düsseldorf.
- Preuss H-P (1992). Fuzzy-Control - heuristische Regelung mittels unscharfer Logik. *atp – Automatisierungstechnische Praxis* 34: 176–184 and 239–246.
- Preuss H-P, Tresp V (1994). Neuro-Fuzzy. *atp – Automatisierungs-technische Praxis* 36: 10–24.
- Raab U (1993). Modellgestützte digitale Regelung und Überwachung von Kraftfahrzeugaktoren. Dissertation TH Darmstadt. Fortschr.-Ber. VDI Reihe 8 no. 313. VDI-Verlag, Düsseldorf.
- Rosenblatt F (1958). The perceptron: A probabilistic model for information storage and organization in the brain. *Psychol. Rev.* 65: 386–405.
- Schmitt M (1995). Untersuchungen zur Realisierung mehrdimensionaler lernfähiger Kennfelder in Großserien-Steuergeräten. Dissertation TH Darmstadt. Fortschr.-Ber. VDI Reihe 12 no. 246. VDI-Verlag, Düsseldorf.
- Strobel H (1975). Experimentelle Systemanalyse. Akademieverlag, Berlin.
- Töpfer S (2002). Hierarchische Neuronale Modelle für die Identifikation nichtlinearer Systems. Dissertation TU Darmstadt.
- Widrow B, Hoff M (1960). Adaptive switching circuits. *IRE WESCON Convention Record*: 94–104, New York.
- Young PC (1984). Recursive Estimation and Time-series Analysis. Springer, Berlin.
- Zadeh LA (1965). Fuzzy sets. *Information and Control* 1965: 338–353.

## CHAPTER 8

- Akaike H (1974). A new look at the statistical model identification. *IEEE Trans. on Automatic Control*, 19: 716–723.
- Box GEP, Jenkins GM (1970). Time Series Analysis. Holden Day Press, San Francisco.
- Brigham EO (1974). The Fast Fourier Transform. Prentice Hall, Englewood-Cliffs.
- Burg JP (1967). Maximum entropy spectral analysis. In: Proceedings of the 37th Meeting of the Society of Exploration Geophysicists.
- Burg JP (1968). A new analysis technique for time series data. NATO Advanced Study Institute on Signal Processing with Emphasis on Underwater Acoustics, August 12–23.
- Cooley IW, Tuckey I (1965). An algorithm for the machine calculation of complex Fourier series. *Math. Comput.* 19: 297.
- Edward JA, Fitelson MM (1973). Notes on maximum-entropy processing, *IEEE Transaction on Information Theory* 19 no. March
- Führer J, Sinsel S, Isermann R (1993). Erkennung von Zündaussetzern aus Drehzahlsignalen mit Hilfe eines Frequenzbereichsverfahrens. In: 13. Tagung Elektronik im Kraftfahrzeug, Essen.
- Hess W (1989). Digitale Filter. Teubner, Stuttgart.
- Isermann R (1988). Digital Control Systems. Springer, Berlin.
- Isermann R (1992). Identifikation dynamischer Systeme, 2nd edn., vol. 1 and 2. Springer, Berlin.
- Kammeyer KD, Kroschel K (1992). Digitale Signalverarbeitung. Teubner, Stuttgart.
- Makhoul J (1975). Linear prediction: a tutorial review. In: *Proceedings IEEE* 63: 561–580.
- Muffert K-H (1980). Ursachen und Beispiele von Schäden an Verbrennungsmotoren. *Der Maschinenschaden* 53: 95–102.
- Neumann D (1991). Fault diagnosis of machine-tools by estimation of signal spectra. In: Proceedings of IFAC/IMACS Symposium on Fault Detection, Supervision and Safety for Technical Processes SAFEPROCESS'91. Baden-Baden, September 10–13, 1: 73–78.
- Neumann D (1994). Analyse periodischer Signale zur Fehlererkennung. In Isermann R (ed) Überwachung und Fehlerdiagnose. VDI-Verlag, Düsseldorf: 43–71.
- Neumann D, Janik W (1990). Fehlerdiagnose an spanenden Werkzeugmaschinen mit parametrischen Signalmodellen von Spektren, VDI-Schwingungstagung. Mannheim, October 11–12. VDI-Bericht no. 846. VDI-Verlag, Düsseldorf.
- Nussbaumer HJ (1981). Fast Fourier Transform and Convolution Algorithms 2nd edn. Springer, Berlin.
- Pandit SM, Wu GM (1983). Time Series and System Analysis with Applications. Wiley, New York.
- Papoulis A (1984). Signal Analysis. McGraw-Hill, New York.

- Press WH, Flannery BP, Teukolsky SA (1988). Numerical Recipes – the Art of Scientific Computing. Cambridge University Press, Cambridge.
- Ribbens WB, Rizzoni G (1990). Onboard diagnosis of engine misfires. SAE-Paper 901768, Detroit.
- Schüssler HW (1988). Digitale Signalverarbeitung, 2nd edn., vol. 1 and 2. Springer, Berlin.
- Stearns SD, Hush DR (1990). Digital Signal Analysis. Prentice Hall, Englewood Cliffs.
- Tong H (1975). Autoregressive model fitting with noisy data by Akaike's information criterion. IEEE Trans. on Information Theory 21: 476–480.
- Tong H (1977). More on autoregressive model fitting with noisy data by Akaike's information criterion. IEEE Trans. on Information Theory 23: 409–410.
- Ulrych TJ, Bishop TN (1975). Maximum entropy spectral analysis and autoregressive composition. Rev. of Geophysics and Space Physics, February 1975.
- Willimowski M, Füssel D, Isermann R (1999). Misfire detection for spark-ignition engines by exhaust gas pressure analysis. Motortechnische Zeitschrift worldwide: 8–12.

## CHAPTER 9

- Bauer H (ed) (1996). Automotive Handbook, 4th edn. Bosch, Stuttgart and SAE, Warrendale.
- Beckwith TG, Marangoni RD, Lienhard JH (1995). Mechanical Measurement, 5th edn. Addison Wesley, Reading
- Christiansen D (ed) (1996). Electronics Engineers' Handbook, 4th edn. McGraw Hill, New York.
- Czichos H (ed) (1989). Hütte – Die Grundlage der Ingenieurwissenschaften. Springer, Berlin.
- Jones BE (1977). Instrumentation, Measurement and Feedback. McGraw-Hill, New York.
- Juckenack D (1990). Handbuch der Sensorik – Messen mechanischer Größen. Teubner, Stuttgart.
- Jüttemann H (1988). Einführung in das elektrische Messen nichtelektrischer Größen. VDI-Verlag, Düsseldorf.
- Jurgen RK (1997). Sensors and Transducers. SAE, Warrendale.
- Kiencke U (1992). Sensorik im Kraftfahrzeug – vom Sensor zum System. VDI-Bericht no. 939. VDI-Verlag, Düsseldorf.
- Kleinschmidt P (1990). Intelligente Sensorsysteme. VDI-Bericht no. 855. VDI-Verlag, Düsseldorf.
- Lauber R, Göhner P (1999). Prozessautomatisierung, 3rd edn. Springer, Berlin.

- Pahl G (ed) (1992). Integrierte Drehmomentmessung. Kolloquium des Sonderforschungsbereiches "Neue integrierte mechanisch-elektronische Systeme für den Maschinenbau". TH Darmstadt, January 16.
- Profos P, Pfeifer T (1992). Handbuch der industriellen Meßtechnik. Vulkan, Essen.
- Schaumburg H (1992). Sensoren. Teubner, Stuttgart.
- Schrüfer E (1993). Elektrische Meßtechnik. Hanser, München.
- Technische Sensoren (1983). Forschungsheft 104, Forschungskuratorium Maschinenbau, Frankfurt.
- Thiel R (1990). Elektrisches Messen nichtelektrischer Größen. Teubner, Stuttgart.
- Tränkler HR, Böttcher (1992). Information processing in sensing devices and microsystems. IFAC Symposium on Intelligent Components, Malaga, May 20–22.
- Tränkler HR (1992). Taschenbuch der Meßtechnik. Oldenbourg, München.
- Webster JG (1999). The Measurement, Instrumentation and Sensors Handbook. CRC Press, Boca Raton.
- Whitaker JC (2000). Signal Measurement, Analysis and Testing. CRC Press, Boca Raton.

## CHAPTER 10

- Anders P (1986). Auswirkung der Mikroeletronik auf die Regelungskonzepte fluidtechnischer Systeme. Dissertation RWTH Aachen.
- Atlas-Copco (1977). Pneumatik-Kompendium. VDI-Verlag, Düsseldorf.
- Backé W (1986a). Grundlage der Pneumatik, 7th edn. RWTH Aachen.
- Backé W (1986b). Servohydraulik, 5th edn. RWTH Aachen.
- Backé W (1992). Fluidtechnische Aktoren. In: Aktoren – Grundlagen und Anwendungen. Janocha H (ed). Springer, Berlin.
- Ballé P, Fischer M, Füssel D, Nelles O, Isermann R (1998). Integrated control, diagnosis and reconfiguration of a heat exchanger. IEEE Control Systems 18: 52–63.
- Bauer G (1998). Ölhydraulik. Teubner, Stuttgart.
- von Bechen P (1989). Präzise und dynamisch – Konzepte und Wirkprinzipien moderner Positionsantriebe. Elektronik 38, no. 7.
- Blanke M, Izadi-Zamanabadi R, Bogh SA, Lunau CP (1997). Fault-tolerant control systems – a holistic view. CEP – Control Engineering Practice 5: 693–702.
- Block H, Kelly J P (1988). Electro-rheology. Journal of Physics, D: Applied Physics 21: 1661.
- Cady W (1964). Piezoelectricity. Dover Publishers Inc., New York.
- Chandler PR (1997). Reconfigurable flight control at Wright laboratory. Neuilly-sur-Seine, France, vol. III, AGARD advisory report

- 360, Aerospace 2020.
- Chen J, Patton RJ (1999). Robust Model-based Fault Diagnosis for Dynamic Systems. Kluwer Academic Publishers, Boston.
- Chen J, Patton RJ, Chen Z (1999). Active fault-tolerant flight control systems design using the linear matrix inequality method. Transactions Institute of Measurement and Control 21: 77–84.
- Chen MSX, Leufgen M (1987). Erfassung des Reibverhaltens von Kolbendichtungen und deren Einfluß auf die Positionierung von pneumatischen Systemen. O + P, Ölhydraulik und Pneumatik 31, no. 12.
- Clark RN (1989). State estimation schemes for instrument fault detection. In: Patton RJ, Chen J, Clark RN (eds) Fault diagnosis in dynamic systems. Prentice Hall, New York.
- Clarke DW (1995). Sensor, actuator, and loop validation. IEE Control Systems 15: 39–45.
- Culshaw B (1996). Smart Structures and Materials. Artech House Publishers, Norwood.
- Deibert R (1997). Methoden zur Fehlererkennung an Komponenten im geschlossenen Regelkreis. Dissertation TH Darmstadt. Fortschr. Ber. VDI Reihe 8 no. 650. VDI-Verlag, Düsseldorf.
- Duclos T, Carlson J, Chrzan M., Coulter J P (1992). Electro-rheological fluids – materials and applications. In: Intelligent Structural Systems, Tzou and Anderson (eds), Kluwer Academic Publishers: 213–241.
- Ehrfeld W, Ehrfeld U, Kieswalter S (2000). Progress and profit through microtechnologies. In: Proc. MICRO.tec 2000, VDE World Microtechnology Congress, Hannover, September 25–27, 1: 9-17. VDE-Verlag, Berlin.
- Gad-El-Hak M (2002). The MEMS Handbook. CRC Press, Baco Raton.
- Gertler JJ (1999). Fault Detection and Diagnosis on Engineering Systems. Marcel Dekker, New York.
- Gevatter HJ (2000). Automatisierungstechnik 3: Aktoren. Springer, Heidelberg.
- Gfröer R (1988). Servo-Schrittmotor Systeme. Antriebstechnik 27, no. 8.
- Glotzbach J (1996). Adaptive Sekundär-Drehzahlregelung hydraulischer Rotationsantriebe. Dissertation TH Darmstadt. Fortschr. Ber. VDI Reihe 8 no. 588. VDI-Verlag, Düsseldorf.
- Heinbach H. et al. (1977). Pneumatik-Kompendium. VDI-Verlag, Düsseldorf.
- Henneberger G (1989). Elektrische Stell- und Positionsantriebe - Komponenten, Konzepte, Definitionen. Report, Institut für Elektrische Maschinen RWTH, Aachen.
- Henry MP, Clarke DW (1993). The self-validating sensor: rationale, definitions, and examples. CEP – Control Engineering Practice 1:

- 585–610.
- Hodgson D (1989). Using Shape Memory Alloys. Shape Memory Applications Inc., Sunnyvale.
- Höfer B (1991). Servo- und Schrittmotor im Vergleich. Antriebstechnik 30, no. 5.
- IEC 61508 (1997). Standard draft IEC 61508, Part 1–7. Functional Safety of E/ E/ PES: (complex) Electrical/ (complex) Electronic/ Programmable Electronic Systems. Version 4.0.
- IFAC Journal Control Engineering Practice (1996). Special section on supervision, fault detection and diagnosis of technical processes, Tutorial Workshop IFAC Congress 1996, 5: 637–719.
- Isermann R (1994a). Überwachung und Fehlerdiagnose. VDI-Verlag, Düsseldorf.
- Isermann R (1994b). Integration of fault detection and diagnosis methods. In IFAC Symposium on Fault Detection, Supervision and Safety for Technical Processes (SAFEPROCESS), Espoo, Finland.
- Isermann R, Keller H (1993). Intelligente Aktoren. atp – Automatisierungstechnische Praxis 35: 593–602.
- Isermann R, Raab U (1993). Intelligent actuators – ways to autonomous systems. Automatica 29: 1315–1331.
- Isermann R, Schwarz R, Stölzl S (2000). Fault-tolerant drive-by-wire systems. In: IFAC Symposium on Fault Detection, Supervision and Safety, Budapest. Proc. Elsevier, London, see also IEEE Control Magazine 2002.
- ISO/DIN 6358 (1982). Pneumatic fluid – methods of test.
- Janocha H (ed) (1992). Aktoren – Grundlagen und Anwendungen. Springer, Berlin.
- Jaffe B, Cook WR, Jaffe H (1971). Piezoelectric Ceramics. Academic Press, London.
- Jendritzka DJ (1998). Technischer Einsatz neuer Aktoren: Grundlagen, Werkstoffe, Designregeln und Anwendungsbeispiele. Expert Verlag, Renningen.
- Jung R, Schneider J (1984). Elektische Kleinmotoren. Konstruktionskatalog und Marktübersicht. Feinwerktechnik und Meßtechnik, 92: 153–165.
- Kallenbach E, Eick R, Quendt P (1994). Elektromagnete. Teubner, Stuttgart.
- Keller H (1994). Wissensbasierte Inbetriebnahme und adaptive Regelung eines pneumatischen Linearantriebs. Dissertation TH Darmstadt. Fortschr. Ber. VDI Reihe 8 no. 412. VDI-Verlag, Düsseldorf.
- Korkmaz F (1982). Hydrospeicher als Energiespeicher. Springer, Heidelberg.
- Kpordonsky W (1993). Elements and devices based on magneto-rheological effect. Journal of Intelligent Material Systems and Structures 4: 65–69.
- Krautstrunk A, Mutschler P (1999). Remedial strategy for a permanent magnet synchronous motor drive. In: Proceedings of EPE'99, Lau-

- sanne, Switzerland.
- Kreuth HP (1988). Schrittmotoren. Oldenbourg, München.
- Lauber R (1988). Prozessautomatisierung, 2nd edn., vol. 1. Springer, Berlin.
- Lenz *et al.* (1990). Neue Aktoren. Mikroperipherik 6/1990, VDI/VDE Technologiezentrum Informationstechnik, Bremen.
- Leveson N (1995). Safeware. System Safety and Computer. Addison-Wesley, Reading.
- Maron C (1990). Methoden zur Identifikation und Lageregelung mechanische Prozesse mit Reibung. Dissertation TU Darmstadt. Fortschr. Ber. VDI Reihe 8 no. 246. VDI-Verlag, Düsseldorf.
- Matthies HJ (1995). Einführung in die Ölhydraulik. Teubner, Stuttgart.
- Merrit HE (1967). Hydraulic Control Systems. Wiley, New York.
- Minxue C, Koluuenbach H, Ohlischläger O (1986). Charakterisierung kompressibel durchströmter Widerstandsnetze. O+P, Ölhydraulik und Pneumatik 30, no.12.
- Moseler O, Heller T, Isermann R (1999). Model-based fault detection for an actuator driven by a brushless DC motor. In: 14th IFAC World Congress, Beijing, China, vol. P: 193–198.
- Nordmann R, Isermann R (eds) (1999). Kolloquium Aktoren in Mechatronische Systemen. Darmstadt, March 11. Fortschr.-Ber. VDI-Verlag, Düsseldorf.
- Oehler R, Schoenhoff A, Schreiber M (1997). Online model-based fault detection and diagnosis for a smart aircraft actuator. In: IFAC Symposium on Fault Detection, Supervision and Safety for Technical Processes (SAFEPROCESS), Kingston upon Hull, UK 2: 591–596.
- Oppelt W (1980). Kleines Handbuch technischer Regelvorgänge. Verlag Chemie, Weinheim.
- Oppelt W (1986). Der Steller im Regelkreis. msr – Messen, Steuern, Regeln 29, no. 8.
- Patton RJ (1997). Fault-tolerant control: the 1997 situation. In: IFAC Symposium on Fault Detection, Supervision and Safety for Technical Processes (SAFEPROCESS), Kingston Upon Hull, UK, 2: 1033–1055.
- Pfeufer T (1997). Application of model-based fault detection and diagnosis to the quality assurance of an automotive actuator. CEP – Control Engineering Practice 5: 703–708.
- Raab U (1990). Stell- und Positionierantriebe im Kraftfahrzeug. FVV-Zwischenberichte. Heft 457, Forschungsvereinigung Verbrennungskraftmaschinen e.V., Frankfurt.
- Raab U (1993). Modellgestützte digitale Regelung und Überwachung von Kraftfahrzeugaktoren. Dissertation TH Darmstadt. Fortschr. Ber. VDI Reihe 8 no. 313. VDI-Verlag, Düsseldorf.
- Raab U, Isermann R (1990). Actuator principles with low power. VDI/VDE-Tagung ACTUATOR 90, Bremen.

- Rau G (1974). Thermobimetalle. Company G. Rau, Pforzheim.
- Rauch HE (1995). Autonomous control reconfiguration. IEEE Control Systems Magazine 15: 37–48.
- Rusterholz R (1985). Grundlagenbetrachtung zur Auslegung pneumatischer Servoantriebe. O + P, Ölhydraulik und Pneumatik 29, no. 10.
- Saffee P (1986). Moderne servohydraulische Antriebe, Robotersysteme 2. Springer, Berlin.
- Schaffnit J (2002). Simulation und Control Prototyping zur Entwicklung von Nutzfahrzeug Motorsteuergerätefunktionen. Dissertation TU Darmstadt. Fortschr.-Ber. VDI Reihe 12 no. 473. VDI-Verlag, Düsseldorf.
- Scheffel G (1989). Antreiben mit geregelten Zylinderanrieben. O + P, Ölhydraulik und Pneumatik, 33: 197–208.
- Schriek J, Sonemann R (1988). Elektronische Regelung und Steuerung mit pneumatischen Aktoren. VDI-Bericht 687. VDI-Verlag, Düsseldorf.
- Srinivasan AV, McFarland DM (2000). Smart Structures: Analysis and Design. Cambridge University Press, Cambridge.
- Storey N (1996). Safety-critical Computer Systems. Addison Wesley Longman Ltd., Harlow.
- Suryanaryanan S, Tomizuka M (2000). Fault-tolerant lateral control of automated vehicles based on simultaneous stabilization. In: 1st IFAC Conference on Mechatronic Systems, Darmstadt, Germany.
- Takuro I (1996). Fundamentals of Piezoelectricity. Oxford University Press, Oxford.
- Tautzenberger P (1989). Thermische Stellelemente. Feinwerk und Meßtechnik 97, no. 4.
- Traeger F (1979). Schrittmotoren für feinwerktechnische Anwendungen. Feinwerk und Meßtechnik 87, no. 4.
- Waram T (1993). Actuator design using shape memory alloys, 2nd edn. Mondo-Tronics, San Anselmo.
- Weck M (1989). Elektrische Stell- und Positionierantriebe - Systemaspekte und Anwendungen bei Werkzeugmaschinen, ETG.
- Weck M (1990). Werkzeugmaschinen. VDI-Verlag, Düsseldorf.
- Wietschorke S, v. Willich J (1986). Stellantriebe mit Gleichstrom-Kleinmotoren für die Kfz-Regeltechnik. Feinwerk und Mechanik 94, no. 7.
- Wilke W (1988). Bürstenlose Gleichstrommotoren. Feinwerk und Meßtechnik 96, no. 4.

## CHAPTER 11

- Bähring H (1994). Mikrorrechner-Systeme, 2nd edn. Springer, Berlin.
- Bender K (ed) (1990). PROFIBUS, Der Feldbus für die Automation. Hanser, München.

- Bleck *et al.* (1996). Praktikum des modernen VLSI-Entwurfs. Teubner, Stuttgart.
- Bosch (ed) (1995). Kraftfahrtechnisches Taschenbuch, 22nd edn. VDI-Verlag, Düsseldorf.
- Bradley DA, Dawson D, Burd D, Loader AJ (1991). Mechatronics-electronics in Products and Processes. Chapman and Hall, London.
- Carter JW (1995). Microprocessor Architecture and Microprogramming. Prentice Hall, Englewood Cliffs.
- Chen W-K (ed) (2000). The VSLI Handbook. CRC Press, Boca Raton.
- Christiansen D (ed) (1996). Electronic Engineers's handbook. McGraw-Hill, New York.
- Conzelmann G, Kiencke U (1995). Mikroelektronik im Kraftfahrzeug. Springer, Berlin.
- Dais S, Unruh J (1992). Technisches Konzept des seriellen Bussystems CAN. ATZ – Automobiltechnische Zeitschrift 94: 66–77 and 208–215.
- DIN 19245 (1988). Messen, Steuern, Regeln. PROFIBUS. Beuth Verlag, Berlin.
- El-Sharkawy M (1997). Digital Signal Processing Applications with Motorola's DSP56002 Processor. Prentice Hall, New Jersey.
- Embacher M (1995). Automobilvernetzung nach Maß. Elektronik 44: 64–72.
- Etschberger K (1994). CAN Controller-area-network. Hanser, München.
- Etschberger K, Suters T (1993). Offene Kommunikation auf CAN-Netzwerken. Elektronik 42: 60–66.
- Färber G (ed) (1987). Bussysteme. Parallele und serielle Bussysteme in Theorie und Praxis, 2nd edn. Oldenbourg, München.
- Färber G (1994). Feldbus-Technik heute und morgen. atp – Automatisierungstechnische Praxis 36: 16–36.
- Fleck R, Bauer P (1989). SAB 80C166 – auf Schnelligkeit getrimmt. Special print, Siemens Aktiengesellschaft, Bereich Halbleiter.
- Gibson V (1994). Microprocessors: Fundamental Concepts and Applications. Delmar, New York.
- Gilmore C (1989). Microprocessor Principles and Applications. McGraw-Hill, New York.
- Glesner M, Herpel HJ, Windirsch P (1993). Anwendungsspezifische Mikroelektronik für den Einsatz in der Mechatronik. Fachtagung Integrierte mechanisch-elektronische Systeme. Fortschr. Ber. VDI Reihe 12 no. 179: 190–209. VDI-Verlag, Düsseldorf
- Grant PM (1996). Signal processing hardware and software. IEEE Signal Magazine 13: 86–89.
- Hanselmann H (1996). Automotive control: from concept to experiment to product. In: IEEE International Symposium on Computer-Aided Control System Design. Dearborn, Michigan, USA, September 15–18.

- Herpel HJ (1995). Rapid Prototyping heterogener Echtzeitsysteme für die Mechatronik. Dissertation TH Darmstadt.
- Höfling J (1994). Mikrocontroller aus dem Baukasten. Elektronik 45: 156–160.
- Ifeachor EC, Jerves BW (1993). Digital Signal Processing. Addison Wesley, Reading.
- ISO-DIS 11989 (1992). Road vehicles – interchange of digital information - CAN for high speed communication 8/1992.
- ISO-DIS 11519-1 Road vehicles – low speed serial data communication part I: low speed CAN.
- Kiel E, Schumacher W (1994). Der Servocontroller in einem Chip. Elektronik 45: 48–60.
- Kreisel R, Madelung O (ed) (1995). ASI – The actuator-sensor-interface automation. Hanser, München.
- Kleitz, W (1990). Digital and Microprocessor Fundamentals. Prentice Hall, Englewood Cliffs.
- Kurz K, Wagner W (1991). Signalprozessoren-Praxis. Franzis, München.
- Lane J, Martinez E (2000). DSP Filters (Electronics Cookbook Series). Prompt Publications, New York.
- Lauber R (1989). Prozeßautomatisierung I. Springer, Berlin.
- Meierau ES (1996). Kostensenkung in der Chip-Fertigung. Siemens-Zeitschrift, Special Forschung und Entwicklung: 6–10.
- Morgan D (1996). Numerical methods for DSP systems. Wiley, Indianapolis.
- Morgenroth K (1995). Formel I – Marktreport: 32-Bit-Mikrocontroller. ELRAD – Magazin für Elektronik und technische Rechneranwendung 20: 52–59.
- N.N. (1994). Marktübersicht: 1b-Bit-Mikrocontroller. Markt & Technik – Wochenzeitung für Elektronik 1994: 56–60.
- N.N. (1995). Marktübersicht: 8-Bit-Mikrocontroller. Markt & Technik – Wochenzeitung für Elektronik 1995: 40–47.
- Patterson DA (1995). Mikroprozesse im Jahre 2020. Spektrum der Wissenschaften. Spezial 4: Schlüsseltechnologie. VDO. Heidelberg, October.
- van den Plassche R (1994). Integrated Analog-to-digital and Digital-to-analog Converters. Kluwer Academic Publishers, Boston.
- Post HU (1989). Entwurf und Technologie hochintegrierter Schaltungen. Teubner, Stuttgart.
- Profos P, Pfeifer T (1992). Handbuch der industriellen Meßtechnik. Vulkan, Essen.
- Rammig FJ (1989). Systematischer Entwurf digitaler Systeme. Teubner, Stuttgart.
- Reissenweber B (2002). Feldbusssysteme zur industriellen Kommunikation, 2nd edn. Oldenbourg, München.
- Rembold U, Levi P (1994). Realzeitsysteme zur Prozeßautomatisierung. Hanser, München.

- Rorabough CB (1998). DSP primer. McGraw-Hill, New York.
- Sax H (1993). Super-Smartpower. Elektronik 42: 79–82.
- Schrüfer E (1983). Elektrische Meßtechnik. Hanser, München.
- Schrüfer E (1992). Lexikon Meß- und Automatisierungstechnik. VDI-Verlag, Düsseldorf.
- Stallings W (1994). Data and computer communications, 4th edn. Macmillan, New York.
- Stiller A (1995). Architektur enthüllt. c't magazin für computer technik 1995: 230–236.
- Stiller A (1996). SPECulatius. c't magazin für computer technik 1996: 60–61.
- Strauss H (1995). Signal Processing. ELRAD – Magazine für Elektronik und technische Rechneranwendung 19: 50–53.
- Thomson A (1994). Understanding Microprocessors: a Practical Approach. Delmar.
- Tietze U, Schenk C (1989). Halbleiter Schaltungstechnik, 9th edn. Berlin, Springer.
- Unruh J, Methony HJ, Kaiser KH (1990). Error detection analysis of automotive communication protocols. SAE International Congress, No. 900699, Detroit.
- Volz M (1993). Profibus-DP – der schnelle Bruder. Elektronik 42: 50–60.
- Whitacker J (ed) (2000). Microelectronics. CRC-Press, Boca Raton.
- Wieder AW (1996). Mikroelektronik quo vadis? Siemens-Zeitschrift, Special Forschung und Entwicklung: 2–5.
- Wunderlich HJ (1991). Hochintegrierte Schaltungen: Prüfgerechter Entwurf und Test. Springer, Berlin.

## CHAPTER 12

- Abou-El-Ela A (1995). Adaptive external torque observation of robotiv joint drives based on friction signal models. In: Proceedings of IFAC Symposium on Motion Control, Munich.
- Alleyne A, Hedrick JK (1995). Non-linear adaptive control of active Suspensions. IEEE Trans. on Control Systems Technology 3: no. 1.
- Böhm J (1994). Kraft- und Positionsregelung von Industrierobotern mit Hilfe von Motorsignalen. Dissertation TH Darmstadt. Fortschr.-Ber. VDI Reihe 8 no. 405. VDI-Verlag, Düsseldorf.
- Bosch (1996). Automotive Handbook. Robert Bosch GmbH, Stuttgart.
- Bußhardt J (1995). Selbsteinstellende Feder-Dämpfersysteme für Kraftfahrzeuge. Fortschr.-Ber. VDI Reihe 12 no. 240. VDI Verlag, Düsseldorf.
- Butsuen T (1989). The design of semi-active suspensions for automotive vehicles. PhD-thesis, Massachusetts Institute of Technology,

- Department of Mechanical Engineering.
- Choi SB, Choi YT, Chang EG (1998). Control characteristics of a continuously variable ER damper. *Mechatronics* 1998: 143–161.
- Choi SB, Lee HK, Chang EG (2001). Field test results of a semi-active ER suspension system associated with skyhook controller. *Mechatronics* 2001: 345–253.
- Craig J (1989). *Introduction to robotics: mechanics and control*, 2nd edn. Addison-Wesley, Reading.
- Darenberg W, Gall H, Acker B (1984). Chancen und Probleme aktiver Kraftfahrzeugfederungen. *VDI Berichte* no. 515. VDI-Verlag, Düsseldorf: 187–194.
- Denavit R, Hartenberg RS (1955). A kinematic notation for lower-pair mechanism based on matrices. *ASME Journal of Applied Mechanics* 22: 215–221.
- Fees G (2001). Study of the static and dynamic properties of a highly dynamic ER servo drive. *Ö + P, Ölhydraulic und Pneumatic* 45, no. 1.
- Freyermuth B (1993). Wissensbasierte Fehlerdiagnose am Beispiel eines Industrieroboters. Dissertation TH Darmstadt. Fortschr.-Ber. VDI Reihe 8 no. 315. VDI-Verlag, Düsseldorf.
- Halfmann C (2001). Adaptive semiphysikalische Echtzeitsimulation der Kraftfahrzeugdynamik im bewegten Fahrzeug. Dissertation TU Darmstadt. Fortschr.-Ber. VDI Reihe 12 no. 467. VDI-Verlag, Düsseldorf.
- Hanselmann H (1996). Automotive control: from concept to experiment to product. In: *IEEE International Symposium on Computer-Aided Control System Design*. Dearborn, Michigan, USA, September 15–18.
- Hayakawa K, Matsumoto K, Yamashita M, Suzuki Y, Fujimori K, Kimura H (1999). Robust  $H\infty$ -output feedback of decoupled automobile active suspension systems. *IEEE Trans. on Automotive Control* 44: 392–396.
- Held V (1992). Parameterschätzung und Reglersynthese für Industrieroboter. Dissertation TH Darmstadt. Fortschr.-Ber. VDI Reihe 8 no. 275. VDI-Verlag, Düsseldorf.
- Held V, Maron C (1988). Estimation of friction characteristics, inertial and coupling coefficients in robotic joints based on current and speed measurements. *Proceedings of the IFAC-Symposium on Robot Control (SYROCO)*, Karlsruhe, Germany: 86.1-86.6.
- Isermann R, Börner M, Fischer D (2002). Mechatronic Semi-active vehicle suspensions. In: *Proceedings ISOM 2002*, Chemnitz.
- Isermann R, Keller H (1993). Intelligente Aktoren. *atp – Automatisierungstechnische Praxis* 35: 593–602.
- Isermann R, Lachmann K-H, Matko D. (1992). *Adaptive Control Systems*. Prentice Hall, New York.
- Isermann R, Raab U (1993). Intelligent actuators – ways to autonomous systems. *Automatica* 29: 1315–1331.

- Isermann R, Schaffnit, J, Sinsel S (1999). Hardware-in-the-loop simulation for the design and testing of engine control systems. CEP – Control Engineering Practice 7: 643–653.
- Karlsson N, Dableh M, Hrovat D (2001). Nonlinear active suspension with preview. In: Proceedings AAC'01: 2640–2645.
- Kim WK, Choi SB (1999). Vibration control of a semi-active suspension featuring electro-rheological fluid dampers. Journal of Sound and Vibration 234: 537–546.
- Kraus H, Dantelle H (1970). Berechnung und Messung von Stoßdämpfer-Ventilen. atz – Automobiltechnische Zeitschrift 75: 234–237.
- Krtolica R, Hrovat D (1990). Optimal active suspension control based on a half car model. In: Proceedings Decision and Control, 29<sup>th</sup> IEEE Conference.
- Majjad R (1997). Estimation of suspension parameters. In: Proceedings of the IEEE International Conference on Control Applications, Hartford, CT.
- Mitschke M (1997). Dynamik der Kraftfahrzeuge, Schwingungen vol B. Springer, Berlin.
- Moosheimer J, Waller H (1999). Reduction of vibrations by bang-bang controlled electrorheological dampers. Archive of Applied Mechanics 70: 0715–0737.
- Nomura S, Takeshita S (1993). New GALANT & ETERNA. JSAE Review 14: 71–77.
- Oya M, Araki Y, Harada H (1998). Robust control of active automotive suspensions with model uncertainties. In: Proceedings of the AVEC 1988, Amiens: 467–472.
- Paul RP (1989). Robot Manipulators: Mathematics, Programming and Control, vol. 1, 2nd edn. MIT Press, Cambridge and London.
- Pfeufer T (1999). Modellgestützte Fehlererkennung und Diagnose am Beispiel eines Kraftfahrzeugaktors. Dissertation TU Darmstadt. VDI-Verlag, Düsseldorf.
- Pfeufer T, Isermann R (1996). Intelligent electromechanical servosystems. IFAC World Congress, San Francisco, CA, USA, July 1–5.
- Raab U (1993) Modellgestützte digitale Regelung und Überwachung von Kraftfahrzeugaktoren. Dissertation TH Darmstadt. Fortschr.-Ber. VDI Reihe 8 no 313. VDI-Verlag, Düsseldorf
- Reimpell J, Stoll H (1989). Fahrwerktechnik: Stoß- und Schwingungsdämpfer, 2nd edn. Vogel Buchverlag, Würzburg.
- Reimpell J, Stoll H (1996). The Automotive Chassis. Arnold.
- Rieth P (1999). Brake by wire - Bremsentechnologie im Wandel. Fahrzeug- und Motortechnischen Seminar der Technischen Universität Darmstadt, February 11, 1999.
- Roukied S, Titli A (1993). Robust sliding mode control of semi-active and active suspension for private cars. In: Proceedings of the 12th IFAC World Congress 1993, Sidney 3: 155-160.

- Salman M (1988). Reduced design of active suspension control. In: Proceedings of the 27<sup>th</sup> Conference on Decision and Control, Austin, Texas.
- Schaffnit J, Isermann R (2000). Hardware-in-the-loop simulation and rapid prototyping for the development of control functions for Diesel engines. In: Proceedings of the 1st IFAC Conference on Mechatronic Systems, MECHATRONICS2000, Darmstadt, Germany.
- Schwarz R (1999). Rekonstruktion der Bremskraft bei Fahrzeugen mit elektromechanisch betätigten Radbremsen. Dissertation TU Darmstadt. Fortschr.-Ber. VDI Reihe 12 no. 393. VDI-Verlag. Düsseldorf.
- Sciavicco L, Siciliano B (2000). Modelling and Control of Robot Manipulators, vol. 1, 2nd edn. Springer, London, Berlin and Heidelberg.
- Sinsel S (1999). Echtzeitsimulation von Nutzfahrzeug-Dieselmotoren mit Turbolader zur Entwicklung von Motormanagementsystemen. Dissertation TU Darmstadt. Logos-Verlag, Aachen.
- Streiter R (1996). Entwicklung und Realisierung eines analytischen Regelkonzepts für eine aktive Federung. Dissertation, TU Berlin.
- Ursu I, Ursu F, Vladimirescu M (1997). The synthesis of two suboptimal electrohydraulic suspensions, active and semiactive, employing the receding horizon method. Non-linear Analysis, Theory, Methods & Applications 30, no. 4.
- Venhovens PJT, Paceika HB (1992). Semi-active vibration and attitude control. In: Proceedings of the International Symposium on Advanced Vehicle Control (AVEC), Yokohama, JSAE-paper No. 923032.
- Wang J, Wilson DA, Halikias GD (2001).  $H^\infty$  robust-performance control of decoupled active suspension systems based on LMI method. American Control Conference, Arlington, VA.
- Weispfenning T (1996). Fault detection of components of the vehicle vertical dynamics. In: Proceedings of the 1<sup>st</sup> Int. Conference on Control and Diagnostics in Automotive Applications, Genova.
- Yokoyama M, Hedrick JK, Toyama S (2001). A model following sliding mode controller for semi-active suspension systems with MR dampers. In: Proceedings of the American Control Conference, Arlington, VA.
- Yue C, Butsuen T, Hedrick JK (1989). Alternative control laws for automotive active systems. Trans. of the ASME, Journal of Dynamic Systems, Measurements and Control, Juni 1989: 286–291.

# Subject Index

---

Absorber	158	- ports	475
AC Motor	168, 205, 273, 398	- shape memory alloys	458
- control	209	- structure	384
- field oriented control	211	- thermal expansion	462
- induction	205	- thermo-bimetal	458
- slip-ring	208	- time behavior	389
- squirrel-cage	208	- unconventional	457
- steady state	212, 219	ADC (analog-to-digital converter)	376, 502
- synchronous	215		
AC-DC converter	233	Algorithm	
Across-through classification	55, 91, 95, 100	- Burg	351
Across-variable	36, 54	ALU (arithmetic logical unit)	493
Actuators	25, 383	Amplitudes	
- application areas	471	- estimation	351
- as system components	474	- modulation	334
- auxiliary energy	387	- spectrum	334
- basic structure	384	Analog input	
- comparison	471	- ADC	502
- components	476	- analog filter	502
- electrochemical	458	- hold element	502
- electromagnetic	527, 529	- multiplexor	502
- electromechanical	392, 404	- optoelectronic couplers	504
- electrorheological	463	- potential separation	502
- fault detection	480, 527	Analog output	
- fault-tolerant	484	- digital converter	504
- functionality	475	- potential separation	505
- hydraulic	406	- power amplifier	505
- inchworm motor	468	Analog-to-digital converter (ADC)	376
- integration	475	Analogies	
- magnetorheological	463	- mechanical and electronic systems	94
- magnetostrictive	458, 469	ANN (artificial neural networks)	309
- micro	470	Apparatus	10
- motor driven	392	ARMA (autoregressive moving average	
- piezoelectric	458	model	349
- pneumatic	439	-difference equation	349

- Sarma MS (1996). Electric Machines. Steady-State Theory and Dynamic Performance. PWS Press, New York.
- Schröder D (1995). Elektrische Antriebe 1. Springer, Berlin.
- Sen PC (1989). Principle of Electrical Machines and Power Electronics. Wiley, Chichester.
- Stadler W (1995). Analytical Robotics and Mechatronics. McGraw-Hill, New York.
- Störling HD (1996). Stand der Technik und Entwicklungstendenzen konventioneller Antriebe. VDI-Bericht no. 1269. VDI-Verlag, Düsseldorf.
- Störling HD, Beisse A (1987). Elektrische Kleinmaschinen. Teubner, Stuttgart.
- Töpfer H, Kriesel W (1983). Funktionseinheiten der Automatisierungs-technik. VEB-Verlag Technik, Berlin.
- Trzynadlowski AM, Legowski S (1998). Introduction to Modern Power Electronics. Wiley, New York.
- Vas P (ed) (1990). Vector Control of AC Machines. Clarendon Press, Oxford.
- Vogt K (1988). Elektrische Maschinen - Berechnung rotierender elektrischer Maschinen. VEB Verlag Technik, Berlin.
- Weißmantel H (1991). Elektrische Kleinantriebe. Lecture TH Darmstadt. Institut für Elektromechanische Konstruktionen.
- Wildi T (1981). Electrical power technology. Wiley, New York.

## CHAPTER 6

- Åström KJ, Wittenmark B (1997). Computer-controlled Systems. Theory and Design. Prentice Hall, Upper Saddle River.
- Bosch (1996). Automotive Handbook, Robert Bosch GmbH.
- Böhm J (1994). Kraft- und Positionsregelung von Industrierobotern mit Hilfe von Motorsignalen. Dissertation TU Darmstadt. Fortschr.-Ber. VDI Reihe 8 no. 405. VDI-Verlag, Düsseldorf.
- Dixon SL (1966). Fluid Mechanics, Thermodynamic of Turbomachinery. Pergamon Press, Oxford.
- Freyermuth B (1993). Wissensbasierte Fehlerdiagnose am Beispiel eines Industrieroboters. Dissertation TH Darmstadt. Fortschr.-Ber. VDI Reihe 8 no. 315. VDI-Verlag, Düsseldorf.
- Fuchs A (1992). Parameteradaptive Regelung des Außenrund-Einstellschleifens. Dissertation TH Darmstadt. Fortschr.-Ber. VDI Reihe 2 no. 266. VDI-Verlag, Düsseldorf.
- Gasch R, Nordmann R, Pfützner H (2001). Rotordynamik. Springer, Berlin.
- Germann S (1997). Modellbildung und modellgestützte Regelung der Fahrzeuglängsdynamik. Dissertation TH Darmstadt. Fortschr.-Ber. VDI Reihe 12 no. 309. VDI-Verlag, Düsseldorf.

- static behavior	192	- types	170
d'Alembert's principle	106	Electromotive force (EMF)	187, 210
Damping ratio	130	Electromotor	
Dead-time	300	- alternating current (AC)	168, 205, 398
Dead-zone, see backlash		- externally commutated	234, 398
Decaying constant	130	- commutator	221
Design		- compound	394
- mechatronic systems	24, 527, 588	- capacitor	222
Defuzzification	323	- direct current (DC)	184
Degradation		- Ferraris	223
- graceful	479	- for actuators	393
Diesel engines	572	- internally commutated	234, 394
Digital-to-analog converter (DAC)	504	- linear model	392, 462
Digital signal processor (DSP)	510	- mechanical-commutated	394
Displays	506	- shunt-wound	394
Displacement	53	- self-commutated	394
Distributed parameters	34	- series-wound	394
DMLP (dynamic multi-layer		- servo	397
perceptron)	321	- single-phase	221
DMA (direct memory access)	511	- squirrel-cage	222
DRAM (dynamic random access		- synchronous	399, 400
memory)	500	- stepper	201, 390, 401
Drivetrain	12, 241	- three-phase capacitor	398
- automotive	279	- universal	221, 398
- belt	151	Elements	
- dynamic model	278	- active	41
- model	280	- electrical	95
- multi-mass	288	- mechanical	95, 115
DSP (digital signal processors)	510	- passive	41
EBC (external bus controller)	508	- storages	59
EEPROM (electrically erasable and		Encoder	366
programmable read only memory)	489	Engine	
Effort	36	- combustion	262
EGR (exhaust gas recirculation)		- Diesel	572
	321, 572	- spark ignition	262
Electrical drives	167	Engineering	
- dynamic behavior	188	- simultaneous	5
- induced voltage	186	Energy	
- speed control	194	- internal	79
- static behavior	192	- kinetic	74
- position control	194	- potential	73
- torque generation	187	Energy balance	48, 71, 85
- types	167	- electrical systems	83
Electrical throttle valve	535	- gases	79
Electromechanical disc brake (EMB)		- mechanical systems	71
	560	- thermal systems	77
Electromagnetic compatibility (EMC)		- steams	79
	377	Energy flow	38
Electromagnets	170, 404	Enthalpy	81
- dynamic behavior	175, 181	EPROM(erasable and programmable	
- holding magnet	170	read only memory)	500
- force-generating magnet	170	EERPOM (electrically erasable and	
- linear behavior	170	programmable read only memory)	500
- position control	181	Equations	
- positioning magnet	170	- balance	47
- static behavior	173, 177	- constitutive	51

- energy balance	71	- resonance angular	130
- fundamental	46, 101	- response	296
- mesh	88	- undamped natural	130
- momentum balance	74	Friction	
- node	88	- compensation	288, 455, 528
- phenomenological	68	- Coulomb	121, 159, 245
- physical state	51	- dry	121, 159, 245
Estimation		- estimation	327
- maximum-entropy spectral	347	- experimental results	271
Euler		- viscous	121, 159, 245, 327
- differential equation	410	Functions	11, 12
Excitation		- Gaussian	314
- basic	132	Fuzzy	
- by unbalance	132	- control	290
Fail		- if-then-rules	323
- operational (FO)	479	- logic	24, 324
- safe (FS)	479	- rules	323
- silent (FSIL)	479	Fuzzification	323
Failure	476	Gas dynamic properties	442
Fault	476	Gas law	443
Fault detection		Gaussian functions	314
-- actuator	480, 533	Gear	143, 401
- sensor	480	Gyrator	64
Fault diagnosis	21, 535, 538	Hacksawing machine	352
Fault-tolerance		Hammerstein model	208
- actuators	481	Hanning-window	346
- components	476	Hall effect	367
- control systems	480	Hardware-architecture	26
- sensors	484	Hardware-in-the-loop simulation (HiL)	569
Feed drive	268	Harvard structure	491
Feedback	255	Hinging hyperplane trees	316
Field bus	514	Human-machine interface	26
- CAN bus	523	Hydraulic	
- functions	517	- actuator	406
- net topologies	515	- control valve	414
- OSI reference model	517	- cylinder	422
- PROFIBUS	519	- losses	427
Field weakening	194	- pressure storages	419
Flow	36, 51	- pump	424
- energy	56	- rotary motor	423
- heat	57	- servo axis	429
- laminar	410	- translatory motor	420
- main	8, 38	- transmission line	418
- mass	57	Hysteresis	
- side	8, 38	- solenoid	531
- turbulent	410	Identification	30, 293
Fluid dynamic properties	408	- application	299
Force		- bandpass filtering	339
- applied	107	- correlation functions	340
Fourier		- closed-loop	299
- analysis	340	- dynamic systems	293
- fast (FFT)	343	- Fourier analysis	340
- transformation	341	- oscillations	333
Frequency			
- damped natural	130		
- modulation	335		

– quarter-car model	551	– flow	8, 38
– spectral estimation	347	– forms	37
Identification methods	293	Maximum-entropy-spectral estimation	347
– classification	294	Measurement	
– least squares	300	– acceleration	370
– modifications	303	– displacement	364
– non-linear processes	308	– force	372
– recursive	303	– oscillation	372
Indicator diagram	308	– pressure	372
Industrial robot	577	– strain gauge	366
– control	583	– torque	373
– modeling	578	– temperature	373
– system structure	585	– velocity	368
Information		– vibration	372
– gaining	19	Mechanical elements	115
– flow	3	– bars	116
– processing	14, 18	– bearings	124
Integration form	14	– springs	118
Interface		– dampers	121
– to process	501	Mechanical engineering	8
Interpolation	326	Mechanical systems	8
Kinematics	101	– backlash	162
Kinetics	102	– classification	7
Kirchhoff laws	89	– friction	159
Lagrange's equations	109	– mobile masses	101
Least squares method	300	Mechatronic Systems	1
Libration	337	– components	481
LRGF (locally recurrent globally feedforward networks)	319	– confinement	10
LOLIMOT (local linear model network)	314	– definitions	4, 11
Look-up table	325	– design	11, 24, 527
LRGF (locally recurrent globally feedforward)	319	– developments	14
Lumped parameters	34	– functions	11, 13
Machines	2, 6, 8, 115, 241	– historical developments	2
– characteristics	248	– integration forms	14
– components	243	– intelligent	6
– power-generating	241	– operation properties	13
– power-consuming	241	– overall	587
– static behavior	257	Memory	497
– dynamic behavior	268	– capacity	497
Machine elements	8	– cycle time	497
Magnetic circuits		Mesh equation	88
– dynamic behavior	175	Methods	20
– static behavior	173	– bond graph	56
Magnetic field	171	– simulation	569
Magnetic flux	172	Microactuator	470
Magnetic flux linkage	174	Microcomputer	489
Main flow	8, 38	– memory	497
Mass		– processor	490
– mobile	101	– structure	489
Mass flow balance	47	Microcontrollers	506
Matter		– architecture	507
		– software	510
		Microelectronics	
		– development	487
		Micromechanics	9
		Micromechanical systems (MEMS)	588

Microprocessors		Node equation	88
– characteristic value	496	Non-linearity	
– digital signal (DSP)	510	– compensation	527
– software		NVRAM (non-volatile random access	
– standard	490	memory)	501
Misfire detection	353	Ohm's law	68
MLP (multi-layer perceptron)	311	– magnetic circuit	174
MMU (memory management unit)	494	One-port element	52
Modeling		Operating point	
– experimental	34	– dependency	283
– object-oriented	588	Oscillation	
– theoretical	33	– harmonic	333
Model		– superposition	334
– adjustment	296	Oscillator	128, 134
– bond-graph	36	– absorbers	158
– brake	564	– belt drives	151
– dynamic	549	– dampers	158
– fuzzy-logic	323	– harmonic	333
– Hammerstein	308	– identification	333, 339
– neuron	311	– longitudinal	128
– non-linear	308	– multi-mass	134
– non-parametric	295	– one-mass	128
– parametric	297, 327	– power transmission	146
– quarter-car	551	– single	334
– reference method	297	– superposition	334
– Volterra	309	– torsional	133, 134, 140, 142
Modulation		OSI-reference model	517
– amplitude	334	Parameter estimation	299, 303
– frequency	335	– continuous time signals	303
– phase	335	– discrete time signals	299
Momentum	53	– least squares	300
– angular	105	– recursive	303
– balance equation	74	– time-varying	307
– flow	85	Parity equation	537
MOS (metal oxide semiconductor)	498	PGA (pin grid arrays)	495
MOSFET (metal oxide field effect		Pneumatic	
transistors)	226	– actuator	437
Navier-Stokes equation	409	– cylinder	441, 454
Neural networks	324	– nozzle	447
– artificial	309	– rotary motor	442
Neuron model	310	– servo axis	452
Net		– storage	448
– topology	515	– translatory motors	452
Network		– transmission online	449
– dynamic systems	318	– valve	440, 445, 456
– local linear model (LOLOMOT)	314	Potential	51
– LRGF	319	Power	
– multi-layer perceptron (MLP)	311	– circuits	226
– neural	324	– component parts	225
– radial basis function (RBF)	313	– transmission	146
– static systems	309	– variables	52, 54
Newton's Laws		Power electronics	225
– kinetics	102	– converter	226
– rotational motion	103	PRBS (pseudo-random-binary signal)	
– second law of momentum	74		298
– translational motion	102		

Precision mechanics	9	- transducers	363
Principle of mechanics	106	- types	363
- d'Alembert	106	- velocity	368
- Lagrange	109	Servo axis	
Process		- hydraulic	452
- non-linear	308	- pneumatic	452
- static	316	Side flow	38
Process elements		Signal	
- causality	91	- preprocessing	19
- classification	37	- processors	510
- connection	88	Simulation	559
- displacement	53	- hardware-in-the-loop	569, 572
- lumped parameters	40	- methods	569
- momentum	53	Sink	41, 69
- distributed parameters	46	SMD (surface-mounted devices)	495
Process engineering	10	Soft computing	24
Processors		Sources	40, 57
- application-specific	512	- current	59
- signal	510	- potential	57
PROFIBUS	519	Spectral estimation	347
PROM (programmable ROM)	500	Spring	118
		- gas	118, 119
RAM (random access memory)	498	- helical	119
RBF(Radial basis function)	313	- metal	118
Redundancy		- rubber	118
- analytical	482	Spring-damper system	119
- dynamic	478	- Coulomb-model	122
- static	477	- Kelvin-Voigt model	119, 122
Requirements engineering	25	- Maxwell-model	122
Reynolds number	411	Spring-mass system	76
Robot		SRAM (static random access memory)	500
- control	589	Stability	
- industrial	577	- machine	251
ROM (read only memory)	498	State-space representation	130
		State-variable filter (SVP)	305
Sensor	359	Stepper motor	201
- acceleration	370	Stiction	159
- analog-to-digital conversion	376	Stiffness	117
- classification	360	Storage	59
- displacement	364	Strain gauge measurement	366
- electrodynamic	368	Stribeck characteristic	160
- encoders	366	Supervision	21
- fault detection	480	Suspensions	
- fault-tolerant	481	- active	542
- force	372	- adaptive	554
- Hall effect	367	- control	554
- incremental inductive	368	- passive vehicle	538
- integrated	378	- semi-active	543
- intelligent	378	Synergy	27
- measuring amplifiers	363	Systems	33
- measurements	364, 370, 372, 373	- adaptive	21
- pressure	372	- autonomous	1
- properties	362	- bus	487
- resistive	364	- electronic	1
- strain gauge	366	- expert	23
- temperature	373	- free	6
- torque	373		

- functions	13
- fuzzy-logic	323, 324
- intelligent	1, 22
- intelligent mechatronic	5
- joint	6
- limitation	11
- mechanical	1, 2, 6
- mechatronic	1
- multi-level control	18
- spring-damper	122
- spring-mass-damper	128
- thermal	77
- time-varying	306
Test signals	298
Thermodynamics	
- first law	79
Throttle valve	535
- electrical	535
Through variable	36, 54
Thyristor	225
Time constant	
- machine	255
Torsion	
- bar	116
- stiffness	118
Transducer	363
Transformer	40, 62
Transistor	
- MOS	498
Transmission	146
Truck	
- drivetrain	282
- simulation	575
Two-port element	3, 52
Universal motor	221
Vehicle	
- brake	560
- quarter car	551
- suspension, see also suspension	558
Vibrations, see oscillations	
Visco clutch	151
V-model	29, 569, 588
Volterra model	209
VTG (variable nozzle turbocharger)	321, 572
Wheel module	562
Windowing function	346
Work	
- displacement	80
- mechanical	79
- usable	81
- virtual	107, 110